

UNCLASSIFIED

AD NUMBER

AD367774

LIMITATION CHANGES

TO:

Approved for public release; distribution is unlimited. Document partially illegible.

FROM:

Distribution authorized to U.S. Gov't. agencies only; Test and Evaluation; 01 DEC 1965. Other requests shall be referred to Air Force Aero Propulsion Laboratory, Research and Technology Division, Wright-Patterson, AFB OH 45433. NOFORN.

AUTHORITY

dna-sst1 ltr dtd 14 Sep 1995

THIS PAGE IS UNCLASSIFIED

UNCLASSIFIED

AD NUMBER

AD367774

CLASSIFICATION CHANGES

TO:

UNCLASSIFIED

FROM:

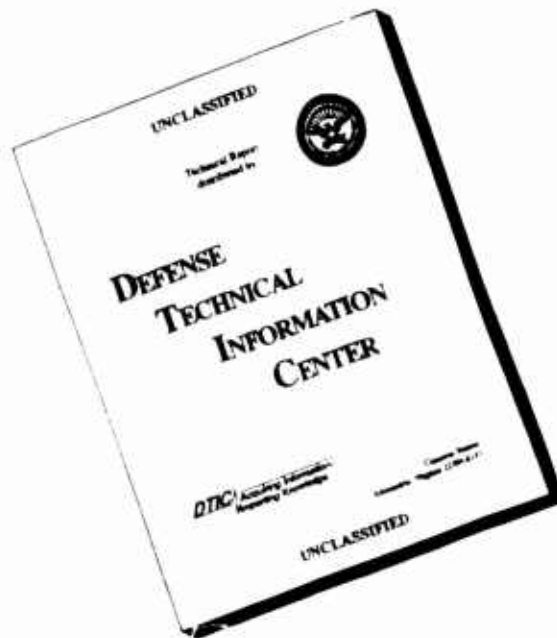
CONFIDENTIAL

AUTHORITY

31 dec 1977, DoDD 5200.10

THIS PAGE IS UNCLASSIFIED

# DISCLAIMER NOTICE



**THIS DOCUMENT IS BEST QUALITY AVAILABLE. THE COPY FURNISHED TO DTIC CONTAINED A SIGNIFICANT NUMBER OF PAGES WHICH DO NOT REPRODUCE LEGIBLY.**

# **SECURITY**

---

# **MARKING**

**The classified or limited status of this report applies to each page, unless otherwise marked.**

**Separate page printouts MUST be marked accordingly.**

---

**THIS DOCUMENT CONTAINS INFORMATION AFFECTING THE NATIONAL DEFENSE OF THE UNITED STATES WITHIN THE MEANING OF THE ESPIONAGE LAWS, TITLE 18, U.S.C., SECTIONS 793 AND 794. THE TRANSMISSION OR THE REVELATION OF ITS CONTENTS IN ANY MANNER TO AN UNAUTHORIZED PERSON IS PROHIBITED BY LAW.**

**NOTICE:** When government or other drawings, specifications or other data are used for any purpose other than in connection with a definitely related government procurement operation, the U. S. Government thereby incurs no responsibility, nor any obligation whatsoever; and the fact that the Government may have formulated, furnished, or in any way supplied the said drawings, specifications, or other data is not to be regarded by implication or otherwise as in any manner licensing the holder or any other person or corporation, or conveying any rights or permission to manufacture, use or sell any patented invention that may in any way be related thereto.

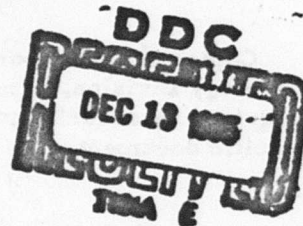
AF APL-TR-65-103  
Volume II

**"ANALYTICAL AND EXPERIMENTAL EVALUATION OF  
THE SUPERSONIC COMBUSTION RAMJET ENGINE" (U)**

**TECHNICAL REPORT AF APL-TR-65-103,  
VOLUME II - "COMPONENT EVALUATION"**

**December 1, 1965**

**Air Force Aero Propulsion Laboratory  
Research and Technology Division  
Air Force Systems Command  
United States Air Force**



**SPECIAL HANDLING REQUIRED  
NOT RELEASABLE TO FOREIGN NATIONALS**

**DOWNGRADED AT 3 YEAR INTERVALS  
DECLASSIFIED AFTER 12 YEARS  
DOD DIR 5200.10**

**Prepared under Contract No. AF33(615)-1586,  
BPSN 4(6399-651E) By the General Electric Company,  
Advanced Engine & Technology Department, Evendale, Ohio**

## NOTICES

When Government drawings, specifications, or other data are used for any purpose other than in connection with a definitely related Government operation, the United States Government, thereby, incurs no responsibility nor any obligation whatsoever; and the fact that the Government may have formulated, furnished, or in anyway supplied the said drawings, specifications or other data, is not to be regarded by implication or otherwise as in any manner licensing the holder or any other person or corporation, or conveying any rights or permission to manufacture, use or sell any patented invention that may in anyway be related, thereto.

In addition to security requirements which apply to this document and must be met, each transmittal outside the agencies of the U. S. Government must have prior approval of the Air Force Aero Propulsion Laboratory, R&TD, Wright Patterson Air Force Base, Ohio.

Copies of this report should not be returned to the Research and Technology Division, Wright Patterson Air Force Base, Ohio unless return is required by security considerations, contractual obligations, or notice on a specific document.

FOREWORD

This report was prepared by the Advanced Engine and Technology Department of the General Electric Company, Evendale, Ohio under Air Force Contract AF33(615)-1586. This advanced technology program, "Analytical and Experimental Evaluation of the Supersonic Combustion Ramjet Engine", was administered and directed by the Air Force Aero Propulsion Laboratory, Research and Technology Division, Mr. Ruben Canny, Project Engineer.

This Volume II presents the work performed under Item II Component Evaluation, Task 2 - "Fuel Injection and Combustion" under contract AF33(615)-1586. This work was conducted under the direction of J. W. Vdoviak, Manager of Combustion and Augmentation. The principle contributors were A. Lingen, Manager of Supersonic Combustion Unit, M. J. Kenworthy, W. C. Colley, P. T. Harsha and D. E. Nieser.

This report (Volume II) was published under General Electric report number R65FPD184 and distributed as directed by Contract No. AF33(615)-1586.

Volume II of this report, which includes SCRAMJET component experimental evaluations and results together with state-of-the-art discussions and vehicle design criteria, is classified Confidential except for sections describing the General Electric Hypersonic Arc Tunnel, the M = 3.25 Cold Flow Wind Tunnel and explanations of the calculation techniques used for data processing.

The classification of Volume II is Confidential as directed by the DD Form 254 Security Check List, included in the contract.

"This document contains information affecting the National defense of the United States within the meaning of the Espionage Laws, Title 18, U. S. C., Sections 793 and 794, the transmission or revelation of which in any manner to an unauthorized person is prohibited by law."

**CONFIDENTIAL****ABSTRACT**

This abstract is classified Confidential.

This final technical report describes the results of analytical and experimental evaluations of the supersonic combustion ramjet engine. The principal objective of this program was to investigate practical component and engine designs, weights and performance levels leading toward the preliminary design of a flight test vehicle. While concentrating primarily on information in support of hypersonic (Mach 6-12) cruise missions, this program imparts supporting technology for flight operations up to orbital velocity.

Volume II of this three volume report is devoted to Item II - Component Evaluation, Task 2 - "Fuel Injection and Combustion".

This was an experimental and analytical investigation to supply design information for the aerothermo design of a supersonic combustor for a flight test vehicle. The experimental investigations were conducted in two separate facilities. The penetration of fuel jets into a supersonic stream was investigated in a cold flow supersonic wind tunnel (Mach - 3.25). Combustion tests of scale model combustors were conducted in General Electric's Hypersonic Arc Tunnel. The results from the cold flow tests and from Mixing Theory were utilized in designing combustors. Combustion tests of several configurations identified a burner having adequate performance characteristics for achieving the vehicle mission. The aero-thermo design of the vehicle combustor was based on this tested configuration.

**PUBLICATION REVIEW**

This technical document has been reviewed and approved by the Air Force Aero Propulsion Laboratory, R&TD, Wright Patterson Air Force Base, Ohio.

Date: 1 November 1965

**CONFIDENTIAL**

TABLE OF CONTENTS

	<u>Page</u>
I INTRODUCTION . . . . .	1
II PROGRAM SUMMARY . . . . .	3
III TECHNICAL DISCUSSION . . . . .	7
ITEM II - COMPONENT EVALUATION . . . . .	7
TASK 2 - FUEL INJECTION & COMBUSTION . . . . .	7
A. TASK OBJECTIVES . . . . .	7
B. SUMMARY OF WORK ACCOMPLISHED . . . . .	7
1. Cold-Flow Penetration Tests . . . . .	8
2. Arc Tunnel Tests of Scale Model Combustors . . . . .	10
3. Combustor Design Considerations . . . . .	14
C. DATA AND RESULTS . . . . .	14
1. Cold-Flow Studies . . . . .	14
a. Introduction . . . . .	14
b. Experimental Techniques . . . . .	16
1) Test Facilities . . . . .	16
a) Mach 3.25 Wind Tunnel . . . . .	16
b) Flat-Plate Centerbody and Injectors . . . . .	16
2) Instrumentation . . . . .	20
a) Wake Rake System . . . . .	25
b) Schlieren System . . . . .	25
3) Test Procedures . . . . .	28
c. Background Analysis . . . . .	28
1) Definition of Penetration . . . . .	30
2) Analytical Models . . . . .	36
3) Proposed Model . . . . .	39

## Table of Contents (continued)

	<u>Page</u>
a) General . . . . .	39
b) Supersonic Injection . . . . .	39
c) Low Aspect Ratio Slots . . . . .	42
d) Row of Holes . . . . .	44
e) Angled Injection . . . . .	44
4) Selected Correlating Parameter . . . . .	44
5) Other Empirical Correlating Parameters . . . . .	49
a) Downstream Length . . . . .	49
b) Duct Diameter . . . . .	50
c) Injector Size . . . . .	50
d) Injection Rate . . . . .	51
e) Mach Number . . . . .	51
d. Discussion and Test Results . . . . .	52
1) Methods of Penetration Measurements . . . . .	52
a) Measurement Criterion . . . . .	52
b) Temperature Measurements . . . . .	53
c) Gas Sample Measurements . . . . .	53
d) Schlieren Measurements . . . . .	57
2) Presentation of Data . . . . .	73
a) Methods of Presentation . . . . .	73
b) Single Hole Injectors . . . . .	76
c) Slot Injectors . . . . .	76
d) Long Row Injectors . . . . .	80
e) Normal/Downstream Injectors . . . . .	83
3) Comparison of Test Data . . . . .	94
a) Data from Mach 3.25 Wind Tunnel . . . . .	94
b) Comparisons with Other Investigators . . . . .	97
4) Injector Designs Selected . . . . .	102
e. Application of Mixing Theory to Penetrating Jets . . . . .	103

## Table of Contents (continued)

	<u>Page</u>
1) Flow Field Downstream of Penetrating Jet . . . . .	103
2) Wake Mixing Theory for Cocurrent Flow . . . . .	105
a) Theoretical Approach . . . . .	105
b) Wake Equations . . . . .	106
3) Two-Dimensional Model of Combustor . . . . .	107
a) Description of Model . . . . .	107
b) Velocity of Penetrated Jets . . . . .	110
c) Composition in Wake . . . . .	111
4) Effect of Static Pressure Field . . . . .	122
5) Effect of Combustion and Mach Number in Mixing . . . . .	123
6) The Eight Injector Configuration . . . . .	124
2. Arc Tunnel Combustor Tests . . . . .	127
a. Experimental Technique . . . . .	127
1) The Arc Tunnel . . . . .	127
a) Combustor Inlet Air Supply . . . . .	129
b) Air Heater Power Supply . . . . .	129
c) Air Heater . . . . .	130
d) Fuel Supply . . . . .	133
e) Exhaust System . . . . .	134
2) Combustor Inlet Air Nozzles . . . . .	134
a) Combustor Inlet Air Nozzles . . . . .	134
b) Fuel Injectors . . . . .	135
c) Tailpipes . . . . .	145
d) Combinations Tested . . . . .	148
3) Measurements . . . . .	152
4) Data Analysis Procedures . . . . .	156
a) Types of Data . . . . .	156
b) Initial Data Reduction . . . . .	158
c) Computed Data . . . . .	172
d) Continuity Check . . . . .	174
e) Eta-NT . . . . .	175

## Table of Contents (continued)

	<u>Page</u>
b. Test Results for Performance. . . . .	177
1) Step Combustors . . . . .	177
a) Configuration AEN. . . . .	177
b) Configuration AFN. . . . .	179
c) Configuration AJN. . . . .	194
d) Configuration BEN. . . . .	194
e) Configuration AGN. . . . .	200
f) Configuration BGN. . . . .	200
g) Configuration BHN. . . . .	200
h) Configurations AGP and AHP . . . . .	205
2) Conical Combustors . . . . .	212
a) Configuration AFQ . . . . .	212
b) Configuration AGQ . . . . .	216
c) Configuration AGFQ. . . . .	222
d) Configuration BHQ . . . . .	222
e) Configuration AKQ and AKFQ. . . . .	227
3) Constant Area Tests for Film Cooling . . . . .	233
4) Step-Cone Combustors . . . . .	237
a) Configuration AHmR. . . . .	237
b) Configuration BHmR. . . . .	240
c) Configuration BHmGR . . . . .	252
5) Summary of Performance Measurements . . . . .	258
a) The Nature of the Flow . . . . .	258
b) Wall Pressure Forces . . . . .	268
c) Combustion Efficiency . . . . .	287
d) Friction Drag . . . . .	294
e) Combined Effects . . . . .	298
c. Burner Nozzle Tests . . . . .	300
1) Objectives . . . . .	300
2) Choked-Burner Exit Conditions . . . . .	300
3) Burner with Fuel/Air Profile . . . . .	301
4) Final Configuration . . . . .	305
5) Applicability of Data Taken from Exhaust Nozzle . . . . .	312

## Table of Contents (continued)

	<u>Page</u>
d. Results of Ignition Tests . . . . .	312
1) Auto-Ignition Experience . . . . .	312
2) Successful Igniter Tests . . . . .	314
a) High Fuel Flow . . . . .	314
b) High Back Pressure. . . . .	317
c) Cold Gas Injection in Step. . . . .	317
d) Cold Gas Injection at Burner Exit . . . . .	317
e) An Explosive Charge in Step. . . . .	317
f) Staged Fuel Injection . . . . .	322
3) The Recommended Igniter System . . . . .	322
3. Combustor Design Considerations . . . . .	322
a. Description of the Problem. . . . .	322
b. Combustor Modes . . . . .	325
1) Supersonic Combustion . . . . .	325
2) Transonic Combustion . . . . .	329
3) Subsonic Combustion . . . . .	331
c. Combustor Features . . . . .	332
1) Area Ratio . . . . .	332
2) Burner Length . . . . .	334
a) Friction Loss . . . . .	334
b) Mixing . . . . .	334
c) Chemical Kinetics . . . . .	335
d) Vehicle Geometry Limitations . . . . .	336
3) Fuel Injection . . . . .	338
a) Struts and Wall Injectors. . . . .	338
b) Geometry . . . . .	339
c) Location . . . . .	339
d. The Recommended Combustor Design. . . . .	339
1) Design Features . . . . .	339
a) Area Ratio . . . . .	341
b) Divergence Rate . . . . .	341
c) Combustor Length . . . . .	343
d) Fuel Staging . . . . .	343
e) Ignition . . . . .	346

Table of Contents (continued)

	<u>Page</u>
2) Combustor Performance Over the Flight Map (Mach 6-12) . . . . .	346
a) Efficiency, Wall Force & Friction from Mach 6 to 9 Tests . . . . .	346
b) Applicability of Performance Parameters to Cycle Analyses . . . . .	353
e. Generalization of the Recommended Design . . . . .	355
1) Mach 3 to 6 . . . . .	355
2) Mach 12 and above . . . . .	356
3) Effects of Size . . . . .	356
D. CONCLUSIONS AND RECOMMENDATIONS . . . . .	357
1. Conclusions . . . . .	357
a) Demonstrated Performance Levels . . . . .	357
b) Increased Knowledge . . . . .	357
1) Ignition . . . . .	357
2) Jet Penetration . . . . .	358
3) Fuel Distribution . . . . .	358
c) Projected Performance Levels . . . . .	358
2. Recommendations . . . . .	359
REFERENCES . . . . .	361
APPENDIX I . . . . .	365

LIST OF ILLUSTRATIONS

<u>Figure</u>	<u>Title</u>	<u>Page</u>
1	Mach 3.25 Wind Tunnel	17
2	Wind Tunnel Schematic	18
3	Wind Tunnel Throat and Test Section	19
4	Flat Plate with Injector and Wake Rake	21
5	Flat Plate and Injector Position	22
6	Injector Plates	23
7	Wake Rakes	26
8	Schlieren System	27
9	Distributed Light Source Schlieren System	29
10	Penetrating Jet	31
11	Jet Concentration Profile (From Reference 5)	33
12	Uniform Concentration Profile	34
13	Wall Effect on Peak Concentration	35
14	Three Simple Analytical Models	37
15	Proposed Penetration Model	40
16	Jet Expansion from Sonic Holes	41
17	Jet Expansion from Supersonic Holes	43
18	Measured Temperature Profile	54
19	Measured Concentration Profile	55

## List of Illustrations (continued)

<u>Figure</u>	<u>Title</u>	<u>Page</u>
20	Measured Impact Pressure Profile	56
21	Initial Schlieren Photograph	58
22	Initial Schlieren Photograph	59
23	Shock Waves on Instrumentation Wake	60
24	Vibration Effects	62
25	Spark Schlieren Photograph	63
26	Full Light Cut-off	65
27	Shadow Graph from Reference 5	66
28	Turbulent Mixing of Helium using Distributed Spark Light Source	67
29	Turbulent Mixing of Nitrogen using Distributed Spark Light Source	68
30	Helium Penetration using Distributed Continuous Light Source	69
31	Nitrogen Penetration using Distributed Continuous Light Source	71
32	Air Penetration using Spot Light Cut-off	71
33	Helium Penetration using Spot Light Cut-off	72
34	Long Row Injector Penetration	74
35	Sonic Slot Injector Flow	75
36	Single Normal Round Sonic Hole Schlieren Data	77
37	Supersonic Normal Round Hole Data	78

## List of Illustrations (continued)

<u>Figure</u>	<u>Title</u>	<u>Page</u>
38	.83" Long Sonic Slot Data	79
39	.83" Long Supersonic Slot Data	81
40	3.0" Long Supersonic Slot Data	82
41	Nine 1/16" Dia. Normal Round Hole Data	84
42	Fourteen 1/16" Dia. Normal Round Hole Data	85
43	Fourteen Normal Round Sonic Holes with Diameter Increasing in Aft Direction	86
44	Fourteen .154" Dia. Normal Round Hole Data	87
45	Protruding Supersonic 30° Round Hole Data	89
46	Comparison of Protruding 30° Supersonic Injector Schlierens	90
47	Twelve 30° 1/16" Dia. Round Hole Data	91
48	Schlieren Photographs of Penetration of the Twelve 30° 1/16" Dia. Holes	92
49	Twelve 30° Square (.06" x .06") Hole Data	93
50	Comparisons of Low Aspect Ratio Penetration Data	95
51	Momentum Correlation of Reference 5 Data	98
52	Momentum Comparison of all Penetration Data	101
53	Fuel Injection and Wake Mixing Models	104
54	Two-Dimensional Model of Circular Duct	108
55	Centerline Decay of Velocity Defect for Stoichiometric Conditions	112
56	Centerline Decay of Massflow Composition	114

## List of Illustrations (continued)

<u>Figure</u>	<u>Title</u>	<u>Page</u>
57	Effect of Initial Velocity Ratio on Mixing	115
58	Wake Velocity Profile	116
59	Profile for Equivalence Ratio of Two	118
60	Mixing Efficiency for Single Jet	119
61	Mixing Efficiency vs. Length	120
62	Construction of Fuel Distribution from Two-Dimensional Solution	125
63	Penetration vs. Flight Mach Number	126
64	Mixing Efficiency vs. ER for several $\frac{X}{D}$	128
65	Electric Arc Air Heater (Schematic)	131
66	Arc Tunnel Combustion Test Apparatus	132
67	Supersonic Combustor Models (Schematic)	138
68	Injector E	139
69	Fuel Nozzle Details, Injectors E & F	140
70	Injector K	142
71	Liner, Injector G	143
72	Injector Casing	144
73	Supersonic Combustor Models (Schematic)	146
74	Combustor Model Installation	147
75	Combustor Model Installation	149
76	Tailpipe R (Schematic)	150

List of Illustrations (continued)

<u>Figure</u>	<u>Title</u>	<u>Page</u>
77	Tailpipe R: Aft Looking Forward	151
78	Combustor Exit Rake	154
79	Gas Sampling System (Schematic)	155
80	Quench Probe Details	157
81	Gas Sample Probe Locations	159
82	Gas Sample Probe Locations	160
83	Gas Sample Probe Locations	161
84	Gas Sample Probe Locations	162
85	Gas Sample Probe Locations	163
86	Gas Sample Probe Locations	164
87	Typical Chromatograph Calibration for Oxygen	166
88	Typical Chromatograph Calibration for Nitrogen	167
89	Typical Chromatograph Calibration for Hydrogen	168
90	Schematic Chromatograms	169
91	Hydrogen Trace Tail Correction	171
92	Wall Static Pressures, Configuration AEN	178
93	Wall Static Pressures, Configuration AEN	180
94	Burner Exit Stream Property Contours	183
95	Burner Exit Stream Property Contours	184
96	Burner Exit Stream Property Contours	185

## List of Illustrations (continued)

<u>Figure</u>	<u>Title</u>	<u>Page</u>
97	Burner Exit Stream Property Contours	186
98	Burner Exit Stream Property Contours	187
99	Burner Exit Stream Property Contours	188
100	Wall Static Pressures, Configuration AFN	190
101	Wall Static Pressures, Configuration AFN	191
102	Burner Exit Stream Property Contours	192
103	Burner Exit Stream Property Contours	193
104	Wall Static Pressures, Configuration AJN	195
105	Wall Static Pressures, Configurations BEN and BHN	196
106	Wall Static Pressures, Configurations BEN and BHN	197
107	Wall Static Pressures, Configurations BEN and BHN	198
108	Wall Static Pressures, Configurations BEN and BHN	199
109	Fuel/Air Profile for Run 191-1 (BEN)	201
110	Wall Static Pressures, Configurations AGN and AFN	202
111	Wall Static Pressures, Configurations BGN and BHN	203
112	Wall Static Pressures, Configurations BGN and BHN	204
113	Fuel/Air Profile for Run 183-1 (BHN)	206

## List of Illustrations (continued)

<u>Figure</u>	<u>Title</u>	<u>Page</u>
114	Fuel/Air Profile for Run 183-2 (BHN)	207
115	Fuel/Air Profile for Run 185 (BHN)	208
116	Fuel/Air Profile for Run 188-1 (BHN)	209
117	Fuel/Air Profile for Run 189 (BHN)	210
118	Wall Static Pressures, Configuration AHP	211
119	Fuel/Air Profile for Run 107 (AHP)	213
120	Wall Static Pressure, Configuration AFQ	214
121	Wall Static Pressure, Configuration AFQ	215
122	Burner Exit Stream Normalized Equivalence Ratio Contours (ER/ERo) - Run 154, Configuration AFQ	218
123	Mach Number Contour at Burner Exit, Run 154 Configuration AFQ	219
124	Wall Static Pressures, Configuration AGQ	220
125	Fuel/Air Profile for Run 164 (AGQ)	221
126	Wall Static Pressure, Configuration AGFQ	223
127	Wall Static Pressure, Configuration AGFQ	224
128	Wall Static Pressure, Configuration BHQ	225
129	Wall Static Pressure, Configuration BHQ	226
130	Normalized Static Pressure, Configuration BHQ	228
131	Fuel/Air Profile, Run 181 (BHQ)	229
132	Wall Static Pressure, Configuration AKQ	230

## List of Illustrations (continued)

<u>Figure</u>	<u>Title</u>	<u>Page</u>
133	Wall Static Pressure, Configuration AKFQ	231
134	Wall Static Pressure, Configuration AKFQ	232
135	Fuel/Air Profile for Run 160 (AKQ)	234
136	Wall Static Pressures, Configuration AK3	235
137	Fuel/Air Profile for Run 157-2	236
138	Film Slot Injector Comparison	238
139	Wall Static Pressures, Configuration AHmR	239
140	Wall Static Pressures, Configuration AHmR	241
141	Fuel/Air Profile For Run 206, Configuration AHmR	243
142	Mach Number Profile for Run 206	244
143	Fuel/Air Profile for Run 208 (AHmR)	245
144	Mach Number Profile for Run 208 (AHmR)	246
145	Wall Static Pressure, Configuration BHmR	247
146	Wall Static Pressure, Configuration BHmR	248
147	Wall Static Pressure, Configuration BHmR	249
148	Wall Static Pressure, Configuration BHmR	250
149	Wall Static Pressure, Configuration BHmR	251
150	Normalized Static Pressure, Configuration BHmR	253
151	Fuel/Air Profile for Run 212 (BHmR)	254
152	Fuel/Air Profile for Run 210 (BHmR)	255
153	Wall Static Pressures, Configuration BHmGR	256

## List of Illustrations (continued)

<u>Figure</u>	<u>Title</u>	<u>Page</u>
154	Wall Static Pressures, Configuration BHmGR	257
155	Theoretical Effect of Heat Addition on Wall Pressure for Transonic Combustor	260
156	Measured Step Base Pressure vs. ER	262
157	Choking Effects in Stream with 2 Step Profile	265
158	V&M Variations, Run 110	267
159	Flow About a Rearward Facing Step (Schematic)	269
160	Effect of Equivalence Ratio on Step Pressure (Mach 2.7 Nozzle)	273
161	Effect of Equivalence Ratio on Step Pressure (Mach 2.7 Nozzle)	274
162	Effect of Equivalence Ratio on Step Pressure (Mach 3.25 Nozzle)	275
163	Effect of Equivalence Ratio on Step Pressure (Mach 3.25 Nozzle)	276
164	Generalized Character of Effect of Equivalence Ratio and Step Pressure	280
165	Effect of Total Enthalpy on Step Pressure (Mach 2.7 Nozzle, H and E Injectors)	281
166	Effect of Heat Addition on Step Pressure (Mach 2.7 Nozzle, H and E Injectors)	282
167	Wall Pressure Comparison	288
168	Dissociated Products in Stoichiometric H <sub>2</sub> -Air at Equilibrium	293
169	Combustion Efficiency vs. Equivalence Ratio	295
170	Thrust Potential vs. Equivalence Ratio	299

## List of Illustrations (continued)

<u>Figure</u>	<u>Title</u>	<u>Page</u>
171	Static Pressure Profiles, Runs 104 and 216	302
172	Theoretical and Measured Dissociation for Run 104 as a Function of Equivalence Ratio	303
173	Measured Dissociation at Nozzle Exit for Runs 202, 216 as a Function of Equivalence Ratio	304
174	Fuel/Air Profile for Run 164 (Configuration AGQ)	306
175	Fuel/Air Profile for Run 203, Configuration AGQS	307
176	Static Pressure Profile for Run 203, Configuration AGQS	308
177	Mach No. Profile at Nozzle Exit for Runs 164 and 205, Configuration AHmRUS	309
178	Fuel/Air Profile - Runs 205 and 215, Configuration AHmRUS	310
179	Measured Dissociation at Nozzle Exit as a Function of Equivalence Ratio for Runs 205, 215 - Configuration AHmRUS	311
180	Static Pressure Distribution Runs 205, 215 and 206	313
181	Predicted Ignition Delay for Hydrogen-Air	315
182	High Fuel Flow Ignition	316
183	High Back Pressure Ignition	318
184	Cold Gas Injection in Step	319
185	Cold Gas Injection at Exit	320
186	Explosive Charge in Step	321
187	Staged Fuel Ignition	323
188	Burner Inlet Conditions	324

List of Illustrations (continued)

<u>Figure</u>	<u>Title</u>	<u>Page</u>
189	Fuel Conditions	326
190	Freezing Point Calculations (Rate of Change of Pressure with Length for Freezing Near Burner Exit)	337
191	Maximum Fuel Injection Pressure	340
192	Burner Contour	342
193	Fuel Staging for Recommended Combustion Design	347
194	Predicted Combustion Efficiency of Recommended (Combustor)	349
195	Predicted Combustion Efficiency of Recommended Combustor Design	350
196	Cycle Performance Level	352

# LIST OF TABLES

<u>Table</u>	<u>Title</u>	<u>Page</u>
I	Injection Configurations Tested in Mach 3.25 Wind Tunnel . . . . .	24
II	Injector Configuration from Literature . . . . .	100
III	Wall Contours, Nozzle "A" . . . . .	136
IV	Wall Contours, Nozzle "B" . . . . .	137
V	Summary of Test Results Step-Burners . . . . .	181
VI	Summary of Test Results Conical Burners . . . . .	217
VII	Summary of Test Results Step-Cone Burner . . . . .	242
VIII	Step-Burner Data . . . . .	277

## LIST OF SYMBOLS

<u>Symbol</u>	<u>Meaning</u>
$a$	Local sonic velocity, ft/sec
$A_f$	Frontal area of penetration jet, ft <sup>2</sup>
$A^*$	Sonic throat area, ft <sup>2</sup>
$A_e^*$	Effective injector hole area, ft <sup>2</sup>
$A_s'$	Flow area of penetration jet after turning . . . , ft <sup>2</sup>
$A_b$	Burner inlet area, ft <sup>2</sup>
$A_d$	Burner exit area, ft <sup>2</sup>
$b$	Wake half-width, ft.
$C_d$	Drag coefficient
$C_f$	Burner friction coefficient, lb/ft
$C_p$	Specific heat at constant pressure, BTU/LBM °R
$C_1, C_2, C_3$	Constants
$D$	Injector hole diameter, ft
$D_0$	Schlichting's drag, or wake momentum defect lb
$D'$	Duct Diameter, ft

# List of Symbols (Continued)

<u>Symbol</u>	<u>Meaning</u>
$D_e^*$	Effective injector hole diameter ft
$D_f$	Friction drag, lb
ER	Equivalence ratio
F	Impulse, lbf/sec
$F_x$	Interaction force in x-direction, penetration model (lbf)
$F_s$	Burner inlet impulse
$F_e$	Burner exit impulse
G	Gravitational acceleration, ft/sec <sup>2</sup>
H	Wake height, ft
Ht	Stagnation enthalpy BTO / LBM
Ht <sub>s</sub>	Burner inlet stagnation enthalpy, BTO/LBM
$K_a$	Mass fraction of air
K <sub>ac</sub>	Mass-fraction of air at c/l
K <sub>a</sub>	Free-stream mass fraction of air
$K_f$	Mass-fraction of fuel
K <sub>fc</sub>	Mass-fraction of fuel at c/l
L	Combustor length, ft
m	Molecular wt, lb/mole

List of Symbols (Continued)

<u>Symbol</u>	<u>Meaning</u>
M	Free-stream mach number
$M_p$	Simulated mach number
$M_x$	Mach number of penetrating jet after being turned downstream and adjusting to free-stream pressure
$M_o$	
$M_1$	
$M_2$	Burner inlet mach number
$M_4$	Burner exit mach number
N (1)	Number of injectors
N (2)	Generalized irreversible flow function (Appendix B)
$P, P_{jet}$	Total pressure of injectant, lb/ft <sup>2</sup>
$P_s$	Free-stream static pressure, lb/ft <sup>2</sup>
$P_t$	Total pressure, lb/ft <sup>2</sup>
$P_w$	Wall static pressure, lb/ft <sup>2</sup>
$P_s$	Burner inlet static pressure
$P_\infty$	Free-stream total pressure, lb/ft <sup>2</sup>
Q	Dynamic head
R (1)	Duct radius, ft
R (2)	Radial coordinate, ft

List of Symbols (Continued)

<u>Symbols</u>	<u>Meaning</u>
$R_0$ (1)	Universal gas constant
$R_0$ (2)	Burner Radius, ft
$S$	Injector spacing, ft
$T$	Static temperature, °R
$T_t$	Total temperature, °R
$T_s$	Inlet static temperature, °R
$T_{0s}$	Inlet stagnation temperature, °R
$T_{0t}$	Burner exit stagnation temperature °R
$U$	Local velocity, ft/sec
$U_c$	Centerline velocity, ft/sec
$U_{fuel}$	Fuel jet velocity after turning downstream...ft/sec
$U_1$	Velocity defect, $U_\infty - U$ ...ft/sec
$U_\infty$	Free-stream velocity, ft/sec
$V$	Velocity component, ft/sec
$V_a$	Burner inlet velocity
$W_a$	Air mass-flow lbm/sec
$W_f$	Fuel mass-flow, lbm/sec
$X$ (1)	Downstream distance, ft

# List of Symbols (Continued)

<u>Symbol</u>	<u>Meaning</u>
X, Y	Cartesian coordinates
Z	Penetration height, ft
f/a	Fuel-air ratio
$\beta$	Constant = 0.18
$\alpha$	Ratio of specific heats
$\eta$	Combustion efficiency
$\eta_{bm}$	Cycle-defined combustion efficiency
$\eta_m$	Mixing efficiency
$\eta_{nt}$	Net thrust potential
$\rho$	Density, lbm/ft <sup>3</sup>
<u>Subscripts</u>	<u>Meaning</u>
2	(Penetration) Penetrating fuel jet elsewhere: burner inlet plane
4	Burner exit plane
h	"Hot" part of stream
c	"Cold" part of stream

**CONFIDENTIAL****SECTION I - INTRODUCTION**

Experiments related to the development of supersonic hydrogen combustion systems for hypersonic ramjet engines have been conducted by the General Electric Company during the past several years. Prior to completion of the Hypersonic Arc Tunnel, these experiments were performed in a combustion heated wind tunnel, using a Mach 2.5 vitiated air stream with stagnation temperatures characteristic of flight speeds up to Mach 6. Early experiments in this facility were reported in Reference 2, and later experiments in References 10, 11 and 12. The major conclusions from these studies were: (1) supersonic combustion was feasible, (2) mixing was slow and ignition difficult when hydrogen was injected parallel to the air stream, (3) cross stream injection facilitated both mixing and flame stabilization, and (4) combustion induced boundary layer separations could be used as flame stabilizers and mixing promoters.

Analytical studies disclosed that there were no performance losses inherent in shock waves and boundary layer separations induced solely by the combustion process (Reference 13), implying that these phenomena could safely be employed as mixers and igniters. These studies also disclosed the inadequacy of some of the performance parameters traditionally applied to subsonic combustors for use with supersonic combustors, and suggested that new performance criteria be developed. This was subsequently done (Reference 14), the result being the Thrust Potential, a parameter related to the ability of the combustor to produce thrust when installed in the engine, and which combines the contributions of individual causes of performance defects.

The initial experiments conducted in the Hypersonic Arc Tunnel Facility were studies of fuel injection from a flat plate into a Mach 3.5 free air jet having a stagnation enthalpy representative of Mach 8 flight. These studies confirmed that burner ignition was facilitated by injection of fuel perpendicular to the air stream. They also revealed advantages of shaping the fuel jet to present minimum frontal blockage. It was found that fuel injected from a slot in the plate oriented with its long axis parallel to the airflow would penetrate the air stream without unduly disrupting the boundary layer.

Use of penetrating fuel jets to best advantage demanded that more extensive penetration data be obtained. The quantitative effects of such variables as jet nozzle geometry, injectant density and injection pressure on the extent of penetration required detailed exploration. The Arc Tunnel Facility was ill suited

**CONFIDENTIAL**

**CONFIDENTIAL**

environment. Since chemical reaction was judged to exert negligible influence on the mechanisms of jet penetration, the needed study was undertaken in a low-cost, low-temperature, supersonic wind tunnel facility.

Most experiments conducted to this point had investigated specific phenomena contributing to the over-all combustion process, such as flame stabilization, fuel-air mixing, or jet penetration. Few experiments had been conducted with the object of fully evaluating over-all combustor performance in a system directly applicable to an engine design. Development tests of a practical combustion system, which were badly needed, are the subject of this report.

**CONFIDENTIAL**

# CONFIDENTIAL

AF APL-TR-65-103

## SECTION II - PROGRAM SUMMARY

Extensive testing of several combustor-injector combinations at conditions simulating flight from Mach 5.1 to 10.5, resulted in the identification of a configuration having suitable performance characteristics for an attractive flight test vehicle. This combustor development was guided by cold flow tests on the penetration of fuel and by analytical work on mixing theory and combustion aerothermodynamics.

Cold-flow penetration tests were conducted to verify a simple penetration theory which was developed. An existing Mach 3.25 wind tunnel was modified for Helium and air injection from a flat plate at the tunnel centerline, thereby, providing a quick and reliable test technique. Many configurations were screened and the relative merits of several geometries were evaluated on the basis of a fixed quantity of injection flow. A general penetration theory, formulated from simple momentum considerations, was found to fit the data well.

A long row of holes was identified as a superior injection configuration. This geometry was found to produce a stream of fuel with a cross section which was very high relative to the width. The latter observation led to the formulation of a simple mixing model which coupled easily with the analytical penetration model to allow definition of the effect of penetration parameters on the combustor process mixing efficiency. The mixing theory was based on classical two-dimensional wake mixing. The unified penetration theory was used to generate the variation of mixing efficiency with combustor length and equivalence ratio.

Presented in this report is a complete detailed description of the General Electric Arc Tunnel Facility which was used as a hot-gas source for tests of scale-model supersonic combustors. A complete combustor environment was provided, with fuel injection type and spacing and all the details of combustor geometry exactly as envisioned in a flight engine. This configuration had a three-inch entrance diameter size and was made up of water-cooled test hardware. Analytical studies were performed and methods of data taking and analysis were reviewed, improved, finally formulated and put into use. A combustor performance criterion was used, the net thrust potential, which expressed the measured combustor performance in terms of system net thrust. Relative merits of combustors are apparent from this criterion, as well as, absolute merits, since the factor is a ratio of actual to ideal system net thrust with a given inlet and nozzle.

CONFIDENTIAL

**CONFIDENTIAL**

The arc tunnel test program consisted of some 92 test runs which comprised a total arc time of nine hours 34 minutes. From this large number of runs, 21 were processed and yielded the measured combustor performance presented in this report. These tests included enthalpy levels which simulate flight over the range of Mach 5.1 to 10.5. The test program was concerned with the following six facets of the combustor performance problem:

- 1) Evaluation of ignition methods for the Mach 6 to 8 range.
- 2) Measurement of performance of step combustors with area ratio 2.5 over the range of enthalpies simulating Mach 6 to 9 flight.
- 3) Measurement of the performance of conical combustors over the same range.
- 4) Some brief observations on the characteristics of a constant-area geometry with a wall-slot injector.
- 5) The formulation of a final design incorporating injectors with downstream thrust and an advanced geometry.
- 6) The acquisition of test experience for a combustor/nozzle combination.

The experimental work in the arc tunnel was supported by continuing evaluations of various combustor phenomena through the use of several analytical models. The concept of "transonic combustion" was dealt with as supersonic heat addition ending at a choked condition. Choking criteria were developed for uniform (one-dimensional) and non-uniform flows. The particular importance of momentum to the choking criteria led to a re-emphasis of early ideas on the importance of the momentum quantity to the one-dimensionalization of non-uniform flows. The study of choking phenomena also provided a basis for correlations of minimum wall forces for "transonic combustion".

The final combustor design was formulated which was very close to the step/cone geometry tested in the arc tunnel. The inlet design, with six "barrels", provides six "struts" which are believed to be effective in maintaining efficiency at levels observed in tests, out to the vicinity of Mach 12. Two stages of fuel injection are provided, one at the step area change and one three diameters upstream of the step area change. Only the fuel injectors at the step are employed from Mach 6 to near Mach 8 and both sets are used to provide a smooth transition up to a point where all fuel flow is to the upstream fuel injectors (at a Mach number near 9.5). All injectors are rows of six sonic holes directed at 30 degrees downstream. There are eight equally spaced sets at the upstream section in each of the six pipes (48 fuel injectors) and six equally spaced sets at the downstream station. The combustor area ratio is 2.0. The geometry is identical to that of the step/cone geometry tested in the arc tunnel with the exception of the multiple pipes.

**CONFIDENTIAL**

Performance values were calculated for the selected configurations over the range from Mach 6 to 12. Heavy emphasis was placed on the experimental information hand. Wall force and friction drag were calculated in keeping with present cycle assumptions and the projected efficiency varied from .85 (at Mach 6 and  $ER = 1.0$ ) to .90 (at Mach 12 and  $ER = 1.6$ ).

**CONFIDENTIAL**SECTION IIIITEM II - COMPONENT EVALUATIONTASK 2 - FUEL INJECTION & COMBUSTIONA. TASK OBJECTIVES

Aerothermodynamic analyses of mixing phenomena and loss mechanisms shall be extended in order to provide theoretical comparisons for test results and permit extrapolation of pertinent parameters over the Mach 6-25 flight spectrum. This effort shall be compared with existing analyses and supported by cold flow tests in the Mach 3 tunnel, which shall also provide preliminary screening of concepts prior to flame tunnel testing.

Combustion testing of selected injector designs shall be accomplished in an existing steady state facility. The most promising designs shall be further evaluated in a closed combustor, in a steady state, arc tunnel facility. An enclosed combustor shall be tested in the existing steady state facility, with a reference velocity and stagnation temperature corresponding to Mach 6 flight. This test model shall be designed such that data will provide adequate information for determining combustion efficiency, wall friction factors, total momentum coefficient for injected fuel, and realistic exit conditions for the definition of nozzle thrust coefficient.

An enclosed duct for the arc tunnel shall be designed, fabricated and tested at contained stream conditions. This model shall incorporate removable sections to permit investigations of fuel injectors and film cooling effects at reference velocities and stagnation temperatures corresponding to flights from Mach 6 to 9.

B. SUMMARY OF WORK ACCOMPLISHED

The work accomplished under the topic of "Fuel Injection and Combustion" is properly divided into three parts:

- 1) Cold flow penetration tests of injectors
- 2) Arc tunnel tests of scale-model combustors
- 3) Combustor design considerations for the flight test vehicle

**CONFIDENTIAL**

**CONFIDENTIAL**

AF APL-TR-65-103

The subsequent summary of this work is divided into three parts, under these three special headings.

Cold flow tests were identified as a convenient technique for screening injectors for use in scale-model and full-scale supersonic combustors. The data correlations of the cold-flow test data allowed generalization of the data for all important variables. Several injectors from this study were evaluated in scale-model combustor tests. The cold-flow tests also were instrumental in allowing simple mixing calculations to be coupled to penetration calculations, a procedure which resulted in a technique which is capable of showing the effects of a wide range of injection variables on combustor mixing efficiency.

The General Electric arc tunnel was used as a hot-gas source for scale-model tests of combustor geometry. An elaborate test setup was used to obtain detailed measurements of all pertinent combustor parameters and multi-stream analysis techniques were employed to obtain combustor performance criteria. Tests were made to identify workable ignition systems for Mach 6 to 8 and to evaluate combustor performance with several injector geometries and several combustor geometries. A step-cone tailpipe, used in conjunction with an 8 injector arrangement of 30 degree sonic holes, was found to have excellent performance over the test range of Mach 6 to 9. This geometry was selected as the basic type on which to base the design for the flight test vehicle discussed in Volume I of this report.

Through consideration of analytical and experimental results, the details of the flight test vehicle combustor were formulated and performance was calculated for the range Mach 6 to 12. It was concluded that the combustor component provided adequate performance for an attractive flight test vehicle.

#### Cold-Flow Penetration Tests

Cold-flow penetration tests were conducted to verify a simple penetration theory which was developed. An existing Mach 3.25 wind tunnel was modified for Helium and air injection from a flat plate at the tunnel centerline, thereby, providing a quick and reliable test technique. Many configurations were screened and the relative merits of several geometries were evaluated on the basis of a fixed quantity of injection flow. A general penetration theory was formulated from simple momentum considerations and was found to fit the data well.

A long row of holes was identified as superior injection configuration. This geometry was found to produce a slug of fuel, the cross section of which was very high relative to the width. The latter observation led to the formulation of simple mixing model which coupled easily with analytical penetration model to allow the definition of the effect of penetration parameters on the combustion process mixing efficiency. The mixing theory was based on classical, two-dimensional, wake mixing. The unified penetration theory was used to generate the variation of mixing efficiency with combustor length and with equivalence ratio.

**CONFIDENTIAL**

# CONFIDENTIAL

AF APL-TR-65-103

These studies provided several important results:

- 1) A general penetration theory which fit the data and provided methods of extrapolation for all of the important injection variables such as size, penetration pressure and temperature, free stream Mach number, and fuel/air ratio.
- 2) The identification of a unique injector geometry of practical proportions providing performance superior to single hole injectors.
- 3) A unified theory of penetration and subsequent mixing which was used to examine trends associated with the effects of combustor length and fuel/air ratios on the mixing efficiency of the combustion process.

A penetration theory was developed by treating the penetrating jet as a simple momentum exchange phenomenon associated with the drag of the obstruction which the injectant poses for the air stream. This theory was found to adequately describe the trends of data from the penetration experiments. Details of the theory are presented in this report. The form of the correlations, based on the theory, allows the evaluation of the effects of all the important injection parameters; i. e., injection pressure and temperature, injection Mach number, freestream Mach number and respective fluid densities.

The penetration tests were conducted with a variety of injector geometries. These terminated when improved configurations which had practical use were identified. The tests were begun with single, normal round holes and correspondence was established with the results obtained by other investigators. The advantage of supersonic penetration was found for the correct restraint of a given fuel flow. Note that, as used throughout this study, the non-dimensionalizing of the penetration distance with the throat diameter of the injector (or the diameter corresponding to the total throat area of an injector) placed on the penetration the proper restraint of a fuel flow. This practice was not adopted by other investigators of penetration into a supersonic stream.

Theoretical grounds for the improved penetration of supersonic injectors were found and used to identify injector configurations which had low aspect ratio (that is, were long in the direction of the air stream and narrow in a dimension perpendicular to the air stream). Of these high slenderness ratio or low aspect ratio configurations, a series of round sonic holes which were axially aligned were identified as the most desirable from a mechanical standpoint. Both normal and 30 degree downstream injecting rows were found to have equivalent penetration and a theoretical reasoning for this was developed from momentum considerations. Both these promising configurations were applied to combustor

CONFIDENTIAL

**CONFIDENTIAL**

geometries for subsequent scale-model testing in the General Electric Arc Tunnel.

The observations of penetration phenomena from tests identified the possibility of a simplified mixing theory which accounted for only the shear mechanism between the injected jet and a freestream flow. Appropriate treatments were found which concerned axisymmetric and two-dimensional mixing models with confluent (cocurrent) flow. From these analyses, a two-dimensional model was chosen for two important reasons; it was the simplest and was the method that best matched the fuel injectors. Mixing calculations were made which accounted for confluent (cocurrent) flow by treating the system as a wake at a distance far downstream of the fuel injection. The calculations identified moderate performance for relatively long combustors, under conditions approximating constant pressure fields. The method was then extended to account approximately for axial static-pressure gradients, such as those normally resulting from combustion, and a degree of performance improvement was identified for several size gradients. Variations in mixing efficiency were generated for a range of combustor length and equivalence ratio with and without axial pressure gradients. These variations are presented in Section C.1.e. Note that a relatively constant pressure environment is typical of a divergent combustor at Mach 12, while Mach 6 performance is believed to tend toward the infinite pressure gradient case provided transonic combustion is involved.

#### Arc-Tunnel Tests of Scale Model Combustors

Presented in this report is a complete detailed description of the General Electric Arc Tunnel Facility which was used as a hot-gas source for tests of scale-model supersonic combustors. A complete combustor environment was provided with fuel injection type and spacing and all the details of combustor geometry exactly as envisioned in a flight engine, but in a 3-inch entrance diameter size and in water-cooled test hardware. Analytical studies were performed and methods of data taking and analysis were reviewed, improved, finally formulated and put into use. A combustor performance criterion was used, the net-thrust potential, which expressed the measured combustor performance in terms of system net thrust. Relative merits of combustor are apparent from this criterion as well as absolute merits, since the factor is a ratio of actual to ideal system net thrust with a given inlet and nozzle.

The Arc Tunnel Test Program consisted of some 92 test runs which comprised a total arc time of 9 hours 34 minutes. From this large number of runs, 62 runs were processed as having yielded good data and 21 were performance runs which yielded measured combustor performance as presented in this report. These tests included enthalpy levels which simulate flight over the range of Mach 5.1 to 10.5. The test program was concerned with six facets of the combustor performance problem:

**CONFIDENTIAL**

# CONFIDENTIAL

AF APL-TR-65-103

- 1) Evaluation of ignition methods for the Mach 6 to 8 range.
- 2) Measurement of performance of step combustors with area ratio 2.5 over the range of enthalpies simulating Mach 6 to 9 flight.
- 3) Measurement of the performance of conical combustors over the same range.
- 4) Some brief observations on the characteristics of a constant-area geometry with a wall-slot injector.
- 5) The formulation of a final design incorporating injectors with downstream thrust and an advanced geometry.
- 6) The acquisition of test experience for a combustor/nozzle combination.

These facets are dealt with separately in the subsequent section on "Data and Results".

The experimental work in the arc tunnel was supported by continuing evaluations of various combustor phenomena using several analytical models. The concept of "transonic combustion" was dealt with as supersonic heat addition ending at a choked condition. Choking criteria were developed for uniform (one-dimensional) and non-uniform flows. The particular importance of momentum to the choking criteria led to a re-emphasis of early ideas on the importance of the momentum quantity to the one-dimensionalization of non-uniform flows. The study of choking phenomena also provided a basis for correlations of minimum wall forces for "transonic combustion".

These studies had several important results: (1) re-affirmation of the need for detailed combustor-exit measurements; (2) development of a workable ignition system for the Mach 6 to 8 range; (3) evaluation of the concept of abrupt area change in combustors having an area ratio of 2.5 for the range Mach 6 to 9; (4) identification of conical geometries as having superior wall-pressure force characteristics to step geometries; (5) formulation of a final configuration incorporating both a step and conical geometry in an area ratio of 2.0; (6) extension of choking criteria from one-dimensional flow to flow with non-uniformity in Mach number and temperature; and, (7) formulation of appropriate one-dimensional equivalent values for non-uniform streams with severe variations in Mach number, composition, temperature and pressure.

CONFIDENTIAL

## CONFIDENTIAL

AF APL-TR-65-103

Analytical consideration was given to the various sources of loss in combustor performance as evident from detailed test observations of the burner exit flow. First among the sources of loss was a profile of fuel/air ratio. Since most cycles require burning at equivalence ratio equal to 1.0, losses due to fuel/air profile are most severe because stoichiometric heat release is a maximum. Rich streaks have unburned fuel and lean streaks have unused oxygen. The independent variable for the variation of profile in fuel/air ratio can be either area or time; and, because the supersonic combustor is basically a turbulent mixing process, the usual case has losses from both sources. (The previously mentioned mixing calculations accounted only for spatial or area profile). Profiles of temperature with area or time are also sources of loss in efficiency. As temperature increases, heat release becomes unavailable due to dissociation at a rate exponential with temperature. Therefore, peaks and valleys of temperature produce different deviations from the average dissociation levels with large net positive losses in heat release. A similar combustor loss results from the heat transferred to the combustor wall. A further loss due to freezing of the composition in the nozzle expansion process is believed to be properly attributable to the combustor design, but is traditionally allocated to the exhaust-nozzle.

The Arc Tunnel Test Program was initiated at the lowest enthalpy level of interest, Mach 6. Even burners with normal fuel injection were found to be unlit at enthalpies as high as that for Mach 7.5. As a result, an experimental study was made of ignition methods. Two appropriate methods were identified. For a single fuel injection plane, a hot-gas source was successfully employed which lit the burner without detrimental effects upstream of the fuel injection station and, hence, without danger of causing inlet unstart. For combustors with two-stage fuel injection, it was found that the fuel-air mixture from the upstream injectors could be lit by normal injection from the downstream injection. In both cases, the burner remained lit after the ignition method was no longer active. It was concluded that Mach 6 to 12 flight test vehicles could easily be fired by either of these convenient methods.

Initial configurations in the performance evaluation program were step combustors, that is, the combustor area changed abruptly from the inlet value to the exit value in one plane. This method of area change was studied as the simplest approach to the area-change design problem. Despite reasonings to the contrary, high step pressures were never obtained under supersonic conditions. However, this type of combustor produced satisfactory performance for flight at Mach numbers up to 8 by virtue of choking phenomena (transonic combustion). These choking effects produced the high step pressures necessary for high performance. Tests at high enthalpies (representative of Mach 8 to 10.5) were conducted with a wide variety of injector configurations and arrangements without success in achieving high values of step pressures, therefore, this method of area change was abandoned in favor of more subtle area variations for Mach 6 to 12 combustors.

CONFIDENTIAL

## CONFIDENTIAL

AF APL-TR-65-103

Tests were conducted with combustors having conical area variation over the entire length (10 entrance diameters as in the case of the step combustors). These geometries were found to have high wall force and moderate efficiency at conditions simulating Mach 8 and, therefore, adequate performance for a flight vehicle at this Mach number. However, two serious drawbacks were noted. First, the geometry was found sensitive to fuel loading at low Mach conditions. A possible fix was identified as staged fuel injection. Second and more important, the efficiency at conditions simulating Mach 9 to 10 was found to be very low. Since the mechanism for obtaining high efficiency was felt to be the use of constant area combustors, this entirely conical geometry was abandoned in favor of a more subtle area variation.

At the conclusion of the preliminary studies of conical and step combustors, a combustion area variation was devised which provided several important characteristics gleaned from the previous geometries. Low Mach fuel loading was to be provided by fuel staging. A geometry incorporating a short constant-area section followed by a small step and a subsequent conical divergence to the exit area was decided upon as having all the right characteristics. The step area change provides a resistance to upstream propagation of disturbances from high fuel loadings at low-Mach conditions. The constant area section provides maximum pressure disturbances for given fuel injection and burning, a necessary situation if high-Mach efficiency is to be good. The over-all area ratio of 20 is required so that stoichiometric fuel flow can be burned in a choked combustor at Mach 6 conditions. Tests were conducted with such a geometry. At Mach 6 burning to an equivalence ratio of 0.7 was achieved with a single fuel injection stage. Measured performance was excellent over the range of enthalpies from Mach 6 to 9.5 and this geometry was selected for use in the design of the flight test vehicle. Minor modifications were made to the geometry in the vehicle design to provide a longer constant-area section after first-stage injection and, thereby, assure the maximum achievable high-Mach performance.

Choking phenomena were studied in analytical work which supported the step-combustor experiments. The usual one-dimensional criterion of Mach 1.0 for choking was examined and found to be usual at real combustor exists. The governing relationship which was selected was the minimum quantity of total momentum for given flow and total temperature. For one-dimensional flow, this minimum level is a characteristic of Mach 1.0 conditions. Two-part streams were studied as characteristic of combustor exit conditions, with the unburned stream at higher Mach number than the burned stream.

The streams were found to be choked where the sum of the total momentum quantities was a minimum for a given total flow and mixed total temperature. When appropriate one-dimensional averages were taken for the case of equal

CONFIDENTIAL

**CONFIDENTIAL**

velocity (which was close to the actual case in the experiments), the average Mach number was 1.0 ( $F$ ,  $W$ ,  $h_t$  and  $A$  correct quantities, see next paragraph).

Particular care was taken in reducing the experimental data to provide combustion efficiency values which would produce correct engine thrusts in the one-dimensional cycle program. As is well known to those schooled in the art of non-uniform flow thermodynamics, the quantities required to be correct for the cycle calculations must be the total (integrated) quantities used by cycle program to determine thrust. In the case of the General Electric cycle program, these determining quantities for the combustor are: area ( $a$ ), Flow ( $W$ ), total enthalpy or energy ( $h_t$ ), and total momentum  $F$ . In the analysis of data, multi-stream techniques were employed and the resultant values reported are those in which  $A$ ,  $W$ ,  $h_t$  and  $F$  are implicit. Hence, the reported values are directly applicable to cycle calculations.

#### Combustor Design Considerations

A final combustor design was formulated which was very close to the step/cone geometry tested in the arc tunnel. The nature of the inlet design, with six "barrels", provides six "struts" which are believed to be effective in maintaining efficiency at levels observed in tests, out to the vicinity of Mach 12. Two stages of fuel injection are provided, one at the step area change and one three diameters upstream of the step area change. Only the fuel injectors at the step are employed from Mach 6 to near Mach 8 and both sets are used to provide a smooth transition up to the point where all fuel flow is to the upstream fuel injectors (at a Mach number near 9.5). All injectors are rows of 6 sonic holes directed at 30 degrees downstream. There are eight equally spaced sets at the upstream section in each of the six pipes (48 fuel injectors) and six equally spaced sets at the downstream station. The combustor area ratio is 2.0. The geometry is identical to that of the step/cone geometry tested in the arc tunnel with the exception of the multiple inlet pipes.

Performance numbers for the selected configurations were derived for a range from Mach 6 to 12. Heavy emphasis was placed on the experimental information on hand. Wall force and friction drag were taken in keeping with present cycle assumptions and the projected efficiency varied from .85 at Mach 6 and  $ER = 1.0$  to .90 at Mach 12 and  $ER = 1.6$ .

### C. DATA AND RESULTS

#### 1. Cold Flow Studies

##### a. Introduction

The mixing of fuel and air has been a major feasibility problem in the design of SCRAMJET combustors. Experimental work at General Electric on mixing of hydrogen and air in 1961-1963 (Reference 1 and 2 ) demonstrated

**CONFIDENTIAL**

**CONFIDENTIAL**

the difficulty of obtaining uniform mixtures in short lengths. This mixing work included data on free-stream struts, injection parallel to a wall, and penetrating jets. Mixing theories were also explored. The available theories in the literature were found to be inadequate for handling the entire complex mixing problem expected in SCRAMJET combustors.

Test combustors for arc tunnel testing were constructed that utilized penetrating wall injectors in order to assure ignition and to obtain any mixing benefits that accrued. Penetrating jets provide a better initial fuel distribution than downstream wall injectors and produce faster mixing because of the large velocity difference and resulting shear gradients between the freestream and the injected gas.

The present cold-flow experimental program was conducted to find additional information on fuel injection penetration into supersonic streams sufficient to permit design of SCRAMJET combustors and to correlate previous data. One objective was to thoroughly investigate the governing relationships of penetration into a supersonic flow stream by: documentation and analysis of the effects of test variables on the penetration phenomena; establishing design criteria for fuel injectors; and defining promising injector configurations to be further evaluated in future closed duct arc tunnel combustion tests. Another major objective was to analyze the distinctions between normal injection and downstream or partly downstream injection by defining the respective penetration characteristics.

The experimental investigation was carried out using a cold flow facility with injection from a flat plate aligned in a Mach 3.25 wind tunnel. Gaseous helium-air mixtures and gaseous nitrogen were used as the injection media. Some of the injection penetration variables investigated were shape, size, aspect ratio, angle of the injector and Mach number, ratio of specific heats and pressure of the injectant.

Most other investigators studied penetration using single round holes or slot injectors stationed crosswise with the freestream flow direction. Before this program was initiated, combustion tests had been performed at General Electric which employed fuel injectors of the following general types: round holes, a long row of holes and a supersonic slot. Except for a limited amount of single round hole data to confirm agreement with other investigators, the major emphasis in this cold flow program was on injector configurations of long rows of holes or low aspect ratio injectors. Although the experimental effort was confined to initial penetration of jets as distinguished from subsequent mixing, a mixing theory was identified which treats the mixing of the penetrated jets.

**CONFIDENTIAL**

**CONFIDENTIAL**

Mixing theories available in the literature was examined under SCRAMJET Air Force funding in 1962-63 and were found to be inadequate for treating the entire mixing problem in SCRAMJET combustors. However, a theoretical approach was identified which handled the effects of cocurrent flow, density, Mach number, combustion and static pressure gradient. This approach was limited because it treated only a single shear-generated mixing mechanism. In general, it could not treat the effects of approach turbulence, overlapping mixing zones, wall shear, or the effects of penetrating jets. The work in 1964 on penetrating jets has led to a quantitative description of the flow field at the injection station that is amenable to treatment by a single mixing mechanism theory. This permitted extending the objectives of this work to include the derivation of simplified mixing expressions, and the application of these equations to the calculations of mixing efficiencies in a combustor, including explanations of the expected effects of combustion and static pressure gradients.

The section of this report on Cold Flow Studies contains a theoretical analysis of penetration, and a presentation of penetration data acquired from Schlieren photographs. A comparison with the penetration data of other investigators is included. Also an extensive section on Schlieren technique is presented. Finally, a mixing theory based on two-dimensional wake theory is applied to the penetrating jets with an example calculation of mixing efficiency for a combustion configuration.

#### b. Experimental Techniques

##### 1) Test Facilities

###### a) Mach 3.25 Wind Tunnel

The supersonic wind tunnel used for this cold flow penetration investigation is shown in Figures 1 and 2. This wind tunnel was designed for Mach 3.25 flow at the 10" x 10" test section.

A schematic of the wind tunnel test section showing the centerbody flat-plate and injector inlet piping is shown in Figure 2. Figure 3 is a photograph of the tunnel throat and test section with the centerbody flat plate installed. The tunnel has a fixed contoured throat, 1.7" x 10" designed for a Mach number of 3.25 with parallel flow at the test section. Air was supplied at 50 pps at 130 psia and heated to 150°F to prevent moisture condensation in the test section. The air supply for the tunnel is tapped off the main high pressure supply line from test facility house compressors. Since there is no suction or return line to the compressors, the tunnel flow is discharged to atmosphere after passing through the tunnel diffuser.

###### b) Flat-Plate Centerbody and Injectors

Gas injection was from the surface of the centerbody flat-plate that spans the wind tunnel at the test section windows. The centerbody was supported by four bolts through the wind tunnel side walls. The injector gas

**CONFIDENTIAL**

**CONFIDENTIAL**

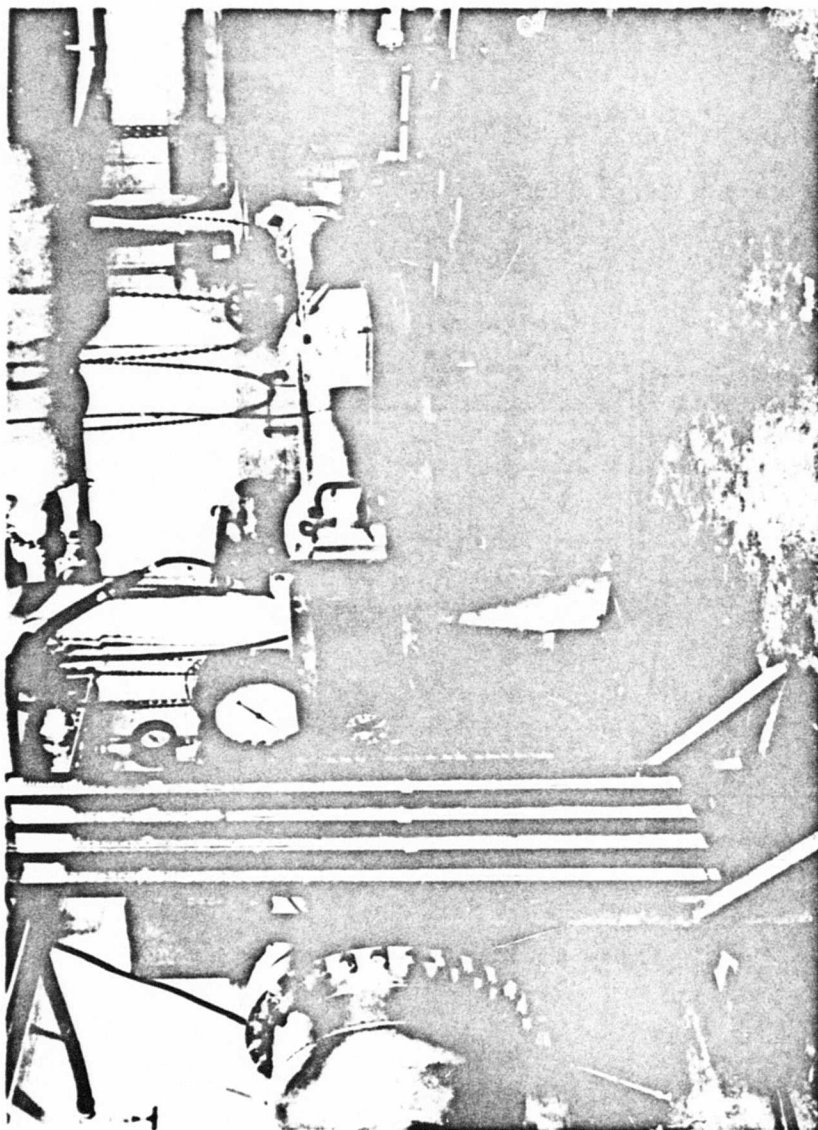


Figure 1 - Mach 3.25 Wind Tunnel.

**CONFIDENTIAL**

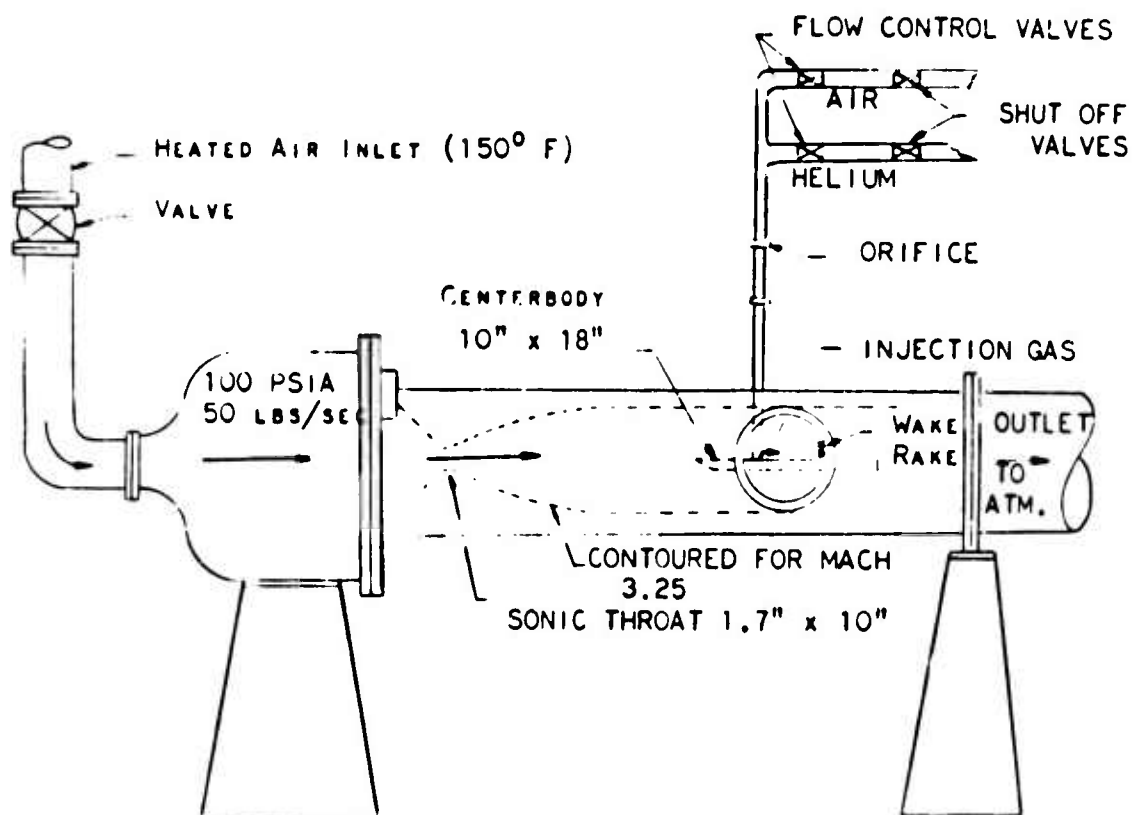
**CONFIDENTIAL**

Figure 2 - Wind Tunnel Schematic.

**CONFIDENTIAL**

**CONFIDENTIAL**

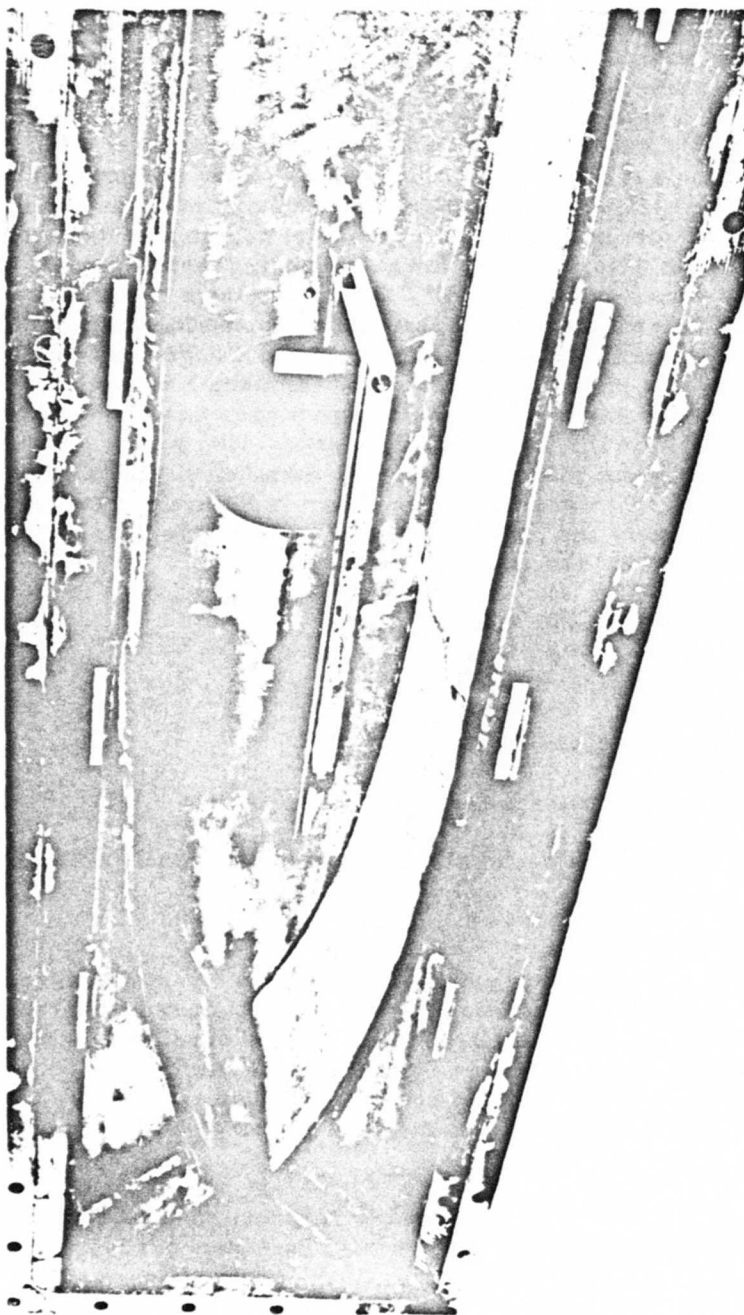


Figure 3 - Wind Tunnel Throat and Test Section.

**CONFIDENTIAL**

# CONFIDENTIAL

AF APL-TR-65-103

was piped through the wind tunnel wall and through a hole in the centerbody to an injector plenum chamber below the injector plate. The single injector hole configurations or the last hole in a long row of holes was located approximately eight inches downstream from the lead edge of the centerbody flat-plate. The injector plates were readily interchangeable by means of four screws through the bottom of the centerbody flat-plate. Bottled helium, nitrogen, and a 100 psig dry air supply were available for injection. The injector piping is shown on the schematic in Figure 2. This injector piping facilitated mixing of the injector gases. During some of the air injection tests, a trace of helium was introduced into the 100 psig dry air line to form a base for gas sampling measurements of concentration. Injectants were supplied at 70°F thus providing a temperature difference between main air and injector gas that could be used for detecting composition by temperature measurements. Figures 3 and 4 show the centerbody flat-plate installed in the wind tunnel. The centerbody contained nine static pressure taps and an instrumentation rake. Both impact pressure and total temperature probes were included in the instrumentation rake. The position of the interchangeable injector plates is shown in Figure 5. Some of the 14 different injector plate configurations that were tested are shown in Figure 6. Two of the original injector configurations, the .1 inch diameter hole and the 9-1/32 inch diameter holes were modified in the following order:

- 9 - 1/16 inch diameter holes
- 14 - 1/16 inch diameter holes
- 14 - holes with increasing diameter aft
- 14 - .154 inch diameter holes

Table I shows the shape and dimensions of all the injector plate configurations tested.

## 2) Instrumentation

The experimental data gathered during this investigation consisted of test section flow conditions, static pressure distributions on the test section walls and on the centerbody flat-plate, injectant flow conditions, and penetration and concentration measurements downstream of the injector port. Penetration and concentration data consisted of Schlieren photographs, total temperature and impact pressure measurements, and gas sample measurements of concentration.

Static pressures were recorded by mercury manometers and high pressure gages were used to measure the wind tunnel plenum pressure and injector plenum pressure.

Copper Constantan thermocouples were used to measure the freestream temperature in the wind tunnel and injector plenum chambers. These

CONFIDENTIAL

**CONFIDENTIAL**

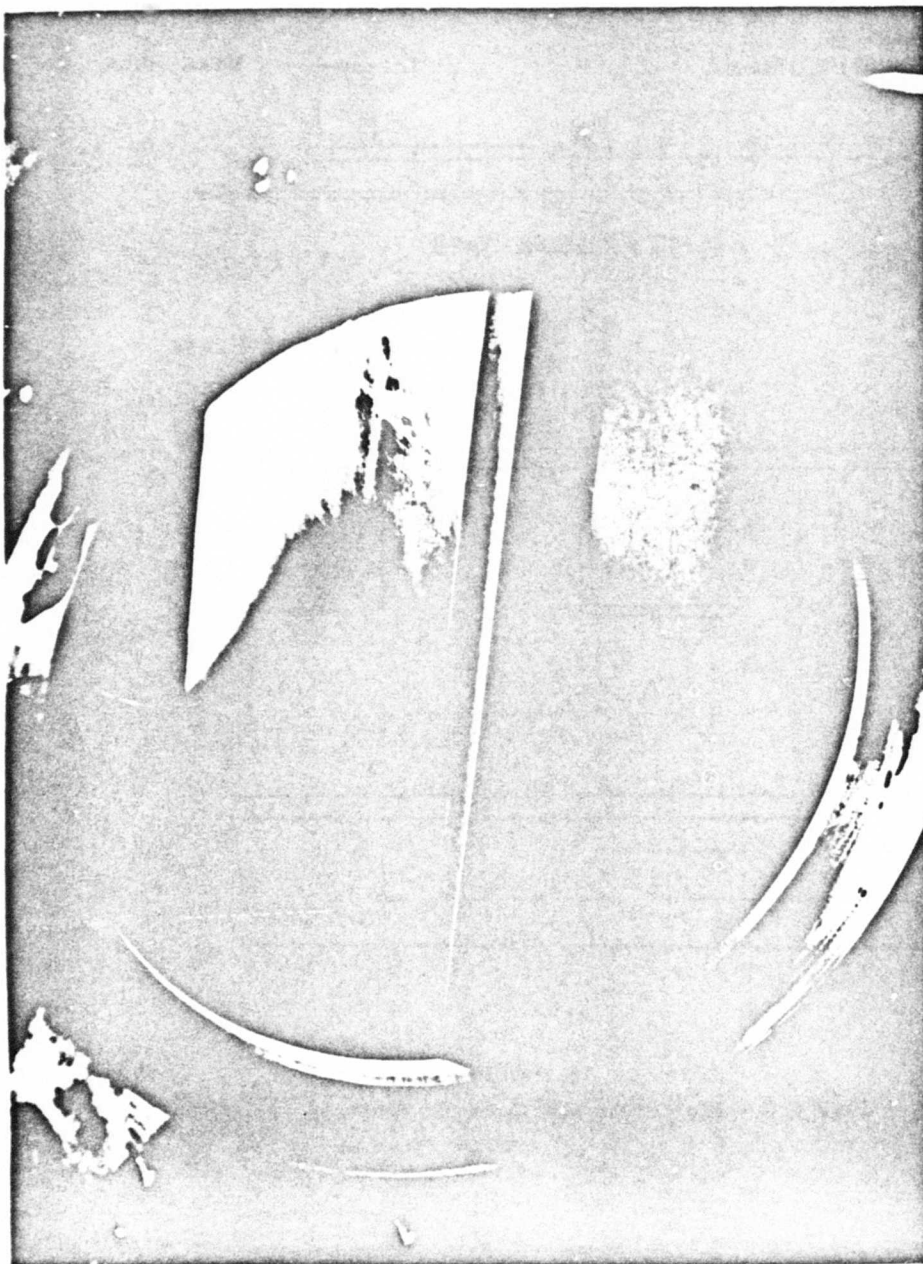


Figure 4 - Flat Plate With Injector and Wake Rake.

**CONFIDENTIAL**

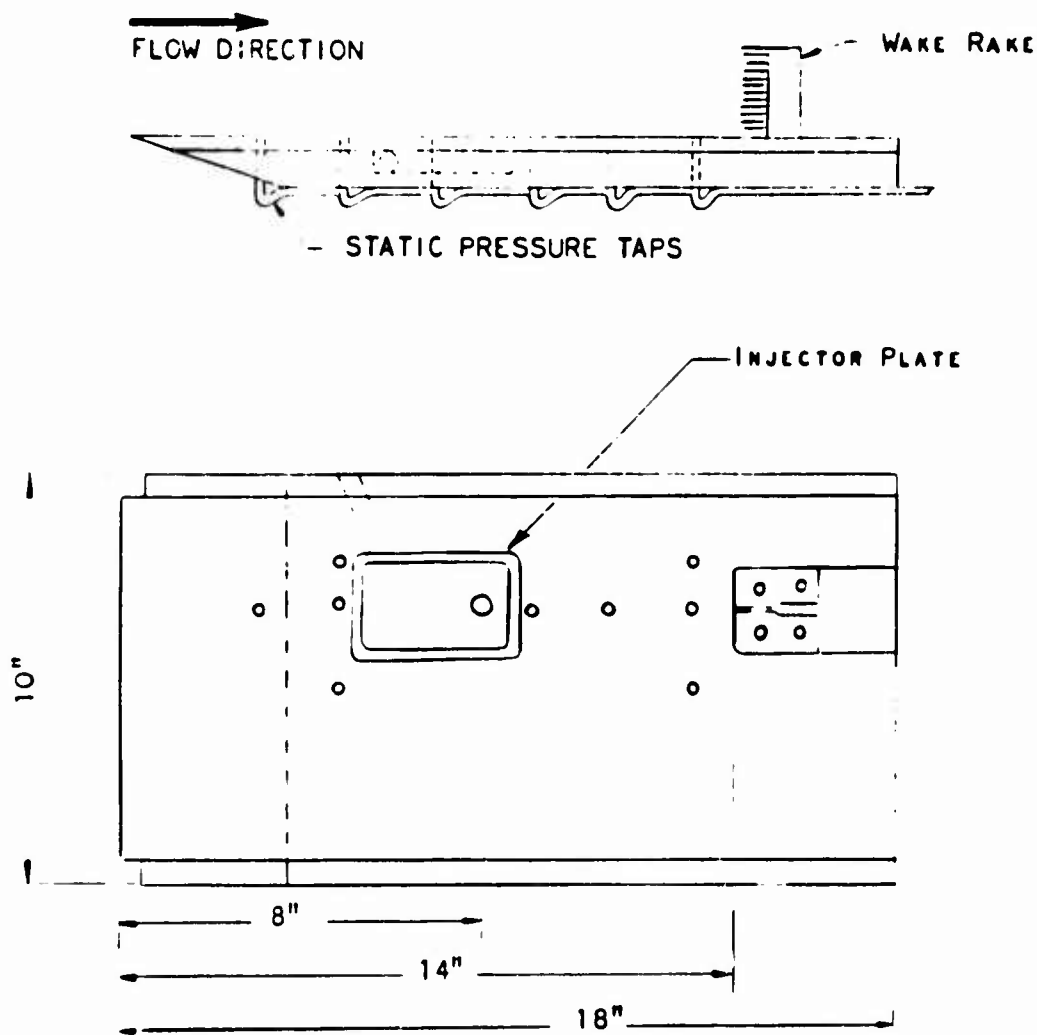
**CONFIDENTIAL**

Figure 5 - Flat Plate and Injector Position.

**CONFIDENTIAL**

**CONFIDENTIAL**

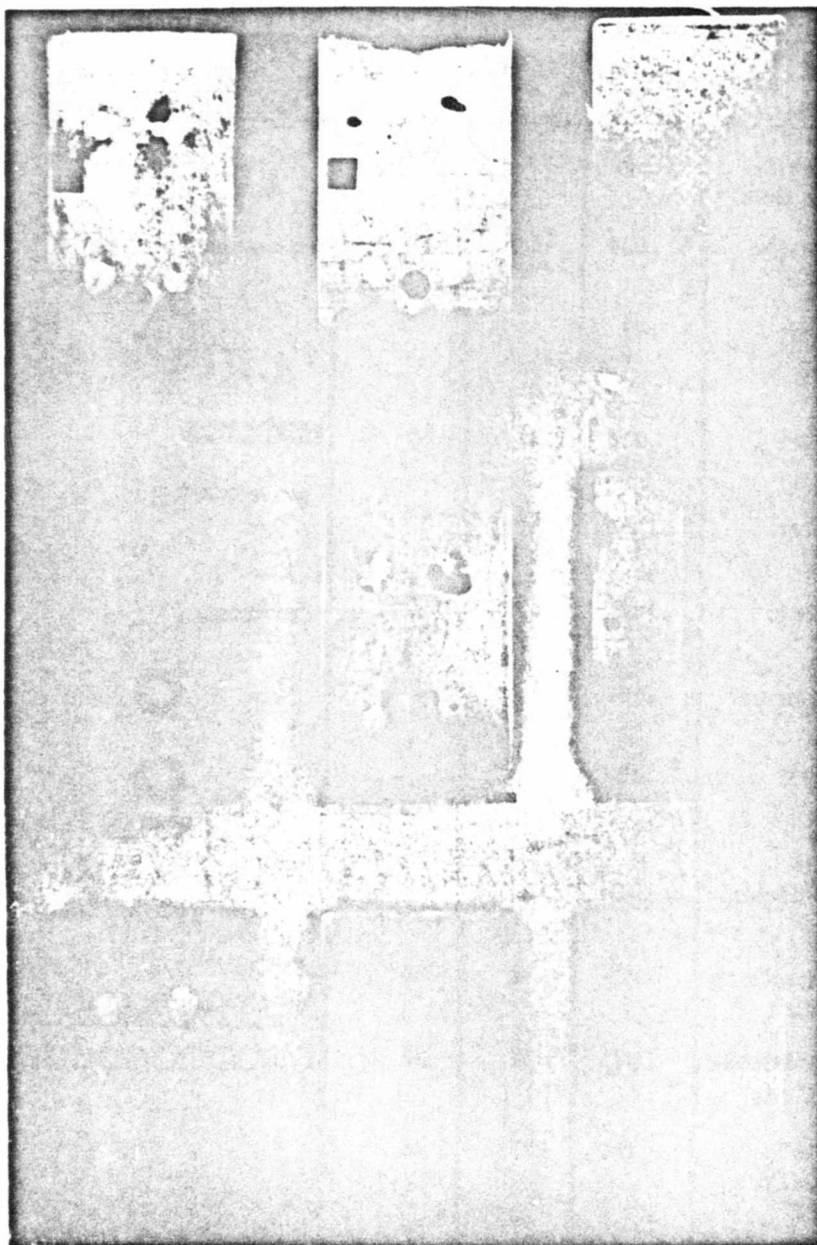





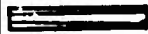






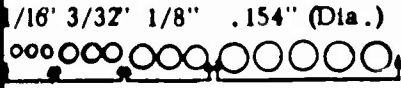

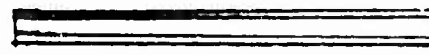

Figure 6 - Injector Plates.

**CONFIDENTIAL**

# CONFIDENTIAL

TABLE I

## INJECTOR CONFIGURATIONS TESTED IN MACH 3.25 WIND TUNNEL

No.	Configuration	De°	L <sup>2</sup> /A°	L/Width	Hole Pattern Sketches
1	0.1" Diameter Normal Sonic Hole	.090			
2	9-1/32" Diameter Holes 1/4" C	.084	183	33	
3	0.3" Diameter Normal Sonic Holes	.27			
4	Supersonic Slot .83 Long	.224	17	10	 
5	9-1/6" Diameter Holes 1/4" C	.168	46	17	
6	.83" Long Sonic Slot	.224	17	17	
7	Supersonic Normal Round Hole	.157			
8	Supersonic 30° Round Hole (Protruding)	.157			
9	14-1/16" Diameter Holes 1/4" C	.216	225	53	
10	14 Holes (Increasing Diameter Aft)	.409	70	22	 1/16" 3/32" 1/8" .154" (Dia.)
11	14 - .154" Diameter Holes 1/4" C	.521	44	22	
12	12 - 30° 1/16" Diameter Holes 1/4" C	.191	227	48	
13	3" Long Supersonic Slot	.409	61	36	
14	12 - 30° Square (.06" x .06") Holes 1/4" C	.23	191	48	

# CONFIDENTIAL

AF APL-TR-65-103

thermocouples, connected to a multipoint scanner and recorder, were located in the low velocity, low turbulence areas of their respective plenum chambers.

## a) Wake Rake System

A stationary wake rake was located directly downstream of the injector, approximately six inches downstream from the injector hole and approximately fourteen inches downstream from the lead edge of the centerbody flat plate. Two different wake rakes were used during this investigation. The wake rakes are shown in Figure 7. The first wake rake contained six pressure probes and six thermocouple probes; the second contained an additional thermocouple probe. The second wake rake was brought into use when approximately 75% of the testing remained.

Structural considerations were important in the thermocouple design. As shown in Figure 7 stainless steel tubing 1/16 inch diameter shrouded the thermocouples. The large shroud with bleed holes facilitated nearly true readings of total temperature. Without a shroud, bare thermocouples read the recovery temperature of the stream instead of the total temperature; the shroud and bleed hole combination reduce the stream velocity to a low subsonic value.

The impact pressure probes were made of .040 inch outside diameter and .008-.010 inch wall thickness stainless steel tubing. Wiancko pressure transducers with a 50 psi range measured the impact pressures from the pressure probes and were also recorded by the multipoint recorder. The tubing leading from the impact pressure probes could be disconnected from the pressure transducers and connected to a vacuum purged gas sampling system which collected the samples in bottles. A Beckman GC-2A gas chromatograph was used to analyze the wake downstream of the injector from the samples drawn through the pressure probes. During initial checkout testing, a directly connected Gow-Mac thermal conductivity analyzer was used, but the response time was too slow to obtain all the desired test data during short test runs.

## b) Schlieren Systems

Figure 8 is a schematic drawing of the Schlieren system that was used for most of the penetration measurement in this program. The system consisted of a 100 watt continuous arc light source, a focusing lens, a rectangular slit, two mirrors, a knife edge, and a speed graphic camera. Measurements of the outer boundary of the penetration jet were made from the Schlieren photographs at approximately 5 inches downstream from the injector hole and approximately 13 inches downstream from the lead edge of the centerbody flat plate.

CONFIDENTIAL

**CONFIDENTIAL**

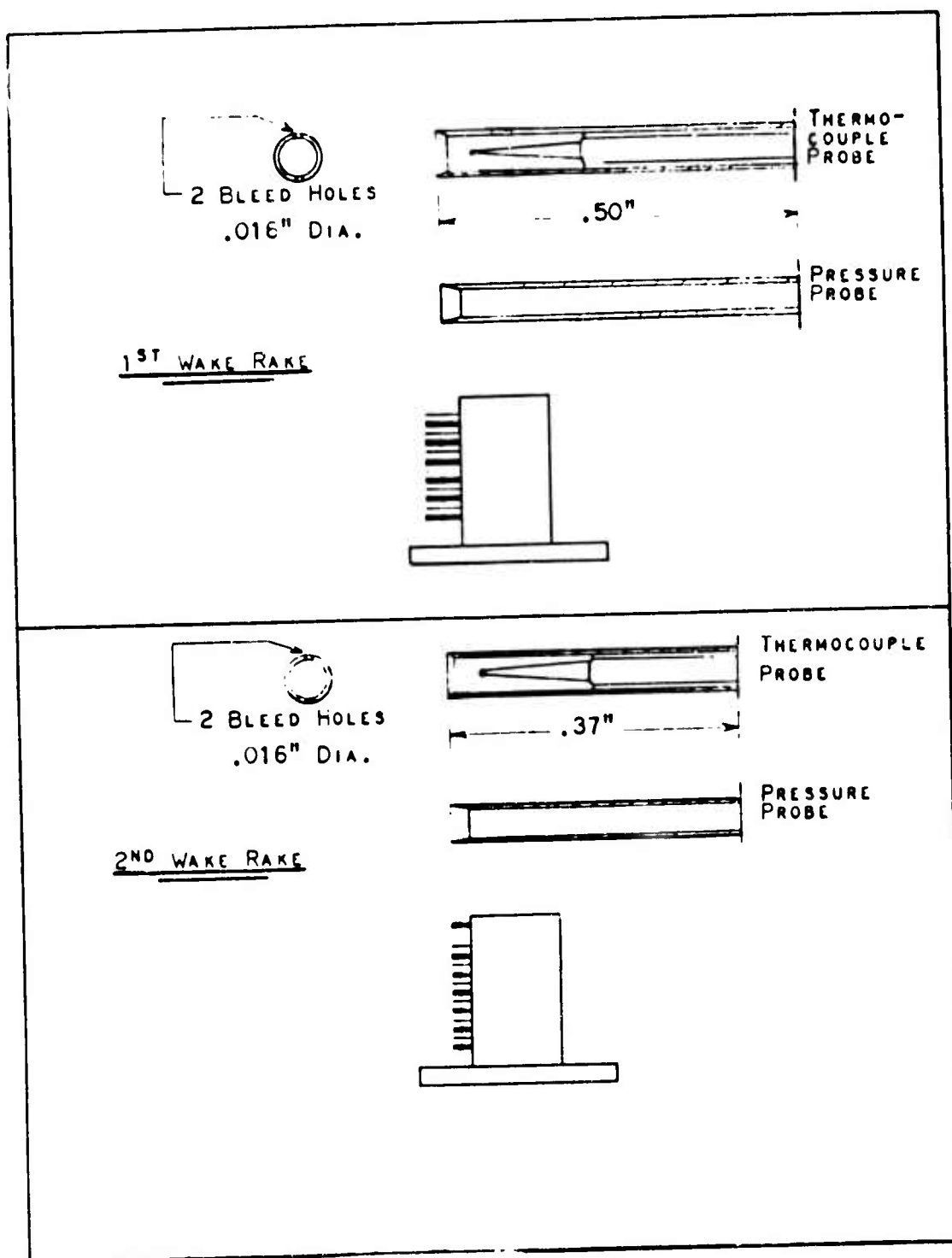


Figure 7 - Wake Rakes.

**CONFIDENTIAL**

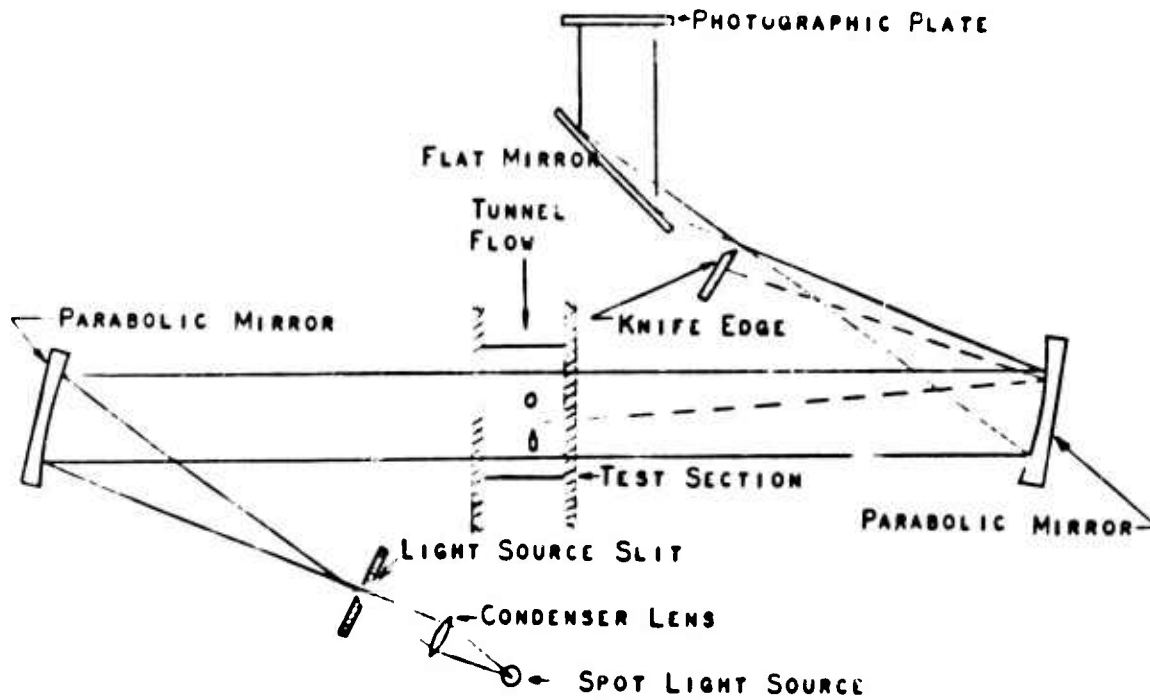
**CONFIDENTIAL**

Figure 8 - Schlieren System.

**CONFIDENTIAL**

**CONFIDENTIAL**

Other Schlieren systems were used for specific effects such as: a spark light source; a distributed light Schlieren system, and a light dispersing prism for color Schlieren. Figure 9 is a schematic of the distributed light Schlieren system that was used with the 100 watt continuous arc light source as well as with a spark light source.

### 3) Test Procedures

Before this test program was initiated, a calibration of the wind tunnel was conducted to verify the flow conditions in the test section. With the centerbody flat plate installed including the wake rake, impact pressures from the Pitot pressure probes were measured. From the ratio of these impact pressures to static pressures measured from tunnel side wall taps and using the Rayleigh-Pitot equation as tabulated in Reference 3, the Mach number in the test section was determined. Two additional measurements of Mach number were available by assuming zero total pressure loss and ratioing the total pressure to static pressure or ratioing the total pressure to the impact pressure. Also, the Mach number was found from measurements of the angles of the Mach lines on Schlieren photographs during conditions of no injector flow. The pressure measurements method of calibration was within approximately  $\pm 2\%$  of the design value of Mach 3.25 for this wind tunnel.

The Wiancko pressure transducers were calibrated before each test run and it was found that only very minute adjustments of the recorder were needed between runs. The injectant mass flow rate for each injector configuration was calibrated previous to a test run by measuring the pressure drop across a standard ASME orifice. Prior to a test run, the Schlieren system was aligned and focused, and a Speed Graphic camera was focused on the plane of the injector in the test section. Dimensional calibration of the Schlieren photographs was established by two static pressure lines where were in view below the plate; these were two inches apart.

The test conducted during this investigation were started by establishing primary flow after a brief facility warm-up time. After the throat of the tunnel was started and supersonic flow was established, the recorder was started and performed continuous scans of temperatures and pressures. At a predetermined injection pressure, gas samples were taken; after which a full range of injection pressures were investigated with Schlieren photographs taken at each pressure point.

### c. Background Analysis

Simplified models of the penetrating mechanism together with analytical calculations based on the proposed models are helpful in understanding the governing relationships that are found experimentally. Appropriate correlating parameters can also be identified from these models. However, the correlating parameters adopted in the available literature on penetration are not all consistent with one another and sometimes suggest inappropriate relationships between the variable.

**CONFIDENTIAL**

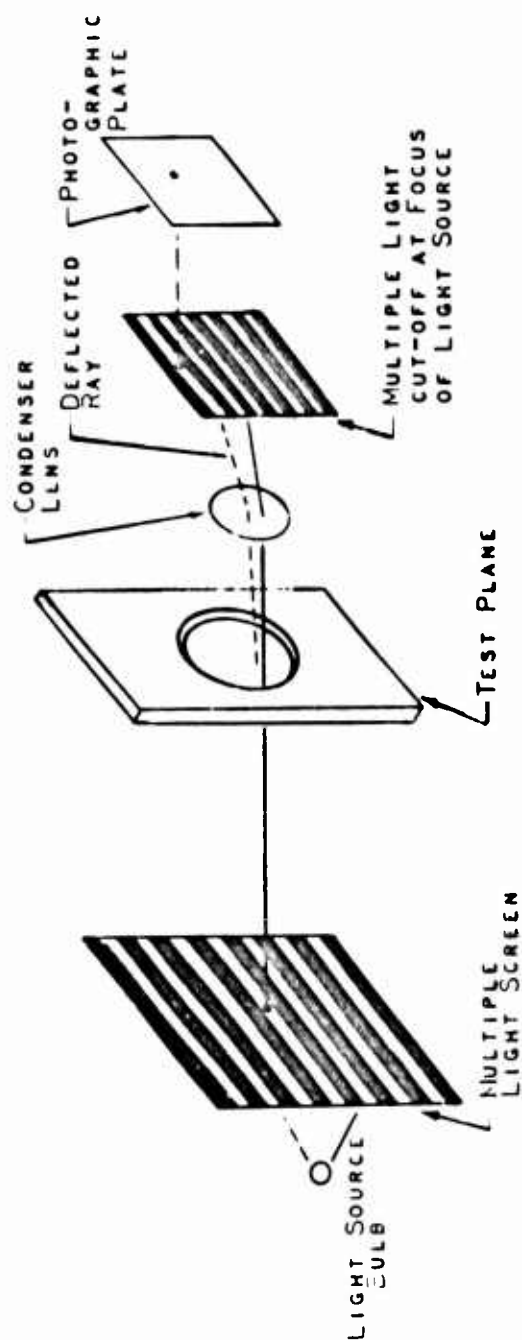
**CONFIDENTIAL**

Figure 9 - Distributed Light Source Schlieren System.

**CONFIDENTIAL**

## CONFIDENTIAL

AF APL-TR-65-103

This section of the report discusses the difficulties with the available data correlations in the literature and explains the reasons for the correlating methods adopted in this report. Analytical models for the penetrating mechanism are discussed and a physical interpretation is given for the effect of the shape of the injection hole, round versus low aspect ratio, and sonic versus supersonic.

### 1) Definition of Penetration

Injecting fluid in a direction normal to another flow aids the spread of fluid across the stream. Experimentally, this effect is not always easily separated from the turbulent mixing that occurs simultaneously with the normal penetration.

Figure 10 is an illustrative sketch of a penetrating jet. The initially normal jet is turned almost parallel to the freestream flow. Even though the penetration is completed, the injected gas continues to spread through the stream by the process of turbulent mixing. Actually, there may also be some continued penetrating effect of the initial jet momentum at all downstream distances. However, in this experimental study of penetration into supersonic flow, the penetration phenomena itself seemed to be essentially completed in a very short downstream distance.

A large body of the literature on jets penetrating into supersonic streams has not included freestream measurements; only wall static pressures were measured. Much of this work was motivated by applications for thrust-vector control exhaust nozzles. While these wall pressure measurements or direct force measurements might be adequate for thrust-vector-control, they are not suitable for estimating the actual penetration distance. The flow separations caused by normal injection and documented in these wall pressure measurements are of interest in designing fuel injectors. Since these separations have been found to be of small extent for the low aspect ratio hole patterns developed in this program, no effort was made to include in this report discussion of the extensive thrust-vector control work. (Reference 4 is a literature survey on work for thrust vector control.)

To properly examine penetration, detailed freestream measurements of mixing jet are needed. To correlate these detailed profile measurements, some simplification is helpful. The locus of maximum concentration of injectant at each downstream station is one simplified description of the penetration. If the injected flow were found to be symmetric about this locus, only an additional spreading parameter would be required to completely describe the jet. Unfortunately, symmetry is not very good for many penetrating jets.

**CONFIDENTIAL**

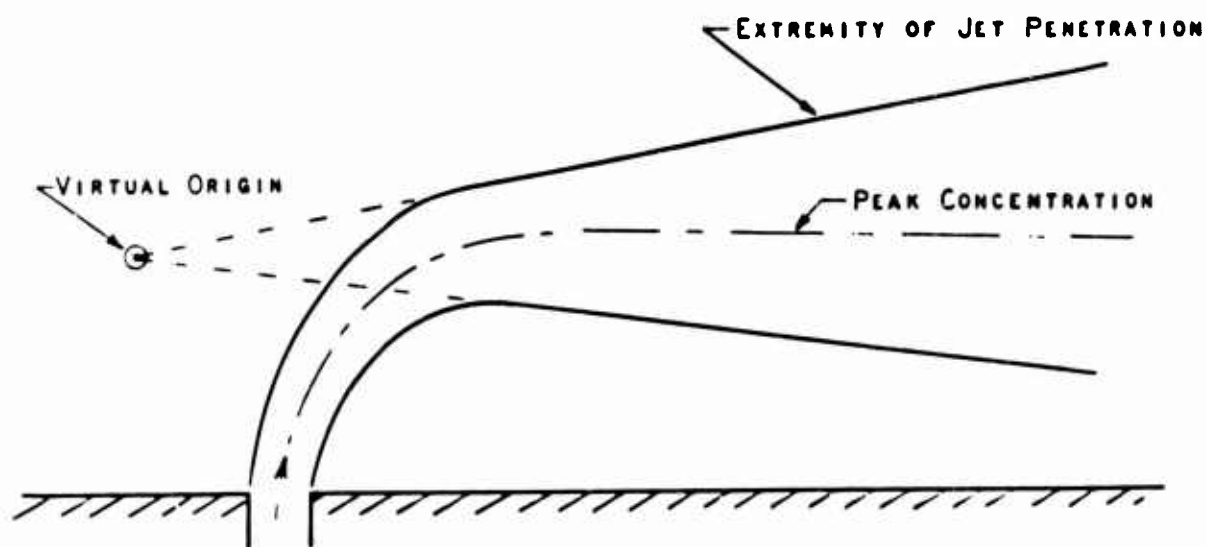


Figure 10 - Penetrating Jet

**CONFIDENTIAL**

## CONFIDENTIAL

AF APL-TR-65-103

Figure 11 indicates that the concentration of a penetrating round sonic jet is not symmetrical. Figure 12 shows that with low aspect ratio holes, the concentration profile is fairly flat from the plane of injection to the extremity of the jet, making the location of a maximum concentration difficult to determine and, therefore, an inappropriate criterion.

Near a wall another difficulty occurs. As illustrated schematically in Figure 13 after the penetration is nearly complete, downstream mixing continues to spread the injected fluid. As the fluid mixes toward the wall, the shape of the concentration curve becomes modified in such a way as to make the peak concentration move toward the wall. This shift occurs because pure air enters the mixing region only from the side away from the wall. When this peak reaches the wall, the penetration based on maximum concentration becomes zero.

In addition to shifting the peak concentration towards the wall, the turbulence levels near the wall are modified, creating a variable non-symmetric mixing field. Under these circumstances, it becomes difficult to separate the concept of penetration from the turbulent mixing phenomena.

Walls are not the only cause of considerable turbulence level variation. Wakes adjacent to a mixing fuel jet, such as occur behind injection spraybars, create high turbulence level fields on one side of the injected flow which result in non-symmetrical mixing patterns.

Another approach to penetration measurements adopts the outermost extremity of the injected fluid as the most significant measurements to correlate. At distances far downstream, this technique suffers because it primarily shows the effect of the turbulent mixing.

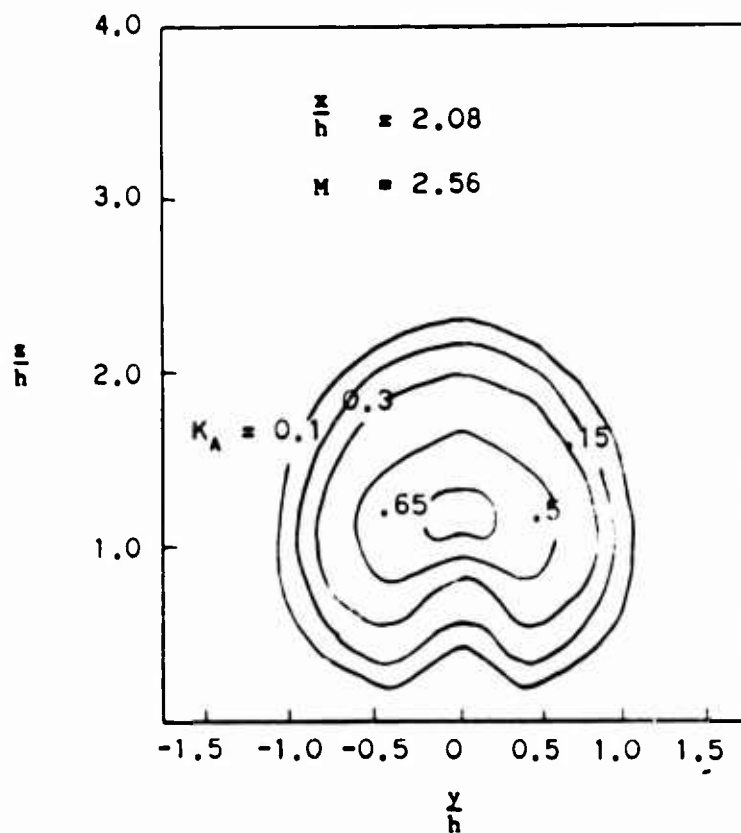
In experiments with subsonic free streams where high intensity turbulence may exist in the approach stream, the outer boundary of the penetration becomes a function of the approach turbulence, greatly complicating comparison with other experiments. In general, supersonic tunnels have very low turbulence, and, therefore, only the turbulence generated by the jet itself and the wall boundary layer affect the results. The Schlieren pictures obtained in this study showed that penetration is essentially completed in a very short downstream distance, and that beyond this distance the outer boundary propagated into the freestream at a very slow rate, making the outer boundary a reasonable measure of the penetration.

The penetration work presented in this report deals primarily with the measurement of the outer extremity of the injected flow. This approach was particularly convenient due to the considerable success of obtaining good

CONFIDENTIAL

**CONFIDENTIAL**

(Reprinted from Reference 5: - Zukoski, E.E. and Spald, F.W., "Secondary Injection of Gases into a Supersonic Flow," California Institute of Technology, Pasadena, California, AIAA Preprint No. 64-110, January 29-31, 1964)



(ALL SYMBOLS AS USED IN REFERENCE 5)

Figure 11 - Jet Concentration Profile (from Reference 5)

**CONFIDENTIAL**

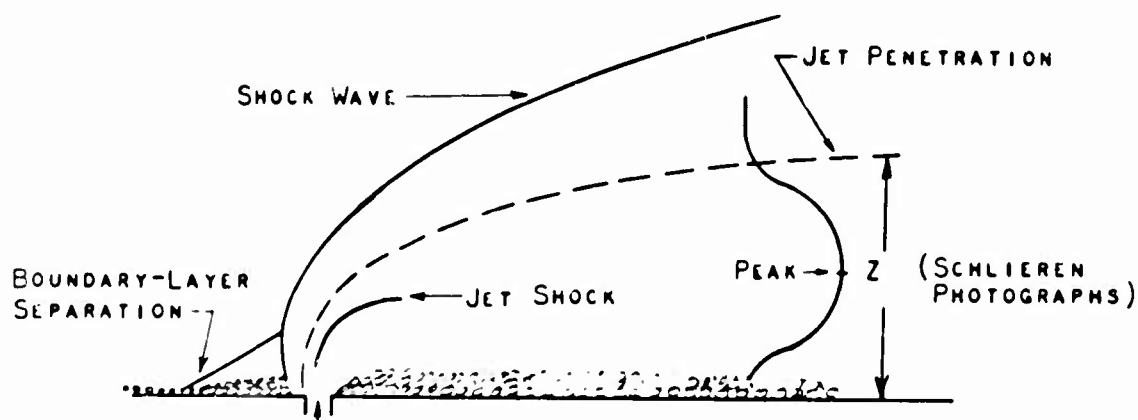
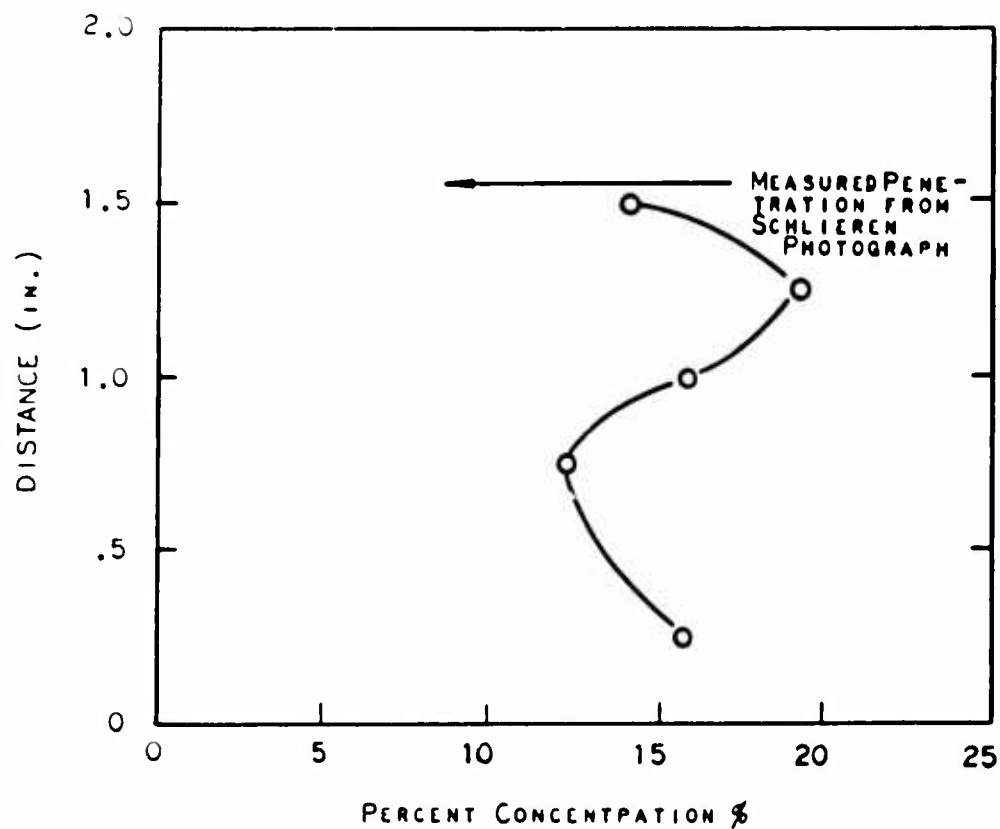
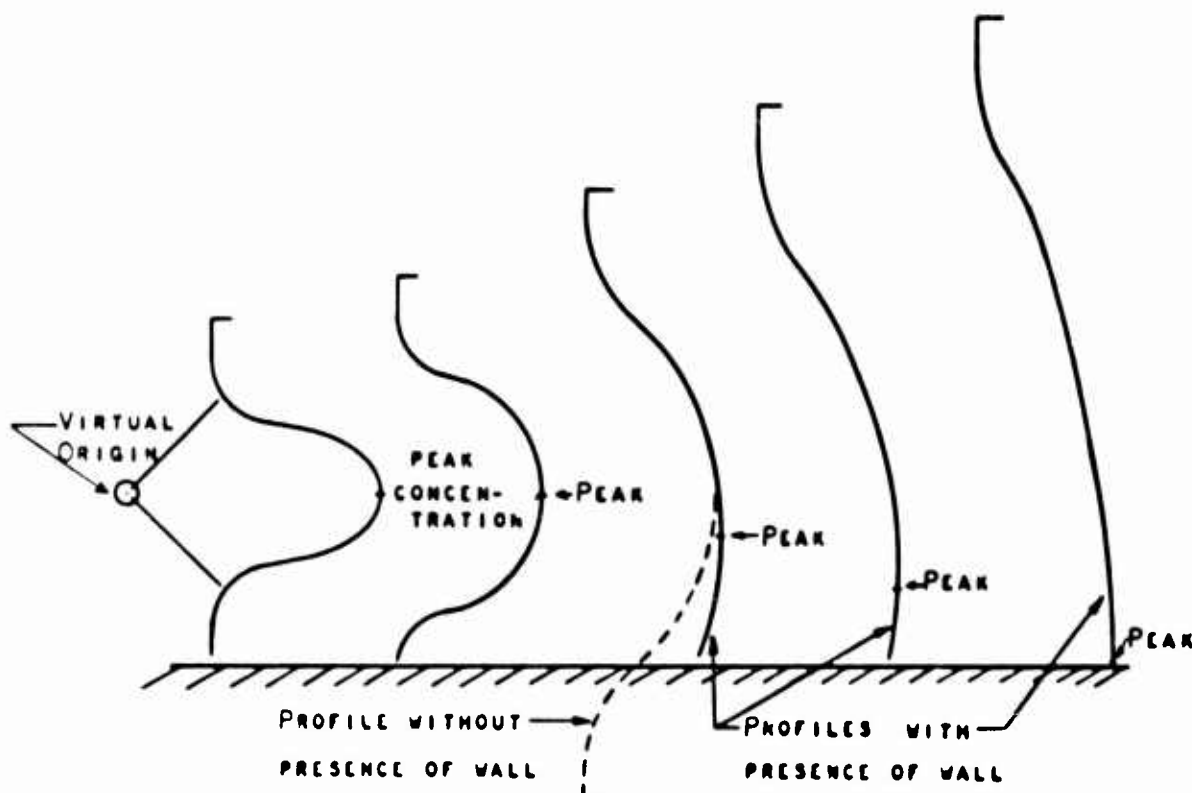
**CONFIDENTIAL**

Figure 12 - Uniform Concentration Profile.

**CONFIDENTIAL**

**CONFIDENTIAL**

FUEL CONCENTRATION PROFILES CHANGED  
BY FUEL BUILD-UP AT THE WALL

Figure 13 - Wall Effect on Peak Concentration

**CONFIDENTIAL**

## CONFIDENTIAL

AF APL-TR-65-103

Schlieren pictures. Schlieren pictures can identify the high concentration gradients near the edge of the injected flow easier than the more gradual changes near the concentration peak. Since the supersonic tunnel flow had a near-zero turbulence level, the edge of the injected gas flow was also the outer edge of the turbulent mixing zone, again making for easy detection by Schlieren technique. The very small increase in the distance to the edge of the jet as length was increased assured that only small effects of turbulent mixing were involved.

Reference 5 correlated the true increase in the distance to the maximum concentration for round sonic jets and found a very small effect of increasing distance. The Schlieren pictures in this study show the rate of change with distance but no attempt was made to correlate this variable. The fairly flat concentration profile detected by gas sample measurements and temperature measurements for low aspect ratio injectors, together with a rapid decrease in concentration at the outer extremity, suggests that this outer edge is an appropriate measurement for characterizing penetration.

The available data in the literature based on maximum concentration determinations can be compared with the data in this report by making use of available profile data to convert maximum concentration data to outer edge correlations.

### 2) Analytical Models

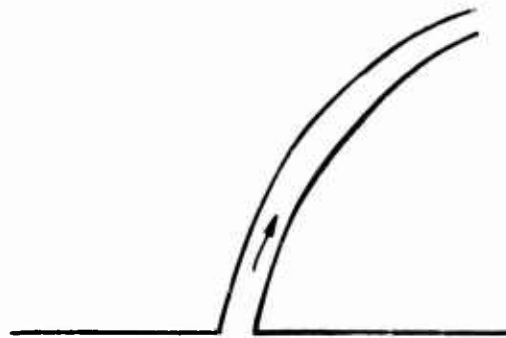
Simple models of a penetrating jet can be postulated and relationships can be calculated from these models. Many of these simple models have obvious limitations. Figure 14 shows three quite different models that might be investigated.

A jet of water into an airstream may retain its cross-sectional area and shape for a considerable distance. The cross stream will exert a force on the water jet similar to that on a cylinder.  $F = C_D q_{air}$ . This force accelerates the water jet in the direction of the air stream. A force balance can be expressed and a trajectory derived.

The limitations of this model are severe. It assumes that no mixing takes place between the jet and the surrounding air stream and that the jet cross section remains at constant size and shape. This would not be expected with gas jets.

The second flow model shows a gas jet which mixes with the surrounding streams as it penetrates. A mixing assumption is required; for example, the mixing can be assumed to be similar to that which would be measured or found in zero velocity surroundings; data are available for this type of mixing. To set up the force balance between this jet and the surroundings, requires assumptions about the character of the form drag. In subsonic free-

**CONFIDENTIAL**



a) WATER JET WITH CONSTANT CROSS SECTION



b) GAS JET MIXING WITH SURROUNDINGS



c) NON-MIXING GAS JET EXPANDING AND TURNING DUE TO PRESSURE FIELD

Figure 14 - Three Simple Analytical Models.

**CONFIDENTIAL**

**CONFIDENTIAL**

stream flow, the form drag on an aspirating jet is probably unknown, it depends heavily on the nature of the wake flow which obviously is affected by the mixing and aspiration phenomena. In supersonic flow where the form drag is primarily due to the pressure on the front surface of the jet, better drag estimates can be made. The momentum transfer from the freestream to the jet because of mixing also enters into the equations.

In the supersonic flows studied in this program, the jets are bent over before mixing should have reached the centerline of the jet. Mixing data in the literature for round holes indicates that the jet core begins to be affected by mixing with an equal-density zero-velocity surroundings after about eight hole diameters. While it is unlikely that this relation will apply exactly to high pressure sonic jets, it is of interest to observe that at an injection pressure for which the injected density is equal to that in the  $M = 3.25$  flow,  $P_j/P_{\text{plenum}} = 0.7$  for helium, the measured penetration was found to be five hole diameters. Thus it is seen that the jet is turned before extensive degeneration of the jet has occurred due to mixing. This observation justified the use of a penetration model that assumes zero mixing.

The third model is a model which assumes zero mixing with the freestream flow and is, therefore, more consistent with the supersonic freestream flow regime. With zero mixing, the frontal drag can be equated to the downstream momentum acquired by the turned jet.

In Reference 6 the flow blockage created by a two-dimensional slot across the stream was set equal to the flow area required to pass the injected gas after it was turned isentropically downstream to the freestream static pressure. The jet was assumed to cause a reaction in the freestream similar to that which would occur from a forward facing step with the same area.

Reference 5 again utilized the assumption of isentropic turning to the freestream pressure, and then suggested that the freestream force on the jet be set equal to this downstream momentum. The penetration height was determined by assuming that the disturbance in the freestream created by the jet involved a flow field of constant shape. A quarter sphere shape was selected. The actual size of this disturbance was determined from a balance between the freestream force on the assumed shape and the downstream momentum acquired by the jet.

The assumption of isentropic turning used in both Reference 5 and Reference 6 supersonic models is obviously not quite valid; non-isentropic shock waves certainly must occur in the jet as it is turned through the 90 degree

**CONFIDENTIAL**

**CONFIDENTIAL**

turn. However, very useful correlations were obtained in Reference 2 using these assumptions. This model, however, fails to offer an approach for determining the difference between a supersonic injection point and a sonic injection point, and is not suitable for explaining the effects of low aspect ratio holes.

### 3) Proposed Model

#### a) General

Figure 15 is the penetration model proposed in this report which leads to a better understanding of supersonic versus sonic holes and other hole shape effects. In this model, it is suggested that the freestream force is related to the blockage created by the jet as it expands to the freestream pressure before turning in the downstream direction. This force should equal the acquired downstream momentum of the jet for normal injection. The penetration height is found from this equality. The turn need not be isentropic, in fact, the available data seem to be consistent with a downstream momentum roughly equivalent to sonic flow. From a physical standpoint, it is not unreasonable to expect that a jet expanding into a low pressure region will develop shock waves and expansion waves which could easily bring the jet Mach number to unity.

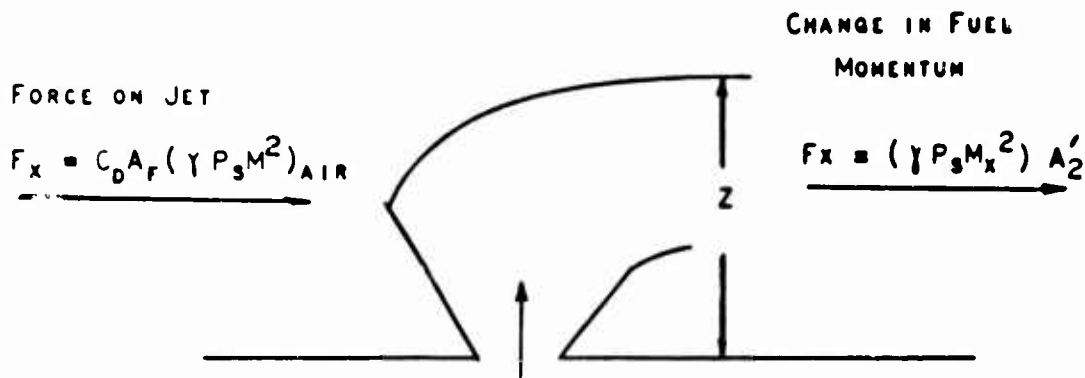
The penetration for a given mass flow of injectant and will be greater if the jet presents a lower blockage to the freestream. The jet will penetrate further into the stream until the blockage area is consistent with the acquired downstream momentum. The advantage of a low aspect ratio hole is easily seen in this model. It presents less frontal blockage width and hence greater height than a round hole. A blockage advantage of supersonic holes can also be seen. A supersonic injector hole if good design involves a lesser flow area at the exit than if the flow had been allowed to expand to the freestream pressure from a sonic flow without the benefit of containing walls. The flow area required for an isentropic expansion in a contoured nozzle can be calculated from the theoretical isentropic flow equations. The flow area required for a jet expanding to freestream from the sonic hole must be determined from detailed method of characteristic solutions.

#### b) Supersonic Injection

In order to get an analytical estimate of the difference in blockage between sonic and supersonic injectors, detailed Method-of-Characteristics solutions were accomplished with an available machine program (F233E). These calculations defined the jet shape that would occur in a zero velocity, non-mixing surroundings. The results showed a significantly greater flow area for a sudden expansion than for a contoured nozzle, qualitatively justifying the increased penetration that is actually found for a contoured, parallel-flow nozzle.

Figure 16 is a correlation of the calculated maximum widths of expanded jets. Calculations reported by NASA are also included. Both axisymmetric and two-dimensional expansions fell on the same line. The para-

**CONFIDENTIAL**

**CONFIDENTIAL**

PROPOSED RELATION:

$$C_D A_F (\gamma P_s M^2)_{AIR} = (\gamma P_s M_x^2)_{FUEL} A'_2$$

WHERE

 $F_x$  IS THE INTERACTION FORCE IN THE X DIRECTION $C_D$  IS THE COEFFICIENT OF DRAG FOR THE SHAPE CREATED BY THE INJECTED GAS $Z$  IS THE PENETRATION HEIGHT OF THE JET $A_F$  IS THE PENETRATION HEIGHT  $Z$  TIMES THE FRONTAL WIDTH OF THE EXPANDED JET $\gamma$  IS THE RATIO OF SPECIFIC HEATS $P_s$  IS THE FREESTREAM STATIC PRESSURE $M$  IS THE FREESTREAM MACH NUMBER OF THE APPROACH FLOW $M_x$  IS THE MACH NUMBER OF THE JET AFTER BEING TURNED DOWNSTREAM AND ADJUSTING TO THE FREESTREAM PRESSURE $A'_2$  IS THE FLOW AREA OF THE FUEL AFTER TURNING AND ADJUSTMENT TO FREESTREAM PRESSURE

Figure 15 - Proposed Penetration Model.

**CONFIDENTIAL**

**CONFIDENTIAL**

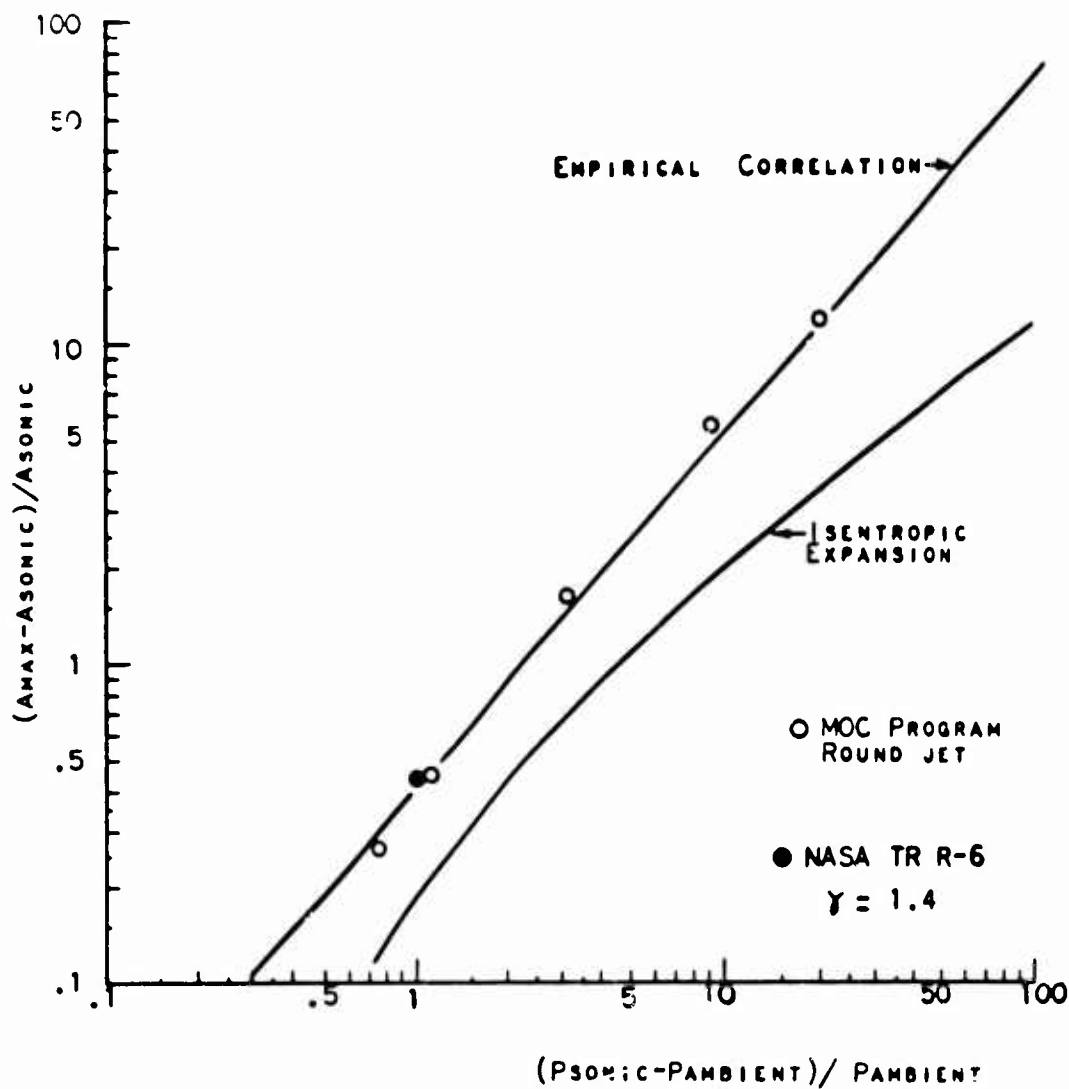


Figure 16 - Jet Expansion from Sonic Holes.

**CONFIDENTIAL**

**CONFIDENTIAL**

meters that were plotted were not derived theoretically, but were found empirically by fitting of the data. However, these parameters have a reasonable form. The axes represent the available pressure ratio for expansion and the resulting increase in jet flow area. Results from nozzles with different design Mach numbers were made to fall on the same curve by using the correction shown in Figure 17.

It is interesting that a ratio of the blockage reduction of a supersonic hole over a sonic hole is almost constant for a configuration at high injection pressure ratios independent of the exact pressure ratio. For a Mach 2 nozzle this correlation indicates 30% less blockage than a sonic hole. For the same  $C_D$ , the penetration would be expected to increase proportional to this percentage change.

At very low freestream  $q$ 's such as occur in low subsonic flows, the supersonic jets may degenerate through shock waves and mixing to the larger size of sonic holes and the blockage of sonic and supersonic injectors may approach each other. The available data are consistent with this hypothesis but not conclusive.

c) Low Aspect Ratio Slots

From a frontal blockage consideration, a two-dimensional slot (long long in the direction parallel to the mainstream flow) should penetrate further than a round hole.

Several features of the flow phenomena can be postulated to have a possible modifying effect on the relations. The turned flow from the upstream portion of the jet must flow around the downstream portion creating an effectively larger blockage to the flow than estimated from two-dimensional method of characteristic calculations. The drag coefficient may increase on the portion of the jet furthest from the wall, limiting its penetration. Also, as the aspect ratio of an injector is made less, its penetration becomes significantly affected by mixing with the surrounding gas. For the actual low aspect ratio injectors investigated in this study, the slots were thin enough that turbulent mixing with the surroundings would be expected to play a part in the penetration phenomena.

With increasing injection pressures, the blossoming jet begins to approach the shape from a round sonic hole. From the correlation in Figure 16, it is possible to make a rough estimate of the pressure at which this should occur. When the calculated maximum width of the expanded jet equals the length of the slot, it would be acting very much like a round hole. This occurs within the range of the experimental measurements in this study for the case of the supersonic slot with an  $L/D$  of 17.

**CONFIDENTIAL**

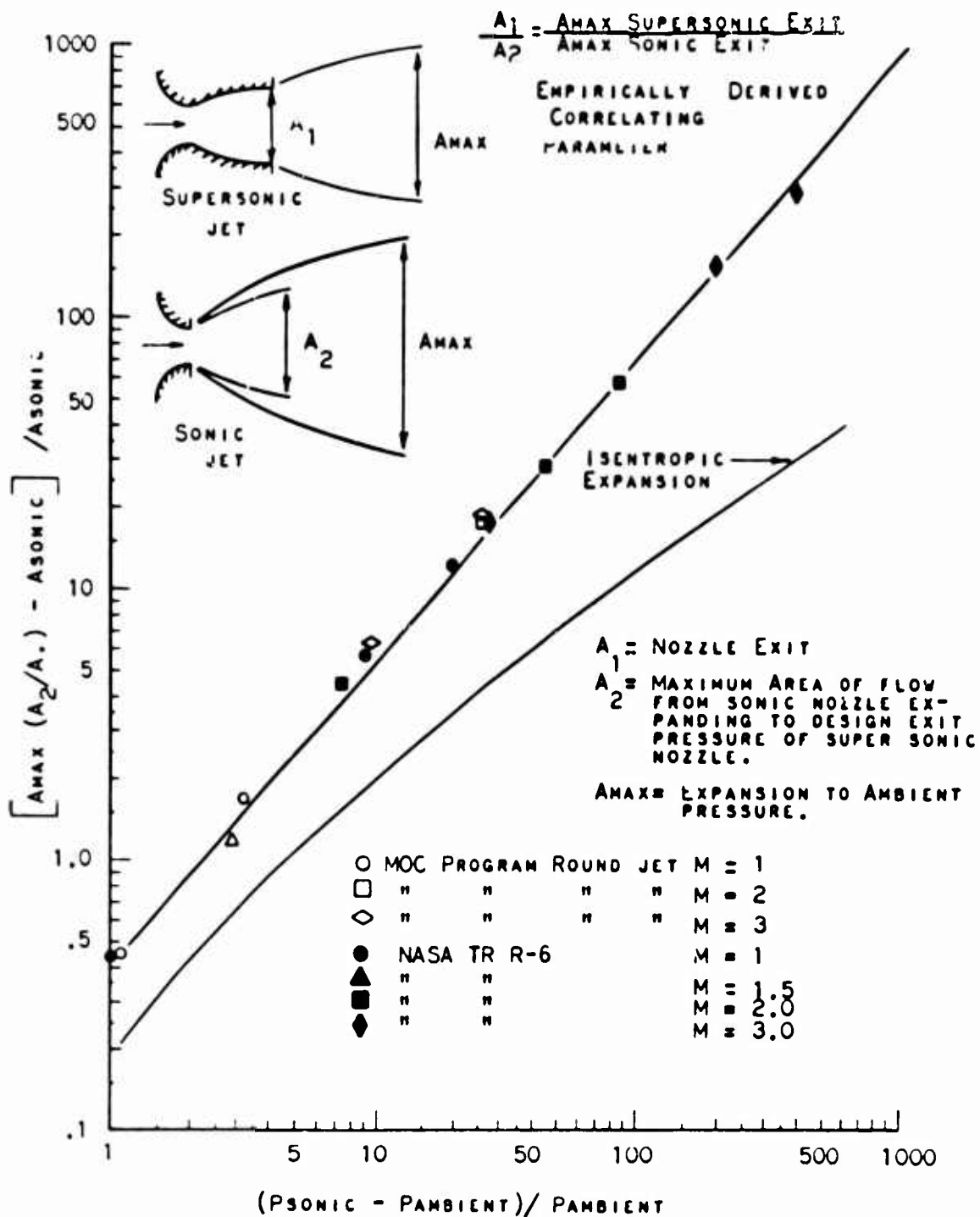
**CONFIDENTIAL**

Figure 17 - Jet Expansion from Supersonic Holes.

**CONFIDENTIAL**

**CONFIDENTIAL**

By the reasoning presented previously as for round holes, the frontal blockage relationship of the expanded jet would suggest that a supersonic slot penetrates better than a sonic slot.

When penetration is affected by mixing, one might expect different results for different density fluids. Injection into quiescent medium shows different effects for different density fluids. However, it is possible in the penetration work described here, that much of the mixing that occurs with the downstream portion of the jet as it penetrates is with the already turned portion of the upstream part of the jet and, therefore, the mixing occurs between equal density fluids and is very similar. The experimental data do not seem to show any difference with injection density other than those accounted for by the correlating parameters that were selected based on zero mixing considerations.

**d) Row of Holes**

In order to minimize tolerance problems, simplify manufacturing requirements, and to minimize friction loss, it might be desirable to replace a long slot with a row of round holes. As the jet from the round hole expands to the low freestream pressure the jets begin to overlap. Under this circumstance, the row would logically act very similar to a long slot.

**e) Angled Injection**

It would be expected that if the direction of the injected flow is angled toward downstream that some of the injection momentum would result in thrust for the engine and that the penetration distance might be somewhat reduced. According to the adopted model, the downstream momentum acquired by the jet injected in a direction normal to the flow, is equal to its final downstream momentum. For angled injectors, it is equal to the final momentum minus the initial downstream momentum. While this momentum difference consideration should reduce the penetration of angled injectors, other features of the jet increase the penetration at high injection pressures. One feature is that the injected flow from a constant cross section angled hole expands around the leading edge of the hole to supersonic velocities. The flow also turns in a direction more normal to the freestream flow direction. Furthermore, a round sonic hole injecting at less than a 90° angle to the wall presents a lower aspect ratio shape to the freestream. These features of the flow tend to increase penetration. Experimentally, the net effect was to produce about the same penetration with normal sonic holes or with angled sonic holes flush with the wall.

**4) Selected Correlating Parameter**

Considerations based on the analytical model and theory suggest that supersonic penetration should be related to the dynamic head, "q" or  $(\rho u^2)$  of the gases. The penetrating flow is turned parallel to the freestream flow by the action of forces at the interface between the two streams. The force due to the main stream is related to the body drag.

$$F_x \propto C_D q \quad (1)$$

**CONFIDENTIAL**

**CONFIDENTIAL**

At Mach numbers above 2, the coefficient of drag for blunt bodies remains constant, so that  $F_x \propto q$  for a given geometry of a blunt body or a given interface between two streams. The opposing due to the injectant is related to the downstream momentum which the injectant acquires in the turn.

The penetration is, therefore, seen to be related to functions involving momentum parameters,  $q$  or  $(\gamma PM^2)$ . Some penetration correlations reported in the literature have utilized mass flow or velocity instead of momentum possibly because the data involved did not include injectants with large density differences.

A long injection hole should present less blockage thickness to the freestream. The reduced force per unit height on the interface permits penetration to a greater height than for a round hole. With moderate aspect ratio holes and high injection pressures, the jet blossoms out to a shape approaching that of a round hole. Thus, only with very long and narrow holes or hole patterns, can significantly greater penetration, than that for round holes, be expected at high injection pressures.

The data in this work are plotted in terms of parameters that illustrate the validity of momentum dependence and the aspect ratio effect. The following discussion explains the selection of parameters that were compared in this study.

Jet penetration should scale linearly. Reynolds number effects are negligible in the penetration mechanism if the boundary layers and boundary layer separations are small compared with the penetration. If the hole diameter is doubled while the injectant pressure remains the same, the shape of the jet should remain exactly similar; and the jet should penetrate twice as far. In comparing penetration data from different hole sizes, the penetration can be made non-dimensional by expressing it as the number of hole diameters, (penetration/D). Round sonic holes with different diameters should exhibit identical (penetration/D) for the same injectant conditions of total temperature, total pressure, molecular weight and specific heat.

To correlate penetration from geometrically dissimilar jets, care must be used in defining the jet diameter. For the injectors used in this work, the penetration was made non-dimensional by using the effective hole diameter,  $D_e^*$ , which is defined as the diameter of a round sonic hole that will pass the same flow as the injector configuration. For the same injectant stagnation conditions, two configurations with different injection hole designs, but the same  $D_e^*$  will pass the same mass flow of gas. In a combustor the fuel mass flow is fixed by the mission and it is desirable to select the injector configuration having the greatest penetration for a given mass flow. The configuration with the

**CONFIDENTIAL**

**CONFIDENTIAL**

better penetrating shape will have the greater (penetration/ $D_e^*$ ) for the same injectant conditions and mass flow. The ratio would not necessarily be greater for the better penetrating shape if the physical injection diameter (which might be much larger for a supersonic hole) were used to make penetration dimensionless. By the scaling consideration discussed in the previous paragraph, comparisons can be made between configurations with different  $D_e^*$ . For identical injectant conditions of total temperature, total pressure, molecular weight, and specific heat a better penetrating shape will exhibit greater (penetration/ $D_e^*$ ) regardless of the differences in flow area.

In these experiments, the total pressure of the injectant,  $P_{jet}$ , was a basic test variable. This parameter can be made nondimensional by dividing it by a pressure in the freestream. Since the Mach number of the freestream was not a variable, the data will correlate in the same manner with either static or total freestream pressures. The total pressure, ( $P \propto$ ), was selected because it is a primary measurement in the testing.

It was proposed to correlate the non-dimensional penetration by one of two parameters: the mass flux of the jet,  $\rho U$ , or the momentum flux  $\frac{\rho U^2}{g}$ . Using the well-known definition of Mach number

$$M = \frac{U}{a}$$

and the perfect gas relations

$$P = \rho R_0 T / M$$

$$a = \sqrt{\gamma g R_0 T / M}$$

$$T_t / T = 1 + \frac{\gamma - 1}{2} M^2$$

$$P_t / P = (T_t / T)^{\frac{\gamma}{\gamma - 1}}$$

the proposed parameters may be expressed as

$$\rho U = \frac{P_t M \sqrt{\frac{\gamma g m}{R_0 T_t}}}{\left(1 + \frac{\gamma - 1}{2} M^2\right)^{\frac{\gamma + 1}{2(\gamma - 1)}}} \quad (2)$$

**CONFIDENTIAL**

**CONFIDENTIAL**

$$\rho U^2 = \frac{\gamma P_t M^2}{\left(1 + \frac{\gamma - 1}{2} M^2\right)^{\frac{\gamma}{\gamma - 1}}}$$

(3)

As long as the total pressure is sufficient to choke the throat of the jet, the Mach number is determined by the jet geometry, and is independent of the total pressure and temperature. Both parameters are thus proportional to the total pressure of the jet. The mass flux,  $\rho U$ , is a function of the temperature and molecular weight of the injectant, whereas, the momentum flux,  $\rho U^2/g$ , is independent of these properties.

Theoretical considerations predict that, of the two proposed correlating parameters, the momentum flux should be superior. When two supersonic perfect-gas flows collide obliquely, the trajectory of the boundary streamline is determined by the Mach numbers, static pressures, and the specific heat ratio existing locally in the two flows. The static pressure is, in turn, a function of the local Mach number and the total pressure and specific heat of each flow. The solution is independent of the molecular weights and total temperatures of the flows. Since the trajectory of the bounding streamline determines penetration of one flow into the other, the correct correlating parameter for penetration should also be independent of molecular weight and total temperature. The momentum flux is independent of these properties, whereas, the mass flux is not.

The superiority of the momentum flux as a correlating parameter was demonstrated experimentally by comparing the penetration of jets of helium and air injected through the same nozzle at the same total pressure and temperature. With these two gases there is a slight but complex modification of the Mach number field due to the difference in specific heat ratio, gamma. The net effect of the differences in gamma and molecular weight at the injection point is to make  $\rho U^2$  larger by a factor of 1.22 for the helium, but the max flux ( $\rho U$ ) is lower by a factor of 2.5. Thus, if mass flux were an adequate correlating criterion, the penetration of helium would be much less than that of air at the same injection pressure. Consistency with the ( $\rho U^2$ ) criteria is established if the experimental data show nearly equal penetration for the two jets; nearly equal penetration was actually found experimentally.

In this report, penetration is represented by the symbol  $Z$  and the term  $(Z/D_e^*)^2$  is plotted against the ratio of the jet total pressure to the freestream total pressure  $P_j/P_\infty$ . This method of plotting was adopted to illustrate an approximate straight line relationship. A straight line through the origin in such a plot is consistent with penetration being proportional to the square root of momentum as illustrated in the following equations:

**CONFIDENTIAL**

# CONFIDENTIAL

AF APL-TR-65-103

$$\left(\frac{Z}{D_e^*}\right)^2 = C_1 P_{jet} = C_2 \left(\frac{\rho U}{g}\right)^2 \quad (4)$$

Critical insight into the effects of the various properties affecting penetration can be gained by expanding this correlation. Using the previously derived expression for the momentum flux of a perfect gas, the correlating equation may be written

$$\left(\frac{Z}{D_e^*}\right)^2 = \frac{C_2 \gamma P_{jet} M^2}{\left(1 + \frac{\gamma-1}{2} M^2\right) \frac{\gamma}{\gamma-1}} \quad (5)$$

Noting that  $A^* = \frac{\pi}{4} (D_e^*)^2$ , the absolute penetration may be expressed as

$$Z^2 = \frac{C_3 \gamma P_{jet} A^* M^2}{\left(1 + \frac{\gamma-1}{2} M^2\right) \frac{\gamma}{\gamma-1}}$$

The equation for the flow through a sonic orifice is

$$w_f = \frac{P_{jet} A^* \sqrt{\frac{\gamma g m}{R_o T_T}}}{\left(\frac{\gamma-1}{2}\right) \frac{\gamma+1}{2(\gamma-1)}}$$

The product  $P_{jet} A^*$  may be eliminated between the last two equations, producing

$$Z^2 = C_3 \gamma w_f M^2 \sqrt{\frac{R_o T_T}{\gamma g m}} \frac{\left(\frac{\gamma+1}{2}\right) \frac{\gamma+1}{2(\gamma-1)}}{\left(1 + \frac{\gamma-1}{2} M^2\right) \frac{\gamma}{\gamma-1}} \quad (6)$$

## CONFIDENTIAL

AF APL-TR-65-103

Inspection of this last equation reveals that, for a given nozzle geometry, injectant and injectant flow and temperature, the penetration is independent of the injection pressure, as long as the pressure is sufficiently high to make the Mach number a function of nozzle geometry only. For a fixed fuel flow, the same penetration is attained by injecting at low pressure through large holes as would be attained by using high injection pressures. The equation also shows that the penetration is proportional to the fourth root of the fuel temperature; heating the fuel from 500°R to 2000°R will produce a 41% increase in penetration.

### 5) Other Empirical Correlating Parameters

Correlating parameters and methods are sometimes selected incorrectly or at least arbitrarily. Frequently a proper relation is not identifiable from either the available data or from analytical models or reasoning. Difficulties with some of the individual correlating parameters that have been used in the literature are discussed in the paragraphs that follow.

#### a) Downstream Length

There should be some effect on the penetration measured depending on the downstream distance at which the measurement is made.  $X/D$  expresses this distance in dimensionless form. In correlating data, the effective downstream distance has been represented as a power of this function  $\frac{Z}{D} \left(\frac{X}{D}\right)^a$ . However, it seems more consistent with the physical phenomena, which involve an initial penetration followed by downstream mixing as illustrated in Figure 2, to use a term of the form:

$$\frac{Z}{D} \sim \left(\frac{Z}{D}\right)_{\text{initial}} + f \left(\frac{X}{D}\right).$$

Alternatively, a virtual origin-upstream of the actual injection point may also be used:

$$\frac{Z}{D} \sim f \left(\frac{X + a}{D}\right).$$

The available data do not seem adequate for determining the most appropriate function; partly because of the very small change with distance that is observed with supersonic flows. It is suspected that basic differences may exist in the length effect between supersonic and subsonic flows. In subsonic freestream flows, the injection momentum of the jet creates a secondary flow field in the mainstream, which is quite different from flow that results from the shock waves in a supersonic stream. In general, the available correlations for subsonic flow show a greater effect of  $(X/D)$ , than the correlations for supersonic freestream flows.

## CONFIDENTIAL

AF APL-TR-65-103

### d) Injection Rate

One of the most significant test variables is the injection flow rate or pressure. For subsonic injection flows, this variable can also be expressed as injection velocity. In high pressure injection from sonic holes; the density of the injected gas is the variable. Data are frequently correlated by terms which include both the density and the velocity. In some experiments, the correlating parameter has been determined from data which did not include independent variations of density and velocity, resulting in the selection of a parameter that was inappropriate for their independent variation. The work in this study investigated both density and velocity effects. This was done by varying injection pressure and molecular weight of the injectant.

One correlation was found in the literature in which the injectant velocity was varied and seemed to be proportional to the penetration that resulted. However, instead of plotting the results vs. velocity or a specific experimental variable such as injection pressure or injected flow, the results were plotted as a function of  $\rho U$ . This plot inferred an experimental result that was not supported by the experiments; it suggested that penetration was proportional to  $\rho U$  for either density or velocity variations. The relations found by other investigators who varied both density and velocity showed that penetration was made nearly proportional to the square root of  $\rho U^2$ .

Another penetration study concluded that the temperature of the injectant was unimportant (Reference 7). While it is true that  $Z/D$  was found to be proportional to the square root of  $\rho U^2$  independent of temperature, the diameter of the hole required to pass a given mass flow is greater for the higher temperature gas; hence, the over-all penetration was greater. Another example of a misleading implication of the  $(Z/D)$  parameter is discussed in the section below on Mach number.

While considerable analytical justification has been used to support the selection of the term  $\rho U^2$ , it can also be argued that the impulse function is appropriate. It is not certain that the existing data are adequate to confirm advantages for the impulse function. In this work  $(\rho U^2)^*$  at the sonic throat was used. The relative comparisons between sonic and supersonic holes does not change when impulse function at the throat is used. However, conditions at the injector exit were used to correlate injection at greater than design pressure ratio, the impulse function is better than  $\rho U^2$  because impulse is a continuously increasing function of Mach number at constant total pressure. The proposed model qualitatively relates the increased penetration of supersonic holes to the reduced flow blockage, instead of to the increased impulse function.

### e) Mach Number

The Mach number of the flows can also be used in correlating the data. Reference 7 found the following correlating expression:

## CONFIDENTIAL

AF APL-TR-65-103

### d) Injection Rate

One of the most significant test variables is the injection flow rate or pressure. For subsonic injection flows, this variable can also be expressed as injection velocity. In high pressure injection from sonic holes; the density of the injected gas is the variable. Data are frequently correlated by terms which include both the density and the velocity. In some experiments, the correlating parameter has been determined from data which did not include independent variations of density and velocity, resulting in the selection of a parameter that was inappropriate for their independent variation. The work in this study investigated both density and velocity effects. This was done by varying injection pressure and molecular weight of the injectant.

One correlation was found in the literature in which the injectant velocity was varied and seemed to be proportional to the penetration that resulted. However, instead of plotting the results vs. velocity or a specific experimental variable such as injection pressure or injected flow, the results were plotted as a function of  $\rho U$ . This plot inferred an experimental result that was not supported by the experiments; it suggested that penetration was proportional to  $\rho U$  for either density or velocity variations. The relations found by other investigators who varied both density and velocity showed that penetration was made nearly proportional to the square root of  $\rho U^2$ .

Another penetration study concluded that the temperature of the injectant was unimportant (Reference 7). While it is true that  $Z/D$  was found to be proportional to the square root of  $\rho U^2$  independent of temperature, the diameter of the hole required to pass a given mass flow is greater for the higher temperature gas; hence, the over-all penetration was greater. Another example of a misleading implication of the  $(Z/D)$  parameter is discussed in the section below on Mach number.

While considerable analytical justification has been used to support the selection of the term  $\rho U^2$ , it can also be argued that the impulse function is appropriate. It is not certain that the existing data are adequate to confirm advantages for the impulse function. In this work  $(\rho U^2)^*$  at the sonic throat was used. The relative comparisons between sonic and supersonic holes does not change when impulse function at the throat is used. However, conditions at the injector exit were used to correlate injection at greater than design pressure ratio, the impulse function is better than  $\rho U^2$  because impulse is a continuously increasing function of Mach number at constant total pressure. The proposed model qualitatively relates the increased penetration of supersonic holes to the reduced flow blockage, instead of to the increased impulse function.

### e) Mach Number

The Mach number of the flows can also be used in correlating the data. Reference 7 found the following correlating expression:

**CONFIDENTIAL**

$$\frac{Z}{D} = 1.56 \left( \frac{\rho_1}{\rho_o} \right)^{.468} \left( \frac{U_1}{U_o} \right)^{.946} (\cos \theta)^{.844} \left( \frac{M_1}{M_o} \right)^{.56} \left( \frac{X}{D} \right)^{.0866}$$

The effect found for the injector Mach number was made dimensionless by ratioing it to the freestream Mach number. However, the freestream Mach number was not a variable in the experiment. Other evidence indicates that it was improper to ascribe this effect to the freestream Mach number.

It is interesting to notice that the correlation predicts a decrease in  $Z/D$  with an increase in the design Mach number of the injector. The penetration itself actually increases with increasing injection Mach number for a given mass flow of injectant in the above correlation although that is not obvious from the parameters used in the correlation. The  $Z/D$  term decreases because the diameter of the injector increases with Mach number for a given massflow. In this study, this difficulty was avoided by ratioing the penetration to the diameter of the sonic throat,  $D^*$ . In the usual combustor problem, the fuel massflow to the injector is the important given quantity; therefore, it is desirable that the correlating equation indicate whether injector modifications increase or decrease the penetration for a given massflow of injectant. It is not of much interest to know how penetration changes in terms of  $D$  as the design Mach number changes. For injectors with the same  $D^*$  and injection pressure, the mass flow will be the same, independent of the supersonic contour of the injector. The correlation, therefore, becomes more closely related to the combustor problem of interest when the penetration is ratioed to  $D^*$  rather than  $D$ .

The effect of injection Mach number on penetration is explained in this present study as an effect of the frontal blockage of the resulting jet.

#### d. Discussion and Test Results

##### 1) Methods of Penetration Measurements

##### a) Measurement Criterion

During this investigation, injector penetration was determined by three methods: temperature measurements, gas samples, and Schlieren photographs. Figure 12 shows a drawing of the idealized penetration. Penetration distance was identified from temperature and gas sample concentration profiles obtained by measuring the height above the flat plate where the concentration had fallen off to within 10-20 percent of the maximum concentration.

**CONFIDENTIAL**

## CONFIDENTIAL

AF APL-TR-65-103

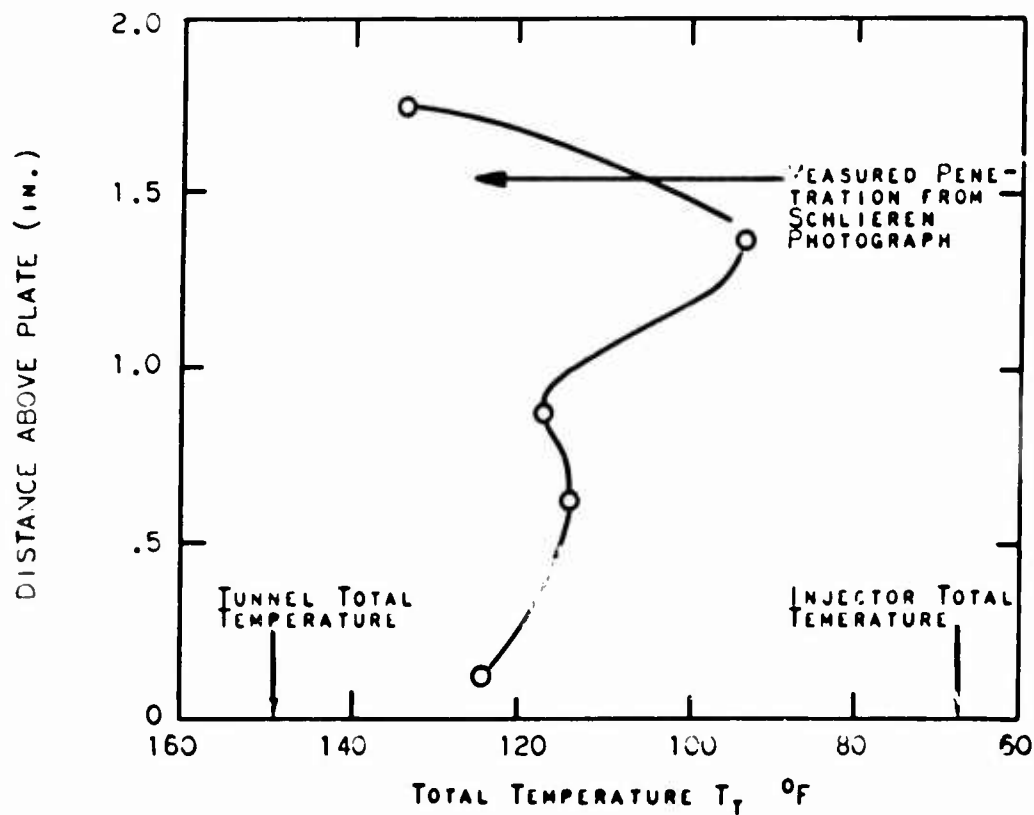
Penetration measurements using Schlieren photographs were made by measuring the height above the flat plate to the line of the outer boundary of the penetrating jet. Schlieren photographs identify the shape of the edge of the mixing region in the main flow direction, while the temperature and gas sample measurements identify the profile at a single downstream location. The three methods were consistent in identifying the position of the outer boundary of the penetrating jet; although the temperature difference measurements indicated richer concentrations of injected gas than did the gas samples. The agreement of identification of the outer boundary of the penetrating jet is shown in Figures 18, 19 and 20. The line for temperature measurements denotes the range where the concentration had fallen off to within 10-20 percent of the maximum or peak concentration. Approximately 5 to 6 inches downstream of the injector, both Schlieren photographs and gas samples indicated a fairly uniform concentration of injectant from the wall to almost the outer boundary of the penetrating jet. From Schlieren photographs, the penetrating jet was found to accomplish most of its penetration in a very short downstream distance. The accomplishment of penetration in a very short distance simplified analytical models for penetration by eliminating the need to consider mixing between the two streams in postulating the penetration mechanism. Also measurements of penetration were simplified because a measurement at only one downstream location provided a reasonable indication of the extent of penetration. The uniformity from the wall, and the rapid completion of penetration suggests that the outer extremity of the jet provides a good characteristic dimension of penetration; the measurement of this edge was, therefore, used extensively in the work for correlation of the data.

### b) Temperature Measurements

Total enthalpy per pound mixes in free turbulent flow by the same mechanism as the mass flow. Hence, it is possible to calculate local composition from local total enthalpy measurements. In low Mach number uniform temperature flow, the total enthalpy or composition can be determined from a thermocouple immersed in the stream. For supersonic flow, a bare thermocouple measures recovery temperature. To get a nearly true reading of total temperature, a shroud is placed around the thermocouple so that a low Mach number flow passes the bead. In a stream which varies with time, thermocouples do not provide a mass average temperature; the averaging process is affected by heat transfer rates to the thermocouple. However, at the outset of this investigation, it was expected that this error would be small and that temperature profiles would be a good indication of composition profiles.

### c) Gas Sample Measurements

To study the mixing of the injectant and the primary flow, a profile of the concentration was produced from the analysis of gas samples drawn at a single downstream location. As mentioned earlier, the temperature measurements indicated a richer concentration of the injected gas than did the

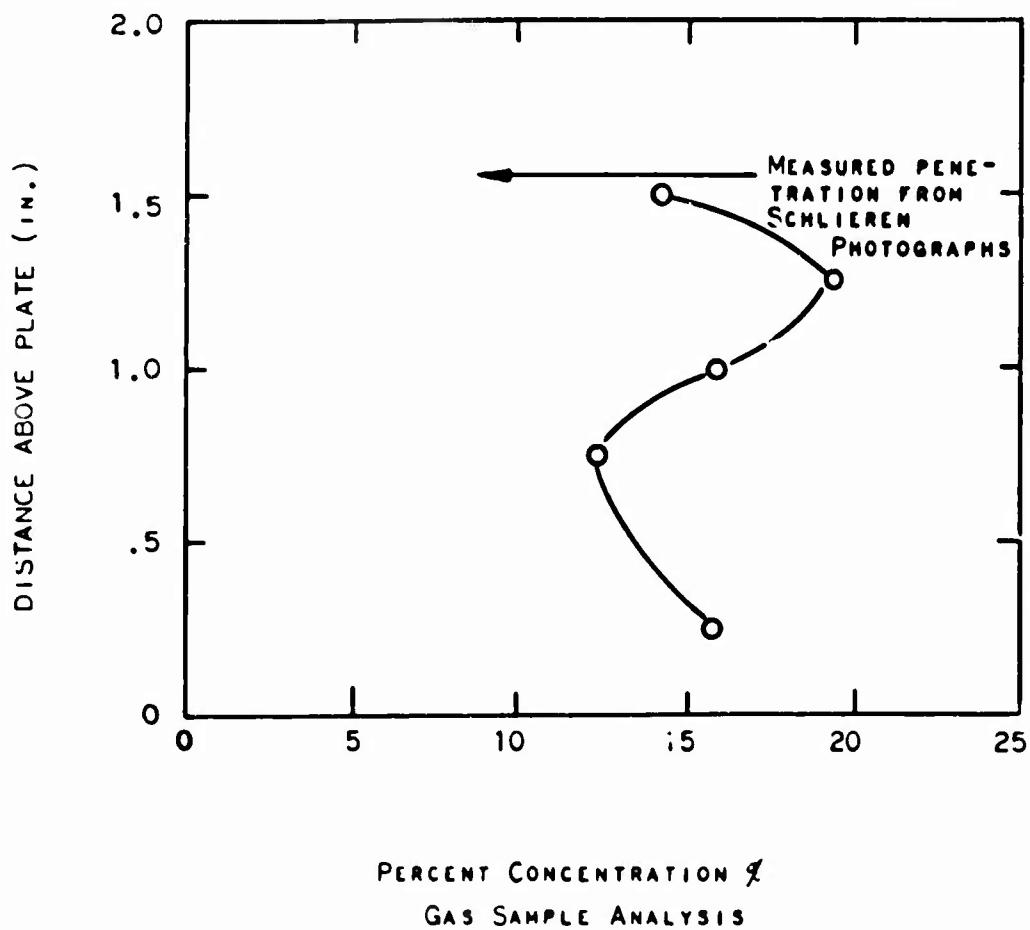
**CONFIDENTIAL**

(14-1/16" ROUND SONIC HOLES)  
(HE-AIR INJECTOR  $P_j/P_\infty = .72$ )

Figure 18 - Measured Temperature Profile.

**CONFIDENTIAL**

**CONFIDENTIAL**

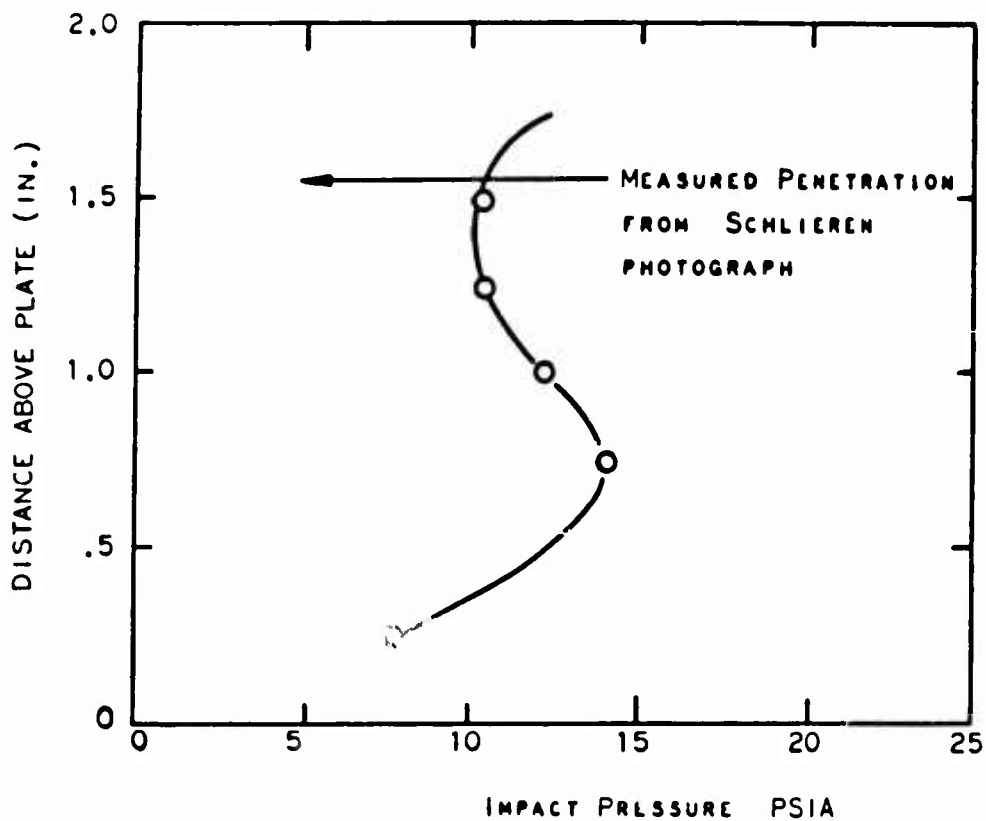


(14-1/16" ROUND SONIC HOLES  
HE-AIR INJECTOR  $P_J/P_\infty = .72$ )

Figure 19 - Measured Concentration Profile.

**CONFIDENTIAL**

**CONFIDENTIAL**



(14-1/16" ROUND SONIC HOLES  
HE-AIR INJECTION  $P_j/P_\infty = .75$ )

Figure 20 - Measured Impact Pressure Profile.

**CONFIDENTIAL**

## CONFIDENTIAL

AF APL-TR-65-103

gas samples. In a series of tests to attempt to discover these differences between gas samples and temperature measurements, a number of modifications were performed on the total temperature probes and on the gas sampling procedure. No significant differences in the original measurements of composition by each method were detected. Considering the difficulties of measurements of freestream temperature, and the difficulties in agreement of concentration profiles, it was decided to place reliance on Schlieren photographs to document the penetration of the injectant gases. Because of the good Schlieren techniques that were developed during this program, providing very rapid data gathering, efforts to improve the other techniques were discontinued.

### d) Schlieren Measurements

Schlieren photographs were obtained to document the penetration and mixing and also to develop techniques suitable for use in combustion tests. The windows for combustion testing in the arc tunnel combustion facility are detrimental to conventional Schlieren systems. A method using a distributed light source which overcomes the window problem was, therefore, investigated in this testing program, in addition to the more conventional Schlieren techniques.

Figures 21 and 22 are some of the first Schlieren photographs obtained. The instrumentation rake is seen at the right of the picture. Straight Mach lines are seen throughout the flow field at an angle consistent with Mach 3.25 flow. The jet orifice is just to the left of the picture. The strong curved line is the interaction shock in the main airstream caused by the jet. The edge of the penetration is a dark region a short distance above and parallel to the boundary layer. The photograph in Figure 21 was taken with the Schlieren system of Figure 8 with the knife edge in the horizontal position. In this position, the density gradients perpendicular to the horizontal were emphasized, and horizontal gradients did not appear. Light passing through the test section was bent toward the high density region. The knife edge cut off the light that was bent downward. The boundary layer was at a higher temperature than freestream and bent the light upward toward the higher density freestream and over the knife edge, showing as white in the photograph. The light passing through the shock wave was bent down toward the higher density region downstream of the shock; and was cut off by the knife edge, appearing black on the film. The shocks at the bottom of the picture appear white by the same physical process. The jet itself was at a slightly lower total temperature than the freestream, but local Mach number was probably a more significant factor affecting the density.

Figure 23 is an enlargement of Figure 21 which shows the shock waves on the front of each probe and also the waves created by the thermocouple bleed holes. The holes themselves can also be seen.

**CONFIDENTIAL**

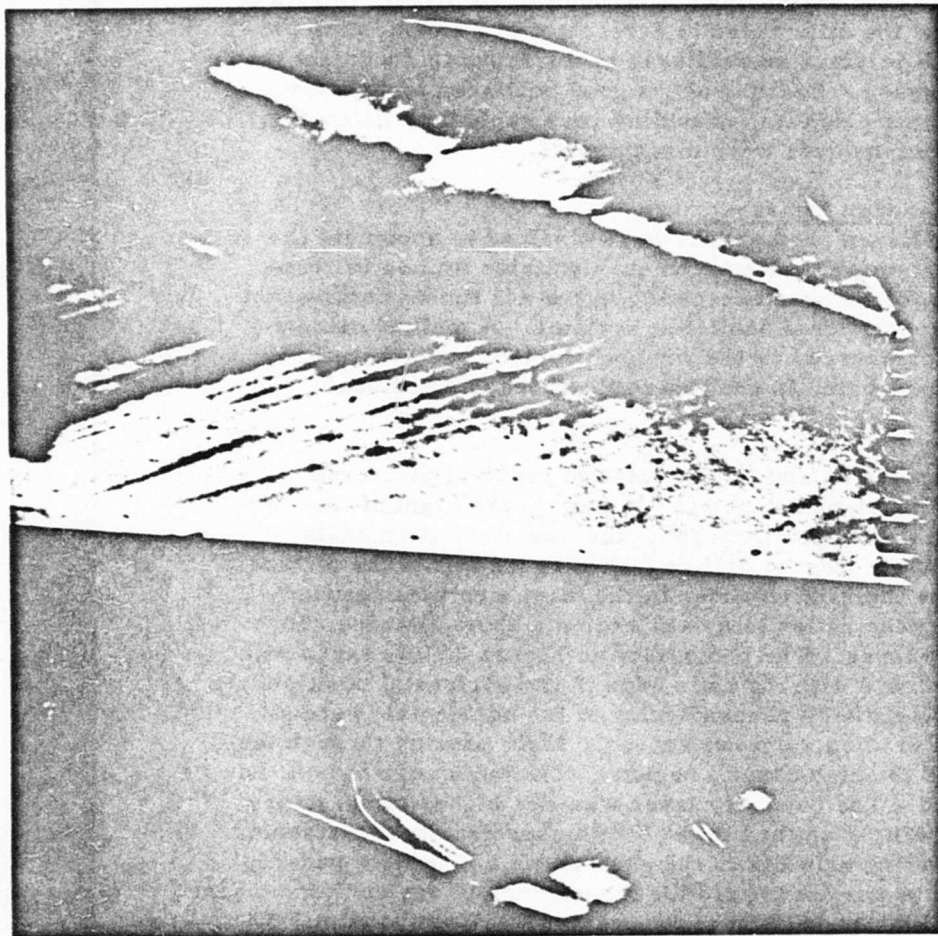


Figure 21 - Initial Schlieren Photograph.

**CONFIDENTIAL**

**CONFIDENTIAL**

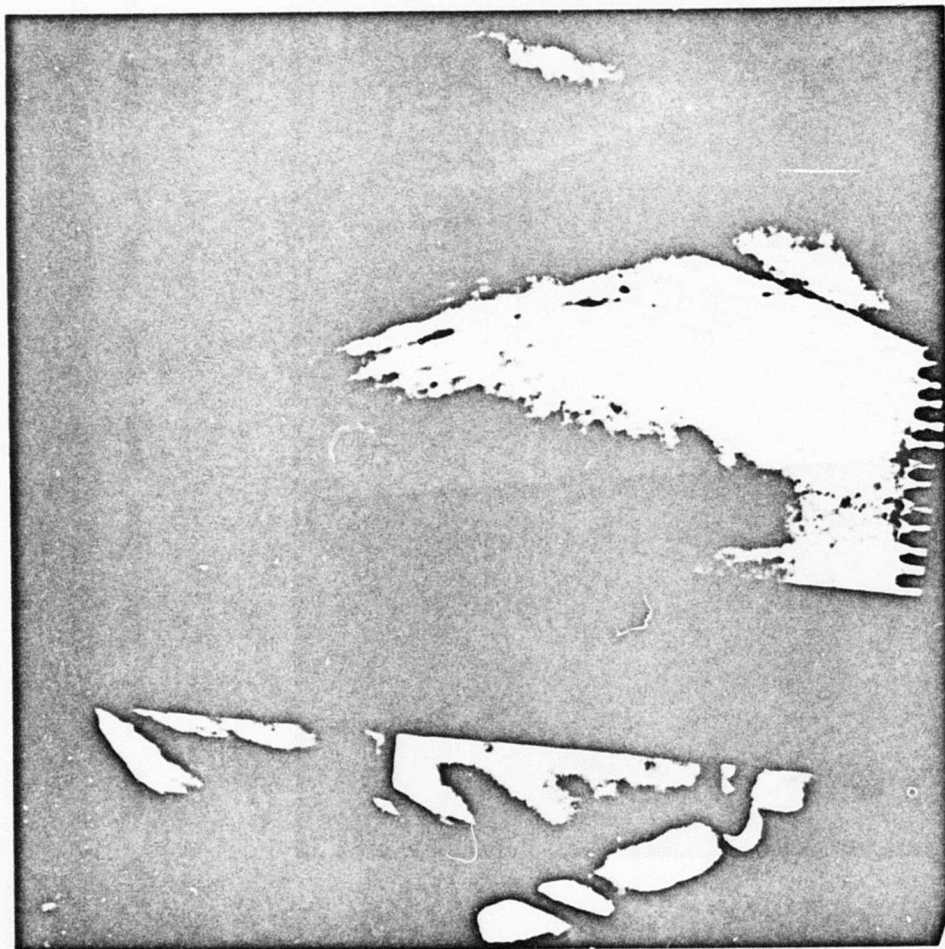


Figure 22 - Initial Schlieren Photograph

**CONFIDENTIAL**

**CONFIDENTIAL**

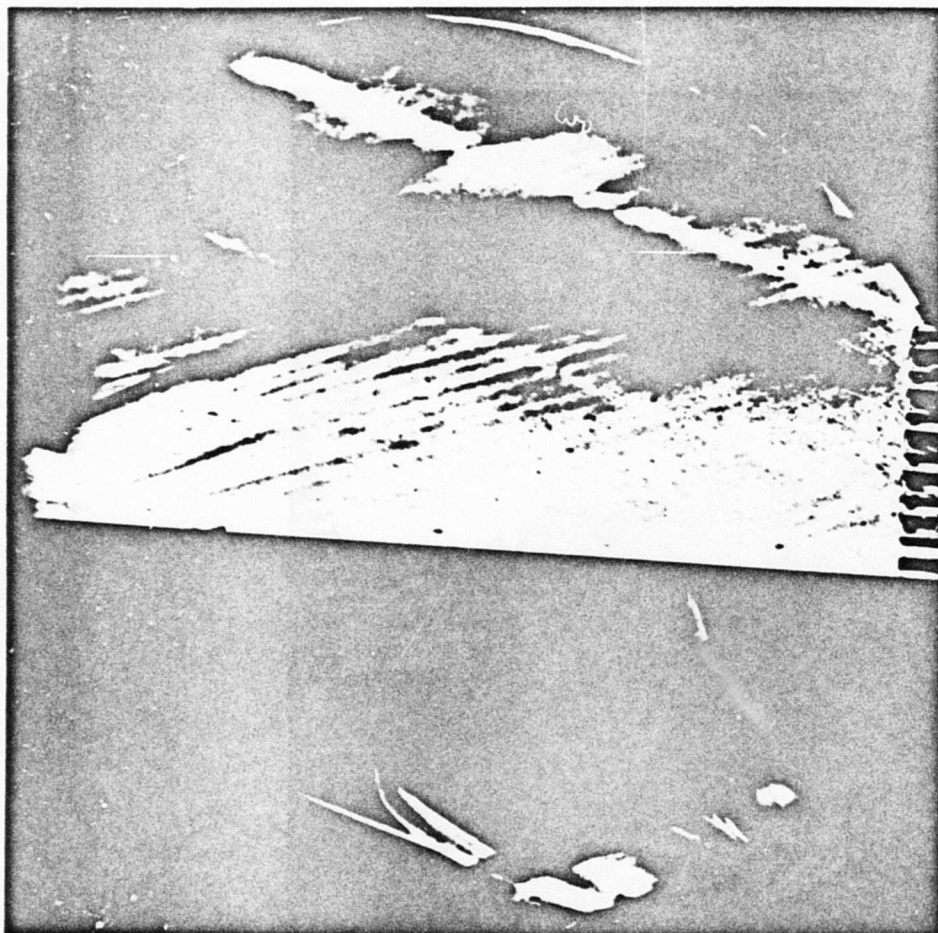


Figure 23 - Shock Waves on Instrumentation Wake.

**CONFIDENTIAL**

## CONFIDENTIAL

AF APL-TR-65-103

Figure 24 shows the same flow phenomena as in Figure 21 with the knife edge turned  $90^\circ$  to emphasize the horizontal density gradients. The boundary layer had gradients primarily in the vertical direction, and is, therefore, not as pronounced as in the first photograph. The jet and shock wave show up dark, consistent with the density increasing in a downstream direction. The jet flow Mach number was low after the interaction phenomena at the injection point, perhaps subsonic. As the injected gas went downstream, its Mach number increased and hence, its density increased.

In addition to providing an indication of the jet path, these photographs also verify that the tunnel was started, both top and bottom, and that the probe was not creating separations in the flow.

One very disturbing feature in both Figures 21 and 23 is the presence of unexplained light intensity variations, the dark region in the upper right hand corner, for example. It was noticed that there was some vibration of the Schlieren components. It was postulated that the amount of light passing over the knife edge was changing due to vibration as the focal plane shutter in the camera moved across the film. To establish if this were so and to eliminate its possible effect on the position of the jet boundary, the camera was turned  $90^\circ$ .

Figure 24 is one example of the vibration effect detected, this was with a particularly severe vibration. It is not believed that variation of intensity of the D. C. light source contributed to this phenomena since attempts to reduce vibration with rubber mounts substantially eliminated the problem in subsequent photographs. The next Schlieren photograph, after identifying the vibration problem, was taken using a spark (3 micro-second) light source. Vibrations did not change the knife edge position significantly during the 3 micro-second exposure.

Figure 25 is one photograph obtained with spark Schlieren. In these photographs the view was moved upstream to show the injection point region. The shock wave is much sharper than in the longer time exposures. Near the injection point two separate shocks are seen apparently crossing. This is partly a three-dimensional effect; the waves do not really cross through one another. The most upstream wave is the interaction shock from the boundary layer separation upstream of the jet. The jet itself is not visible. The mottled effect may be caused by imperfect windows or side wall boundary layers. One prominent feature of the injected jet should be its interaction shockwave. In this photograph, the wave should appear white and was, therefore, masked by the already white boundary layer.

Schlieren photographs are frequently taken with half of the direct light passing over the knife edge. This causes deflections in one

**CONFIDENTIAL**

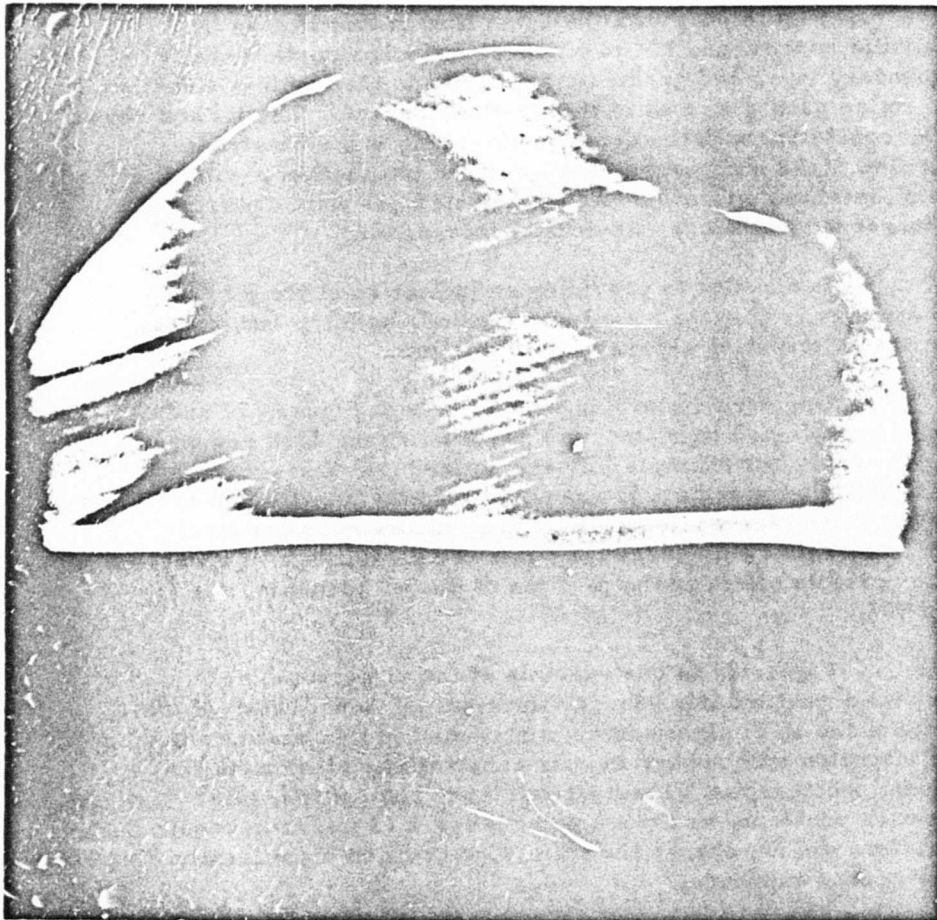


Figure 24 - Vibration Effects.

**CONFIDENTIAL**

**CONFIDENTIAL**

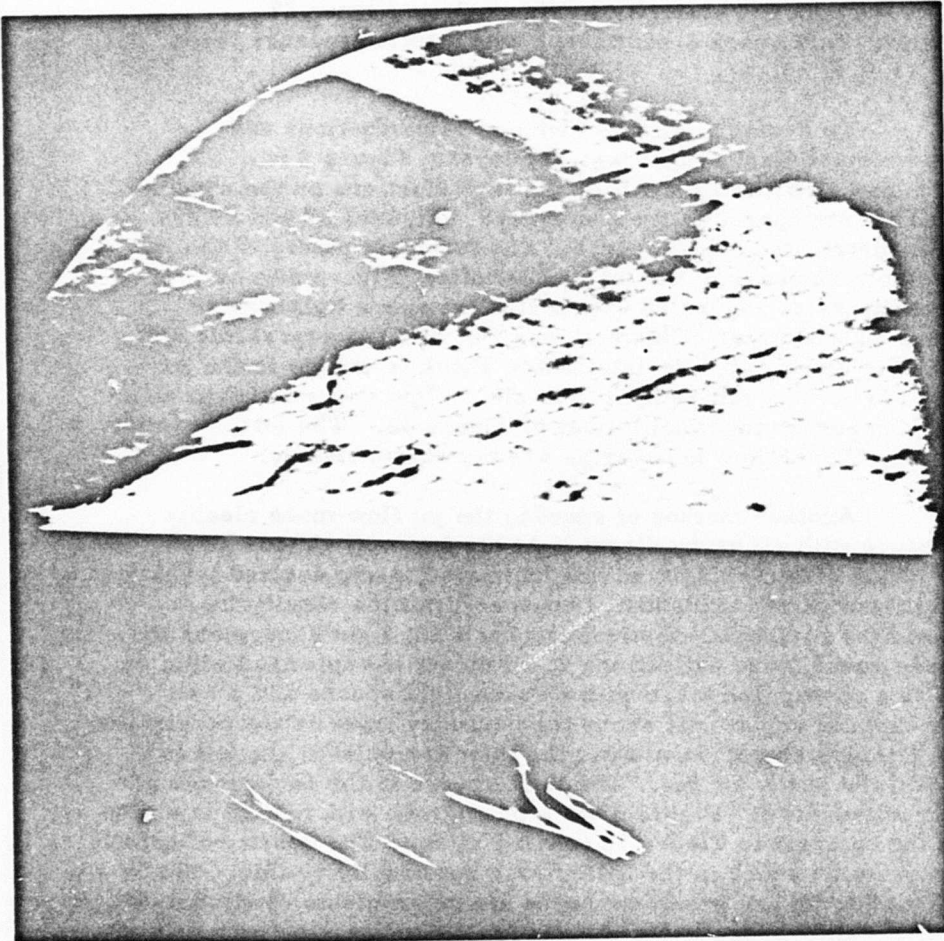


Figure 25 - Spark Schlieren Photograph.

**CONFIDENTIAL**

**CONFIDENTIAL**

direction to appear as dark regions and deflections in the other direction to appear bright. However, the sensitivity of the method is increased if all of the direct light is blocked by the knife edge. Figure 26 is a Schlieren photograph with full cut off. The injection pressure was higher than in Figure 25 bringing the interaction shock in the jet well out beyond the boundary layer. The edge of the separated boundary layer ahead of the jet can also be seen. Of special interest is the very close similarity of Figure 26 to Figure 27 (Reference 9, Figure 17); a spark shadowgraph with a total pressure ratio, jet to freestream of 13.9.

To avoid the effect of window imperfections and boundary layers a distributed light source was employed. Figure 9 is a schematic of the light path. With this method, the imperfections on the windows were out of focus and did not appear in the photograph. Figures 28 and 29 are photographs using the distributed spark source. The turbulent nature of the jet region was illustrated and the edge of the jet was definite. Figure 30 was taken at the same conditions as Figure 28 except that the spark light was replaced by a continuous light source. This test was run with the supersonic slot and with helium as the injected gas. No interaction shock is visible in the jet because the density of helium is low compared to air. Figure 31 was taken with nitrogen injection at a pressure identical to that of Figure 30. The jet interaction shock was visible here, but the flow boundaries are not shown clearly.

Another method of showing the jet flow more clearly involved a time exposure with all of the direct light blocked out. Theoretically, the exposure of the deflected light can be increased to any desired level. However, stray light from partly unidentified sources limit the sensitivity of this method. To avoid the horizontal-vertical emphasis the light source and the light cutoff were made round, thus deflections in all directions appeared white on the film. Figure 32 is a photograph taken with a round light source and a spot cut off. The faintly exposed region just above the boundary layer is the penetration region. The strong triangle shaped wave over the injection point at the left is the interaction shock wave in the jet gas. The light specks in the background are from nicks in the tunnel windows. Figure 33 is a photograph with helium injection and is presented in the contrast to Figure 32 (air injection). The density of helium is so low that the interaction shock in the helium was not usually visible. The density gradients that show up are gradients in the air or gradients of air concentration. The density differences in the mixing region are greater with helium injection than with air injection; this allows the mixing region to be more easily photographed.

Spot Schlieren with helium injection provided the most sensitive indication of a boundary of all the methods attempted. If all the indirect light is blocked out, the gradient regions will have the least exposure, but this method is not as sensitive to the time varying gradients involved in

**CONFIDENTIAL**

**CONFIDENTIAL**

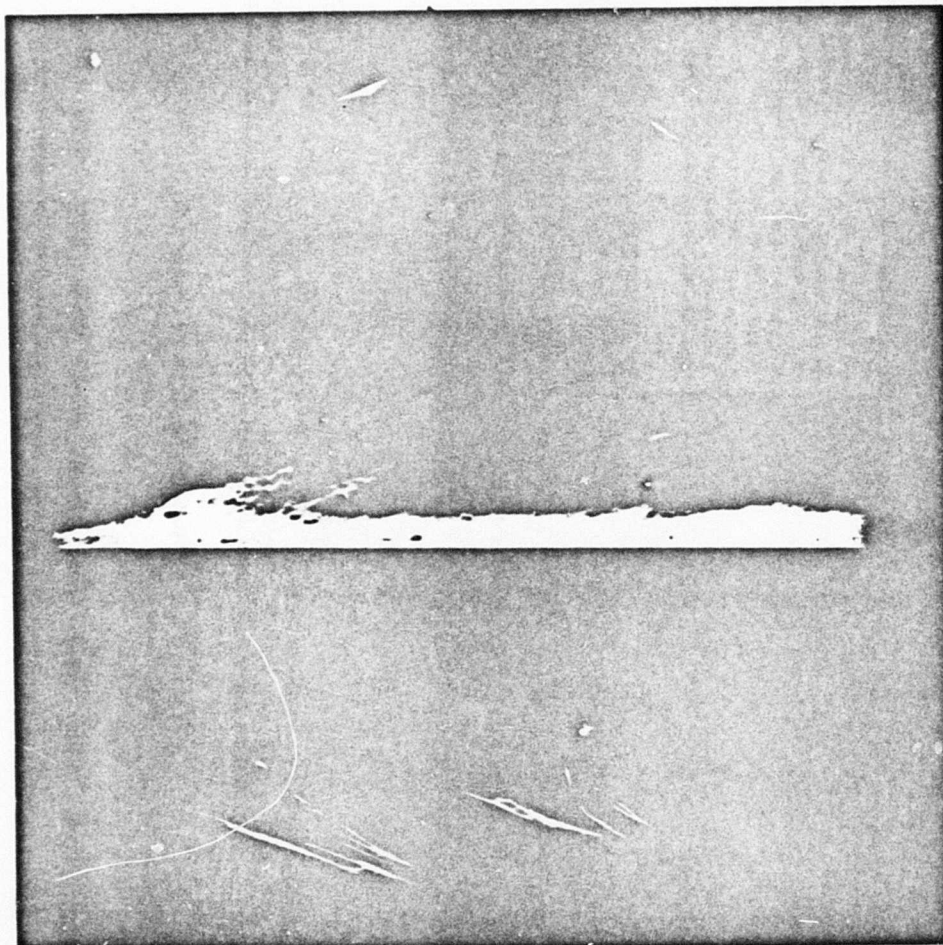


Figure 26 - Full Light Cut-Off.

**CONFIDENTIAL**

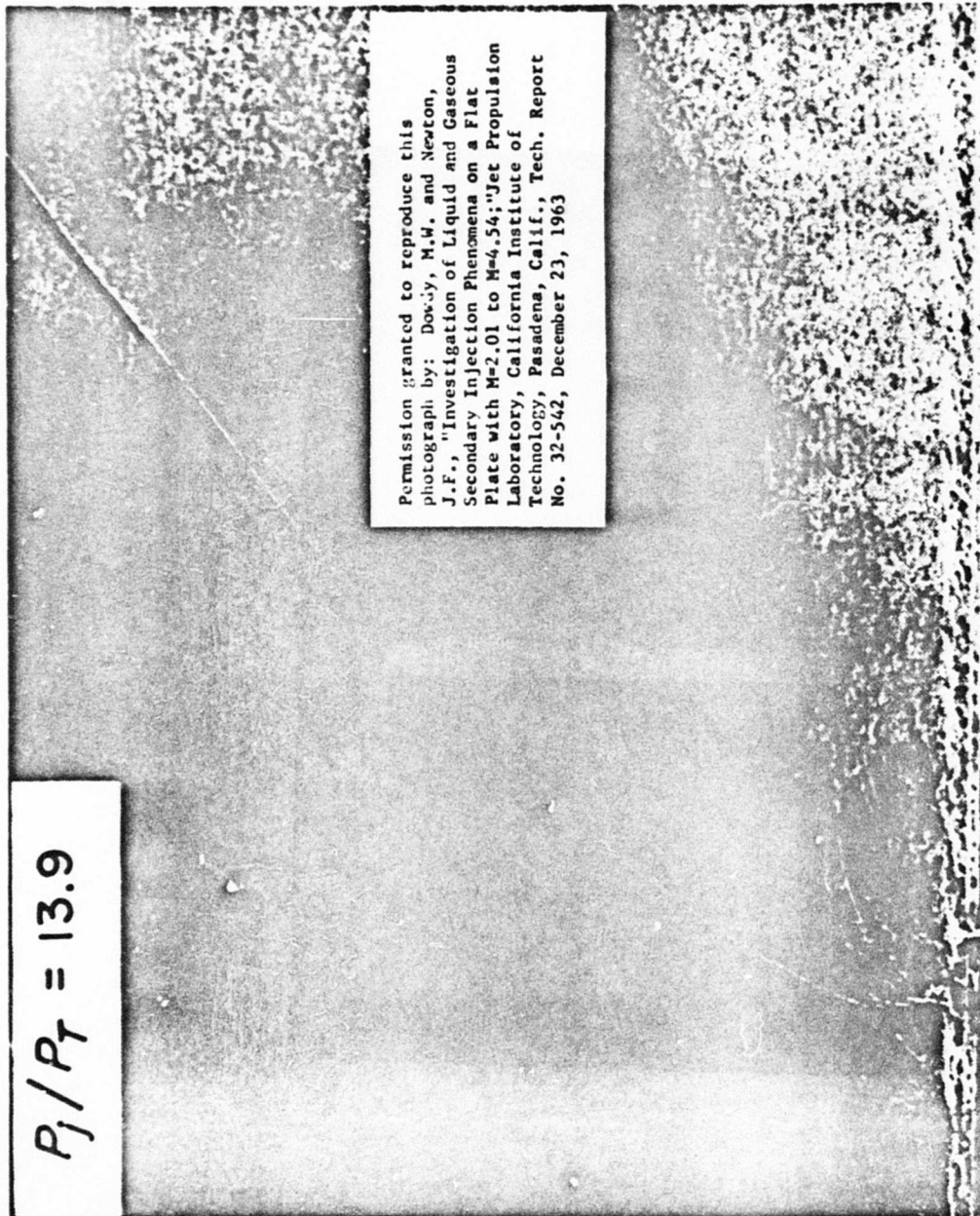
**CONFIDENTIAL**

Figure 27 - Shadow Graph from Reference 5.

**CONFIDENTIAL**

**CONFIDENTIAL**

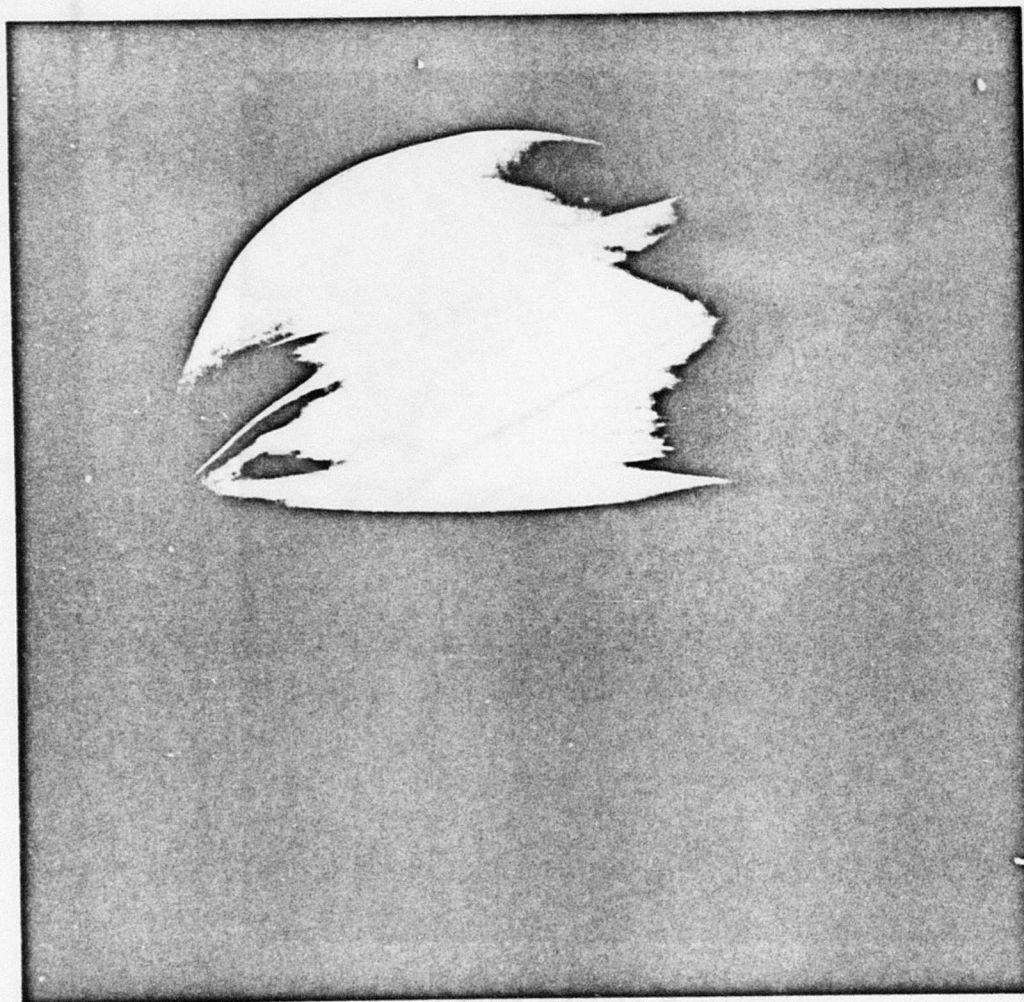


Figure 28 - Turbulent Mixing of Helium Using  
Distributed Spark Light Source.

**CONFIDENTIAL**

**CONFIDENTIAL**

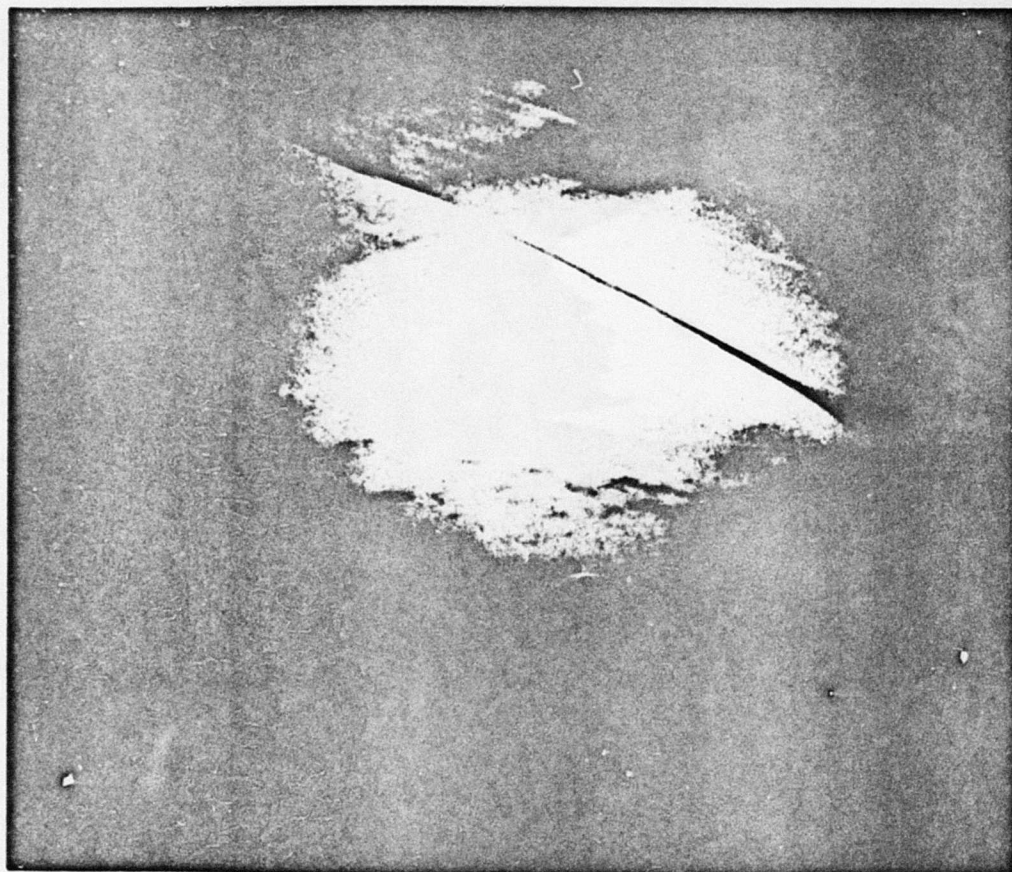
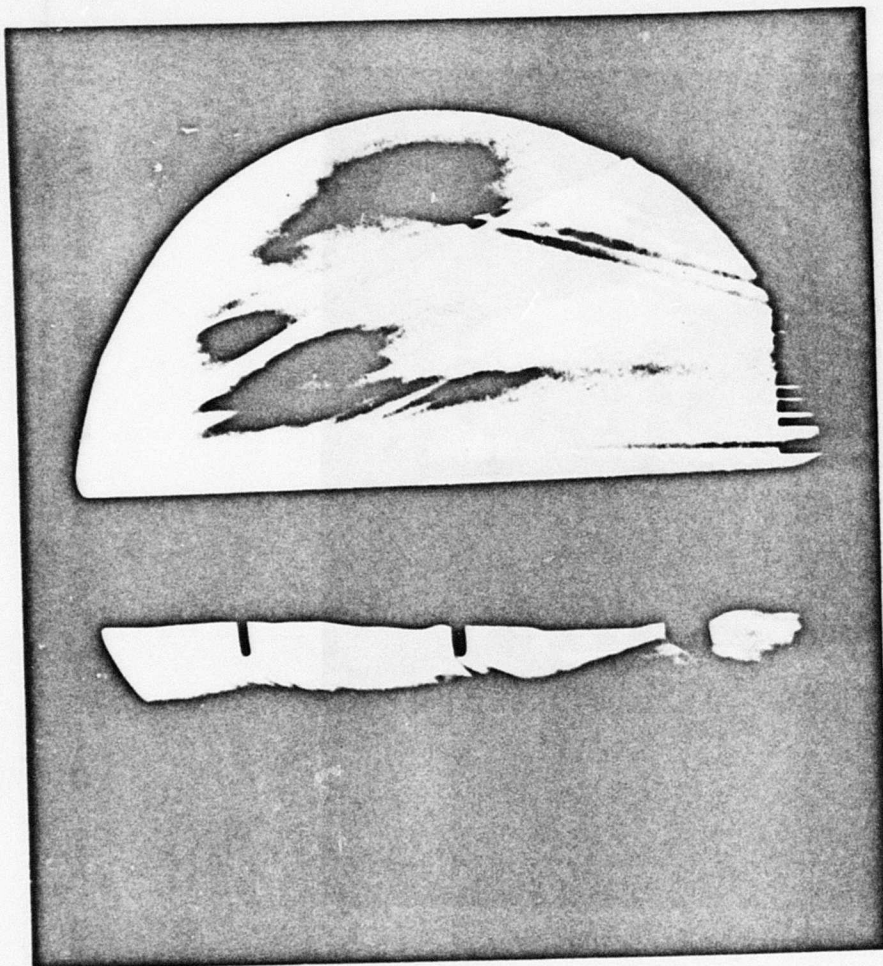


Figure 29 - Turbulent Mixing of Nitrogen Using  
Distributed Spark Light Source.

**CONFIDENTIAL**

**CONFIDENTIAL**



**Figure 30 - Helium Penetration Using Distributed Continuous Light Source.**

**CONFIDENTIAL**

**CONFIDENTIAL**

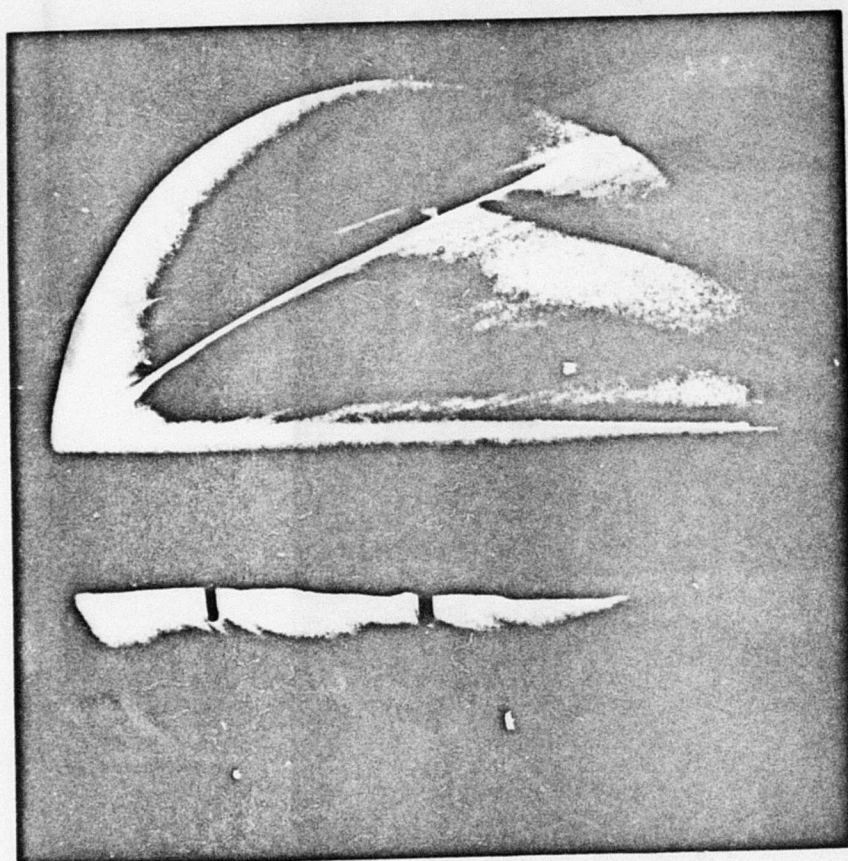


Figure 31 - Nitrogen Penetration Using Distributed Continuous Light Source.

**CONFIDENTIAL**

**CONFIDENTIAL**

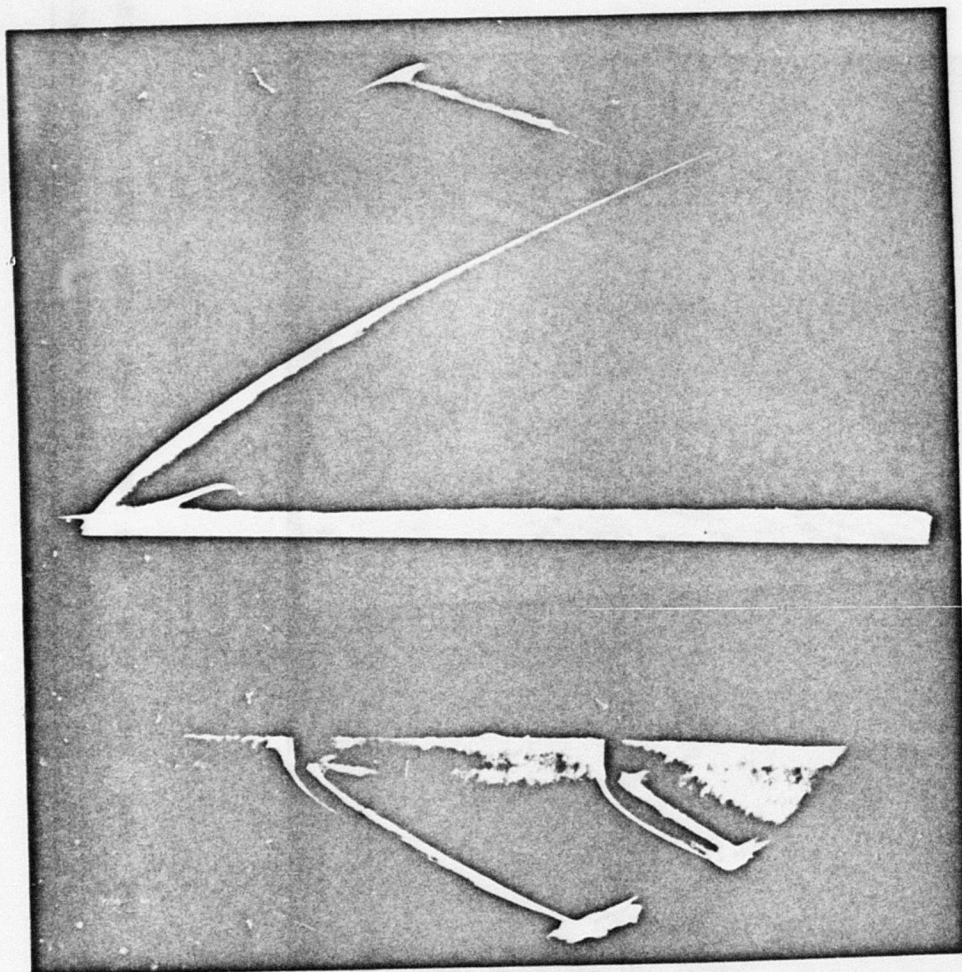


Figure 32 - Air Penetration Using Spot Light Cut-off.

**CONFIDENTIAL**

**CONFIDENTIAL**

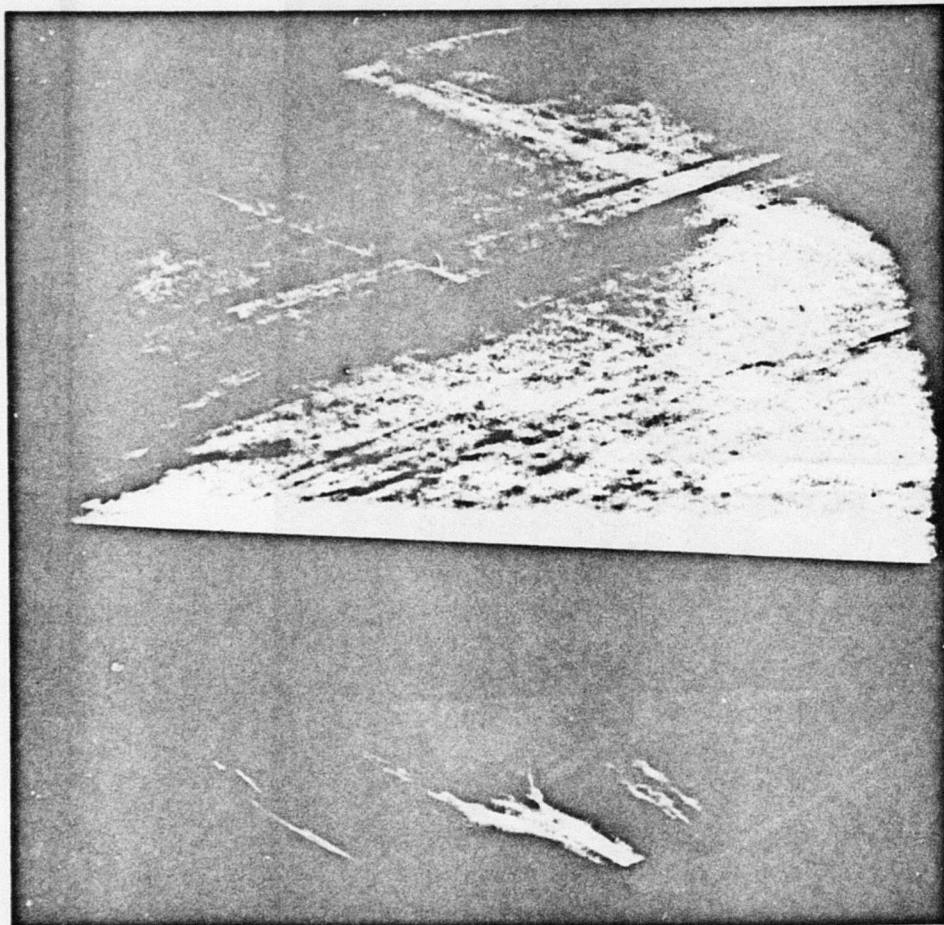


Figure 33 - Helium Penetration Using Spot Light Cut-off.

**CONFIDENTIAL**

## CONFIDENTIAL

AF APL-TR-65-103

turbulent mixing.

Color photographs were also obtained that not only identify the regions of gradients, but also provide qualitative indications of the degree of light bending that occurred and the direction. The white light just upstream of the knife edge was separated into color components by prisms. The color of the light passing by the knife edge or edges was different, depending on the bending that occurred in the test plane. It is interesting that maximum color sensitivity was obtained when the knife edges were not located exactly at the light focal points.

Figure 34 is a close-up of the injection region for Configuration 5. In this photograph some interesting details of the jet structure are visible. The shocks in the jet originate at the apex of the V's at the region where two adjacent jets expand and meet each other. The individual jets remain unaffected by the freestream flow until they are affected by the interaction shock wave. Clearly, the downstream jets penetrate further than the upstream jets before being turned by the pressure field.

Another interesting feature of a jet is illustrated in Figure 35. The photograph is of the sonic slot (Configuration 6) with no freestream flow. The fine shadows in the early part of the jet are from file marks in the throat region. More interesting is the three part structure in the upper portion of the jet. This interesting structure is believed to develop from the expansion and compression waves from the front and back of the jet.

### 2) Presentation of Data

#### a) Methods of Presentation

As mentioned earlier in this report, the objectives were to thoroughly investigate the governing relationships of penetration by: documenting the effects of test variables on the penetration-phenomena; and establishing design criterion for fuel injectors. Before this investigation was initiated, combustion tests had been performed which employed fuel injectors of the following general types; round holes, a long row of holes and a supersonic slot (Reference 1).

Except for a limited amount of single round hole data to confirm agreement with other investigators, the major emphasis in this test program was on injector configurations of long rows or low aspect ratio injectors.

In the following section, the square of the ratio of Schlieren penetration height to effective hole diameter of the particular injector configuration was plotted against the ratio of the total pressure of the jet to the total pressure of the freestream. For identical injectant conditions of total temperature, total pressure, molecular weight and gamma, a better penetrating

**CONFIDENTIAL**

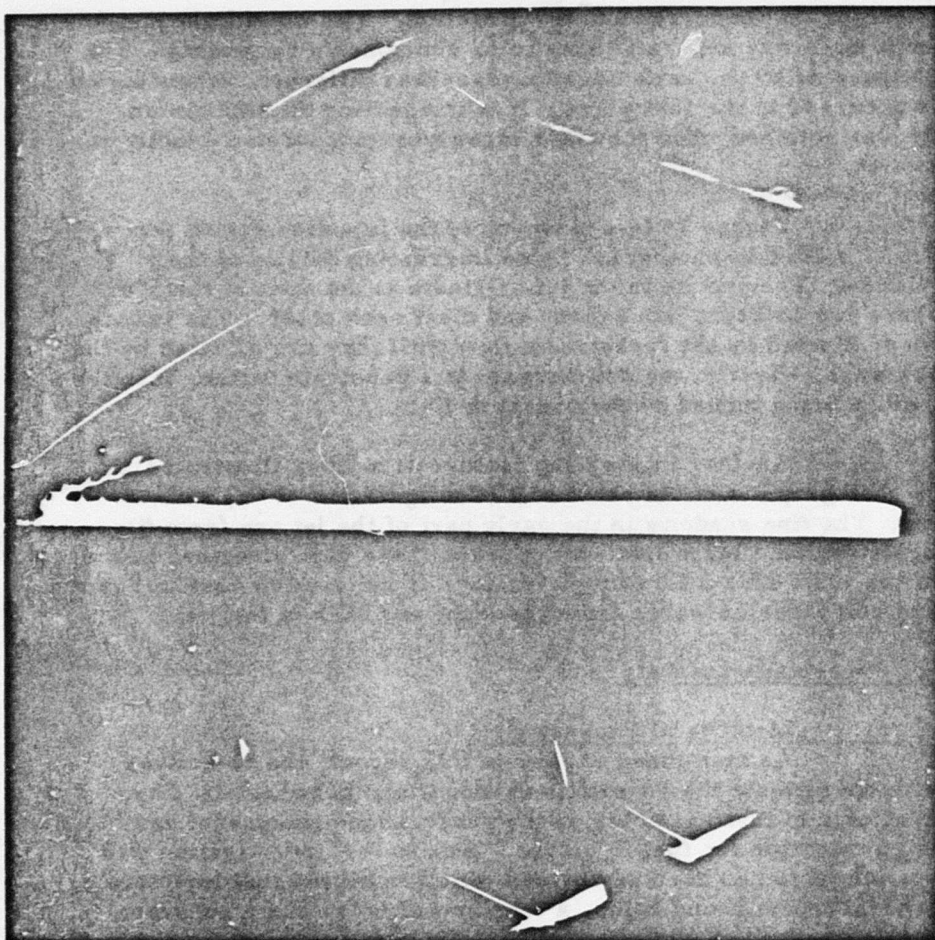


Figure 34 - Long Row Injector Penetration.

**CONFIDENTIAL**

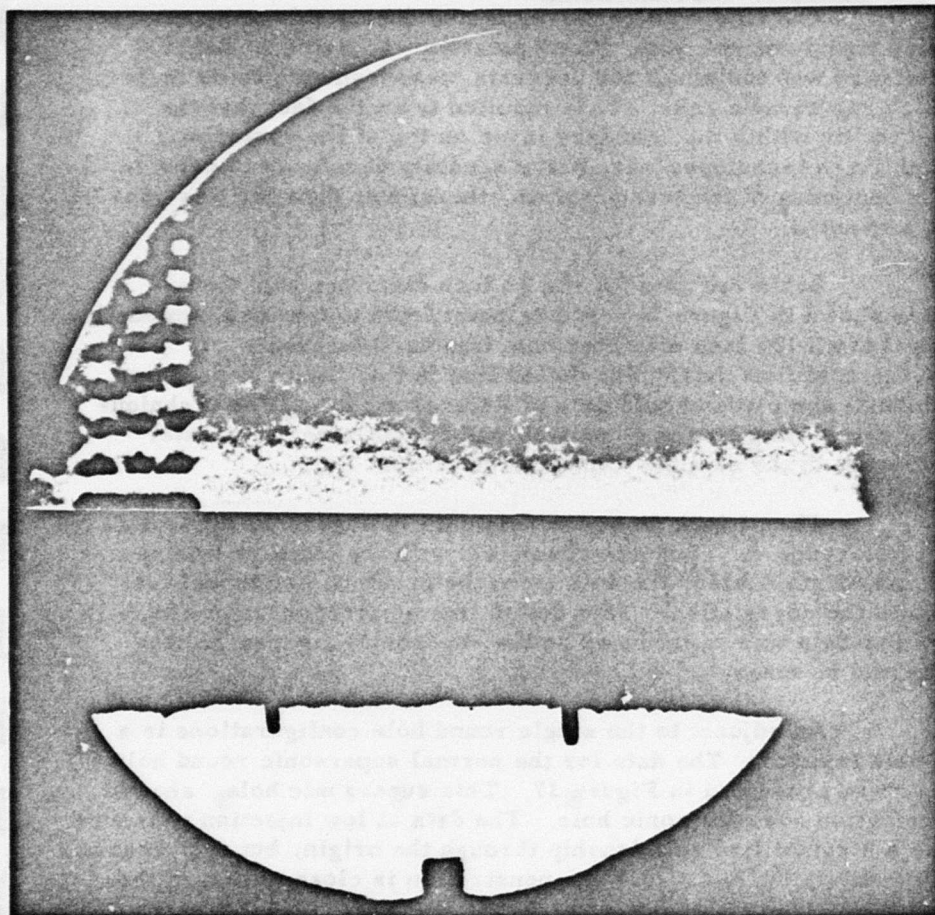
**CONFIDENTIAL**

Figure 35 - Sonic Slot Injector Flow.

**CONFIDENTIAL**

## CONFIDENTIAL

AF APL-TR-65-103

shape will exhibit greater  $(Z/D_e)^2$  regardless of the differences in injection flow area. This method of plotting was adopted to illustrate an approximate straight line relationship. As discussed earlier in the theoretical analysis section of this report, for a straight line the penetration of a given mass of injectant having a sonic velocity was independent of simultaneous changes in injection pressure and hole size.

### b) Single Hole Injectors

The first injector investigated during this program was the .1 inch diameter round normal hole. Configuration 1 listed in Table I. The penetration distance was too small for accurate measurements to be made with the temperature gas sample rake. This resulted from the fact that the injected gas stayed partly within the boundary layer on top of the centerbody flat plate. Also Schlieren techniques were not adequately developed to provide reliable data at the beginning of the test program, therefore, data for this configuration are not presented.

Schlieren data for the .3 inch diameter hole Configuration 3, are shown in Figure 36. A data point from a previous combustion test in the arc tunnel of a .186 inch diameter hole injector (Reference 1) is seen to agree with the cold flow data. The dotted line in this figure represents the extrapolated normal sonic round hole data of Reference 5. The technique used to produce the correlating line in Figure 36 will be explained in greater detail later in the report in the section, Comparison of Test Data.

The .3 inch diameter hole data in Figure 36 agree well with the data from Reference 5 and are consistent with the straight line relationship through the origin. Also, the data from the previous arc tunnel test agree fairly well with the correlation. This dotted line of correlation of single round hole penetration data was reproduced on the succeeding figures so that visual comparisons can be made.

An adjunct to the single round hole configurations is a supersonic round hole injector. The data for the normal supersonic round hole configuration 7, are presented in Figure 37. This supersonic hole showed an increase in penetration over the sonic hole. The data at low injection pressure are consistent with a straight line relationship through the origin, but at pressure ratios above approximately  $P_j/P_\infty = 0.8$  the penetration is close to that of the sonic holes.

### c) Slot Injectors

A slot with the long side in the same direction as the freestream flow was used to achieve a lower aspect ratio and to reduce the frontal blockage of the jet. A sonic slot, configuration 6, was the first slot tested. The data for this injector are shown in Figure 38. The penetration was better than that for the round sonic hole at low injection pressures, but not at high injection pressures.

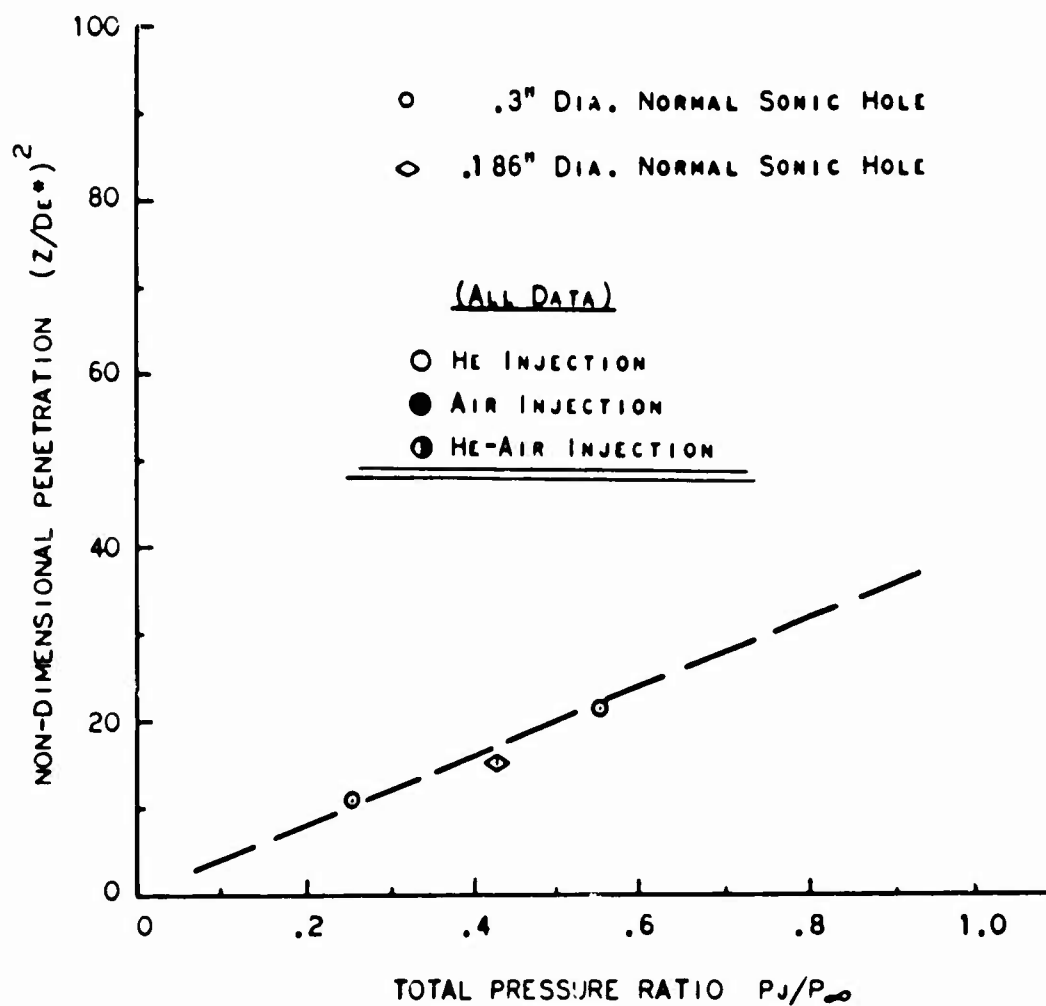
**CONFIDENTIAL**

Figure 36 - Single Normal Round Sonic Hole Schlieren Data.

**CONFIDENTIAL**

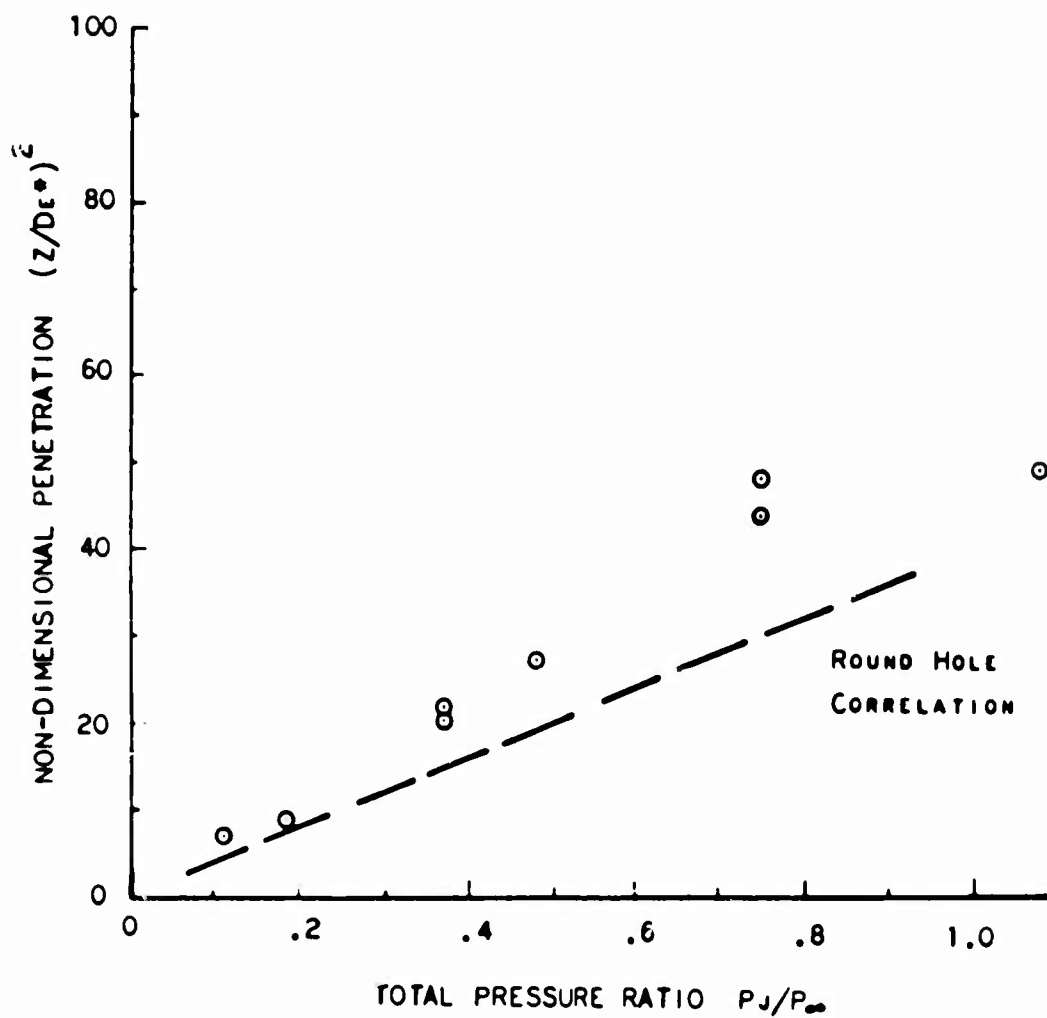
**CONFIDENTIAL**

Figure 37 - Supersonic Normal Round Hole Data.

**CONFIDENTIAL**

**CONFIDENTIAL**

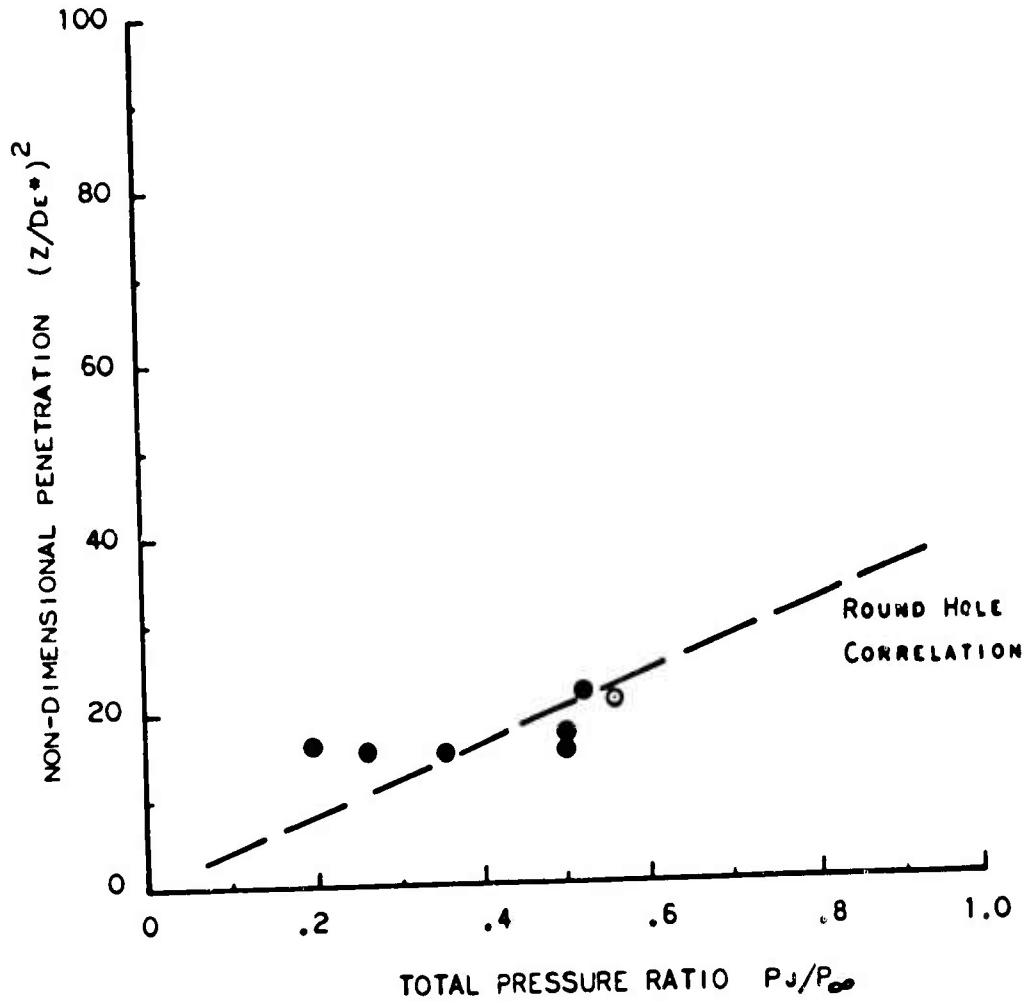


Figure 38 - .83" Long Sonic Slot Data.

**CONFIDENTIAL**

## CONFIDENTIAL

AF APL-TR-65-103

Just as for round holes the blockage relationship of the expanded jet would suggest that a supersonic slot penetrates better than a sonic slot.

The data for configuration 4 , a supersonic slot which was a factor of 2 times the dimensions of a similar supersonic slot used in open jet and closed duct arc tunnel tests (Reference 1 ) is presented in Figure 39. These data show an improvement in nondimensional penetration over the sonic slot of the same size in Figure 38. The nondimensional penetration was similar to that found with a supersonic round hole, except that greater penetration was found for the supersonic slot at low pressure ratios.

The data for configuration 13 , a three-inch long supersonic slot, are shown in Figure 40, these data indicate that by continually reducing the aspect ratio or increasing the  $L_t^2/A$  term of a given supersonic slot, the nondimensional penetration could be increased particularly at the higher injection pressures. These data show a significant increase in penetration over the short supersonic slot and also appear to follow a linear relationship through the origin throughout the complete range of documentation. The range of data was limited to low injection pressure by facility capabilities; but it was postulated that the data are beginning to deviate from the straight line through the origin at the maximum pressure,  $P_j/P_\infty = 0.3$ . Looking back at Figure 39, it can be seen that the nondimensional penetration for low injection pressures of the shorter slot may also have been consistent with this same linear relationship.

### d) Long Row Injectors

In order to minimize tolerance problems of long slots, simplify manufacturing requirements and to minimize friction losses, it might be desirable to replace a long slot with a row of round holes. At high injection pressures at the jet from the round holes expands to the low freestream pressure, the jets begin to overlap and act very similar to the long slot.

The first long row injector tested consisted of nine (9) 1/32 inch diameter holes, configuration 2 . Data are not presented for this configuration because the small mass flows with this injector did not provide enough penetration to be accurately documented by the temperature gas sample rake and the Schlieren techniques were not adequately developed at the time these tests were run. Configuration 2 , the nine (9) 1/32 inch diameter hole injector, was modified into a number of other configurations as mentioned in the Experimental Technique section; the first modification was to a row of nine (9) 1/16 inch diameter holes (Configuration 5 ).

CONFIDENTIAL

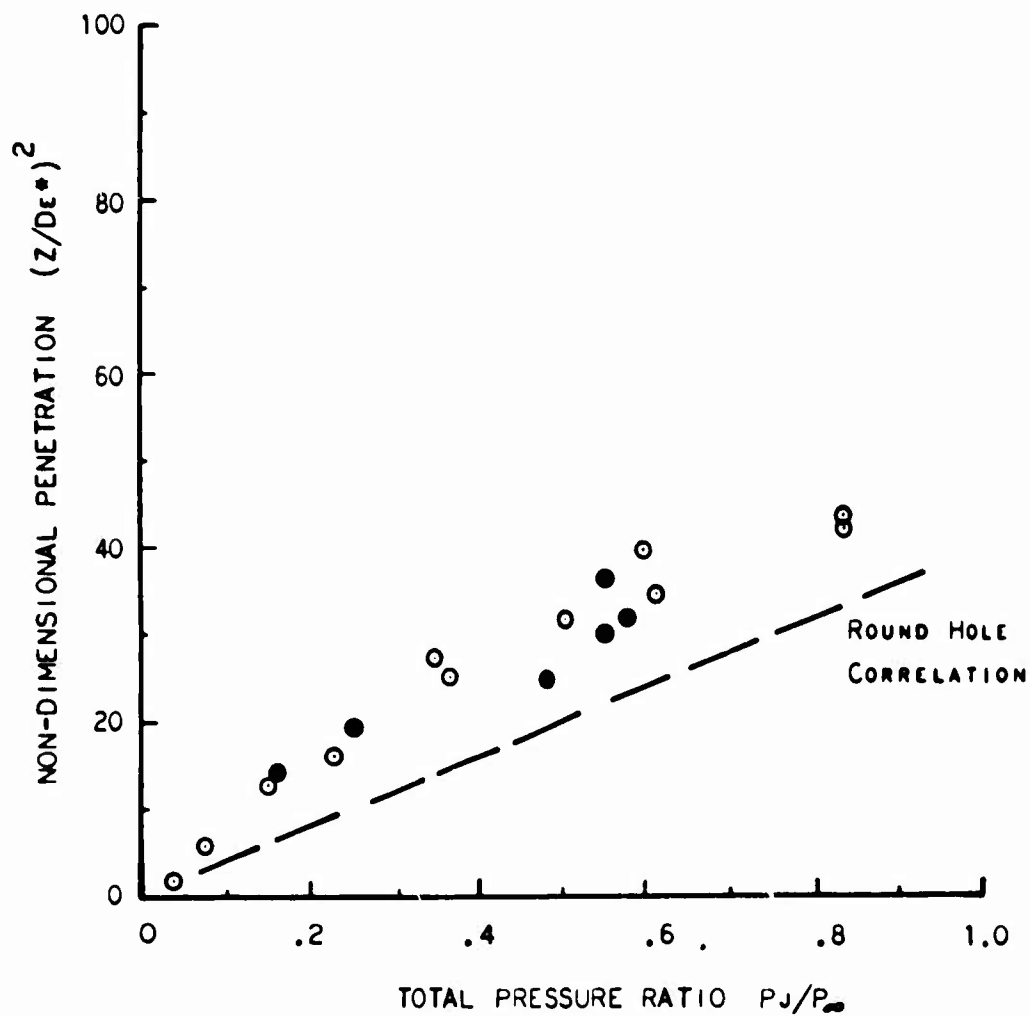
**CONFIDENTIAL**

Figure 39 - .83" Long Supersonic Slot Data.

**CONFIDENTIAL**

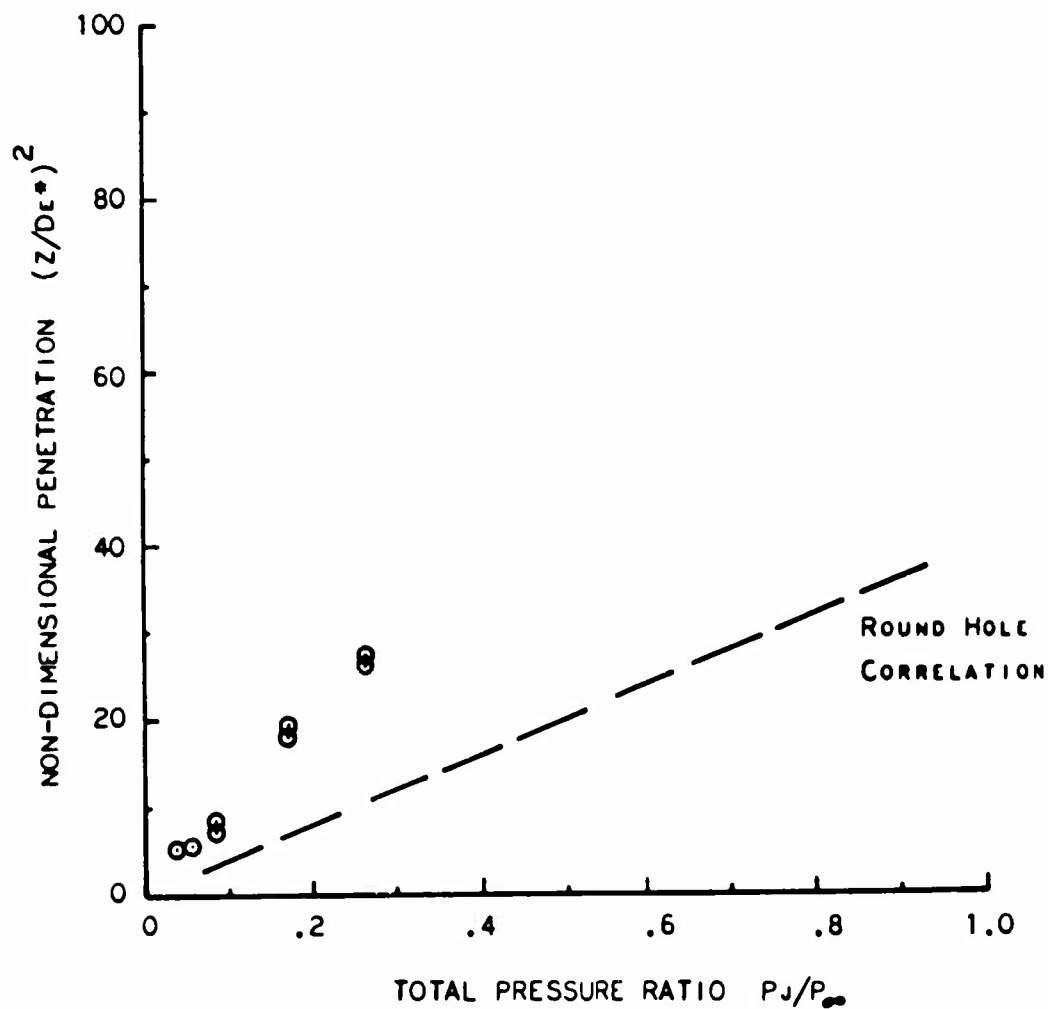
**CONFIDENTIAL**

Figure 40 - 3.0" Long Supersonic Slot Data.

**CONFIDENTIAL**

**CONFIDENTIAL**

Figure 41 is a documentation of the data for the nine (9) 1/16 inch diameter holes. Large nondimensional penetration is exhibited in the low pressure ratio range up to approximately  $P_j/P_\infty = 0.3$ . The data follow a linear relationship through the origin similar to the long slot data, but at higher pressures the penetration begins to approach that for the round hole data. The differences in the data for helium and air were due partly to the Schlieren technique. The air data for this particular configuration were taken with a technique that did not provide a sharp indication of the penetration boundary and were, therefore, not as reliable as the helium data.

The second modification in this series was to a row of fourteen (14) 1/16 inch diameter holes (Configuration 9). This injector exhibited the greatest nondimensional penetration of all the injectors tested during this investigation. The data are shown plotted in Figure 42.

This Configuration 9 had the largest ratio of length squared to area term  $L_t^2/A$  of all the configurations tested as shown in Table I. This large  $L_t^2/A$  or low aspect ratio points out that there was a direct parametric relationship between penetration the  $L_t^2/A$  term. The large nondimensional penetration with associated large ratio of  $L_t^2/A$  is consistent with the deep penetration that was apparently detected from the forty-eight (48) 0.04 inch diameter hole injector configuration of previous cell 5 combustion tests. Figure 42 includes a data point from these cell 5 combustion tests converted to a freestream Mach number  $M = 3.25$  by a technique which utilized Figure 3 of Reference 5.

Figure 43 shows the data for another modification to the original row of holes. This modification was Configuration 10; a row of fourteen holes with diameter increasing in the freestream direction as shown in Table I. This modification did not produce any increase in nondimensional penetration over the fourteen 1/16 inch diameter configuration.

The last modification to the original Configuration 2 that was made was Configuration 11, a row of fourteen (14) .154 inch diameter holes, the data for which appear in Figure 44. The total jet to freestream pressure ratio range was limited because of the large flow area of this injector.

#### e) Normal/Downstream Injectors

As stated earlier, one of the major objectives of this investigation was to design a fuel injector that produced acceptable penetration while conserving a portion of the downstream thrust. It would be expected that if the direction of the injected flow was angled slightly downstream that some of the injection momentum would result in downstream thrust for the engine and also that the penetration height might be somewhat reduced.

**CONFIDENTIAL**

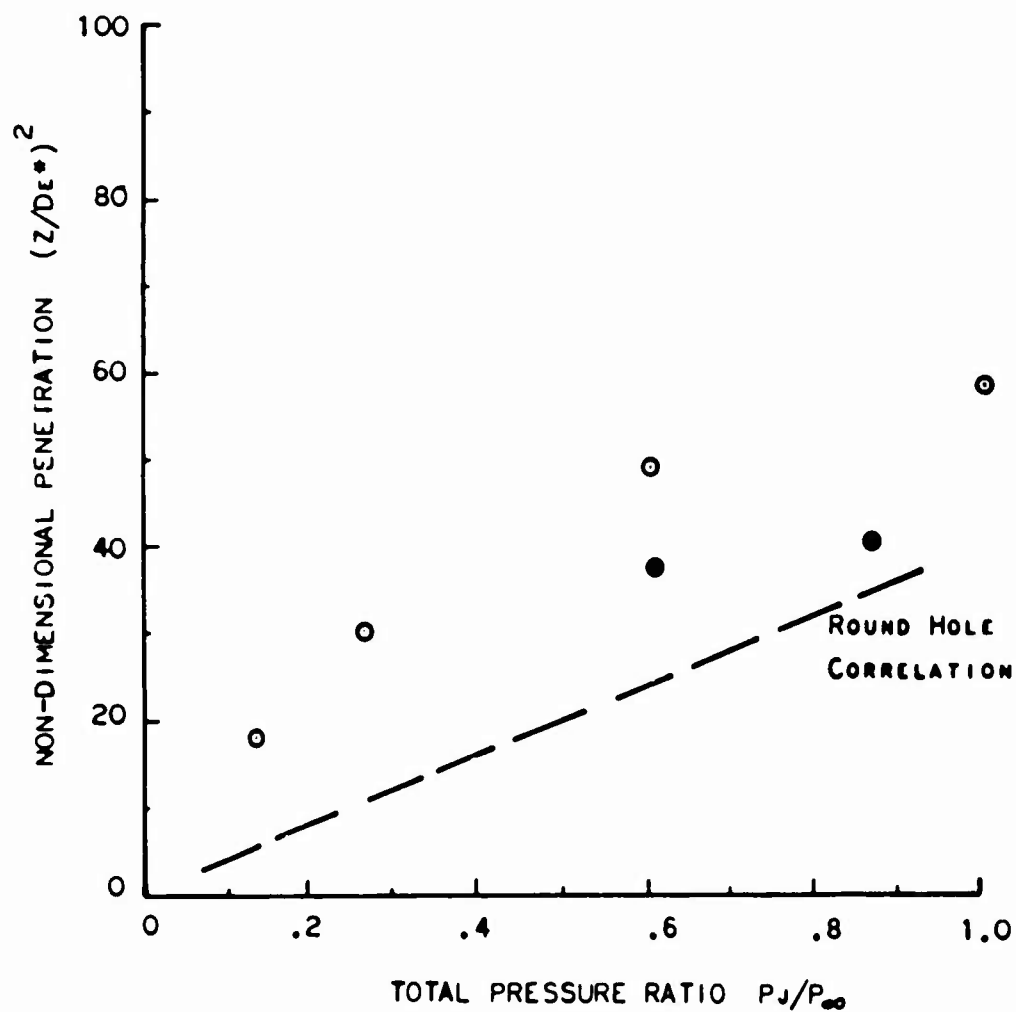
**CONFIDENTIAL**

Figure 41 - Nine 1/16" Dia. Normal Round Hole Data.

**CONFIDENTIAL**

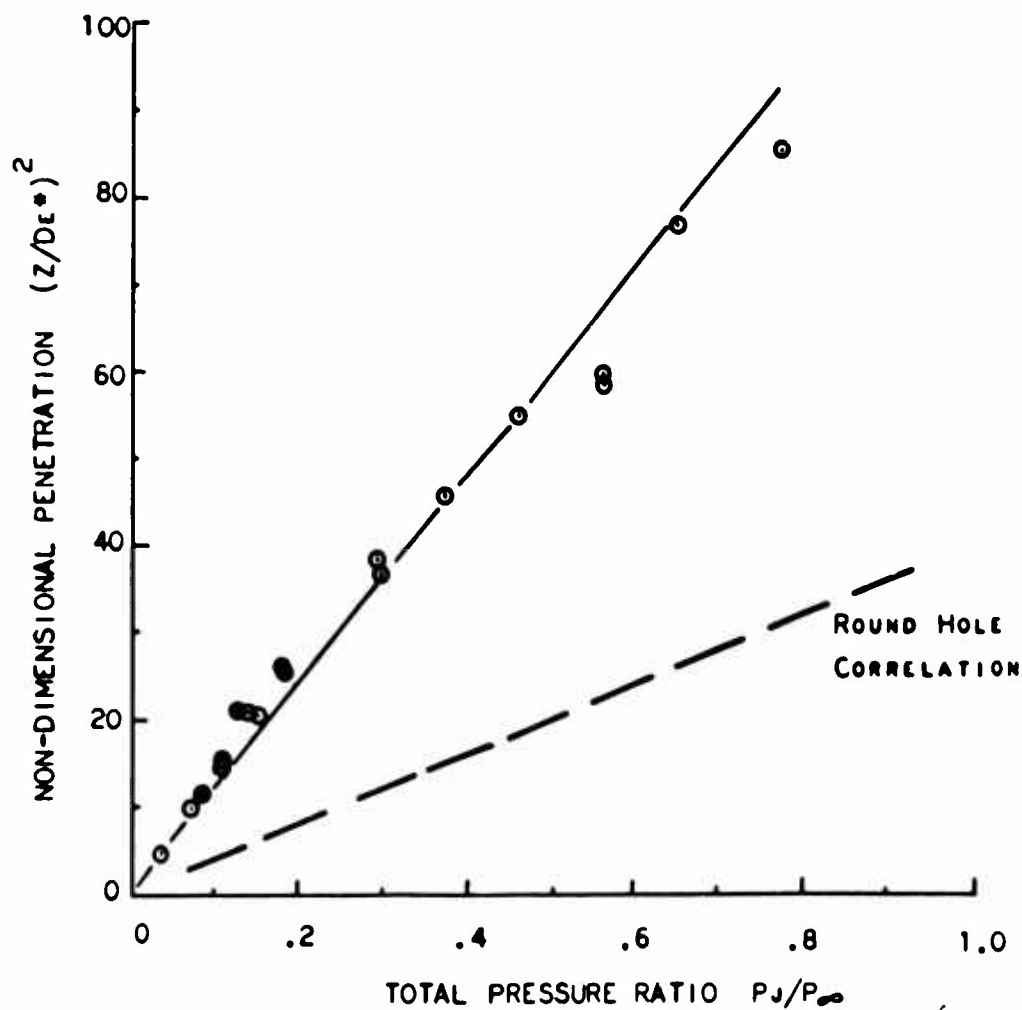
**CONFIDENTIAL**

Figure 42 - Fourteen 1/16" Dia. Normal Round Hole Data.

**CONFIDENTIAL**

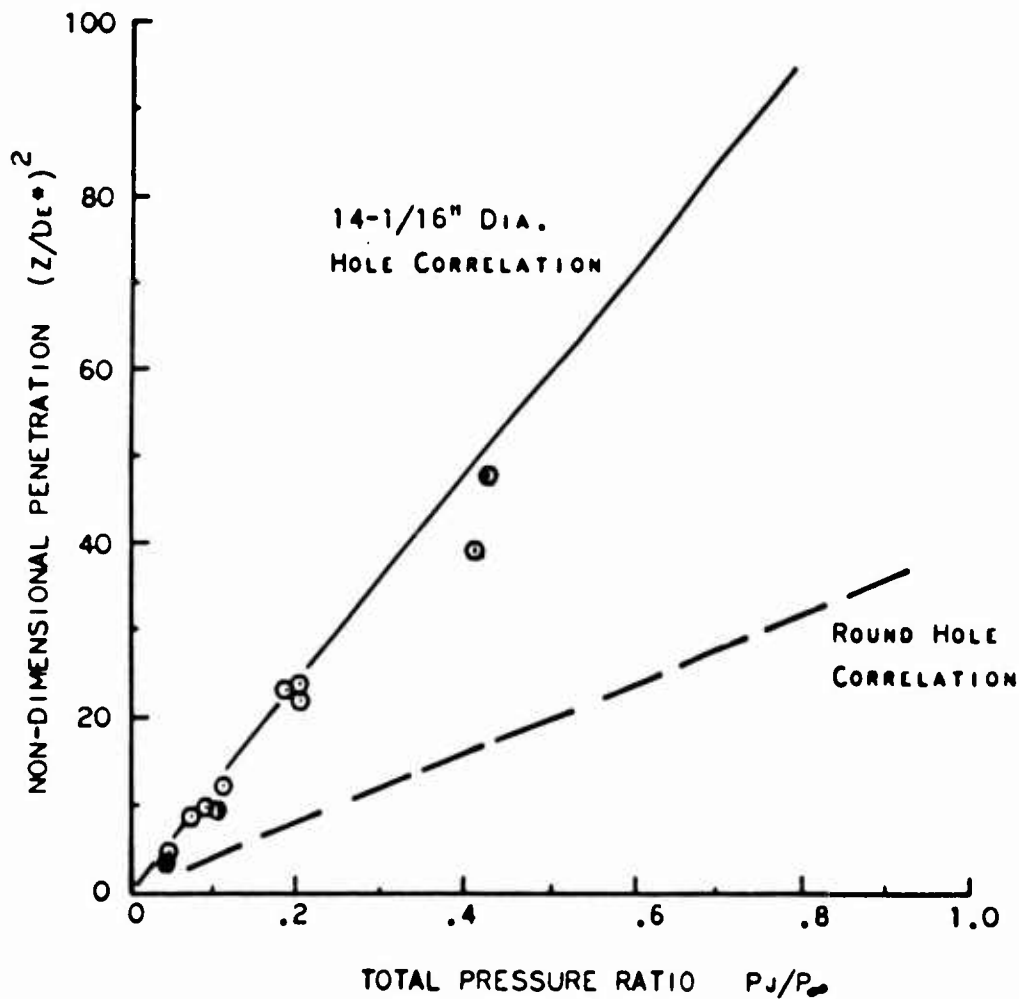
**CONFIDENTIAL**

Figure 43 - Fourteen Normal Round Sonic Holes with Dia. Increasing in Aft Direction.

**CONFIDENTIAL**

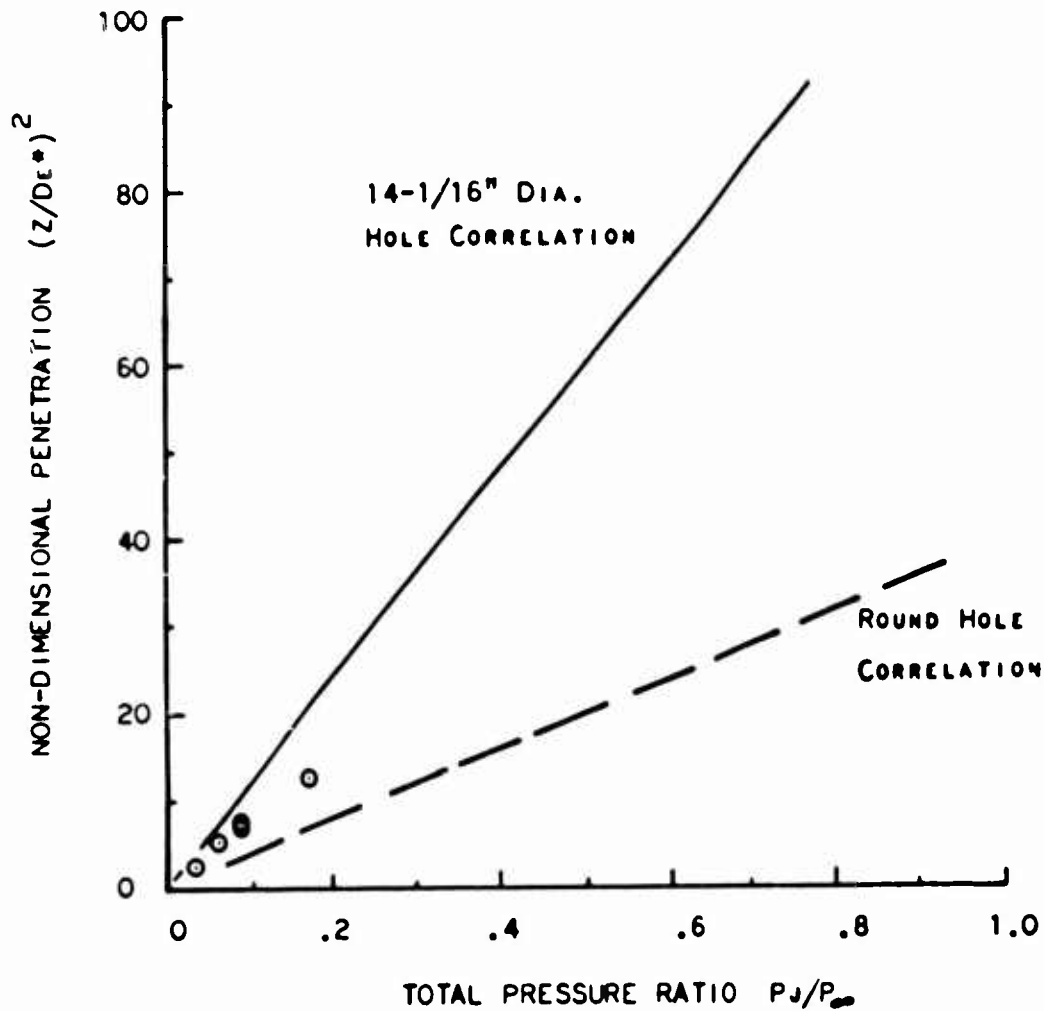
**CONFIDENTIAL**

Figure 44 - Fourteen .154" Dia. Normal Round Hole Data.

**CONFIDENTIAL**

# CONFIDENTIAL

AF APL-TR-65-103

One of the previous arc tunnel tests used as injector the same size as Configuration 7, but angled at 30° downstream and protruding into the freestream (Reference 1). This same injector design and a 30° downstream protruding hole, Configuration 8, were tested in this cold flow investigation. From the results presented in Figure 45, it was evident that this downstream injector suffered some penetration penalties. At low injection pressures the nondimensional penetration is shown to be greater than for the single round hole correlation line, but this is because the injector hardware protruded into the freestream. If the penetration height at the data point,  $P_j/P_\infty = 0.0378$  and  $(Z/D_e^*)^2 = 7.64$ , is adjusted by half the height of the injector protrusion, it moves down to  $(Z/D_e^*)^2 = 2.17$ . This adjusted penetration agrees better with previous observations of other injectors. These Schlieren data also agree qualitatively with the 30° injector Schlieren data from the previous arc tunnel tests (Reference 1). Figure 46 is a comparison of Schlieren photographs at similar total pressure ratios ( $P_j/P_\infty$ ) of the 30° injector in the arc tunnel tests and the 30° injector, (Configuration 8) of this investigation.

Configuration 12, a row of twelve (12) 1/16 inch diameter holes at a 30° downstream angle, was an attempt to combine low aspect ratio and downstream injection. The data are presented in Figure 47. The nondimensional penetration for this configuration was almost the same as the penetration for the row at fourteen (14) 1/16 inch diameter normal holes. Above  $P_j/P_\infty = 0.8$ , the results fall below the straight line correlation for the data of lower injection pressure. This row of twelve (12) 1/16 inch diameter, 30° holes exhibited good nondimensional penetration characteristics while providing some downstream thrust.

A set of Schlieren photographs of the penetration, over a range of pressure ratios, for the row of twelve (12), 1/16 inch diameter, 30° holes (Configuration 12) is shown in Figure 48. With air at high injection pressures the pattern from the individual holes was clearly visible. It is interesting that the individual jets seem to inject at an angle to the freestream considerably greater than 30°. As discussed earlier the jets over expand toward the 90° direction, as they leave the injection hole. The photographs of helium injection produced the most distinct outer boundaries of the penetrating jet while the air injection tests showed some evidence of mixing between the two air streams.

Figure 49 contains the data for the last configuration tested during this investigation. This was Configuration 14, a row of 12 square holes at a 30° downstream angle. The total area of injection between Configurations 12 and 14 was held similar, as shown in Table I, to study the differences between round and square hole injectors. The data deviate from the straight line relationship through the origin at a lower pressure ratio than for the 30° round hole.

CONFIDENTIAL

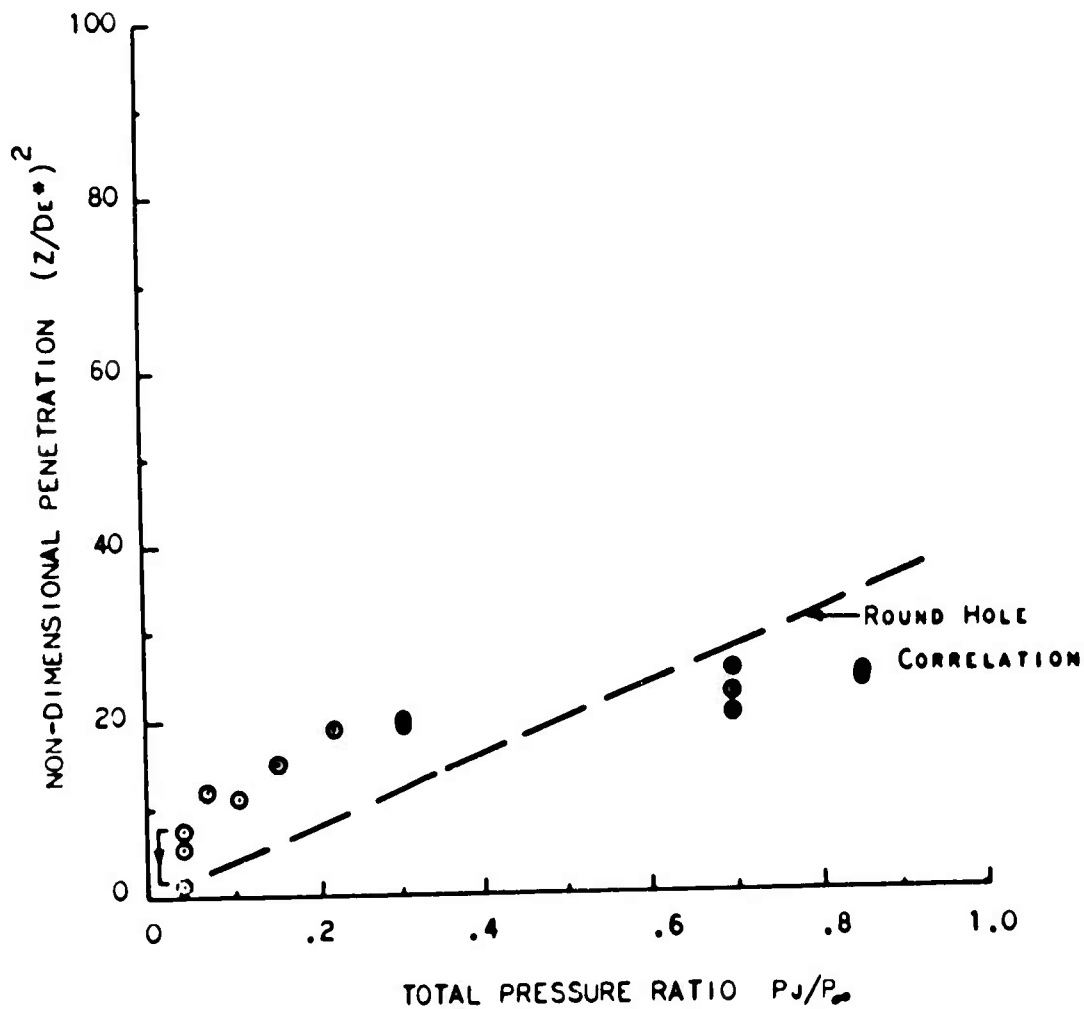
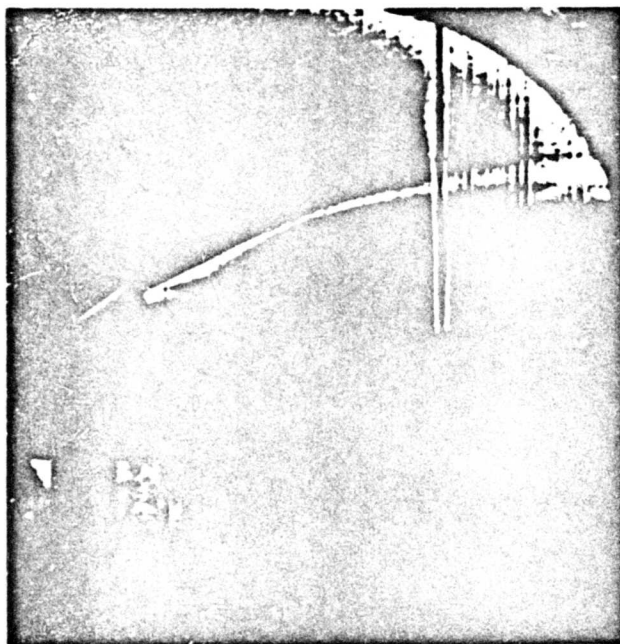
**CONFIDENTIAL**

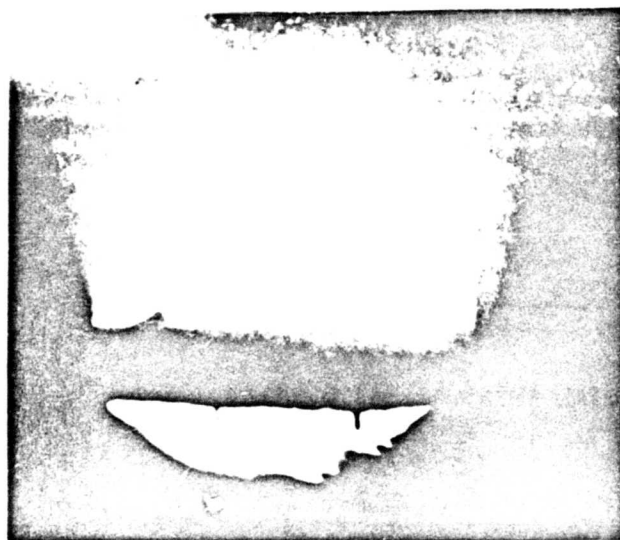
Figure 45 - Protruding Supersonic 30° Round Hole Data.

89  
**CONFIDENTIAL**

**CONFIDENTIAL**



ARC TUNNEL TESTS



COLD FLOW TUNNEL TESTS

Figure 46 - Comparison of Protruding  $30^\circ$  Supersonic  
Injector Schlierens.

**CONFIDENTIAL**

**CONFIDENTIAL**

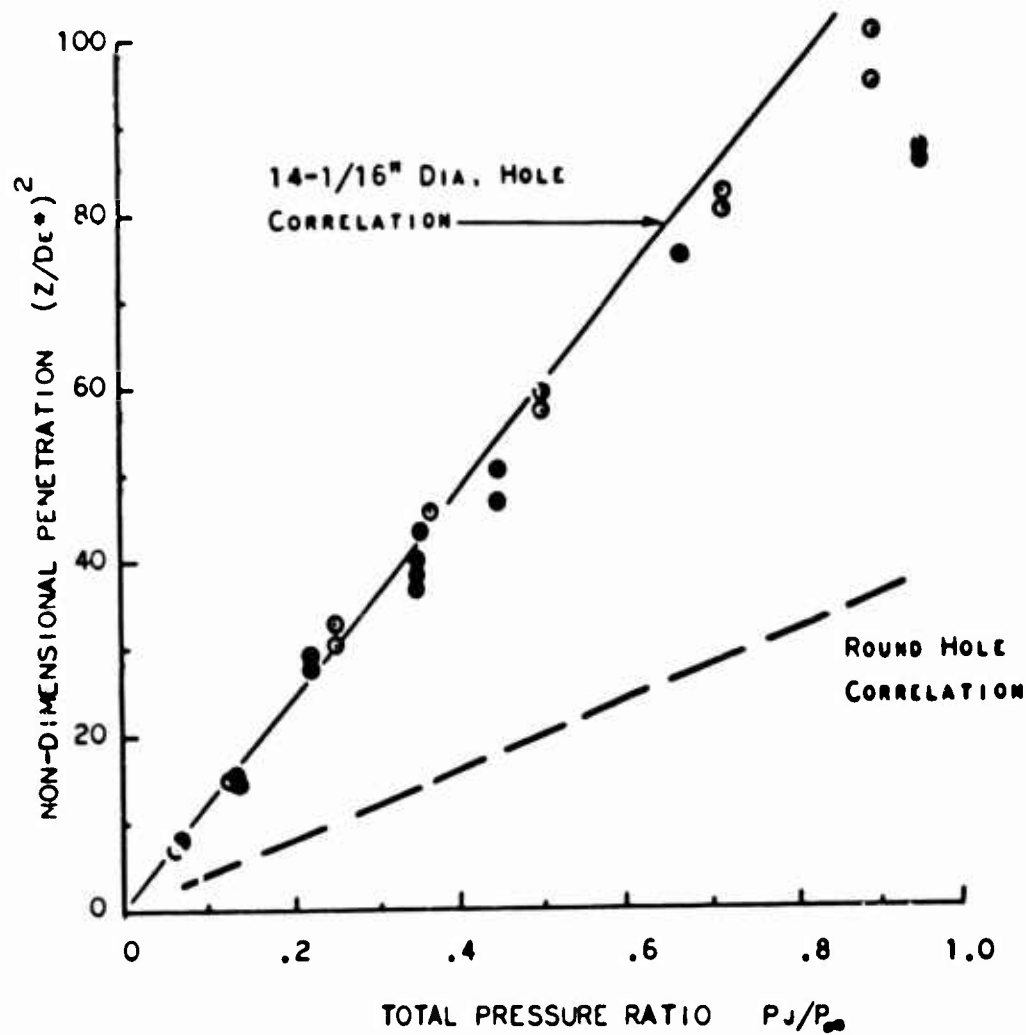


Figure 47 - Twelve 30° - 1/16" Dia. Round Hole Data.

**CONFIDENTIAL**

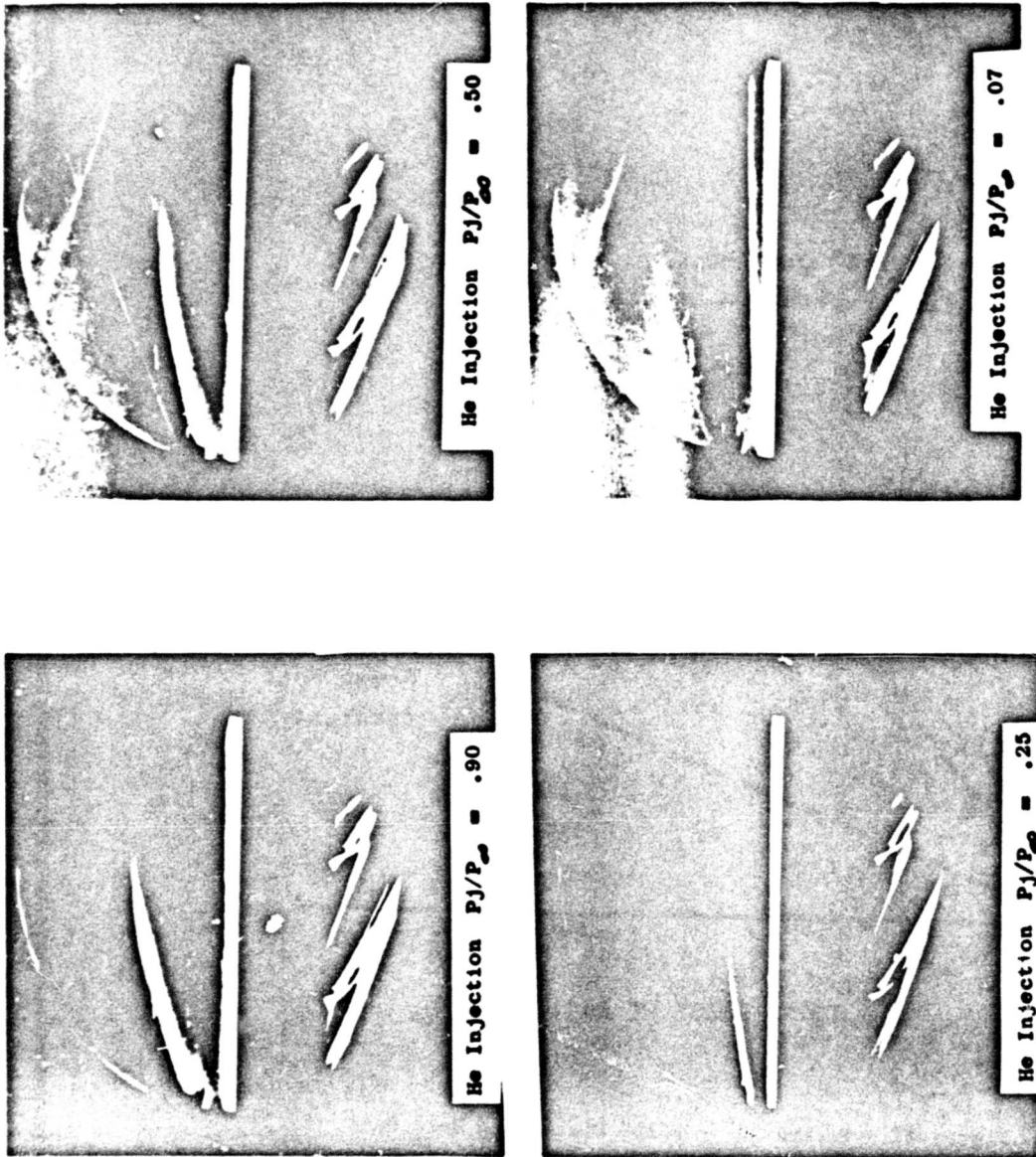
**CONFIDENTIAL**

Figure 48 - Schlieren Photographs of Penetration of the Twelve 30 1/16" Dia. Holes.

**CONFIDENTIAL**

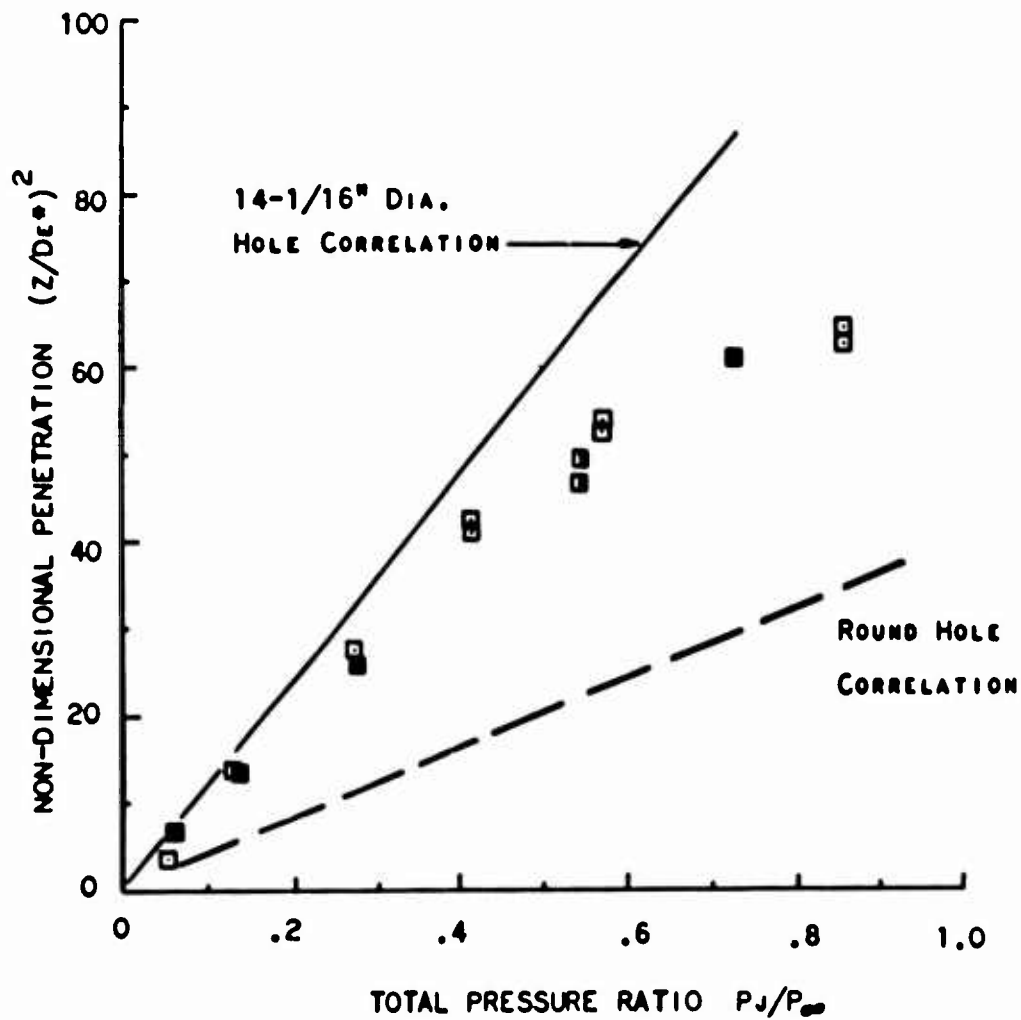
**CONFIDENTIAL**

Figure 49 - Twelve 30° Square (.06" x .06") Hole Data.

**CONFIDENTIAL**

# CONFIDENTIAL

AF APL-TR-65-103

## 3) Comparison of Test Data

### a) Data from Mach 3.25 Wind Tunnel

All of the penetration determinations for the low aspect ratio injectors are plotted in Figure 50. The correlation lines for single round holes and for the fourteen (14) 1/16 inch diameter hole configuration are included for comparison with the data points.

The low aspect ratio holes or hole patterns show greater penetration than the basic round hole. At low injection pressures  $(Z/D_e)^2$  data for all of the low aspect ratio holes fall on the same straight line. This corresponds to 40% more penetration than for a round hole. The lower the aspect ratio, the higher the injection pressure at which the data continue to fall near the straight line. As injection pressure increases, the expanding jet from the low aspect ratio holes approaches the shape of a jet from a round hole, with the penetration decreasing toward that of a round hole. At low pressures, the different aspect ratio injectors fell near the same line suggesting that this may be a penetration limit.

The injectors made up of a series of small holes showed the same increase in penetration over round holes that was achieved with long slots. This may provide significant simplifications in injector design.

The long row of fourteen holes gave better penetration at high injection pressures than the supersonic slot that was constructed for the first arc tunnel combustor tests, Configuration 4. At the pressure ratio expected in the arc tunnel tests, the fourteen hole configuration gave 40% greater penetration than the supersonic slot, or equal penetration for a jet with half the mass flow. This suggests that twice as many of these fourteen hole fuel injectors could be used while maintaining the same penetration distance. Furthermore, the row of twelve, 30° injectors achieves this same improved penetration, while also providing some injection thrust to the engine.

For all configurations, helium exhibits about the same penetration as air at the same injection pressure, even though its mass flow is less by a factor of 2.5 because of its low molecular weight. This establishes not only the effect of a fuel's molecular weight on penetration, but simultaneously the effect of fuel temperature. As discussed earlier in the section on The Selected Correlating Parameters this correlation of helium and air confirms that total momentum is a better correlating parameter than mass flow. Also, as previously explained, in the range of injection pressures over which the straight line relationship is valid, the penetration of a given mass of injectant having a given sonic velocity is independent of simultaneous changes in injection pressure and hole size. This means that high injection pressure is not needed to achieve penetration.

CONFIDENTIAL

**CONFIDENTIAL**

- 12-30° ROUND 1/16" DIA. HOLES
- ◇ 3" SUPERSONIC SLOT
- 14 NORMAL ROUND .154" DIA. HOLES
- 14 NORMAL ROUND HOLES, INCREASING DIA. AFT
- 12-30° SQUARE (.06" X .06") HOLES
- △ .83" LONG SUPERSONIC SLOT
- CELL 5

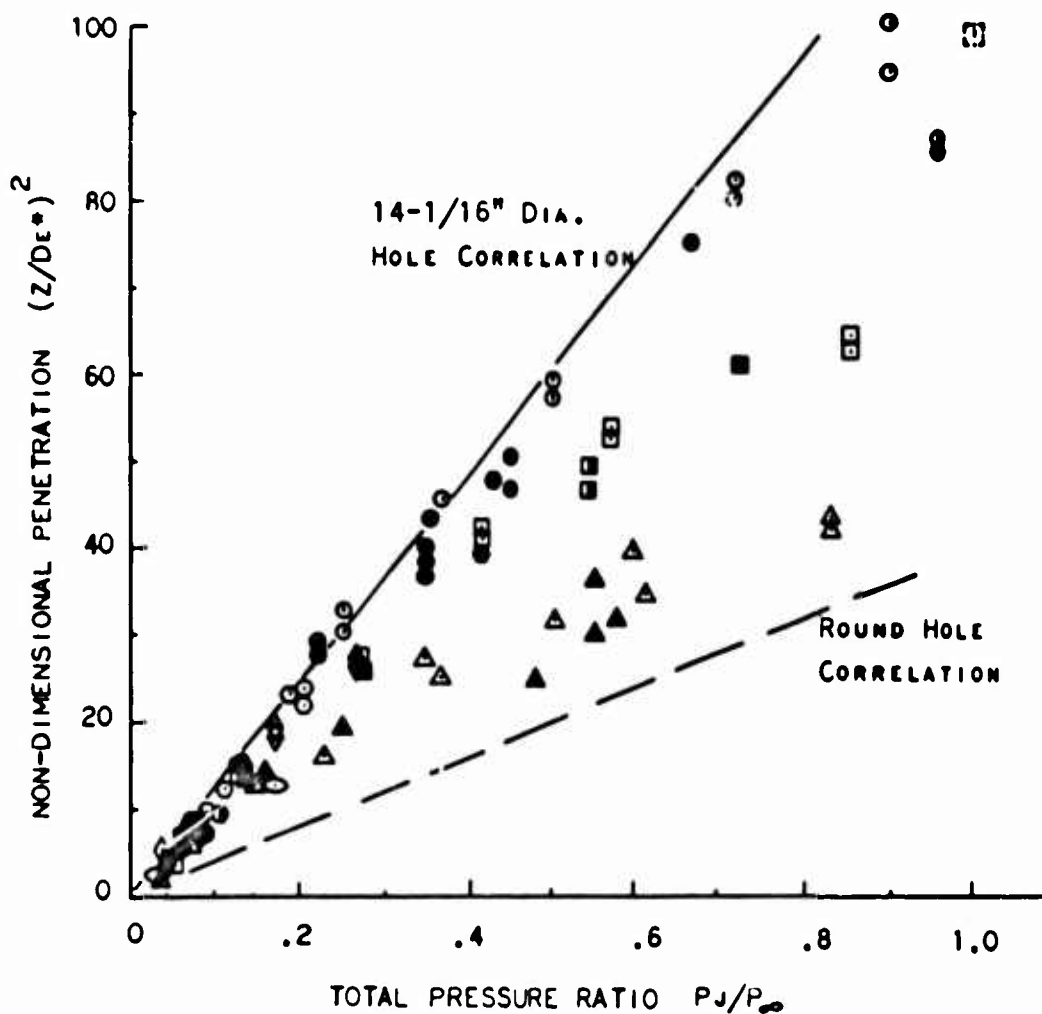


Figure 50 - Comparison of Low Aspect Ratio Penetration Data.

**CONFIDENTIAL**

# CONFIDENTIAL

AF APL-TR-65-103

A straight line, Figure 50, defines the following relation:

$$(Z/D)^2 \propto P_{jet} / P_o \quad (7)$$

Now, since

$$P_{jet} \propto (\rho U^2)^*$$

and

$$P_o \propto (\rho U^2)_o$$

The following relation also holds

$$(Z/D)^2 \propto (\rho U^2)^*_{jet} / (\rho U^2)_o \quad (8)$$

Figure 52 shows the straight lines from Figure 50 replotted with these alternate parameters.

These parameters were selected to be consistent with the analytical models discussed in the Background Analysis Section. The resulting correlations based on momentums are expected to be more general than the previous expressions based on total pressures.

$$\text{For round sonic holes: } (Z/D_o)^2 = 16 (\rho U^2)^* / (\rho U^2)_o \quad (9)$$

$$\text{For low aspect ratio holes: } (Z/D_o)^2 = 41 (\rho U^2)^* / (\rho U^2)_o \quad (10)$$

Since  $(\rho U^2)_o$  was held constant during these tests, experimental verification of its generality will be established by other data in the literature.

CONFIDENTIAL

**CONFIDENTIAL**b) Comparisons with Other Investigators

Zukoski and Spaid (Reference 5) correlated penetration data taken from freestream Mach numbers of 1.38, 2.01, 2.56, 2.61, 3.50 and 4.54. Figure 51 shows most of these data points plotted, as non-dimensional penetration divided by effective diameter ( $Z/D_e$ ) vs. the momentum ratio of the injector to the freestream

$$\frac{(\rho U^2)_{\text{jet}}}{(\rho U^2)_\infty}$$

The correlation of these data from different freestream Mach numbers provides a considerable simplification over the correlating equation 6 of Reference 5 :

$$\frac{h}{d \sqrt{c}} = \left\{ \left( \frac{1}{M_\infty} \right) \left( \frac{P_{0j}}{P_\infty} \frac{\gamma_j}{\gamma_\infty} \frac{2}{C_{p*}} \right)^{1/2} \times \left[ \frac{2}{\gamma_j - 1} \left( \frac{2}{\gamma_j + 1} \right)^{(\gamma_j + 1) / (\gamma_j - 1)} \left( 1 - \left( \frac{P}{P_{0j}} \right)^{(\gamma_j - 1) / \gamma_j} \right) \right]^{1/4} \right\}$$

The simpler equation expressing this present correlation is:

$$(Z/D)^2 = 16 (\rho U^2)_{\text{jet}} / (\rho U^2)_{\text{freestream}}$$

In Reference 5, the penetration was defined as  $h$ , the height above the plate of a dense line above the injector hole. It was suggested that this line of density change was the region of maximum concentration of the injectant. Close examination of Schlieren photographs from this present investigation indicates that this line is a shock wave in the injector gas produced by the interaction with the freestream. The measured concentration profiles in Reference 5, Figure 6, were used to convert penetration measurement ( $h$ ) to numbers consistent with the measurement of the outer boundary in this investigation. It was found that the composition was 10-20% of the peak concentration at 2.7 times the height of the measured penetration ( $h$ ). The following relationship was, therefore, used.

$$Z = 2.7 h \quad (11)$$

**CONFIDENTIAL**

CONFIDENTIAL

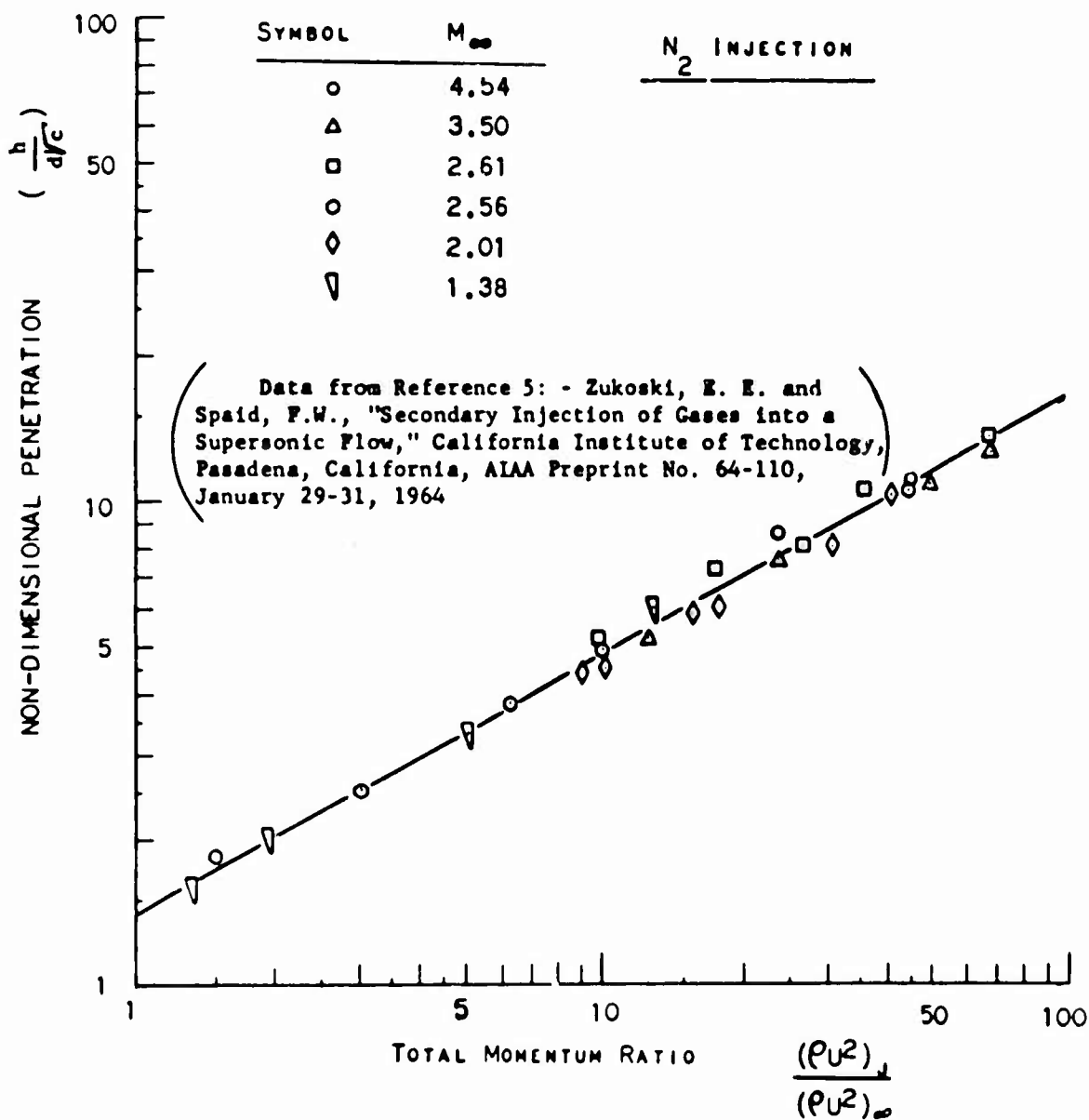


Figure 51 - Momentum Correlation of Reference 5 Data.

CONFIDENTIAL

## CONFIDENTIAL

AF APL-TR-65-103

Table II is a listing of some injector configurations, sizes and shapes for which penetration data are available, other than those tested in this cold flow program. All of these data are presented in Figure 52 together with the data obtained in this study. The 10-20% of peak concentration criteria was again used to define the outer boundary.

The solid line in Figure 52 for the data from Reference 7 was determined from the correlating equation 6, from Reference 7, evaluated at  $M = 3.25$ . The line in Figure 52 representing the data correlation of Reference 7 was obtained from Equation 11.

$$Z/D = 1.68 \left[ \left( \frac{\rho U_j^2}{U^2} \right) \left( \frac{M_\infty}{M_j} \right) (\cos^2 \theta) \right]^{0.5} \left( \frac{X}{D} \right)^{.0866}$$

By evaluating this expression at the Mach number for which the data were taken,  $M = 3$ , and by using a typical  $(X/D)$

$$\left( \frac{X}{D} \right)^{.0866} = (15)^{.0866} = 1.265$$

$$M_j = 1$$

$$\cos^2 \theta = 1$$

The following relationship was found

$$Z/D = 3.7 \left( \frac{\rho U_j^2}{U^2} \right) \quad (12)$$

In Reference 7 the definition of penetration ( $Z$ ) was the vertical distance above the plane of the injector where the mole fraction of injected fluid was 0.005. These measurements were made from concentration profiles produced from gas samples of the downstream wake.

The data for measurements of penetration at the outer boundary of the penetrating jet are shown in Figure 52. The comparisons are shown between the results of this investigation and the correlations of Zukoski and Spaid, (Reference 5), Dowdy and Newton, (Reference 9), and Vranos and Nulan (Reference 1). The penetration characteristics of all round sonic

CONFIDENTIAL







# CONFIDENTIAL

AF APL-IR-5-103

were found to agree well.

$$(Z/D_e)^2 = 16 (\rho U_j^2) / (\rho U^2). \text{ (Single Round Holes)}$$

TABLE II  
INJECTOR CONFIGURATION FROM THE LITERATURE

Configuration	De*	L <sup>2</sup> /A*	L/Width	Hole Pattern Sketches
C. I. T. Ref. Round Sonic Holes	.12 .04			 
J. P. L. Ref. Round Sonic Holes	.1			
G. E. Ref. .186" Dia. Round Sonic Hole - Arc Tunnel Tests	.168			
G. E. Ref. .83" Long Supersonic Slot - Arc Tunnel Tests	.224	17	10	
G. E. Ref. 48 - .04" Dia Hole, .08" C Cell Tests		239	95	

CONFIDENTIAL

CONFIDENTIAL

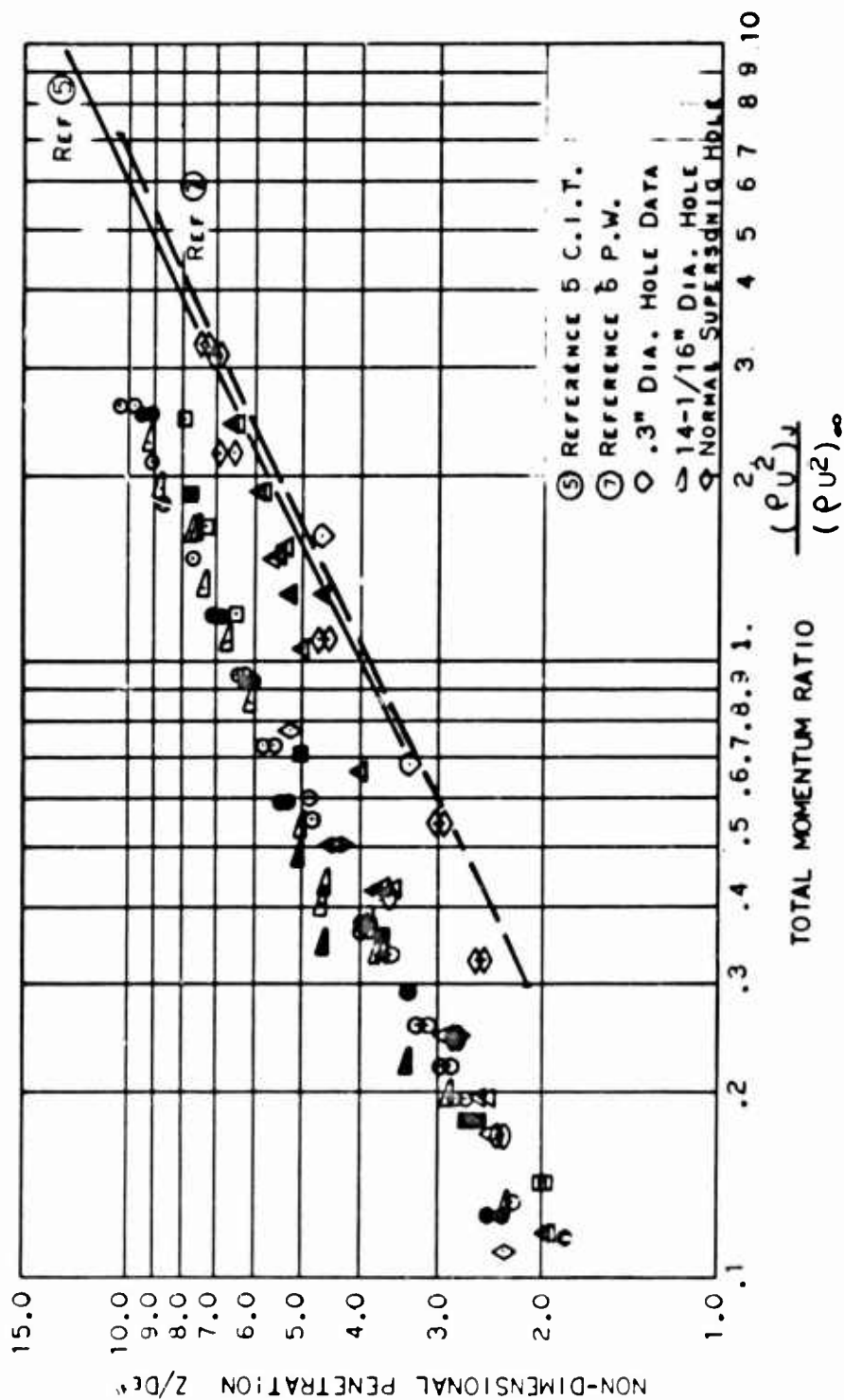


Figure 52 - Momentum Comparison of all Penetration Data.

CONFIDENTIAL

# CONFIDENTIAL

AF APL-TR-65-103

## 4) Injector Designs Selected

A major objective of this investigation was to identify and select alternate injector configurations to be further tested in arc tunnel combustor tests.

The row of fourteen (14) holes produced the best penetration of any of the configurations tested while the twelve (12) 30° holes gave nearly equivalent penetration with some downstream thrust. Arc tunnel configurations were, therefore, constructed incorporating these two injector types.

The generalizations and correlations established in this penetration study not only identified improved configurations, but also suggested that these two injector types should be sufficient for the evaluation of low aspect ratio holes in general. All low aspect ratio holes exhibit the same penetration characteristics at sufficiently low injection pressure. Any injector obeying the relation

$$(Z/D_e)^2 = 41 (\rho U^2)_{\text{jet}} / (\rho U^2)_e$$

will produce the same desired improvement in penetration, thus eliminating the need for tests on other injector types -- long slots for example.

Furthermore, the penetration from an injector obeying the above relation is independent of the flow area of the injector. As explained in the Background Analysis Section, the penetration will be proportional to the square root of the injectant momentum.

$Z^2 \propto (\rho * A_e * \rho U^2)$ , which is the mass flow rate times the sonic velocity.

Thus the flow area of the injector can be selected to achieve convenient injection pressures without affecting the penetration, and only one injector size need be tested.

The only injector design variable affecting the penetration is the number of injectors per combustor, since this affects the mass flow rate to each injector. The penetration for low aspect ratio injectors can be expressed as follows:

$$Z^2 = 26 \times \frac{(\text{total fuel flow rate}) (\text{sonic velocity of injectant})}{(\text{No. of Injectors}) (\text{Freestream } q)} \quad (14)$$

all in consistent units.

CONFIDENTIAL

## CONFIDENTIAL

AF APL-TR-65-103

Eight injectors per combustor were selected for the arc tunnel tests. The penetration data showed that these injectors would penetrate the same distance as the four supersonic slots in the original designs. Improvements in circumferential mixing would be expected while the radial profile might remain unchanged. For the  $M = 6$  arc tunnel conditions and at a fuel equivalence ratio of 1.0, the calculated penetration is .7 combustor radii.

Variations in penetration during combustion tests can be investigated by several techniques. The fuel flow rate or equivalence ratio is easy to vary. With the fuel equivalence ratio constant, the penetration can be increased by increasing the fuel temperature. The increase in the sonic velocity of the injectant resulting from the increased fuel temperature increases the penetration. Alternately an inert, nitrogen, could be added to the fuel in combustor tests to change the penetration without changing equivalence ratio.

### e. Application of Mixing Theory to Penetrating Jets

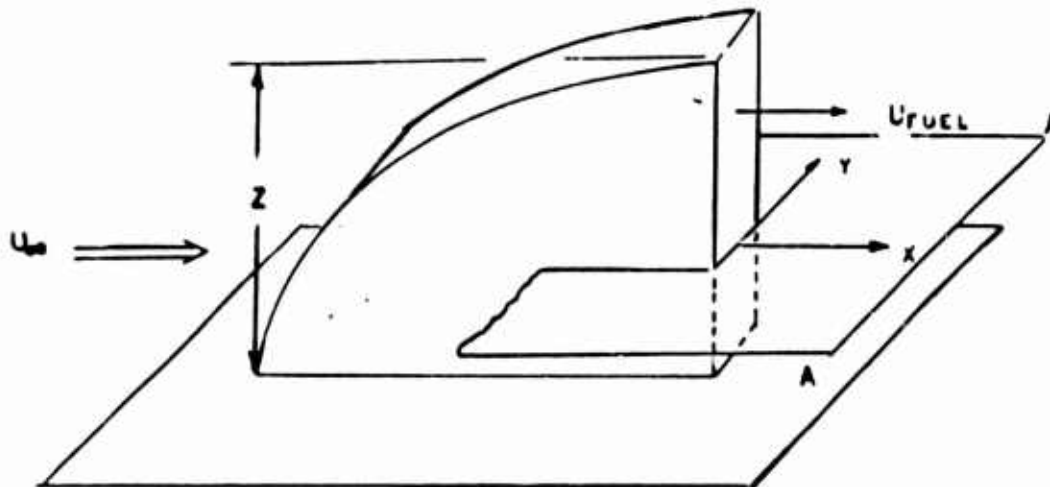
From the work discussed in the previous sections on penetration of jets, it is possible to define the flow field just downstream of the injectors. Since the jets are turned nearly parallel to the freestream flow before appreciable mixing has taken place, the downstream mixing can be estimated by mixing theories for shear gradients in parallel cocurrent flow. Both axisymmetric and two-dimensional wake mixing equations are available which can be applied to the mixing of cocurrent flow. By using these equations, estimates of mixing efficiency for a combustor design can be obtained, and trends due to changes in configuration can be predicted.

#### 1) Flow Field Downstream of Penetrating Jet

Schlieren photographs indicate that jets penetrating into a supersonic stream are turned to the downstream direction in a very short distance. The data on low aspect ratio injectors showed a nearly uniform concentration profile from the wall to nearly the outer boundary of the jet, suggesting that these jets can be approximated by two-dimensional cocurrent flow.

Figure 53 is a schematic representation of the penetrating jet as the flow is turned to a direction parallel to the freestream flow direction. It is postulated that a jet penetrating into a supersonic flow is turned to a downstream direction through strong shock waves that result in a downstream velocity that is near sonic jet after the jet has been turned. The case of a hydrogen jet penetrating into an arc tunnel flow stream simulating  $M = 6$  flight conditions is used in some of the examples that follow. For the case of  $M = 6$  conditions, simulated in arc tunnel tests, the sonic fuel velocity is 80% of the freestream velocity. The penetration was calculated from the correlations of the previous section and found to be .7 times the duct radius. The width of the resulting fuel flow was found to be one-fifth of the penetrating height, calculated by assuming the flow was distributed uniformly along the penetration height at a Mach number of one.

CONFIDENTIAL

**CONFIDENTIAL**

A) FUEL INJECTION MODEL

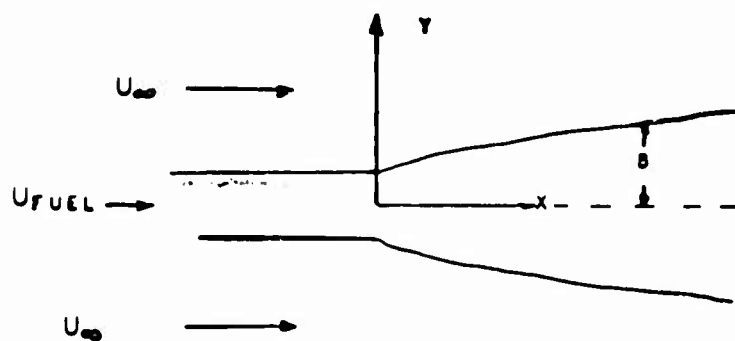
B) COCURRENT FLOW MODEL IN PLANE A-A  
OF FIGURE A.

Figure 53 - Fuel Injection and Wake Mixing Models.

**CONFIDENTIAL**

**CONFIDENTIAL**

The mixing problem to be solved is seen to be a problem of parallel cocurrent flows. Early in the mixing process, the problem is two-dimensional in character, with the end effects near the wall and at the penetration extremity being negligible. Far downstream as the width of the mixing region approaches the penetration height, the end effects become important and the problem approaches that of an axisymmetric problem with an important boundary influence at the wall. In the development that follows, the calculations are confined to a two-dimensional treatment; this permitted the use of some recently derived simple expressions to illustrate the effects of various parameters on the mixing.

## 2) Wake Mixing Theory for Cocurrent Flow

### a) Theoretical Approach

The presentations of classical mixing theories for jets and wakes in the available textbooks, Schlichting (Reference 26) for example, does not include a complete explanation of the effects on a mixing jet of density, Mach number, or of a cocurrent flow. This is partly due to a lack of accurate experimental data for comparison with theories. However, the simple equations available for wake development far downstream of the origin, provide a means for approximating the mixing of cocurrent jet flows.

A jet in a faster, equal-density, parallel, cocurrent flow is very similar to a wake in character, in that both are low velocity regions in a flow field; therefore, these cocurrent flows should be treatable by the same theory which applies to the wake. In the development of a wake, the shape of the velocity profile at a point far downstream is independent of the shape of the original profile in the wake; it is characterized only by its width and its momentum defect.

It is postulated here that the very useful principle of "similar solutions" that has been successful in so many free turbulence and boundary layer problems can also be applied to the mixing region downstream of a cocurrent flow jet; i. e., a jet with the same momentum defect as a wake will develop the same profile shapes as the wake. This momentum defect is the momentum required to bring the jet flow to the freestream velocity.

For a jet with different density than the surroundings, the mixing with the surroundings gradually eliminates the initial density differences. Far downstream from the initial station, the developed jet or wake has the profile shape of a constant density jet. The size of the mixing region for a given centerline defect is characterized by the total momentum defect of the jet or wake. For a jet with different density surroundings, this momentum defect is taken to be the momentum required to bring the jet flow to the velocity of the surroundings. Utilization of this "Momentum Defect Principle" permits problems far downstream of the jet origin to be treated by the equal-density theory.

**CONFIDENTIAL**

## CONFIDENTIAL

AF APL-TR-65-103

This far-downstream theory was considered adequate for estimating mixing trends for this report and for illustrating the important affect of static pressure gradient on mixing. Perhaps the best data in the literature on density differences in the near field are those of Kaegy and Weller (Reference 28 ) for a helium jet issuing into a quiescent surrounding of air. Those results on a jet could have been used to determine near field effects in a cocurrent flow jet, but no such work was done.

### b) Wake Equations

Equations for turbulent wake development are given by Schlichting for both two-dimensional and axisymmetric wakes. Because the penetrating jets to be treated in this analysis are to be approximated by a two-dimensional source; only the two-dimensional mixing theory will be presented here.

Equation 23.37 of Schlichting (Reference 26) for two-dimensional wakes behind circular cylinders is:

$$\frac{U_1}{U_\infty} = \frac{\sqrt{10}}{18\beta} \left( \frac{X}{C_{Dd}} \right)^{-1/2} \left[ 1 - \frac{y^2}{b^2} \right]^{3/2} \quad (15)$$

where  $\beta = 0.18$  and the constant is 0.976.

For the centerline decay,  $\frac{y}{b} = 0$ , and the equation becomes

$$\frac{U_1}{U_\infty} = 0.976 \left( \frac{X}{C_{Dd}} \right)^{-1/2} = 0.976 \left[ \frac{C_{Dd}}{X} \right]^{1/2} \quad (16)$$

where:

$U_1$  is the centerline velocity defect ( $U_\infty - U$ )

$U$  is local velocity

$U_\infty$  is freestream velocity

$X$  is the distance downstream

The  $C_{Dd}$  term was introduced into this expression from the following equation in Schlichting p. 493 (Reference 26 ).

$$D_s = 1/2 C_{Dd} h (\rho U^2) \quad (17)$$

**CONFIDENTIAL**

The momentum defect of the drag,  $D_d$ , was set equal to the wake by Schlichting. The postulate of this present treatment of cocurrent flows is that the momentum defect equals the product of the fuel mass flow and the difference in velocity between fuel jet and freestream. This product is the amount of momentum required to bring the fuel jet to freestream velocity:

$$D_d = W_f (U_\infty - U_{fuel}) \quad (18)$$

By solving these last two equations for  $C_{Dd}$  and substituting into the wake equation, an equation for the centerline velocity of a cocurrent flow jet is obtained.

$$C_{Dd} = \frac{(\text{fuel mass flow})(U_\infty - U_{fuel})}{h (1/2 \rho U_\infty^2)} \quad (19)$$

$$\frac{U_1}{U_\infty} = 1.38 \left[ \frac{(\text{fuel mass flow})(U_\infty - U_{fuel})}{X h (\rho U_\infty^2)} \right]^{\frac{1}{2}} \quad (20)$$

This equation can be further simplified by examining the two-dimensional model of the penetrating jets.

### 3) Two-Dimensional Model of Combustor

#### a) Description of Model

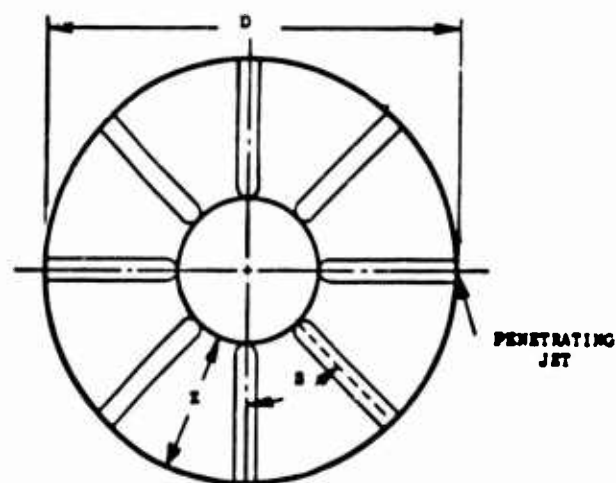
In Figure 54a, fuel jets that have penetrated into a circular duct are represented by two-dimensional cocurrent flows. Figure 54b shows these same jets in a two-dimensional field having the same airflow and area as the carbureted area of the circular cross section which is shown shaded in Figure 54a. With this rectangular, two-dimensional model, the "fuel mass flow" term in equation 20 can be replaced by terms involving the injector spacing

$$(\text{fuel mass flow}) = f/a (\text{air mass flow}) = f/a (\rho AU)_{air} = f/a (\rho U)_{air} NSZ$$

where

- Z is the penetration height
- S is the injector spacing
- N the number of injectors

**CONFIDENTIAL**

**CONFIDENTIAL**

CROSS HATCHING DENOTES CARBURETED AREA  
 D = DUCT DIAMETER  
 Z = JET PENETRATION  
 S = INJECTOR SPACING

Figure 54a - Cocurrent Flow Sources from Penetrating Jets.

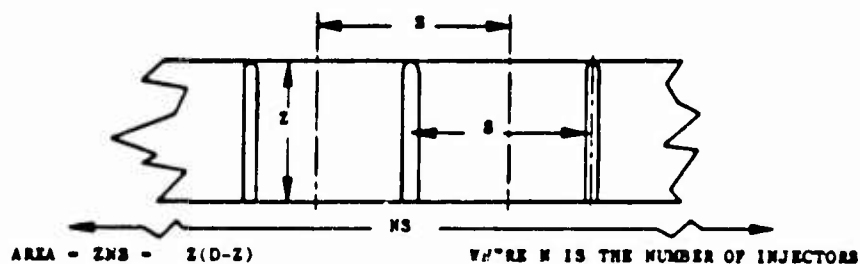


Figure 54b - Injection Jets in Two-Dimensional Field Having Same Airflow and Area as Carbureted Area of Circular Cross Section Shown in Figure 54a (Shaded Area).

**CONFIDENTIAL**

**CONFIDENTIAL**

Substituting this expression for the "fuel mass flow" of one injector into equation 20

$$\frac{U_1}{U_\infty} = 1.38 \left[ \frac{f/a (\rho U)_{\text{air}} SZ (U_\infty - U_{\text{fuel}})}{X h (\rho U_\infty^2)} \right]^{1/2}$$

Reducing this expression and noting that  $h$  and  $Z$  both represent the height of the two-dimensional wake.

$$\frac{U_1}{U_\infty} = 1.38 \left[ \frac{S}{X} (f/a) \frac{U_\infty - U_{\text{fuel}}}{U_\infty} \right]^{1/2} \quad \text{or,} \quad (21)$$

$$\frac{U_1}{U_\infty} = 1.38 \left[ \frac{S}{X} (f/a) \left( 1 - \frac{U_{\text{fuel}}}{U_\infty} \right) \right]^{1/2} \quad (22)$$

This is the desired expression for mixing of a cocurrent fuel jet, in terms of the initial velocity ratio of the fuel and air, the fuel/air ratio of the carbureted region, and the injector spacing.

Returning to the original circular duct, the injector spacing can be replaced by a term containing duct diameter " $D$ " as indicated below:

$$w_f = (f/a) W_a = f/a (\rho U)_{\text{air}} \pi / 4 D^2$$

The area under consideration for the two-dimensional mixing is somewhat smaller than  $\pi / 4 D^2$  since the penetration,  $Z$ , is usually not equal to the duct radius. The relation between these areas is:

$$NSZ = (\pi / 4) [D^2 - (D - 2Z)^2]$$

$$NS = \pi (D - Z)$$

**CONFIDENTIAL**

**CONFIDENTIAL**

Combining this relation into equation 21

$$\frac{U_1}{U_\infty} = 1.38 \left[ \frac{f/a}{N X} \frac{D-Z}{N X} \frac{U_\infty - U_{\text{fuel}}}{U_\infty} \right]^{1/2} \quad (23)$$

b) Velocity of Penetrated Jets

A fuel jet injected normal to the freestream flow has zero downstream momentum. It creates a momentum defect in an infinite flow field equal to its mass flow times the freestream velocity.

$$\text{Momentum Defect} = (\text{fuel mass flow}) U_\infty$$

If this momentum defect were concentrated in the mixing region, the term  $(U_\infty - U_{\text{fuel}}) / U_\infty$  in the wake expressions should be set equal to 1.0, giving from equation 15:

$$\frac{U_1}{U_\infty} = 1.38 \left[ \frac{S}{X} f/a \right]^{1/2} \quad (24)$$

However, the penetrating jet absorbs momentum from the freestream as it is turned in a downstream direction, by mechanisms other than mixing. The resulting momentum defect is not all concentrated near the jet flow. In a supersonic stream the shockwaves generated in the freestream by the penetrating jet, transfer momentum to great distances from the jet origin. This entire momentum defect is encompassed by the mixing wake only at infinitely long distances.

The actual momentum defect most appropriate to the earlier portion of the mixing problem may be more closely associated with the momentum defect of the jet itself just after it has been turned downstream. It is postulated that the supersonic jet is turned to a downstream direction through strong shock waves that result in a downstream velocity that is near sonic. For this case, the wake equation becomes

$$\frac{U_1}{U_\infty} = 1.38 \left[ \frac{S}{X} f/a \frac{U_\infty - U^*_{\text{fuel}}}{U_\infty} \right]^{1/2} \quad (25)$$

Both equations 24 and 25 are of interest, since as discussed later, the effect of a combustion generated static pressure rise is to drive the initial fuel velocity from sonic to lower values.

**CONFIDENTIAL**

**CONFIDENTIAL**

Figure 55 shows the relation for the decay of the centerline velocity difference for both conditions expressed by equations 24 and 25 at an equivalence ratio of one. The lines were drawn for hydrogen fuel at stoichiometric overall,  $f/a = 0.0291$ . The term  $(U_{\infty} - U_{\text{fuel}}^*) / U_{\infty}$  was evaluated for conditions expected in arc tunnel combustion tests at inlet air enthalpies simulating  $M = 6$  conditions.

$$(U_{\infty} - U_{\text{fuel}}^*) / U_{\infty} = 0.2 \quad (25)$$

c) Composition in Wake

If composition or mass is assumed to mix at the same rate as momentum, then equation 24 for the centerline velocity decay can be simply converted to composition decay.

$$\frac{U_1}{U_{\infty}} = \left( \frac{U_{\infty} - U_c}{U_{\infty}} \right) = \left( 1 - \frac{U_c}{U_{\infty}} \right) = \left( 1 - \frac{K_{Ac}}{K_{A_{\infty}}} \right) \quad (27)$$

if  $K_{Ac} = 0$  when  $U_c = 0$

where

$K_{Ac}$  is the mass fraction of air at the centerline and

$K_{A_{\infty}}$  is the mass fraction of air in the freestream

since

$K_{A_{\infty}} = 1.0$ , and since the mass composition of fuel,  $K_{F_c} = (1 - K_{A_c})$

$$1 - \frac{K_{Ac}}{K_{A_{\infty}}} = (1 - K_{Ac}) = K_{F_c}, \text{ or}$$

$$\frac{U_1}{U_{\infty}} = K_{F_c} \quad (28)$$

This gives:

$$K_{F_c} = 1.38 \left[ (S/X) (f/a) \right]^{1/2} \quad (29)$$

**CONFIDENTIAL**

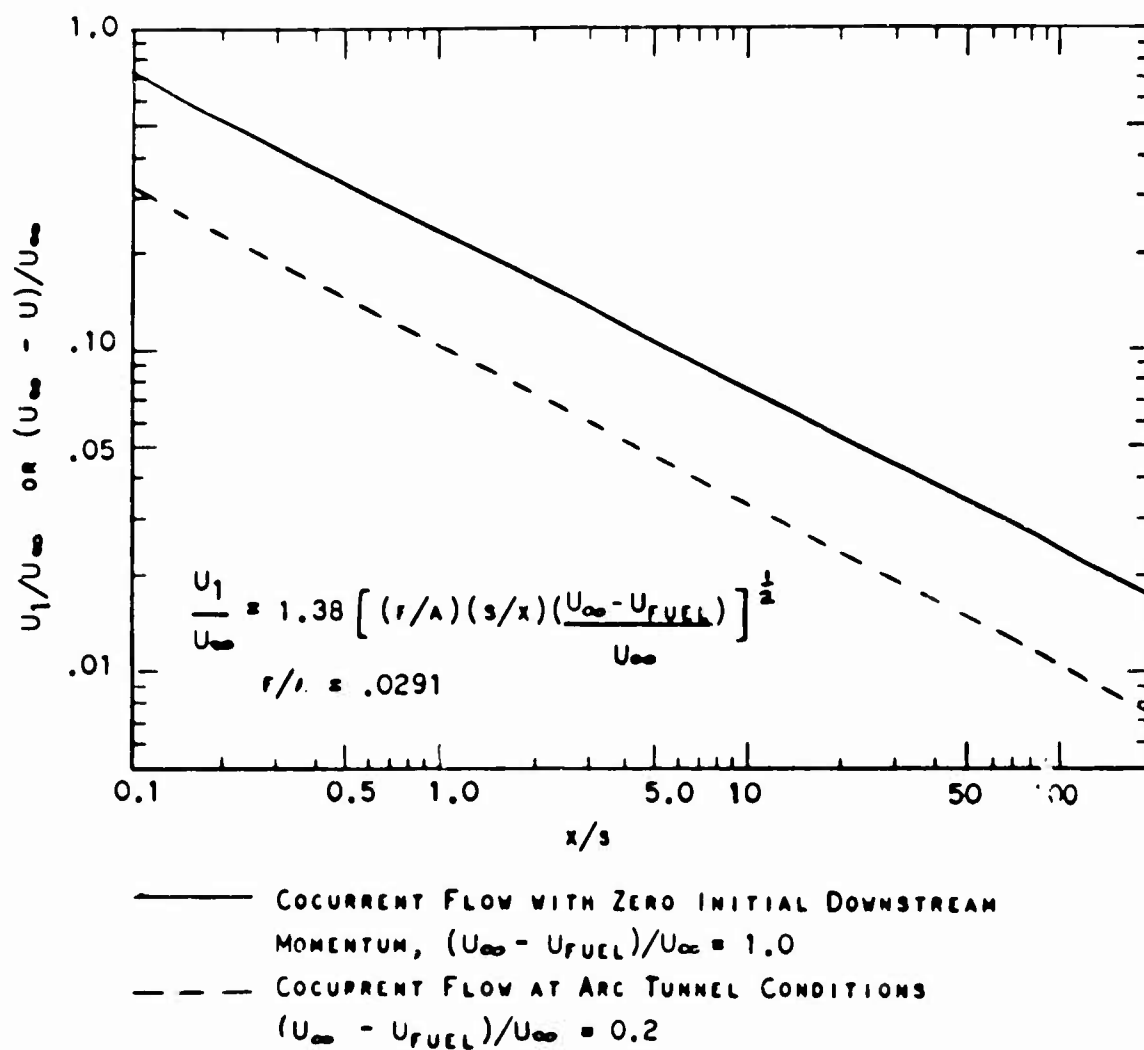
**CONFIDENTIAL**

Figure 55 - Centerline Decay of Velocity Defect for Stoichiometric Conditions.

**CONFIDENTIAL**

# CONFIDENTIAL

AF APL-TR-65-103

Thus the line for velocity decay in Figure 55 also represents the line for centerline mass flow composition for an initial downstream momentum of the fuel flow equal to zero.

When the initial downstream momentum of the fuel is different from zero, pure fuel exists in the wake when  $U_1 = (U_\infty - U_{fuel})$ . The composition decays at the same ratio that  $U_1$  decays giving

$$K_{Fc} = \frac{U_1}{U_\infty - U_{fuel}}$$

Using equation 41

$$K_{Fc} = 1.38 \left( \frac{U_\infty}{U_\infty - U_{fuel}} \right) \left[ (S/X) (f/a) (U_\infty - U_{fuel}) / U_\infty \right]^{1/2} \quad (30)$$

Figure 56 shows this composition decay for two cases. With the initial downstream momentum of the fuel equal to zero, the composition curve is the same as the velocity defect curve shown in Figure 55. The second case is the composition decay for an initial downstream fuel velocity equal to sonic fuel velocity at the conditions expected in the arc tunnel. Much longer distances are required to achieve good mixing. To mix the centerline concentration to below stoichiometric requires a downstream length of 63 injector spacings for zero downstream velocity, and 320 for sonic fuel velocity.

For the eight injectors in the circular arc tunnel combustor, the predicted penetration is .7R and the corresponding injector spacing in the two-dimensional model is:

$$S = \pi (D' - Z) / N = .51D'$$

The mixing lengths in terms of duct diameters are indicated in Figure 56 on the top of the plot.

Figure 57 indicates the length required to mix below stoichiometric for different initial fuel velocities. The relation is plotted two ways to illustrate the straight line relationship  $X/S \propto U_\infty / (U_\infty - U_{fuel})$  as well as to illustrate infinite mixing length required when the fuel and air are at equal velocity

Figure 58 illustrates the shape of the wake profile. The expression for this wake shape consistent with equation 15 is,

$$\frac{U}{U_c} = \left[ 1 - (y/b)^{3/2} \right]^2 \quad (31)$$

as in Schlichting.

CONFIDENTIAL

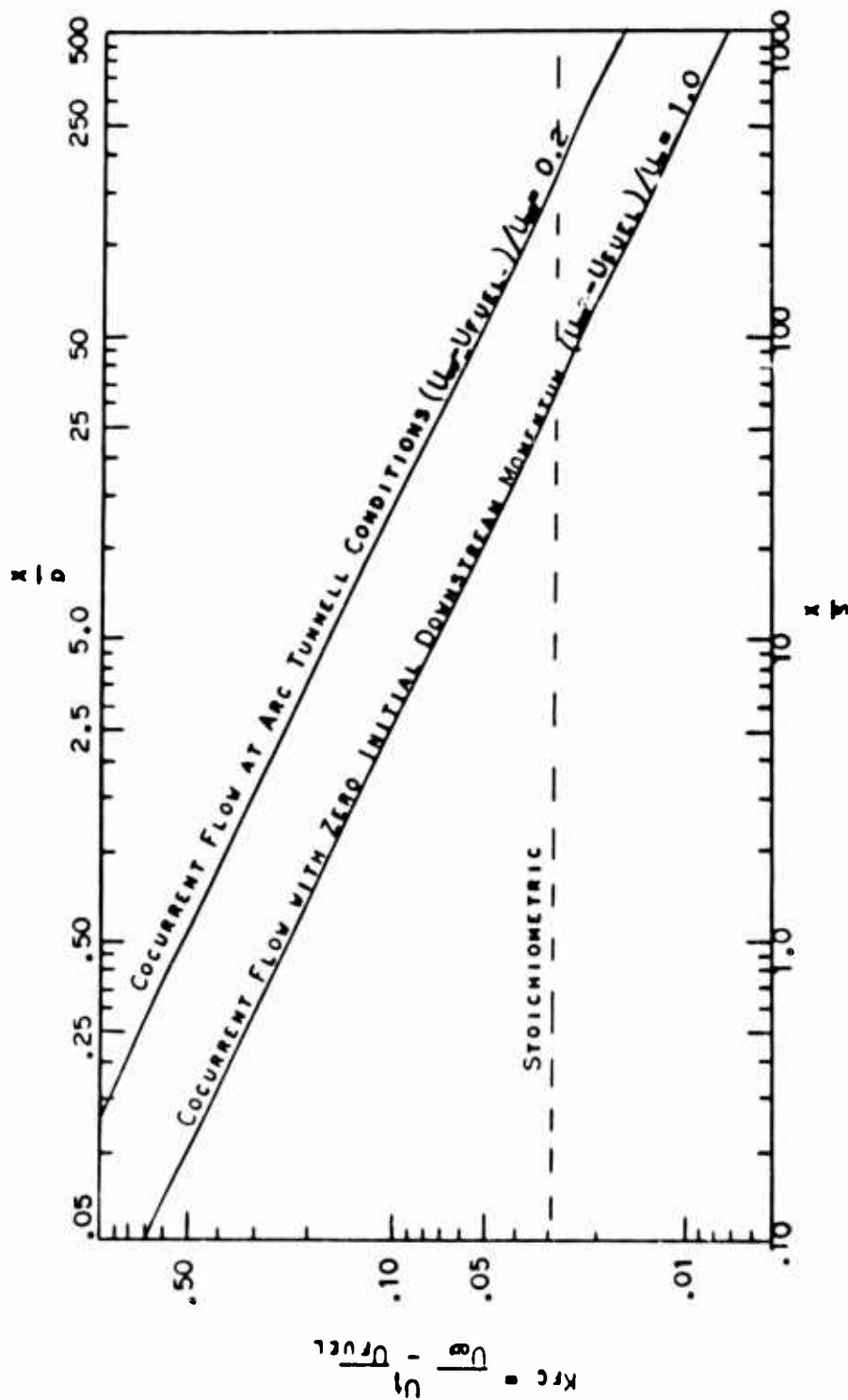


Figure 56 - Centerline Decay of Mass Flow Composition.

CONFIDENTIAL

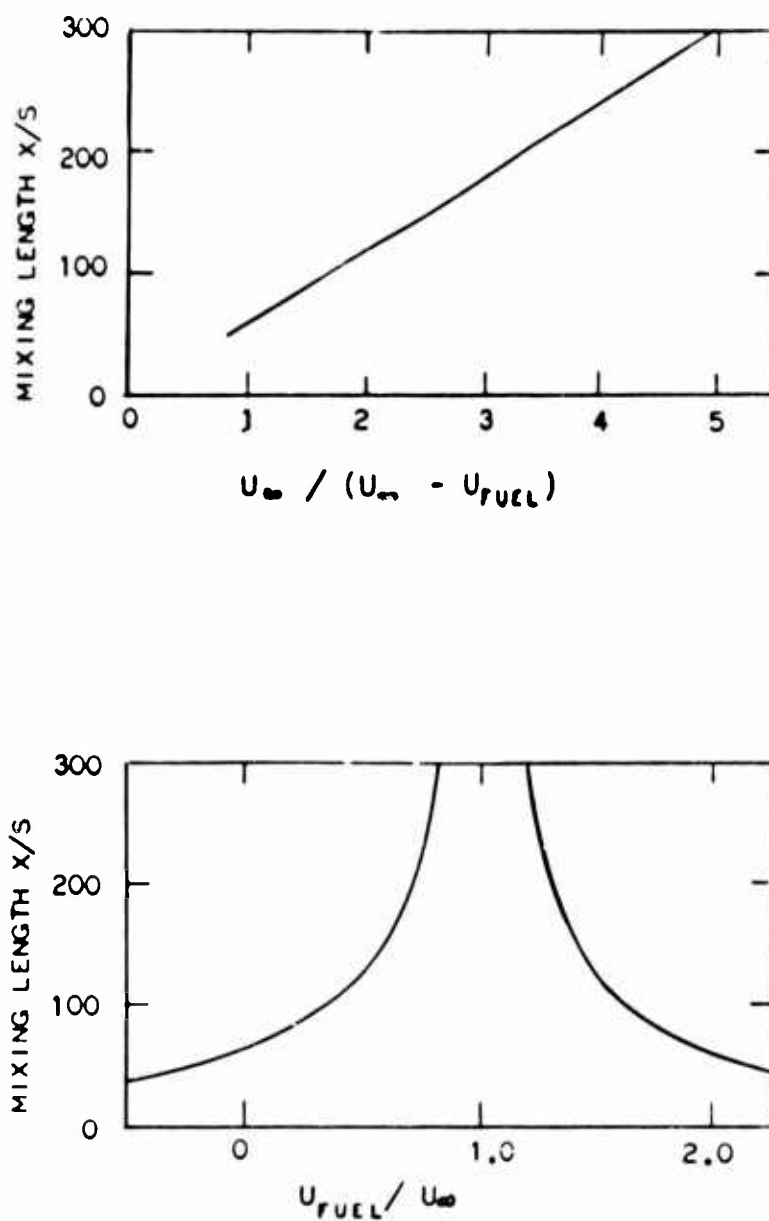
**CONFIDENTIAL**

Figure 57 - Effect of Initial Velocity Ratio on Mixing.

**CONFIDENTIAL**

**CONFIDENTIAL**

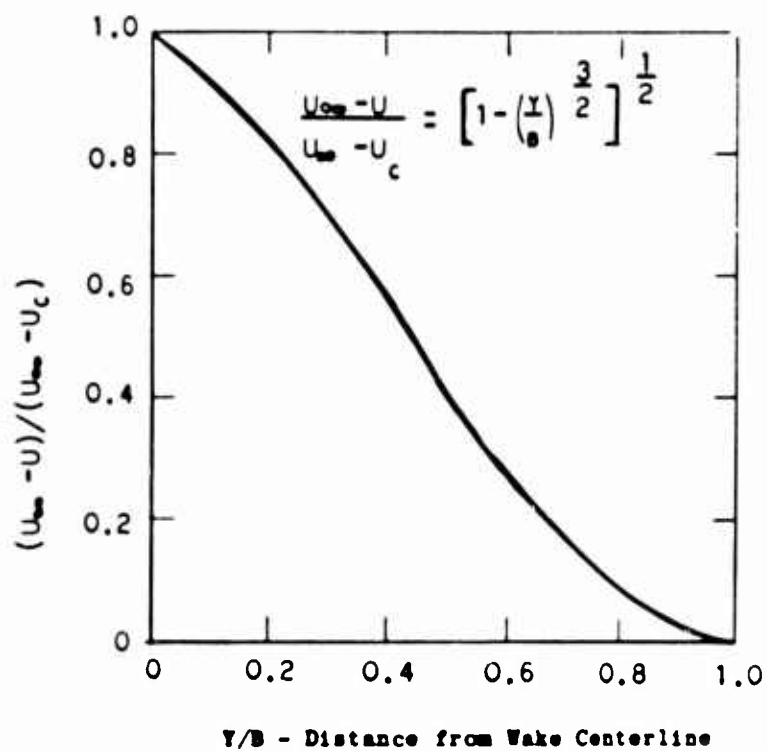


Figure 58 - Wake Velocity Profile.

**CONFIDENTIAL**

**CONFIDENTIAL**

For equivalent mixing of mass and momentum

$$U/U_c = K_F/K_{Fc}$$

Figure 59 represents a fuel jet that has mixed to a peak equivalence ratio of 2.0.

To indicate the quantity of fuel that is over stoichiometric and, therefore, unavailable for combustion, a "mixing efficiency" will be defined.

$$\text{Mixing efficiency} = \eta_m = 1 - \frac{\text{Quantity of fuel unmixed with air because of poor mixing}}{\text{Total fuel up to stoichiometric overall}}$$

This excess fuel is shown cross hatched in Figure 59.

Figure 60 is a plot of the "mixing efficiency" versus the centerline fuel concentration. In Figure 61 this mixing efficiency is plotted versus length, by utilizing values from Figure 60 and Figure 56.

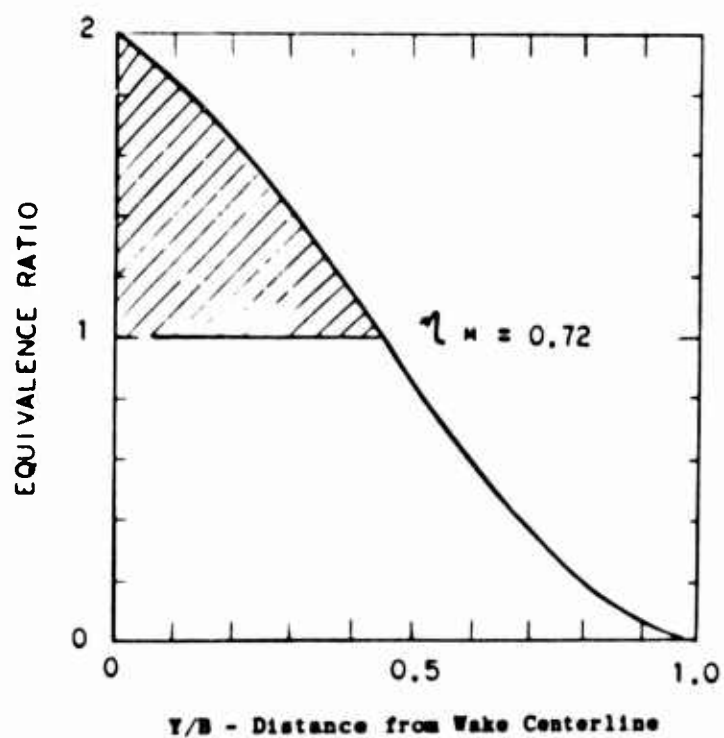
The rigorous application of wake equation theory beyond the point where adjacent wakes touch each other, was not investigated under this contract. It should be noted, however, that Schlichting's text includes an approach in Chapter 23, Section 4, presented by R. Gran Olsson, for the treatment of overlapping mixing zones. For the calculations presented below, mixing efficiencies were determined in this overlap region by simply adding the fuel concentrations predicted for each wake. The condition at which one mixing zone reaches the centerline of the adjacent zone can be determined as follows. To find the region of overlap, the half width of the wake is taken from Schlichting's equation 23.36

$$b = \sqrt{10} \beta (X C_{Dd})^{1/2} \quad \text{for } \beta = .18$$

Again, substituting the relation derived here for  $C_{Dd}$  for a cocurrent flow, equation 20, and the expression for (fuel mass flow), equation 21 for one injector:

$$\begin{aligned} b &= 0.57 (X)^{1/2} \left[ \frac{(f/a (\rho U)_{\text{air}} S Z (U_{\infty} - U_{\text{fuel}}))^{1/2}}{h (1/2 \rho U^2)_{\infty}} \right]^{1/2} \\ &= .805 (X)^{1/2} \left[ \frac{(f/a) S (U_{\infty} - U_{\text{fuel}})}{U_{\infty}} \right]^{1/2} \end{aligned} \quad (13)$$

**CONFIDENTIAL**

**CONFIDENTIAL**


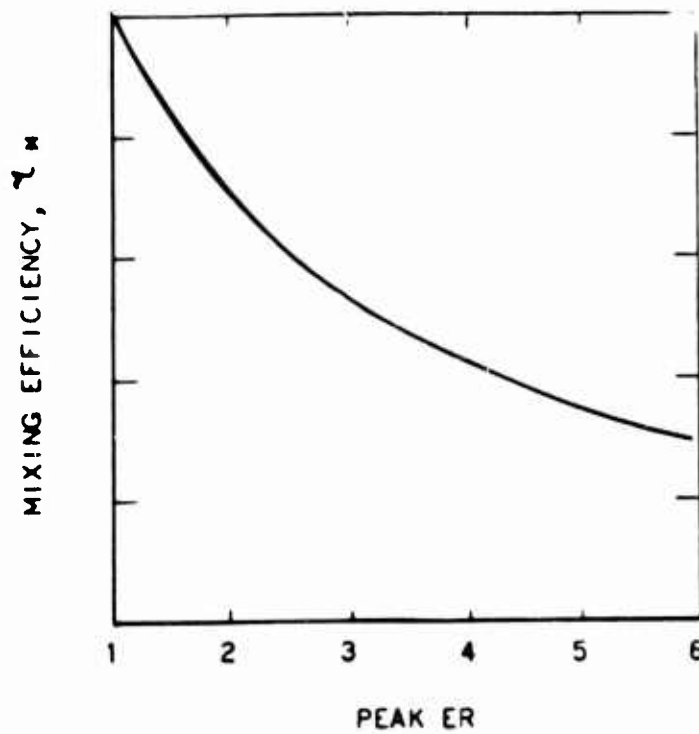
 - FUEL IN EXCESS OF STOICHIOMETRIC

Figure 59 - Profile for Equivalence Ratio of Two.

**CONFIDENTIAL**

**CONFIDENTIAL**

$$\eta_m = 1 - \frac{(\text{FUEL IN EXCESS OF STOICHIOMETRIC})}{(\text{TOTAL FUEL})}$$

Figure 60 - Mixing Efficiency for Single Jet.

**CONFIDENTIAL**

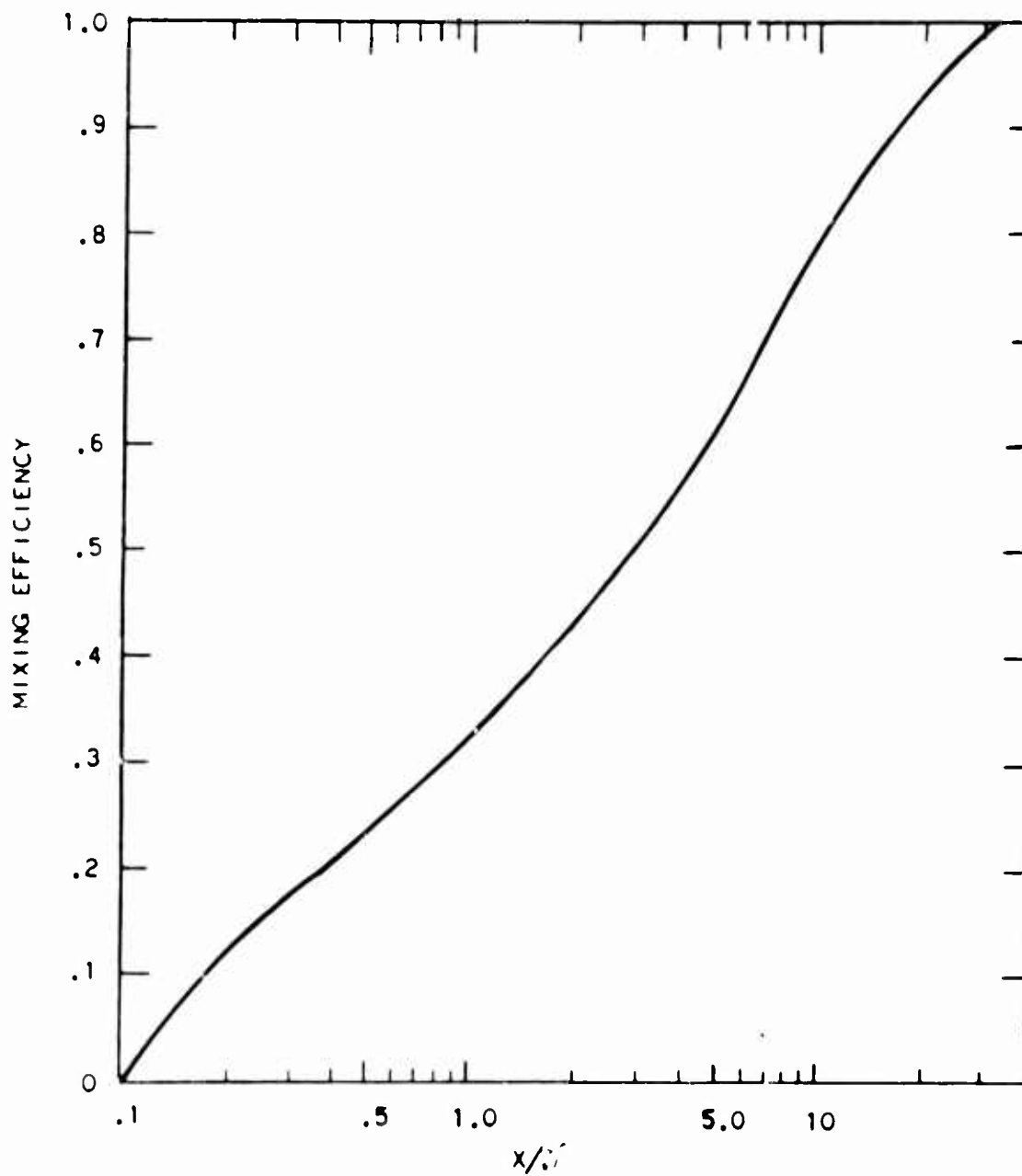
**CONFIDENTIAL**

Figure 61 - Mixing Efficiency vs length

**CONFIDENTIAL**

# CONFIDENTIAL

AF APL-TR-65-103

Solving for the composition at which complete wake overlap occurs,

$$S = b, \text{ and} \\ \sqrt{\frac{b}{a}} = .805 (X)^{1/2} \left[ \frac{(f/a) \frac{U_{\infty} - U_{\text{fuel}}}{U_{\infty}}}{1} \right]^{1/2} = S^{1/2} \quad (34)$$

and by substituting for S in equation 30 and cancelling terms:

$$K_c \text{ (at centerline overlap)} = 1.12 (f/a) \quad (35)$$

For a stoichiometric over-all fuel/air ratio, the overlap of one mixing wake to the centerline of the adjacent wake occurs when the centerline concentration has mixed to very near stoichiometric, indicating that a nearly uniform mixture exists at this condition.

The mixing zones began to first touch each other when  $S = 2b$  giving

$$X_c = 2.25 (f/a) \text{ for touching mixing zones} \quad (36)$$

The assumption of equivalent mixing of mass and momentum used in the above derivations is known to be incorrect. Mass composition and temperature mix faster than momentum. A discussion on mixing of scale quantities such as temperature and composition in two-dimensional wakes is presented in Hinze's textbook (Reference 27), section 6-5.

The simple expression comparable to equation 21 for agreement with temperature profile data in a two-dimensional wake is

$$\frac{K}{K_c} \propto \left[ 1 - \frac{y}{b} \right]^{3/2} \quad (37)$$

Equal mass and momentum mixing is equivalent to assuming that the Schmidt number equals one, for relations that utilize this dimensionless group. On page 426 of Hinze's text a Schmidt number of  $1/1.85 = .54$  is indicated from the available two-dimensional wake and jet measurements. This value is a more accurate representation of the data than equation (36), it is consistent with a profile shape of

$$\frac{K}{K_c} \propto \left( \frac{U}{U_c} \right)^{1/1.85} \text{ or } \left[ 1 - \left( \frac{y}{b} \right)^{3/2} \right]^{1.08} \quad (38)$$

**CONFIDENTIAL**

and is consistent with a faster centerline decay for mass composition corresponding to:

$$K_c = .54 \left( \frac{U_1}{U_{\infty} - U_{\text{fuel}}} \right) \quad (39)$$

The measured profiles predicted by the above expressions are averages of the instantaneous values, taken over a period of time. The mixing is not as complete as indicated by these time-average measurements. For example, when the centerline concentration on a time-average basis in a mixing fuel jet has decreased to stoichiometric, some of the fuel is still at over stoichiometric conditions. A sampling probe mixes this over stoichiometric region with lean regions to indicate an average composition near stoichiometric. One measure of this time-average feature is the intermittency factor in the wake, discussed in section 6-6 of Hinze's text, (Reference 27); this intermittency factor indicates significantly less mixing than the time-average measurement. Another indication of the problem is observable in the work of Hawthorne, Weddell and Hottel (Reference ). They showed that mixing was not sufficient to complete combustion in an axisymmetric turbulent, diffusion flame, until the centerline time-average composition had mixed to less than 1/2 of stoichiometric.

This time-average consideration predicts a reduction in instantaneous mixing greater than the increased mixing rate found for mass when compared with momentum mixing. The equations and illustrations used for composition mixing in this report give a slower more conservative estimate of the mixing rate than if the Schmidt Number = 0.54 is used. This reduced mixing rate assumption partly compensates for the time-average problem.

#### 4) Effect of Static Pressure Field

Most mixing theories are developed for application in a constant static pressure field. However, in supersonic combustors large variations in static pressures are expected to occur at axial distance from the injectors increases. The static pressure field affects the mixing by changing the velocity gradients or in the case of wakes, by changing the magnitude of the momentum defect in the wake.

A change in static pressure along the mixing path results in a velocity change. If the Mach number is uniform, all the velocities will be changed by the same ratio and the resulting velocity gradients would not indicate a change in the mixing. However, large Mach number variations are expected throughout the mixing process. Even if large Mach number gradients do not exist in the early part of the mixing, the combustion process will lower the Mach number in the burned portion of the flow.

**CONFIDENTIAL**

**CONFIDENTIAL**

Quantitatively, the effect of static pressure is to alter the velocity field and, thereby, alter the momentum defect of the mixing wake. In the case of a  $M = 2.7$  freestream and a  $M = 1$  cocurrent fuel flow, a pressure rise of a factor of two will stop the  $M = 1$  flow while permitting the freestream to remain supersonic. The subsequent mixing will occur at the rate for  $M = 1$  injection but at the faster rate of the cocurrent flow with zero downstream momentum.

In constant area burners or step burners, the calculations accounting for axial pressure gradient are simplified because the pressure field is fairly uniform, except for an initial pressure rise. For these cases, the pressure rise can be approximated by assuming it occurred all at one stage of the mixing process.

The magnitude of the pressure rise changes with flight Mach number or inlet air enthalpy and is also a function of the combustor geometry. The arc tunnel step-combustor operating at  $M = 6$  conditions has a pressure rise greater than a factor of two. Thus, if the downstream velocity of the fuel after completion of penetration were sonic, the pressure rise in the burner would reduce the average fuel velocity to zero or even to a negative value. At higher flight Mach numbers, the pressure rise decreases, but the supersonic combustor configurations tested at General Electric that attained high efficiency, also involved pressure rise near the burner inlet of at least two. This provides justification for using a zero downstream momentum in the cocurrent flow equations to simulate arc tunnel combustor conditions.

#### 5) Effect of Combustion and Mach Number on Mixing

The effects of Mach number and combustion on mixing are accountable as effects due to density and static pressure.

Combustion in a constant static pressure field does not change the flow velocities; instead, the flow area increases to accommodate the hotter, lower density burned gases. Since the velocities do not change, the momentum defect of the wake also remains unchanged by combustion. The wake equations predict that the mixing will not be affected by combustion in a constant static pressure field. However, some density effect, not accounted for by the far-field equations, may be involved because of the near-field type of problem that is associated with the large density differences generated by combustion.

More important than the direct density effects on mixing are the effects of the static pressure gradients that are generated in SCRAMJET combustors. The combustion process in a constant area duct results in a pressure rise. The effect of this static pressure rise, as described in the last section, is to change the flow velocities and also the momentum defect.

**CONFIDENTIAL**

**CONFIDENTIAL**

The result is a large increase in the mixing rate for combustors that have large pressure rises early in the combustion process.

One important influence of Mach number, may be associated with its effect on the rate of static pressure rise. At very high burner inlet Mach numbers, oblique shock waves may require long axial distances to transmit pressure disturbances across the burner. The beneficial effects of pressure rise on mixing may be delayed at high Mach numbers. The other effects of Mach number either through density effects or due to interaction with a static pressure field, are properly treated, in the wake equations with the momentum defect adjusted as indicated in the last section on pressure gradients.

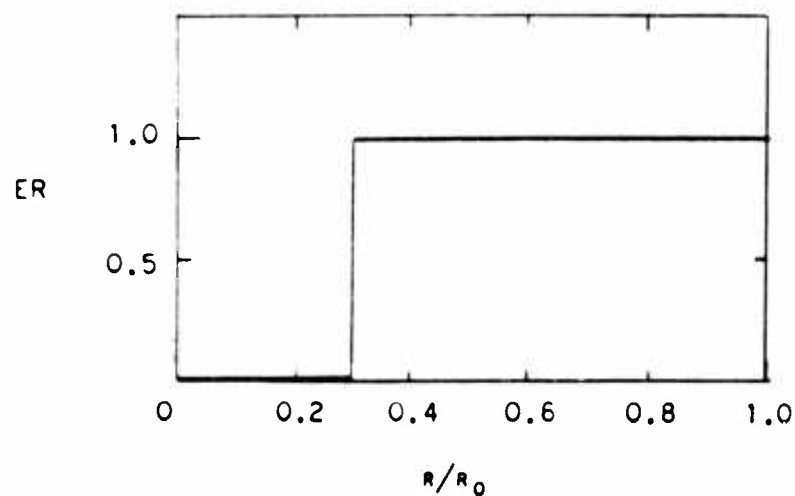
#### 6) The Eight Injector Configuration

A fourteen (14) hole normal injector was selected for incorporation into a combustor design, having a total of eight wall injectors, for testing in the arc tunnel. This injector, configuration 4 in the penetration work, was labeled Injector "G" when incorporated into arc tunnel combustor hardware.

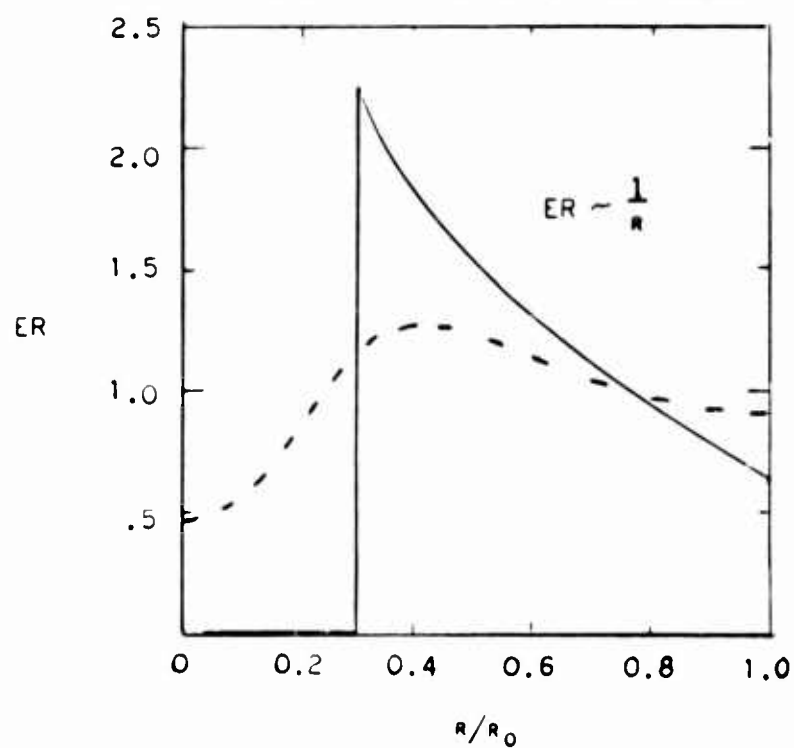
From Figure 61, the predicted mixing efficiency for the two-dimensional model of this configuration is 80%. This is for an equivalence ratio of 1.0, and a combustor length of ten (L/D)'s. This corresponds to a nearly uniform  $f/a$  profile in a two-dimensional region. However, if the jets are actually two-dimensional sources, then the  $f/a$  in the round combustor will tend to decrease toward the outer wall. This was experimentally observed in some arc tunnel tests. Figure 62 shows three constructions to illustrate this three-dimensional problem. First the carbureted region is shown uniform. Then, the fuel is distributed inversely proportional to the radius in the carbureted region. Finally a construction of mixing toward the centerline is added. This final construction was made assuming that fuel mixed toward the center of the duct from the carbureted region at a rate consistent with the two-dimensional jet mixing. The lean center, prominent in all of the constructions, was a significant feature in many of the measured  $f/a$  profiles in arc tunnel combustor tests. The presence of the wall and the shear gradients in the wall boundary layer should have a significant affect on the mixing in the outer region, however, no effort was made in this study to treat the mixing due to the wall shear.

Figure 63 shows the calculated penetration for a set of cycle data for a Mach 6-12 vehicle. This particular vehicle for which the curve was obtained, required a cooling equivalence ratio of 2.21 for cooling at  $M = 12$ . The calculated penetration from equation 14 shows that the penetration remained almost constant over the entire mission. Obviously, this greatly simplifies the problem of optimizing penetration for all flight speeds. The

**CONFIDENTIAL**

**CONFIDENTIAL**

A) RESULT OF TWO-DIMENSIONAL MODEL

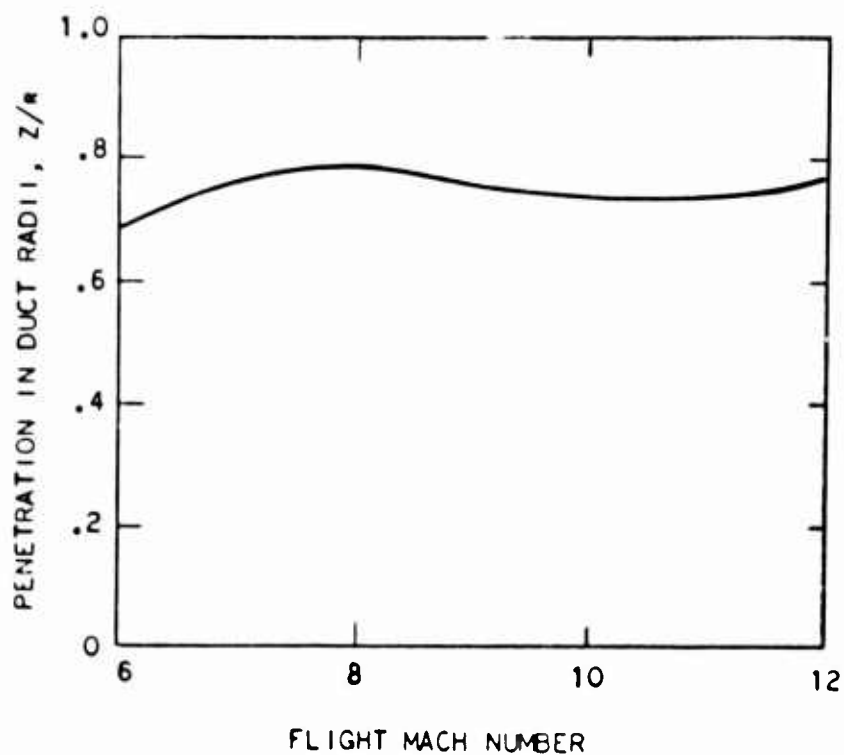


- - - - ESTIMATE OF EFFECT OF MIXING  
TOWARDS CENTER

B) TWO ADDITIONAL CONSTRUCTIONS CONSISTENT  
WITH ROUND DUCT

Figure 62 - Construction of Fuel Distribution from Two-Dimensional Solution.

**CONFIDENTIAL**

**CONFIDENTIAL**

CYCLE CONDITIONS

MP	ER
6	1.0
8	1.0
10	1.41
12	2.21

Figure 63 - Penetration vs Flight Mach Number.

**CONFIDENTIAL**

**CONFIDENTIAL**

effect on fuel penetration of the increasing velocity of the freestream with increasing flight Mach number is approximately compensated by either the fuel velocity increase due to increased fuel temperature or at high flight speeds by the equivalence ratio increase required to maintain the maximum permissible temperature.

A Mach 6-12 vehicle requiring only an equivalence ratio of 1.5 at Mach 12 for cooling, would have a penetration the same as in the Mach 6 arc tunnel tests,  $Z = .7R$ . Fuel jets in arc tunnel tests with a total fuel temperature limited to 500-550R, will penetrate less than .7R at air enthalpies greater than  $M = 6$ .

The "G" injector is in a constant area section at the burner inlet. It is instructive to examine the mixing efficiency in the short distance from the injector to the diverging portion of the burner. In Figure 61, a mixing efficiency of 50% is given to  $X/D$  equals 3.0. However, if the pressure rise upstream of the divergence is small, the mixing should proceed at the slower rate predicted for sonic fuel velocity. From Figure 57, it requires five times the length to achieve the equivalent mixing for sonic fuel velocity, this corresponds to a mixing efficiency of only 25% in the 3 ( $X/D$ )'s upstream of the divergence.

Figure 64 is a mixing efficiency performance map made from calculations for several over-all equivalence ratios. Lowest performance always occurs at stoichiometric fuel/air ratios. With rich mixtures, all of the oxygen is mixed with fuel before the fuel distribution becomes uniform. For lean mixtures, it is only necessary to mix the peaks below stoichiometric, not to uniformity, to achieve a mixing efficiency of 100%.

The results in the figure were for an assumption of zero downstream fuel momentum at the origin of mixing consistent with an initial sonic downstream velocity, followed by a two-to-one pressure rise. The location and extent of the pressure rise due to the combustion should have an important effect on the mixing efficiencies actually achieved, lower mixing efficiency estimates result for constant pressure processes.

## 2. Arc Tunnel Combustor Tests

### a. Experimental Technique

#### 1) The Arc Tunnel

The tests reported herein were performed on water-cooled heavyweight supersonic combustor models assembled into the Hypersonic Arc Tunnel, located in AETD Cell 2 at the Evendale Plant. A description of the

**CONFIDENTIAL**

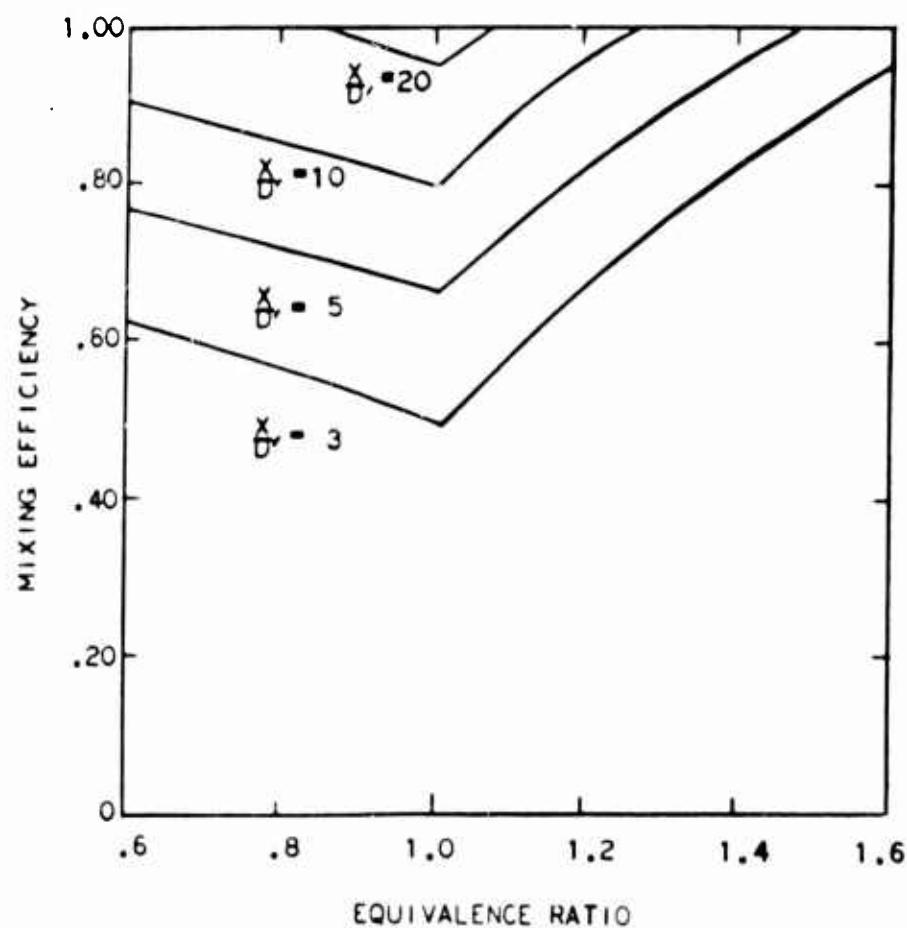
**CONFIDENTIAL**

Figure 64 - Mixing Efficiency vs ER for Several  $(X/D)$ 's.

**CONFIDENTIAL**

**CONFIDENTIAL**

facility follows:

a) Combustor Inlet Air Supply

Air for combustion tests was compressed by a piston-type air compressor and stored in pressure tanks. The compressor was rated 100 scfm (.123 pps) at 3100 psi output pressure. The tanks contained 3000 pounds of air at 3000 psig pressure. A portion of this air was used for pumping the remainder, and was not available to the combustor. The fraction of air available for test was dependent upon the flow rate required and the combustor inlet total pressure.

The airflow rate was controlled automatically by a pressure regulator which maintained a pre-set pressure upstream of two venturi flowmeters sized for choked flow at their throats. The air from the two venturis was delivered to two air injection points on the air heater by electrically insulating flexible hoses. The flow split through the two systems was fixed by the relative size of the venturis. Piping was sized for a maximum flow rate of four pounds per second.

b) Air Heater Power Supply

Electrical power for the arc air heater was drawn from the commercial source through a three phase autotransformer having a power capacity of 25,700 KVA for 15 minutes. Output voltage to ground for each phase could be regulated from zero to 4000 volts. Output current capacity was a function of voltage setting, with a maximum of 4350 amperes per phase at the 2000 volt setting. Voltage regulation was accomplished by a mechanism which varied the location of the autotransformer's secondary taps. A coarse control changed the output voltage in 400 volt steps over the entire 4000 volt range, and could only be actuated with no current flowing. A verrier control provided 12.5 volt steps over a 400 volt range, and could be changed during operation.

Circuit breakers interrupted power to the transformer when the electrical system became overloaded or unbalanced.

Arc ballast was provided by a reactor coil in series with the arc gap in each phase. The inductance of each coil could be changed by manually connecting the power cable to one of six coil taps provided. Inductive reactance from .352 to 1.73 ohms was available. The function of the arc ballast was to limit the current when the arc gap resistance was low, and to allow high gap voltage when the resistance was high (as when the arc was extinguished). The latter function is particularly important in alternating current arcs, as the arc is extinguished and must be re-struck twice during each current cycle. Note that the reactor coil dissipated little power, but reduced the power factor considerably.

**CONFIDENTIAL**

**CONFIDENTIAL**

c) Air Heater

Combustion air was heated by dissipation of electrical energy in an arc within the air stream. By this method, a continuous flow of air could be heated to temperatures above the melting points of structural materials. The construction of the air heater is shown schematically in Figure 65. The air heater, partly disassembled, is visible in Figure 66.

The arc was struck within a cavity termed the "arc chamber", enclosed by a stainless steel pressure vessel designed for 1500 psi pressure and conforming to the ASME Boiler Code. The vessel was cylindrical, 24 inches inside diameter, and was 31 inches long. One end was closed by an integral head having an opening in its center into which was fitted the hot air exit nozzle. The opposite end was flanged, and was closed by a 41 inch OD, six-inch thick, bolted blind flange, termed the "end closure", on which were mounted the arc electrodes and air inlet fittings. The pressure vessel was protected from the hot air within it by close-wound helical coils of one-inch copper tubing through which water was pumped at high velocity. The end closure was similarly protected by a water-cooled fabricated copper liner.

Three identical sets of arc electrodes were mounted within the arc chamber, projecting from the end closure as shown in Figure 65. Each set consisted of a center electrode and an outer ground electrode. The center electrode consisted of a copper disc 0.9 inches thick and 3.0 inches in diameter, mounted on a 1.5 inch diameter support post. The support post passed through the end closure and was electrically insulated from the closure. To each center electrode post was connected one of the three power cables from the three-phase electrical power supply. Within the post were passages carrying air and cooling water. The cooling water circulated through passages within the rim of the center electrode disc. The air was injected into the arc chamber through holes drilled diagonally through the boron nitride insulating sleeve.

In addition to the air injected through the center electrode insulators, additional "by-pass" air could be injected through the end closure into the space between the pressure vessel and its cooling coil. This air entered the arc chamber by bleeding between the turns of the coil.

The ground electrode was a water-cooled copper ring positioned concentrically around the center electrode disc. The diameter of the ring determined the arc gap, which was varied to suit the arc chamber pressure and power level. The ring was attached by two tubular supports to the end closure and was electrically grounded to the closure.

**CONFIDENTIAL**

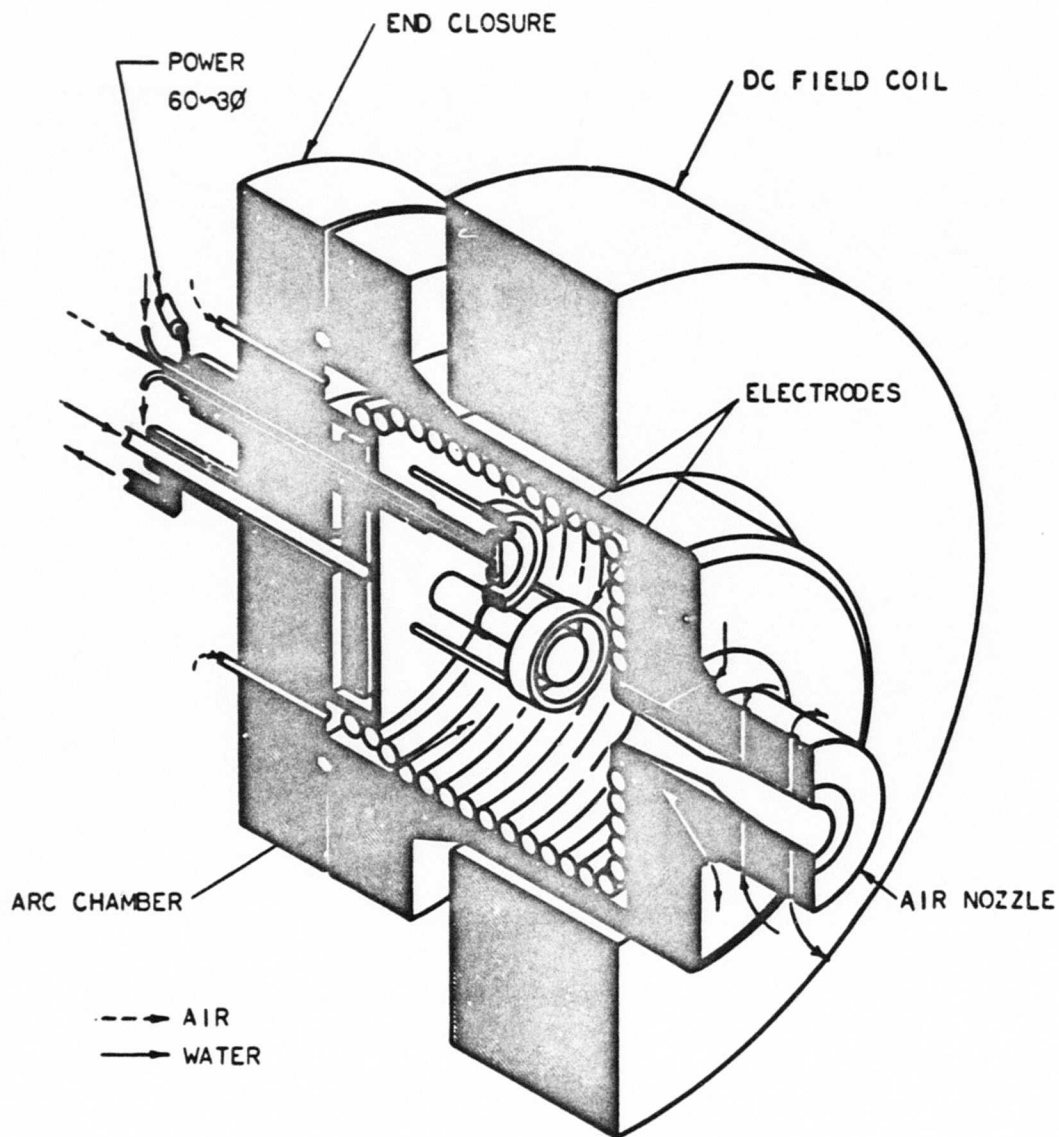
**CONFIDENTIAL**

Figure 65 - Electric Arc Air Heater (Schematic).

**CONFIDENTIAL**

**CONFIDENTIAL**

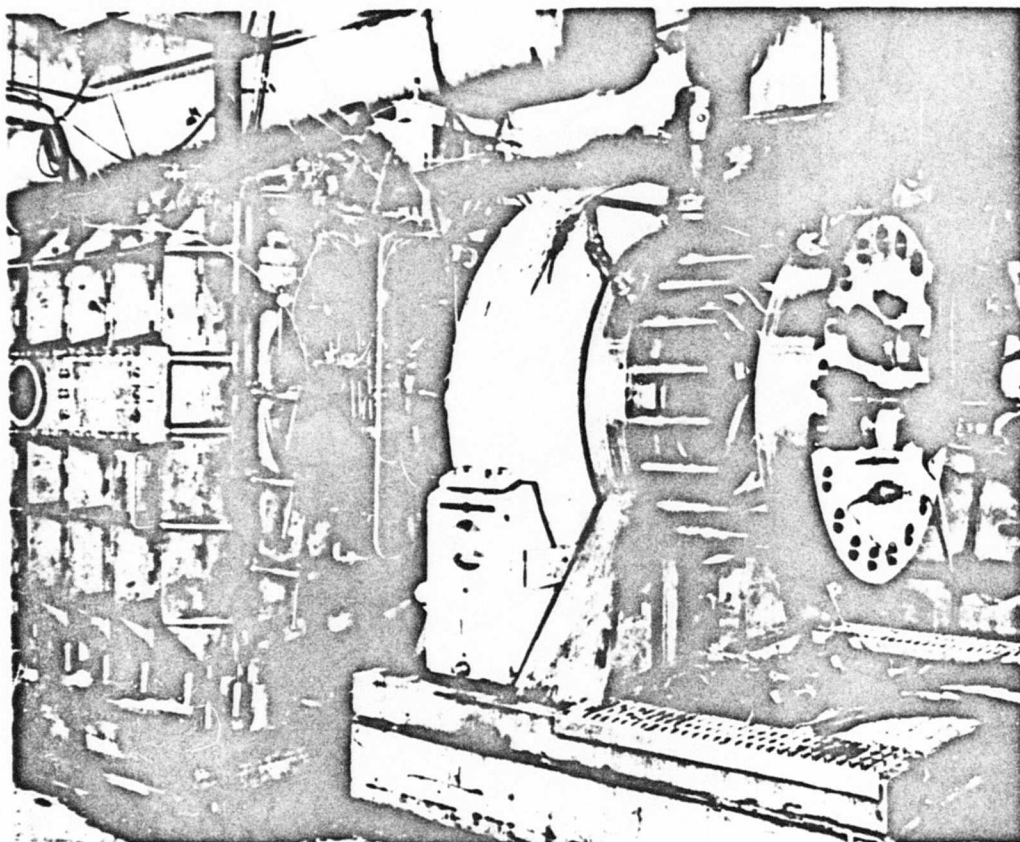


Figure 66 - Arc Tunnel Combustion Test Apparatus.

**CONFIDENTIAL**

**CONFIDENTIAL**

The arc was struck across the annular gap between the center and ground electrodes. The intensity of the arc was such that, had the arc been allowed to remain stationary, the electrode material would have been consumed within seconds, despite the vigorous water-cooling. Electrode life was extended by forcing the arc to rotate around the annular gap. Each point on the electrode surface was thus exposed to the arc column only for brief instants. Rotation of the arc column was accomplished by establishing a powerful magnetic field within the arc chamber, oriented parallel to the axes of the electrodes. Since the current flow through the arc column was radial, hence perpendicular to the field, a force was exerted on the arc column in a direction perpendicular to both the field and the current. The force caused the arc to rotate about the annulus. The magnetic field was generated by a water-cooled D. C. coil outside of the pressure vessel. To prevent distortion of the field, only non-magnetic structural materials were used in and about the air heater.

Electrode life was normally in excess of ten minutes, depending upon power level and chamber pressure. Contamination of the air stream by electrode material was very low, about .05 percent. Electrode failure was evidenced by the appearance of small holes in the electrode cooling water passages. When the hot air pressure was less than the cooling water pressure, water was sprayed directly into the arc column, extinguishing the arc without further damage. Had the arc chamber pressure been higher than the water pressure, hot air would have entered the cooling water passages, causing catastrophic damage to electrode supports and the end closure. As the maximum cooling water supply pressure available was 700 psi, the arc chamber pressure was limited to 500 psi by this consideration.

The electrical voltages used were insufficient to strike an arc with cold air in the arc gap. Starting was accomplished by bridging each gap with a stainless steel fuse wire. The initial surge of current vaporized the wire, establishing a conductive path for the arc. The normal restrike that occurred at the beginning of each current alternation was easily accomplished, as ionized gases remained in the gap from the previous alternation. Starting was accomplished with reduced airflow. Full airflow was established ten to fifteen seconds after ignition.

d) Fuel Supply

Gaseous hydrogen fuel was supplied to the combustor from transport trailers through two parallel systems each capable of delivering 0.15 pounds per second at 1500 psi. Flow control was accomplished by dome-loaded pressure regulators which maintained a pre-set pressure upstream of standard thinplate orifice flowmeters. On-off control was provided by electro-pneumatically actuated bail cocks.

**CONFIDENTIAL**

**CONFIDENTIAL**

Parallel systems permitted nitrogen to be substituted for the hydrogen flow for purging or for non-burning combustor operation.

An automatic switching system normally started the hydrogen flow when full air had been established. This system could be overridden when necessary. An interlock stopped the hydrogen flow when the arc power was interrupted.

e) Exhaust System

The combustor exit stream was dumped abruptly into a large rectangular chamber, about four feet square, shown in Figure 66. The burner exit instrument rake was mounted through the roof of this chamber. A movie camera observed the burner exit stream through windows in the chamber side walls. The chamber walls were heavily constructed of stainless steel, and were uncooled.

Any fuel not consumed in the combustor was burned in the dump chamber as the kinetic energy of the jet from the combustor was dissipated. To assist this purging action, secondary air was drawn from the shop air supply and injected into the dump chamber through a distributor pipe. The combustor could be operated at equivalence ratios up to about 1.2 without discharging unburned hydrogen to the exhausters.

From the dump chamber, the exhaust gases flowed through a large pipe to the exhaust cooler. The pipe was 27.6 inches in diameter for 12 feet, then enlarged gradually to the ten foot diameter of the exhaust cooler. The cooler was a shell-and-tube heat exchanger capable of transferring 9000 BTU/sec of heat to its cooling water.

The cooled gases were pumped to the atmosphere by multiple stages of mechanical compression followed by a steam ejector. The functions of the steam ejector were to assist the mechanical compressors, to maintain the entire system at subatmospheric pressure to avoid release of nitrogen dioxide through seal leakage, and to dissolve the nitrogen dioxide, preventing formation of a frightful brown cloud at the exhaust stack. The exhaust system was capable of maintaining the dump chamber pressure at less than 3 psia at the maximum facility flow rates.

2) Combustor Hardware

a) Combustor Inlet Air Nozzles

The arc heated air was expanded to supersonic velocity and delivered to the combustor. This was accomplished by one of two water-cooled axisymmetric converging-diverging nozzles close-coupled to the

**CONFIDENTIAL**

**CONFIDENTIAL**

air heater. One of these nozzles is depicted in Figure 65.

The nozzles used for these tests had an exit diameter of 3.0 inches, and were contoured to provide a uniform exit flow. The ratio of exit area to throat area was 3.86 for nozzle "A" and 7.00 for nozzle "B", providing exit Mach numbers of approximately 2.7 and 3.2 respectively, varying slightly with the enthalpy level for each test. Current engine cycles show burner inlet Mach numbers of 2.7 and 3.2 at flight speeds of Mach 6.7 and 7.7, respectively.

The nozzle contours, established by the method of characteristics are tabulated in Table III and IV. No correction for boundary layer was made. The boundary layer was calculated by the technique of Henderson (Reference 15), which predicted a displacement thickness of 0.03 inches for nozzle A sufficiently small to be neglected.

The nozzle walls were constructed of beryllium copper, this material providing a reasonable compromise between high strength and high thermal conductivity. Wall thickness was .06 inches. The walls were cooled by an axial flow of high pressure water over the outer surface. Water velocity at the nozzle throat was 110 feet per second.

b) Fuel Injectors

The fuel injectors employed for these tests were of two types: step injectors and cylindrical injectors.

The step injectors, shown schematically in Figure 67, were denoted as injectors "E", "F", and "J". All were similar in that they were of circular cross section, had flanged ends 9.0 inches apart, and were water-cooled. Their outer casings were of stainless steel, their flanges of monel, and their inner liners of copper. Heated air at supersonic velocity entered one end, having a 3.0 inch diameter bore. Fuel and air flowed out through the opposite end, which had a 4.75 inch bore. Inlet and exit bores were concentric. The increase in bore diameter occurred in a single step located part way through the injector. The injectors differed in the location of the step, and in the method of fuel injection.

In injector "E", the step was located 6.0 inches from the exit end. Approximately 0.75 inches aft of the step, four pedestals 1.0 inches in diameter protruded radially inward from the 4.75 inch bore to the height of the step as shown in Figure 68. These were oriented at the 3, 6, 9 and 12 o'clock positions. The fuel nozzles were located in the radially innermost surfaces of the pedestals. The exit of each nozzle was rectangular, 0.031 inches wide and 0.31 inches long set flush with the surface of the pedestal, as shown in Figure 69. The long axis was oriented parallel to the airflow. The fuel was directed radially inward, perpendicular to the airflow.

**CONFIDENTIAL**

# CONFIDENTIAL

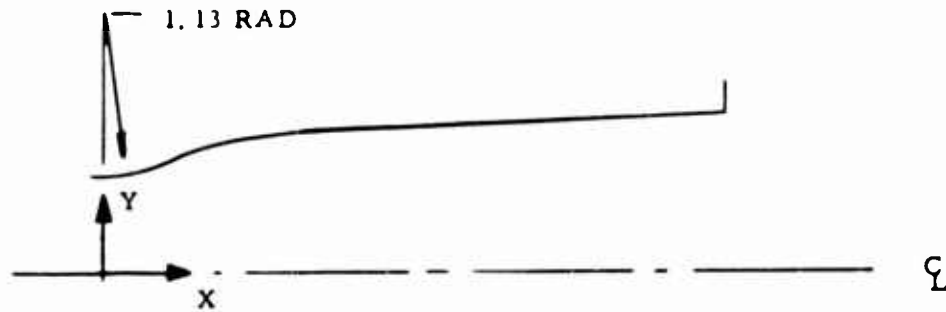
TABLE III: WALL CONTOURS, NOZZLE "A"



X IN.	Y IN.
0	.760
.333	.797
.400	.812
.600	.863
.800	.914
1.000	.965
1.500	1.084
2.000	1.190
2.500	1.274
3.000	1.341
3.500	1.395
4.000	1.439
4.500	1.462
5.000	1.481
5.500	1.491
6.000	1.500
7.900	1.500

# CONFIDENTIAL

TABLE IV: WALL CONTOURS, NOZZLE "B"



X IN.	X IN.
0	.5670
.310	.6105
.323	.6140
.386	.6325
.487	.6630
.577	.6915
.618	.7050
.645	.7135
.671	.7215
.675	.7230
1.078	.8470
1.325	.9180
1.620	.9960
1.775	1.0340
2.228	1.1335
2.643	1.2105
2.902	1.2525
3.591	1.3435
3.638	1.3485
4.422	1.4195
4.708	1.4385
5.260	1.4665
6.005	1.4890
7.053	1.5000

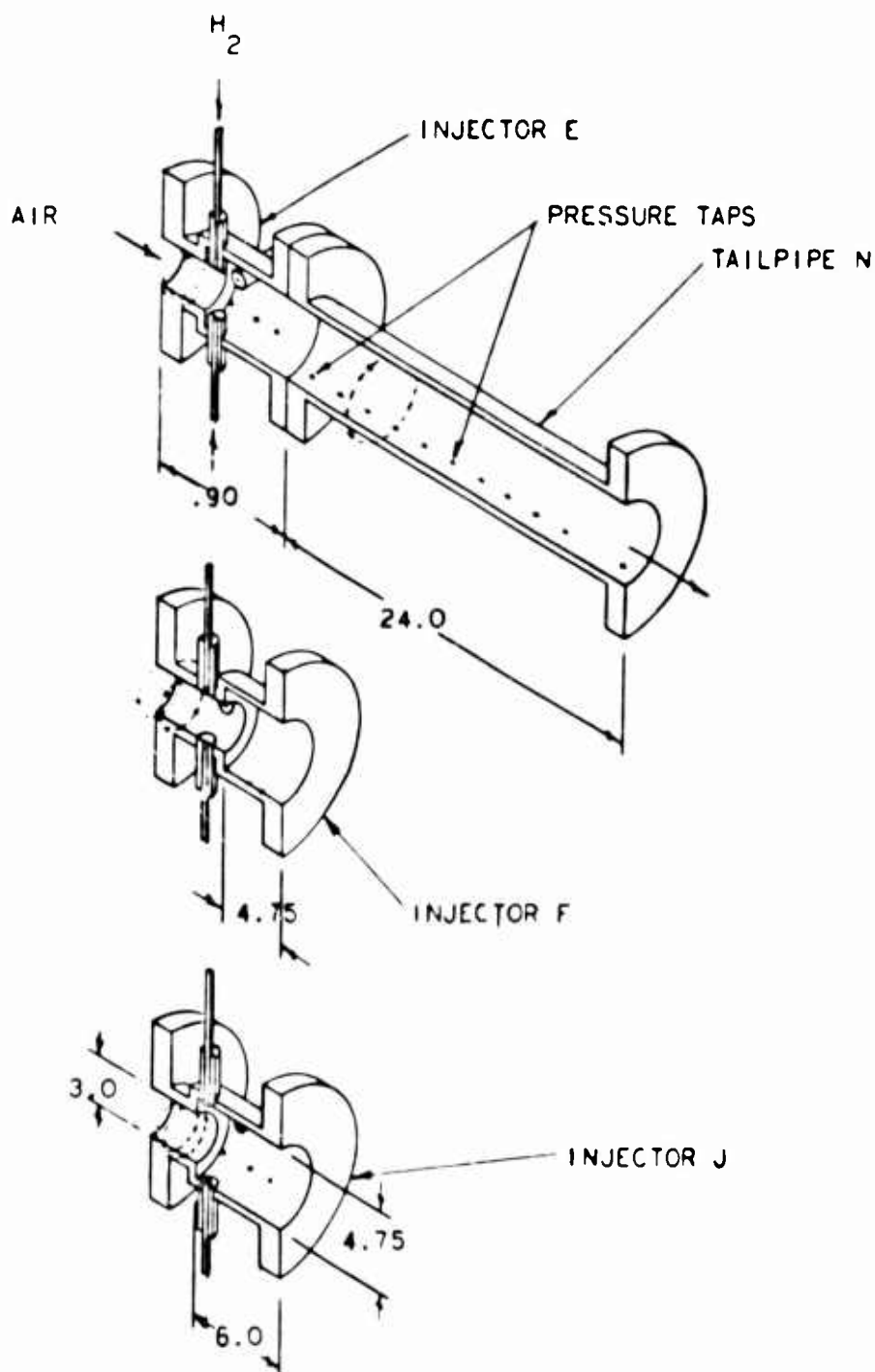
**CONFIDENTIAL**

Figure 67 - Supersonic Combustor Models (Schematic).

**CONFIDENTIAL**

**CONFIDENTIAL**

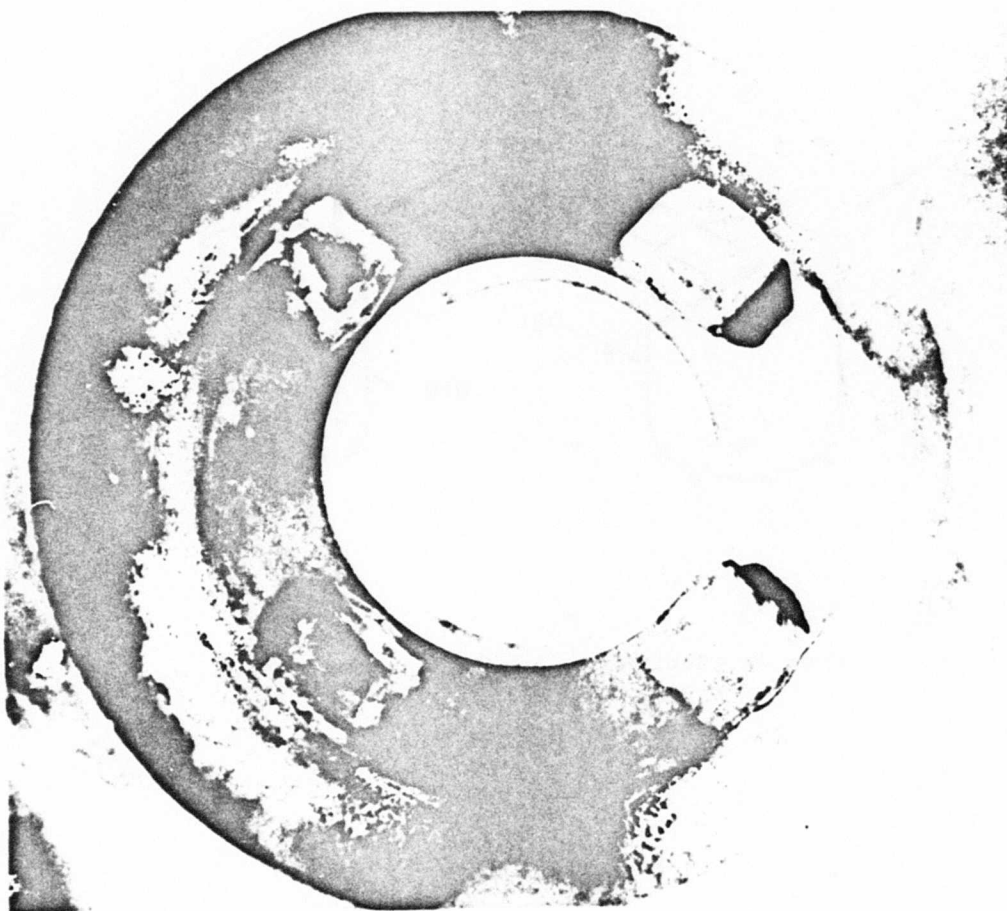


Figure 68 - Injector E.

**CONFIDENTIAL**

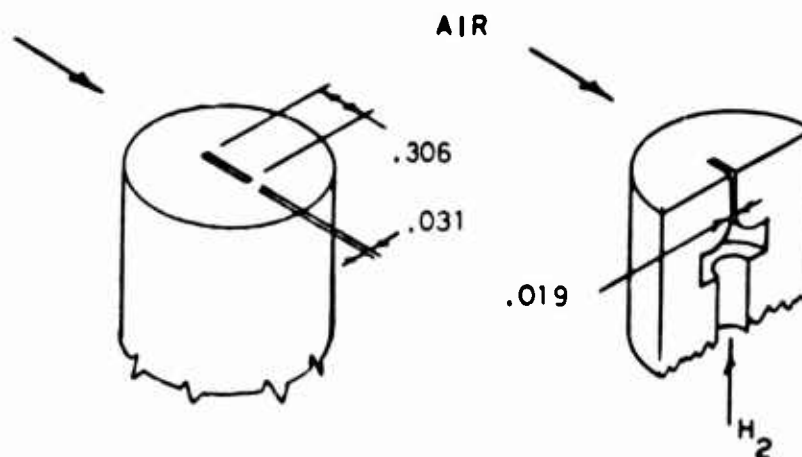
**CONFIDENTIAL**

Figure 69 - Fuel Nozzle Details, Injector E and F.

**CONFIDENTIAL**

**CONFIDENTIAL**

The fuel nozzles were converging-diverging, of constant length, but having a throat width of 0.019 inches.

The step of the injector "F" was located only 4.25 inches from the exit end. The fuel nozzles were similar to those of injector "E", but were set flush with the 3.0 inch diameter bore 1.2 inches upstream from the step. The bore was thus left unobstructed. Again, the fuel was directed radially inward from four points around the periphery of the injector.

The step of injector "J" was located 6.0 inches from the exit end. Fuel was admitted from four small, irregular protrusions spaced around the periphery of the 4.75 inch bore, 0.75 inches aft of the step. The fuel nozzles were shaped to direct the fuel roughly circumferentially, in a swirling manner, perpendicular to the airflow.

The intended purpose of the step in the wall of the injectors was twofold: it provided a seat for combustion-induced boundary layer separations, stabilizing their location and preventing their propagating further upstream and it provided a sheltered region for stabilization of a pilot flame to maintain combustion when conditions prevented auto ignition of the fuel-air mixture.

Five cylindrical type injectors were employed. These were denoted as injectors "K", "G", "H", "Hm", and an "F-type" injector integral with Tailpipe "Q".

Injector "K" is depicted in Figure 70. This injector was constructed of stainless steel and formed a "flange", 1.5 inches thick, which was sandwiched between the air nozzle and the end flange of the tailpipe.

Hydrogen was injected from an annular slot circling the perimeter of the 3.0 inch bore. The slot was oriented to direct the fuel downstream as a film on the tailpipe wall. The slot had an exit height of .040 inches, with a minimum height of .024 inches further upstream, so that the injection velocity was supersonic. Injector "K" was cooled only by the fuel flowing through it.

Injectors "G", "H" and "Hm" also formed "flanges" to be sandwiched between the air nozzle and tailpipe, but were water-cooled. They were of two-piece construction, having an outer casing of brass or aluminum and an inner liner of copper. An injector liner is shown in Figure 71 and a casing in Figure 72. Liner and casing were joined mechanically with o-ring seals, this method of construction proving much more reliable than welding. These injectors were all 4.0 inches long, and had 3.0 inch bases.

**CONFIDENTIAL**

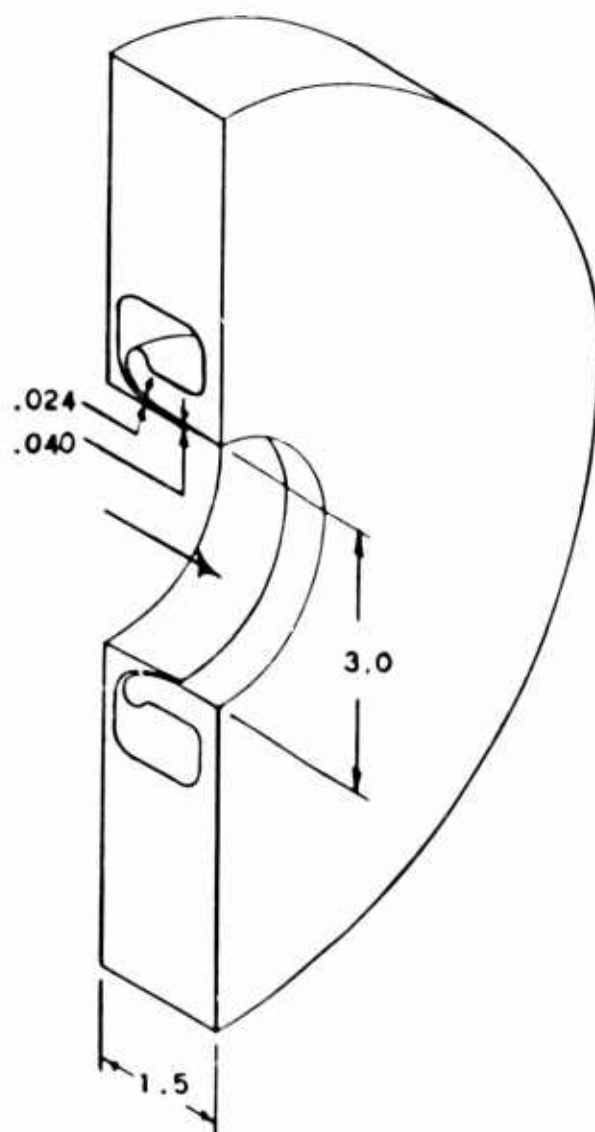
**CONFIDENTIAL**

Figure 70 - Injector K.

**CONFIDENTIAL**

**CONFIDENTIAL**

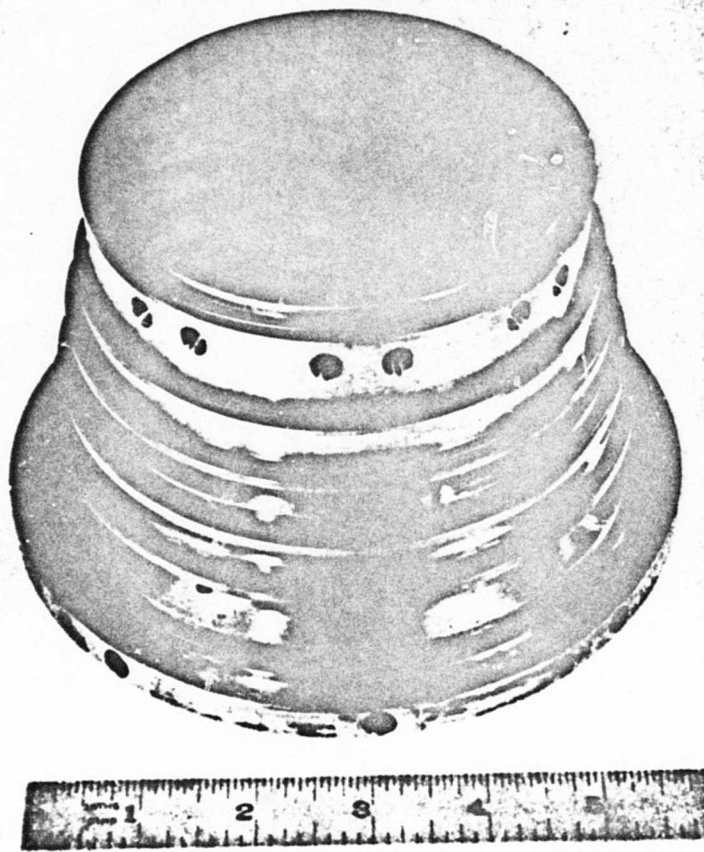


Figure 71 - Liner, Injector G

**CONFIDENTIAL**

**CONFIDENTIAL**

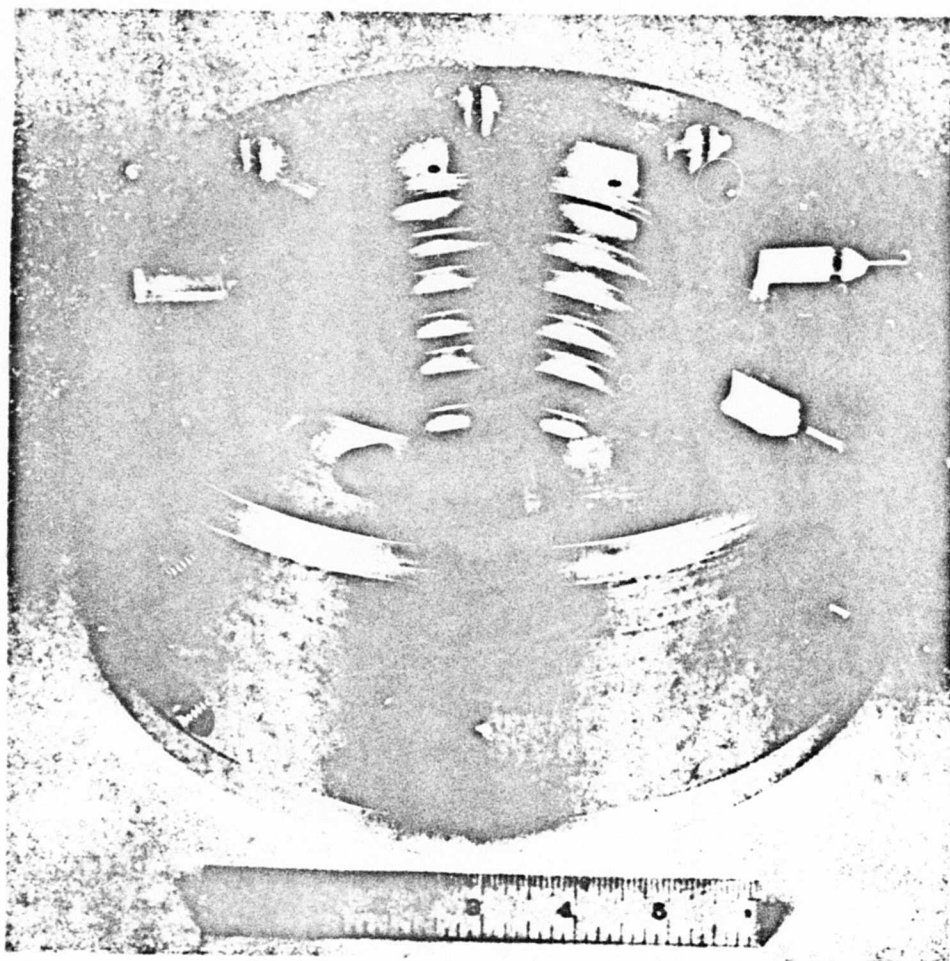


Figure 72 - Injector Casing.

**CONFIDENTIAL**

**CONFIDENTIAL**

They differed in the method of fuel injection.

Injector "G" is shown in Figure 73. Fuel was admitted normal to the airflow through 112 holes, .06 inches in diameter, drilled radially through the wall of the 3.0 inch base. The holes were arranged in eight rows of 14 holes each. The axis of each row was oriented parallel to the airflow. The rows were spaced 45 degrees apart around the circumference of the base. The hole spacing in each row was .25 inches.

Injector "H" is also shown in Figure 73. Fuel was admitted through 96 holes, .06 inches in diameter, arranged in eight rows of 12 holes each. This arrangement was similar in Injector "G", except that the holes were drilled at an angle of 30° to the axis of the base, so that the fuel was directed obliquely downstream.

Injector "Hm", not shown, was a modification of Injector "H". The modification was to close, by brazing, every other hole in every other row. This injector thus contained 72 holes, arranged in four rows of 12 holes each, with .25 inch spacing, separated by four rows of six holes each, with .50 inch spacing. The purpose of this modification was to allow part of the fuel to penetrate further than the rest, to improve the initial distribution.

Tailpipe "Q", described below, contained provisions for mounting fuel nozzles near its 3.0 inch diameter entrance. These nozzles were identical to those of step-type Injector "F", hence are referred to as "F-type" injectors. Tailpipe "Q" did not contain a wall step. This arrangement is illustrated in Figure 73.

c) Tailpipes

The fuel injectors were followed by one of five mixing pipes or "tailpipes", in which mixing and burning of the fuel and air occurred.

Tailpipes "N" and "P" were used with the step injectors, and tailpipes "Q", "R" and "3" were used with the cylindrical injectors. A cylindrical injector could be assembled to tailpipe "N" or "P" only by using a step injector as a transition piece.

Tailpipe "N" is shown schematically in Figure 67. It consisted simply of a 24 inch length of water-cooled flanged pipe having a 4.75 inch diameter bore. The outer structural shell was fabricated of stainless steel, the flanges were of monel, and the inner liner was copper. Tailpipe "N" is faintly visible beneath the tangled plumbing in Figure 74. Tailpipe "P", not shown, was similar to tailpipe "N", except that its length was 12 inches.

**CONFIDENTIAL**

**CONFIDENTIAL**

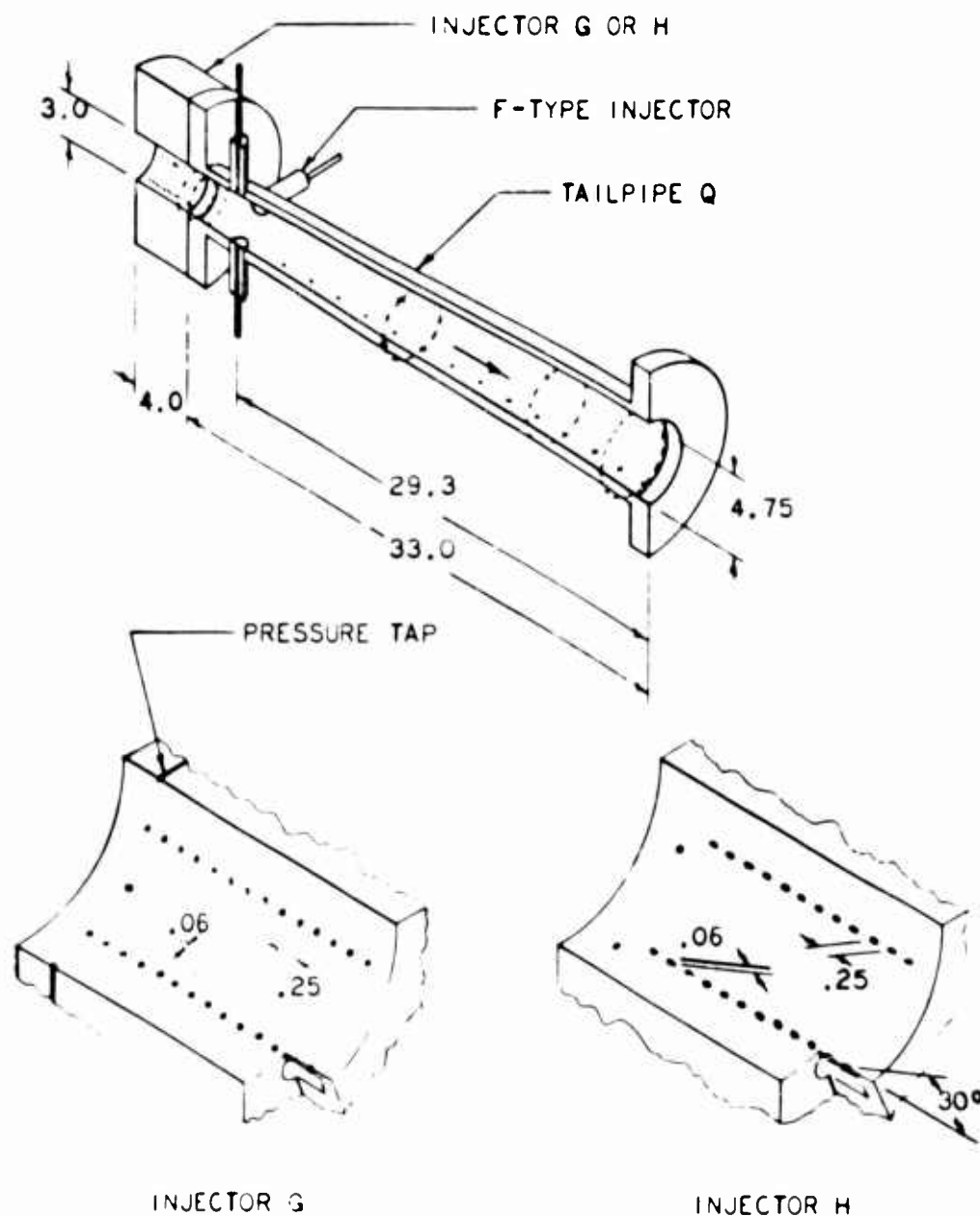


Figure 73 - Supersonic Combustor Models (Schematic).

**CONFIDENTIAL**

**CONFIDENTIAL**

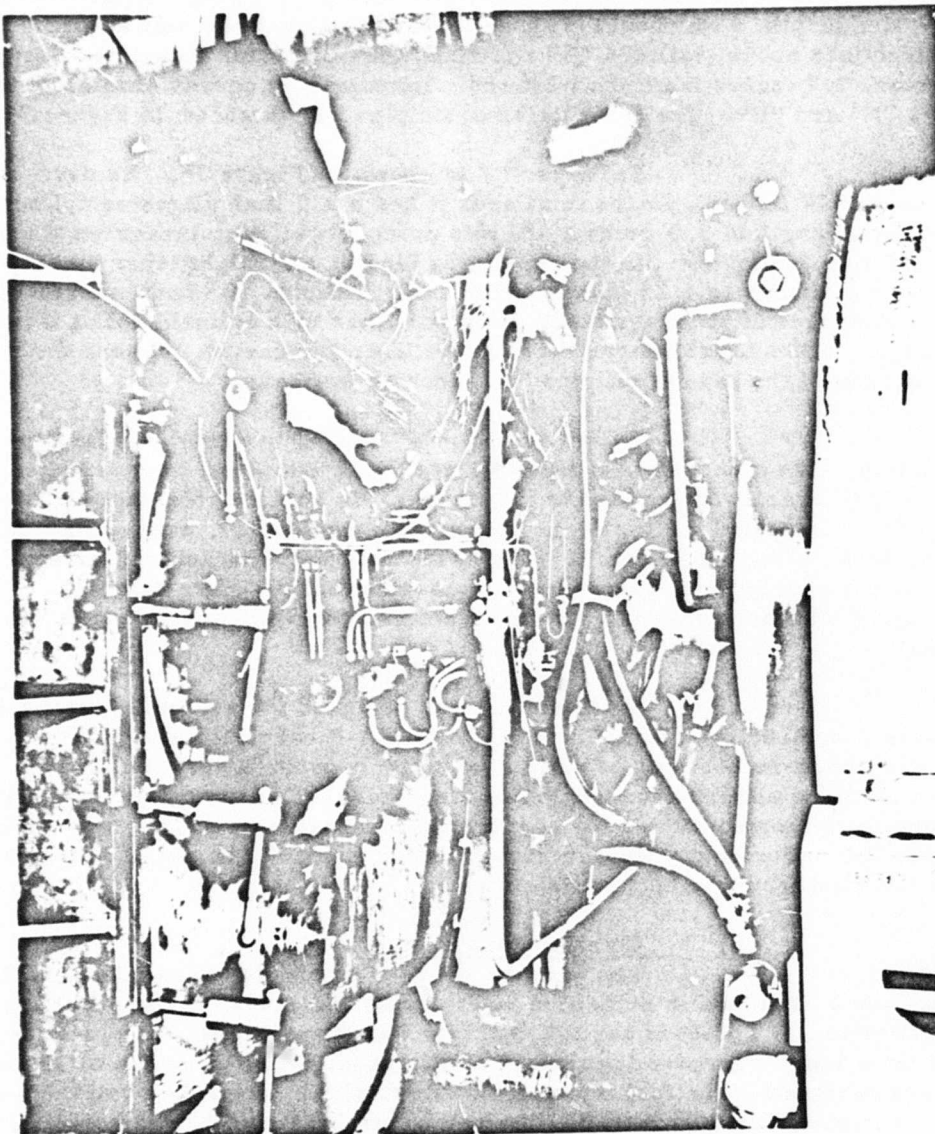


Figure 74 - Combustor Model Installation.

**CONFIDENTIAL**

**CONFIDENTIAL**

Tailpipe "Q" is shown in Figure 73. Its length was 33 inches. It had a 3.0 inch diameter bore at the inlet, and a 4.75 inch diameter bore at the exit. Its internal contour was a straight taper over nearly its entire length, with short (.75 inch long) cylindrical sections at either end. As explained above, tailpipe "Q" contained provisions for mounting "F-type" injectors 3.7 inches from the inlet end. Its construction was similar to tailpipes "N" and "P". The installation of tailpipe "Q" is shown in Figure 75.

Tailpipe "R" is shown in Figure 76. Its over-all length was 27 inches. At the inlet end, it had a 3.0 inch diameter cylindrical bore for a length of 3.0 inches. At this point, a wall step increased the base diameter to 3.5 inches. In the remaining length, a straight taper increased the bore diameter to 4.25 inches at the exit. Tailpipe "R" had an outer casing and end flanges of stainless steel, a copper liner with helical cooling water passages, and a brass spacer between the liner and casing. Figure 77 is a photograph of the base of tailpipe "R", looking upstream.

Tailpipes "N", "P" and "Q" were of welded construction. The monel flanges were welded to the stainless steel casings, and the copper liners were welded to the flanges. In service, thermal expansion resulted in repeated flexing of the copper-to-monel welds, producing troublesome water leaks. Tailpipe "R" was assembled with mechanical fasteners and o-ring seals, which allowed some movement of the liner within the casing. While more expensive to manufacture, this part was free of water leaks.

Tailpipe "E" was designed for use in heat transfer studies described in Volume III of this report. It consisted of a 3.06 inch ID cylinder 18 inches long, constructed entirely of stainless steel and designed to be either water-cooled or air-cooled. The base was heavily instrumented with thermocouples for heat transfer measurements. It is included in this list of combustor apparatus because some useful combustion information was obtained from the heat transfer tests.

#### d) Combinations Tested

The various items of combustor hardware described above were combined in numerous ways during the course of the experimental investigations. The code used to describe an individual test configuration consists of a letter representing the air nozzle used, followed by one or more letters designating the fuel injector(s), and finally a letter denoting the tailpipe. For example: Configuration BHN contained air nozzle "B", injector "H", injector "E" used only as a transition piece between the cylindrical injector and the larger tailpipe, and tailpipe "N". No fuel was injected from injector "E" when used as a transition piece. Configuration AGFQ contained air

**CONFIDENTIAL**

**CONFIDENTIAL**

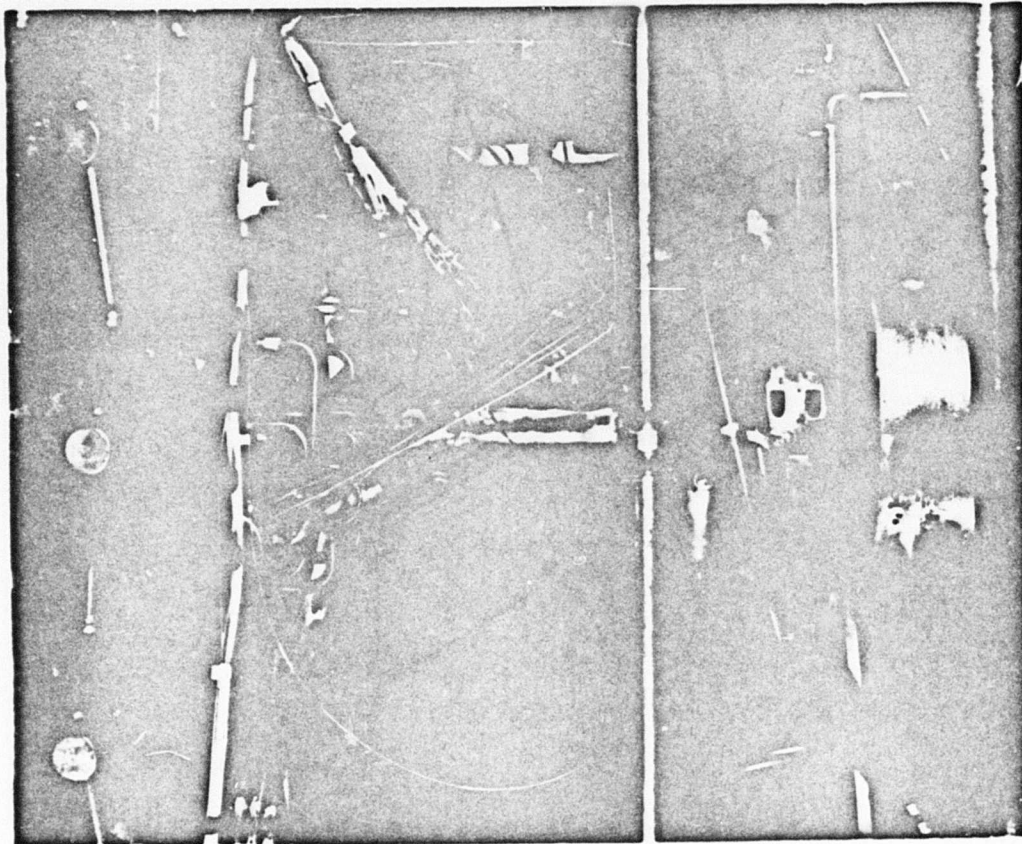


Figure 75 - Combustor Model Installation.

**CONFIDENTIAL**

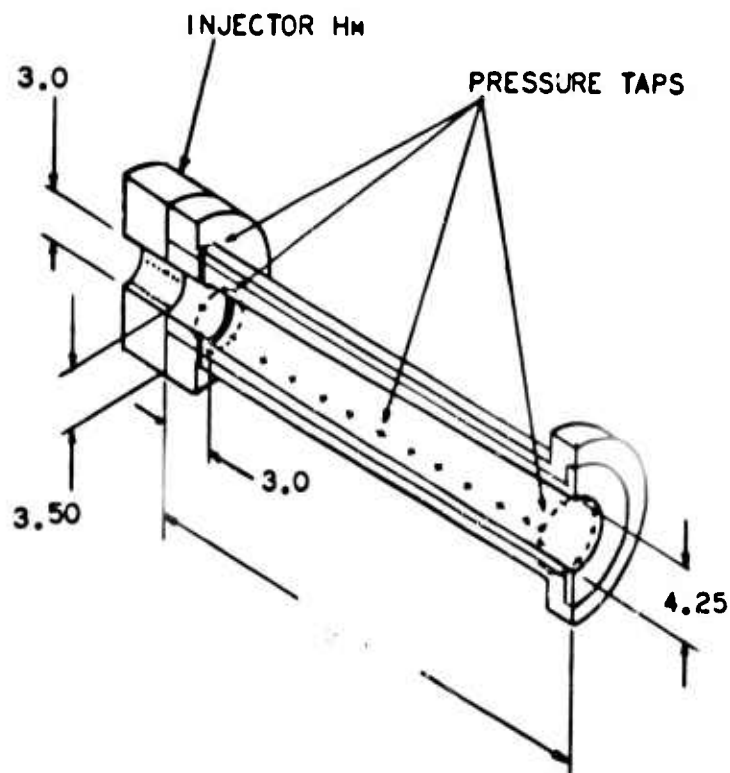
**CONFIDENTIAL**

Figure 76 - Tailpipe E (Schematic).

**CONFIDENTIAL**

**CONFIDENTIAL**

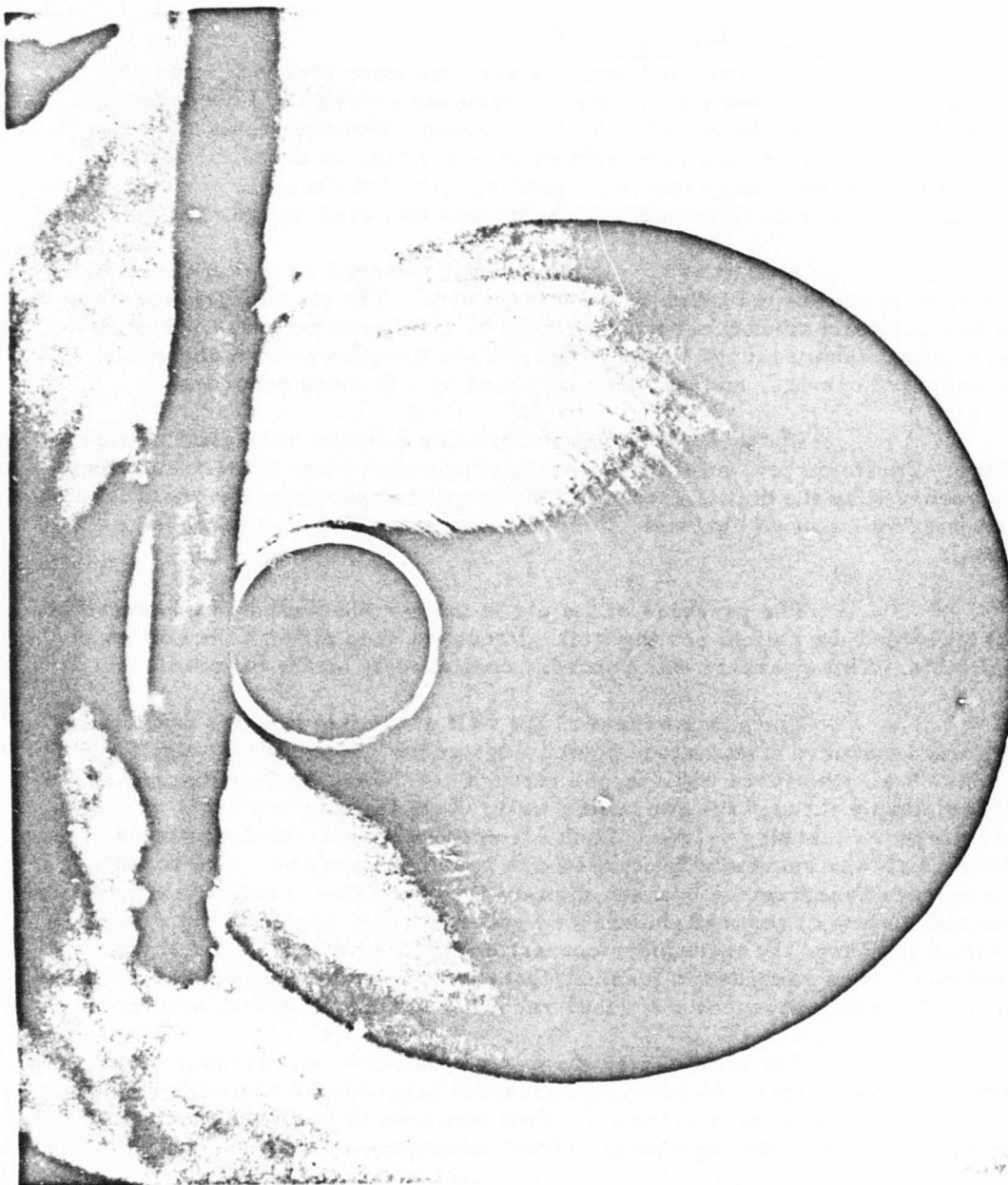


Figure 77 - Tailpipe R - Aft Looking Forward.

**CONFIDENTIAL**

**CONFIDENTIAL**

nozzle "A", injector "G" and tailpipe "Q" with its integral "F-type" injectors. Both injectors were active.

### 3) Measurements

Pressure and temperature data were recorded in one of two ways. Measurements requiring a continuous record were recorded by two eight-channel Sanborn strip-chart recorders. Measurements requiring only intermittent sampling were printed on paper tape by a digital recorder. The digital recorder was capable of handling up to 600 channels of data. Its normal sampling rate for combustion tests was five readings per second.

Airflow to the combustor was metered by a pair of critical-flow venturi meters fed from a common plenum. The plenum pressure was fed to a pressure transducer and recorded by a Sanborn recorder. The air temperature was measured in the vicinity of the flowmeters by a chromel-alumel thermocouple, and was also recorded by a Sanborn recorder.

Hydrogen flow was metered by a Daniel thin-plate orifice meter. Upstream pressure and differential pressure were fed to transducers and recorded by the digital recorder. Hydrogen temperature was measured near the meter by a capped chromel-alumel thermocouple and also recorded on the digital.

The pressure of the air in the arc chamber was measured at a point behind the helical cooling coil. Pressure drop through the coil was negligible. This pressure was recorded continuously on the Sanborn.

The gas pressure at the wall of the fuel injector and mixing pipe was measured at numerous points, located as indicated in Figure 67, 73 and 76. Wall pressures were tapped through a 0.04 or .06 inch diameter hole drilled cleanly through the combustor wall. Each tap was connected to one of four pressure scanning valves. Each scanning valve contained a pressure transducer which was sequentially connected to each pressure tap. The scanning valves were synchronized with the digital recorder. In operation, the pressure indicated by one of the transducers was recorded, then the scanning valve was actuated to change the transducer connection to the next tap. Each of the four transducers was recorded in turn, so that the cycle was repeated 0.8 seconds later. The wall pressures were thus recorded at the rate of five per second.

For some tests, six to eight selected wall pressure taps were connected directly to individual pressure transducers and were recorded continuously on a Sanborn recorder. This was done to facilitate monitoring of combustor behavior during changes in test conditions.

**CONFIDENTIAL**

**CONFIDENTIAL**

Heat loss to the water-cooled combustor walls was derived from measurements of cooling water flow and temperature rise. Water flow was measured by a thin plate orifice meter. The differential pressure was recorded on the digital. Water temperatures were measured by chromel-alumel thermocouples at the inlet and discharge, and were recorded on the digital.

The combustor exit stream was surveyed by the gas sampling and impact pressure rake illustrated in Figure 78. The rake was 0.33 inches wide, and had a wedge-shaped, sharp leading edge with a 35 degree included angle. The leading edge was constructed of copper, and was water-cooled. Measurements were obtained through six holes 0.04 inches in diameter spaced 0.5 inches apart along the apex of the wedge. The rake was oriented vertically in the burner exit stream, with the leading edge approximately 0.6 inches aft of the exit plane. A remote-controlled actuating mechanism swung the rake laterally to one of four preset locations in the stream or to a fifth location outside the stream.

Connection to the measuring ports of the rake was made initially through about 5 inches of 0.04 inch ID copper tubing, followed by 38 inches of stainless steel tubing of similar size within the water-cooled body of the rake, and finally through larger diameter tubing leading out of the test rig. A system of solenoid valves permitted each of the six ports to be connected to a pressure scanning valve to record the impact pressure, or selectively to one of four gas sampling bottles. A total of 24 gas samples could be obtained during each test. This system is illustrated in Figure 79.

The procedure for gas sampling, at a preset rake position, was to first purge the sample lines. This was accomplished by opening solenoid valves on both sides of the selected set of sample bottles to allow gas to be drawn through the lines and bottles by a vacuum pump for 20 seconds. The downstream valves were then closed and the bottles allowed to fill for 10 seconds, after which the upstream valves were closed to isolate the samples.

Closing the upstream valves connected the rake ports to the pressure scanning valves. When the pressure had been recorded, the rake was moved to another position and the procedure repeated.

Following a test, the bottled gas samples were removed to a laboratory and analyzed quantitatively for hydrogen, oxygen, nitrogen and nitric oxide on a dry basis by gas chromatography, and for nitrogen dioxide by wet chemistry. The latter technique was to react the sample with sulfanilic acid and measure the color change of the liquid.

**CONFIDENTIAL**

**CONFIDENTIAL**

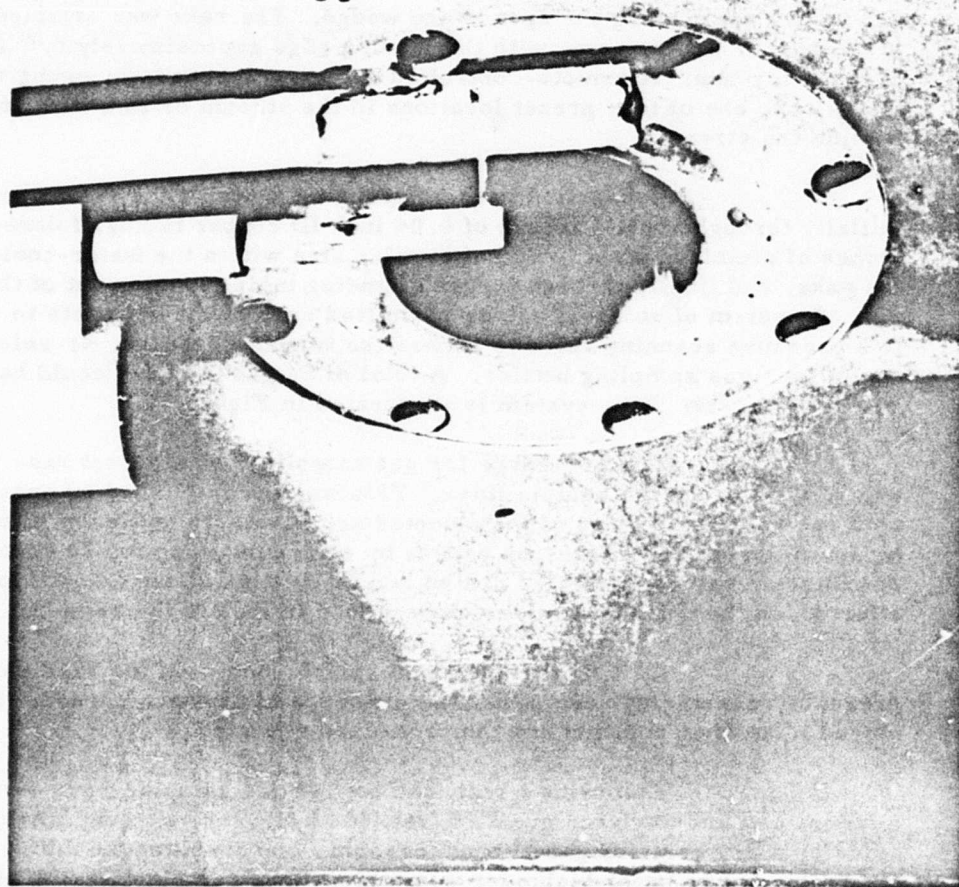


Figure 78 - Combustor Exit Rake.

**CONFIDENTIAL**

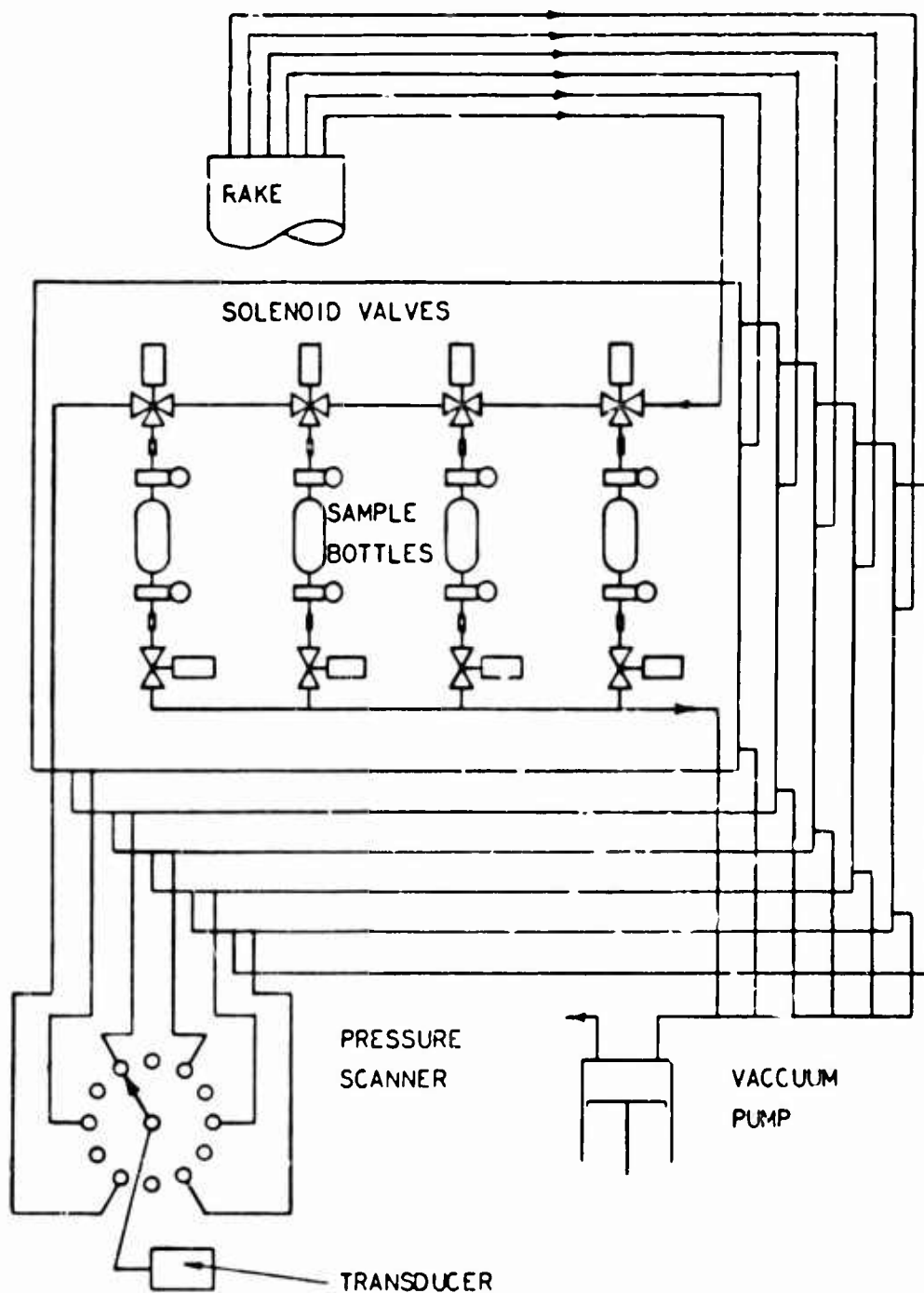
**CONFIDENTIAL**

Figure 79 - Gas Sampling System (Schematic).

**CONFIDENTIAL**

**CONFIDENTIAL**

A special rake was designed to permit the sample to be expanded quickly to a very low pressure before cooling. Rubins and Rhodes (Reference 16), used such a probe and successfully obtained samples from a supersonic combustion zone which had combustion efficiencies throughout the range from 0 to 100%, with the efficiency increasing as length increased in the experimental combustion zone. Although these measured combustion efficiencies could not be quantitatively verified, the qualitative results were very encouraging.

By cooling or quenching the samples at the low pressures in the probe, the reaction rates of the three-body heat-releasing reactions are suppressed in comparison with the faster two-body reactions. It is postulated that the radicals H, O and OH are converted to stable molecules by these fast two-body reactions, which release or absorb very little heat.

Figure 80 shows the dimensions of this quick-quench probe. The samples from this probe were drawn into large (1 to 1.5 liters) evacuated samples bottles. The collected samples at less than 1 psia pressure, were then analyzed with the chromatograph.

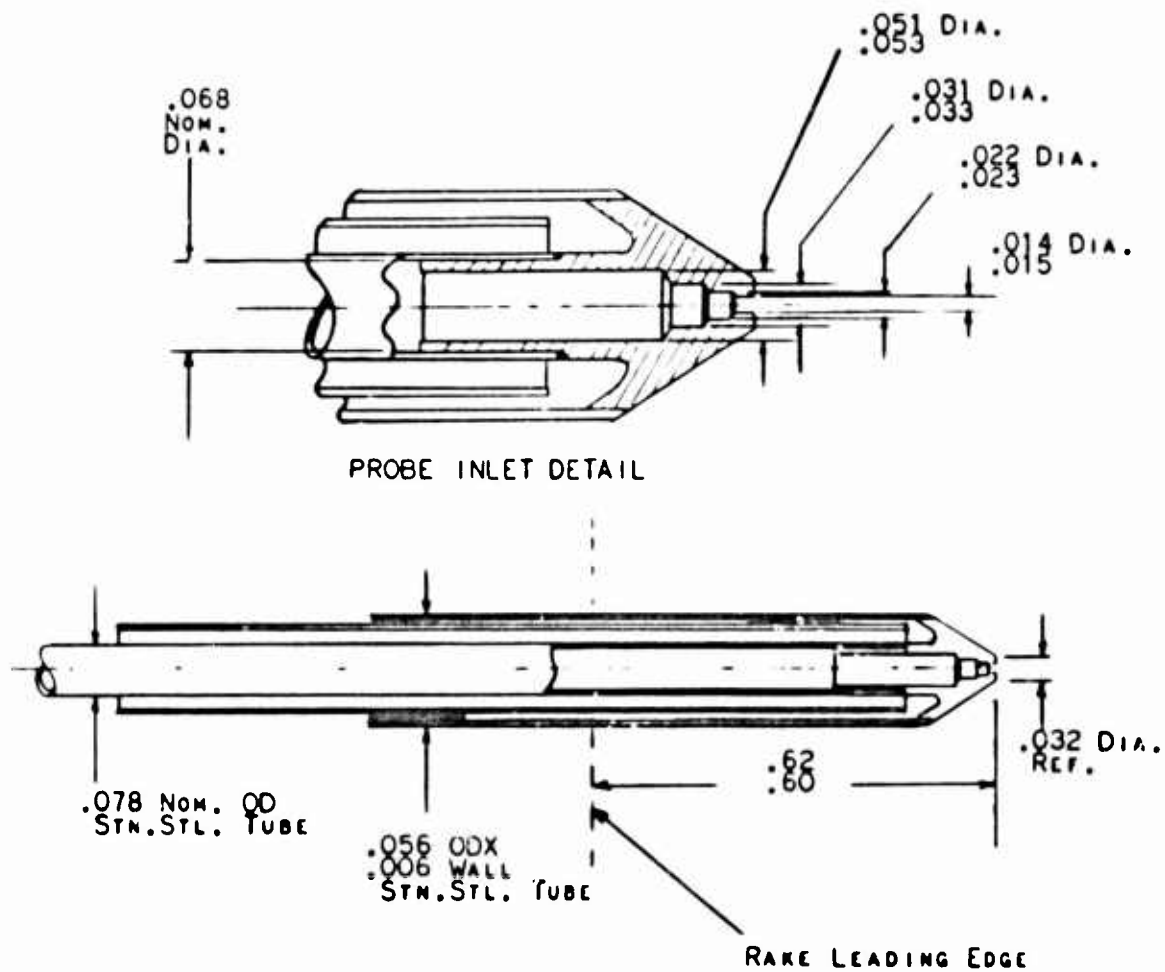
In addition to the rake survey of the burner exit stream, a traversing line reversal pyrometer was also employed. This instrument is fully described in Reference 17. The sensing device was mounted on the same traversing mechanism which held the rake, and measured an average stream static temperature along a path parallel to the rake, 1.75 inches from the rake and 1.2 inches from the burner exit plane.

#### 4) Data Analysis Procedures

##### a) Types of Data

For the tests reported herein, two different types of data were taken. Pressure and temperature data from Sanborn charts and digital tapes were transposed into tabular form as part of the test operation. This transposition operation also included the conversion of thermocouple readings from millivolts to degrees F or degrees R, and the conversion of pressure transducer readings into psi or psia. Pressure and temperature data were comprised of static pressure measurements within the arc chamber, along the length of the combustor, and in the test chamber section, measurements of the pressures and temperatures of the air, hydrogen and cooling water flows, gas sample rake impact pressure and the dump chamber wall temperature and arc power measurements. In all, pressure and temperature data comprised approximately eighty measurements per reading, with each reading corresponding to one set of six gas samples.

**CONFIDENTIAL**

**CONFIDENTIAL**

CONSTRUCTION OF SINGLE ELEMENT OF SIX-ELEMENT RAKE

Figure 80 - Quench Probe Details.

**CONFIDENTIAL**

**CONFIDENTIAL**

Gas samples taken with the gas sample rake located 0.6 inches aft of the combustor exit plane formed the second distinct series of measurements that were taken during an arc tunnel test. Normally twenty-four individual samples were taken at known locations in the exit stream. The gas sampling positions were altered occasionally during the course of the experimental program. The locations of the sampling positions for the various test runs are charted in Figures 81, 82, 83, 84, 85 and 86.

For Run 154 and all succeeding tests, the gas samples were first analyzed for  $\text{NO}_2$  by wet chemistry. In this procedure, the bottle containing the gas sample was connected to a second bottle containing a liquid reagent which would change color upon reacting with  $\text{NO}_2$ . The amount of liquid in the two bottles was adjusted until the pressure was atmospheric and the displaced liquid measured to determine the quantity of gas present. The color intensity of the liquid was then measured to determine the amount of  $\text{NO}_2$  originally present in the gas sample.

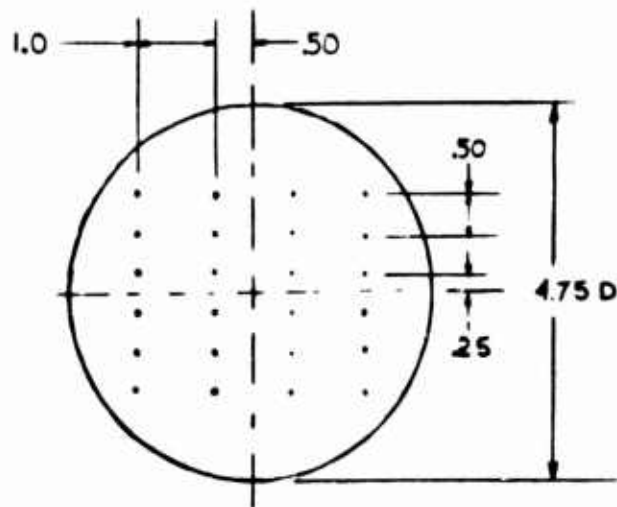
Next, all the gas samples were analyzed for  $\text{O}_2$ ,  $\text{H}_2$ ,  $\text{N}_2$  and  $\text{NO}$  by means of gas chromatography. In this operation the concentration of each of these three constituents in the sample was determined through use of a thermal conductivity cell after the sample had been passed through a molecular sieve. In addition to the sieve, which was used to separate the constituents sufficiently to allow the thermal conductivity cell to react to each individually, the sample was also passed through a cold trap to freeze out whatever water exists in the same before it entered the fractionating column. The result of this procedure was a set of curves of the response of the cell to each sample from which the concentration was determined in a manner described below. In addition to traces corresponding to each gas sample, calibrating mixtures were run through the chromatograph before and after each set of twelve gas samples to provide a consistent sensitivity determination.

b) Initial Data Reduction

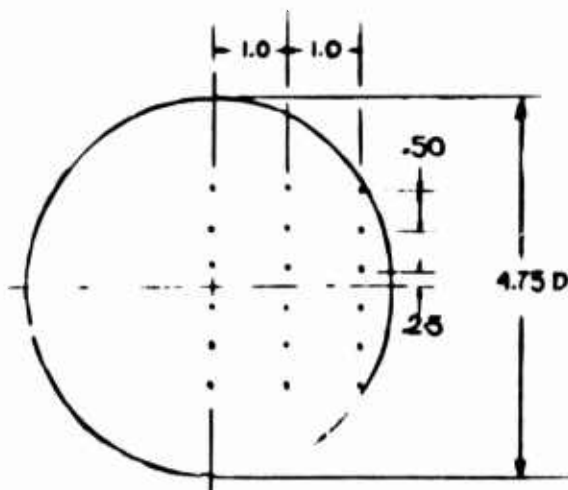
The analysis of the data obtained from an arc tunnel combustion test was a complex process which required the use of high-speed computers. Four separate computer programs, were written for use in the data analysis and were used in the reduction of the data from the tests that are the subject of this report. However, before the computer program could be used a certain amount of hand analysis of the data was both necessary and desirable.

From the pressure and temperature data, the input air and fuel flows were calculated, as well as the over-all equivalence ratio and the approximate air enthalpy, from which the simulated flight Mach number of the tests was determined. The approximate air enthalpy is obtained from a relation developed in NASA TN D 2132 (Reference 18) suitably modified to fit the relatively narrow range of conditions encountered in these tests. The NASA relation, suitable over a wide variety of conditions, is

**CONFIDENTIAL**

**CONFIDENTIAL**

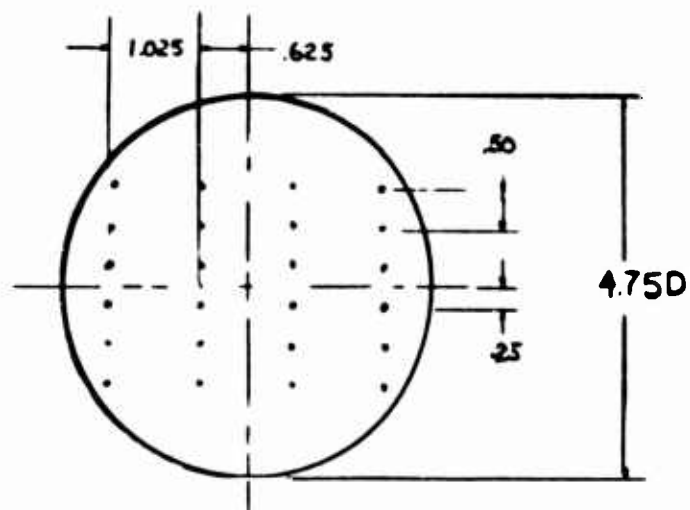
PROBE LOCATIONS FOR RUNS 104-110  
AND FOR RUNS 117-129



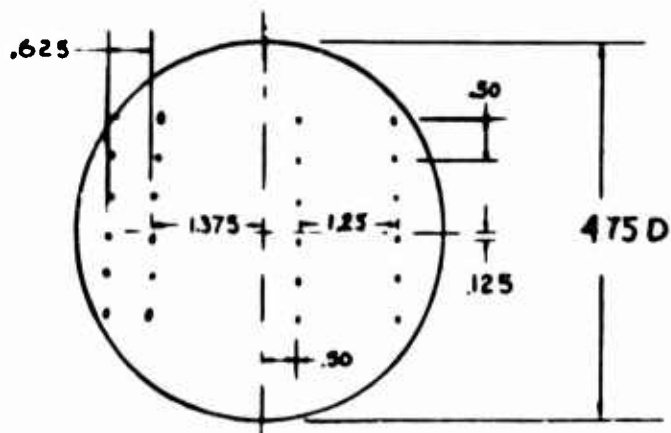
PROBE LOCATIONS FOR RUN 111

Figure 81 - Gas Sample Probe Locations.

**CONFIDENTIAL**

**CONFIDENTIAL**

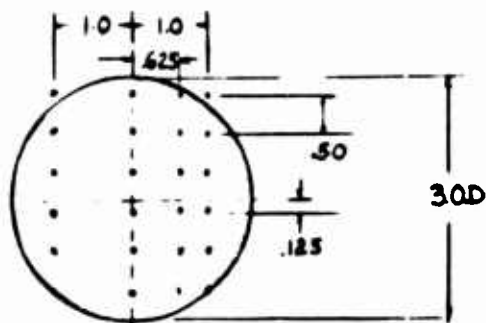
PROBE LOCATIONS FOR RUNS 154-160



PROBE LOCATIONS FOR RUNS 163-198

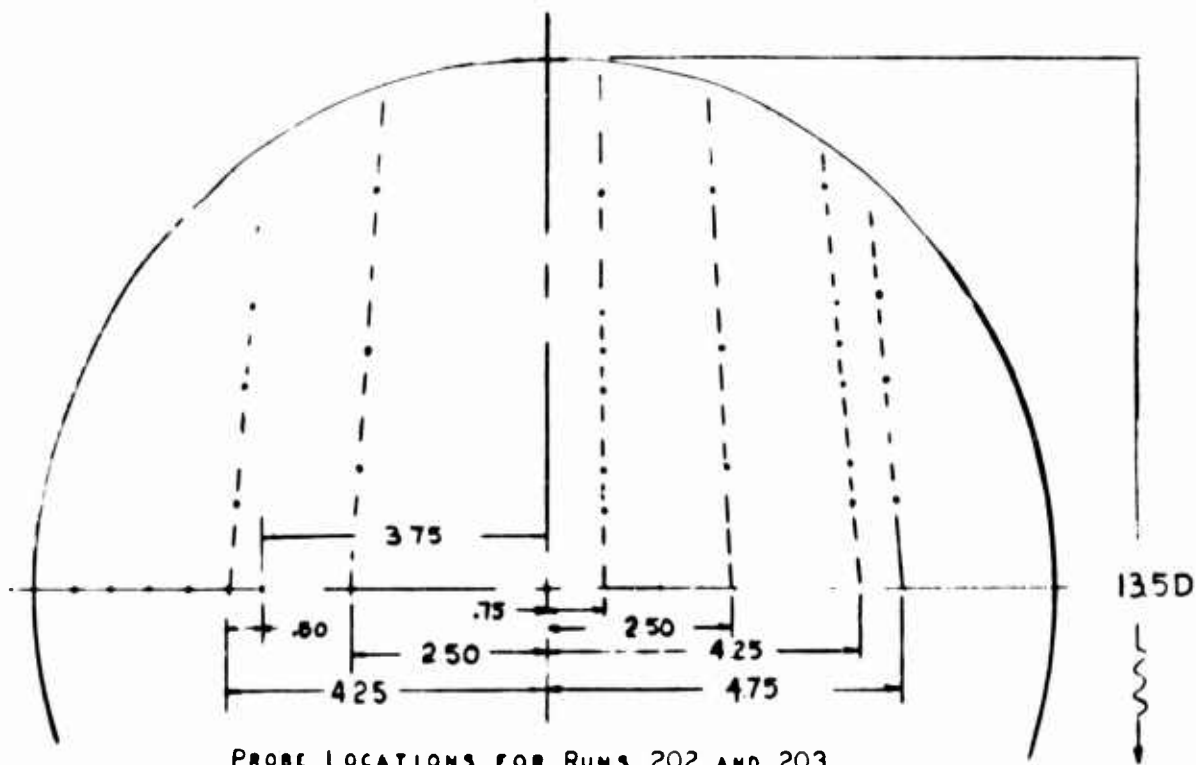
Figure 82 - Gas Sample Probe Locations.

**CONFIDENTIAL**

**CONFIDENTIAL**

PROBE LOCATIONS FOR RUNS 198-201

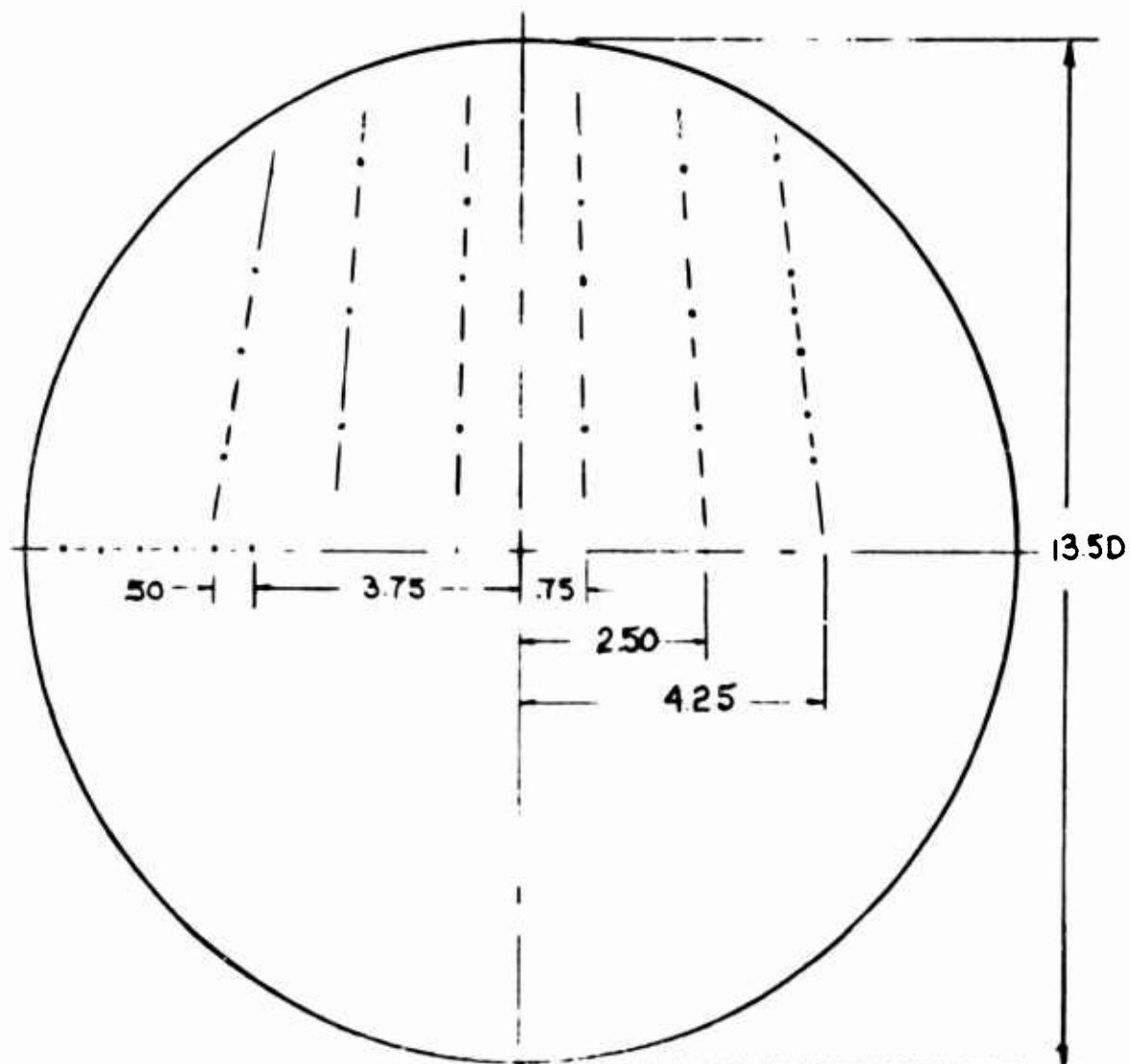
NOTE: RUNS 198 AND 201 USED ONLY  
CENTERLINE PROBE



PROBE LOCATIONS FOR RUNS 202 AND 203

Figure 83 - Gas Sample Probe Locations.

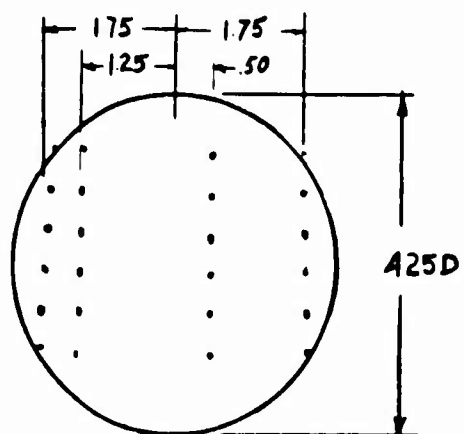
**CONFIDENTIAL**

**CONFIDENTIAL**

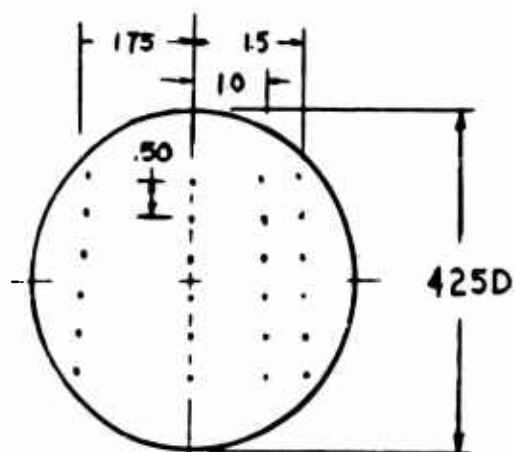
PROBE LOCATION FOR RUNS 203-205

Figure 84 - Gas Sample Probe Locations.

**CONFIDENTIAL**

**CONFIDENTIAL**

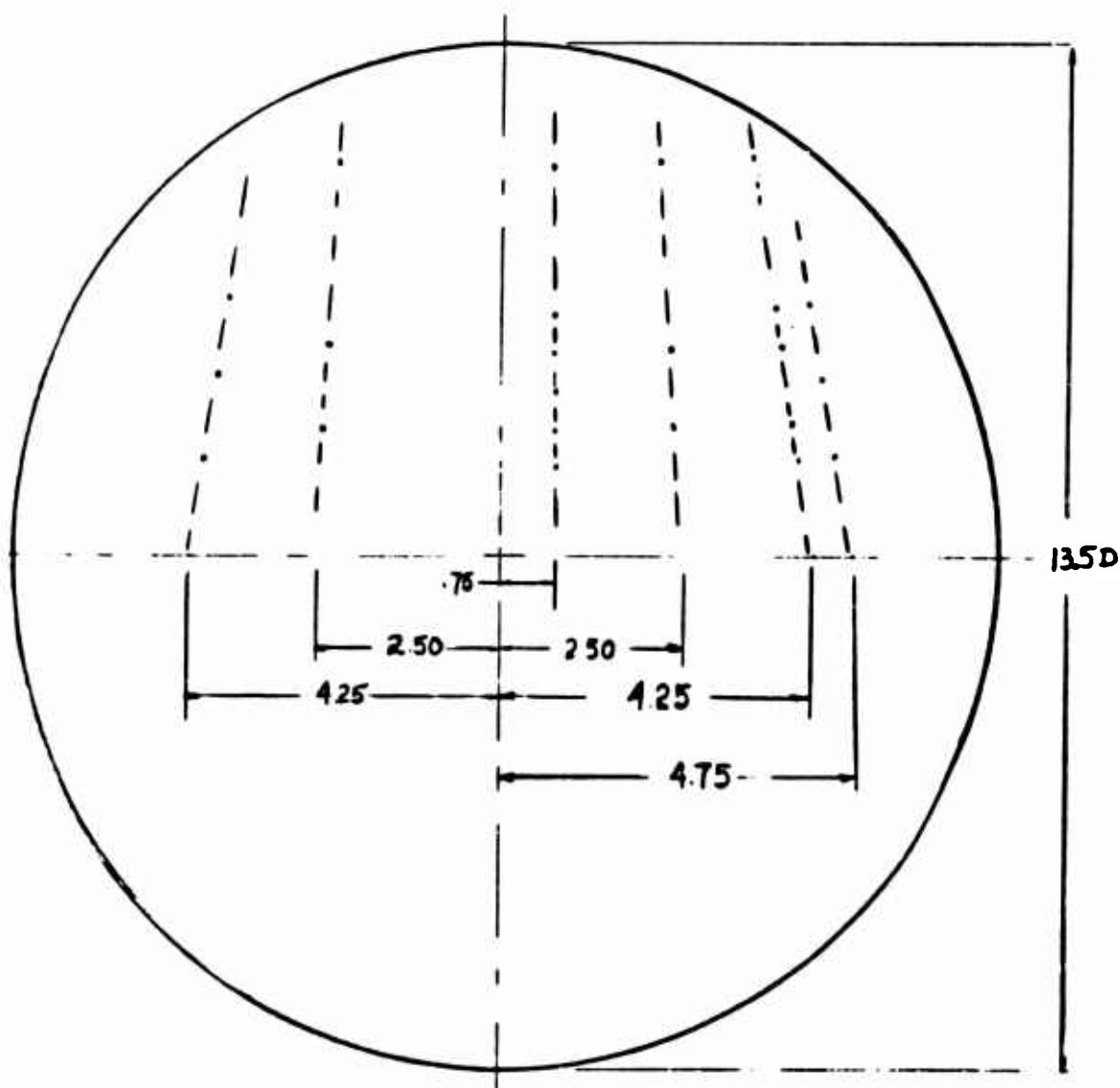
PROBE LOCATIONS FOR RUNS 206 AND 207



PROBE LOCATION FOR RUNS 208-212

Figure 85 - Gas Sample Probe Location.

**CONFIDENTIAL**

**CONFIDENTIAL**

PROBE LOCATIONS FOR RUNS 213-216

Figure 86 - Gas Sample Probe Locations.

**CONFIDENTIAL**

**CONFIDENTIAL**

$$\frac{W}{A \cdot P_t} = \frac{280}{h_t \cdot 397}$$

where W is the airflow rate in pps, A\* the nozzle throat area in square feet,  $P_t$  the air stagnation pressure in atmospheres and  $h_t$  is the air enthalpy, Btu/lbm. For the conditions of these tests, it was found that a more accurate representation is given by:

$$\frac{W}{A \cdot P_t} = \frac{425}{h_t \cdot 457} \text{ for nozzle "A" and } \frac{W}{A \cdot P_t} = \frac{388}{h_t \cdot 444} \text{ for nozzle "B"}$$

Further, the static pressure distribution along the length of the combustor was plotted directly from data supplied by the digital recorder.

In the gas sample analysis, point equivalence ratios and mole fractions of each sample point were hand-calculated directly from the gas analysis output sheets and charts. As mentioned above, before each set of twelve gas samples was run through the chromatograph, a calibration mixture of hydrogen, oxygen and nitrogen of known composition and total pressure was tested, and the output of the thermal-conductivity cell recorded. Since the composition and total pressure of the mixture was known, the partial pressure of each component was known, and from this and the peak output of the thermal conductivity cell, the "sensitivity" of the cell to each component was determined. The "sensitivity" was expressed as mm (partial pressure) / div (T. C. C. output) and was determined for several different mixture total pressures. The resulting data were used to develop sensitivity curves which were then used in analysis of the test samples. Since the calibrating mixture used contained less hydrogen than the average sample, a special pure hydrogen calibration was made for an additional sensitivity determination. Figure 87, 88 and 89 present sample sensitivity curves developed from test data from Run 110.

In the actual sample analysis, the contents of each sample bottle at a known pressure were passed through the chromatograph. Each constituent of a given sample produced a specific output of the thermal conductivity cell, which was recorded on a chart. Ideally, the cell output for each component would be a discrete curve, as shown schematically in Figure 90a, but due to the finite response time of the cell and the manner of separation of the components the output was recorded as a smooth curve. This curve shown schematically in Figure 90b. The peak of this curve and the sensitivity determined the partial pressure and thus the concentration of the component being analyzed. In rich samples a further determination was made before the actual peak output of the cell could be measured. This determination was made necessary by the fact that, with a large amount of hydrogen present in the sample, some hydrogen back-diffused through the molecular sieve resulting in the peaks for the oxygen and nitrogen curves falling on the tail of the hydrogen

**CONFIDENTIAL**

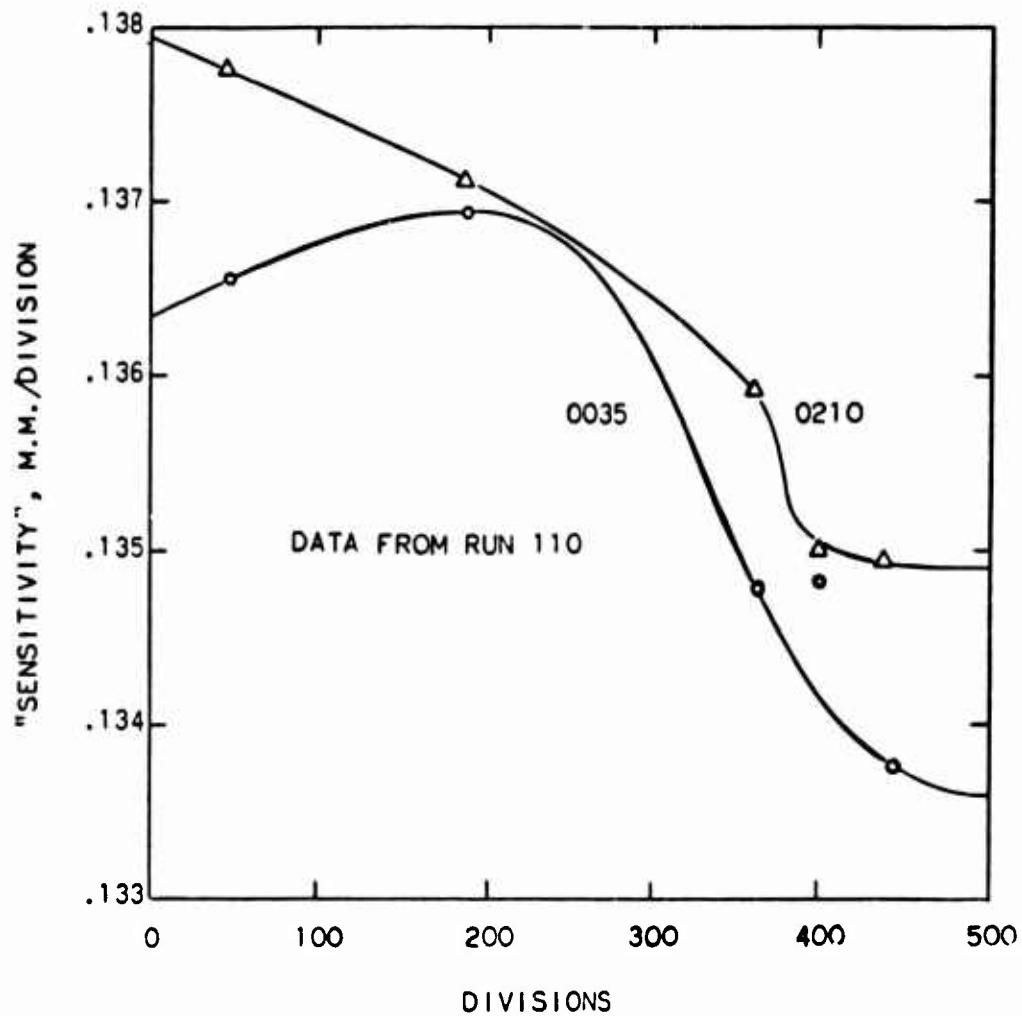
**CONFIDENTIAL**

Figure 87 - Typical Chromatograph Calibration for Oxygen.

**CONFIDENTIAL**

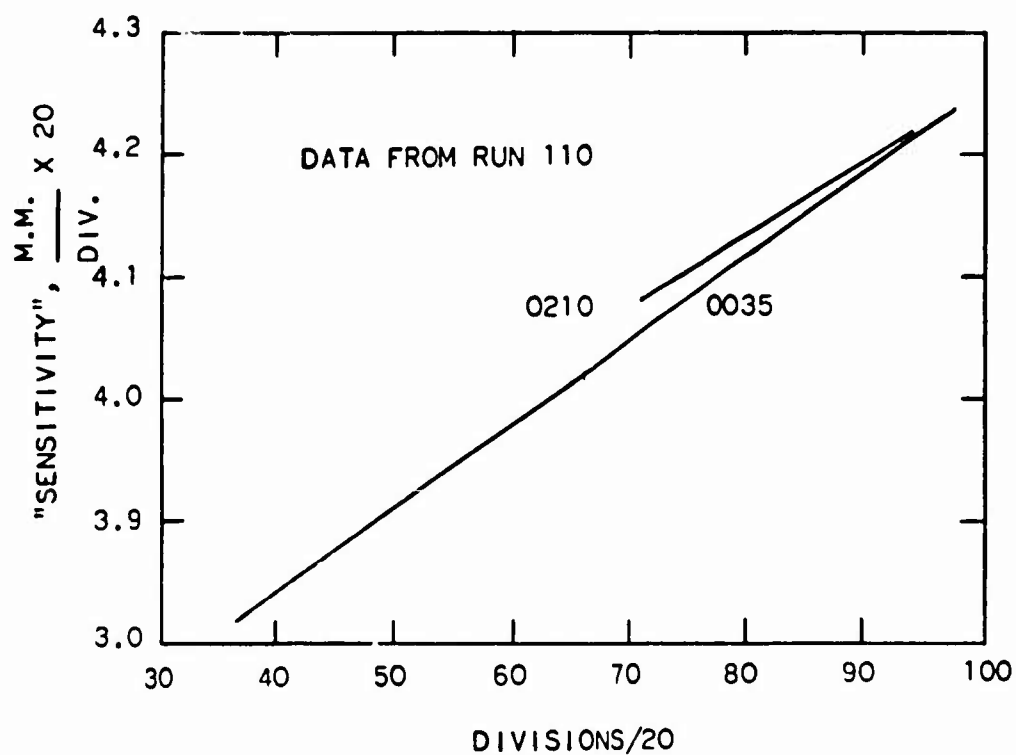
**CONFIDENTIAL**

Figure 88 - Typical Chromatograph Calibration for Nitrogen.

**CONFIDENTIAL**

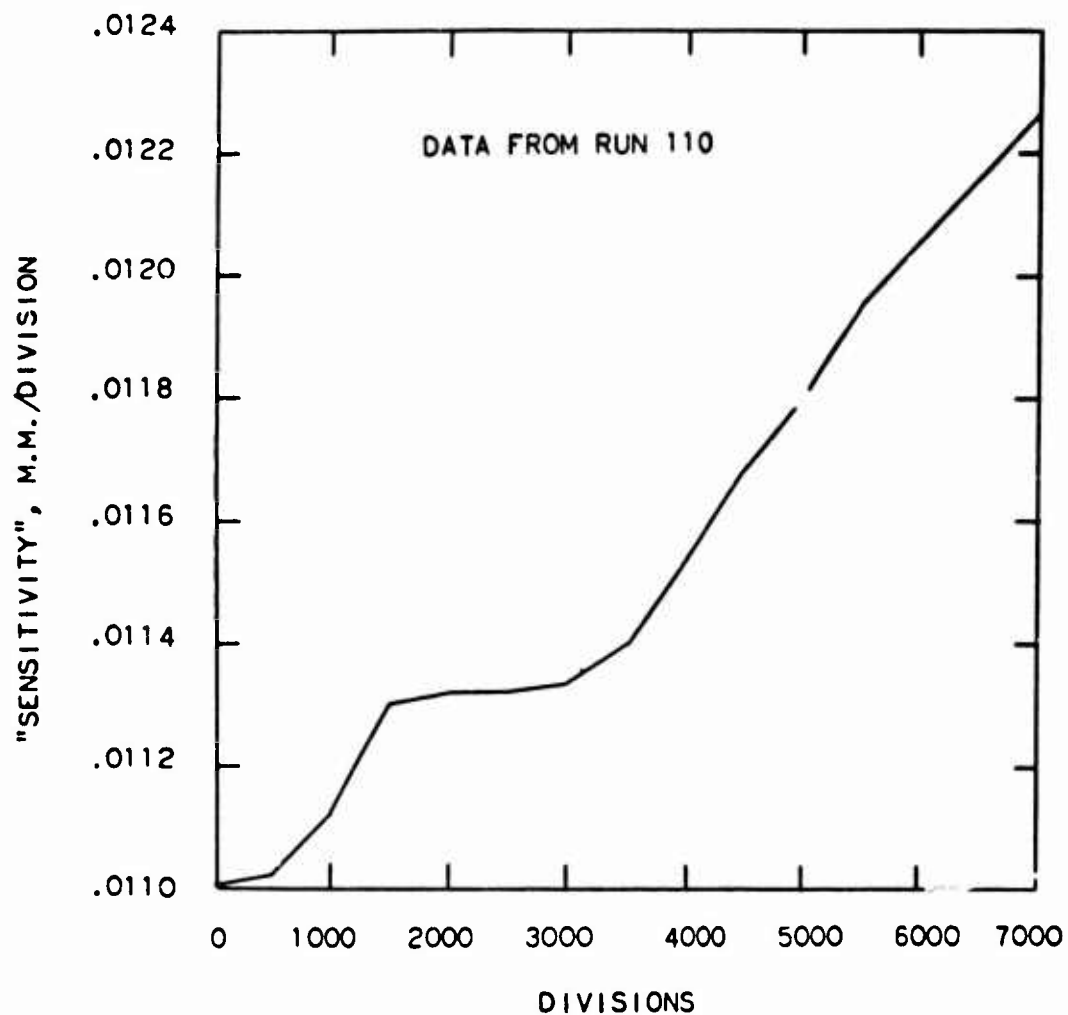
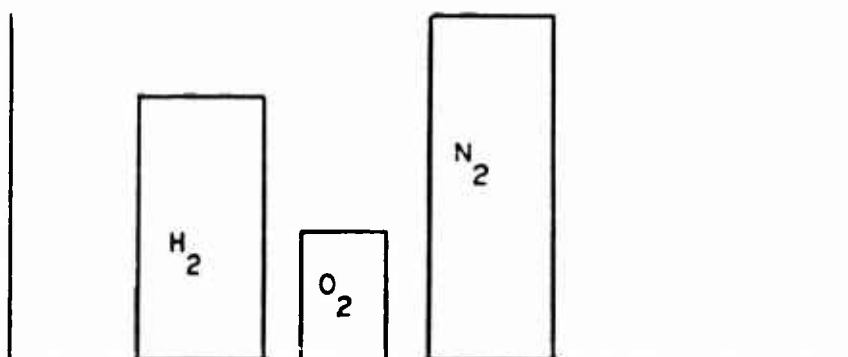
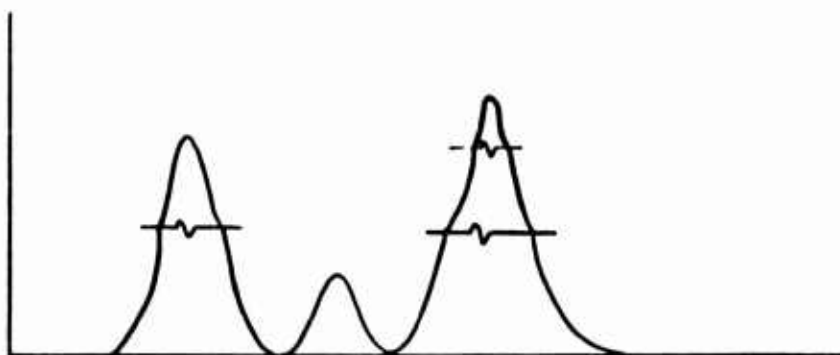
**CONFIDENTIAL**

Figure 89 - Typical Chromatograph Calibration for Hydrogen.

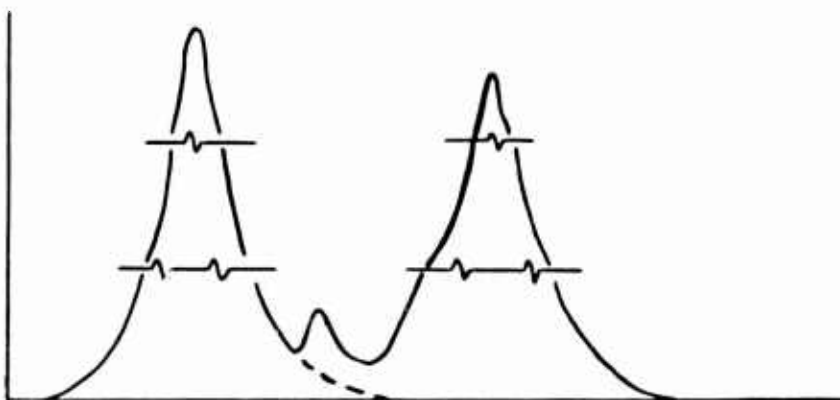
**CONFIDENTIAL**

**CONFIDENTIAL**

A. IDEAL CHROMATOGRAM



B. ACTUAL CHROMATOGRAM-LEAN SAMPLES



C. ACTUAL CHROMATOGRAM-RICH SAMPLES

Figure 90 - Schematic Chromatograms.

**CONFIDENTIAL**

**CONFIDENTIAL**

curve, as shown in Figure 90c. A systematic correction was developed and used in this test series to allow for this possibility in rich samples. This involved determining the time taken for the hydrogen trace to return to the zero of the recording chart using the hydrogen sensitivity curves. The result of these calculations expressed as hydrogen-curve trace height/peak height was plotted vs. time and used as a systematic correction for the apparent peak heights of the oxygen and nitrogen traces. A sample curve is shown on Figure 91.

Once the actual peak heights of all constituents were known, the concentration of hydrogen, oxygen, nitrogen in each sample was determined and thus the point equivalence ratio. The expression used to obtain the point equivalence ratio, given the mole fraction of hydrogen, oxygen and nitrogen after decomposing any NO or NO<sub>2</sub> present is:

$$ER = 1 + 1.8638 \text{ M.f. H}_2 - 2 (\text{M.f. O}_2) / \text{m.f. N}_2$$

The derivation of this expression is given in Colley and Kenworthy (Reference 2) report. This process was repeated for each sample point, and the result plotted as an exit equivalence ratio profile.

As an aid to the clarification of the above discussion, a sample calculation is given below. Selecting data point 5 from Run 110, the following data were available from the chromatograph output chart and data sheet:

Sample pressure	= 420 mm
H <sub>2</sub> divisions	= 837.5
O <sub>2</sub> divisions	= 59.6
N <sub>2</sub> divisions	= 1860
NO divisions	= 0

The latter four pieces of data are the peak heights, uncorrected, of the traces of H<sub>2</sub>, O<sub>2</sub>, N<sub>2</sub> and NO for data point 5 appearing on the chromatograph chart. The absence of NO is normal for a sample containing O<sub>2</sub>, as NO oxidizes spontaneously at room temperature to form NO<sub>2</sub>. Measurable quantities of NO were found only in samples containing no O<sub>2</sub>. From calibrating mixtures, the sensitivity of the chromatograph to these three components was determined and is given as Figures 87, 88 and 89. Since calibration for oxygen and nitrogen was made before each set of 12 samples, two curves appear on the sensitivity figures for each of these components. From the data sheet

**CONFIDENTIAL**

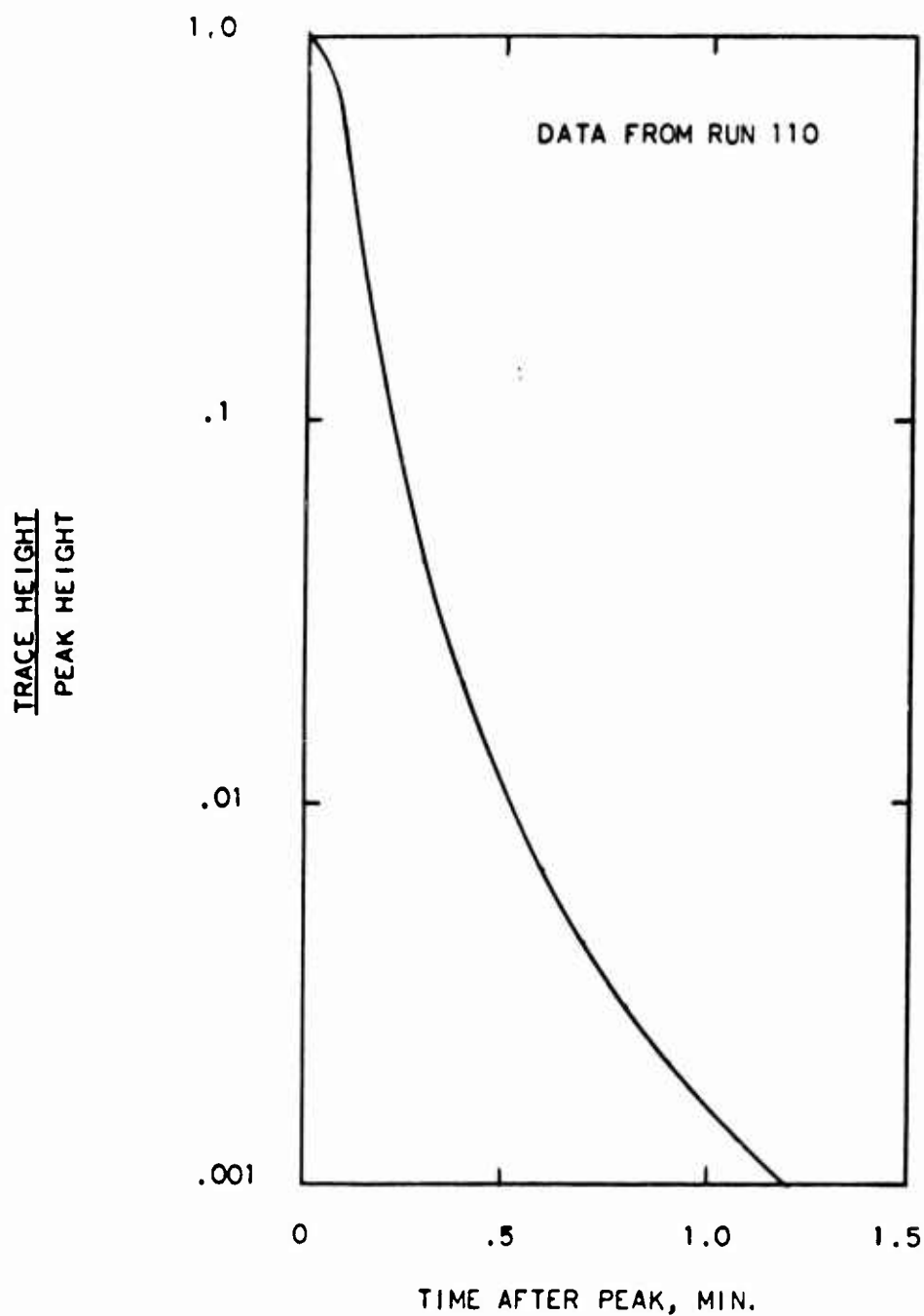
**CONFIDENTIAL**

Figure 91 - Hydrogen Trace Tail Correction.

**CONFIDENTIAL**

**CONFIDENTIAL**

included with the chromatograph output, it was known that the curves labeled 0035 are the ones that correspond to data point 5.

From Figure 89, the sensitivity for  $H_2$  at 837.5 division was found to be .01108. Multiplying the peak height of the trace by the sensitivity and dividing by the total pressure gave the mole fraction of hydrogen in the sample:

$$\frac{837.5 \times .01108}{420} = .02209$$

The apparent height of the  $O_2$  trace was given by the data as 59.6 divisions. From the chromatograph chart, it was found that the time lag between the hydrogen peak and the oxygen peak was 0.53 minutes. From the previously determined hydrogen tail curve, Figure 91, the  $H_2$  tail height at this  $\Delta t$  was 8.38 division, thus the actual oxygen peak height was 51.22 divisions, and from Figure 87, the sensitivity at this point was .13769 mm/div. Thus the mole fraction of  $O_2$  in the sample was given by

$$\frac{51.22 \times .13769}{420} = .01679$$

Determination of the mole fraction of nitrogen in the sample was exactly the same as for oxygen. In this case  $t = 0.86$  min., the hydrogen tail height was 2.09 div., and thus the actual nitrogen peak height was 1857.9 div. Using Figure 88, the sensitivity was found to be 0.21035. Thus, the mole fraction of  $N_2$  in the sample was:

$$\frac{1857.9 \times .21035}{420} = .93054$$

With the mole fraction known, the equivalence ratio was determined as:

$$ER = 1 + 1.8638 \left\{ \left[ .02209 - 2 (.01679) \right] / .93054 \right\} = 0.977$$

and the initial gas analysis for point 5 was complete.

c) Computed Data

The first use of computer programs in the data reduction procedure involved use of program SSCPAI (see Appendix A). This program was used to compute the input air and fuel flows and conditions, and by assuming an ideal combustion process, to compute an ideal burner nozzle thrust.

**CONFIDENTIAL**

**CONFIDENTIAL**

Input data for this program were taken from the pressure and temperature data section of the test output, and from the hand calculated input parameters discussed above. Given the air and fuel plenum conditions and flows, SSCPAI computed flow parameters such as Mach number, impulse, temperature, pressure molecular weight, etc., at the burner inlet plane for air and fuel and for combined inputs at the burner inlet plane. This was accomplished in the program, given plenum conditions, by computing equilibrium isentropic expansions through area ratios that corresponded to the actual physical air and fuel nozzles.

Since the air and fuel enthalpies are known only approximately from the raw data, it was desirable to obtain more exact values through iteration of the program. This was possible because SSCPAI, given the approximate enthalpy for the air and fuel plenum conditions, and the nozzle area ratio, computed as part of its procedure the nozzle throat area. Since this was a physical nozzle, throat area was measured, and thus iterations were performed on the enthalpies until the calculated throat area was identical to the actual throat area (see NASA TND-2132, Reference 18 ). In this manner exact burner inlet conditions were calculated.

The ideal combustion process was arbitrarily defined as a constant area, adiabatic, frictionless combustion process from actual inlet streams to a uniform stream in chemical equilibrium. If thermal choking made the process as defined above impossible, the combustion process was redefined as a diverging area process with wall pressure equal to terminal pressure and terminal velocity equal to sonic velocity. Once the calculation of either of the two possible processes was made, the ideal burner nozzle thrust was obtained by allowing the calculated exit stream to undergo a frozen expansion through a hypothetical nozzle. The nozzle exit area was the same as that used to determine the thrust produced by the test combustor under the same inlet conditions. Once the thrust potential of the test combustor was known, a relative thrust potential efficiency was obtained.

The input weight flow of air and the iterated air and fuel enthalpies from program SSCAI were used, along with composition determined from the gas sample data, wake impact pressures, and exit static pressures, in program SSCDR. The function of this program was to calculate stream composition, temperature and pressure, exit Mach numbers and point combustion efficiencies for each gas sample point. A description of the details of these calculations appears in Colley and Kenworthy (Reference 2 ). These calculations were performed using the following quenching process assumption:

**CONFIDENTIAL**

**CONFIDENTIAL**

1. No  $H_2O$  is formed during the gas sampling process.
2.  $OH$ ,  $NO$ ,  $H$ ,  $O$  formed are in equilibrium with the  $H_2$ ,  $O_2$ ,  $N_2$  present.

Point combustion efficiencies greater than 100% were commonly encountered. It was postulated that this was a consequence of the first assumption listed above, and that the assumption was, at least in the case of rich samples, not entirely valid. Thus a correction was made during the analysis which involved modifying the sample data. The correction postulated that a certain amount of water was formed during the quenching process at a lower temperature than that of the sample stream. The amount formed was estimated from the sample composition computed by the CDR Program, and this amount was analytically decomposed into hydrogen and oxygen which was then added to the sampled amounts of hydrogen and oxygen. This procedure was then iterated until the point efficiency was reduced to 100%. In the case where a point efficiency less than 100% was computed from the initial data, no correction was made.

A further correction to the measured gas sample for the runs prior to Run 154 involved a correction for the  $NO_2$  in the stream. The presence of  $NO_2$  was a consequence of the operation of the arc tunnel, but it was not possible to measure this concentration using techniques available until Run 154. However, later tests succeeded in measuring the  $NO_2$  levels at various simulated Mach numbers, and the results of these tests were applied back to the earlier tests. Measured amounts of  $NO$  and  $NO_2$  were analytically decomposed to  $N_2$  and  $O_2$  before being input to program SSCDR.

d) Continuity Check

With the completion of the iteration on the point combustion efficiencies, the data available comprised the input flow condition (from SSCPAI) and the measured flows and conditions at the burner exit (from SSCDR). These burner exit flow parameters must, of course, satisfy continuity conditions. The measured gas sample points were taken essentially in the core of the burner streams, leaving an unprobed area around the circumference of the burner duct. This unprobed zone was used to satisfy continuity conditions in the following manner.

To each probed point, a portion of the burner exit area was arbitrarily assigned, and property values in each area were assumed to be constant at the level of the values at the probed point. The sum of these areas was less than the burner exit area. For each of these areas, program SSCPAI calculated flow parameters from the SSCDR output of temperature, pressure, stagnation enthalpy and composition. The fuel and airflows were then summed

**CONFIDENTIAL**

**CONFIDENTIAL**

and the enthalpy mass-averaged, and these results were compared with the input conditions calculated as part of program SSCPAI. The difference in these quantities was then assumed to be satisfied by the properties of the stream in the unprobed area.

An additional correction to the measured data was made at this point. Since the combustor was water-cooled, a certain amount of heat was lost to the cooling water during the combustion process and this heat loss had to be accounted for. This heat loss resulted in a enthalpy decrease of the burner exit stream, and was calculated from the known cooling water flow and temperature rise. This enthalpy correction was also applied to the ideal thrust calculation of program SSCPAI, necessitating an additional use of this program to avoid biasing the thrust-potential efficiency calculation against the actual combustor. It is worth noting at this point that in an actual engine design, the combustor would be regeneratively cooled and thus the heat loss described above would not occur. Rather, the heat transferred to the combustor walls would return to the combustor in the fuel stream.

The estimation of the flow properties in the unprobed portion of the stream was done in this manner for the following reasons. First, the wide variation in flow parameters across the exit stream that was exhibited in each run made it impossible to extrapolate the known data into the unprobed area. Further, in three runs at nominally similar conditions (Run 107, 110 and 111), no significant pattern was found. Thus, determination of properties in the unprobed area by other means than a continuity balance could not be justified.

Once the properties of the outer zone, such as air and fuel flow rates and enthalpies were known, the composition was calculated by assuming a pressure on the basis of the known data and using tables of H<sub>2</sub>-Air combustion data. This involved calculating the temperature of the unprobed stream (assumed uniform), the known mass flow and interpolating in the tables to reach the correct temperature and equivalence ratio. In the early tests, these calculations and interpolations were made by hand; in later tests, they were incorporated into program SSCPAII.

e) Eta-NT

With continuity satisfied and the composition and other properties of the burner exit stream known, the "net thrust potential" of the actual combustor was determined. This thrust potential was determined in two ways. In both methods a hypothetical nozzle was assumed, as for the ideal burner nozzle thrust calculation. In one method, each zone of the burner exit stream was expanded isentropically with frozen composition to a uniform

**CONFIDENTIAL**

**CONFIDENTIAL**

pressure at the arbitrarily assigned total nozzle exit area. In the second method used the burner exit stream was mixed without reaction at constant area and the resultant mixed stream expanded isentropically through the nozzle. These two means of determining the thrust potential give results that vary by only a few percent. The quoted performance figures were derived by the first method.

The net thrust potential efficiency,  $\eta_{NT}$  was defined as

$$\eta_{NT} = \frac{\text{nozzle exit impulse} - \text{engine inlet impulse}}{\text{ideal engine net thrust}}$$

For this calculation, the nozzle exit impulse was obtained from the thrust calculation for the actual burner as made in program SSCPAII while the ideal nozzle exit impulse was obtained from program SSCPAI. The engine inlet impulse was computed from the burner inlet stream of program SSCPAI, using equations of continuity of mass and energy. As here defined, Eta-NT relates the calculated performance of the actual burner to that of an arbitrarily defined ideal burner.

The next step in the data analysis procedure was to evaluate the over-all combustion efficiency,  $\eta_{BM}$ . This combustion efficiency calculation related the data for the actual burner to a cycle-defined combustion efficiency which itself is defined essentially in terms of an enthalpy loss. For this calculation, the combustor exit flow was considered as a single stream. Using the appropriate analytical expression for the effect of combustor efficiency as total enthalpy,

$$(h_t)_{eff} = h_t - (1 - \mu) f' (\text{LHV}) / (i + f)$$

where

$h_t$  = stagnation enthalpy, Btu/lbm

$\mu$  = combustion efficiency

LHV = 51,600 Btu/lbm

$f$  = fuel/air ratio

$f' = f$  for  $f \leq .0291618$

$f' = .0291618$  for  $f > .0291618$

the enthalpy of this single stream was calculated for various  $\mu_{BM}$ . Program SSCCKO was then used to determine the composition, temperature, and pressure

**CONFIDENTIAL**

**CONFIDENTIAL**

of a single stream at enthalpy values corresponding to various  $\mu_{BM}$ . After the computation and properties were calculated, the resulting data were used in Program SSCPAII to calculate the nozzle exit impulse corresponding to various combustion efficiencies. With the nozzle exit impulse of the actual burner known from the thrust-potential calculation, the combustion efficiency at the test conditions was determined as that producing the same impulse as the actual combustor.

The final series of calculations made as part of a normal data reduction procedure involved the hand-calculation of the wall shear stress, skin friction coefficient and wall force factor of the actual combustor under test conditions. These calculations used data from all four data reduction programs and also raw data from the test cell data sheets and completed the data reduction procedure.

b. Test Results for Performance

1) Step Combustors

a) Configuration AEN

Thirteen tests in which nozzle A and Injector E were employed produced useful data. Nozzle A provided a burner inlet Mach number of about 2.7, corresponding to the engine cycle at flight Mach 6.7.

Plotted in Figure 92 are combustor wall pressures measured at various stations along the length of the combustor. Test conditions include various burner equivalence ratios. The enthalpy levels are relatively low, typical of flight Mach numbers in the range 5.2 to 6.0. With no fuel flowing, the pressures were at a relatively low level, especially in the wake of the step. Equivalence ratios up to about 0.20 produced pressures little different from the no-fuel case, indicating little or no combustion. Higher equivalence ratios produced pressures much higher than the no-fuel level. The step wake pressure increased with increasing equivalence ratio. Step wake pressures nearly twice the inlet static pressure were attained with no apparent effect on the inlet stream. Pressure increased still more downstream of the step, characteristically reaching a plateau along the length of the mixing pipe, then falling somewhat toward the burner exit.

At none of the enthalpy levels shown in Figure 92 did ignition of the burner occur with a low pressure in the dump chamber behind the combustor. When fuel was admitted with a dump chamber pressure of say, 3 psia the pressures in the combustor remained at the no-fuel level. Movies of the burner exit confirmed no combustion. When the dump chamber pressure was increased to about 10 psia, the burner pressures rose to the higher levels.

**CONFIDENTIAL**

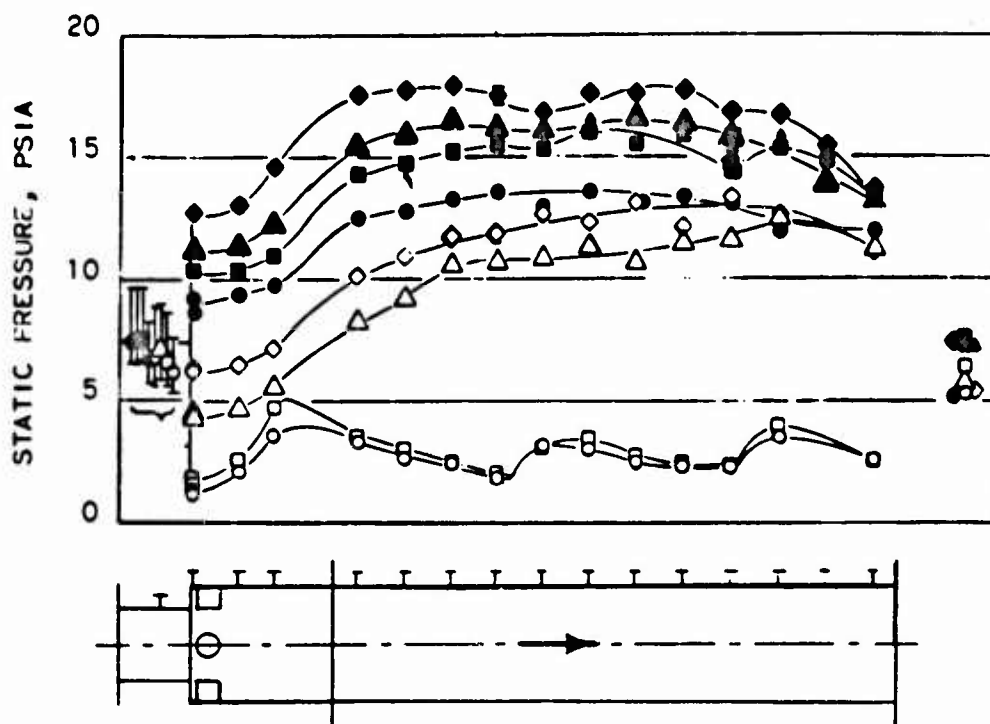
**CONFIDENTIAL**

Figure 92 - Wall Static Pressure, Configuration AEN

**CONFIDENTIAL**

**CONFIDENTIAL**

When the equivalence ratio was greater than about 0.29, the burner would remain lit when the dump chamber pressure was reduced. Gas samples drawn from the step wake region indicated little fuel in the wake with burner pressures at the lower level.

Similarly plotted in Figure 93 are combustor wall pressures at higher enthalpy levels, typical of flight Mach number of 7.8 to 8.0. At equivalence ratios below about 0.7, the step wake pressure was low and nearly independent of equivalence ratio. The pressures downstream from the step increased gradually along the length of the mixing pipe. As equivalence ratio was increased above 0.7, the step wake pressure increased and the pressures downstream assumed the peaked characteristic of the lower enthalpy levels.

At stagnation enthalpies above about 1200 Btu/lbm, burner ignition occurred spontaneously at all equivalence ratios, even with low dump chamber pressure.

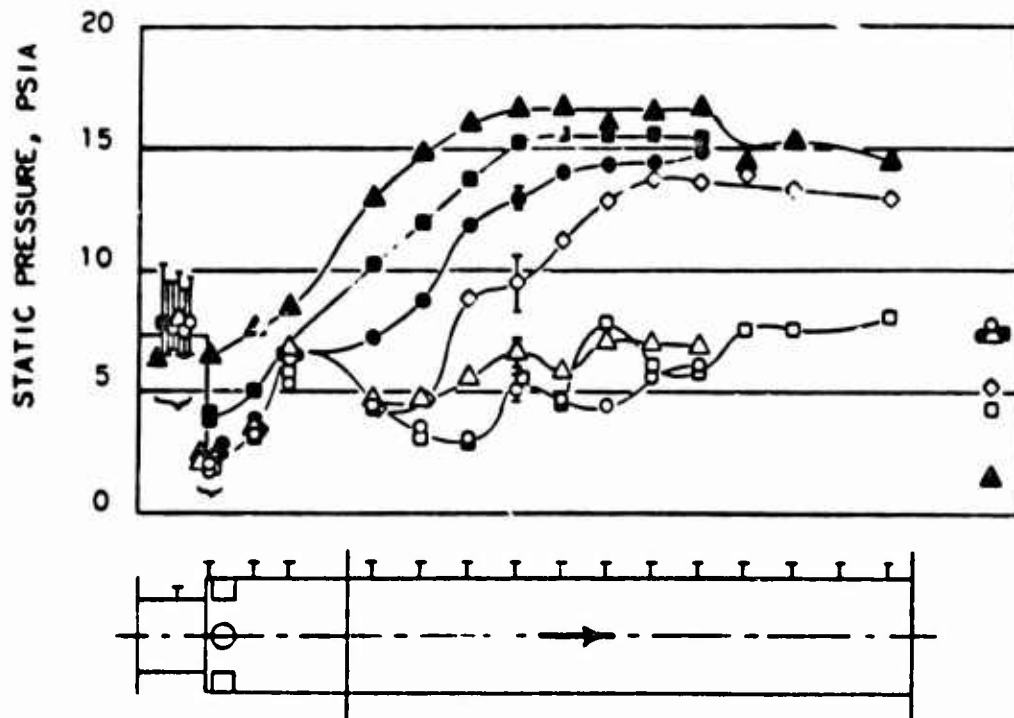
Six of the tests produced burner exit surveys sufficiently complete to permit full analysis of burner performance. The test conditions and the derived performance parameters, are tabulated in Table V. Combustion efficiencies were generally high. Wall friction and step base drag were major contributors to the over-all performance deficit. Net thrust potential was in the range .76 to .84 at the lower enthalpy levels, falling to .49 to .73 at the higher enthalpies.

Figures 94 through 99 show contours of Mach number and equivalence ratio derived from rake surveys in the burner exit plane. All plots are drawn looking upstream. Arrowheads at the perimeter of the stream indicate the circumferential location of the fuel injectors. The eighth-segment maps were plotted by averaging equivalence ratio measurements at points similarly located with respect to the fuel injectors.

Figure 96 is typical of conditions of high equivalence ratio and low enthalpy, characterized by wall pressures high in the step wake, rising to a higher plateau further downstream, then diminishing slightly toward the burner exit. The tests conditions of Figure 91 correspond to those of curve  $\square$  of Figure 92. The local equivalence ratios in the burner exit plane were circumferentially uniform but were lean in the center of the stream and rich near the walls. The Mach numbers are seen to be highest in the lean regions of the stream. The density in these regions is also higher than in the rich regions, due to the lower temperature and higher molecular weight in the lean regions. The lean regions, therefore, contain mass flows disproportionately higher than their relative areas.

**CONFIDENTIAL**

**CONFIDENTIAL**



SYMBOL	$H_{T2}$	ER
○	1233	.33
○	1229	.43
△	1296	.51
◇	1279	.59
●	1233	.71
●	1222	.88
▲	1291	1.26

Figure 93 - Wall Static Pressure, Configuration AEN

**CONFIDENTIAL**

**CONFIDENTIAL**

TABLE V - SUMMARY OF TEST RESULTS - STEP BURNERS

Run Number	104	107	110	111	117	126	128
Configuration	AEN	AEN	AEN	AEN	AEN	AEN	AFN
Air Stagnation Enthalpy, $HT_2$ , $\frac{BTU}{LBF}$	1328	963	906	870	598	1314	773
Simulated Flight Mach Number, $M_p(1)$	8.1	6.8	6.6	6.4	5.2	8.1	6.0
Burner Inlet Mach Number, $M_2$	2.71	2.75	2.76	2.76	2.80	2.72	2.78
Burner Inlet Velocity, $V_2$ , FT/SEC	6130	5310	5160	5070	4260	5930	4810
Burner Inlet Static Temperature, $T_2$ , $^{\circ}R$	2260	1610	1510	1450	980	2040	1280
Burner Inlet Static Pressure, $P_2$ , PSIA	7.53	7.09	7.09	6.54	6.08	7.37	7.08
Burner Inlet Impulse, LBF	569.4	561.3	565.4	524.3	505.4	559.9	576.3
Burner Equivalence Ratio, ER	1.193	.817	.769	.785	.290	.592	.729
Step-Base Pressure Ratio, $P_W/P_2$	.870	1.225	1.312	1.371	.683	.309	1.762
Burner Friction Coefficient, $C_f(2)$	.0038	.0025	.0025	.0019	.0035	.0023	.0017
Burner Exit Impulse, LBF	577.2	612.9	623.6	595.7	498.0	527.1	669.2
Ideal Thrust of Optimum Burner, LBF(3)	264.3	306.4	311.8	308.9	188.4	207.2	347.5
Ideal Thrust of Actual Burner, LBF(3)	211.3	218.5	214.6	203.2	164.6	184.1	224.4
Combustion Efficiency, $\eta_{AEM}$	.946	.955	.925	.882	.988	.919	.954
Net Thrust Potential, $\eta_{TANT}$	.725	.838	.830	.824	.765	.489	.889

Notes: (1)  $M_p$  based on an Ambient Temperature of  $390^{\circ}R$   
 (2)  $C_p$  based on Burner Inlet Velocity Head  
 (3) Thrust based on Hypothetical Exhaust Nozzle of Exit Area =  $1.27 \text{ FT}^2$ .

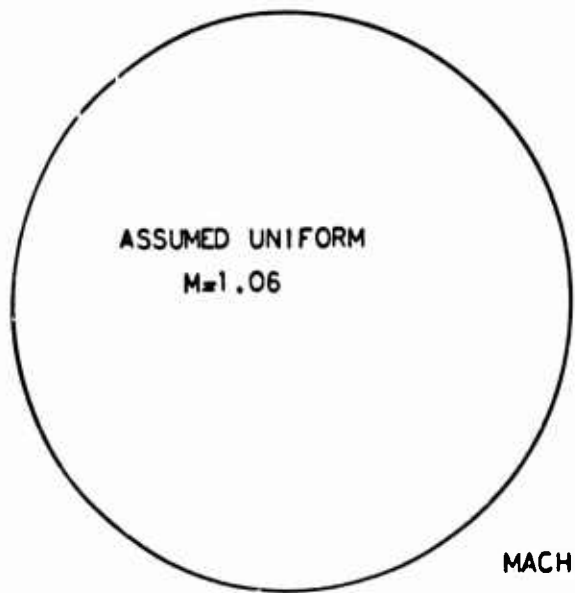
**CONFIDENTIAL**

**CONFIDENTIAL****TABLE V CONCLUDED - SUMMARY OF TEST RESULTS - STEP BURNERS**

Run Number	129	183-1	183-2	185	188-1	189	191-1
Configuration	AFN	BHN	BHN	BHN	BHN	BHN	BEN
Air Stagnation Enthalpy, $HT_2$ , BTU/LBM	1315	976	1272	1234	1443	1161	1526
Simulated Flight Mach Number, $M_p(1)$	8.1	6.9	7.9	7.8	8.5	7.6	8.7
Burner Inlet Mach Number, $M_2$	2.71	3.31	3.25	3.26	3.22	3.27	3.21
Burner Inlet Velocity, $V_2$ , FT/SEC	6100	5750	6490	6400	6870	6230	7040
Burner Inlet Static Temperature, $T_2$ , $^{\circ}R$	2240	1290	1730	1675	1990	1570	2120
Burner Inlet Static Pressure, $P_2$ , PSIA	7.43	7.24	4.35	7.16	6.83	7.01	7.03
Burner Inlet Impulse, LBF	562.2	821.5	472.7	780.6	725.1	771.6	727.1
Burner Equivalence Ratio, ER	.445	.692	1.086	.798	.752	.763	.903
Step-Base Pressure Ratio, $P_W/P_2$	.194	.894	.782	.287	.299	.424	.473
Burner Friction Coefficient, $C_f(2)$	.0017	.0014	.0025	.0026	.0025	.0026	.0029
Burner Exit Impulse, LBF	549.3	850.6	468.7	734.2	686.9	734.9	692.1
Ideal Thrust of Optimum Burner, LBF(3)	183.4	348.2	196.8	298.6	242.7	302.8	260.5
Ideal Thrust of Actual Burner, LBF(3)	154.0	263.4	157.7	246.2	202.9	253.8	209.5
Combustion Efficiency, $\eta_{TAE}$	.892	.909	.870	.784	.808	.852	.755
Net Thrust Potential, $\eta_{TANT}$	.502	.798	.711	.746	.518	.622	.478

Notes: (1)  $M_p$  based on an Ambient Temperature of  $390^{\circ}R$   
 (2)  $C_f$  based on Burner Inlet Velocity Head  
 (3) Thrust based on Hypothetical Exhaust Nozzle of Exit Area =  $1.27 \text{ FT}^2$ .

**CONFIDENTIAL**

**CONFIDENTIAL**

RUN 104  
CONFIGURATION AEN  
 $H_{t2} = 1328$  BTU/LBM  
 $ER=1.193$

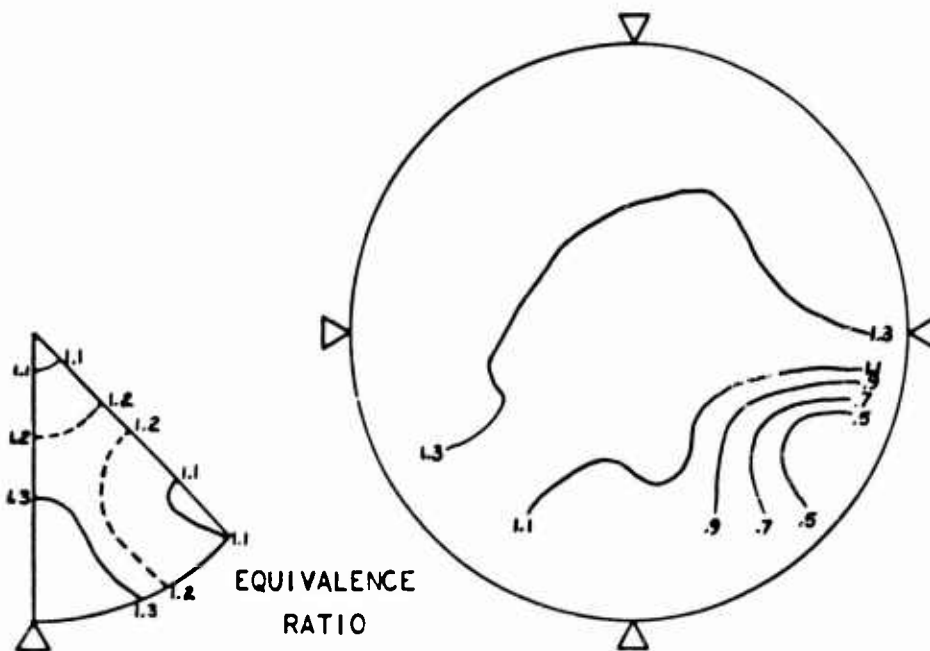
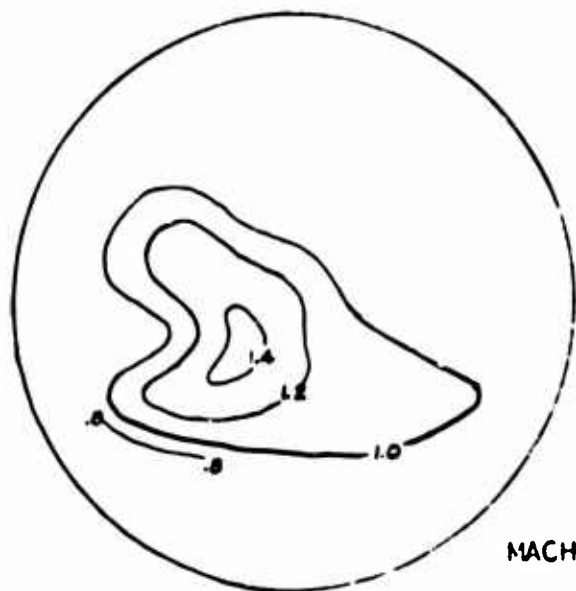


Figure 94 - Burner Exit Stream Property Contours

**CONFIDENTIAL**

**CONFIDENTIAL**

RUN 107  
CONFIGURATION AEN  
 $H_{12} = 963$  BTU/LBM  
ER=.817

MACH NUMBER

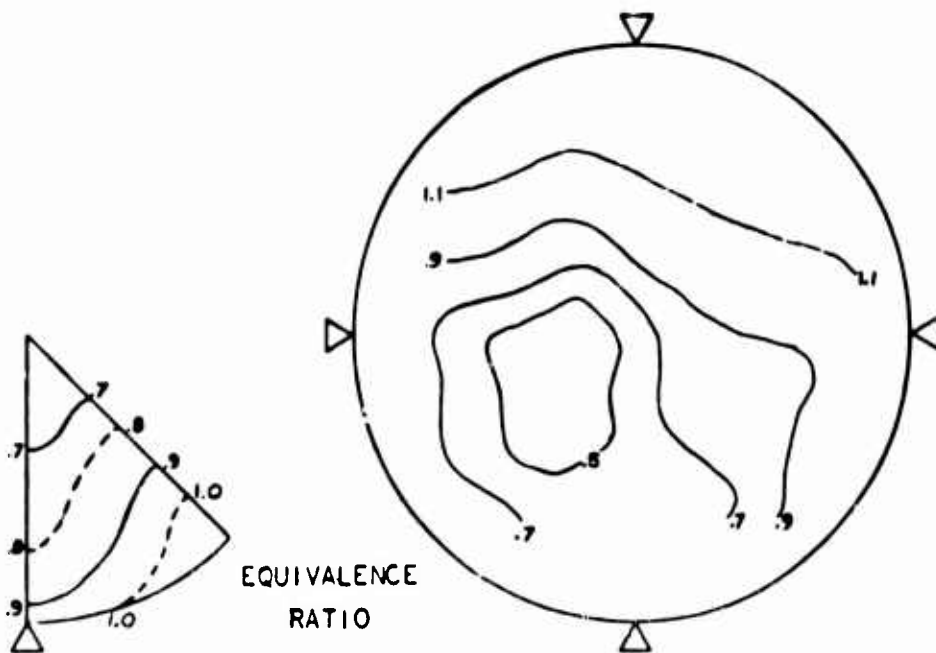
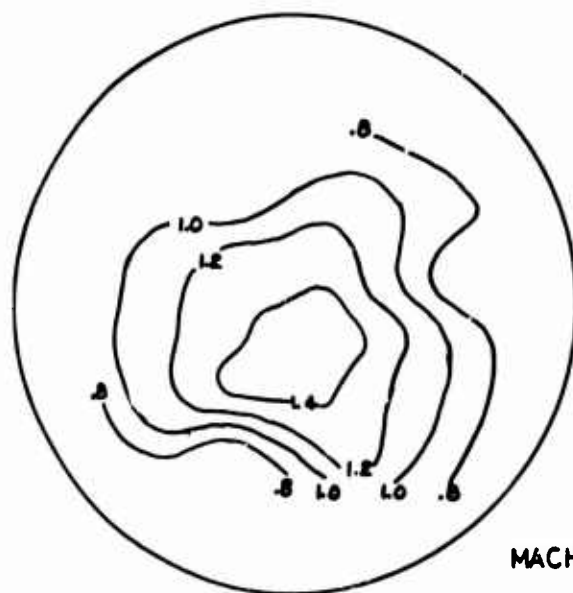
EQUIVALENCE  
RATIO

Figure 95 - Burner Exit Stream Property Contours

**CONFIDENTIAL**

**CONFIDENTIAL**

RUN 110  
CONFIGURATION AEN  
 $H_{T2} = 906$  BTU/LBM  
ER = .769

MACH NUMBER

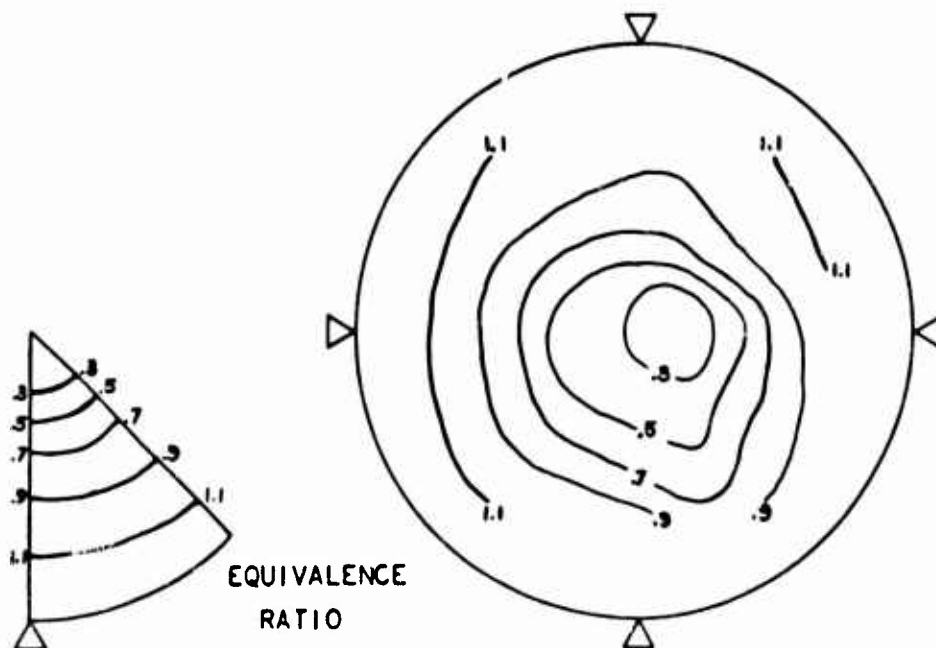
EQUIVALENCE  
RATIO

Figure 96 - Burner Exit Stream Property Contours

**CONFIDENTIAL**

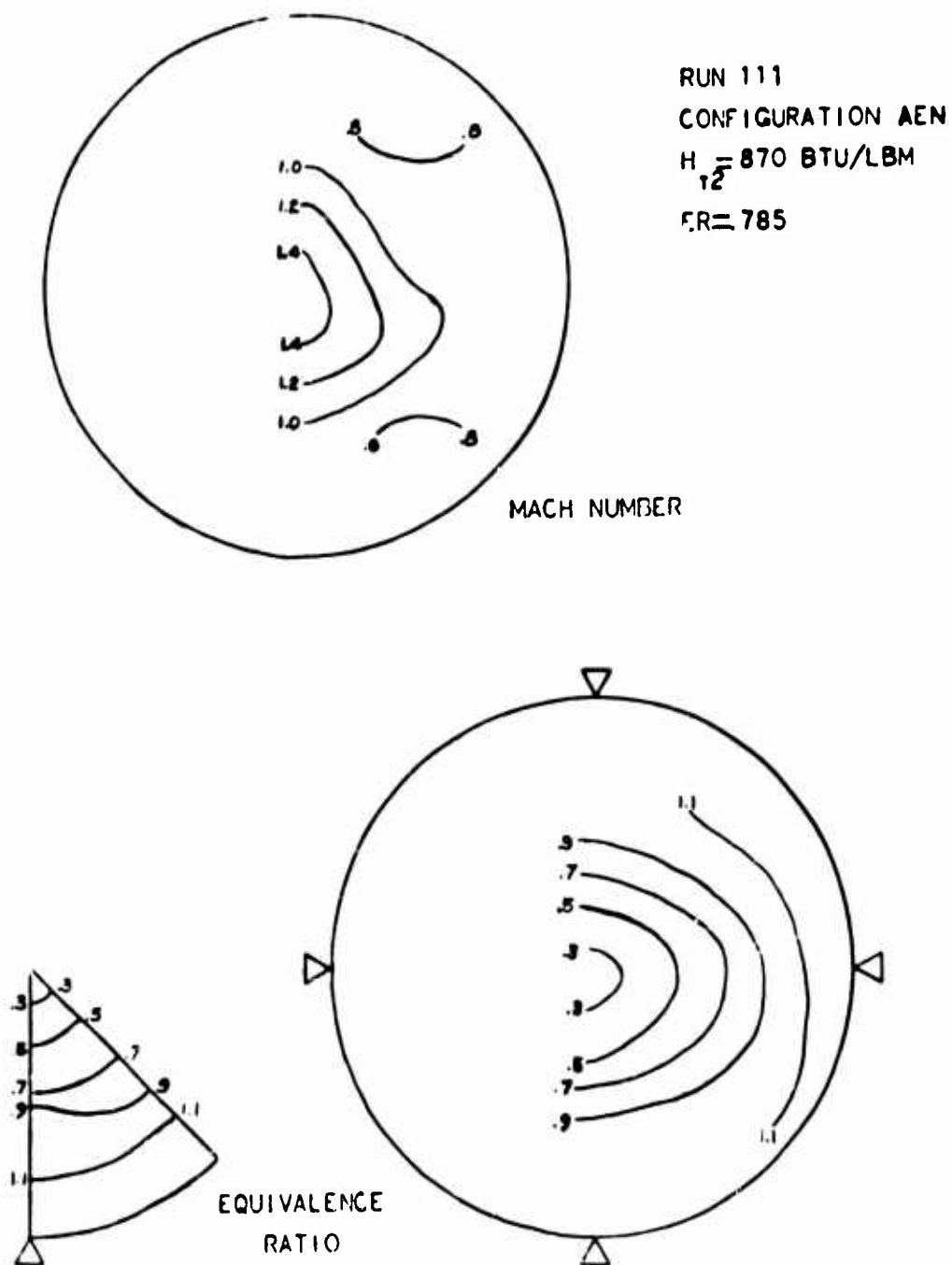
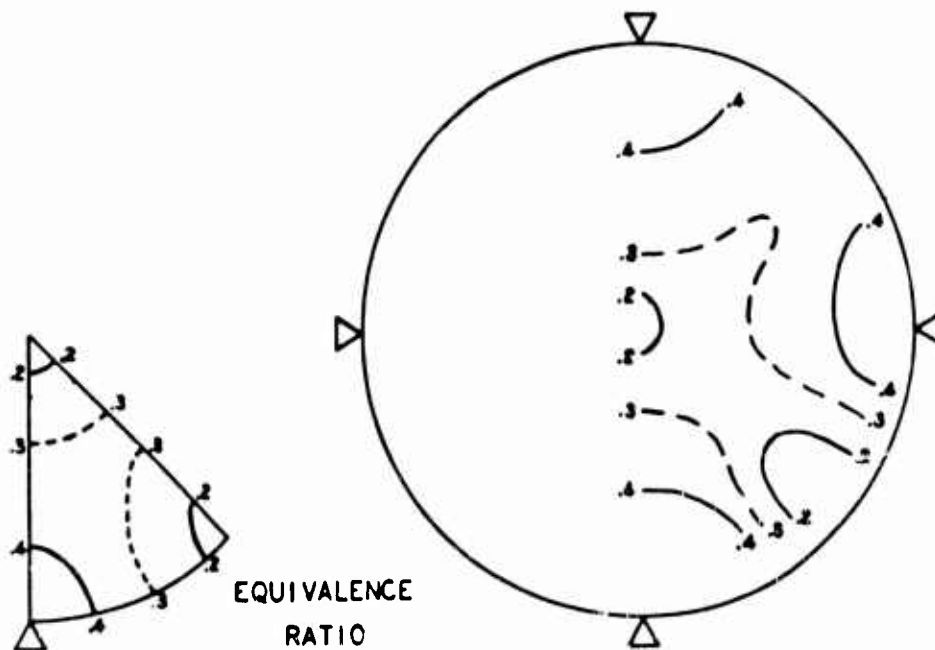
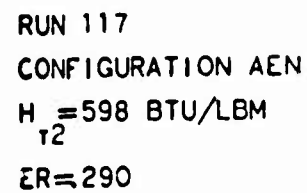
**CONFIDENTIAL**

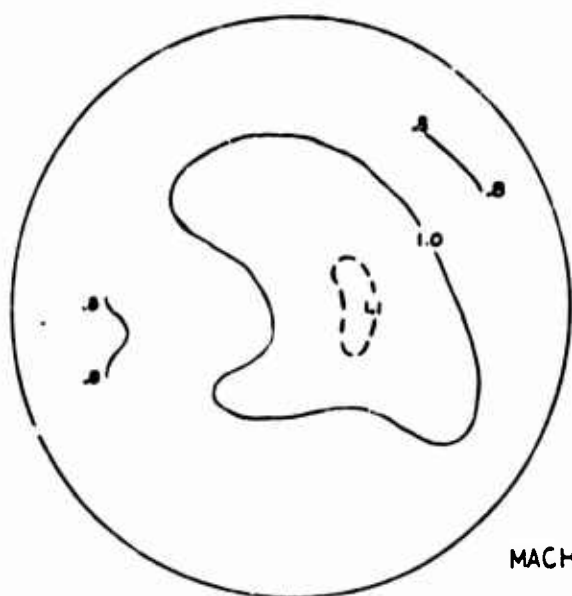
Figure 97 - Burner Exit Stream Property Contours

**CONFIDENTIAL**

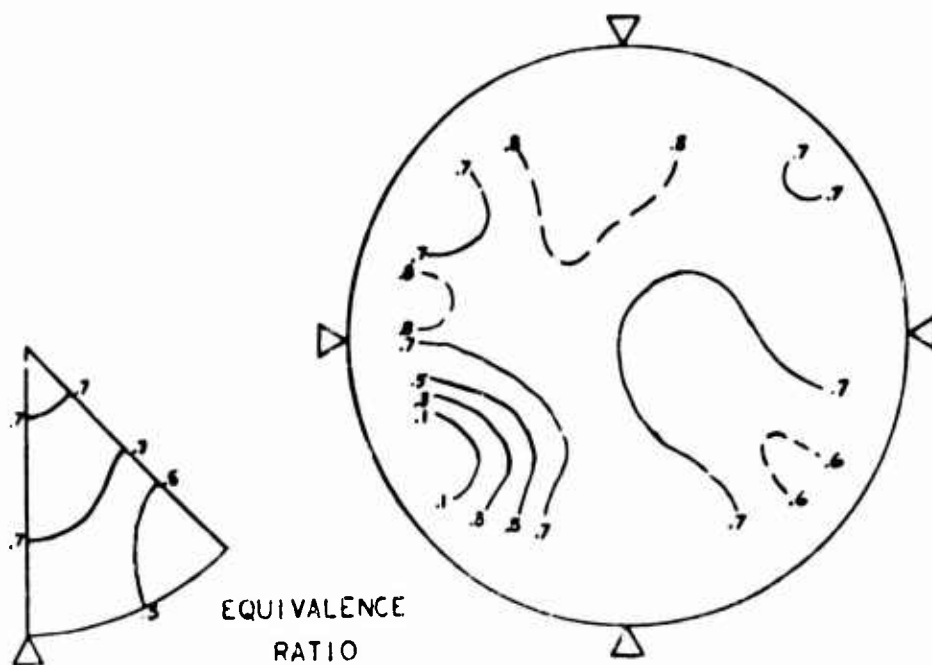


**Figure 98 - Burner Exit Stream Property Contours**

**CONFIDENTIAL**



RUN 126  
CONFIGURATION AEN  
 $H_{12} = 1314 \text{ BTU/LBM}$   
ER=592



**Figure 99 - Burner Exit Stream Property Contours**

**CONFIDENTIAL**

**CONFIDENTIAL**

In Run 104 the burner exit survey was made with very low pressure in the dump tank. The expansion of the essentially sonic jet so adversely affected the impact pressure measurements that it was necessary to assume a uniform exit Mach number.

In Runs 107, 110 and 111 the dump tank pressure was intentionally matched to the burner exit pressure. This procedure proved difficult, as tank pressure and exit pressure tended to drift together to higher levels.

In Run 117 and all subsequent runs, the dump tank pressure was adjusted to approximately 60 percent of the exit static pressure when surveying the exit stream.

Figure 99 is typical of conditions of lower equivalence ratio and high enthalpy, characterized by wall pressures low in the step wake and rising gradually toward the burner exit, as shown in curve  $\diamond$  of Figure 93. The fuel distribution at the burner exit assumed a lobed pattern directly related to the location of the four injection points.

Results of the line reversal pyrometer measurements of the burner exit stream have been separately reported in Reference 19.

b) Configuration AFN

Four tests in which Injector F was employed produced useful data. Combustor wall pressures at low and high enthalpy levels are plotted in Figures 100 & 101. The combustor pressures were generally similar to those of Injector E. Step base pressures were slightly higher than for Injector E at similar conditions.

Curves  $\square$  and  $\Delta$  of Figure 101 show significantly different combustor pressure distributions for two fairly similar operating conditions, both with combustion. The condition producing the highly peaked pressure distribution had a slightly lower enthalpy and a slightly higher ER. The suggested bistable flow field was supported by the movies of the burner exit, in which occasional sudden changes in flame pattern were seen.

The ignition characteristics of Injector F closely paralleled those of Injector E. The burner ignited spontaneously at the 1200 Btu/lbm enthalpy level, but not at lower levels.

Two tests of Injector F provided burner exit surveys adequate for burner performance analysis. Results of these tests are included in Table V, and the corresponding burner exit Mach number and equivalence ratio contours are plotted in Figures 102 and 103.

**CONFIDENTIAL**

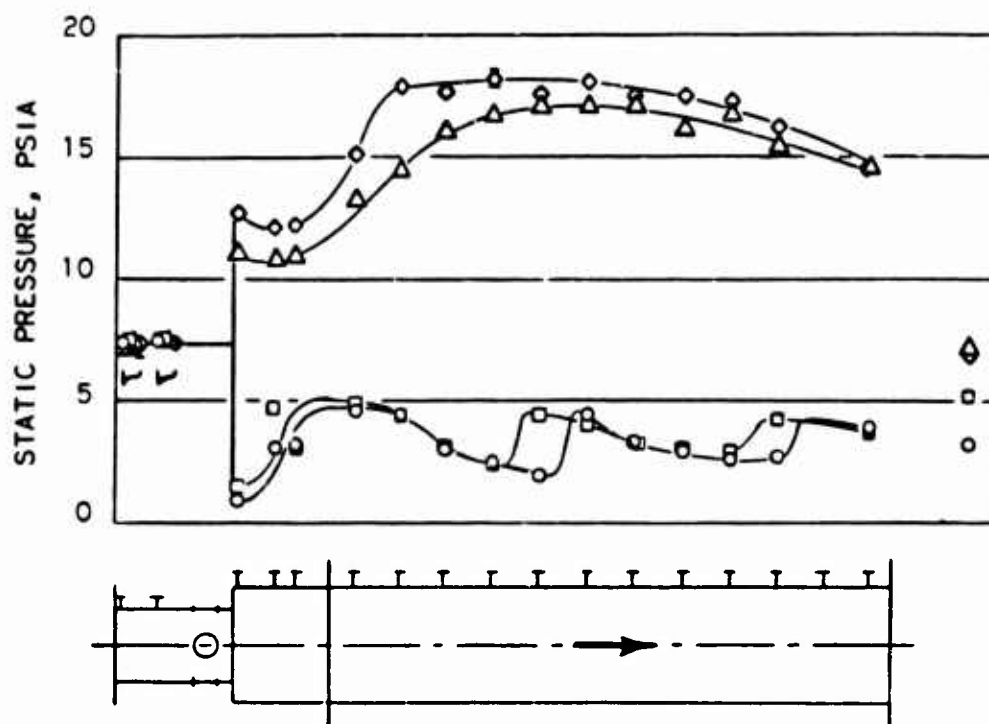
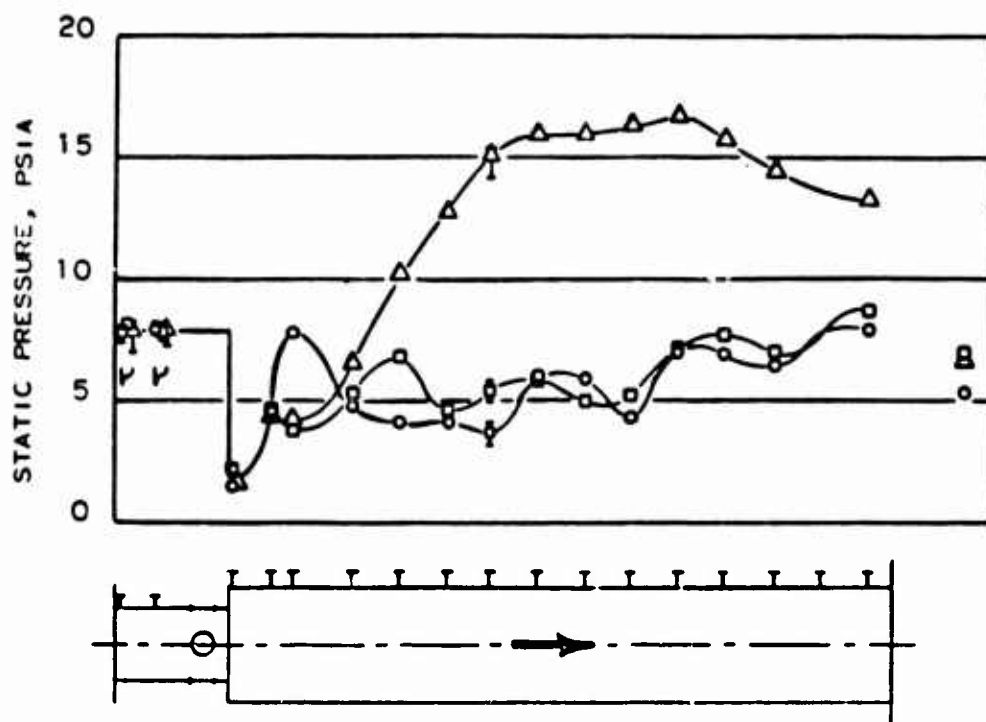
**CONFIDENTIAL**

Figure 100 - Wall Static Pressures, Configuration AFN

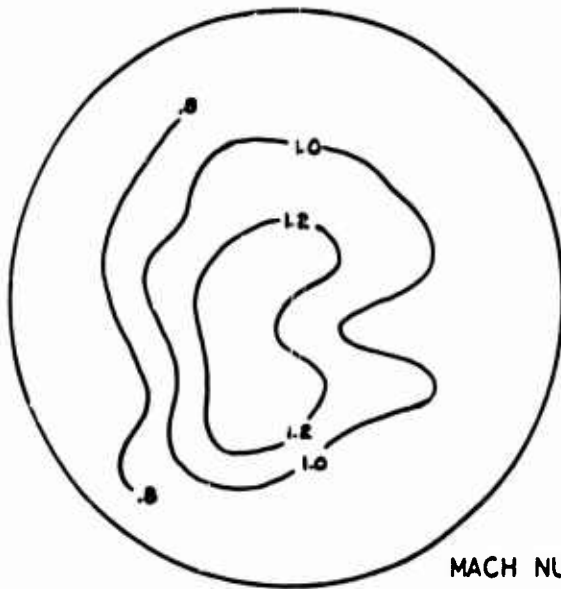
**CONFIDENTIAL**

**CONFIDENTIAL**

SYMBOL	H <sub>T2</sub>	ER
○	1296	.44
◻	1369	.57
△	1290	.59

Figure 101 - Wall Static Pressures, Configuration AFN

**CONFIDENTIAL**

**CONFIDENTIAL**

RUN 128  
CONFIGURATION AFN  
 $H_{T2} = 773$  BTU/LBM  
 $ER = 729$

MACH NUMBER

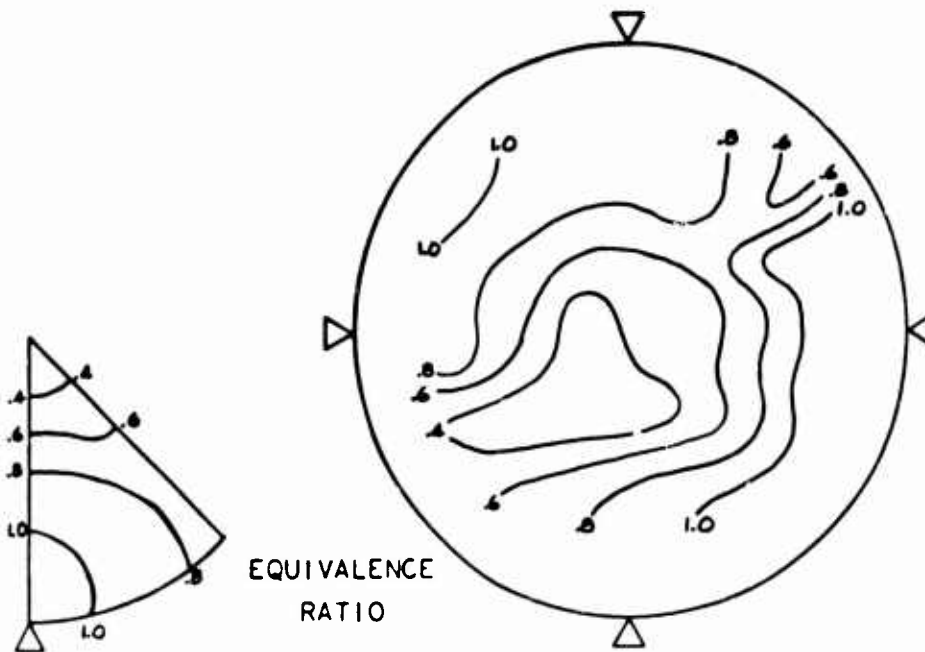
EQUIVALENCE  
RATIO

Figure 102 - Burner Exit Stream Property Contours

**CONFIDENTIAL**

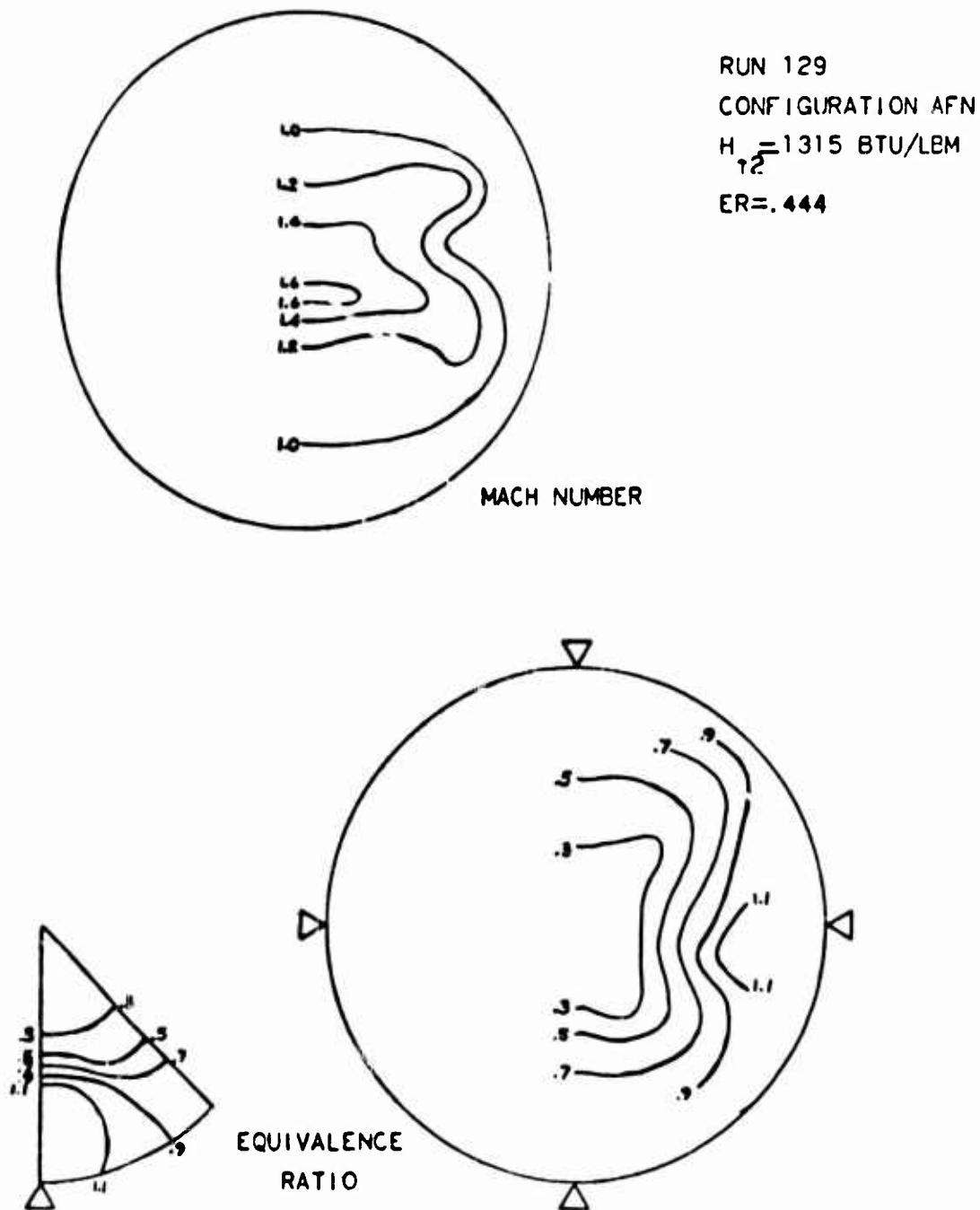
**CONFIDENTIAL**

Figure 103 - Burner Exit Stream Property Contours

**CONFIDENTIAL**

**CONFIDENTIAL****c) Configuration AJN**

One test of Injector J was performed. Its purpose was to determine if direct fueling of the step wake region would establish combustion in the wake, permitting stable burner operation at low enthalpies and equivalence ratios, perhaps with increased wake pressure.

Combustor wall pressures are shown in Figure 104. The lean operating limit for low enthalpy levels was reduced somewhat. The step base pressure was no higher than for the corresponding conditions with Injector E.

A gas sample drawn from the step wake region contained only hydrogen.

**d) Configuration BEN**

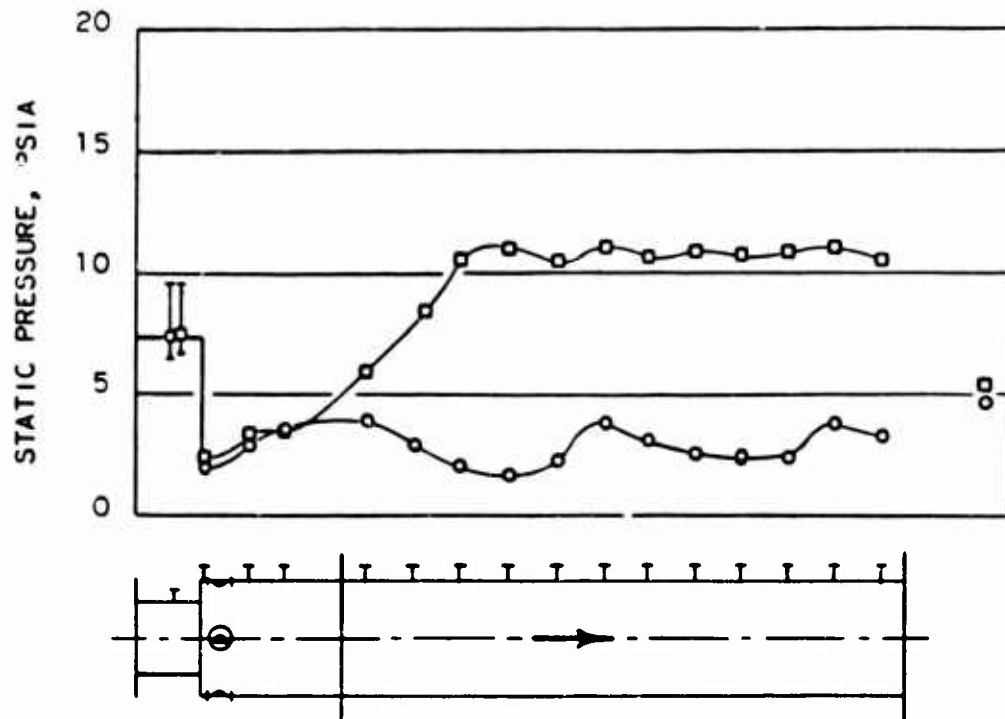
In three tests, Injector E was used with the higher inlet Mach number nozzle, B, to better simulate higher flight speed conditions. Nozzle B provided a burner inlet Mach number of about 3.2, corresponding to that of the engine cycle at flight Mach 7.7. In these tests, Injector H was installed between the nozzle and Injector E. While Injector H was partly water cooled, it relied partly upon fuel cooling for structural integrity. Since the air enthalpy levels were high (1170 to 1620 Btu/lbm), it was necessary to maintain a small flow of nitrogen through Injector H while evaluating hydrogen injection from Injector E.

At the highest enthalpy levels (above 1400 Btu/lbm), it was necessary to reduce the burner airflow somewhat to avoid overloading the facility aftercooler at high equivalence ratios. This resulted in burner inlet pressures lower than the normal 7.3 psia.

Combustor wall pressure data from these tests are included in Figures 104, 105, 106 and 107. The test conditions of Figure 104 are comparable with those at which Configuration AEN was tested, Figure 93. The higher inlet Mach number of Nozzle B resulted in a higher burner exit pressure than with Nozzle A. The pressures in the downstream half of the tailpipe showed the same high plateau characteristic of lower speed tests at high equivalence ratios. The step base pressure was about the same as with Nozzle A.

Figures 106, 107 and 108 show data at higher air enthalpy levels. With increasing enthalpy, the high step base pressure and the peaked pressure became more difficult to attain. At an air stagnation enthalpy of 1620 Btu/lbm (Figure 108), representative of flight at Mach 9, the step pressure was low and the burner pressures rose gradually along the length of the tailpipe, even with an equivalence ratio of 1.4.

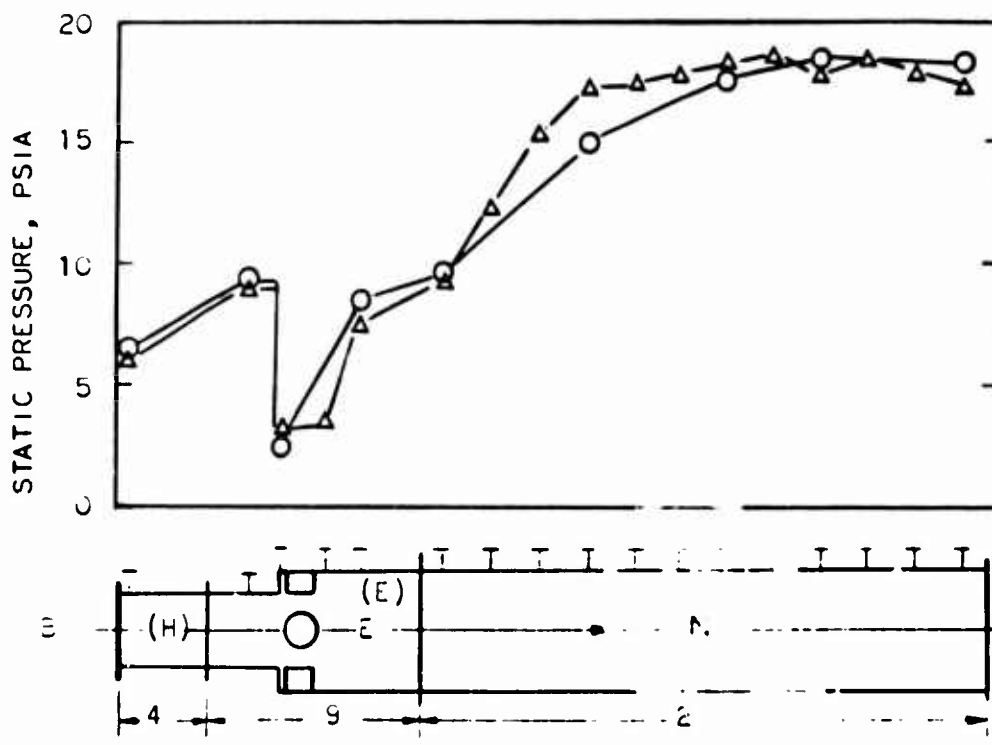
**CONFIDENTIAL**

**CONFIDENTIAL**

SYMBOL	$H_{T2}$	ER
○	761	.15
□	769	.23

Figure 104 - Wall Static Pressures, Configuration AJN

**CONFIDENTIAL**

**CONFIDENTIAL**

SYMBOL	INJ.	$H_{T2}$	$M_P$	ER	UN	Rdg
O	(E)	1170	7.58	.71 * N <sub>2</sub> to (H)	189	5E
Δ	(H)	1165	7.56	.76	189	4A

Figure 105 - Wall Static Pressures, Configurations BKN  
and BHN

**CONFIDENTIAL**

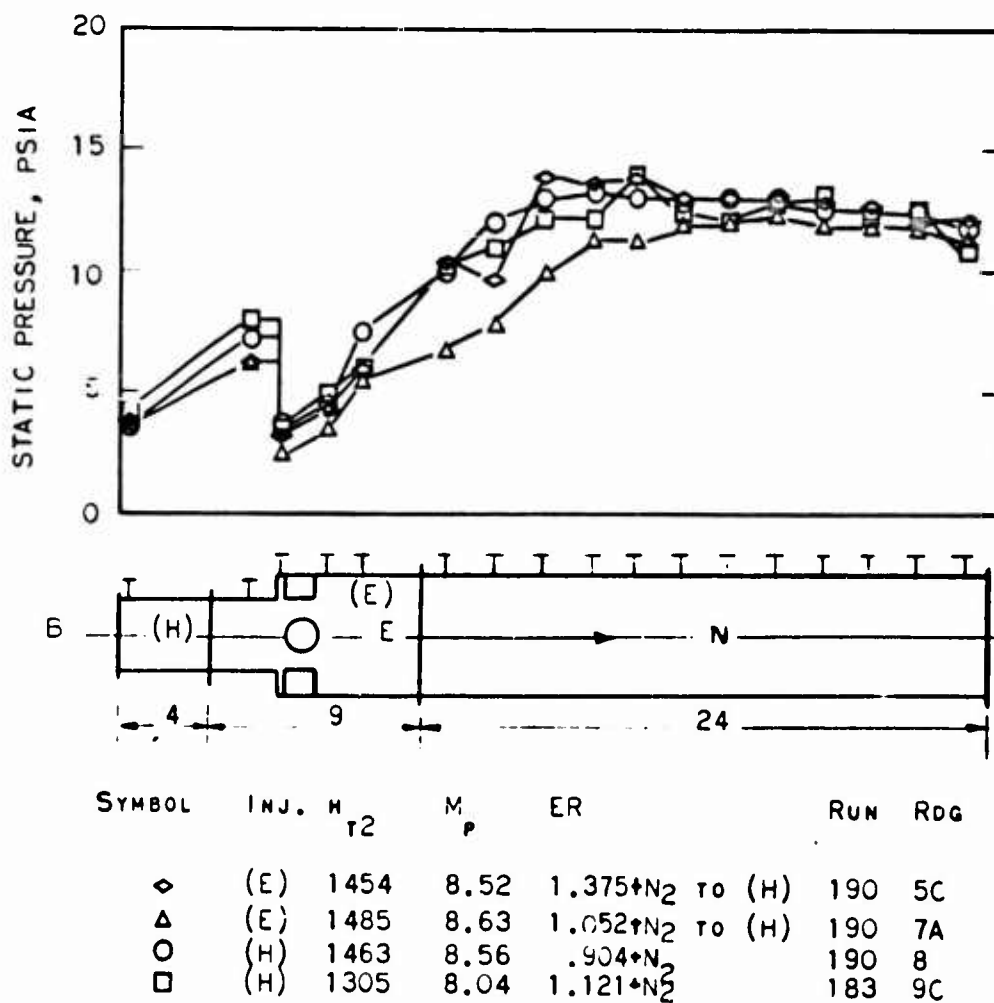
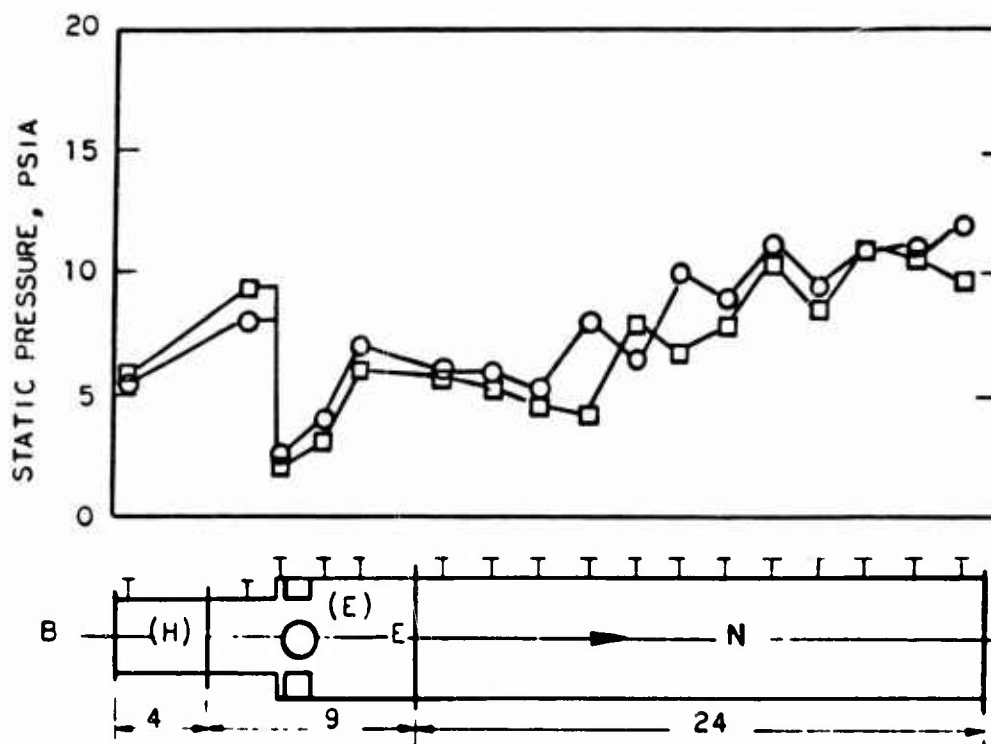
**CONFIDENTIAL**

Figure 106 - Wall Static Pressures, Configuration BEN  
and BHN

**CONFIDENTIAL**

**CONFIDENTIAL**

SYMBOL	INJ. W	$M_p$	ER	Run	Rdg
○	(E) 1430	8.45	.884 $\times$ N <sub>2</sub> to (H)	191	12C
□	(H) 1455	8.53	.749	188	6B

Figure 107 - Wall Static Pressures, Configurations BEN  
and BHN

**CONFIDENTIAL**

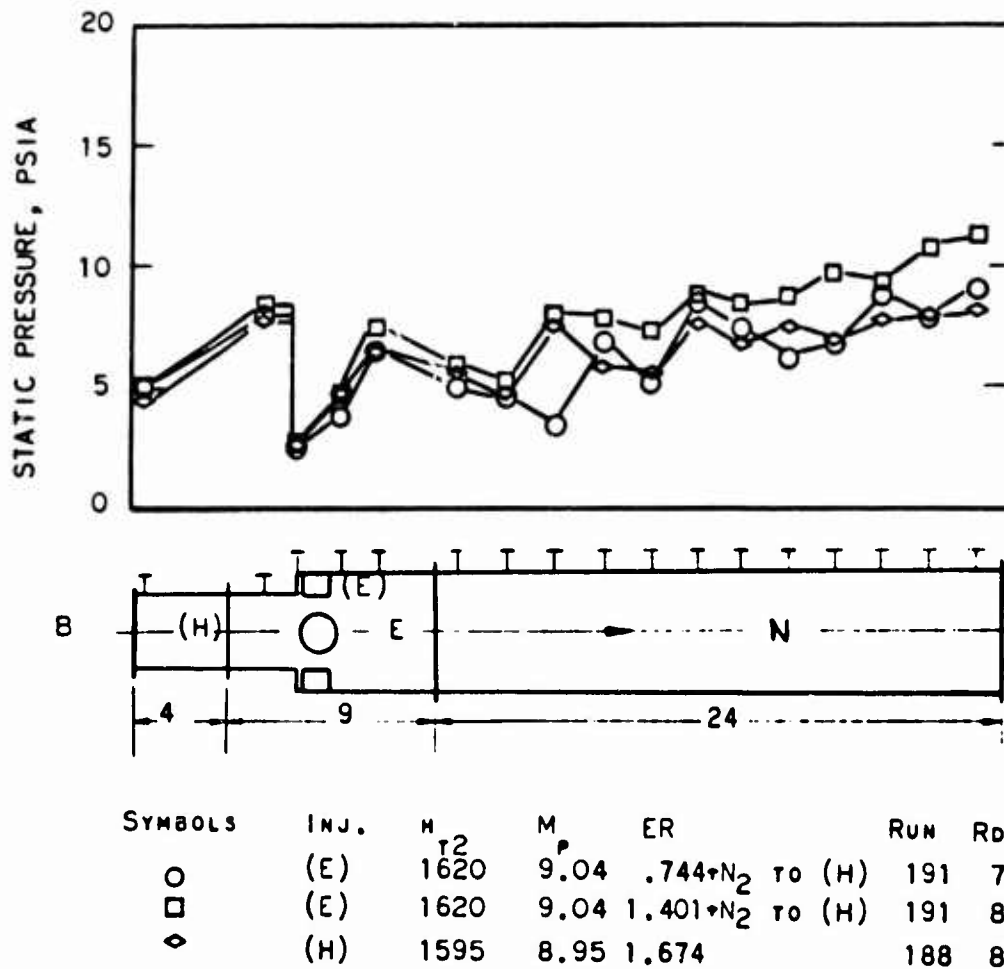
**CONFIDENTIAL**

Figure 108 - Wall Static Pressures, Configuration BKN  
and BEN

**CONFIDENTIAL**

**CONFIDENTIAL**

Run 191 produced data suitable for full analysis of burner performance. These data are included in Table V. The high air enthalpy (1530 Btu/lbm) and near-stoichiometric equivalence ratio (.9) produced a relatively low combustion efficiency (.76). This, together with the low step base pressure, resulted in a low thrust potential.

The local equivalence ratios measured in the burner exit stream were plotted in Figure 109 as a function of radial position, instead of in a contour map as before. Circumferential fuel distribution is seen to be uniform. The concentration of fuel near the outer wall indicates slightly less than optimum jet penetration, although appreciable radial mixing had occurred.

e) Configuration AGN

In one test Injector G was combined with the Mach 2.7 air nozzle, A, and Tailpipe N, with Injector E used as a transition piece. The test was conducted with a relatively low air enthalpy level, representative of flight at Mach 5.8

The burner wall pressures are plotted in Figure 110. Aft of the wall step, the pressures produced by Injector G were very similar to those of Injector F at comparable conditions. Upstream of the step, Injector G produced a high rise in wall pressure in the 3.0 inch diameter section, detected by pressure taps 1.75 inches aft of the four inch long injector.

The data from this test were inadequate for a full evaluation of burner performance.

f) Configuration BGN

Two tests were made with the Mach 3.2 air nozzle, B, with Injector G, Tailpipe N, and Injector E used as a transition piece. These tests were at high air enthalpy levels, simulating flight at Mach 8.3 to 9.0.

The measured wall pressures are presented in Figures 111 and 112. The wall static pressure characteristics were typical of high enthalpy conditions, showing low step base pressure and gradually rising pressure along the tailpipe. At the highest enthalpy level, Figure 112, the response of the wall pressure to increasing equivalence ratio was very weak relative to low enthalpy tests of other configurations, even though equivalence ratios up to 1.2 were used. The high pressure rise just aft of Injector G and upstream of the step was again in evidence of Nozzle B, as with Nozzle A.

The data from these tests were inadequate for a full evaluation of burner performance.

g) Configuration BHN

Useful data were obtained from six tests of Injector H combined with Tailpipe N, using Injector E as a transition piece. All these tests used the Mach 3.2 Air Nozzle B.

**CONFIDENTIAL**

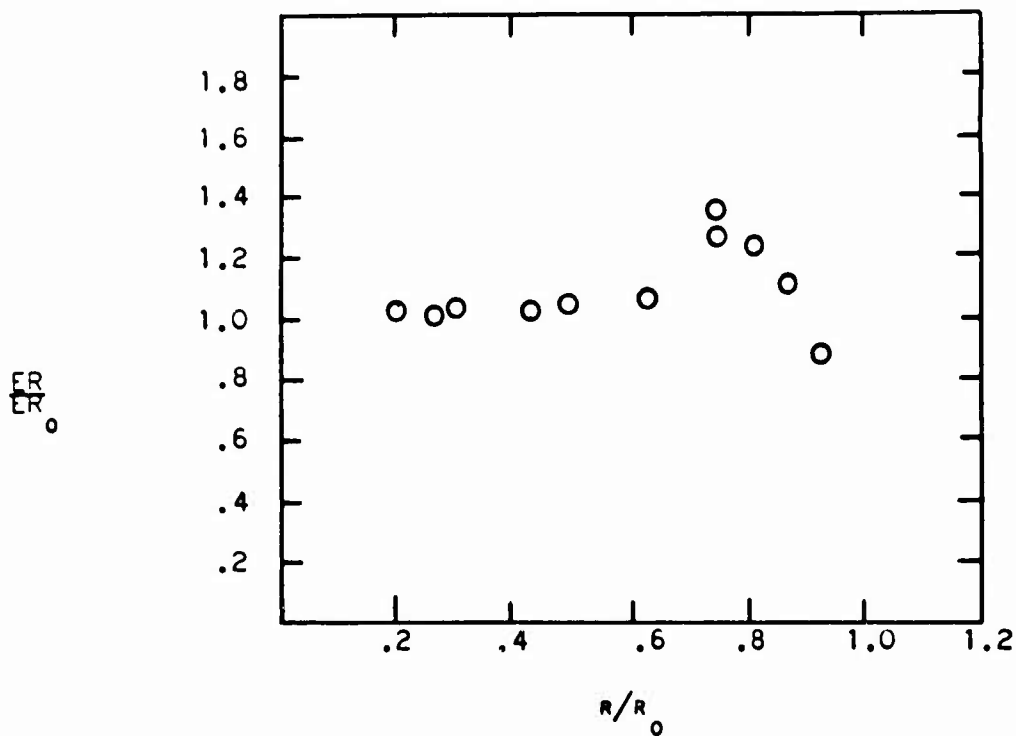
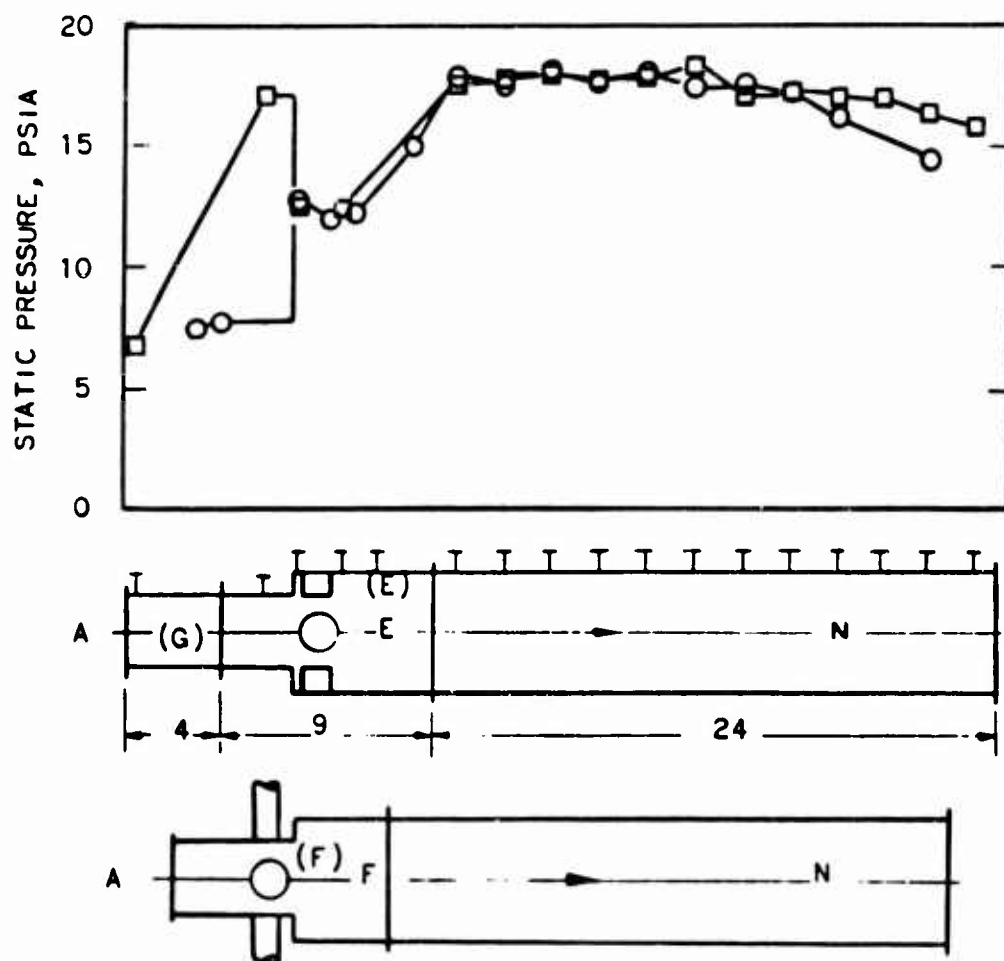
**CONFIDENTIAL**

Figure 109 - Fuel/Air Profile for Run 191-1 (BKN)

$$M_p = 9.0$$

$$FR_0 = 0.90$$

**CONFIDENTIAL**

**CONFIDENTIAL**

CONFIGURATION	SYMBOL	INJ.	$M_{T2}$	$M_p$	ER	RUN	Rdg
AFN	○	(F)	794	6.12	.727	128	1V
AGN	□	(G)	725	5.81	.746	194	2C

Figure 110 - Wall Static Pressures, Configuration AGN  
and AFN

**CONFIDENTIAL**

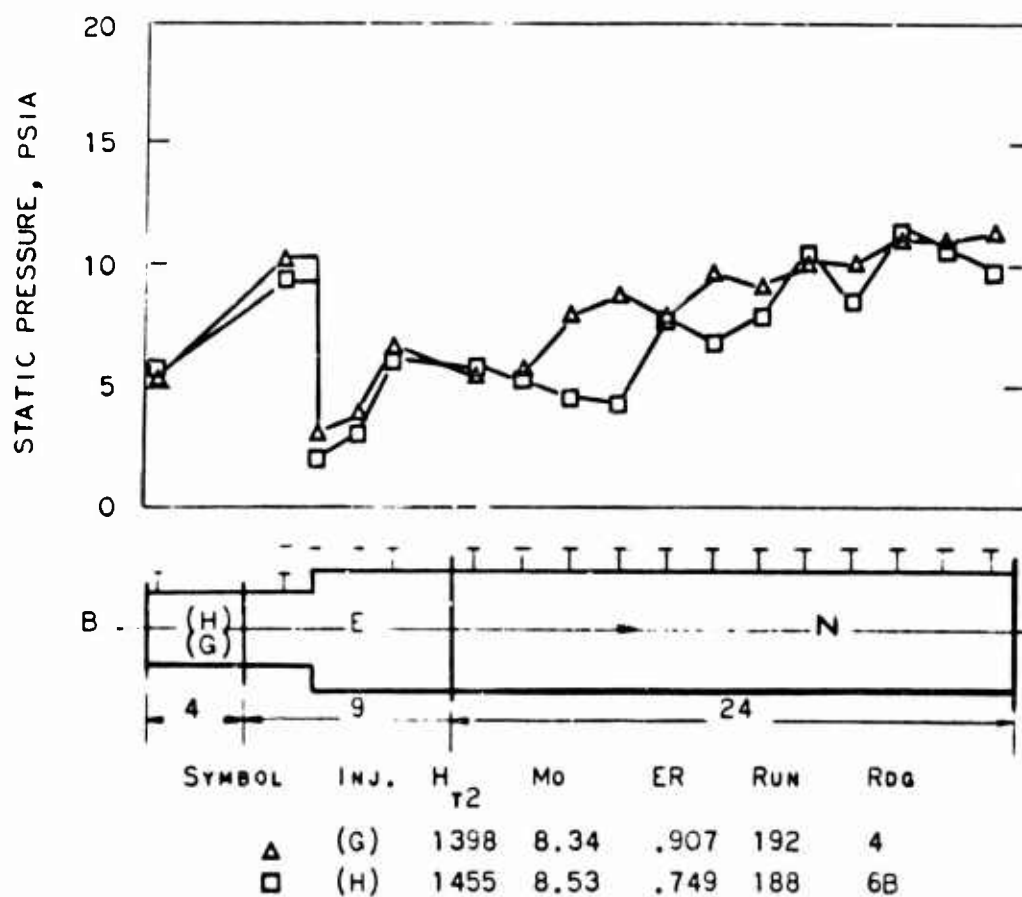
**CONFIDENTIAL**

Figure 111 - Wall Static Pressures, Configuration BGN  
and BEN

**CONFIDENTIAL**

CONFIDENTIAL

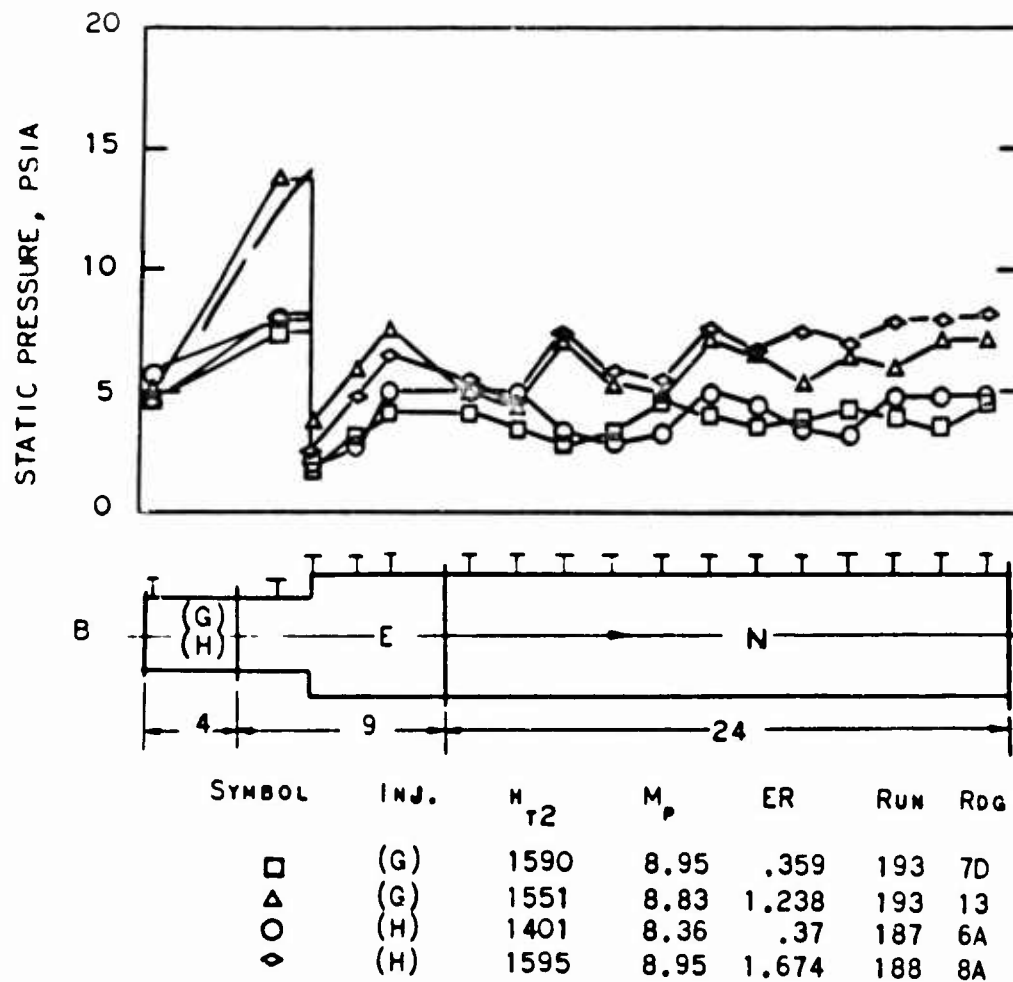


Figure 112 - Wall Static Pressures, Configurations  
BGN and BHN

CONFIDENTIAL

**CONFIDENTIAL**

Wall static pressure data from these tests are included in Figures 105 through 108 and 111 through 112, plotted to facilitate comparison with other configurations. Step base pressures and tailpipe pressures showed little significant difference from those of other configurations under comparable conditions. Figure 112 shows that the wall pressure rise induced by Injector H between the injector and step was less than that induced by Injector G. This factor affects the tendency of the injector to separate the boundary layers of the burner inlet stream.

Four of the six tests produced data sufficient for full evaluation of burner performance. In one of these, Run 183, performance evaluation at two different conditions was achieved by taking half the gas samples, then reducing airflow to increase enthalpy level and equivalence ratio before taking the remaining gas samples. These data are included in Table V. Performance levels were generally comparable to those of Configurations AEN and AFN. This indicates that Injector H is capable of producing more thrust than Injectors E or F, since its ideal thrust includes the benefit of a downstream component of fuel momentum.

Local equivalence ratios measured in the burner exit stream are plotted as a function of radial position in Figures 113 through 117. Circumferential distribution was uniform in all cases. At equivalence ratios above .75, the radial fuel distribution indicated near-optimum jet penetration except at the highest air enthalpy level (1440 Btu/lbm, flight Mach 8.5). An equivalence ratio of .69 produced somewhat less than optimum penetration, even at a relatively low enthalpy level (980 Btu/lbm, flight Mach 6.9).

h) Configurations AGP and AHP

Four tests were performed using the short Tailpipe P. All used Air Nozzle A. One used Injector G; the rest used Injector H. As these tests were primarily evaluations of ignition devices described in Section C.2. d. Injector E served not only as a transition piece, but also as a holder for the igniters. The enthalpy level was representative of flight speeds around Mach 6.

Ignition of Injector G with the excessively powerful igniters resulted in choking in the 3.0 inch bore of Injector E, upstream of the step, with accompanying separation of the flow in the air nozzle. To expediate the igniter tests, Injector H was substituted, in the belief that the added fuel momentum would lessen the chance of upstream choking.

Wall static pressures with Configuration AHP are shown in Figure 118. Shortening the tailpipe appeared to have little effect on the character of the static pressures. At high equivalence ratios, the high step base pressure and peaked tailpipe pressure were still observed. At equivalence ratios in excess of 1.0, choking could be induced in the 3.0 inch diameter bore upstream of the step, as with Injector G. Once the flow in the air nozzle was

**CONFIDENTIAL**

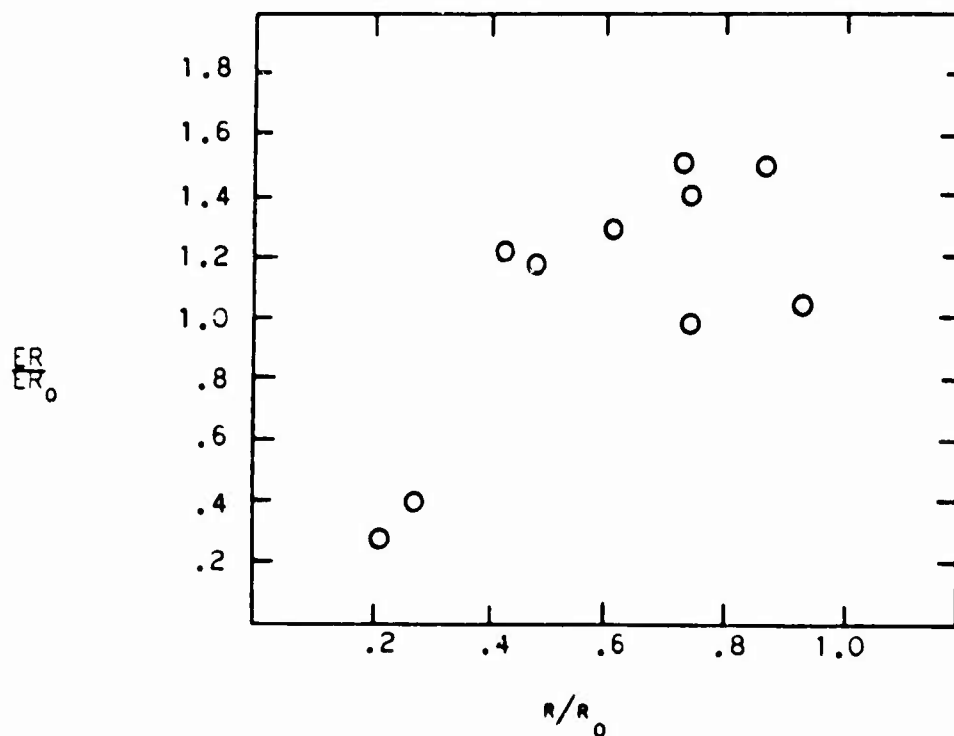
**CONFIDENTIAL**

Figure 113 - Fuel/Air Profile for Run 183-1 (BHN)

$$M_p = 7$$

$$ER_0 = .675$$

**CONFIDENTIAL**

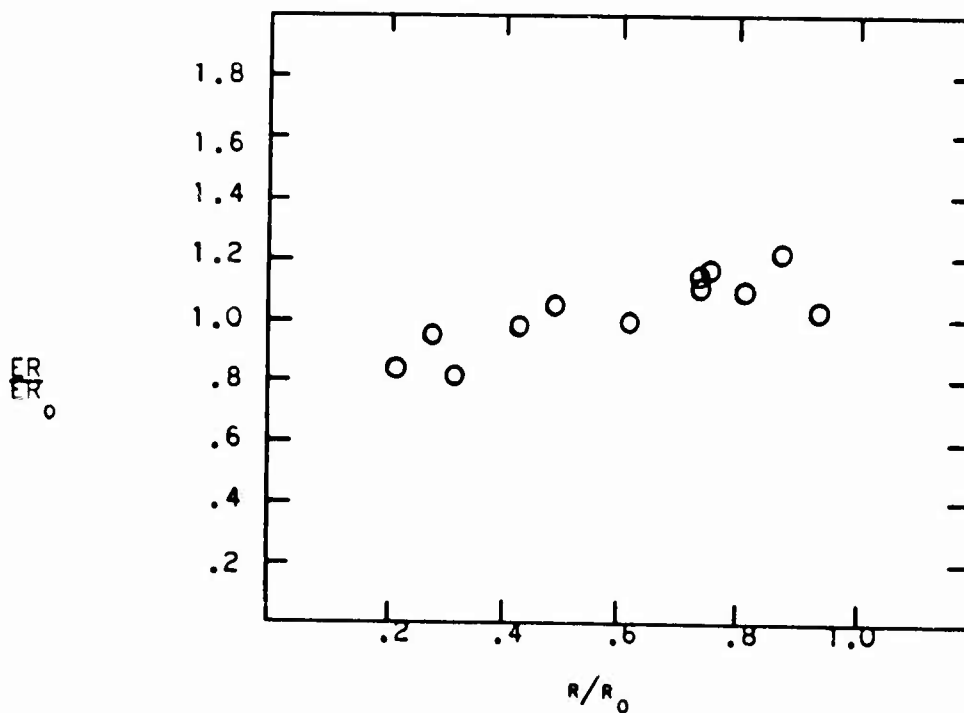
**CONFIDENTIAL**

Figure 114 - Fuel/Air Profile for Run 183-2 (BHN)

$$M_p = 8$$

$$ER_0 = 1.25$$

**CONFIDENTIAL**

**CONFIDENTIAL**

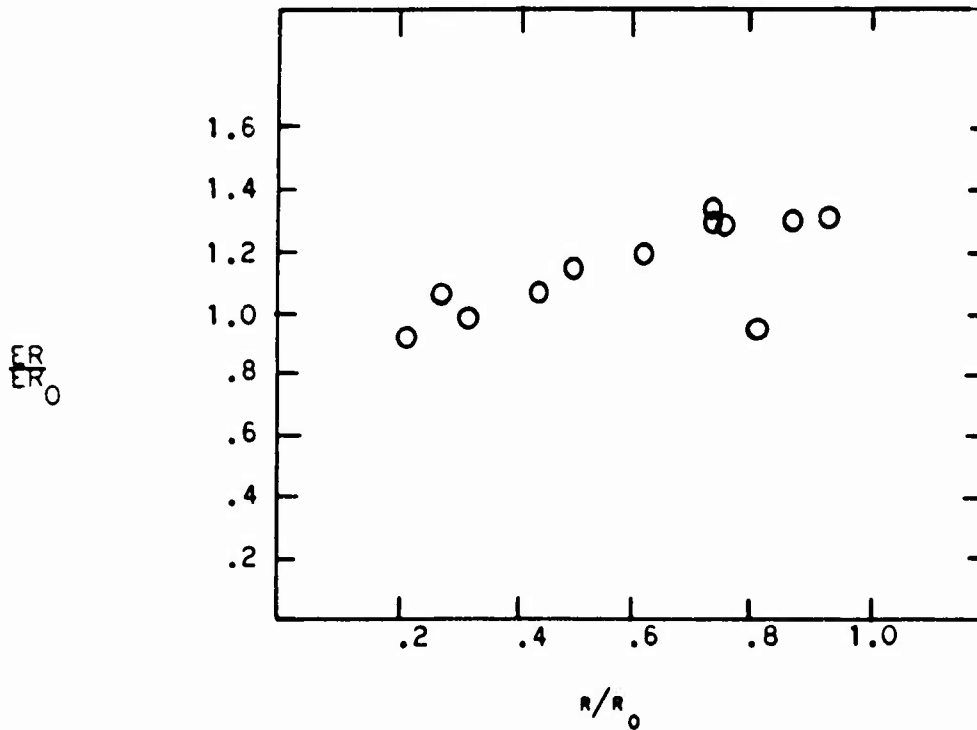


Figure 115 - Fuel/Air Profile for Run 185 (BHN)

$$M_p = 8$$

$$ER_0 = .80$$

**CONFIDENTIAL**

CONFIDENTIAL

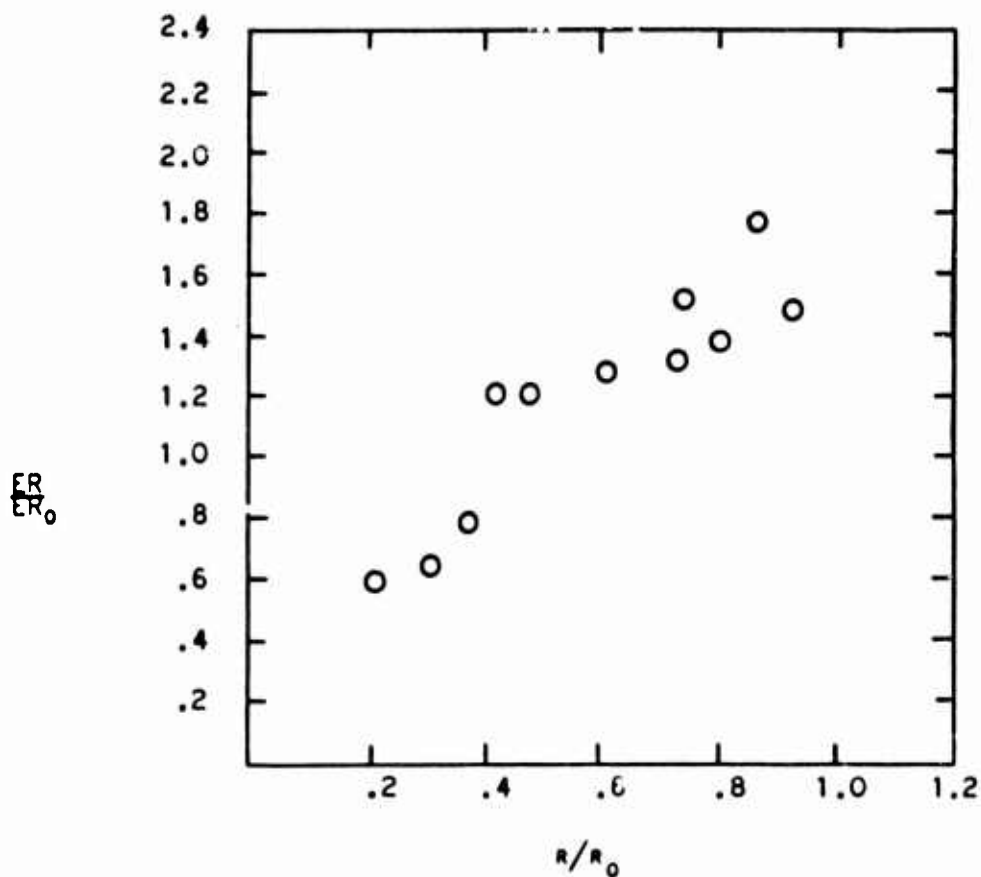


Figure 116 - Fuel/Air Profile for Run 188-1 (BHN)

$$M_p = 8.5$$

$$ER_0 = .745$$

CONFIDENTIAL

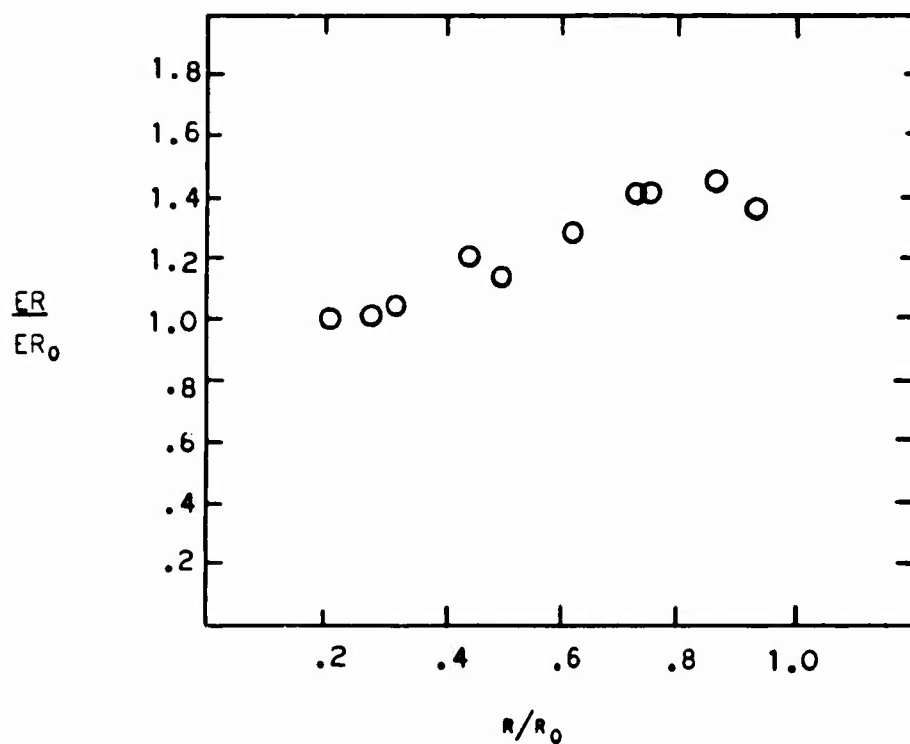
**CONFIDENTIAL**

Figure 117 - Fuel/Air Profile for Run 189, Configuration BHM

$$M_p = 8$$

$$ER_0 = .758$$

**CONFIDENTIAL**

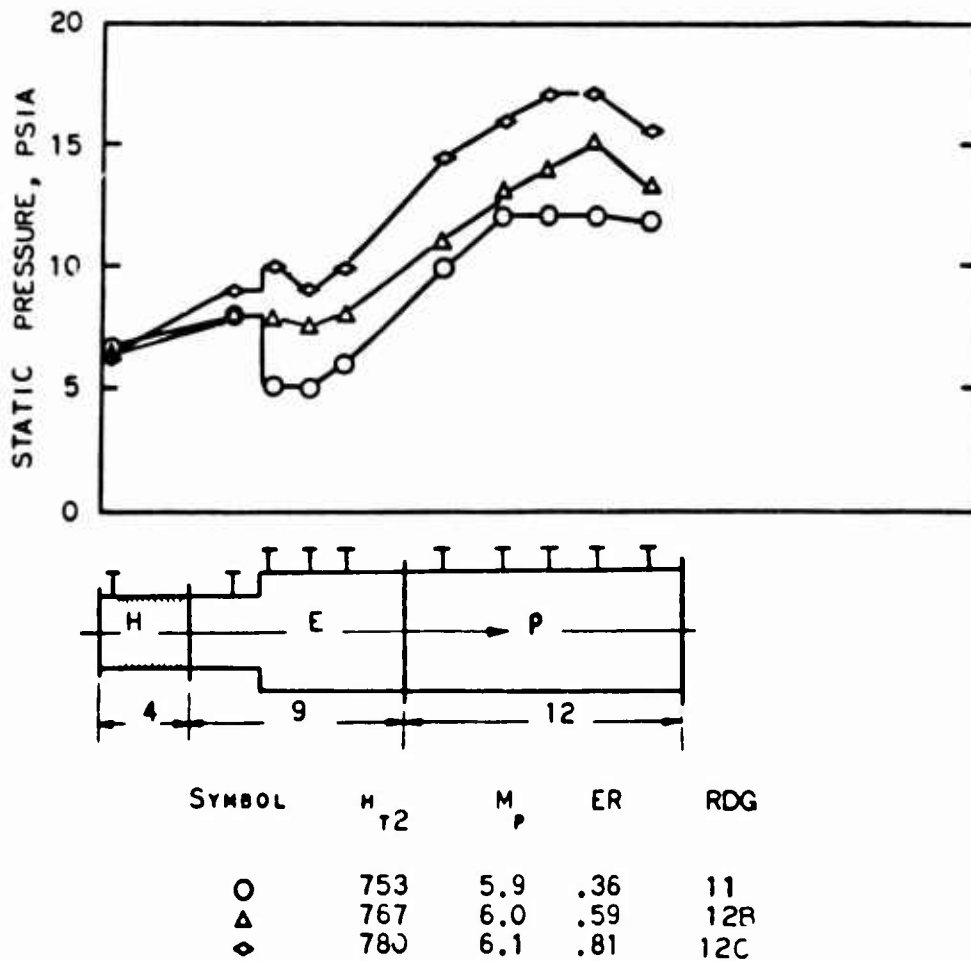
**CONFIDENTIAL**

Figure 118 - Wall Static Pressure, Configuration AHP

**CONFIDENTIAL**

**CONFIDENTIAL**

separated, it was necessary to reduce the equivalence ratio to a very low value before the burner inlet would again flow full.

A burner exit survey was obtained from one test, but the data were defective. A satisfactory continuity check could not be established; hence, meaningful performance parameters could not be calculated. The equivalence ratio profile measured at the burner exit is shown in Figure 119. The circumferential distribution was good, considering the short burner length. The radial distribution showed near-optimum penetration, but a lack of radial mixing.

## 2) Conical Combustors

### a) Configuration AFQ

In four tests, the conical Tailpipe Q was used with its integral F-type injectors and the Mach 2.7 air nozzle, A.

Wall static pressures measured along the tailpipe at low enthalpy levels, simulating flight speeds of Mach 5.2 to 6.0, are presented in Figure 120. At an equivalence ratio of .5, a sharp pressure rise occurred at the point of fuel injection, with the wall pressure reaching a peak about 1.5 inches downstream from the fuel nozzles. From its peak, the pressure declined as the flow expanded down the diverging duct, in an irregular manner suggesting repeated reflection of waves in the supersonic flow. At higher equivalence ratios, the pressure rise occurred upstream of the fuel nozzles, indicating separation of the flow in the air supply nozzle. At an equivalence ratio of 1.1, the peak pressure was six times the nominal burner inlet static pressure, and occurred slightly upstream from the fuel nozzles. As the air supply nozzle was not instrumented, the upstream extent of the pressure rise was not determined.

This test was started with a high fuel flow and high dump tank pressure to ensure ignition. It was not determined whether ignition could be attained with low dump tank pressure.

Wall static pressures measured at higher enthalpy levels, simulating flight speeds of Mach 7.9 to 8.0, are presented in Figure 121. At this enthalpy level, the pressure rise did not extend upstream from the fuel nozzles and the pressure peak was much less prominent than at the lower enthalpy level. At an equivalence ratio of 1.0, the pressure peak was about the same as that noted at  $ER = .5$  at the lower enthalpy level, but the pressure further down the tailpipe remained much higher.

The burner exit survey performed at the lower enthalpy level was made at an equivalence ratio of .78, when the air nozzle was separated. As this condition is intolerable for application to the engine, these data are not presented.

**CONFIDENTIAL**

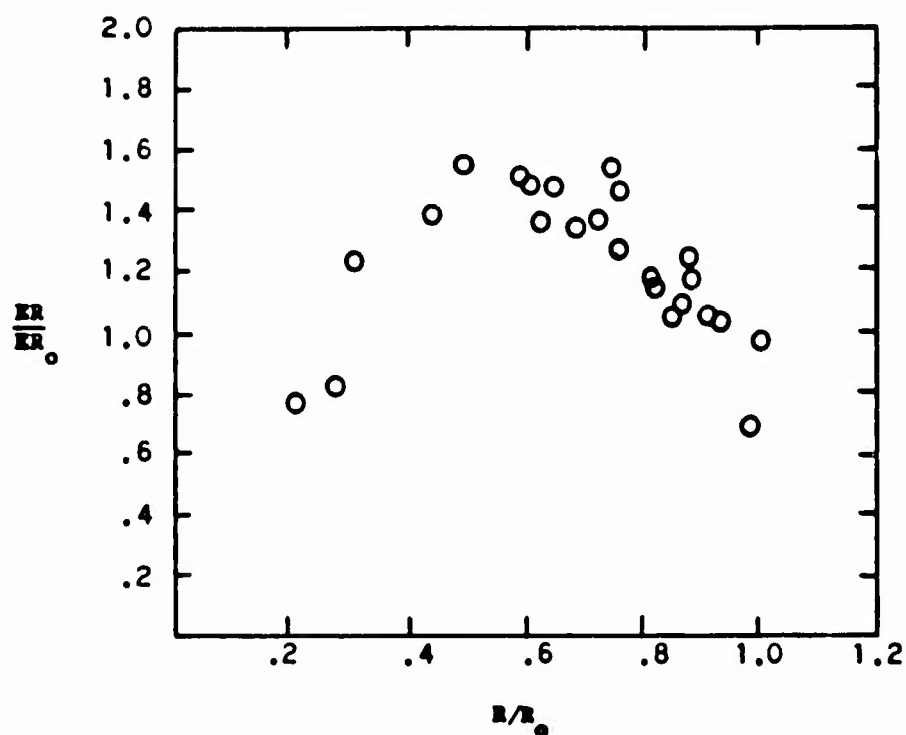
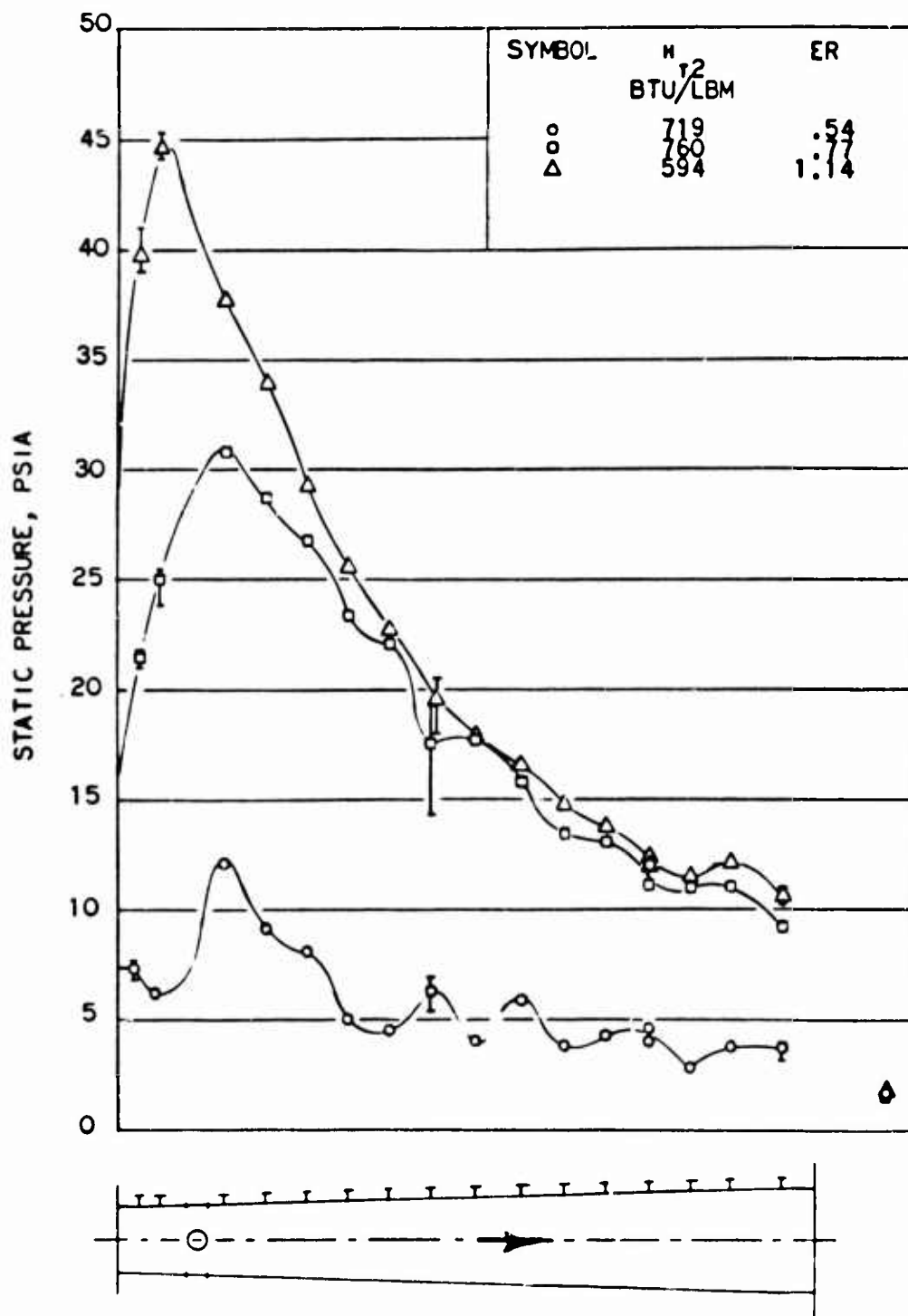
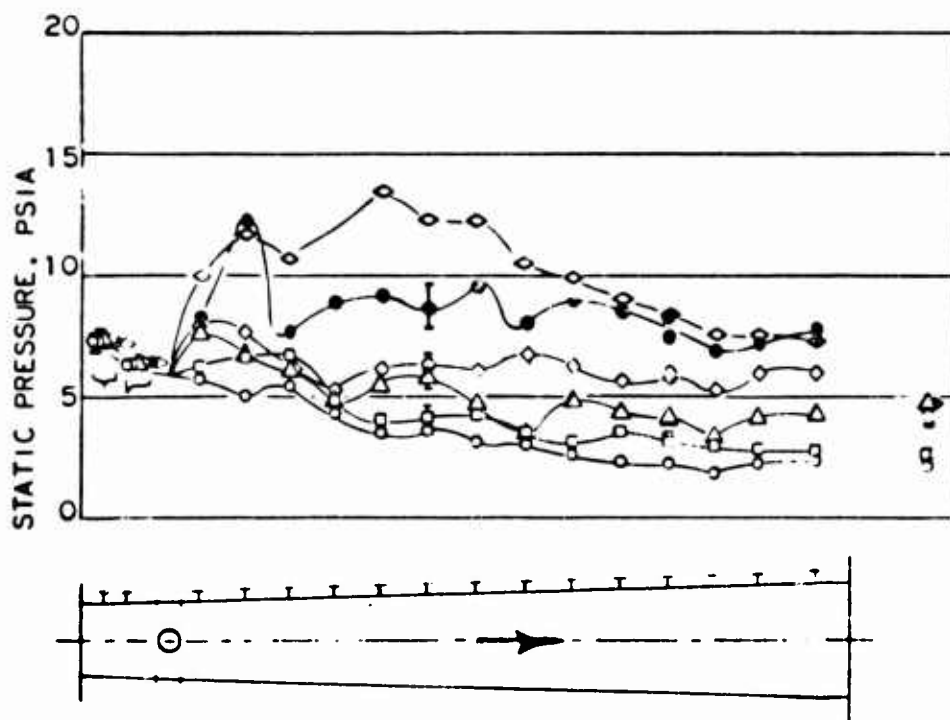
**CONFIDENTIAL**

Figure 119 - Fuel/Air Profile for Run 107 (AEP)

$$M_p = 6 \quad KR_0 = .760$$

**CONFIDENTIAL**

**CONFIDENTIAL****CONFIDENTIAL**

**CONFIDENTIAL**

SYMBOL	$h_{T2}$ BTU/LBM	ER
○	1285	0
△	2800	.38
○	2688	.57
○	275	.74
●	268	.96
△	300	1.19

Figure 121 - Wall Static Pressures, Configuration APQ

**CONFIDENTIAL**

**CONFIDENTIAL**

Burner performance was evaluated at an enthalpy level simulating Mach 7.6 flight, and an equivalence ratio of .76. These data are tabulated in Table VI. The combustion efficiency was low (.55) relative to step combustors under comparable conditions. The thrust potential was not so low, due to the higher mean wall pressure.

Burner exit Mach number and equivalence ratio maps are drawn in Figures 122 and 123. A lobed fuel distribution pattern is evident, indicating that radial and circumferential mixing were inadequate for high performance. The necessity of assuming low local combustion efficiencies (like .70) in order to achieve a satisfactory continuity check was taken as evidence that the instantaneous ER profiles were much less uniform than the time-average profiles shown in Figures 122 and 123.

b) Configuration AGQ

In three tests, Injector G was installed between Air Nozzle A and Tailpipe Q, with the F-type injectors of Tailpipe Q inactive.

Wall static pressures measured at enthalpy levels simulating flight at Mach 7.9 and 8.2 are plotted in Figure 124. At this condition, Injector G produced separation of the air supply nozzle at equivalence ratios greater than .5. At lower ER's strong pressure peaks in the tailpipe were absent, except for a narrow range of ER's just prior to inlet separation.

Since Injector C was prone to separate the inlet, it was not evaluated at lower enthalpy levels, where inlet separation occurs more readily.

Burner exit surveys were made at equivalence ratios of .42 and .83. As inlet separation existed at the latter condition, these data are considered invalid and are not presented. Burner performance figures at the lower equivalence ratio are included in Table VI. The combustion efficiency was less than for the step combustors under comparable conditions, but greater than that of Configuration AFQ, due primarily to the lower equivalence ratio. Mixing deficiencies produce greater efficiency decrements near stoichiometric equivalence ratio.

Local equivalence ratios measured in the burner exit stream are plotted as a function of radial position in Figure 125. The increased injection point density of Injector G resulted in a more uniform circumferential distribution than with the F-type injector of Tailpipe Q. The radial distribution is poor, due both to weak radial mixing and to less than optimum fuel jet penetration at the low equivalence ratio.

**CONFIDENTIAL**

**CONFIDENTIAL**TABLE VI - SUMMARY OF TEST RESULTS - CONICAL BURNERS

Run Number	154	164	181
Configuration	AFQ	AGQ	BHQ
Air Stagnation Enthalpy $HT_2$ , BTU/LBM	1138	1249	1788
Simulated Flight Mach Number, $M_p$ (1)	7.6	7.8	9.5
Burner Inlet Mach Number, $M_2$	2.73	2.72	3.16
Burner Inlet Velocity, $V_2$ , FT/SEC	5830	5970	7540
Burner Inlet Static Temperature, $T_2$ , $^{\circ}R$	2010	2120	2525
Burner Inlet Static Pressure, $P_2$ , PSIA	7.321	7.838	4.832
Burner Inlet Impulse, LBF	562.7	544.4	487.7
Burner Equivalence Ratio ER	.759	.417	1.191
Step Base Pressure Ratio, $P_W/P_2$	.943	.959	1.175
Burner Friction Coefficient, $C_f$ (2)	.0026	.0034	.0015
Burner Exit Impulse, LBF	663.5	565.4	527.7
Ideal Thrust of Optimum Burner, LBF (3)	248.7	171.1	165.9
Ideal Thrust of Actual Burner, LBF(3)	144.8	112.9	99.6
Combustion Efficiency, ETABM	.549	.779	.682
Net Thrust Potential, ETANT	.533	.525	.746

Notes: (1)  $M_p$  based on an Ambient Temperature of  $390^{\circ}R$   
 (2)  $C_p$  based on Burner Inlet Velocity Head  
 (3) Thrust based on Hypothetical Exhaust Nozzle of Exit Area =  $1.27 \text{ FT}^2$ .

**CONFIDENTIAL**

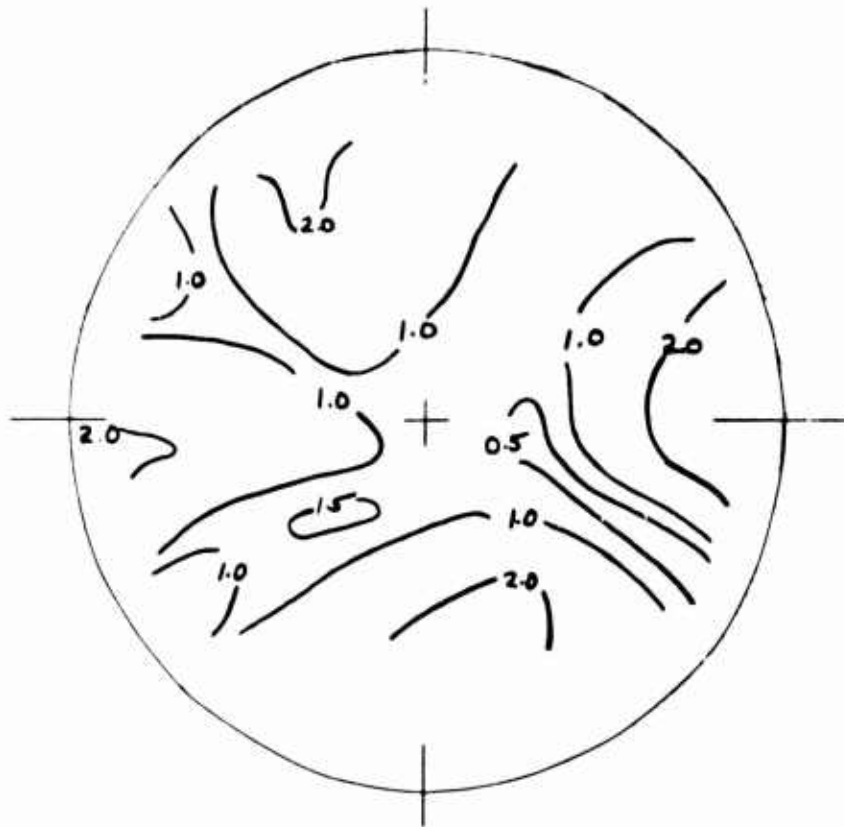
**CONFIDENTIAL**

Figure 122 - Burner Exit Stream Normalized Equivalence Ratio  
Contours ( $KR/KRo$ ) - Run 154, Configuration APQ  
 $KRo = 0.74$      $Mp = 8$

**CONFIDENTIAL**

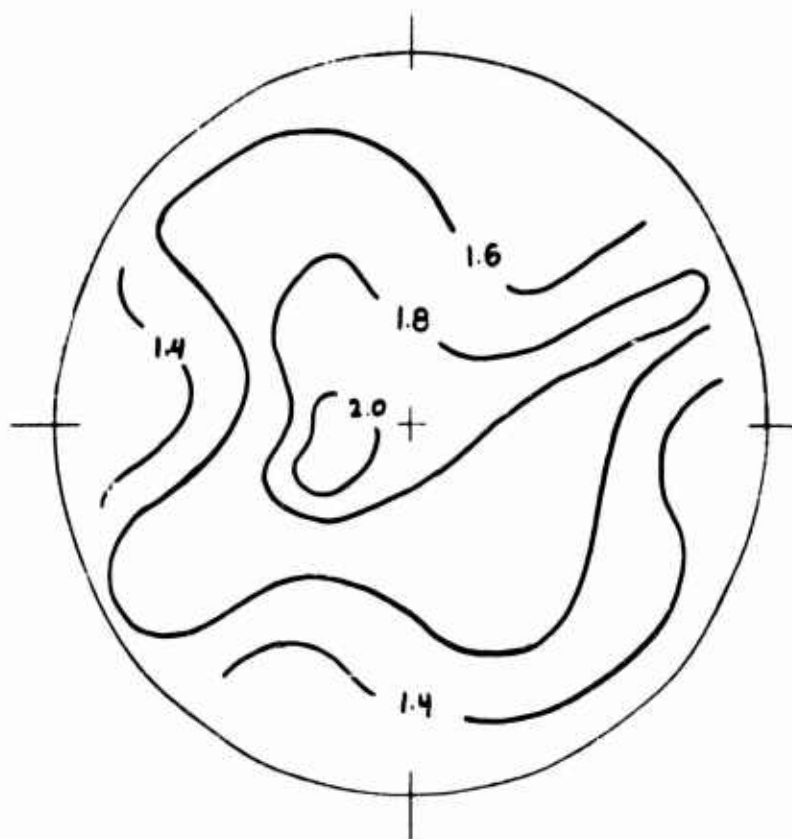
**CONFIDENTIAL**

Figure 123 - Mach Number Contour at Burzor Exit  
Run 154, Configuration AFQ

**CONFIDENTIAL**

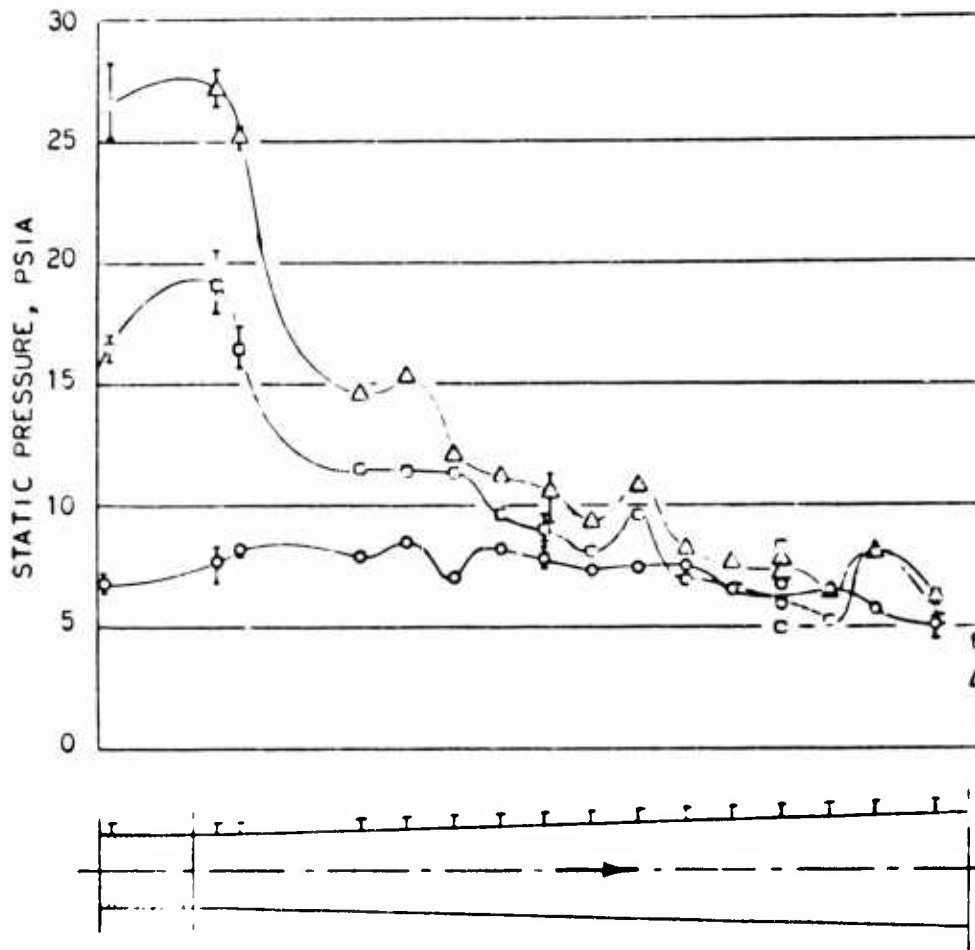
**CONFIDENTIAL**

Figure 124 - Wall Static Pressures, Configuration AGQ

**CONFIDENTIAL**

**CONFIDENTIAL**

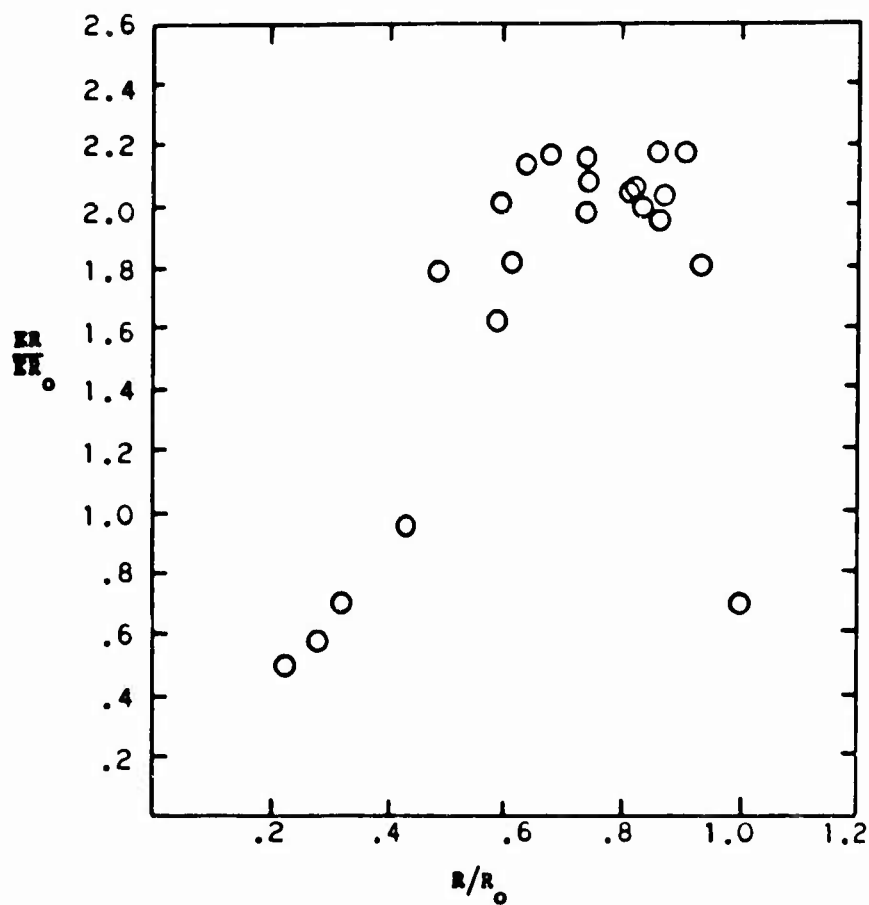


Figure 125 - Fuel/Air Profile for Run 164 (AQQ)

$$M_p = 8$$

$$KR_0 = .42$$

**CONFIDENTIAL**

**CONFIDENTIAL**

c) Configuration AGFQ

During portions of two tests, both Injector G and the F-type injectors of Tailpipe Q were operated simultaneously. This was done to combine the advantages of each injector: the uniform circumferential distribution of Injector G and the resistance to inlet separation of the F-type injectors. The tests used enthalpy levels simulating flight at Mach 7.9.

The wall static pressure data are displayed in Figures 126 and 127, together with data from Configurations AFQ and AGQ for comparison. Figure 126 shows the effect of holding a constant fuel flow from Injector G while increasing the flow from the F-type injector. As the equivalence ratio increased, a strong pressure peak developed in the vicinity of the F-type injector. Peak pressures as high as 3.5 times the nominal inlet static pressure were recorded, with no evidence of separation upstream of Injector G. Equivalence ratios up to 1.3 were satisfactorily attained.

Figure 127 shows the effect of varying the flow split between the two injectors, with an approximately constant, near-stoichiometric total fuel flow. With all the fuel flowing from Injector G, the burner inlet was separated. With all the fuel injected from the F-type injectors, the pressure along the diverging tailpipe was approximately constant. With 43% of the fuel injected from Injector G and 57% through the F-type injectors, the pressure peaked strongly in the vicinity of the F-type injectors, but no inlet separation occurred.

No burner exit surveys were made with this configuration.

d) Configuration BHQ

Two tests were made of Tailpipe Q, with its F-type injectors inactive, fitted with Injector H and the Mach 3.2 Air Nozzle B. These tests were made at high enthalpy levels, simulating flight speeds from Mach 8.2 to 9.7. To attain the highest enthalpy levels, it was necessary to operate the combustor with an inlet static pressure somewhat less than the normal 7.4 psia.

Wall static pressures, measured at several equivalence ratios with an enthalpy level simulating flight at Mach 8.5, are shown in Figure 128. Data at a higher enthalpy level, simulating flight at Mach 9.7, are displayed in Figure 129. The response of the static pressure to increasing equivalence ratio was definite, but not as strong as with Configuration AGQ at lower enthalpy levels. Strong pressure peaks were absent, even with an equivalence ratio of 1.2. The data of Figures 128 and 129 were taken at different burner inlet

**CONFIDENTIAL**

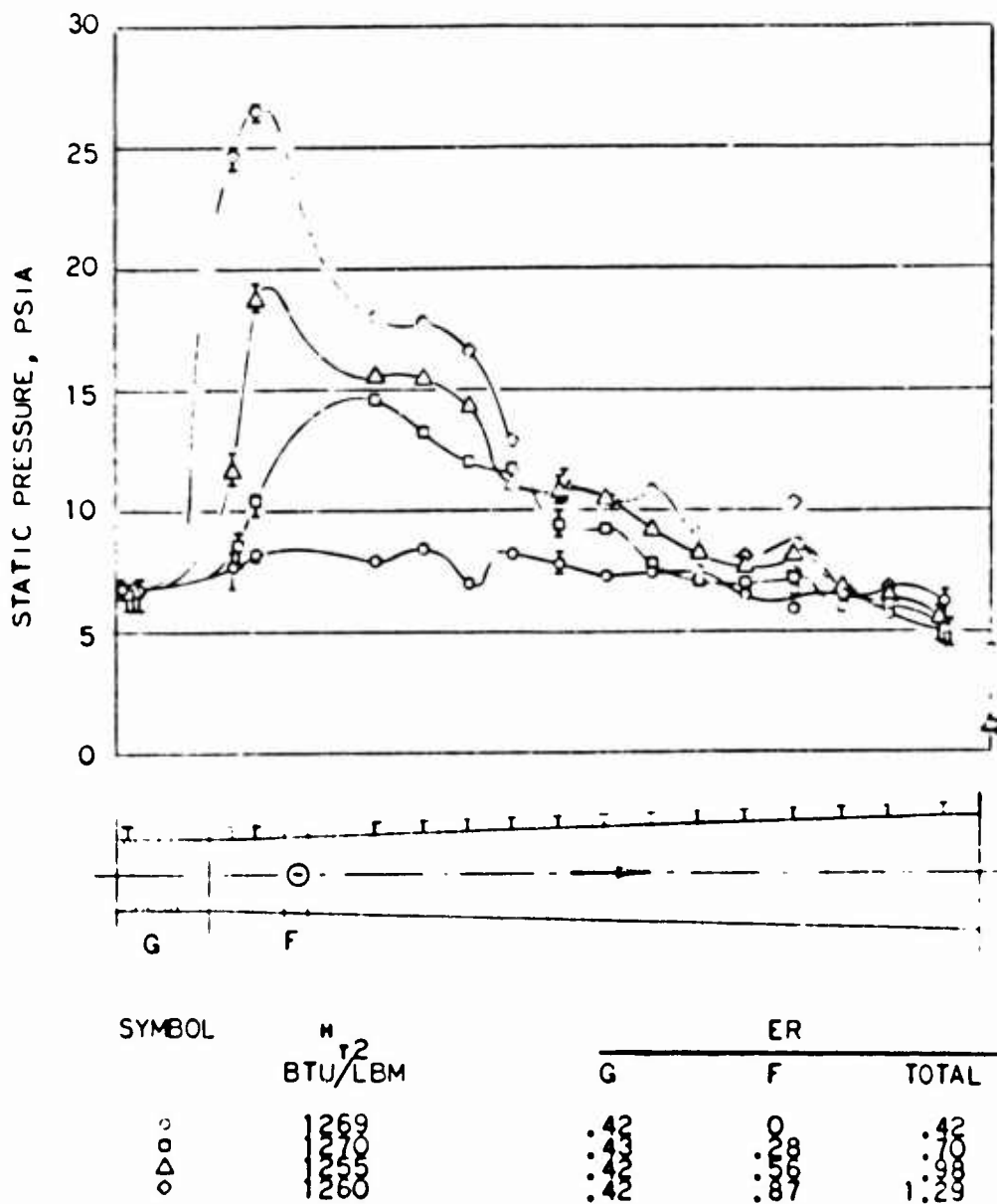
**CONFIDENTIAL**

Figure 126 - Wall Static Pressures, Configuration AGPQ

**CONFIDENTIAL**

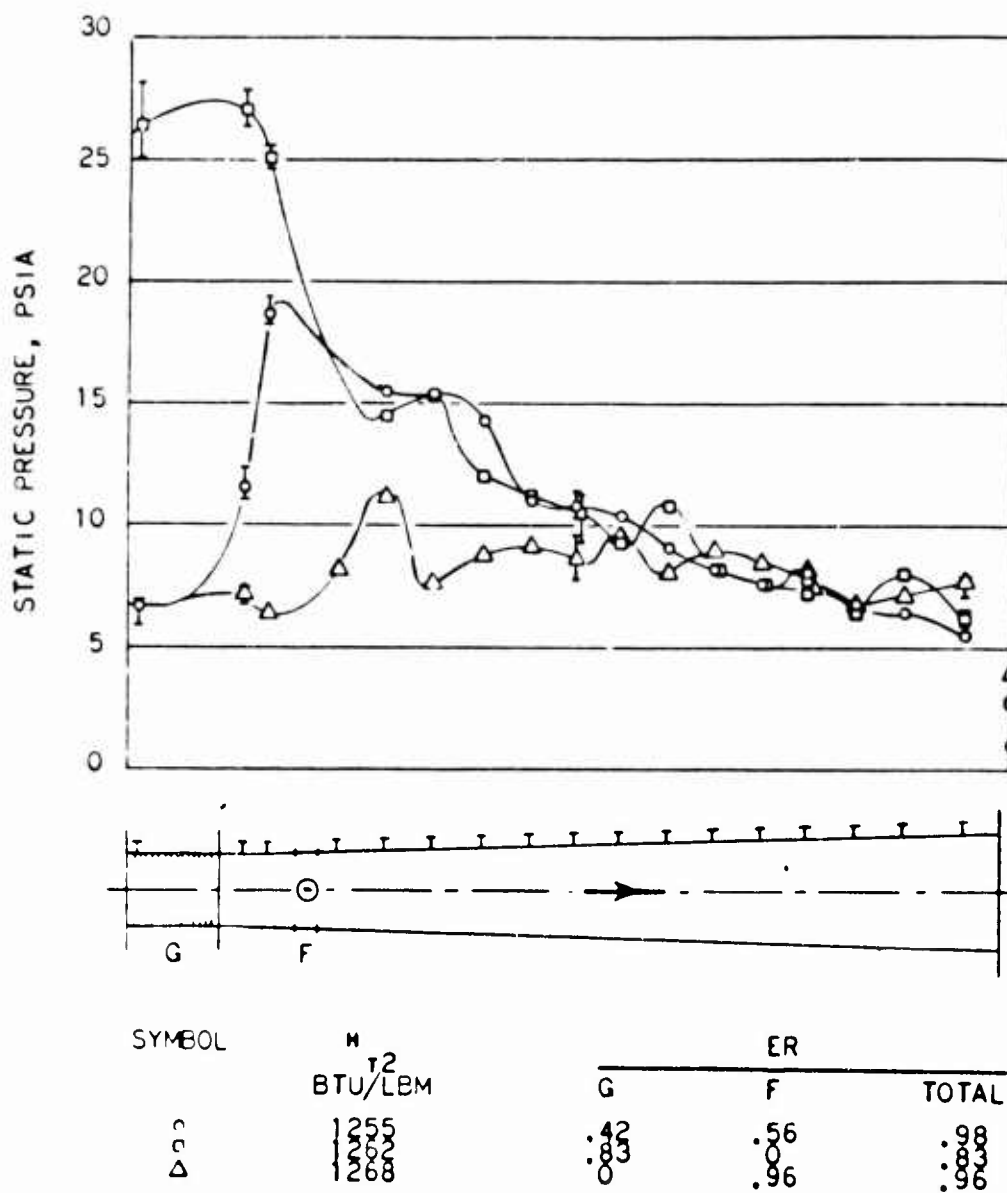
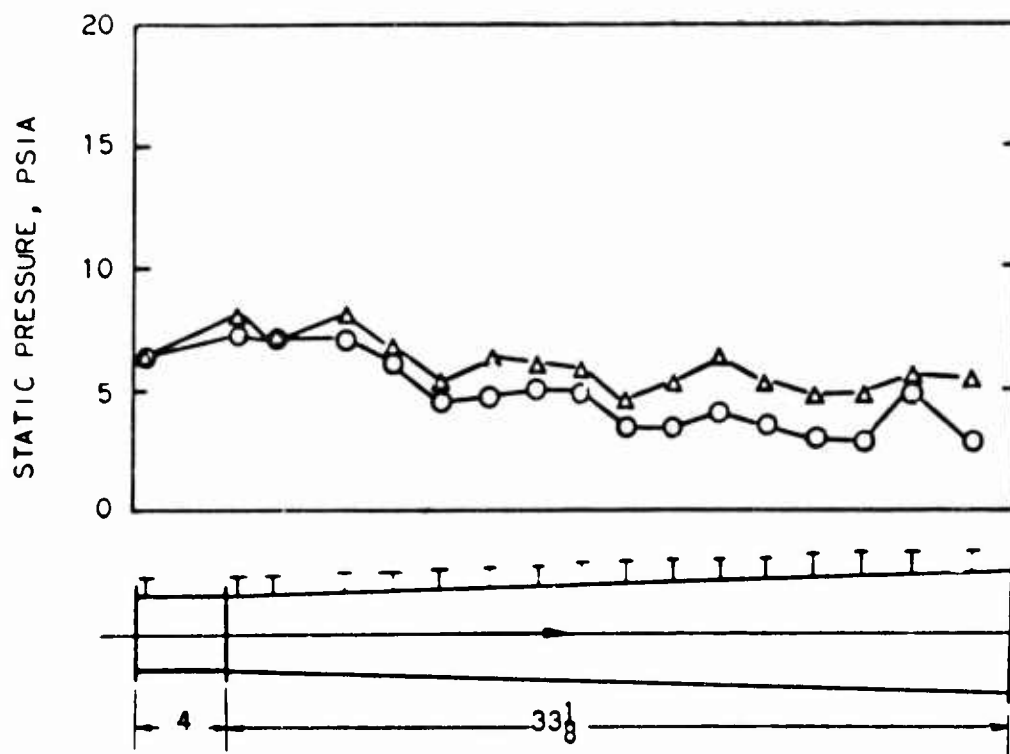
**CONFIDENTIAL**

Figure 127 - Wall Static Pressures, Configuration AGPQ

**CONFIDENTIAL**

**CONFIDENTIAL**

SYMBOL	$M_{T2}$	ER	RDG
O	1433	.170	4
Δ	1471	.712	6C

Figure 128 - Wall Static Pressure, Configuration B1Q

**CONFIDENTIAL**

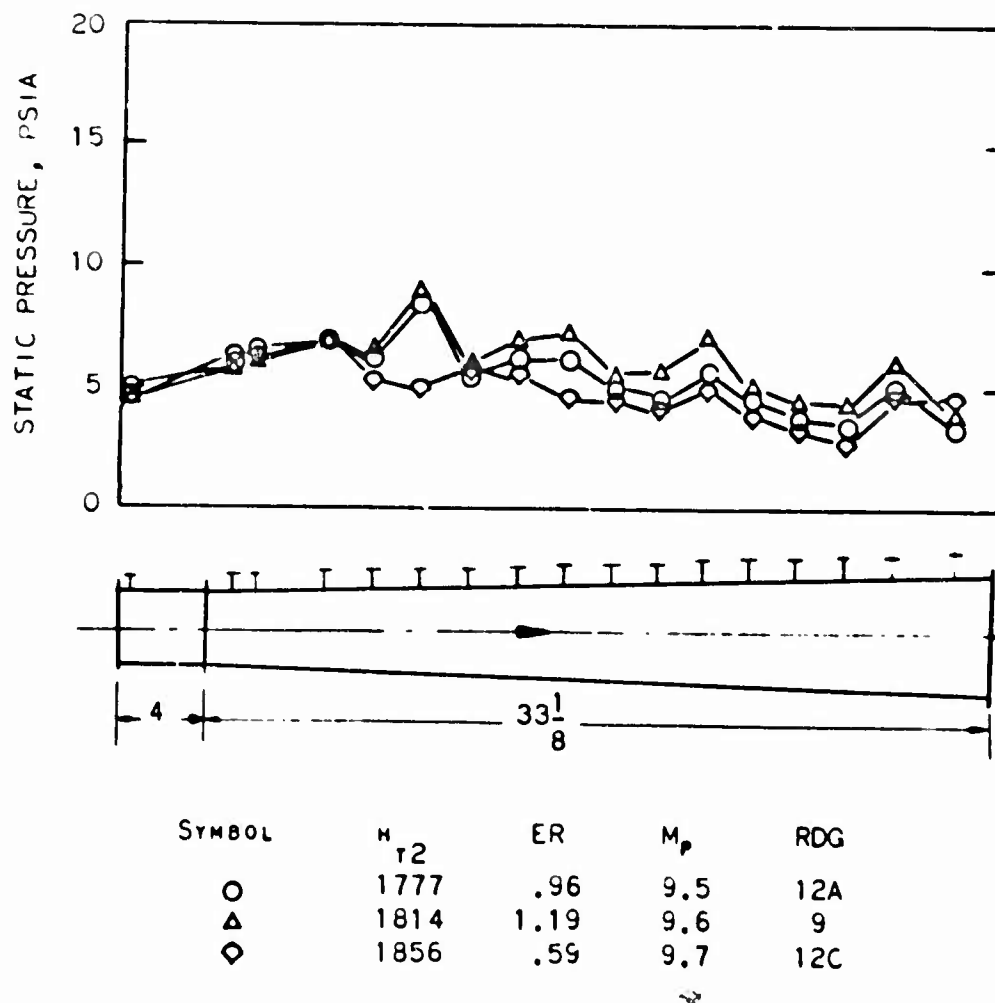
**CONFIDENTIAL**

Figure 129 - Wall Static Pressure, Configuration BBQ

**CONFIDENTIAL**

**CONFIDENTIAL**

pressure levels. To facilitate comparison, these data have been normalized by dividing local static pressure by nominal burner inlet static pressure. The comparison plot is given in Figure 130. At comparable equivalence ratios, the higher enthalpy level produced static pressures higher than those of the lower enthalpy level.

A burner exit survey was made at an equivalence ratio of 1.2 and an enthalpy level simulating flight at Mach 9.5. These data are included in Table VI. Combustion efficiency was low (.68), due partly to deficient mixing and partly to slow reaction kinetics at the low pressure level ( $\sim 7$  psia). The thrust potential was, however, acceptable, due to the high mean wall pressure.

Local equivalence ratios measured in the exit stream are plotted in Figure 131. The circumferential distribution was uniform, a characteristic of the high injection-point-density injectors. The mixing deficiency was in the radial and axial directions. Jet penetration into the high-energy air stream appeared less than optimum, despite the high equivalence ratio.

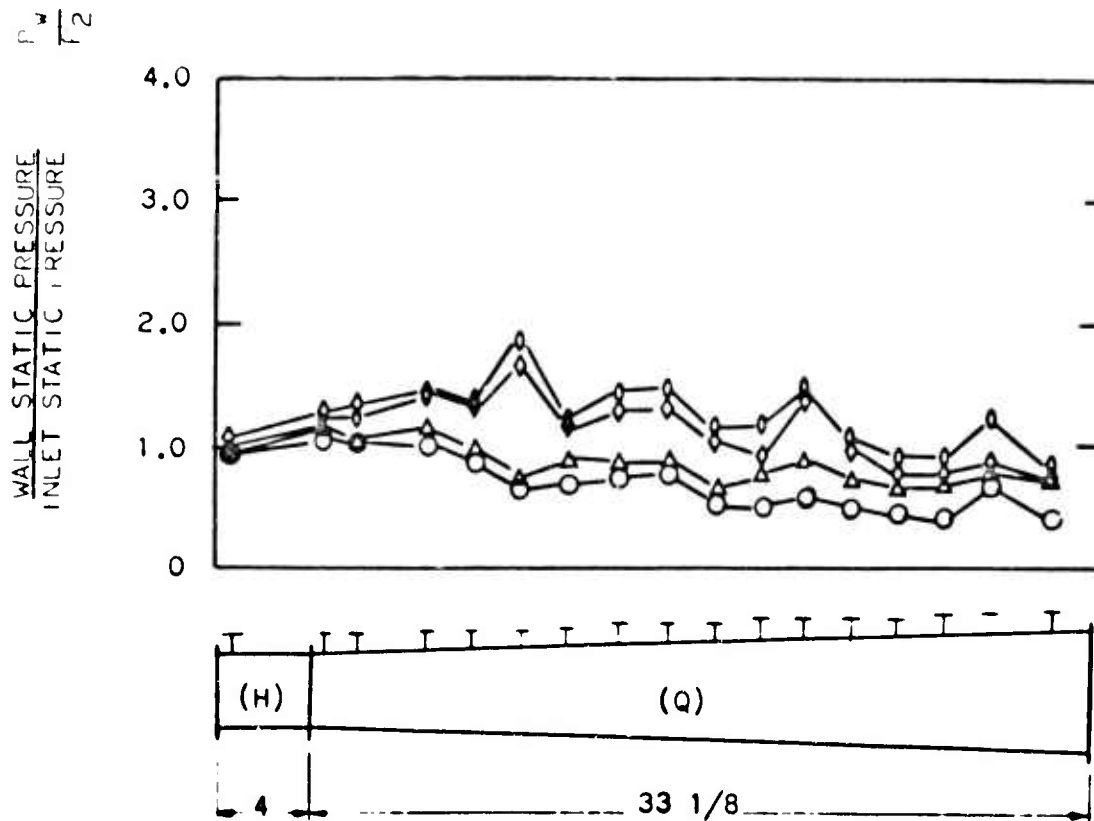
e) Configuration AKQ and AKFQ

Two tests were made with Air Nozzle A, the film slot Injector K, and Tailpipe Q, with its F-type injectors both active and inactive. These tests were at enthalpy levels simulating flight speeds around Mach 8.

Wall static pressures measured with Injector K operating alone are plotted in Figure 132. The wall pressures responded very weakly to large variations in equivalence ratio, indicating little or no combustion was occurring.

Wall static pressures measured with Injector K and the F-type injectors of Tailpipe Q operating together are plotted in Figures 133 and 134. Plotted for comparison are data from tests of Configuration AFQ (Figure 121). In Figure 133, the total equivalence ratio of Configuration AKFQ is .78, with an equivalence ratio of .55 being injected from the F-type injectors. The two sets of pressures from Configuration AFQ tests have equivalence ratios corresponding approximately to the total equivalence ratio of the AKFQ test and to the F injector ER of the AKFQ test. The AKFQ pressures are more similar to the AFQ pressures for the total equivalence ratio than to the AFQ pressures for the F-injector ER, indicating that much of the K-injector fuel had been induced to burn by injection of fuel from the F-type injectors. In Figure 134 the total ER of the AKFQ test was about 1.2. Two sets of pressures are shown for AKFQ: one with an F-injector ER of .47 and the other with an F-injector ER of .61. Again, the two sets of AFQ pressures shown are for

**CONFIDENTIAL**

**CONFIDENTIAL**

SYMBOL	$M_{T2}$	ER	$P_{s2}$ (PSIA)	RDG	RUN
O	1433	1.70	6.86	4	181
Δ	1471	.71	6.98	6C	181
◊	1777	.96	4.81	12A	181
◻	1814	1.19	4.87	9	181

Figure 130 - Normalized Static Pressures (BHQ)

**CONFIDENTIAL**

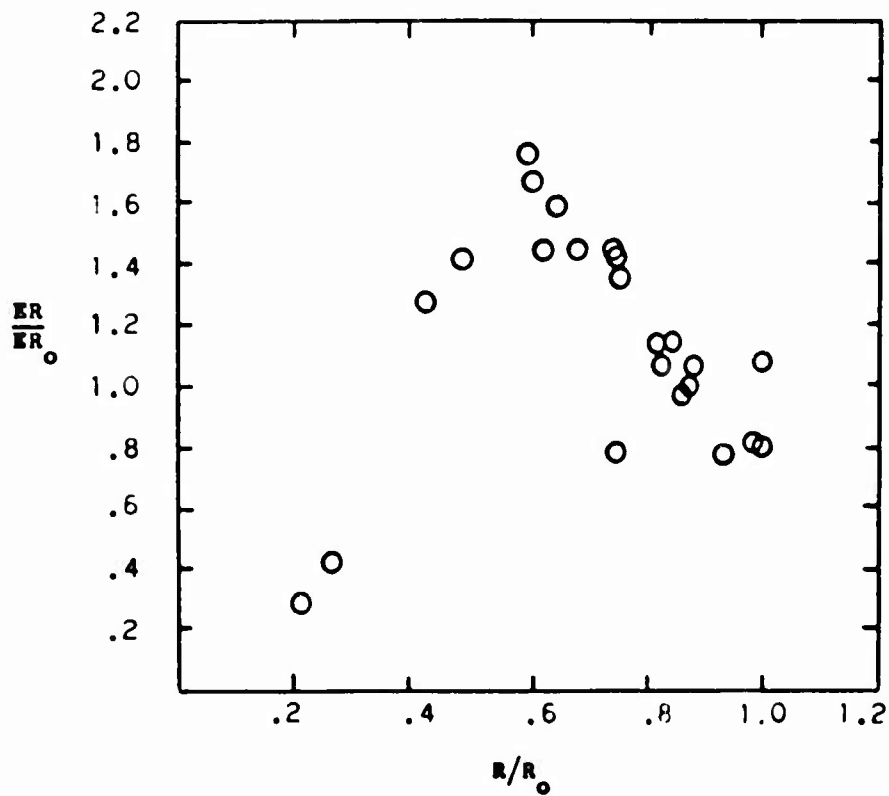
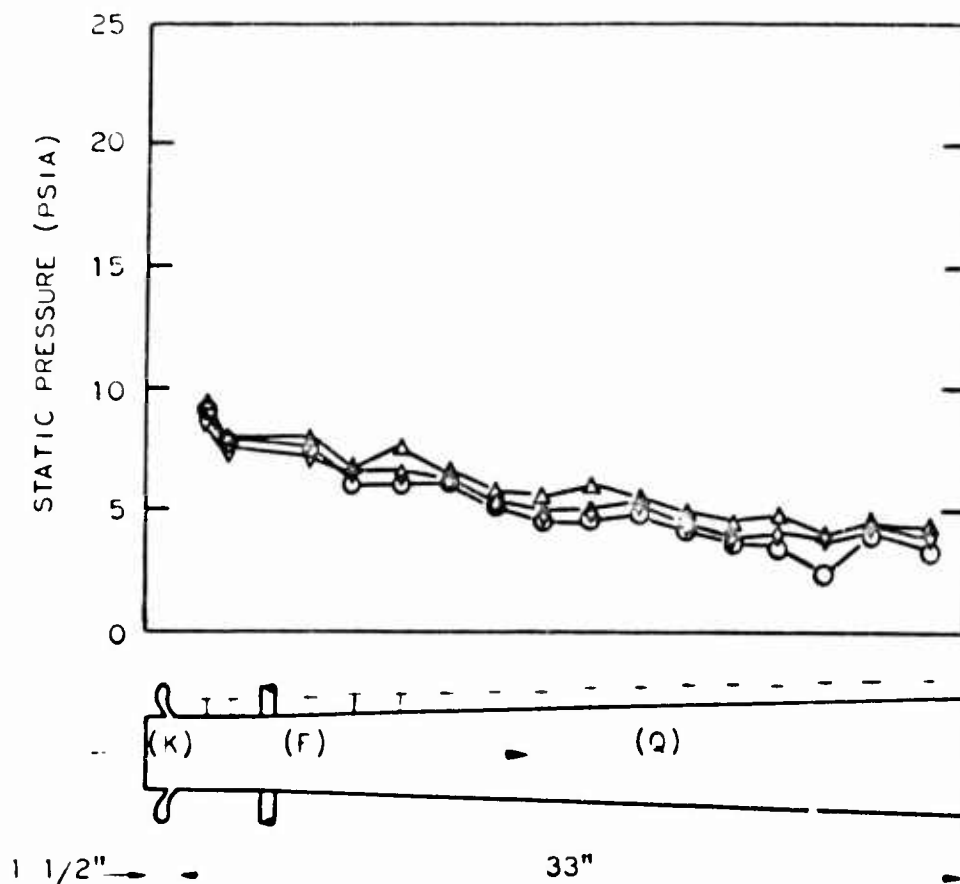
**CONFIDENTIAL**

Figure 131 - Fuel/Air Profile for Run 181 (BHQ)

$$M_p = 9$$

$$ER_0 = 1.23$$

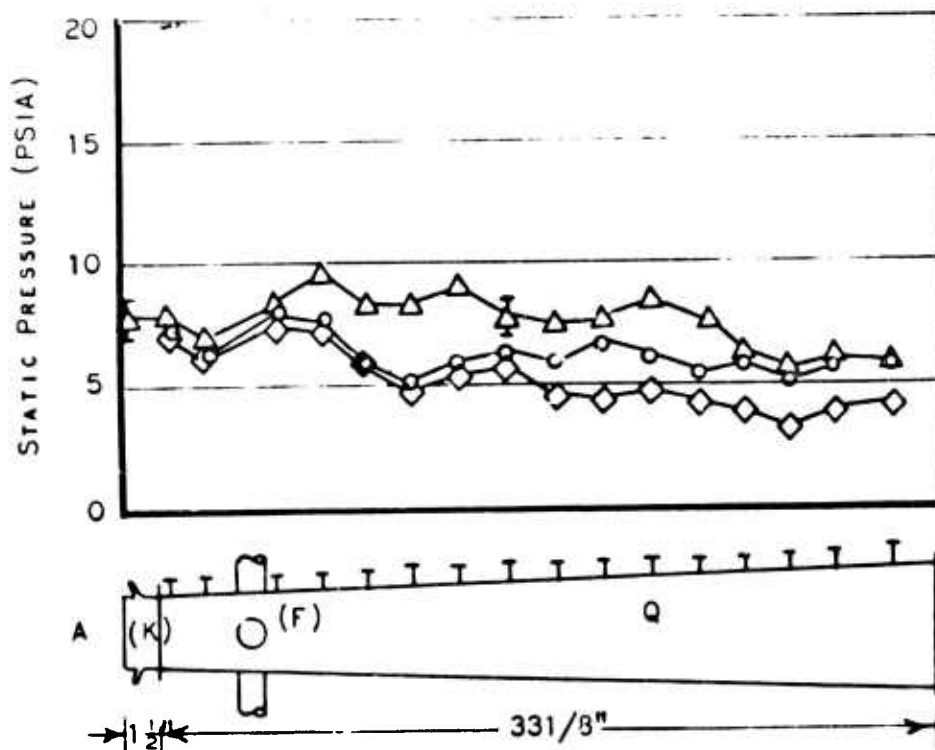
**CONFIDENTIAL**

**CONFIDENTIAL**

SYMBOL	$M_{T2}$	MP	ER	RDG
O	1276	7.98	.580	1 RUN 160
◊	1393	8.33	.968	3 RUN 160
Δ	1332	8.13	1.275	5 RUN 160

Figure 132 - Wall Static Pressure, Configuration AKQ

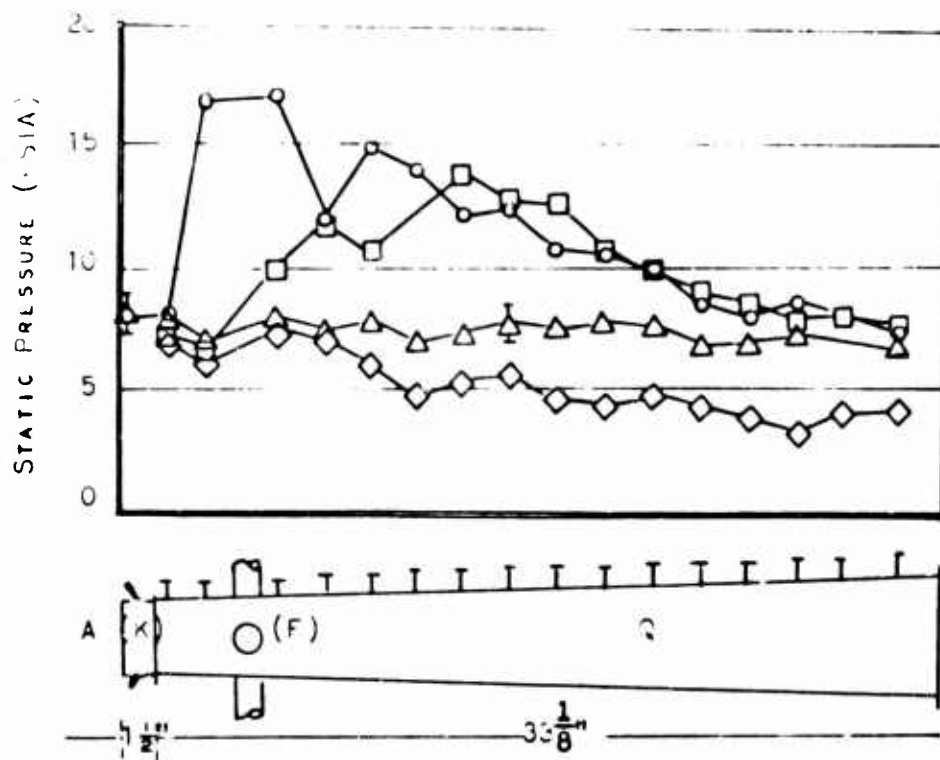
**CONFIDENTIAL**

**CONFIDENTIAL**

SYMBOL	M <sub>T2</sub>	M <sub>P</sub>	ER (K)	ER (F)	TOTAL ER
○	1275	7.9		.745	.745
△	1261	7.9	.236	.545	.781
◇	1268	7.9		.566	.566

Figure 133 - Wall Static Pressure, Configuration AKPQ

**CONFIDENTIAL**

**CONFIDENTIAL**

SYMBOL	M <sub>T2</sub>	M <sub>P</sub>	ER(K)	ER(F)	TOTAL ER	RUN
○	1261	7.9	.694	.611	1.305	161-20B
△	1261	7.9	.708	.474	1.182	161-20C
□	1300	8.0		1.19	1.19	153-5
△	1268	7.9		.566	.566	151-4

Figure 134 - Wall Static Pressure, Configuration AXFQ

**CONFIDENTIAL**

**CONFIDENTIAL**

equivalence ratios approximately matching the total and F-injector ER's. The set of AKFQ pressures having the lower F-injector ER corresponds more closely to the AFQ set for the F-injector ER, indicating that only part of the K-injector fuel had burned. The AKFQ set having the higher F-injector ER resembles the AFQ set for the total ER, indicating that the higher F-injector fuel flow had induced combustion of much of the K-injector fuel.

A burner exit survey was performed with an equivalence ratio of .94 from Injector K alone. Since little combustion was in evidence, performance parameters were not calculated. Local equivalence ratios measured in the exit stream are plotted in Figure 135 as a function of radial position. A heavy concentration of fuel was found at the burner wall, with little radial mixing having occurred. With the stream so unmixed, combustion efficiency would have been very low, whether or not ignition occurred.

### 3) Constant Area Tests for Film Cooling

Five tests with the film-slot (K) injector and the 3" constant area tailpipe produced useful data. All tests were made with the Mach 2.7 air nozzle, A. Three of these tests were run at simulated Mach 8 enthalpy levels, and two at simulated Mach 6 conditions.

Static pressure profiles are presented in Figure 136 for the two runs made at Mach 6 enthalpies and one run at a Mach 8 enthalpy level, (run 200, which was lit). Auto-ignition was not observed to occur at any Mach 6 condition with the 3" tailpipe, but did occur in this configuration at Mach 8 enthalpy as the equivalence ratio was raised to 0.4. The fact that auto-ignition did not occur at Mach 6 condition is evidenced by the gentle pressure rise shown in Figure 136 for Runs 198 and 201, which are typical of non-burning runs. The steep combustion-induced pressure rise shown in the figure for Run 200 is evidence of auto-ignition at these conditions. Noticeable from Figure 136 is the large increase in the magnitude of the pressure rise with increasing equivalence ratio. Once lit at an equivalence ratio of .4, the combustor remained lit as the equivalence ratio was lowered to .2. At equivalence ratios above .7, the large pressure rise caused the flow in the inlet to separate.

A gas-sample profile for Run 157 is shown in Figure 137. This test was made at a Mach 8 enthalpy level and the gas samples were taken at a lean equivalence ratio. Little or no combustion was taking place during the sampling in Run 157, as was indicated by visual observation. This profile is typical of runs where no burning occurred. Noticeable is the high concentration of hydrogen near the wall, which is characteristic of the film-slot injector.

**CONFIDENTIAL**

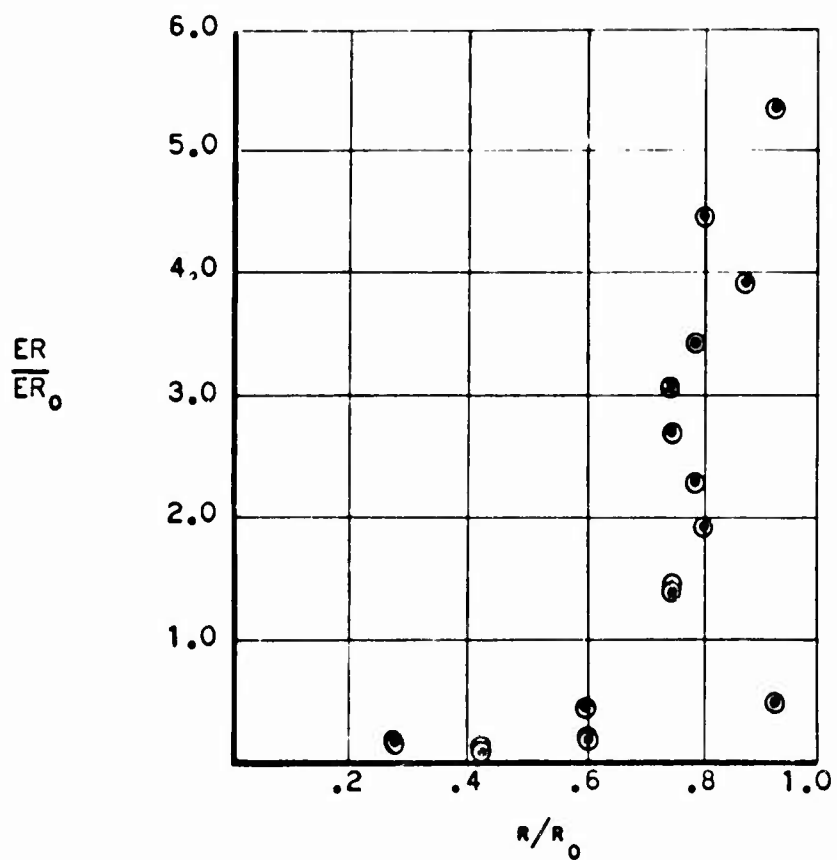
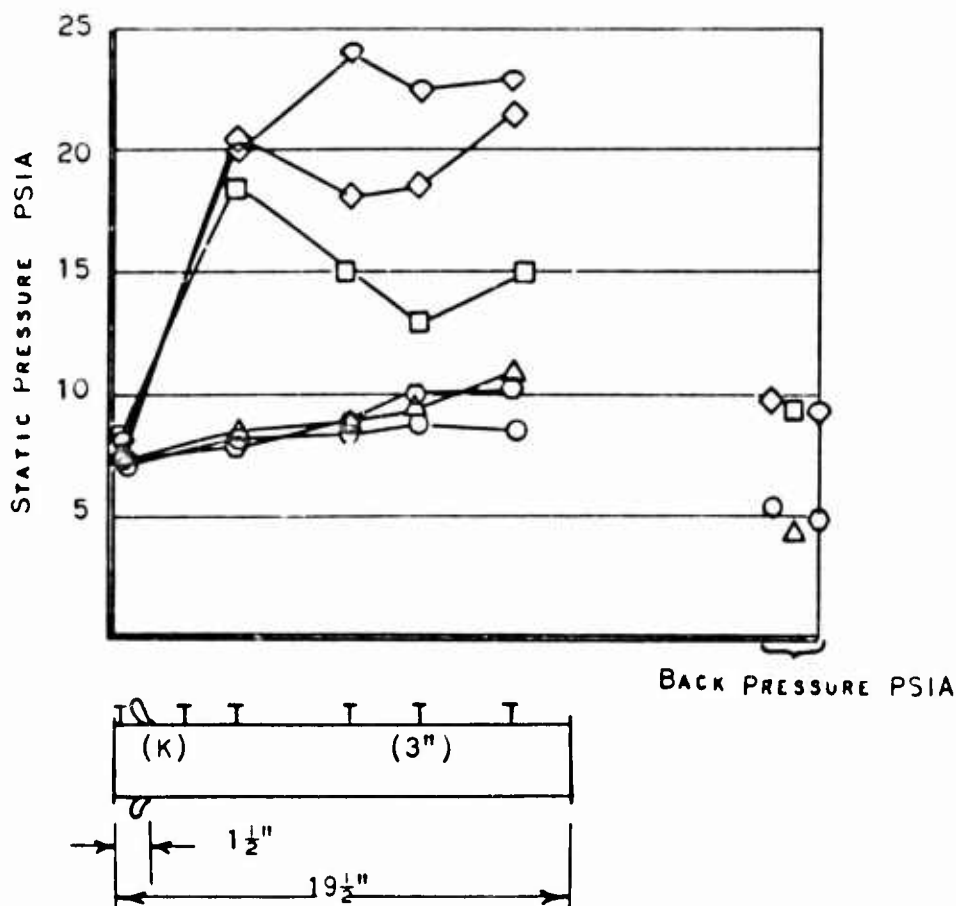
**CONFIDENTIAL**

Figure 135 - Fuel/Air Profile for Run 160 (AEQ)

$$ER_0 = .941$$

$$M_p = 8$$

**CONFIDENTIAL**

**CONFIDENTIAL**

SYMBOL	M <sub>T2</sub>	M <sub>p</sub>	LR	RUN	RDG
○	735	5.9	.22	201	8
△	735	5.9	.96	201	12
○	730	5.8	.70	198	10
◇	1250	7.9	.39	200	2A
□	1320	8.1	.19	200	7
◇	1530	8.8	.66	200	98

Figure 136 - Wall Static Pressures, Configuration AEX

**CONFIDENTIAL**

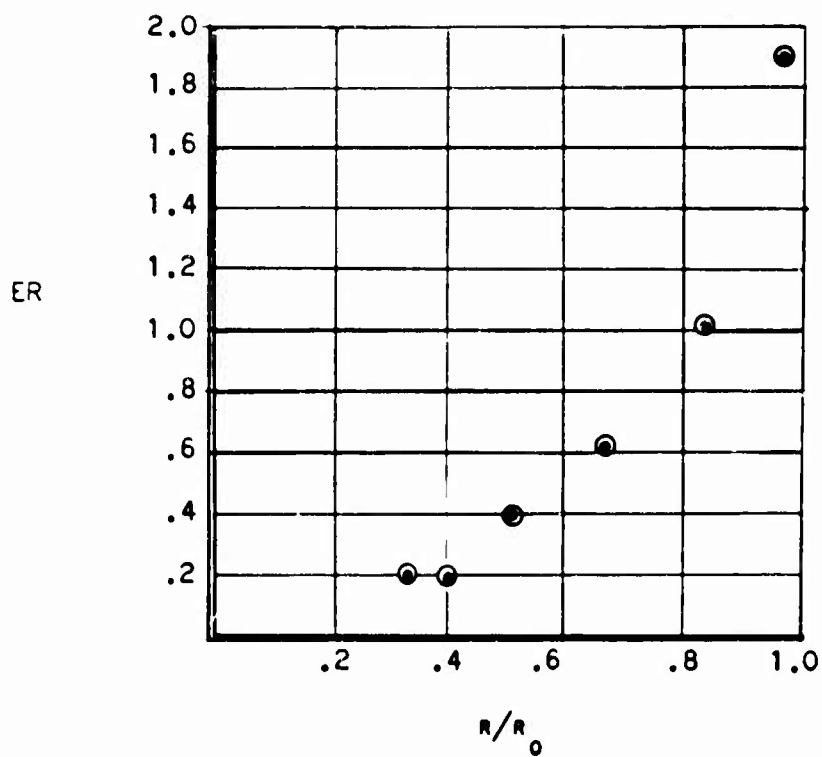
**CONFIDENTIAL**

Figure 137 - Fuel/Air Profile for Run 157-2

AK3"

M = 8

**CONFIDENTIAL**

**CONFIDENTIAL**

Figure 138 shows the gas sample profile obtained from Run 200. Also shown on the same figure, are the peak fuel/air ratios recorded at varying over-all equivalence ratios in Runs 198 and 200. It is clear from the figure that much better mixing exists in Run 200 than in the non-burning samples. The large pressure disturbances created by the combustion in Run 200 have a beneficial effect on the mixing, resulting in a much less exaggerated fuel/air profile than exists in the unlit runs.

Data for one additional run with the film-slot (K) injector and the conical Q tailpipe were presented in the previous section. The static pressure profile for this run, number 160, Configuration AKQ at simulated Mach 8 conditions, is shown in Figure 132 and the associated gas sample profile in Figure 135. The data for Run 160 further illustrate the difficulty in obtaining good mixing and auto-ignition with the film-slot injector. The decrease in wall static pressure with downstream distance shown in Figure 132 demonstrates that auto-ignition did not occur with the Q tailpipe even at conditions at which the 3" constant-area tailpipe lit. The dropping static pressure and static temperature in the expansion downstream of the injection point are responsible for the suppression of ignition in the Q tailpipe. Figure shows the gas sample profile obtained during this run; the steep profile is characteristic of those K injector runs which did not light. Because of the apparent poor characteristics of the K injector, no performance numbers were calculated for these runs.

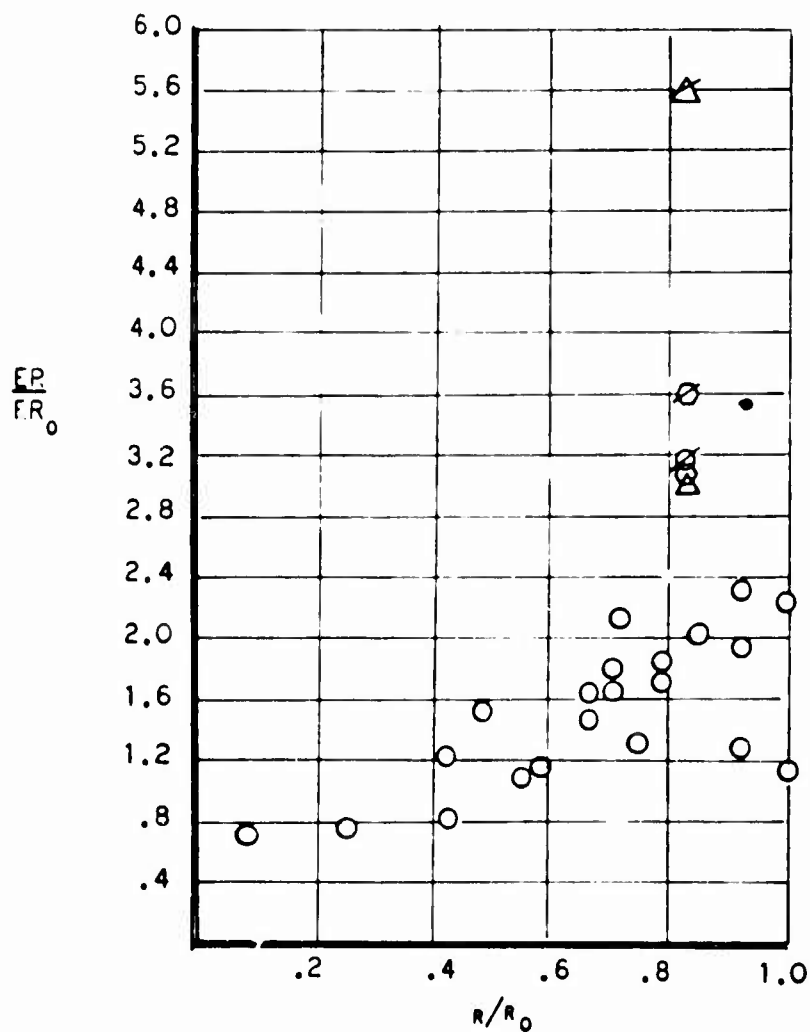
#### 4) Step-Cone Combustors

##### a) Configuration AHmR

Five tests were made of the combination of the Mach 2.7 air Nozzle A, the modified oblique Injector Hm, and the step-cone Tailpipe R. Air stagnation enthalpies ranged from 713 to 1280 Btu/lbm, simulating flight speeds from Mach 5.8 to 8.0. Equivalence ratios ranged from .33 to 1.26.

Wall static pressures measured along the combustor at a relatively low enthalpy level, simulating flight speeds around Mach 6.4, are plotted in Figure 139. The burner equivalence ratio was nearly constant at about .7. A moderate pressure rise occurred in the 3.0 inch diameter section ahead of the step. Base pressure on the rather small step was high, about twice the nominal burner inlet static pressure. Wall pressures remained high along the conical length of the tailpipe. Also shown in Figure 139 are pressures for a condition in which the equivalence ratio was about the same, but enthalpy level had drifted to a slightly lower level, simulating Mach 5.8 flight. This condition existed after a surge in fuel flow, caused by a defective control, had separated the flow in the air supply nozzle.

**CONFIDENTIAL**

**CONFIDENTIAL**

○ RUN 200, AK3", MP = 8, ER<sub>0</sub> = .390  
 ○ PEAK F/A, RUN 198-2, MP = 6, ER<sub>0</sub> = .219  
 ● PEAK F/A, RUN 198-3, MP = 6, ER<sub>0</sub> = .700  
 ○ PEAK F/A, RUN 201-2, MP = 6, ER<sub>0</sub> = .209  
 △ PEAK F/A, RUN 201-3, MP = 6, ER<sub>0</sub> = .911  
 △ PEAK F/A, RUN 201-4, MP = 6, ER<sub>0</sub> = .629

Figure 138 - Film Slot Injector Comparison

**CONFIDENTIAL**

CONFIDENTIAL

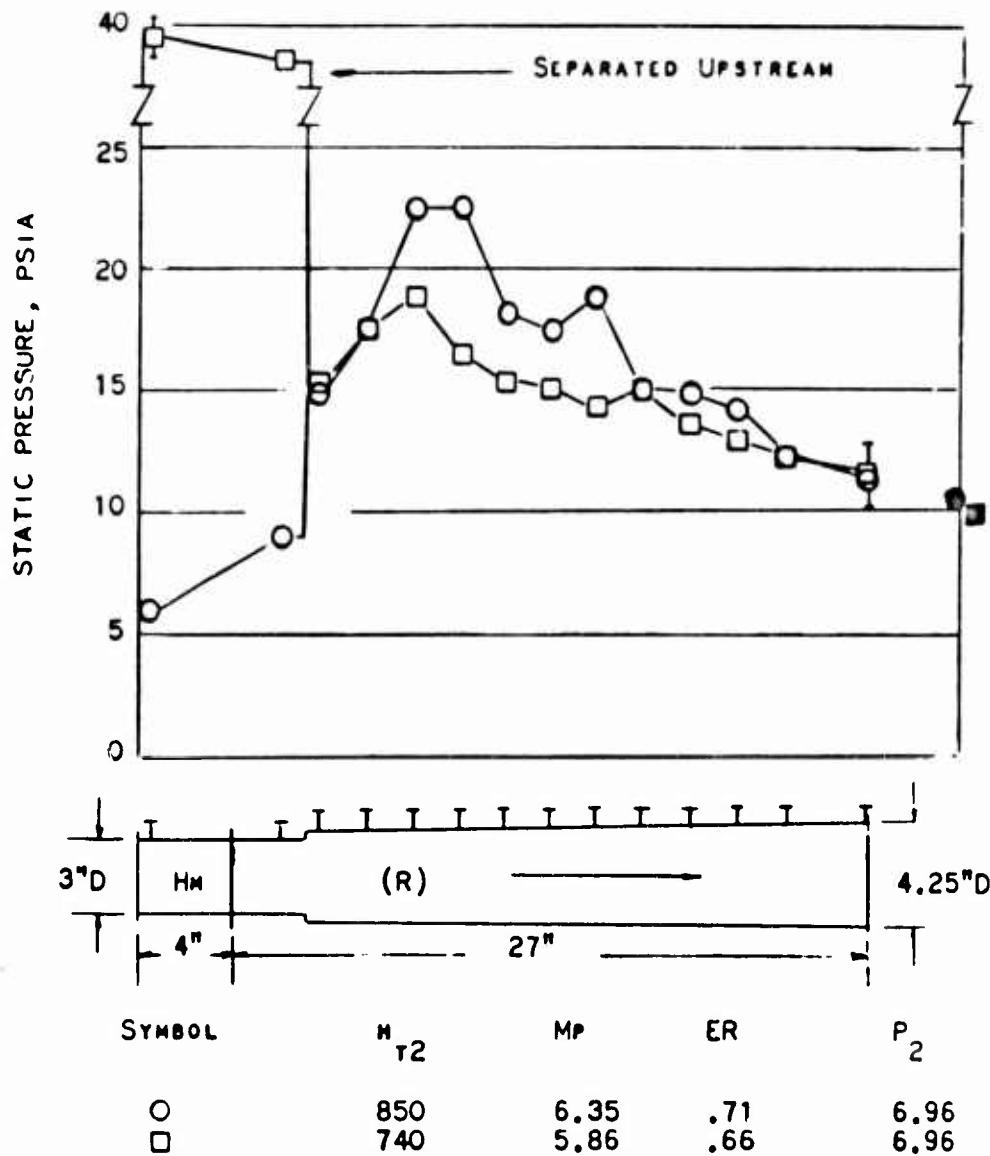


Figure 139 - Wall Static Pressures, Configuration ABR

CONFIDENTIAL

**CONFIDENTIAL**

The low enthalpy ignition characteristics of Configuration AHmR were not determined. The test was started with a high dump tank pressure to ensure ignition. No effort was made to determine if ignition would have occurred with a lower dump tank pressure.

Wall static pressures measured at a higher enthalpy level, simulating flight speeds around Mach 7.8, are shown in Figure 140. Step base pressures were lower than at the lower enthalpy level, but were significantly higher than those of previous step combustors. Pressures along the conical portion of the tailpipe were generally quite high. At this enthalpy level, separation of the burner inlet could be induced only by elevating the fuel flow to the highest ER shown, then adding nitrogen to the fuel to increase its bulk.

A burner exit survey was made at the lower enthalpy level, but the data are considered invalid, and are not presented. The burner inlet stream was separated at the time the survey was made, and this condition was not detected until after the test.

Two burner exit surveys at the higher enthalpy level produced burner performance figures at equivalence ratios of 1.0 and 1.2. These data are presented in Table VII at the end of this discussion. The combustion efficiency was .75 at stoichiometric equivalence ratio, rising to .84 at ER = 1.2. These efficiency levels are considered quite acceptable. The relatively high efficiencies, together with the high mean wall pressures, resulted in excellent thrust potentials.

Local equivalence ratios and Mach numbers measured in the burner exit stream are plotted in Figures 141, 142, 143 and 144 as a function of radial position. Circumferential fuel distribution was reasonably uniform. Both ER profiles showed leaner-than-average equivalence ratios in the center of the stream, indicating less than optimum fuel jet penetration or insufficient radial mixing. The profile for the higher over-all equivalence ratio was slightly more uniform. The Mach number profiles indicate that the flow was fully supersonic except for thin boundary layers.

b) Configuration BHmR

Three tests were made with the Mach 3.2 air nozzle, B, fitted to Injector Hm and Tailpipe R. High air stagnation enthalpies were used, ranging from 1095 to 1649 Btu/lbm, simulating flight speeds from Mach 7.3 to 9.1. Equivalence ratios ranged from .46 to 1.97.

Figures 145 through 149 present wall static pressure measurements at various equivalence ratios, with increasingly higher enthalpy

**CONFIDENTIAL**

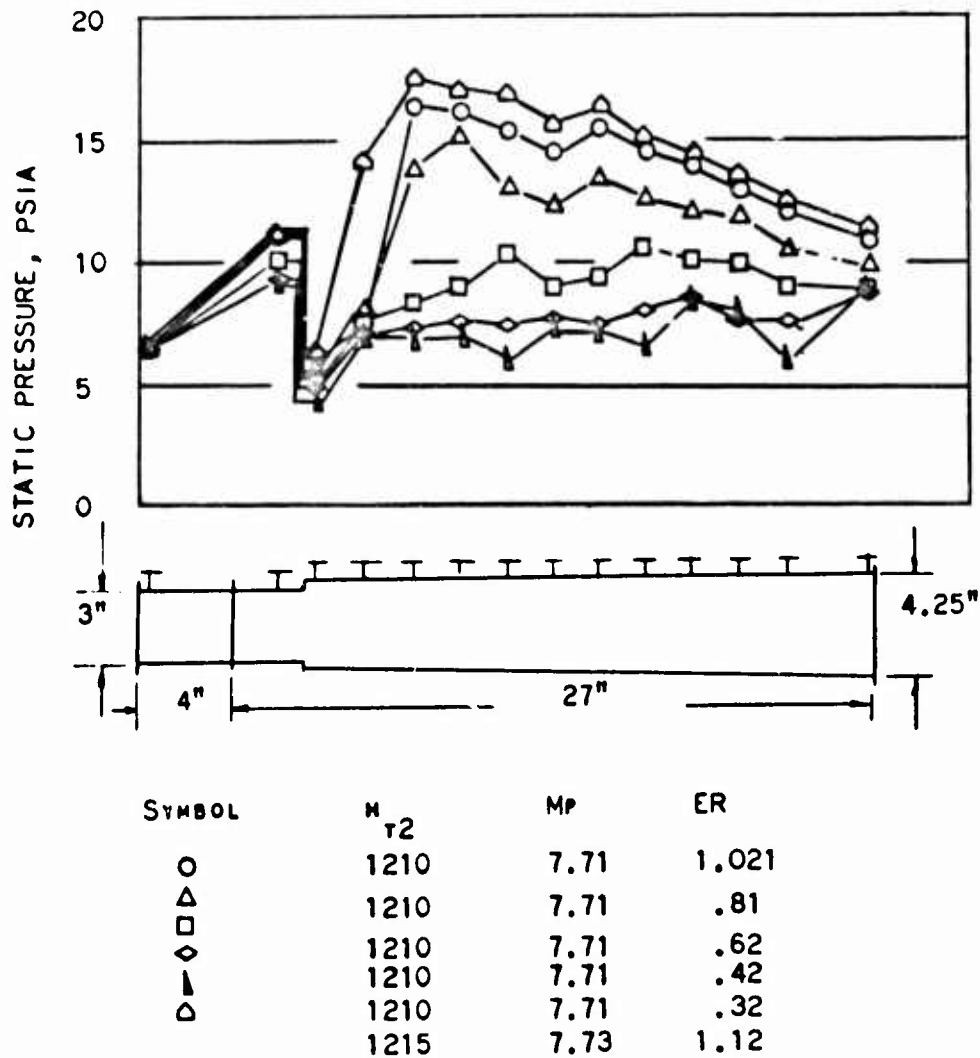
**CONFIDENTIAL**

Figure 140 - Wall Static Pressures, Configuration ABaR

**CONFIDENTIAL**

**CONFIDENTIAL**TABLE VII - SUMMARY OF TEST RESULTS STEP-CONE BURNER

Run Number Configuration	206 AHmR	208 AHmR	210 BHmR	212 BHmR
Air Stagnation Enthalpy $HT_2$ , BTU/LBM	1223	1238	1408	1240
Simulated Flight Mach Number, $M_p$ (1)	7.8	7.8	8.4	7.8
Burner Inlet Mach Number, $M_2$	2.72	2.72	3.23	3.26
Burner Inlet Velocity, $V_2$ , FT/SEC	5910	5900	6790	6410
Burner Inlet Static Temperature, $T_2$ , °R	2070	2070	1935	1685
Burner Inlet Static Pressure, $P_2$ , PSIA	7.011	7.160	5.415	5.766
Burner Inlet Impulse, LBF	570.0	554.1	577.5	630.9
Burner Equivalence Ratio, ER	1.194	.986	1.084	.984
Step-Base Pressure Ratio, $P_w/P_2$	1.674	1.351	.986	2.208
Burner Friction Coefficient, $C_f$ (2)	.0022	.0026	.0021	.0017
Burner Exit Impulse, LBF	626.2	587.6	584.8	693.8
Ideal Thrust of Optimum Burner, LBF (3)	286.6	244.6	217.0	265.5
Ideal Thrust of Actual Burner, LBF (3)	205.6	173.3	148.2	176.0
Combustion Efficiency, ETAEM	.844	.745	.657	.749
Net Thrust Potential, ETANT	.878	.763	.583	.868

Notes: (1)  $M_p$  based on Ambient Temperature of 390°R  
 (2)  $C_f$  based on Burner Inlet Velocity Head  
 (3) Thrust based on Hypothetical Exhaust Nozzle of Exit Area = 1.27 FT<sup>2</sup>.

**CONFIDENTIAL**

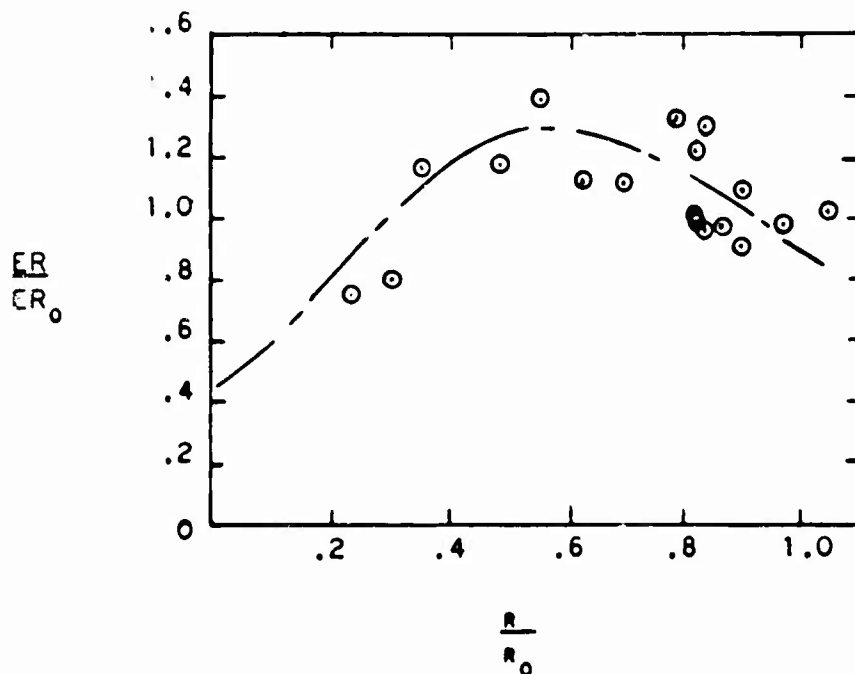
**CONFIDENTIAL**

Figure 141 - Fuel/Air Profile for Run 206, Configuration ABaR

$$ER_0 = 1.183 \quad M_p = 8$$

**CONFIDENTIAL**

**CONFIDENTIAL**

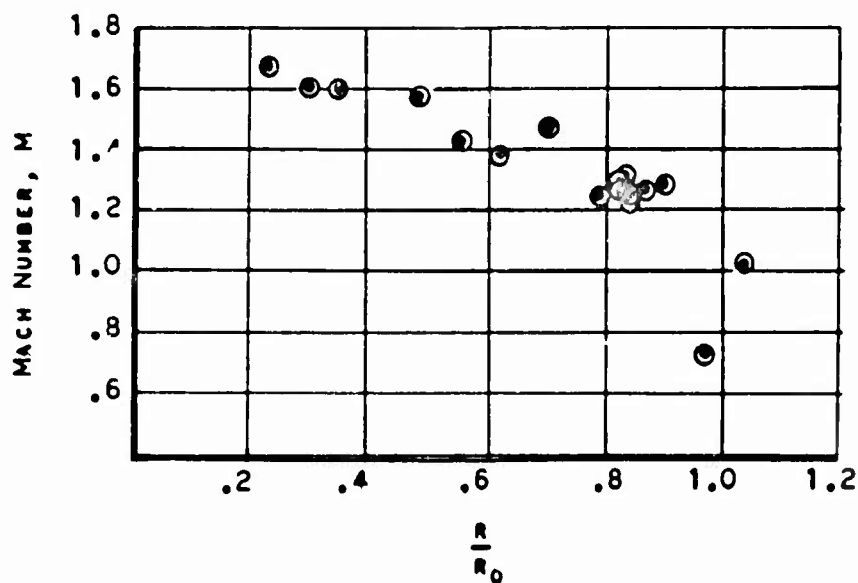


Figure 142 - Mach Number Profile for Run 206 ABaR

$$M_p = 8$$

$$R_{r_0} = 1.183$$

**CONFIDENTIAL**

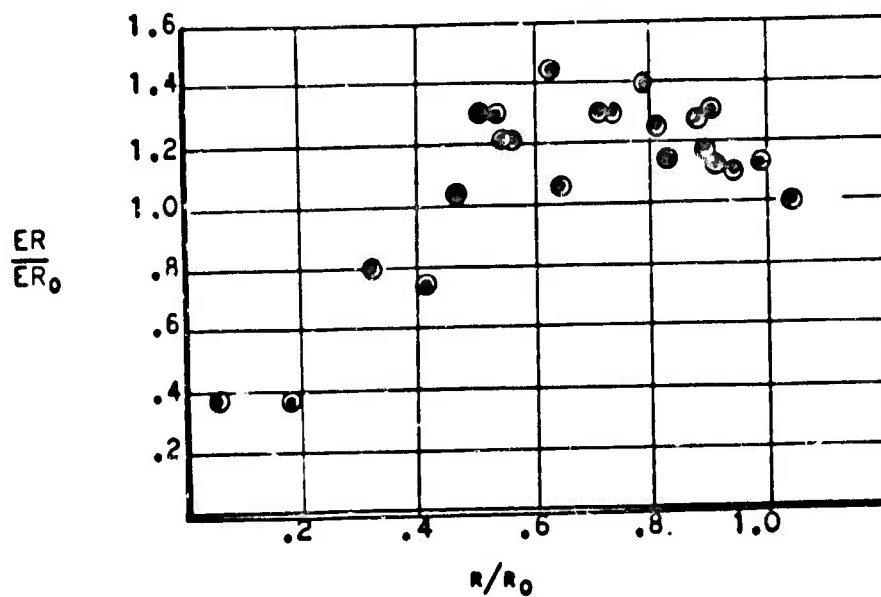
**CONFIDENTIAL**

Figure 143 - Fuel/Air Profile for Run 208 (ABMR)

$$ER_0 = .986 \quad M_p = 7.84$$

**CONFIDENTIAL**

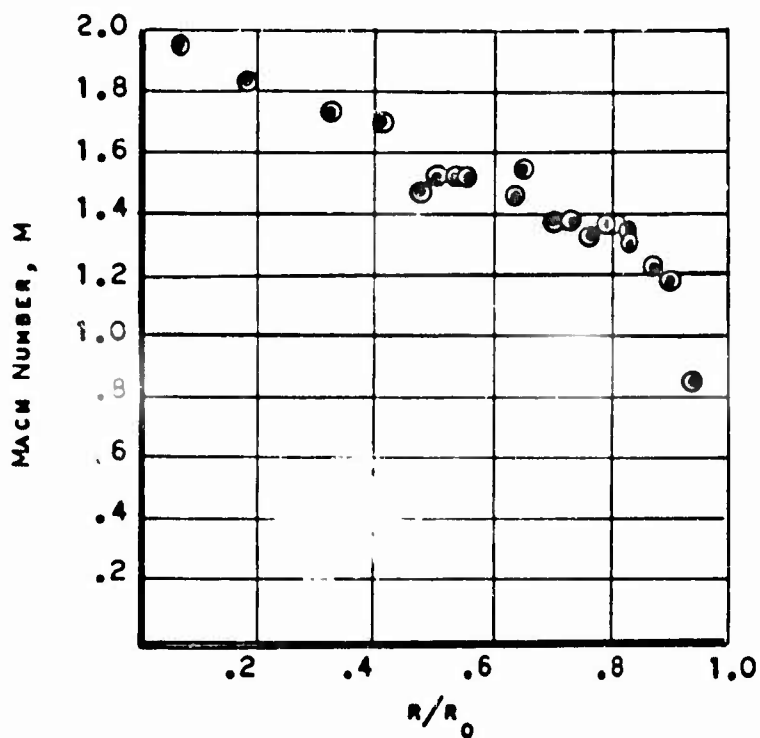
**CONFIDENTIAL**

Figure 144 - Concluded Mach Number Profile for Run 208 (AER)

$$M_p = 7.84$$

$$KR_0 = .986$$

**CONFIDENTIAL**

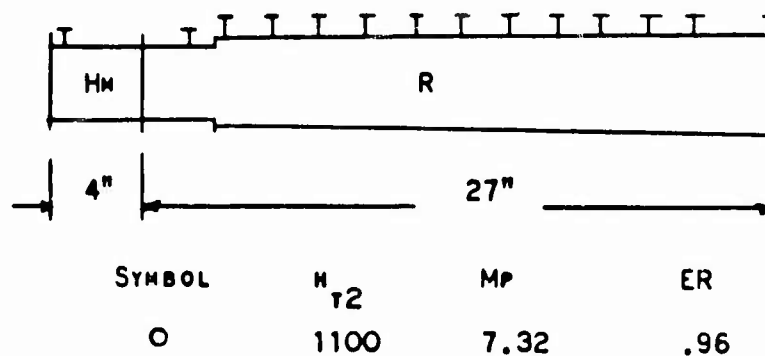
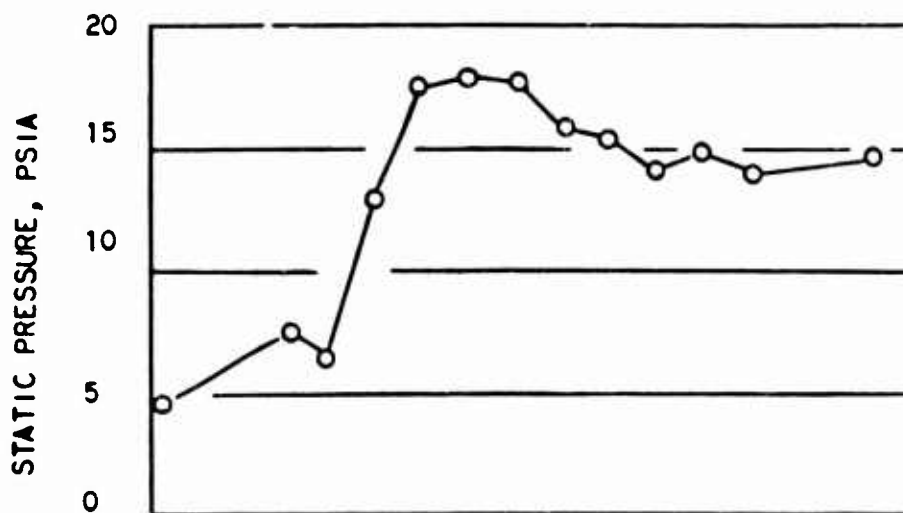
**CONFIDENTIAL**

Figure 145 - Wall Static Pressure, Configuration B3aR

**CONFIDENTIAL**

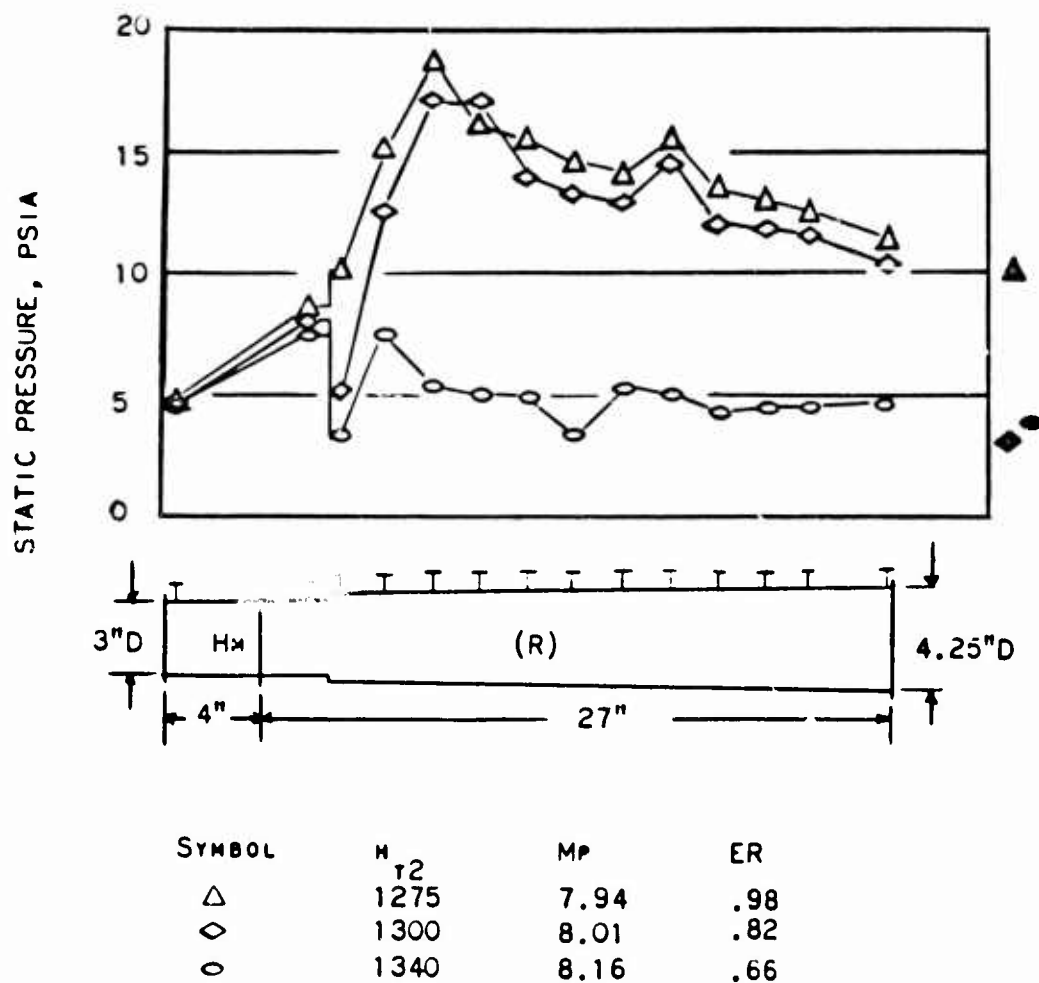
**CONFIDENTIAL**

Figure 146 - Wall Static Pressure, Configuration BHR

**CONFIDENTIAL**

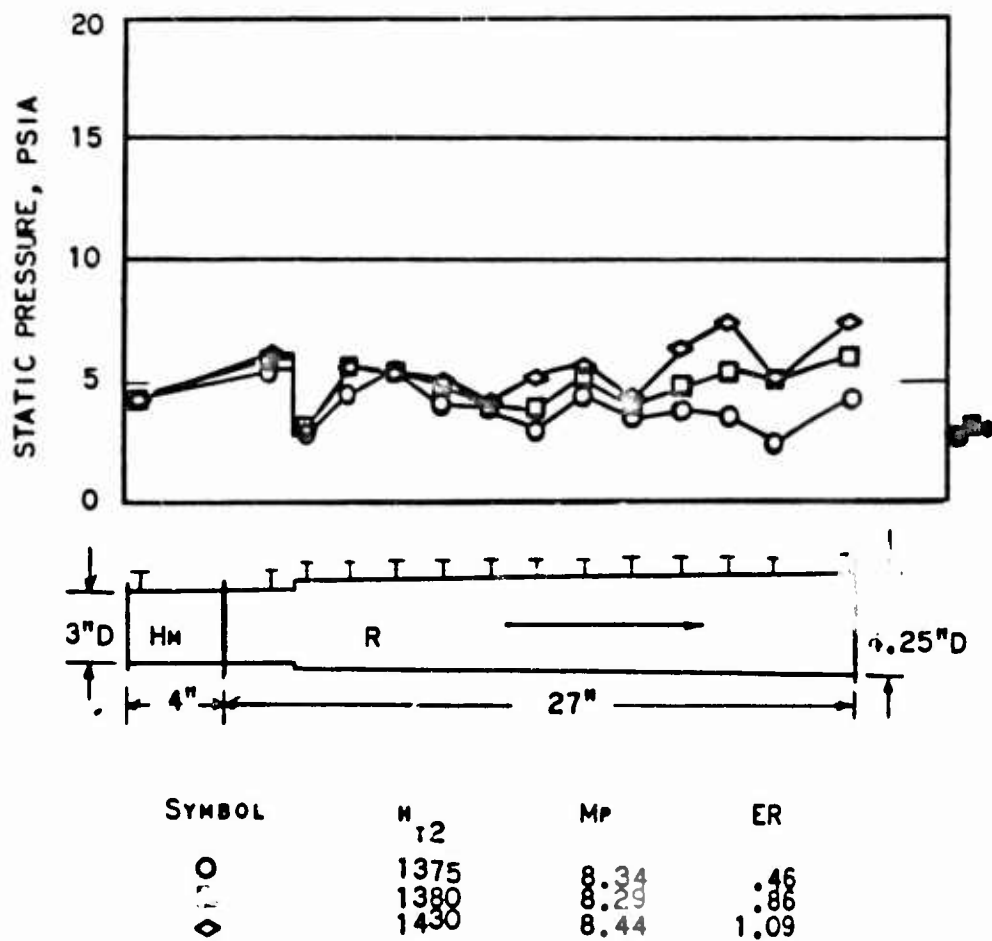
**CONFIDENTIAL**

Figure 147 - Wall Static Pressure, Configuration BBaR

**CONFIDENTIAL**

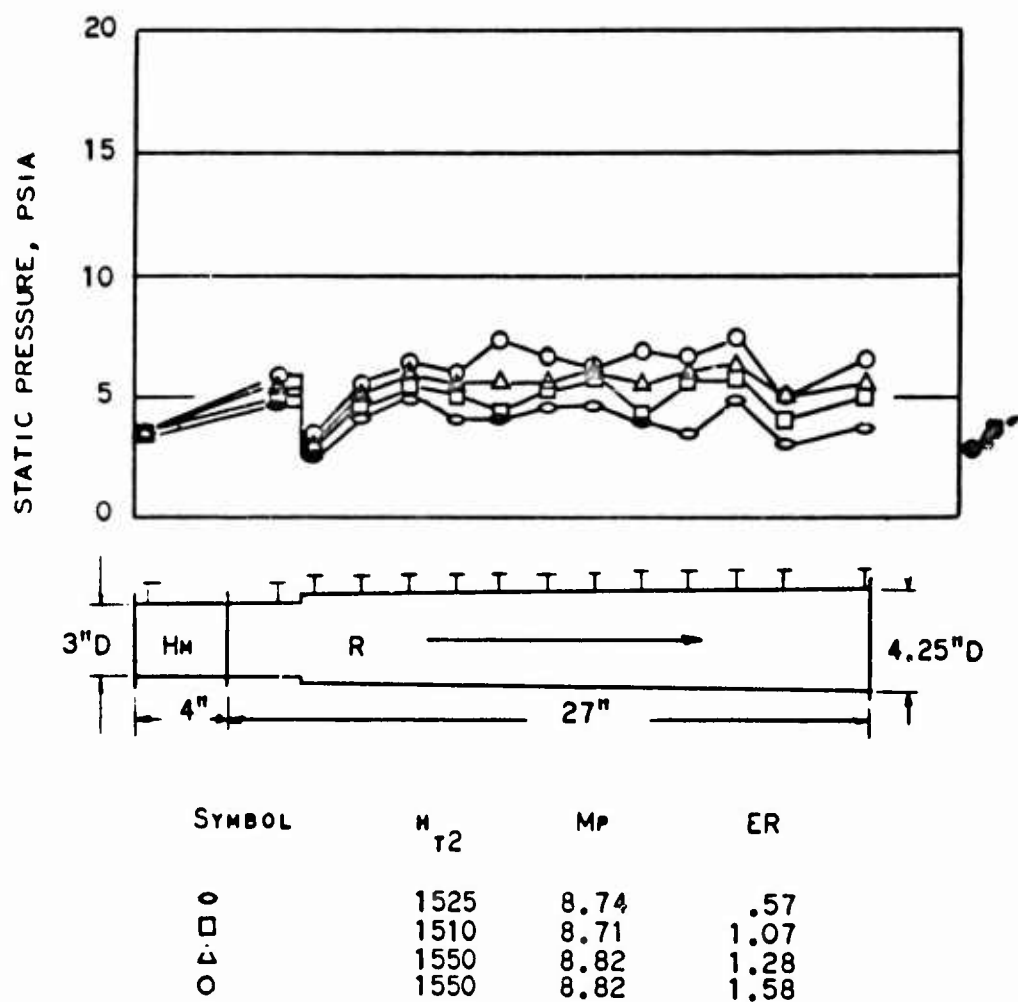
**CONFIDENTIAL**

Figure 148 - Wall Static Pressure, Configuration BHM2

**CONFIDENTIAL**

**CONFIDENTIAL**

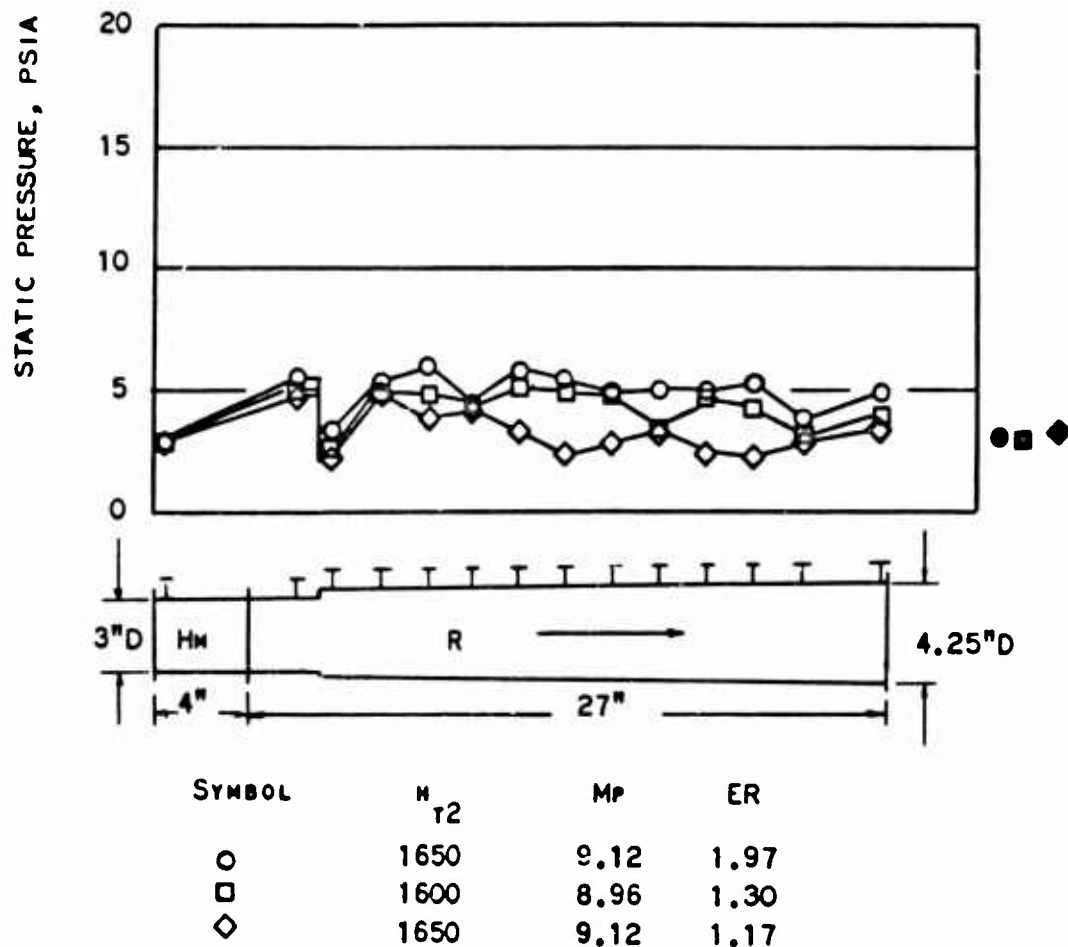


Figure 149 - Wall Static Pressure, Configuration R

**CONFIDENTIAL**

**CONFIDENTIAL**

levels. The response of the wall pressures to increasing equivalence ratio diminished as enthalpy level increased. As in previous tests, it was necessary to reduce the nominal burner inlet static pressure to attain high enthalpy levels, because of facility limitations. To facilitate comparison of wall pressures at various enthalpy levels, selected sets of pressures for near-stoichiometric equivalence ratios are presented as ratios of measured wall pressure to nominal burner inlet pressure in Figure 150. Included also is a set of pressures from a test of Configuration AHmR. The higher burner inlet Mach number is seen to produce relatively higher pressure rise in the combustor at comparable ER's and enthalpy levels. The pressure rise diminishes with increasing enthalpy level with comparable ER's and burner inlet Mach numbers.

Two burner exit surveys were performed on Configuration BHmR. Both employed near-stoichiometric equivalence ratios, but differed in enthalpy level. The performance parameters generated are included in Table VII. The data at the flight Mach 7.8 enthalpy level are directly comparable with data from Configuration AHmR. The higher burner inlet Mach number resulted in a combustion efficiency about equal to that of the lower inlet Mach number. The mean wall pressure for the higher inlet Mach number was higher than that for the lower Mach number, with the net result that the thrust potential was higher. The higher enthalpy data for Configuration BHmR showed reduced combustion efficiency, wall pressure and thrust potential.

Local equivalence ratios measured in the burner exit stream are plotted as a function of radial position in Figures 151 and 152. The circumferential distribution was reasonably uniform at both enthalpy levels. At the lower enthalpy level, the radial distribution was also uniform, indicating near-optimum fuel jet penetration and good radial mixing. The higher enthalpy data showed a lean core in the stream, indicating reduced penetration or radial mixing.

c) Configuration BHmGR

One test was performed in which Injectors Hm and G were operated in tandem between Air Nozzle B and Tailpipe R. No burner exit survey was made with this configuration. The purpose of this arrangement was to improve performance, as evidenced by wall static pressures, by increasing the length of the constant-area duct ahead of the step. The total length of 3.0 inch diameter duct attained was 11 inches, or nearly four diameters.

Wall static pressures measured at two enthalpy levels, simulating flight speeds around Mach 9 and 10, are presented in Figures 153 and 154. Data were taken with various total equivalence ratios, and with various flow splits between the two injectors. Figure 153, when compared with data from Configuration BHmR as comparable conditions, Figure 149, shows that

**CONFIDENTIAL**

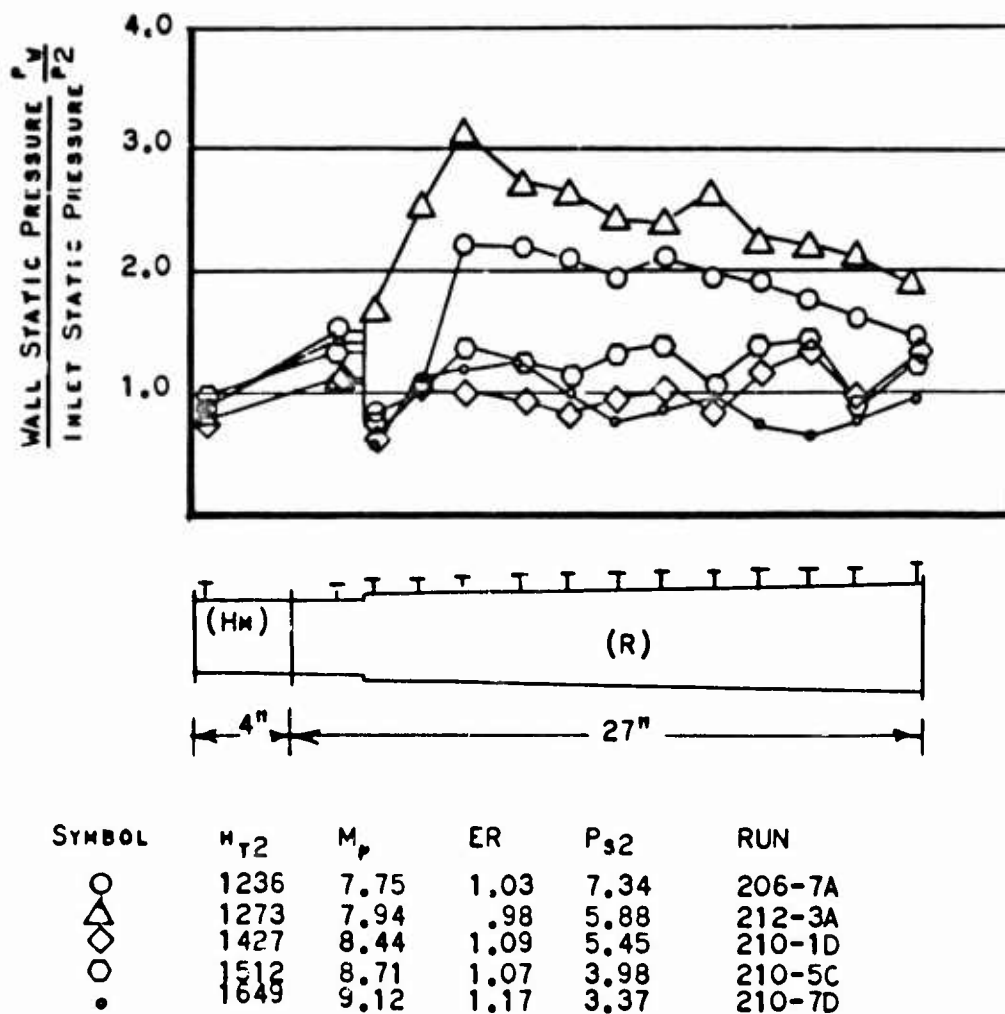
**CONFIDENTIAL**

Figure 150 - Normalized Static Pressure, Configuration BPaR

**CONFIDENTIAL**

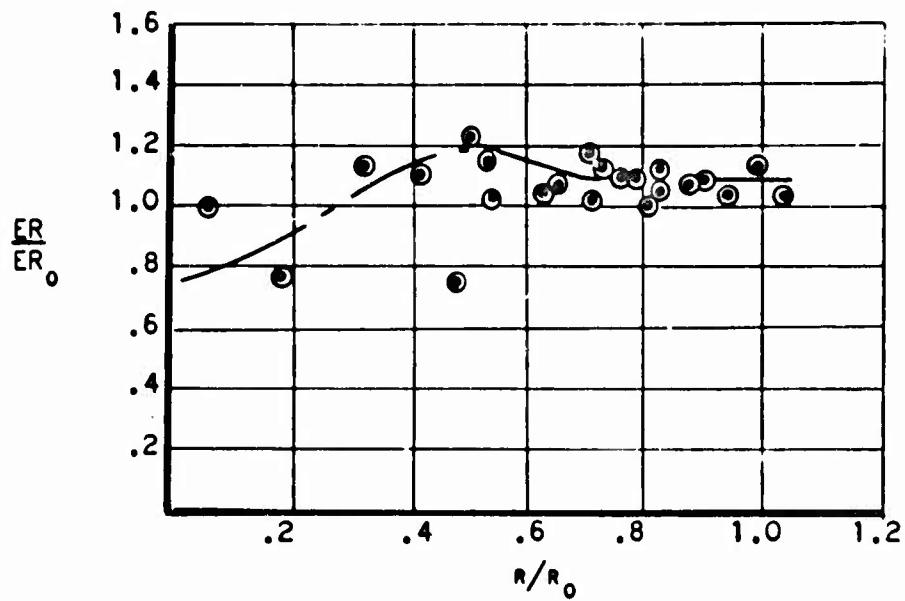
**CONFIDENTIAL**

Figure 151 - Fuel/Air Profile for Run 212 (BHAR)

$$ER_0 = .985$$

$$M_p = 8$$

**CONFIDENTIAL**

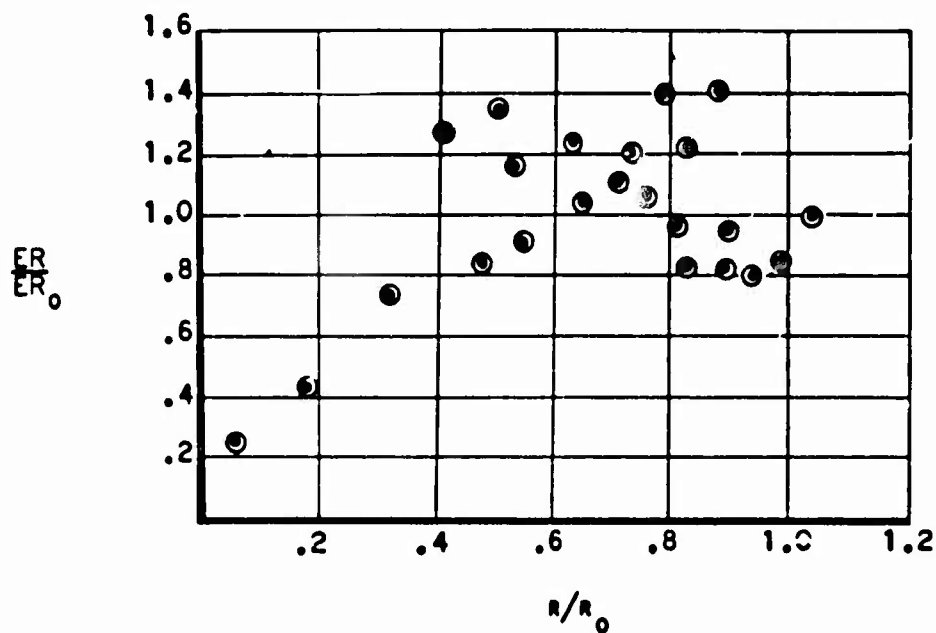
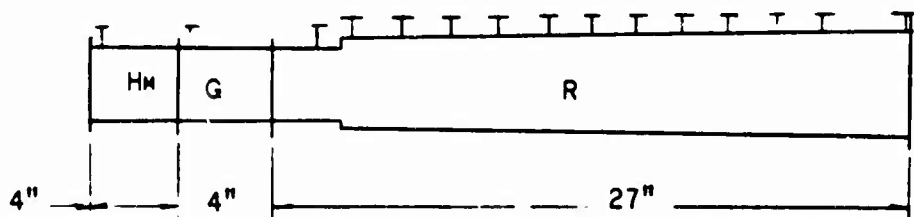
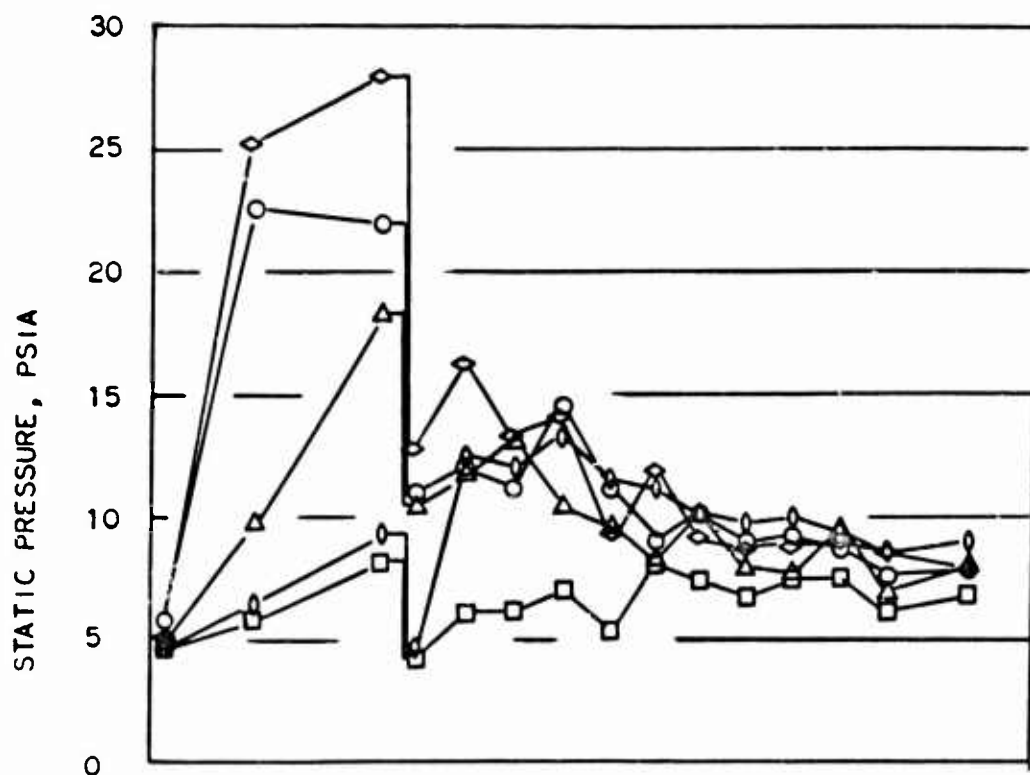
**CONFIDENTIAL**

Figure 152 - Fuel/Air Profile for Run 210 (E2AR)

$$ER_0 = 1.083 \quad M_p = 8.375$$

**CONFIDENTIAL**

**CONFIDENTIAL**

SYMBOL	$N_{T2}$	MP	ER (HM)	ER (G)
O	1575	8.89	.199	.925
Δ	1575	8.89	.204	.775
◇	1580	8.92	.200	.375
0	1625	9.04	.751	.187
□	1575	8.89	.973	.187

Figure 153 - Wall Static Pressures, Configuration RBmGR

**CONFIDENTIAL**

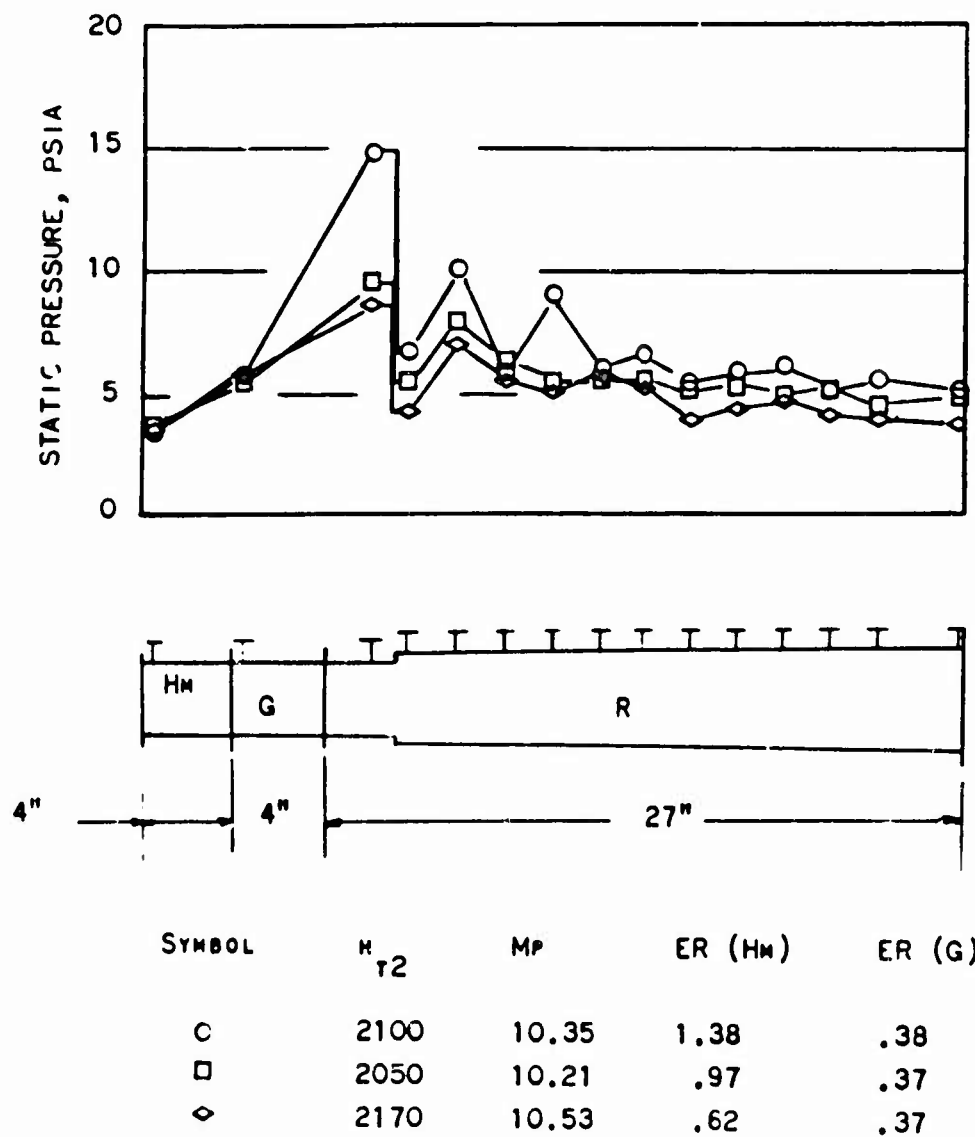
**CONFIDENTIAL**

Figure 154 - Wall Static Pressures, Configuration BH-GR

**CONFIDENTIAL**

**CONFIDENTIAL**

significantly higher burner pressures were measured with both injectors than with Injector Hm alone. The highest pressure rises in the constant-area section were attained with a large proportion of the fuel injected cross-stream from Injector G, which followed the oblique Injector Hm.

## 5) Summary of Performance Measurements

### a) The Nature of the Flow

Before beginning a detailed discussion of the performance of these combustors, a definition of terms will be helpful. Three terms are to be defined: subsonic combustion, supersonic combustion and transonic combustion. The definitions of the first two are established, whereas the last is, heretofore, undefined.

Conventional subsonic combustion is a process in which air enters the combustion chamber after having been decelerated to subsonic velocity. Fuel is added and mixed, and burning occurs at subsonic velocity. The hot, burned gases depart the chamber at subsonic velocity, to be reaccelerated to sonic velocity in the converging portion of a nozzle.

In supersonic combustion, the air enters the chamber at supersonic velocity. The flow throughout the process of fuel injection, mixing and burning remains supersonic in a one-dimensional sense. This does not disallow minor local regions of subsonic flow, such as strut wakes or boundary layers. As the burned gases depart the combustor at supersonic velocity, no constriction of the flow through the exhaust nozzle is required.

Transonic combustion resembles supersonic combustion in that the air stream entering the combustor is supersonic, and constriction of the discharge stream is unnecessary. The distinguishing feature of transonic combustion is that the burner stream is choked at some axial position within the burner, behaving as would a one-dimensional stream at sonic velocity. This does not imply that the actual stream at the choked station is of uniformly sonic velocity. The flow elsewhere within the combustion chamber may be supersonic, subsonic, or both.

It is apparent from the data that the step combustors tested here operated in the transonic combustion mode over much of the range of conditions used, with the choked station located at the combustor exit. To show that this is so, it will be expedient first to study the behavior of a simplified analytical step combustor model operating with sonic exit velocity, then to show the parallels of behavior between the step combustors tested and the analytical model.

**CONFIDENTIAL**

**CONFIDENTIAL**

The one-dimensional Mach number of a flow of perfect gas at a point in a duct is determined by the parameter

$$N(\delta, M) = \frac{RT_0}{\gamma g} \left(\frac{w}{F}\right)^2 \quad 41$$

This equation is derived in Appendix I. In general, the equation has two roots of Mach number,  $M$ ; one subsonic, the other supersonic. As the value of  $N$  increases, the two roots converge toward  $M = 1$ . The value  $N^* = N(\gamma, 1)$  is the maximum value of  $N$  for which real roots exist. No one-dimensional flow can have a value of  $N$  greater than  $N^*$ .

A flow having the maximum possible value of  $N$  is said to be choked. Its Mach number is one. Any change in the properties of the flow tending to increase  $N$ , such as an increase in stagnation temperature,  $T_0$ , must be accompanied by a simultaneous change in another property sufficient to maintain  $N$  constant, such as a reduction in mass flow,  $w$ , or an increase in total momentum,  $F$ .

With this insight into the nature of choked flows, the hypothetical, one-dimensional, perfect-gas "combustor" of Figure 155 may be examined. Here, a supersonic gas flow enters the duct from the left (station 2). Within the duct, the area undergoes an abrupt increase by a factor of 2.5, and heat is added to increase the stagnation temperature of the gas. The gas leaves the duct at station 4 in a choked condition ( $M_4 = 1$ ). The process of transonic combustion is thus simulated.

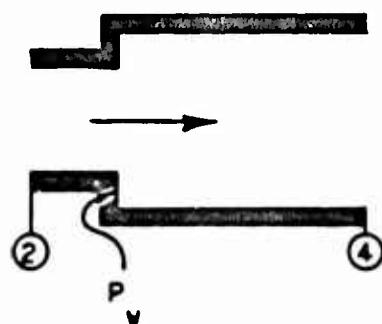
The mass flow through the duct is constant for a given inlet condition. The total momentum of the exit stream is determined by the inlet stream and by the pressure on the base of the step (friction is neglected):

$$F_4 = F_2 + P_w (A_4 - A_2) \quad (42)$$

Since the stream at station 4 is choked, an increase in the stagnation temperature must be accompanied by an increase in the total momentum. As the inlet stream is invariant, this can be accomplished only by an increase in the step base pressure.

Figure 155 shows the minimum step base pressure required to maintain flow through the hypothetical combustor as a function of its stagnation temperature ratio. With base pressures higher than the minimum shown,  $N_4$  will be less than  $N^*$ , and the exit stream will be supersonic.

**CONFIDENTIAL**

**CONFIDENTIAL**

$$\begin{aligned}\gamma &= 1.3 \\ A_4/A_2 &= 2.5 \\ M_4 &= 1 \\ C_f &= 0\end{aligned}$$

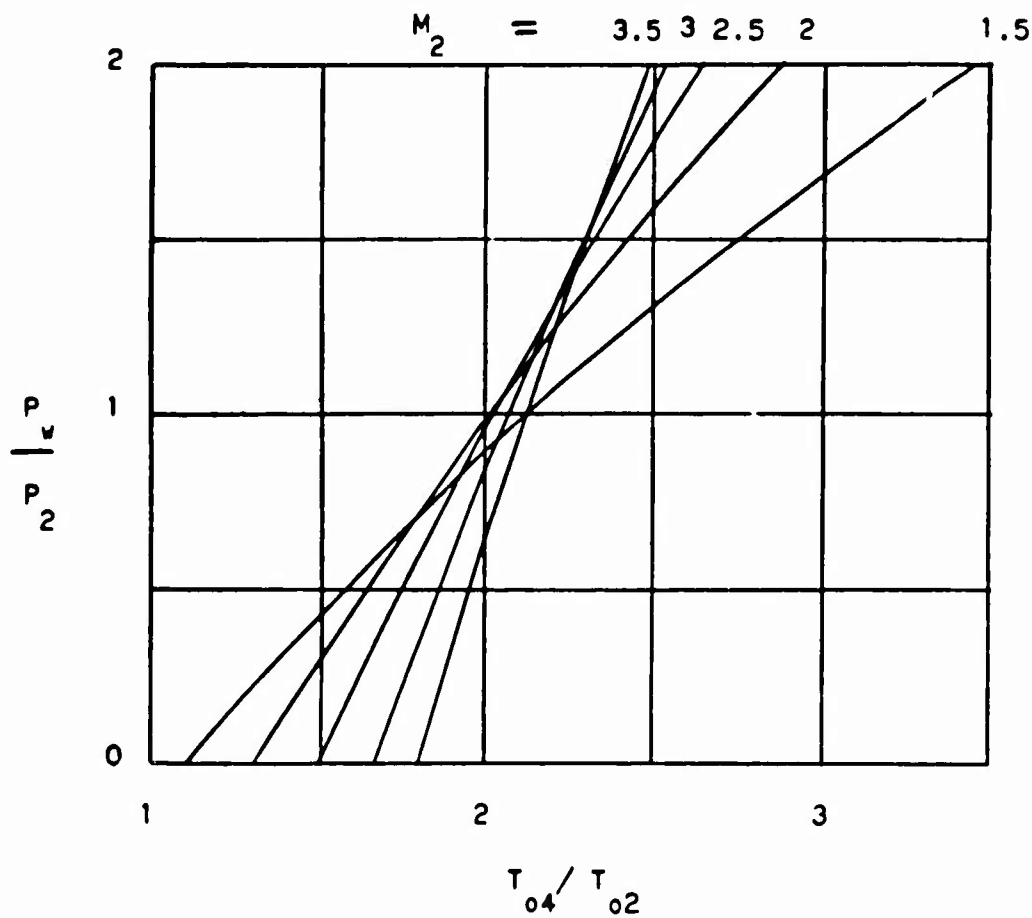


Figure 155 - Theoretical Effect of Heat Addition on  
Wall Pressure for Transonic Combustor

**CONFIDENTIAL**

**CONFIDENTIAL**

At low temperature ratios, the minimum base pressure is negative, indicating that the transonic combustion mode is impossible in this frictionless model. Only the supersonic combustion mode is possible. At higher temperature ratios, the transonic mode becomes possible. In the transonic mode, the base pressure increases with increasing temperature ratio. The theoretical maximum heat release occurs when the base pressure equals the static pressure aft of a normal shock in the inlet passage.

The behavior of the measured step base pressure of the step combustor tested may now be shown to be similar to that of the hypothetical transonic combustor. Figure 156 shows the measured base pressures as a function of burner equivalence ratio, ER. The data are segregated into two groups by enthalpy level. Closed symbols represent tests at enthalpy levels approximating Mach 6 flight, and open symbols represent tests at Mach 8 enthalpies. The burner equivalence ratio is roughly analogous to the stagnation temperature ratio of the hypothetical combustor, although the relationship is by no means linear, being influenced by the inlet enthalpy, the variation of combustion efficiency with equivalence ratio, and the maximum temperature rise occurring near  $ER = 1$ . At the higher equivalence ratios, the measured step base pressure exhibited the steep rise characteristic of the hypothetical transonic combustor. This is considered strong evidence, that the test combustors operated in the transonic combustion mode at these conditions.

At low equivalence ratios and the Mach 6 enthalpy level, combustion could not be sustained. Only when the equivalence ratio was increased well into the transonic combustion mode could combustion be sustained. This accounts for the discontinuity in the step pressure curve in Figure 156.

At low equivalence ratios and the Mach 8 enthalpy level, combustion was stable, as shown by the wall pressure curves of Figures 93 and 101, but the step base pressure remained at its no-fuel level. Only above  $ER = .6$  did the base pressure begin to increase. This is considered good evidence that the supersonic combustion mode prevailed at equivalence ratios less than  $ER = .6$ .

It was previously stated that the flow within a transonic combustor may be both subsonic and supersonic. This is obviously true in the regions immediately downstream from the wall step. The step wake is necessarily subsonic, but the core of the flow is supersonic, crossed by compression or expansion waves depending upon whether the base pressure is greater or less than the inlet pressure. In such a non-uniform flow, the pressure measured at the wall has no direct relation to the one-dimensional equivalent of the flow. This has been demonstrated analytically and experimentally (Reference 10). Further downstream, the high and low speed flows begin to mix, and the stream becomes more uniform.

**CONFIDENTIAL**

**CONFIDENTIAL**

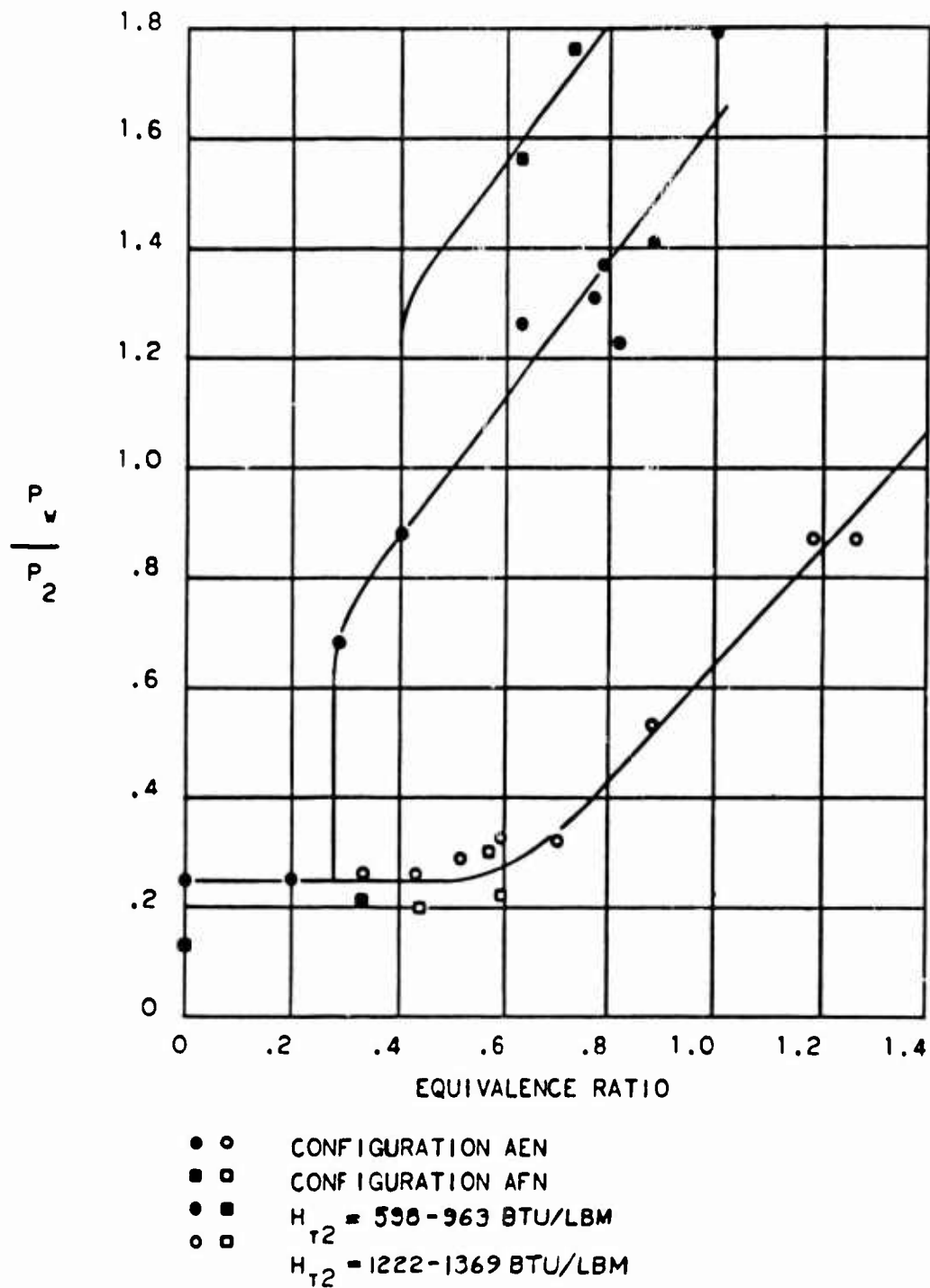


Figure 156 - Measured Step Base Pressure VS. ER

**CONFIDENTIAL**

**CONFIDENTIAL**

The nature of choking in a non-uniform stream may be tentatively explored with the aid of a second simplified analytical model. A flow of perfect gas past a point in a duct is assumed to be divided into two parts, each piecewise uniform. Each part contains half the total mass flow,  $w$ . The stagnation temperature of one part is twice that of the other. The hot part is denoted by the subscript  $h$ , and the cold part by  $c$ . The total mass flow and energy are fixed.

The flow will be defined as choked when it has the minimum total momentum sufficient to pass the given mass flow. This definition is consistent with that used for the uniform flows discussed previously.

The total momentum of the combined stream is the sum of that for its parts:

$$F = F_h + F_c \quad (43)$$

This may be expressed in terms of the flow parameter  $N$ , defined in Equation (41):

$$F = w_h \sqrt{\frac{RT_{oh}}{\gamma g N_h}} + w_c \sqrt{\frac{RT_{oc}}{\gamma g N_c}} \quad (44)$$

The boundary conditions imposed are:

$$w_h = w_c = 1/2w \quad (45)$$

and

$$T_{oh} = 2T_{oc} \quad (46)$$

The mean total temperature of the combined stream is

$$\bar{T}_o = \frac{w_h}{w} T_{oh} + \frac{w_c}{w} T_{oc} \quad (47)$$

**CONFIDENTIAL**

**CONFIDENTIAL**

Combining Equations (44), (45), (46) and (47) and performing some algebraic manipulations, a non-dimensional expression for the total momentum is obtained as a function of  $N_c$  and  $N_h$ :

$$\frac{F}{w} \sqrt{\frac{\gamma g}{R T_0}} = \sqrt{\frac{1}{6}} \left( \frac{1}{N_c} + \frac{2}{N_h} \right) \quad (48)$$

$N_c$  and  $N_h$  are, in turn, functions of the respective Mach numbers of the two parts of the flow. This function may be found in Appendix B.

The total momentum is plotted as a function of the two Mach numbers in Figure 157. The total momentum is a minimum when both Mach numbers are unity. With no further constraints, the flow thus chokes when the Mach number is uniformly one, with the total momentum less than required to pass the flow were it mixed to uniform temperature.

The attainability of a choked two-part flow having both Mach numbers unity may be challenged on intuitive grounds. Since the temperatures of the two parts are unequal, the parts must have unequal velocities in order to have equal Mach numbers. The two parts would be separated by a slip streamline or shear layer. Flows strongly influenced by pressure gradients can contain thin mixing layers approximating slip streamlines for short distances. Such a flow would be the approach to the throat of a converging nozzle. A flow approaching the choking point through a long duct with only mild pressure gradients is much less likely to contain velocity discontinuities. Viscous interaction and turbulent transport between the two parts of the stream tend to equalize their velocities. If the hot part, which has the higher sonic velocity, is adjacent to the solid boundary of the duct, viscous interaction with the boundary will tend to retard its velocity. These effects may impose additional constraints on the system.

Superimposed on Figure 157 are lines on constant  $V_h / V_c$ . If the relative velocities of the two parts of the stream are constrained to a fixed ratio, and this ratio is nearer unity than that for equal Mach numbers, the minimum total momentum required to pass the flow is greater than that for the unconstrained flow. Choking occurs with the Mach number of the hot part of the stream subsonic, and that of the cold part supersonic. If the two velocities are held equal, the minimum total momentum is the same as that which would result in choking of the stream if mixed to uniform temperature (and, incidentally, the pressure of the two-part choked stream is the same as that of the mixed choked stream, a phenomenon peculiar to the condition of equal velocities).

**CONFIDENTIAL**

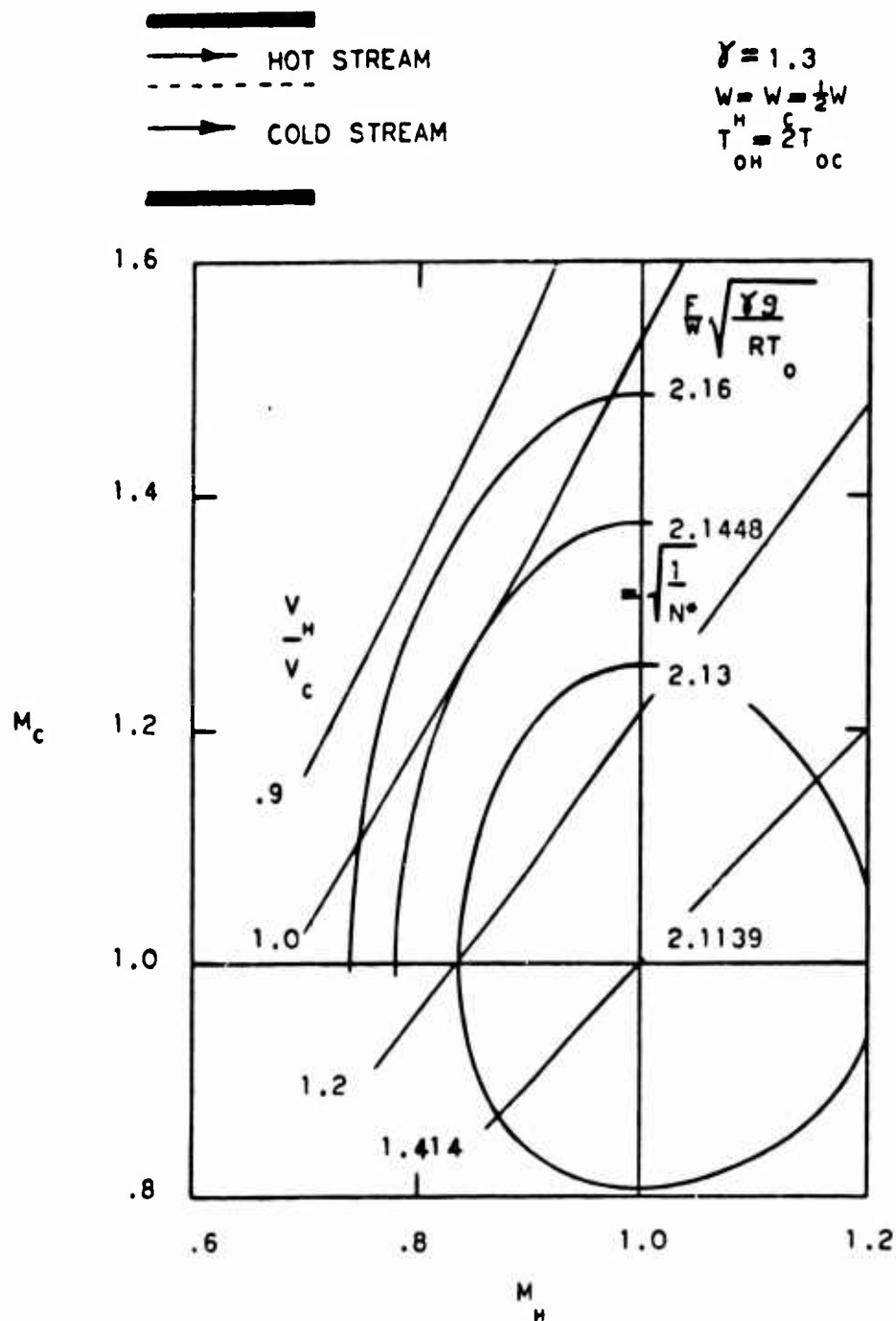
**CONFIDENTIAL**

Figure 157 - Choking Effects in Stream with Two-Step Profile

**CONFIDENTIAL**

**CONFIDENTIAL**

These considerations help to explain the presence of significant variations in local Mach number in the exit streams of the test combustors that otherwise appear to be choked. Figures 95 through 98 and 102 show supersonic peak Mach numbers, generally in regions having leaner than average equivalence ratios, and large areas of slightly subsonic Mach numbers, usually coinciding with the richer equivalence ratios.

Local velocity and Mach number are plotted against the local frozen total temperature in the exit stream from a typical choked combustor in Figure 158. Mach numbers in the hotter parts of the stream were subsonic, while those in the cooler parts were supersonic. Velocities in the hot parts of the stream were equal to or less than those in the cooler parts. The velocity appears slightly more uniform than the Mach number, having a standard deviation of 17% of the average, as compared to 25% for the Mach numbers.

The wall pressures measured in the aft portions of the step combustor provide further evidence that the combustors operated in the transonic mode. Since mixing has progressed to some extent, the velocity profiles are much more uniform than in the forward sections of the combustors, and it may be postulated that the behavior of the stream pressure has some relationship to the one-dimensional equivalent of the actual flow. These one-dimensional equivalent flows may be termed subsonic or supersonic, even though the actual flow is non-uniform and contains both subsonic and supersonic local Mach numbers.

Since the pressure in the dump chamber was maintained much lower than the combustor exit static pressure, the combustor exit stream was necessarily either supersonic or choked. With the exit flow supersonic, it is improbable that the flow immediately upstream would be subsonic. With the flow immediately upstream of the exit supersonic, its pressure would be rising under the influence of friction and heat addition. Figures 92, 93, 100, and 101 show that, at the highest equivalence ratios, the pressure of the stream approaching the exit was falling, indicating a subsonic flow approaching the sonic exit.

At lower equivalence ratios, the pressure of the stream approaching the exit is seen to be rising, indicating a supersonic flow approaching a sonic or supersonic exit. The point of demarcation between sonic and supersonic exit flows is not well defined.

In the proceeding discussion, it was assumed that the station at which the flow choked was located at the burner exit. In step combustors having fuel injection near the step, such as Configuration AEN, this is generally the case, as heat release is restricted to the region between the step and exit. In configurations having fuel injection upstream from the step, such as Configuration AGN, choking can also occur in the smaller inlet bore of the combustor at the plane of the step. Should this occur, there is no mechanism within the combustor, upstream from the choked plane, by which the total momentum of the flow can be

**CONFIDENTIAL** 266

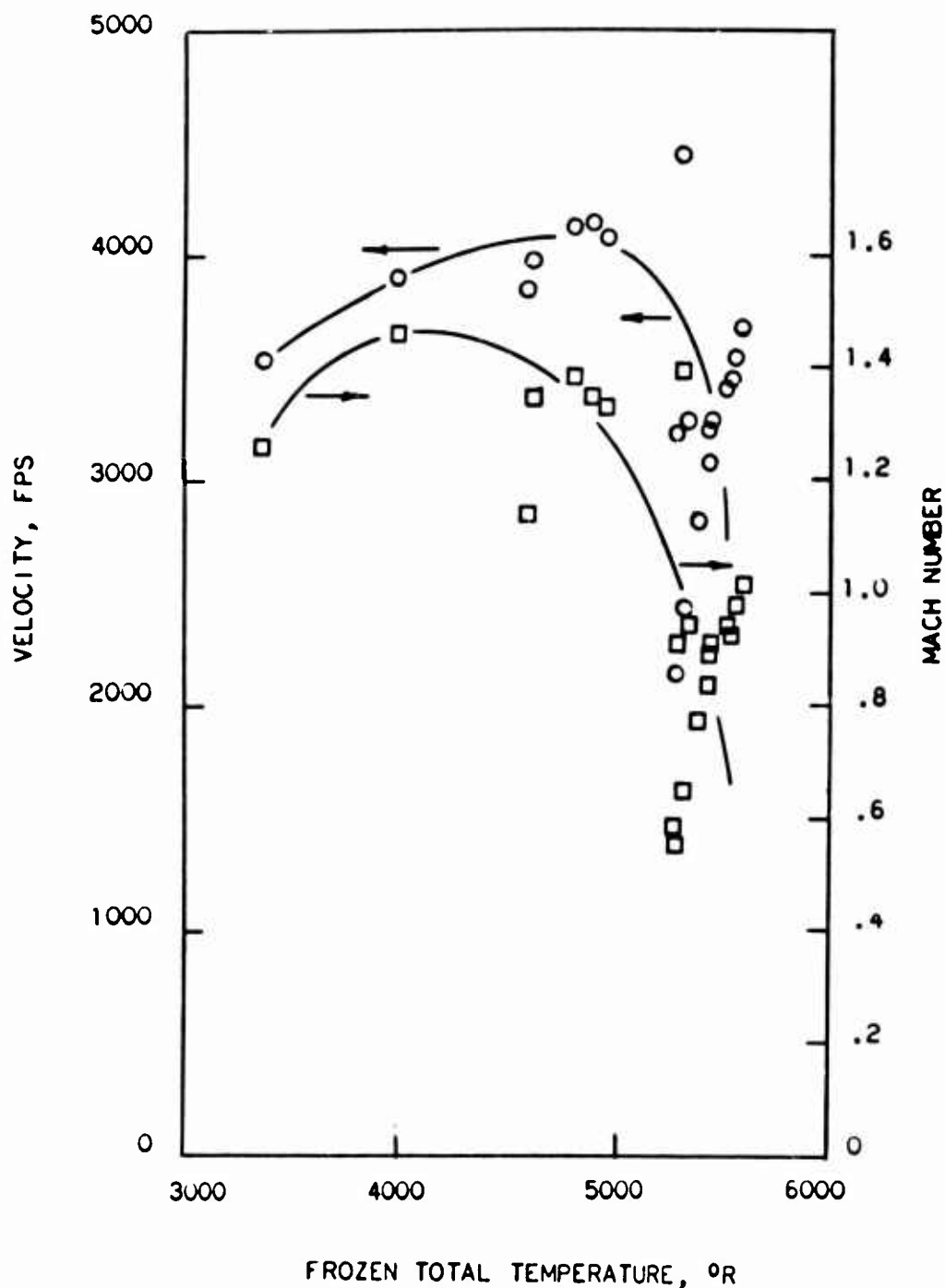
**CONFIDENTIAL**

Figure 158 - V and M Variations, Run 110

**CONFIDENTIAL**

**CONFIDENTIAL**

adjusted to the level necessary to sustain flow. The flow seeks an adjustment of momentum upstream from the combustor. In the component test, this momentum adjustment occurs through separation of the flow in the air supply nozzle, the diverging portion of the nozzle acting as a "step" upon which an increase in pressure may act to increase the momentum of the flow. In an engine, the adjustment would be one of mass flow, rather than total momentum; the inlet would spill excess flow, and allow to enter the combustor only the flow sustainable at the choked plane by the available total momentum.

A separated burner inlet stream does not always imply a choked flow at any plane. The boundary layers of the burner inlet stream may be separated by excessive pressure gradients imposed by fuel injection or combustion, even though the flow is far from choked.

In combustors having a gradual increase in flow area with length, the mode of combustion is less easily defined than in step combustors. In a step combustor, the flow can choke at one or both of only two axial locations: the burner exit and the brink of the step. In a conical combustor, the flow can choke at any axial location at which the rising total momentum fails sufficiently to keep pace with the rising stagnation temperature. If choking occurs partway along the conical divergence, the combustor can operate in the transonic mode even though both inlet and exit are supersonic. The supersonic exit occurs, in this case, due to expansion of the flow aft of the choked plane.

The existence of a choked plane in a conical combustor is difficult to detect. A high pressure peak along the length of the combustor does not necessarily imply choking, as non-uniformities in the flow can create high pressures without choking. Separation of the burner inlet is considered a fairly reliable indication of the existence of a choked plane, provided the inlet boundary layers are thin, capable of negotiating large pressure gradients.

#### b) Wall Pressure Forces

In the step combustors, pressures on the base of the wall step were sufficiently high to provide good burner performance when the equivalence ratio was high enough to cause the burner to operate well within the transonic combustion mode, as shown in Figure 156. At lower equivalence ratios, the pressure fell rapidly to levels much lower than desired.

With no fuel injection, a low base pressure was expected. Figure 156 shows the no-fuel pressure to be about 0.2 times the pressure of the burner inlet stream. The flow phenomena that establish this pressure are complex. A qualitative explanation can be formulated with the aid of the conceptual flow diagram of Figure 159. For a more informed discussion of these phenomena, see Reference 20.

**CONFIDENTIAL**

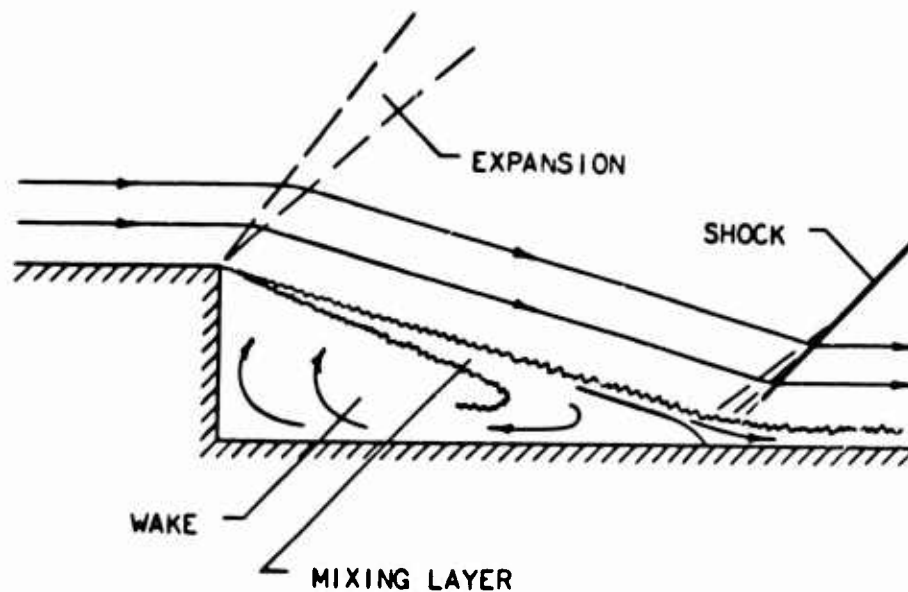
**CONFIDENTIAL**

Figure 159 - Flow About A Rearward-Facing Step (Schematic)

**CONFIDENTIAL**

**CONFIDENTIAL**

The supersonic flow across the step undergoes an expansion turn to the lower pressure existing in the step wake. The flow then proceeds toward the downstream wall with a "free boundary". This boundary is actually a turbulent layer in which low-speed gas from the wake is mixing with the main-stream flow. Upon contact with the downstream wall, the main-stream flow is forced to negotiate a compression turn to its initial direction. This is the "reattachment point".

The effect of the pressure rise at the reattachment point on the mixing layer determines the pressure in the wake. The higher velocity portion of the layer, adjacent to the main-stream flow, is able to negotiate the compression, and continues downstream with the main-stream flow. The lower velocity portion, adjacent to the wake, is unable to negotiate the compression, and is turned back ("recirculated") into the wake. The amount of recirculated gas depends upon the strength of the compression.

If the pressure in the wake were reduced from its equilibrium value, the expansion of the approaching air would be greater, and the main stream would approach the downstream wall at a greater angle. The reattachment compression would thus be stronger, causing a greater proportion of the mixing layer to be recirculated. The added flow into the wake would tend to increase the wake pressure. Conversely, if the pressure in the wake were increased, the reattachment compression would be weakened, and the recirculated flow reduced, tending to reduce the wake pressure.

It was expected that combustion of fuel in the wake would increase the wake pressure substantially, even with the combustor operating in the fully supersonic mode. Heating a gas reduces its density, therefore, it was expected that low-density gases entering the mixing layer would reduce the momentum of the flow, so that a greater volume of gas would be unable to negotiate the reattachment compression and would recirculate to increase the wake pressure. Also, partially burned gases recirculating into the wake would complete their reactions while in the wake, expanding to increase wake pressure. This anticipated effect was demonstrated by Townend (Reference 21 ), who burned hydrogen in the wake of the blunt base of a cylindrical missile in a supersonic stream. With sufficient burning, Townend was successful in elevating the base pressure to that of the surrounding stream. This effect was also demonstrated by Bowyer and Carter (Reference 22 ), in experiments using a wall step in a rectangular duct.

In the present tests, efforts to elevate the base pressure by burning fuel with the combustor in the supersonic mode were unsuccessful. Four possible explanations may be advanced:

**CONFIDENTIAL**

**CONFIDENTIAL**

- (1) A combustible fuel-air mixture was not established in the wake. Gas samples drawn from the wake region of Injector E, with the burner fully supersonic, indicated little fuel in the wake. The pedestals of Injector E evidently placed the fuel too far into the stream to be recirculated. Injector J placed all its fuel directly into the wake. Wake gas samples indicated that all air had been excluded. Wake gas samples were not obtained with Injectors G, H or F; these had better opportunity to establish a combustible mixture in the wake.
- (2) Wake pressures were too low for stable combustion. Flameholder theory (Reference 23 ) holds that a bluff-body flame stabilizer is stable if the residence time in the mixing layer is greater than the ignition delay of the mixture of hot combustion products and unburned fuel and air existing in the mixing layer. Low pressures tend to lengthen ignition delay times, and could be responsible for the ineffectiveness of the step as a flameholder.
- (3) The reattachment compression was weaker than that in the Townend experiment. The collision of flows converging on the axis of symmetry aft of Townend's cylindrical missile would produce a much stronger compression than the diverging axisymmetric, flows meeting the wall aft of the step. The stronger compression innately tends to recirculate more of the mixing layer.
- (4) The attainable temperature rise was relatively much less than in Townend's experiment. Townend's air stagnation temperature was only 540°R, whereas the air temperatures used in the present tests were in excess of 2500°R.

In the transonic combustion mode, the step base pressure was forced to acceptably high levels. Unfortunately, it is expected that transonic combustion will be increasingly more difficult to attain at higher flight speeds. The heat release afforded by a given equivalence ratio may be approximated by a fixed stagnation temperature rise  $T_o = T_{o4} - T_{o2}$  in the simplified analytical model of Figure 155 . The base pressure of the analytical model is determined by the ratio of stagnation temperatures

$$\frac{T_{o4}}{T_{o2}} = 1 + \frac{T_{o4} - T_{o2}}{T_{o2}} = 1 + \frac{\Delta T_o}{T_{o2}} \quad (9)$$

**CONFIDENTIAL**

**CONFIDENTIAL**

Thus, with a burner inlet Mach number of, say 3, an equivalence ratio producing a base pressure 1.5 times the inlet pressure of flight Mach 6 ( $h_{02} = 767.5$  Btu/lbm) would be insufficient to choke the burner at flight Mach 9 ( $h_{02} = 1610.4$  Btu/lbm).

Tabulations and correlations were made of step pressure data obtained from step burners tested. The step-to-inlet pressure ratio was correlated with equivalence ratio, total enthalpy, and a semi-empirical function of total enthalpy-equivalence ratio.

Good agreement was shown between similar injectors over the range of flight Mach numbers tested. A map of step-to-inlet pressure ratio vs. total enthalpy was generated to facilitate extrapolation of step pressures over a range of burner operating conditions.

The slope of  $P_w/P_{s2}$  with respect to ER varies for different levels of flight Mach number, the largest slope being at the lowest  $M_p$ , see Figures 160, 161, 162 and 163. Differences between injectors are evident in Figure 160. Injectors (G) and (F), located upstream of the step and injecting normal to the air stream, produce similar results. Injector H located upstream from the step and injecting obliquely, and Injector E, injecting normally downstream of the step produce similar results. The normal/upstream injectors have higher base pressures. Table VIII is a tabulation of the step burner data collected.

A drawing of the general character of the effects of ER on the step-to-inlet static pressure ratio for all step burners showing the steep slope which is indicative of burner exit choked conditions is shown in Figure 164.

The lines correlating the data in Figures 160 and 161 at Mach 6 and 8 were replotted to produce an empirical relation between step-to-inlet pressure ratio and enthalpy for an ER range. Only data correlations of the (H) and (E) injectors with the A arc-tunnel nozzle were used. This map, Figure 165, facilitates prediction of step pressure over an ER range from .4 to 1.2 and  $M_p$  range from 6 to 8. A few points to  $M_p = 5.5$  from Figure 160 are also shown in Figure 165. Next this data was replotted in Figure 166 against a semi-empirical function of heat addition.

Figure 166 is a semi-empirical correlation of the effects of heat addition on the step-to-inlet pressure ratio. The points on the plot were obtained from the lines of data correlation for  $M_p$  5.5, 6 and 8 in Figures 160 and 161. The derivation that follows indicates that an ideal frictionless gas. The step pressure should be correlated by one line. All

**CONFIDENTIAL**

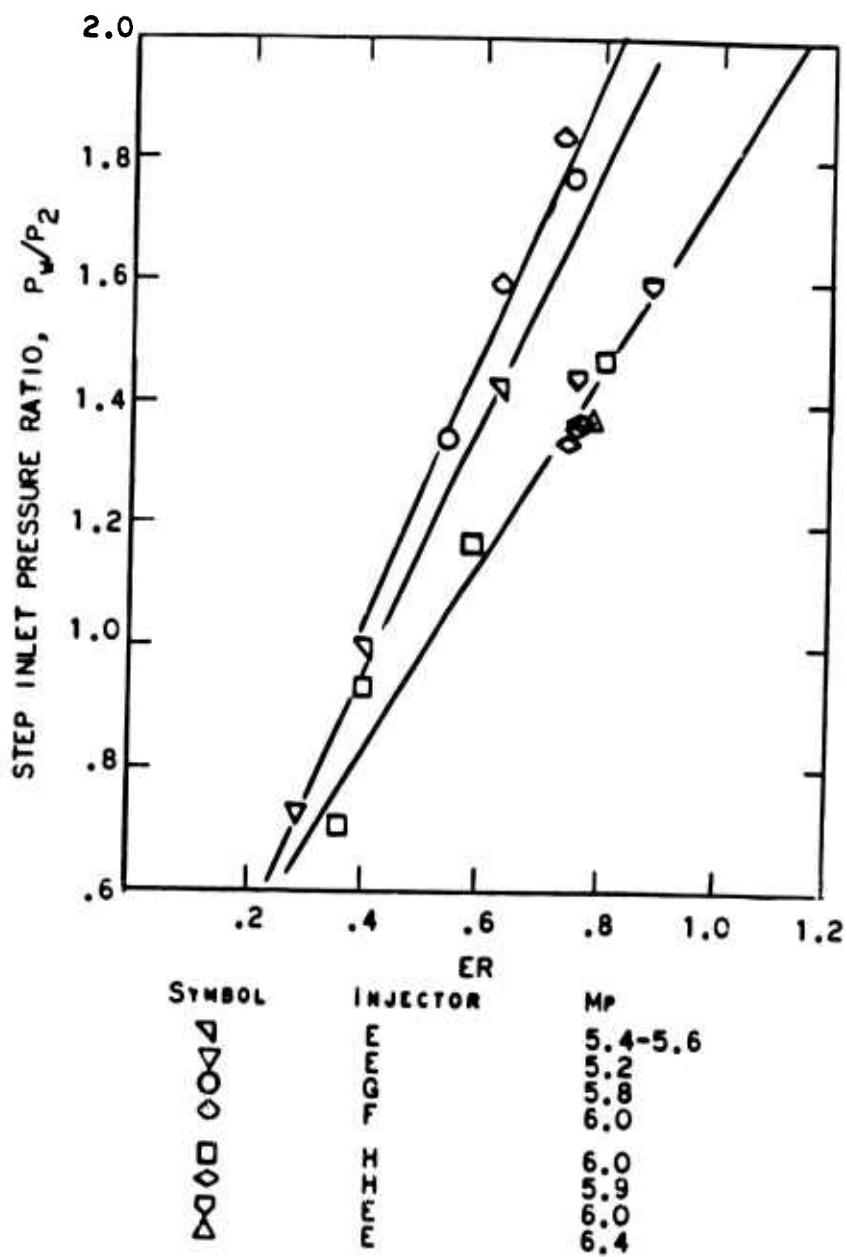
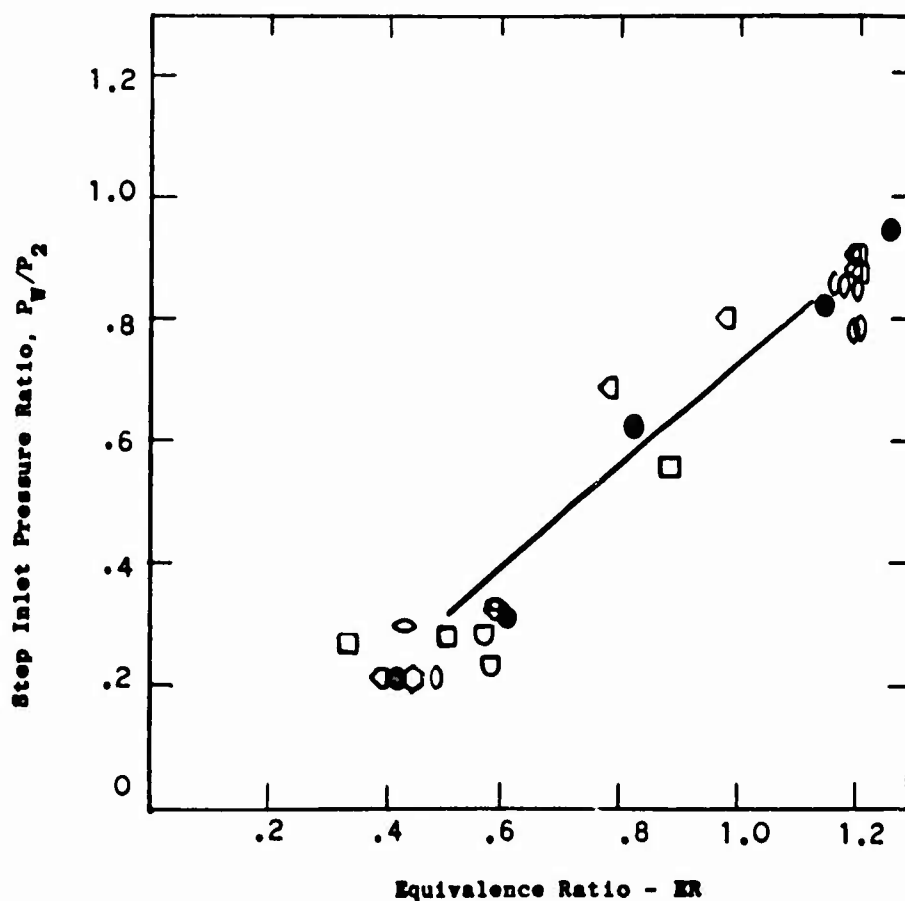
**CONFIDENTIAL**

Figure 160 - Effect of Equivalence Ratio on Step Pressure (Mach 2.7 Nozzle)

**CONFIDENTIAL**

**CONFIDENTIAL**

SYMBOL	INJECTOR	MP
●	E	7.7-7.85
△	E	7.7-7.9
○	E	7.8-8.1
□	E	7.8-8.0
◇	E	7.8-8.1
○	F	8.0-8.25
○	E	8.05

Figure 161 - Effect of Equivalence Ratio on Step Pressure,  
Mach 0.7 Nozzle

**CONFIDENTIAL**

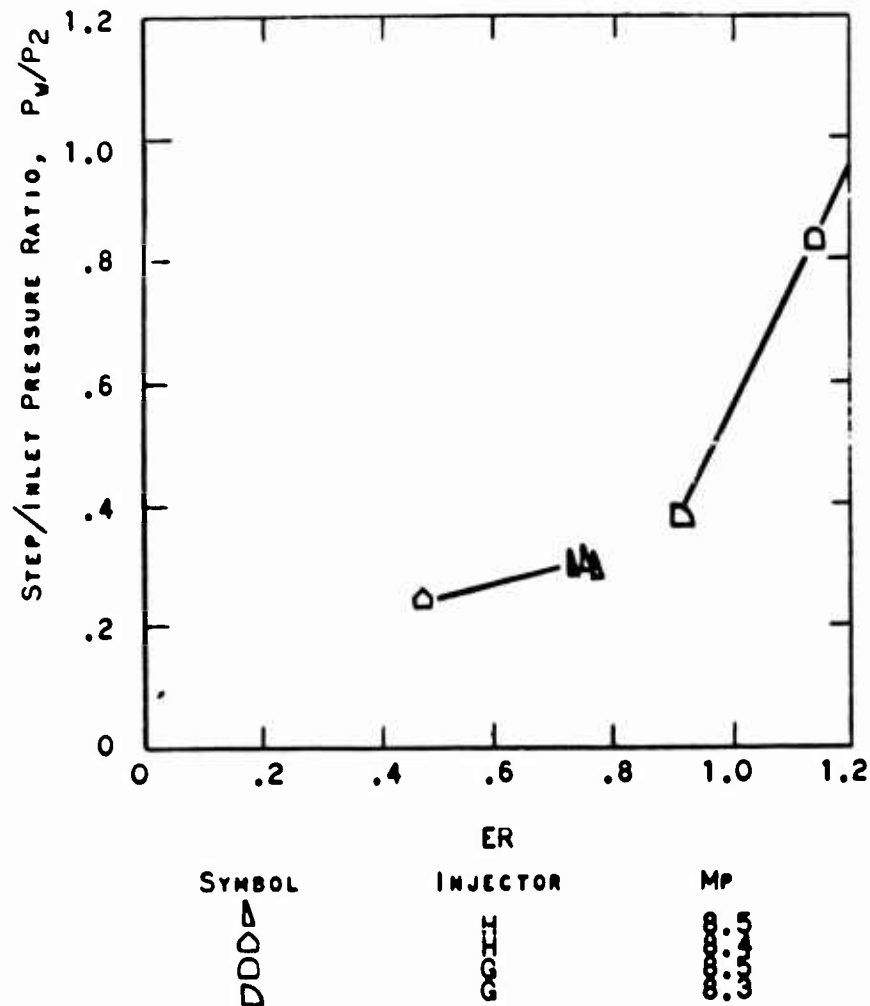
**CONFIDENTIAL**

Figure 162 - Effect of Equivalence Ratio on Step Pressure  
(Mach 3.25 Nozzle)

**CONFIDENTIAL**

**CONFIDENTIAL**

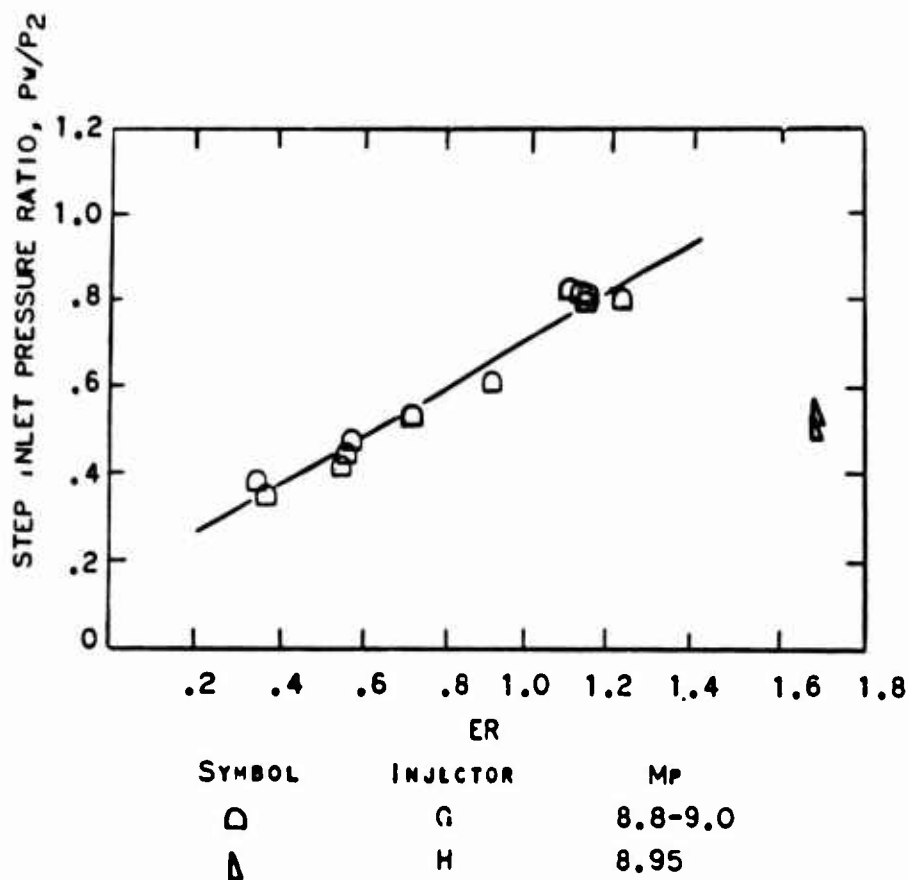


Figure 163 - Effect of Equivalence Ratio on Step Pressure  
(Mach 3.25 Nozzle)

**CONFIDENTIAL**

# CONFIDENTIAL

TABLE VIII - STEP-BURNER DATA

(Only data points where nitrogen was  
not on are tabulated)

Symbol	Run	Rdg.	Config.	$h_{42}$	$M_p$	ER	$\frac{P_s \text{ step}}{P_{s2} \text{ inlet}}$
	117		AEN	598	5.20	.2912	.726
	116	IV	AEN	645.2	5.43	.4029	1.009
	116	V	AEN	688.5	5.64	.6327	1.432
	128	V	AFN	761.6	5.98	.6321	1.60
	128	IV	AFN	773	6.03	.729	1.84
	146	II	AEN	770.4	6.02	.758	1.442
	146	III	AEN	765.4	6.0	.8818	1.6
	194	2B	AGO	720	5.79	.5467	1.34
	194	2C	AGO	725	5.81	.7462	1.77
	176	11	AHP	747	5.91	.363	.706
	176	12A	AHP	758	5.96	.404	.935
	176	12B	AHP	761	5.97	.587	1.168
	176	12C	AHP	775	6.04	.806	1.470
	177	6A	AHP	756	5.96	.741	1.336
	177	6B	AHP	755	5.95	.765	1.361
	177	6C	AHP	751	5.94	.763	1.371
	177	6D	AHP	735	5.86	.770	1.370
	111		AEN	870	6.44	.785	1.371
	110		AEN	906	6.60	.769	1.312
	107		AEN	963	6.82	.817	1.225
	183	7A	BHO	975	6.87	.6831	.87
	183	7B	BHO	985	6.91	.6685	.865
	217	2	AEOS	1192	7.66	1.26	.943
	217	3A	AEOS	1210	7.75	1.144	.82
	217	3B	AEOS	1218	7.75	.824	.623
	217	3C	AEOS	1247	7.85	.418	.213
	217	4A	AEOS	1243	7.84	.612	.3135

# CONFIDENTIAL

# CONFIDENTIAL

Symbol	Run	Rdg.	Config.	$h_{t2}$	$M_p$	ER	$\frac{P_s \text{ step}}{P_{s2} \text{ inlet}}$ <sup>2</sup>
	216	2A	AEOS	1229	7.79	1.189	.901
	216	2B	AEOS	1219	7.75	1.198	.904
	216	2C	AEOS	1251	7.87	1.20	.88
	216	2D	AEOS	1247	7.85	1.194	.879
	216	2E	AEOS	1280	7.96	1.205	.866
	216	2F	AEOS	1259	7.89	1.203	.877
	216	3A	AEOS	1174	7.60	.975	.80
	216	3B	AEOS	1202	7.70	.785	.693
	216	3C	AEOS	1227	7.78	.588	.324
	216	3D	AEOS	1210	7.73	.392	.214
	185	4A	BHO	1245	7.84	.8038	.286
	185	4B	BHO	1220	7.76	.7925	.288
	185	6A	BHO	1220	7.76	.6126	.272
	185	6B	BHO	1295	8.01	.4406	.264
	202	3	AEOS	1245	7.84	.4917	.215
	202	5	AEOS	1265	7.91	1.1544	.856
	202	7A	AEOS	1290	7.99	1.172	.857
	202	7B	AEOS	1290	7.99	1.2023	.876
	202	7C	AEOS	1290	7.99	1.1964	.851
	202	7D	AEOS	1320	8.09	1.1926	.784
	202	7F	AEOS	1330	8.12	1.2028	.781
	122	I	AEN	1233.2	7.8	.3335	.277
	122	III	AEN	1221.8	7.76	.8847	.554
	122	IV	AEN	1295.7	8.01	.5059	.281
	126	II	AEN	1228.9	7.79	.4317	.302
	126	IV	AEN	1314	8.07	.592	.329
	132	I	AFN	1369.1	8.25	.5747	.285
	132	II	AFN	1290.4	7.99	.5863	.2299
	129	II	AFN	1315	8.05	.445	.215
	192	4	BGO	1397	8.34	.90664	.373
	187	6A	BHO	1401	8.36	.37	.242
	188	6A	BHO	1425	8.44	.7292	.298
	188	6B	BHO	1455	8.53	.7489	.305
	188	6C	BHO	1455	8.53	.7637	.292

# CONFIDENTIAL

# CONFIDENTIAL

Symbol	Run	Rdg.	Config.	ht2	M <sub>p</sub>	ER	$\frac{P_s \text{ step}^3}{P_{s2} \text{ inlet}}$
	193	5A	BGO	1502	8.68	1.152	.829
	188	8A	BHO	1595	8.95	1.6739	.544
	188	8B	BHO	1595	8.95	1.6701	.521
	193	5B	BGO	1595	8.96	1.149	.815
	193	5C	BGO	1568	8.88	1.155	.809
	193	5D	BGO	1569	8.88	1.135	.813
	193	5E	BGO	1568	8.88	1.157	.799
	193	7A	BGO	1618	9.03	.942	.611
	193	7B	BGO	1630	9.06	.717	.53
	193	7C	BGO	1637	9.08	.567	.462
	193	7D	BGO	1575	8.9	.357	.389
	193	7F	BGO	1641	9.09	.383	.352
	193	7G	BGO	1640	9.09	.555	.433
	193	11	BGO	1589	8.94	.572	.483
	193	13	BGO	1595	8.96	1.166	.804

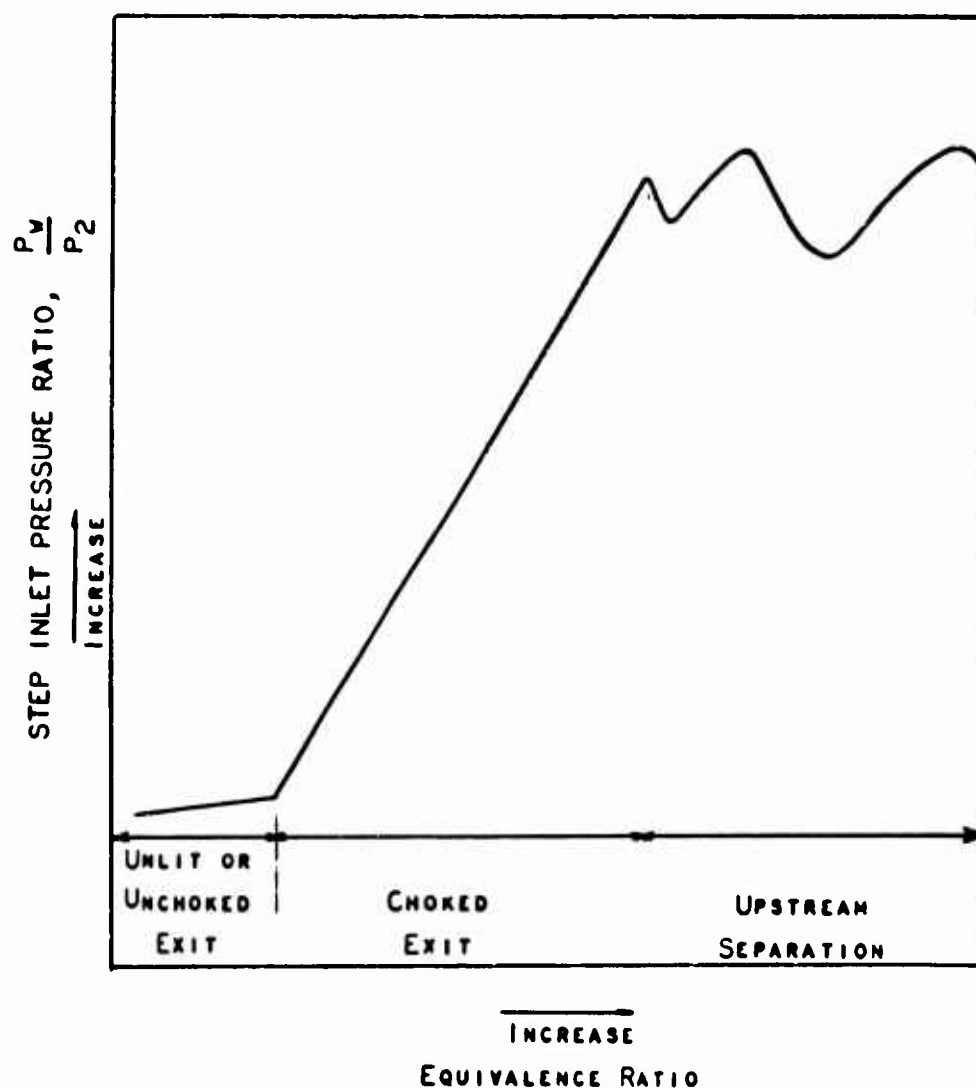
**CONFIDENTIAL**

Figure 164 - Generalized Character of the Effects of Equivalence Ratio on Step Pressure

**CONFIDENTIAL**

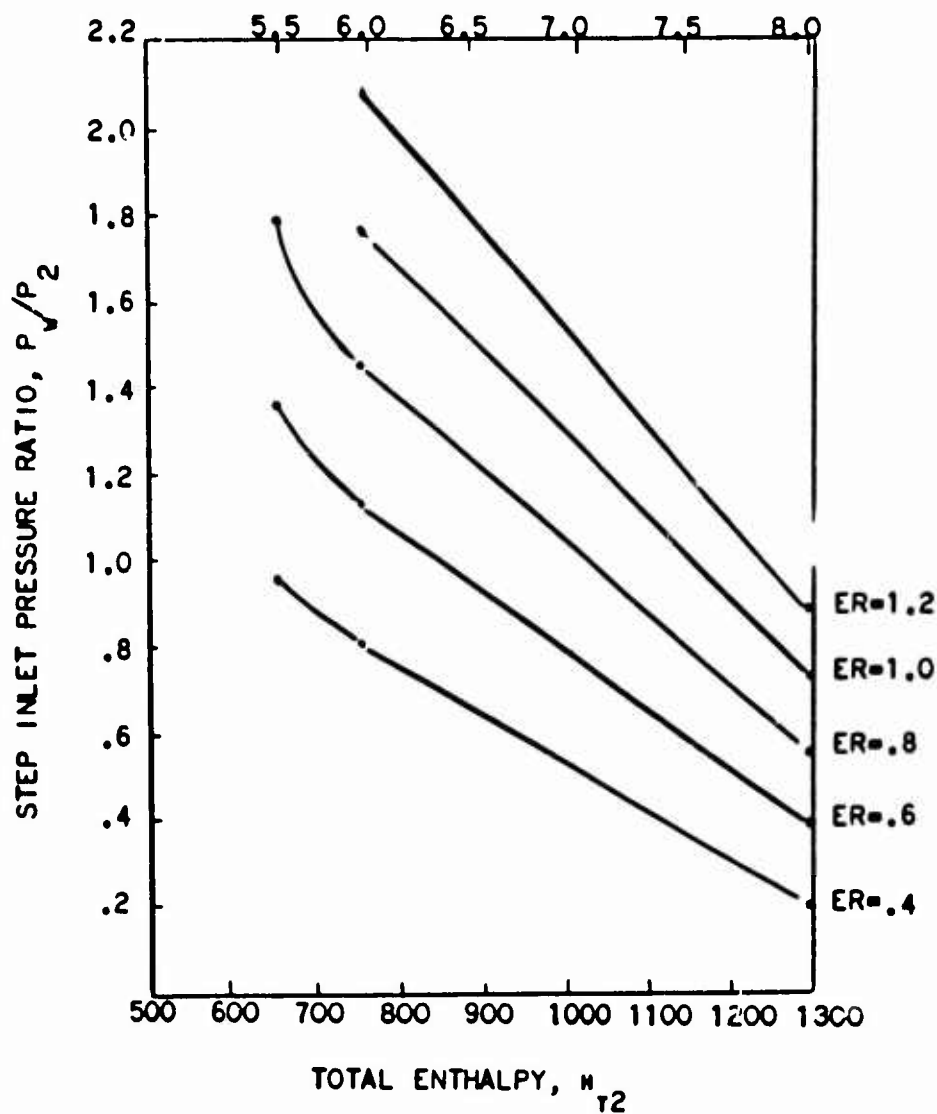
**CONFIDENTIAL**

Figure 165 - Effect of Total Enthalpy on Step Pressure  
(Mach 2.7 Nozzle, H and E Injectors)

**CONFIDENTIAL**

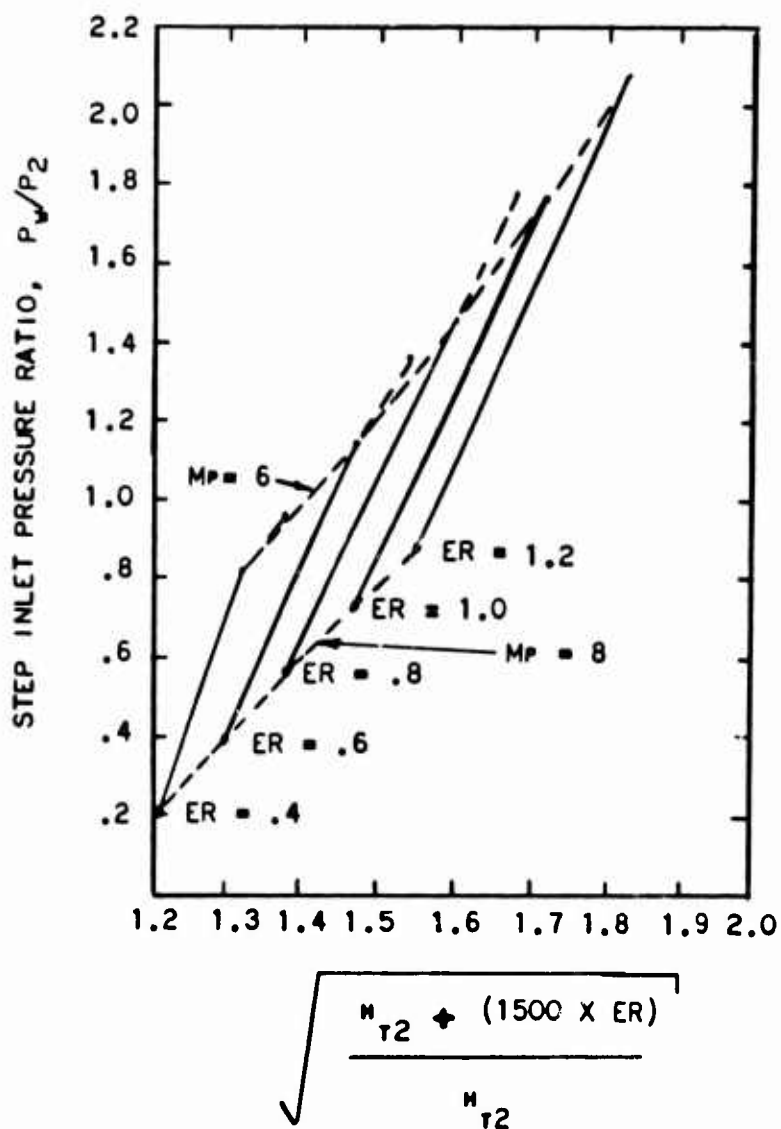
**CONFIDENTIAL**

Figure 166 - Effect of Heat Addition on Step Pressure  
(Mach 2.7 Nozzle, H and E Injectors)

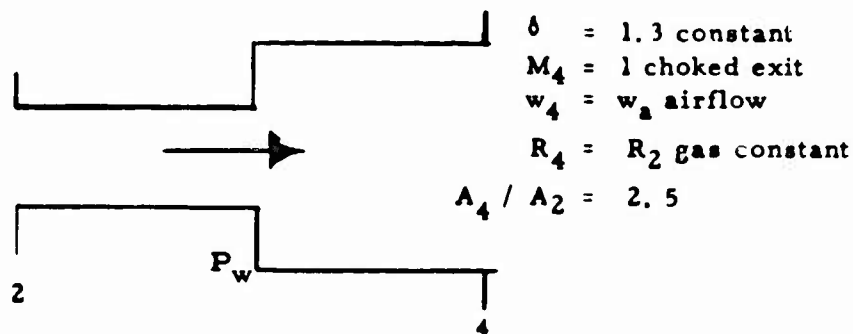
**CONFIDENTIAL**

**CONFIDENTIAL**

points in Figure 166 do not lie on one line because of the large deviations from an ideal frictionless gas. The parameter  $\frac{h_{t2}}{h_{t2} + (1500) ER}$  was arrived at by using the derivation of Generalized Irreversible Flow Function,  $h_{t2}$  Appendix I.

A step burner operating thermally choked at the exit was analyzed. The following assumptions were made to simplify the analysis:

1. Isentropic flow
2. Ideal frictionless gas
3. Constant airflow
4. Heat addition only - no mass addition



Algebraic manipulation of the one-dimensional momentum equation results in the

Step to Inlet Static Pressure Ratio

$$\frac{P_w}{P_2} = \frac{\left(\frac{F_4}{F_2} - 1\right)(1 + \gamma M_2^2)}{A_4/A_2 - 1} \quad (50)$$

In Appendix I, the following ratios were derived:

Impulse Function Ratio

$$\frac{F_4}{F_2} = \sqrt{\frac{T_{o2}^*}{T_{o2}}} \left(\frac{N_2}{N^*}\right) \quad (51)$$

**CONFIDENTIAL**

**CONFIDENTIAL**Flow Function Ratio

$$\frac{N_2}{N^*} = \frac{2(\gamma + 1) M_2^2 \left(1 + \frac{\gamma - 1}{2} M_2^2\right)}{1 + \gamma M_2^2} \quad (52)$$

where:

$$T_0^* = (T_{04}) M_4^2 = 1$$

$$N^* = (N_4) M_4^2 = 1$$

Combining equations (51 and 52)

$$\frac{P_w}{P_2} = \frac{(1 + \gamma M_2^2)}{(A_4/A_2 - 1)} \left[ \sqrt{\frac{T_0^*}{T_{02}}} \left( \frac{N_2}{N^*} \right) - 1 \right] \quad (53)$$

Combining equations (53 and 54)

$$\frac{P_w}{P_2} = \frac{(1 + \gamma M_2^2)}{(A_4/A_2 - 1)} \left[ \sqrt{\frac{T_0^*}{T_{02}}} \left( \frac{2(\gamma + 1) M_2^2 \left(1 + \frac{\gamma - 1}{2} M_2^2\right)}{(1 + \gamma M_2^2)^2} \right) - 1 \right]$$

Simplifying (55)

$$\begin{aligned} \frac{P_w}{P_2} &= \frac{(1 + \gamma M_2^2)}{(A_4/A_2 - 1)(1 + \gamma M_2^2)} \left[ \sqrt{\frac{T_0^*}{T_{02}}} \sqrt{\frac{2(\gamma + 1) M_2^2 \left(1 + \frac{\gamma - 1}{2} M_2^2\right)}{(1 + \gamma M_2^2)^2}} - 1 \right] \\ \frac{P_w}{P_2} &= \frac{\sqrt{2(\gamma + 1) M_2^2 \left(1 + \frac{\gamma - 1}{2} M_2^2\right)}}{(A_4/A_2 - 1)} \sqrt{\frac{T_0^*}{T_{02}}} \frac{(1 + \gamma M_2^2)}{A_4/A_2 - 1} \end{aligned}$$

But using the original assumptions of ideal frictionless gas, and constant  $M_2$ ,  $\gamma$ ,  $C_p$ ,  $R$  and  $A_4/A_2$  some of the terms may be lumped together into constants.

$$\frac{P_w}{P_2} = C_1 \sqrt{\frac{T_0^*}{T_{02}}} - C_2 \quad (55)$$

**CONFIDENTIAL**

**CONFIDENTIAL**

where

$$C_1 = \sqrt{2(\gamma + 1) M_2^2 \left(1 + \frac{\gamma - 1}{2} M_2^2\right)}$$

$$C_2 = \frac{(1 + \gamma M_2^2)}{(A_4/A_2 - 1)}$$

Therefore, the step-to-inlet static pressure ratio can be defined as a function of the square root of the total temperature ratio:

$$\frac{P_w}{P_2} = f\left(\sqrt{\frac{T_o^*}{T_{o2}}}\right) \quad (56)$$

Also, by keeping in mind the assumption of heat addition and no mass addition, the following approximation can be made:

$$C_p T_o^* \approx h_{t2} + (1500) ER \quad (57)$$

Where the weight of fuel per weight of air is the equivalence ratio times the stoichiometric fuel/air ratio of  $H_2$  and air:

$$\frac{W_f}{W_a} = ER \times \left(\frac{W_f}{W_a}\right)_{ER=1} = \frac{\text{lb fuel}}{\text{lb air}}$$

where:

$$\left(\frac{W_f}{W_a}\right)_{ER=1} = .029 \text{ Stoichiometric } H_2 \text{ fuel/air ratio}$$

Heating value of  $H_2 = 51,600 \text{ Btu/lb}$

$$\frac{W_f}{W_a} \times 51,600 \text{ Btu/lb fuel} = \frac{\text{Heating value of fuel}}{\text{lb of air}}$$

**CONFIDENTIAL**

**CONFIDENTIAL**

then:

$$ER \times \left( \frac{W_f}{W_a} \right)_{ER=1} \times (51,600 \text{ Btu/lb fuel}) = \frac{\text{Heating value of fuel}}{\text{lb of air}}$$

therefore:

$$(1500) ER = \frac{\text{Heating value of fuel}}{\text{lb of air}}$$

Again from equation (8)

$$\left( \frac{T_{o^*}}{T_{o2}} \right) = \frac{h_{t2} + (1500) ER}{h_{t2}} \quad (58)$$

Therefore, the step-to-inlet static pressure ratio is a function of the square root of the total temperature ratio as well as a function of a total enthalpy-equivalence ratio term:

$$\frac{P_w}{P_2} = f \left( \sqrt{\frac{T_{o^*}}{T_{o2}}} \right) = G \left( \sqrt{\frac{h_{t2} + (1500) ER}{h_{t2}}} \right) \quad (59)$$

The effect of the semi-empirical total enthalpy-equivalence ratio function, equation (59), on the step-to-inlet pressure ratio is shown in Figure 166. The effects of the ideal frictionless gas assumptions not holding true during the heat addition can be seen by the fact that all the data are not correlated by one line.

The conical combustors are more suited to use at high flight speeds than the step combustors, from the consideration of high wall pressure forces. In the conical combustors, the rearward-facing surface is distributed along the length of the combustor. With no combustion, the mean pressure on the rearward-facing surfaces is higher than that of the step combustors, since the flow is attached to the surface. Any combustion producing an increase in stream pressure will increase the mean wall pressure, since it is not necessary to transmit the pressure rise through a wake region to the rearward-facing surface.

The data substantiate the wall force advantage of the conical combustors. Tables V and VI show a mean wall pressure ratio of .96

**CONFIDENTIAL**

**CONFIDENTIAL**

for Configuration AGQ and .19 for Configuration AFN under comparable conditions ( $h_T = 1250-1300$  Btu/lbm,  $ER = .4$ ). A graphic comparison of the wall force of the various combustor types is provided in Figure 167.

A disadvantage of the conical combustors appears at low enthalpy levels, where thermal choking occurs readily. Should the flow tend to choke at a location near the burner entrance, sufficient rearward-facing surface is not available to provide the necessary increase in total momentum to sustain the flow. The flow then seeks relief upstream from the combustor by separating the flow in the air supply nozzle. This phenomenon limited the maximum useful equivalence ratio of Configuration AFQ to .5 at the flight Mach 6 enthalpy level, and limited the maximum ER of Configuration AGQ to .5 at an even higher Mach 8 enthalpy level.

The step-cone combustor was a compromise between the step combustors and the conical combustors. A small step near the burner entrance provided for stabilization of transonic combustion at low enthalpy levels, while a conical section following the step, together with a smaller combustor area ratio, enhanced the mean wall pressure at higher enthalpy levels. It was possible to operate Configuration AHmR at equivalence ratios as high as .7 at low enthalpy levels without separating the burner inlet stream. With Configuration BHmR, a wall pressure ratio of .99 was achieved at flight Mach 8.4 enthalpy level and stoichiometric equivalence ratio, a substantial improvement over the pressure ratios of the step combustors.

#### c) Combustion Efficiency

The combustion efficiency is a measure of the degree to which the conversion of chemical energy to sensible energy has been completed. Combustion efficiency is difficult to define with perfect rigor for a number of reasons. Principal reasons are the fact that a certain amount of chemical energy remains unconverted when the stream has reached equilibrium, and that the residual chemical energy depends upon the interchange of sensible and kinetic energy occurring simultaneously with the combustion process.

The combustion efficiency for the combustors reported here is based upon an approximate definition commonly used to facilitate engine cycle calculations. By this definition, the burner exit stream is assumed to be in chemical equilibrium, but an amount of heat equal to the fraction of the nominal heating value of the fuel represented by the combustion inefficiency is discarded from the system. The use of equilibrium gas properties thereby permitted greatly simplifies cycle calculations. The studies of Reference 14 have shown that the difference in results between this and more rigorous definitions is minor.

**CONFIDENTIAL**

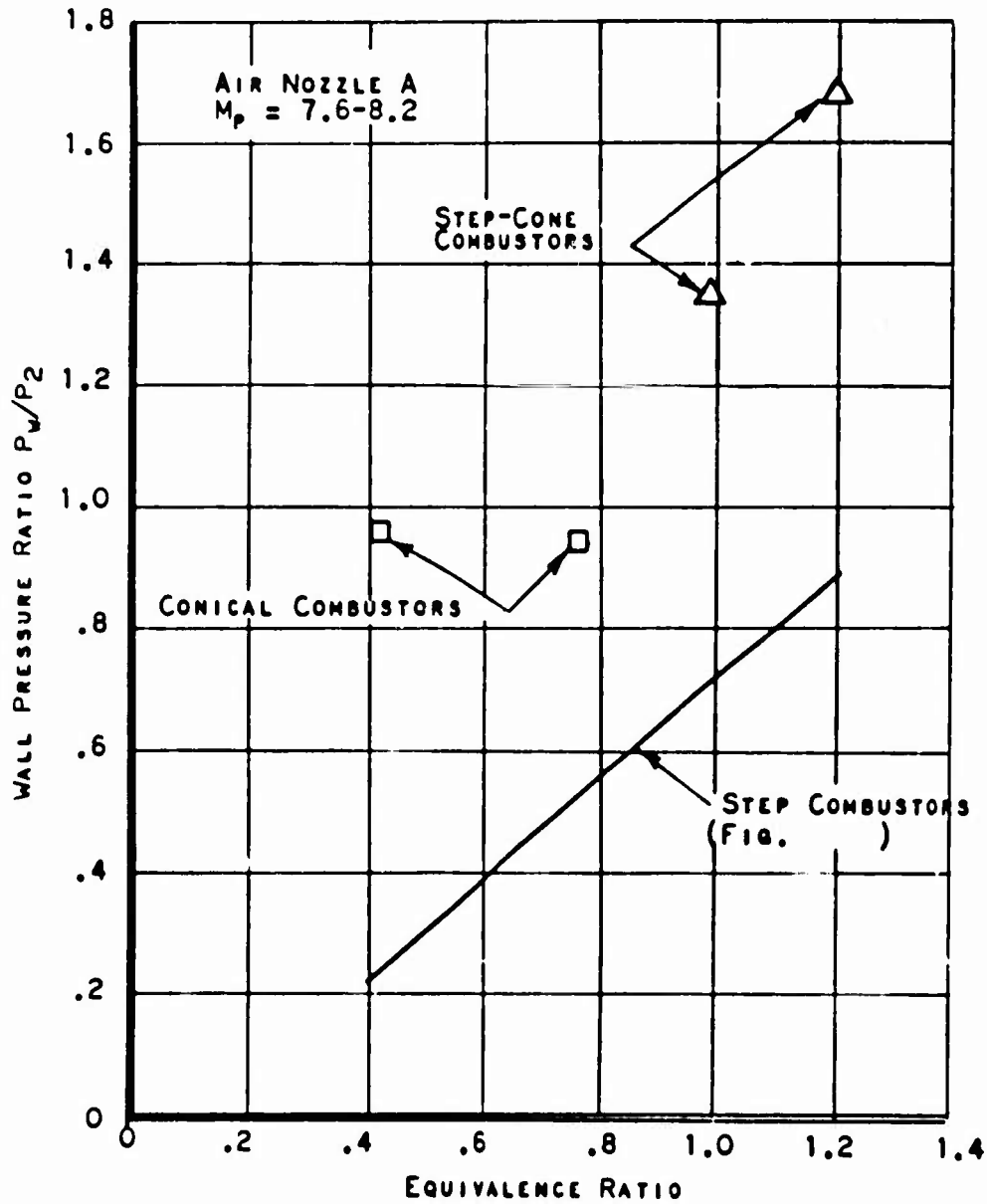
**CONFIDENTIAL**

Figure 167 - Wall Pressure Comparison

**CONFIDENTIAL**

**CONFIDENTIAL**

In a high-temperature combustor, two requirements must be satisfied in order to complete conversion of chemical energy to sensible energy to occur: (1) the fuel and air must be intimately mixed, and (2) sufficient time must be allowed for the reaction to proceed to equilibrium. It is believed that the former was the primary contributor to the combustion inefficiency of the test combustors.

When the combustors were operating in the transonic combustion mode, the gas stream pressure rose quickly to about 1.0 atmospheres and remained at that level for much of the length of the mixing pipe. At this pressure level, reaction rates are relatively fast. The chemical kinetics calculations of Zakkay and Krause (Reference 24 ) predict a reaction time of  $2 \times 10^{-4}$  seconds under these conditions. At a velocity of 6000 feet per second, this would require 1.2 feet for completion of the reaction, as compared to the 2.5 feet of mixing length available.

Means of detecting incomplete chemical reactions were not available for these tests. The gas sampling rake used at the burner exit was incapable of freezing the composition of the gas sample. Many of the samples contained less than the freestream equilibrium amounts of reactants, indicating that the chemical reactions had proceeded toward equilibrium during cooling of the gas sample within the probe. Since the kinetics calculations predicted that the reactions should be locally complete, these samples were corrected to indicate chemical equilibrium in the freestream. The quoted combustion efficiencies for the combustor thus reflect only mixing imperfections, but are believed to be reasonably accurate.

In the mixing process, the objective is to transport the fuel from discrete sources (the fuel nozzles) to a uniform dispersion in the air stream within the length of the burner. This process is accomplished in two phases. The first consists of the breaking up and scattering of the fuel jets by turbulence existing or induced in the stream. The second phase is the intimate mixing of fuel and air molecules accomplished by molecular diffusion. Chemical reaction can occur only after the latter phase has been accomplished. Since molecular diffusion is a relatively slow process, the approach to the problem of reducing mixing length is to reduce the transverse distance a fuel molecule must diffuse to reach an air molecule.

The first consideration in improving mixing is the distribution of the fuel sources in the air stream. If the fuel sources were located only at the duct walls, some of the fuel would have to be transported by turbulence and diffusion the full radius of the duct to reach the air at the center. If, on the other hand, the fuel sources were projected into the air stream, the transverse distance to be traversed is reduced. The purpose of

**CONFIDENTIAL**

**CONFIDENTIAL**

injecting the fuel at angles to the flow in the present combustors was to project the fuel sources away from the duct walls by the mechanism of jet penetration.

Jet penetration in many of the test combustors was insufficient to fully fuel the center of the stream, especially when the fuel flow was relatively low. The fuel concentration profiles of Figures 96, 103, 116, 125 and 141 all show fuel-lean regions near the center of the duct at the burner exit plane. This indicates that the distance the fuel had to traverse to reach the center was excessive. All these data were taken with less than stoichiometric fuel flow. As jet penetration increases with fuel flow, higher equivalence ratios would be expected to produce better fueling of the centerline. The data of Figures 94, 114 and 151 were taken with an equivalence ratio of stoichiometric or higher, and show a much more uniform distribution. High flight speed simulation appears to render penetration more difficult. The data of Figures 131 and 152 show evidence of deficient penetration, despite high fuel flow.

The function of turbulence is to break the stream of fuel from the fuel sources into lumps, to distribute these lumps throughout the air stream, and to break the large lumps into smaller lumps until the distance between lumps is small enough for molecular diffusion to complete the mixing process. If the turbulence existing in the inlet air stream is inadequate to accomplish this, additional turbulence must be induced within the combustor. Penetrating fuel jets may be expected to induce turbulence. Combustion induces turbulence by creating non-uniformity in the flow field. The strong non-uniformity of the flow field associated with transonic combustion would be expected to be especially effective in creating turbulence.

The data substantiate the expected beneficial effect of transonic combustion in promoting turbulence. The fuel distribution profile data of Figures 94 through 97 and 102 were obtained with equivalence ratios high enough to strongly choke the combustor. These data were generated by injectors E and F, having only four fuel sources. The fuel profiles show radial gradients, but relatively slight circumferential gradients. In contrast, the profiles of Figure 98, 99, 103 and 122, obtained at lower equivalence ratios at which the burner was supersonic or only weakly choked, show distinct circumferential patterns which were related to the locations of the fuel injectors.

Induced turbulence may account for the observed trend toward more uniform fuel distribution with decreasing enthalpy level observed among burners operated at high equivalence ratios. An example of this trend may be found in comparing Figures 151 and 152. Increased turbulence tends to compensate for insufficient penetration.

**CONFIDENTIAL**

**CONFIDENTIAL**

The fuel distribution profiles presented here are indicative of the degree to which turbulence had dispersed the fuel in the air stream, but do not show the degree to which molecular scale mixing had progressed. The point equivalence ratios were computed from analysis of gas samples. Each gas sample was taken by a probe that ingested a small part of the flow at a point in space over a relatively long period of time in order to fill the sample bottle. In all probability, the composition of the gas stream at the sampled point was not constant with time. More likely, the flow consisted of lumps of fuel broken from the fuel jets by turbulence, separated by regions of air, with blending of the fuel and air having occurred to some degree due to molecular diffusion. Lumps and spaces might be expected to be of the order of .01 to .1 ft. in size, producing a period of fluctuation of  $2 \times 10^{-6}$  to  $2 \times 10^{-5}$  seconds. The probe thus sampled a continuously varying composition cooling the sample and mixing it in the sample bottle to provide an approximately time-average composition.

It is significant that a probe that was incapable of quenching the high-temperature reactions in the gas sample could, by sampling a heterogeneous stream, obtain a sample that appeared to indicate incomplete reaction. In one increment of time, the probe might ingest a fuel-rich mixture. All residual oxygen would be consumed in the probe during cooling of the sample, and the products, with excess hydrogen, dumped into the sample bottle. Once cooled completely, the sample would not react with other mixtures present in the bottle. In another increment of time, the probe might ingest a lean sample. After completely reacting, this sample would contribute its excess oxygen to the mixture in the bottle. The mixed sample in the bottle would thus contain both hydrogen and oxygen, as it would had the probe quenched a homogeneous, incompletely reacted mixture. The probability of this occurrence increases, of course, as the time-average composition of the stream approaches stoichiometric. Experimental observations and more detailed discussion of this phenomenon are found in Reference 25.

High over-all combustion efficiency is most difficult to attain when the burner equivalence ratio is near stoichiometric. To attain high efficiency with lean equivalence ratios, it is only necessary to mix enough to bring at least one oxygen molecule into proximity with each two hydrogen molecules. The performance defect resulting from allowing the excess oxygen to remain unmixed is of secondary magnitude. With rich equivalence ratios, it is only necessary to bring at least two hydrogen molecules into proximity with each oxygen molecule, and the excess hydrogen may be left unmixed. But at stoichiometric, there are no excess reactants, and mixing must be complete to attain high performance.

**CONFIDENTIAL**

## CONFIDENTIAL

AF APL-TR-65-103

In the event that the burner equivalence ratio is significantly less than stoichiometric, and mixing has progressed, not to complete uniformity, but to the extent that all the fuel is in proximity with at least the stoichiometric amount of oxygen, combustion inefficiency of secondary magnitude can still exist. The same is true for burner equivalence ratios well above stoichiometric, when local equivalence ratios are not uniform, but are above stoichiometric everywhere in the stream. This inefficiency arises from temperature gradients in the flow. The regions having local equivalence ratios near stoichiometric have higher static temperatures than the regions far from stoichiometric. The extent of dissociation of combustion products in chemical equilibrium increases exponentially with temperature. The equilibrium dissociation corresponding to the mean temperature of the flow may be moderate. The dissociation of the cooler regions will be somewhat less. The dissociation of the hotter regions, however, will be disproportionately high, so that the mean extent of dissociation is greater than that corresponding to the mean temperature.

Combustion inefficiency also arises from temperature profiles caused by heat transfer to the burner walls. This heat is, in general, extracted primarily from the regions of the flow adjacent to the walls, leaving these regions cooler than average, and the core of the stream hotter than average.

To illustrate this effect, the theoretical curve of Figure 168 may be employed. This curve presents the extent of equilibrium dissociation of stoichiometric combustion products at one atmosphere pressure as a function of temperature. If the mean temperature of a stream were, say, 4600°R, the extent of dissociation corresponding to this temperature would be 15%. If, however, half the stream were actually at a temperature of 4000°R, and the other half at 5200°R, then the two parts would be 4% and 50% dissociated, respectively, and the mean extent of dissociation would be 26%. The mean extent of dissociation would thus be 11% higher than that corresponding to the mean temperature, and an efficiency decrement of about 11 points would result.

An example of combustion inefficiency due to a temperature profile was found in Run 164, a test of Configuration AGQ at  $ER = .42$  and an enthalpy level simulating Mach 7.8 flight. The measurements indicated that the combustor exit stream was everywhere in chemical equilibrium. Local equivalence ratios were found to vary from .14 to .91, all below stoichiometric. Heat rejected the burner walls was assumed to have been extracted from the outer third of the mass flow, rendering the stagnation enthalpy of this region 370 Btu/lbm lower than the average. The method of calculating combustion efficiency was such that the rejected heat would not have resulted in an efficiency decrement had it been extracted uniformly from the stream. The combustion efficiency computed for this burner was 78, despite

CONFIDENTIAL

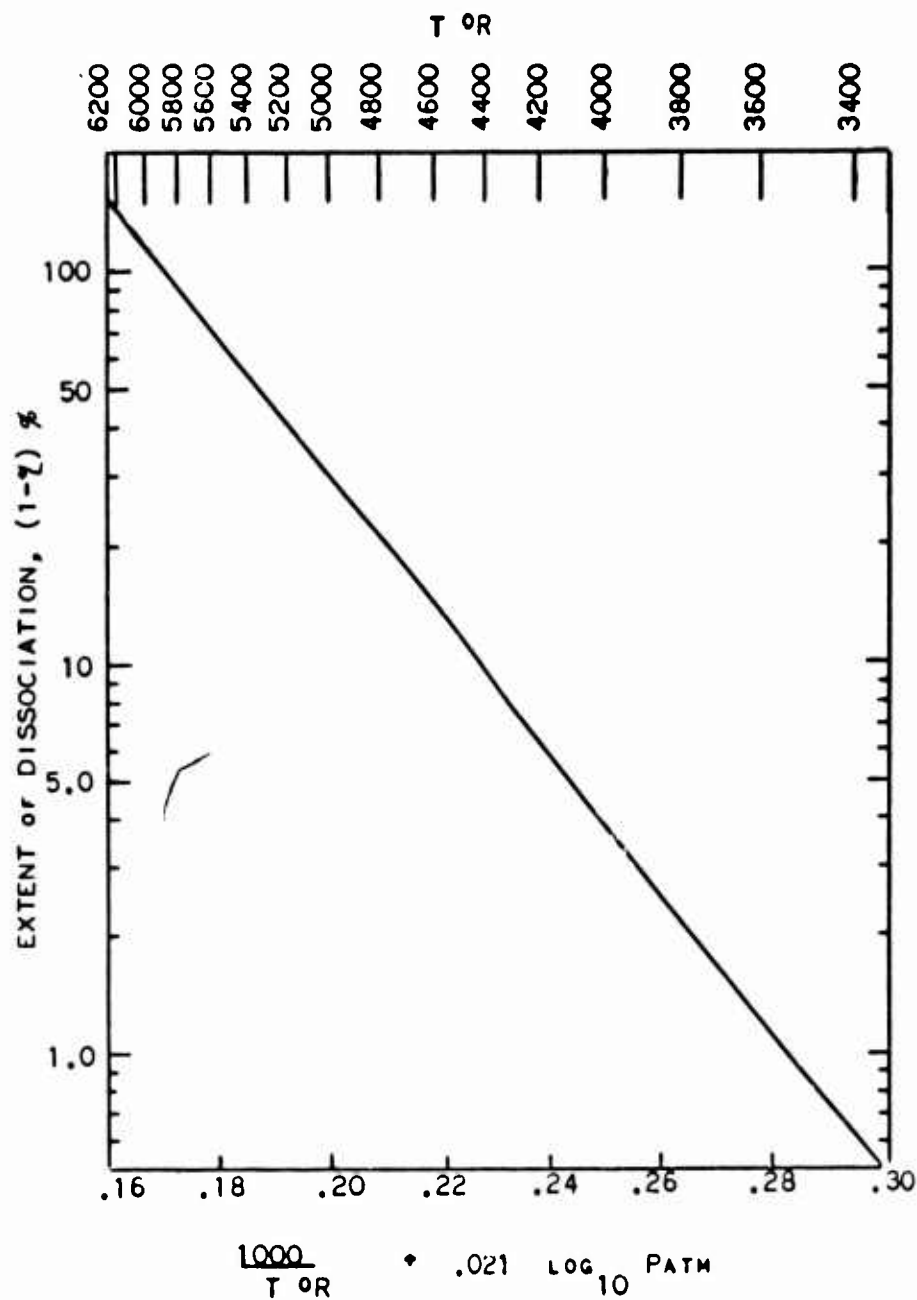
**CONFIDENTIAL**

Figure 168 - Dissociated Products in Stoichiometric  
 $H_2$ -Air at Equilibrium

**CONFIDENTIAL**

**CONFIDENTIAL**

apparently adequate mixing and combustion. The entire efficiency decrement for this run was attributed to the above effects of temperature non-uniformities in the burner exit stream.

The measured combustion efficiencies of the various configuration types have been plotted against equivalence ratio, roughly segregated by enthalpy level, in Figure 169. Superimposed on this plot is the target combustion efficiency curve established at the outset of the program. The efficiency target was met or exceeded by the combustors when operated at the lower enthalpy level, where the transonic combustion mode is readily established. At higher enthalpy levels, the target combustion efficiency was less frequently attained, especially at lean equivalence ratios, where the combustors tended to operate fully supersonic. In general, the step combustors displayed the highest efficiency levels, attributed to the strong turbulence induced by the flow about the step. The step-cone combustors displayed next highest efficiencies, followed by the conical combustors, which had the least turbulence generation.

d) Friction Drag

Friction drag was calculated from the change in total momentum of the gas stream through the combustor, using the principle of conservation of momentum:

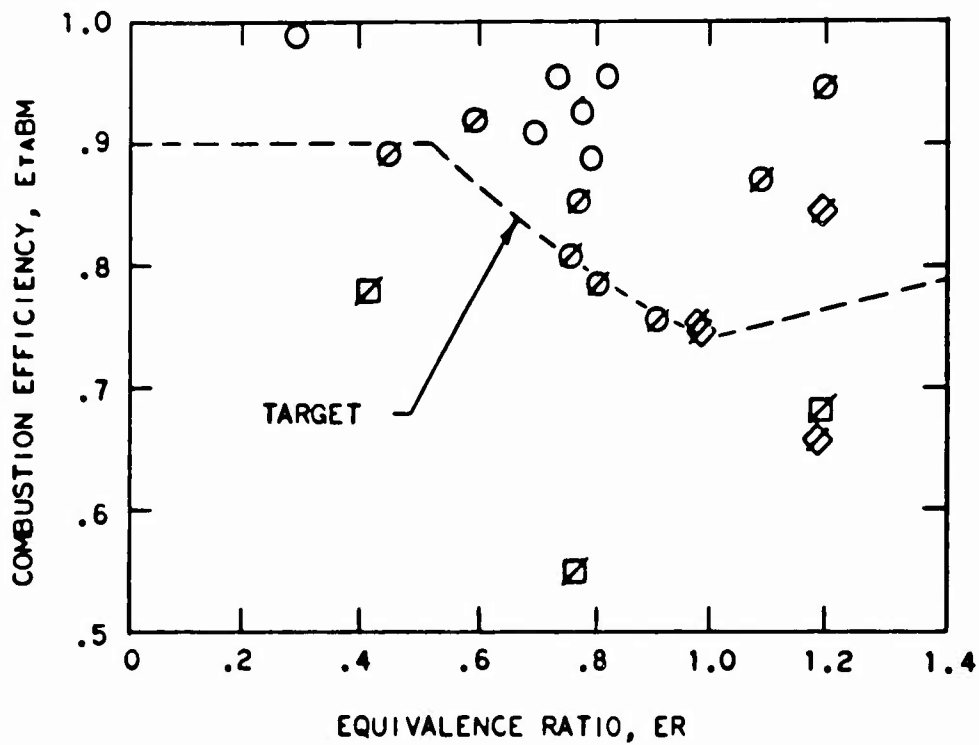
$$D_f = F_2 + P_w(A_4 - A_2) - F_4 \quad (60)$$

The burner inlet total momentum,  $F_2$ , was calculated assuming isentropic flow through the air supply nozzle. When fuel was injected downstream, the fuel momentum was included in this total. For normal injection, the fuel being injected perpendicular to the axis adds no momentum to the stream. The exit momentum,  $F_4$ , was computed from the burner exit surveys, corrected to meet mass and energy continuity. As the velocity head of the non-uniform exit stream was difficult to evaluate, the friction coefficients reported in Tables V, VI and VII were based on inlet velocity head and the wall surface in shearing contact with the flow:

$$C_f = \frac{D_f}{A_s q_2} \quad (61)$$

The friction coefficient is probably the least accurate of the performance parameters reported. In Equation (60), the two total momentum terms are large relative to the friction drag, so that a one percent error in evaluating either total momentum will result in an error of the order of 20% in the friction drag.

**CONFIDENTIAL**

**CONFIDENTIAL**

- STEP COMBUSTORS,  $M_p < 7$
- ◐ STEP COMBUSTORS,  $M_p > 7$
- ◑ CONICAL COMBUSTORS,  $M_p > 7$
- ◒ STEP-CONE COMBUSTORS,  $M_p > 7$

Figure 169 - Combustion Efficiency VS Equivalence Ratio

**CONFIDENTIAL**

**CONFIDENTIAL**

The calculated friction coefficients average .0025 with a standard deviation of .0007. That this average is higher than would be predicted for fully developed pipe flow is probably justifiable on such grounds as: the turbulence generating mechanisms, such as the penetrating fuel jets and separated flows, tend to destroy established boundary layers; the combustor length is too short to allow fully developed flow; etc.

A brief analytical combustion study was performed to investigate the effect of measurement errors on the accuracy of combustor friction forces calculated from measurement of the combustor exit profiles.

A stream composed of two parts was selected for analysis, in each part occupying equal areas and having equal static pressures, total momentums and air and hydrogen stagnation enthalpies. Enthalpy levels were approximately equivalent to a SCRAMJET burner exit stream at  $M_p = 8$ . The two parts of the stream differed in that part (a) had an equivalence ratio of 0.8 and part (b) had an equivalence ratio of 1.2. Both were in chemical equilibrium. This stream was selected as being representative of a burner exit stream which might be encountered in a SCRAMJET engine in flight at Mach 8. The stream properties were as follows:

Area	ft <sup>2</sup>	Part a	Part b
		1.0	1.0
Static pressure	atm	1.0	1.0
Static temperature	°R	4885	4956
Equivalence ratio		0.8	1.2
Velocity	ft/sec	5431	5728
Total momentum	lbf	8465	8465

It was assumed that the following measurements were made: impact pressure in part (2), equivalence ratio in part (a), static pressure in both parts and total fuel and airflows and stagnation enthalpies. The impact pressure and equivalence ratio measurements determined the flow in part (a). The flow in part (b) was adjusted to maintain over-all continuity of mass and energy.

The errors introduced and the resultant errors in the calculated total momentum are outlined in the following table:

**CONFIDENTIAL**

**CONFIDENTIAL**

Measurement Error	Magnitude of Error - Percent	Resultant Total Momentum Errors		
		Part a	Part b	Overall
Static pressure in both parts too low	10	-.87	+7.7	+3.4
Static pressure of part (b) only measured low	10	0	+3.3	+1.6
Impact pressure of part (a) too low	10	-9.1	+9.6	+.26
Equivalence ratio of part (a) too high	12.5	+.003	+.59	+.29
Stagnation enthalpy of both parts too low	10	0	-4.3	-2.1
Stagnation enthalpy of part (a) too low; over-all enthalpy correct	10	0	-.41	-.20

A ten percent reduction in the static pressure of both parts of the stream resulted in a 3.4 percent increase in the over-all total momentum of the stream. Since the combustor friction forces are determined by the difference between combustor entrance and exit, an error in the exit total momentum might be magnified ten times in computing the friction. It was concluded that the static pressure measurement is critical to the friction determination.

A ten percent reduction in the static pressure of part (b) only resulted in a 1.6 percent increase in the over-all total momentum.

A ten percent reduction in the impact pressure measurement in part (a) resulted in a 9.1 percent reduction in the total momentum of part (a), but this was compensated by adjustment of the flow in part (b) to maintain continuity, so that the over-all increased only 0.26 percent. It was concluded that the impact pressure measurement is less critical than the static pressure measurement, provided over-all continuity is maintained.

A 12.5 percent increase in the equivalence ratio measurement in part (a) produced a 0.29% increase in the over-all total

**CONFIDENTIAL**

**CONFIDENTIAL**

momentum. This measurement is also of lesser importance in determining friction than the static pressure.

When the stagnation enthalpy of both parts were reduced ten percent, the over-all total momentum was reduced 2.1 percent; but when the enthalpy of part (a) only was reduced ten percent, with the over-all heat balance maintained correct, the resultant decrease in total momentum was only 0.20 percent. This indicates that the accurate measurement of combustor heat losses is critical to the determination of friction, but that a knowledge of the distribution of these heat losses throughout the exit stream is of lesser importance.

Errors in measuring the degree of departure from chemical equilibrium in the stream would produce much the same error in total momentum as errors in heat loss measurement.

e) Combined Effects

It is apparent that combustion efficiency alone is insufficient to fully describe the performance of a combustor. High combustion efficiency can be attained by increasing burner length, but the friction drag of extremely long burners renders them useless for production of thrust in an engine. A true measure of combustor effectiveness must combine the relative effects of combustion efficiency, friction drag, wall pressure, etc., and must be related to the ability of the combustor to produce thrust when integrated with an engine.

The over-all combustor effectiveness parameter used here is the net thrust potential, defined as the net axial force on the combustor and a hypothetical inlet and exhaust nozzle, compared to the axial force on an ideal combustor inlet, and nozzle having the same combustor inlet stream and exhaust nozzle exit area.

Net thrust potential is plotted as a function of equivalence ratio in Figure 170. The data are segregated by configuration type. The numerals beside each data point represent the flight Mach number simulated by the air stagnation enthalpy of each test. Superimposed on the plot are curves of net thrust potential obtained from engine cycle calculations using target values of wall pressure force, friction coefficient, and combustion efficiency established at the outset of the program. These curves correspond to fuel injection at a 30 degree angle to the airflow, curves for normal injection are generally .01 to .02 higher.

**CONFIDENTIAL**

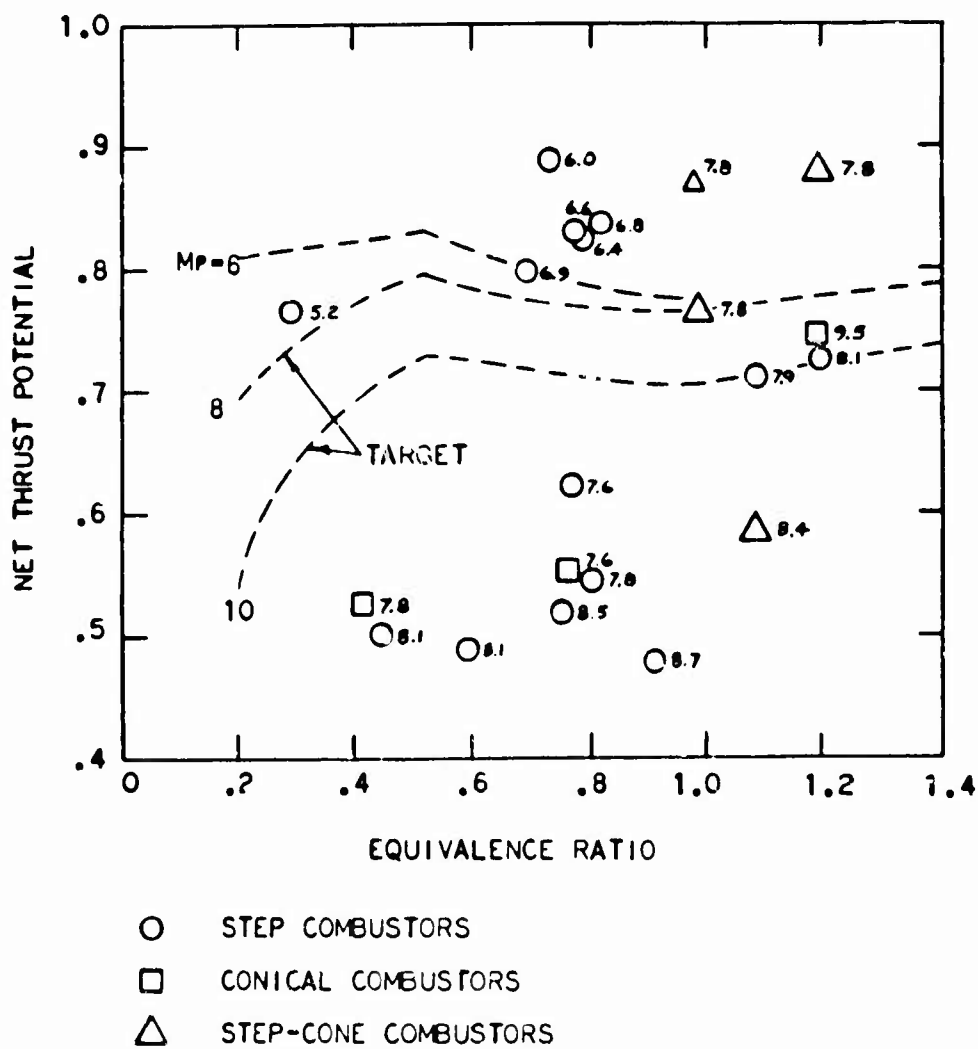
**CONFIDENTIAL**

Figure 170 - Thrust Potential VS Equivalence Ratio

**CONFIDENTIAL**

**CONFIDENTIAL**

The net thrust potentials of all three configuration types, step, conical and step-cone were approximately equal. The combustion efficiencies of the conical combustors were much lower than those of the step combustors (See Figure 100), but this deficiency was compensated by higher mean wall pressures. At the enthalpy level simulating Mach 7.8 flight; the step-cone combustor appears superior to the other types, but its performance depreciated badly at the Mach 8.4 enthalpy level.

Target levels of net thrust potential were exceeded at the lower enthalpy levels (Mach 6-7 flight) with equivalence ratios greater than 0.7. At higher enthalpy levels, performance was below target for all equivalence ratios below 1.2.

### c. Burner Nozzle Tests

#### 1) Objectives

The early experimental work on fuel injectors was extended to combustor tests in 1964. In 1965 this progress was further extended to GE's first tests on the combination of two water cooled SCRAMJET components, the combustor and exhaust nozzle. This testing provides initial background on the mutual effect of the two components in one another, and indicates the usefulness of data obtained from tests of two combined components.

The specific objectives of these initial exploratory tests were to:

1. Develop appropriate test techniques and establish the suitability of the available facility.
2. Identify any effects on the burner due to the presence of the exhaust nozzle.
3. Obtain wall pressures and freestream exit impact pressures for an exhaust nozzle with burner exit conditions similar to those expected in a vehicle, for comparison with analytical calculations.
4. Provide an indication of the extent of mixing and combustion occurring in the exhaust nozzle.
5. Examine the suitability of measurements made at the end of an exhaust nozzle, as indicators of combustion performance.

#### 2) Choked-Burner Exit Conditions

Step-burner combustor tests run at simulated Mach 8 enthalpy levels, resulted in a choked (near sonic) burner exit condition. These tests using a step-burner Configuration AEN, were rerun with an exhaust

**CONFIDENTIAL**

**CONFIDENTIAL**

nozzle to provide results from a uniform, well defined burner exit stream, with a high level of dissociation at the nozzle inlet.

Figure 171 compares the static pressure distributions from the burner nozzle test Run 216 with Run 104, the comparable test without a nozzle. It is seen that the nozzle did not significantly affect the burner pressures and that the pressure distributions for the two runs were nearly identical.

Figure 172 presents the results of gas samples taken at the combustor exit shown as percent dissociation. The percentage dissociation is defined as the percentage of the fuel's heating value that is still unreleased at the combustor exit and is tied up in partly-dissociated latent-chemical-energy of the products. The heating value used does not include the heating value for that portion of the fuel that is over stoichiometric. This percentage dissociation could also be defined in terms of molecular weight change which would give very close to the same values. The measured quantities of dissociated products found in the gas samples was less than the theoretical equilibrium quantity that should have existed based on calculations from the local freestream static temperature and pressure. The probe did not successfully quench the products, and recombination took place within the sampling probe.

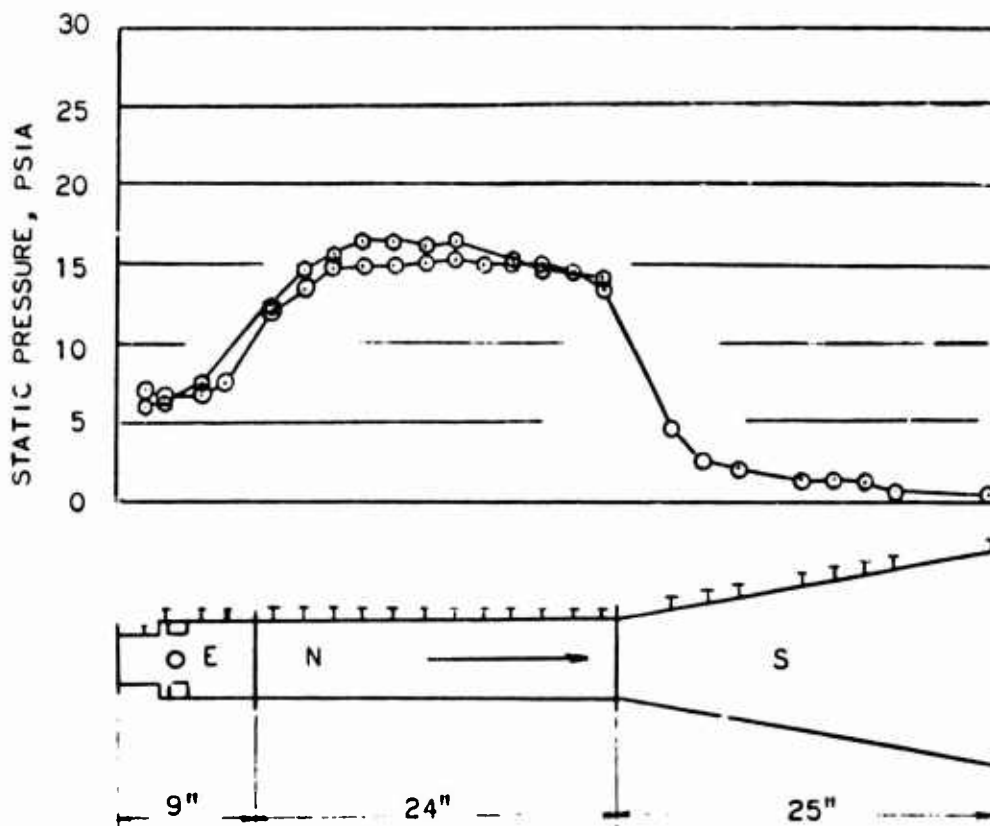
Figure 173 shows that the measured dissociation level at the end of the nozzle was greater than that measured at the end of the burner. The samples at the end of the nozzle were obtained at a much lower total pressure where quenching should be much easier, 5 psia at the end of the nozzle vs. 30 psia at the end of the burner. Also the quenching in the exhaust nozzle itself may have helped in quenching the reactions. In addition to the 5 psia samples, four samples were drawn through the specially designed quenching probe (See Figure 80) which cools the sample at a pressure of 1/2 psia. The compositions found for these samples were in general agreement with the 5 psia samples.

The measured dissociation level at the nozzle exit is significantly below the theoretical level at the exit of the burner. These samples may be measuring the extent of recombination occurring in the exhaust nozzle. The nozzle recombination does not, however, go all the way to equilibrium. The equilibrium level of dissociation at the exhaust nozzle exit is less than 0.1%.

### 3) Burner with Fuel/Air Profile

To demonstrate the lack of mixing in the supersonic nozzle, a burner with a significant fuel/air profile was run. Run 164, Configuration AGQ, a conical burner which had shown a significant fuel/air profile at simulated

**CONFIDENTIAL**

**CONFIDENTIAL**

SYMBOL	$M_{T2}$	$M_P$	ER	CONFIGURATION
○	1230	7.8	1.19	AENS
○	1290	8.0	1.26	AEN

Figure 171 - Static Pressure Profiles, Runs 104 and 216

**CONFIDENTIAL**

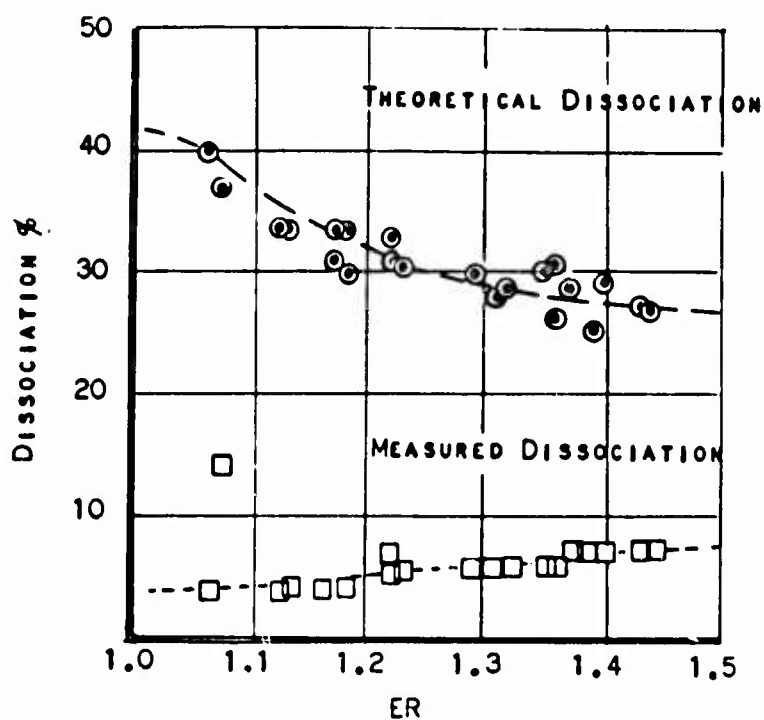
**CONFIDENTIAL**

Figure 172 - Theoretical and Measured Dissociation for Run 104 As A Function of Equivalence Ratio

**CONFIDENTIAL**

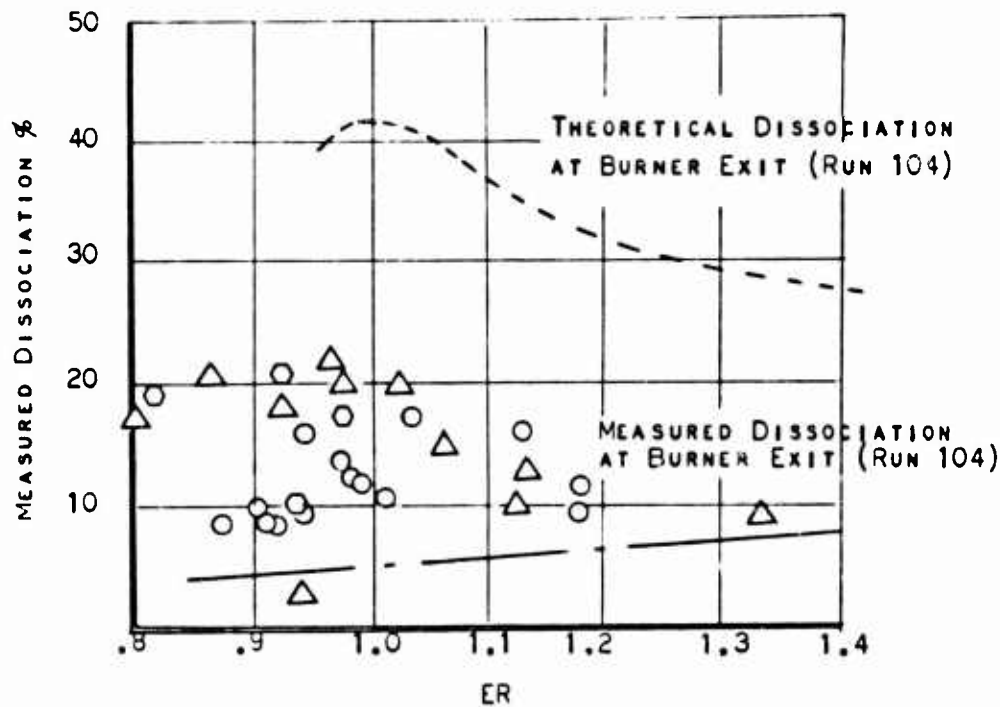
**CONFIDENTIAL**

Figure 173 - Measured Dissociation At Nozzle Exit for Runs 202, 216 As A Function of Equivalence Ratio

Run 202  
Run 216  
Run 216 Quench

**CONFIDENTIAL**

**CONFIDENTIAL**

Mach 8 conditions and an equivalence ratio of 0.4, was retested with an exhaust nozzle as Run 203, Configuration AGQS. Gas samples were obtained at the end of the nozzle, and the samples from both tests are shown in Figures 174 and 175. The prominent characteristic of a large, very lean center region is evident in both profiles, indicating that little mixing occurs in the nozzle.

Figure 176 compares the static pressure profiles for Runs 203 and 164. As was the case with the choked step burners already discussed, the presence of the nozzle did not significantly alter the combustor pressure distribution.

#### 4) Final Configuration

The final configuration, the R tailpipe, was also tested with an exhaust nozzle. This combustor has a supersonic exit with uniform exit profile except for some leanness at the center.

Figure 177 contains the measured Mach number at the end of the exhaust nozzle. One-dimensional expansions from the burner exit were made with constant  $\gamma$  calculations from the data previously presented in Figure 142, to show the approximate agreement of the shape of the profile at the two stations.

Figure 178 compares the fuel/air data measured in Run 205, a burner-nozzle test at simulated Mach = 8 conditions, with a line representing the data at the burner exit which was previously presented in Figure 141, for Run 206. The somewhat lean center region of the burner exit profile is also evident in the exhaust nozzle profile.

Figure 179 presents the measured percentage of dissociation at the nozzle exit. If the samples were properly quenched in the probe, then these results are measurements of the combined effect of combustion efficiency and nozzle recombination. By comparison with the curve determined for theoretical dissociation at the burner exit, it is seen that the results are reasonably consistent with the assumption of frozen nozzle flow, the assumption used in cycle calculations and in EtaNT determinations. This consistency is dependent on the existence of high local combustion efficiencies at the burner exit. The actual one-dimensional combustion efficiency numbers used in cycle calculation and in EtaNT calculations are significantly less than 100% because of profile effects, especially that due to convection heat loss to the walls. This heat loss results in an average enthalpy level for the one-dimensional burner exit stream that is less than the local level in the freestream. The theoretical dissociation level is, therefore, lower for the one-dimensional stream. For the data points presented here, the one-dimensional dissociation level for the burner exit was seventeen (17) percent.

**CONFIDENTIAL**

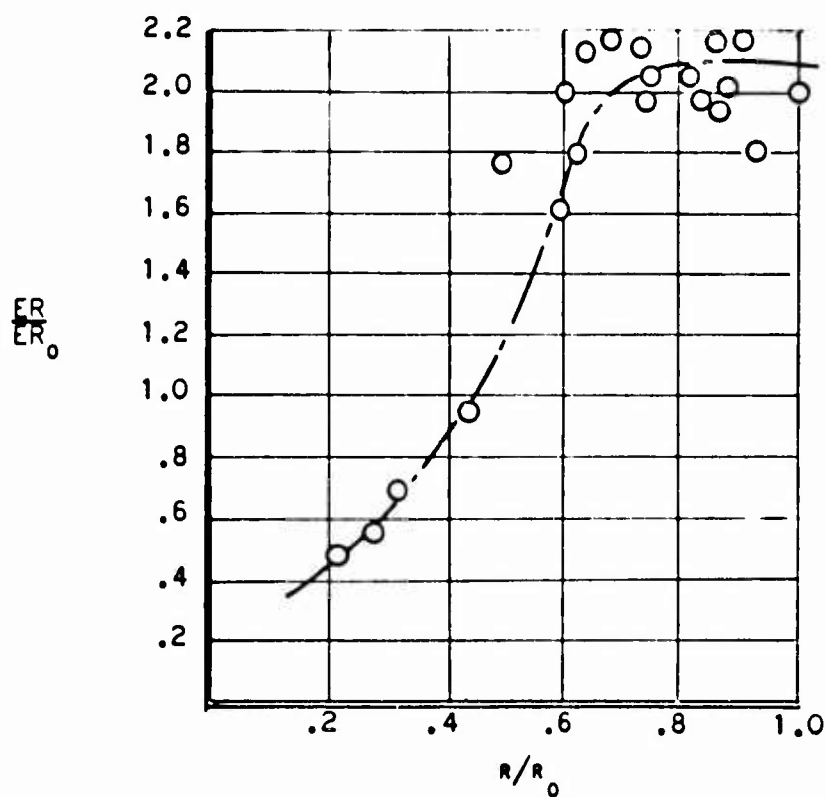
**CONFIDENTIAL**

Figure 174 - Fuel/Air Profile for Run 164, Configuration AGQ

$$M_p = 8$$

$$ER_0 = .420$$

**CONFIDENTIAL**

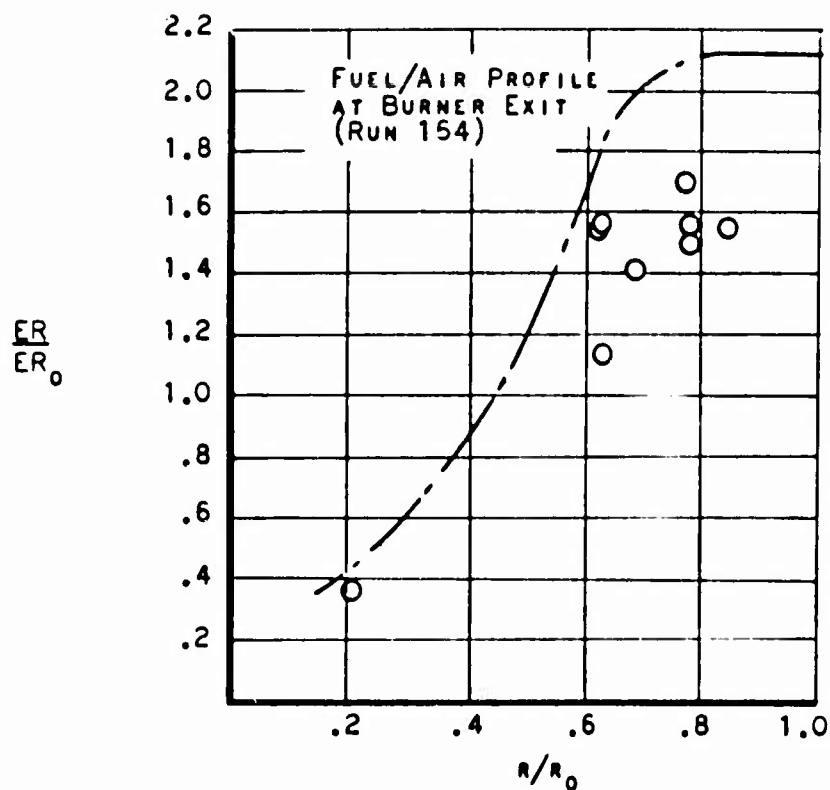
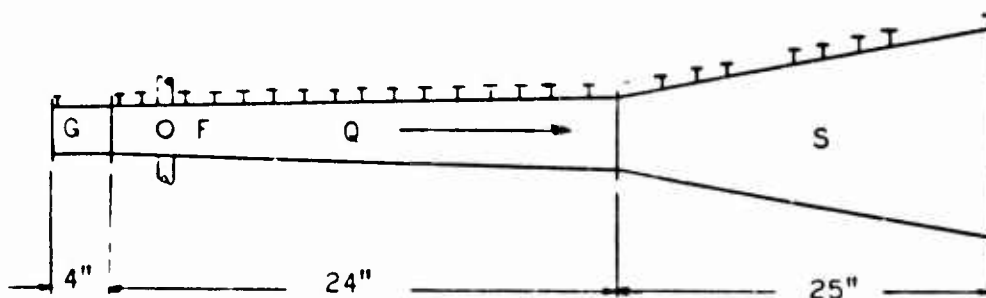
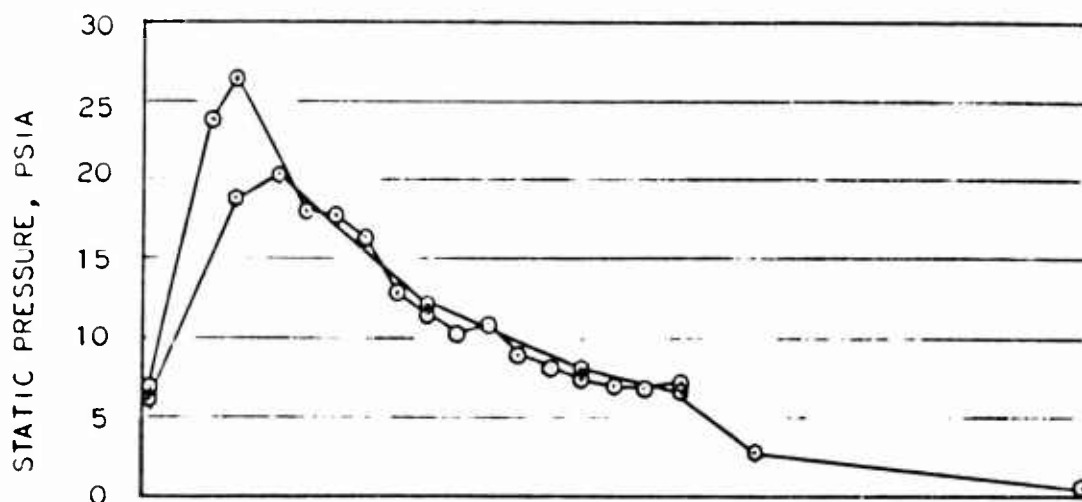
**CONFIDENTIAL**

Figure 175 - Fuel/Air Profile for Run 203, Configuration AQQ3

$$M_p = 8$$

$$ER_0 = .373$$

**CONFIDENTIAL**

**CONFIDENTIAL**

SYMBOLS	$M_{T2}$	$M_P$	ER (G)	ER (F)	CONFIGURATION
○	1260	7.89	.42	.87	AGFQ
○	1320	8.09	.35	.88	AGFQS

Figure 178 - Static Pressure Profile, Runs 164 and 203

**CONFIDENTIAL**

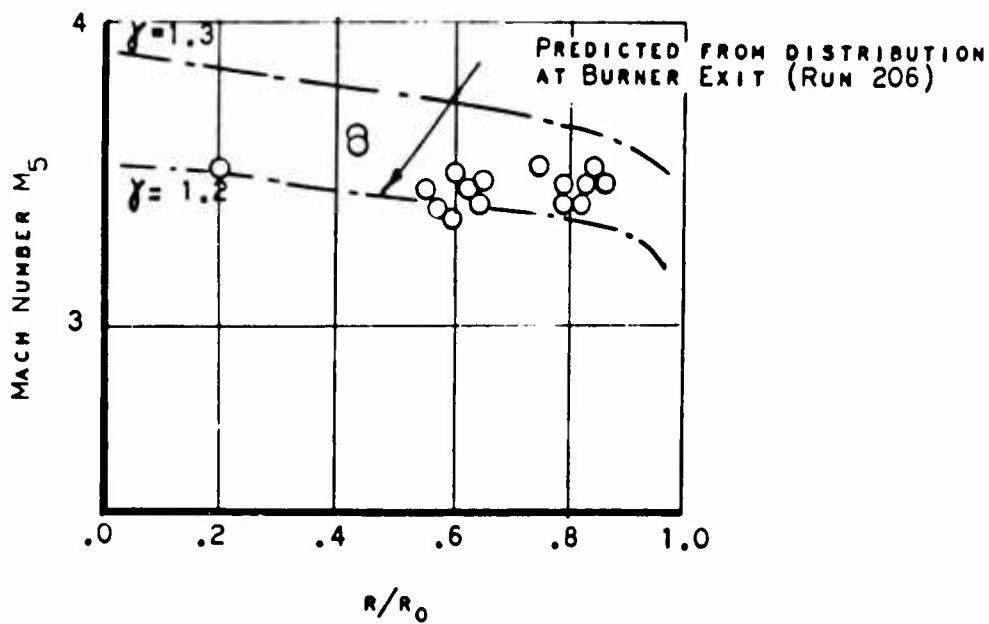
**CONFIDENTIAL**

Figure 177 - Mach Number Profile At Nozzle Exit Run 205,  
Configuration ABaRUS

**CONFIDENTIAL**

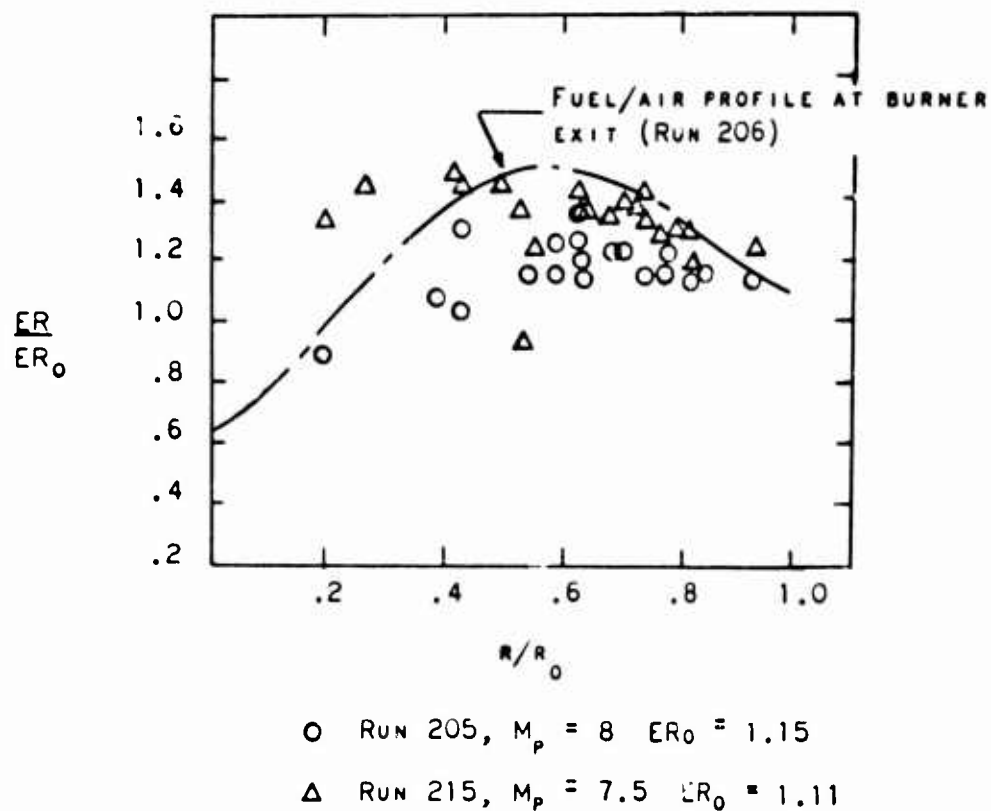
**CONFIDENTIAL**

Figure 178 - Fuel/Air Profile for Runs 205, 215,  
 Configuration AHMUS

**CONFIDENTIAL**

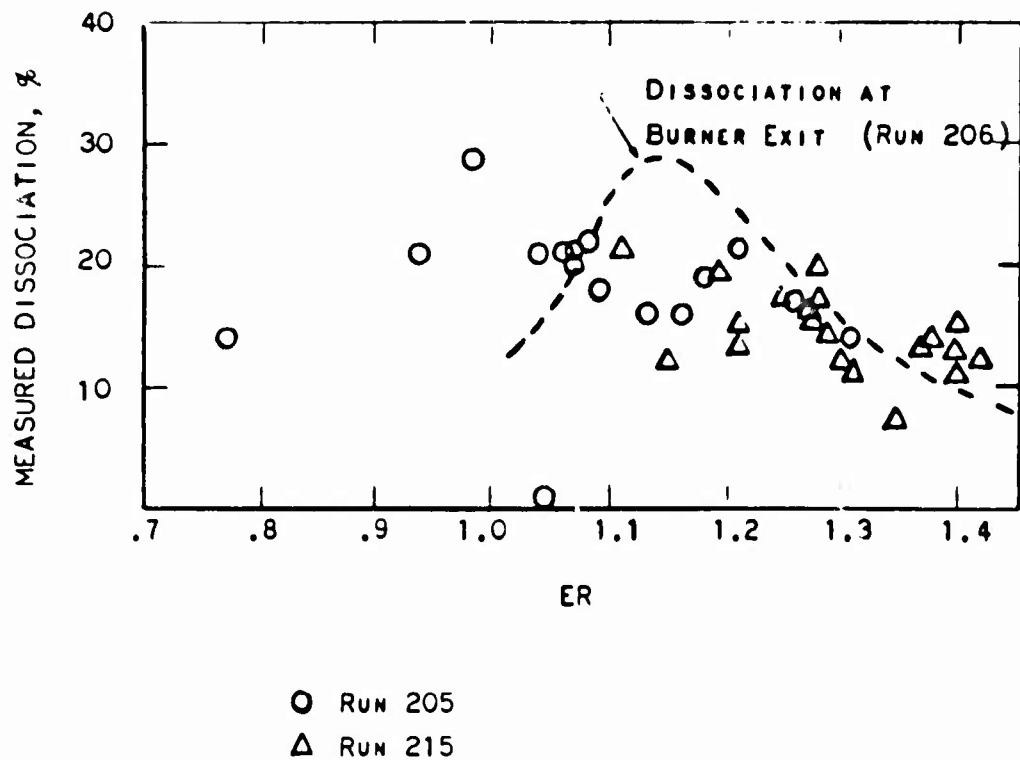
**CONFIDENTIAL**

Figure 179 - Measured Dissociation At Nozzle Exit  
As A Function of Equivalence Ratio for  
Runs 205, 215 - Configuration AHaRUS

**CONFIDENTIAL**

**CONFIDENTIAL**

Static pressure profiles for Runs 205, 215 and 206, Figure 180 shows that for the step-cone geometry, as for all other geometries, there is no significant effect of the nozzle on the combustor pressure distribution.

5) Applicability of Data Taken from an Exhaust Nozzle

Burner-nozzle combinations were successfully tested at simulated Mach 8 conditions. Gas samples were successfully obtained from the low pressure nozzle exit. Combustor wall static pressure measurements were obtained which showed that there was no effect of the nozzle on the combustor pressure distribution, confirming that nozzle measurements can be compared directly with burner measurements.

Low-pressure gas samples were successfully obtained at the nozzle exit. Comparison of samples made at the burner exit with samples at the exhaust nozzle exit showed that very little large scale mixing occurred down the nozzle. Thus some features of inadequate mixing in the burner can be detected in the measured profile at the nozzle exit. Furthermore, the exhaust nozzle samples showed more dissociation than samples taken at the burner exit (at least for choked burners), suggesting better quenching of the reactions. These samples may be measuring the recombination taking place in the nozzle. No quantitative verification of the sampling technique is available. The sum of chemical reactions taking place in the combustor and the nozzle is possibly more significant value than reactions in the combustor alone.

The impact-gas-sampling probe is much less subject to damage when used downstream of the exhaust nozzle. The flow at the nozzle exit is at lower pressure and at a lower mass flow rate per square inch than at the burner exit, resulting in significantly lower heat transfer rates. The life of the probe is increased and the relaxation of cooling requirements makes it possible to design probes with improved aerodynamic design.

The wall pressures on the nozzle are a bonus from combustor tests with an exhaust nozzle. These measurements provide an indication of the thrust produced by the combination. A comparison of these nozzle measurements with analytical calculations is reported in Volume III, which contains a discussion of exhaust nozzle performance, under Task 3a of Item II.

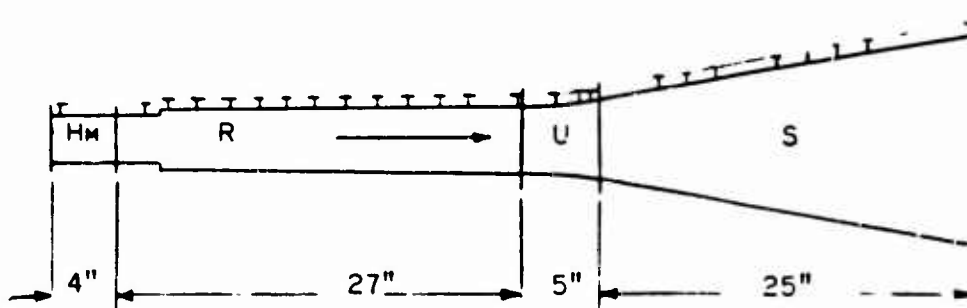
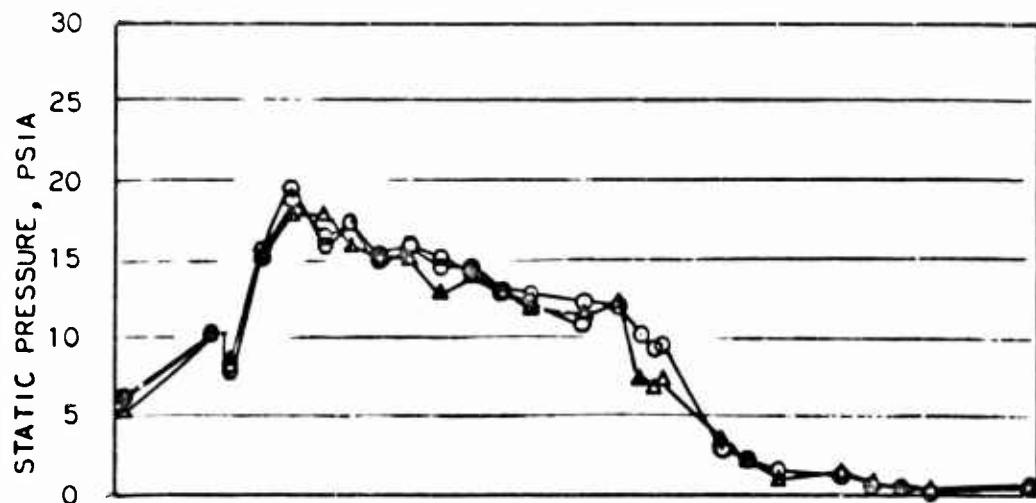
d. Results of Ignition Tests

1) Auto-ignition Experience

Ignition of the test combustors and stabilization of combustion after ignition proved to be somewhat more severe problems than originally anticipated. It was recognized at the outset that for the lower Mach number cycle conditions, the freestream static temperatures were too low to result in auto-ignition. However, it was hoped that sufficient recovery of total temperature would occur in the fuel injection and mixing process or in boundary

**CONFIDENTIAL**

**CONFIDENTIAL**



SYMBOL	$H_{T2}$	MP	ER	CONFIGURATION
O	1260	7.9	1.17	AHMRUS
$\Delta$	1230	7.8	1.16	AHMRUS
O	1230	7.8	1.19	AHMR

Figure 180 - Static Pressure Distribution Runs 205, 215, 206

**CONFIDENTIAL**

**CONFIDENTIAL**

layers, to result in ignition.

The term "auto-ignition" means that the static temperature of the fuel and air streams are sufficiently high so that the combustion reaction begins spontaneously shortly after the streams begin to mix.

The distance required for auto-ignition to occur at given conditions of temperature, pressure and velocity is approximately calculable. The ignition lag curve of Figure 181 is derived from the empirical correlation of shock tube data by Schott and Kinsey (Reference 31 ). Similar predictions can be obtained by calculation of chemical kinetics.

At the flight Mach 6 enthalpy level, the air stream entering the test combustors had a static temperature of about 1300°R. Figure 181 shows that this temperature is too low for auto-ignition to occur. Cross-stream injection of the fuel was expected to raise the static temperature at the leading edge of the jet; but this region is small and could not be relied upon to provide ignition. The step in the step burner was expected to allow ignition of the burner by providing a low velocity, hence high temperature, region in which a fuel-air mixture could be retained for a sufficient length of time for auto-ignition to occur.

When neither of these ignition mechanisms succeeded in lighting the burner at M = 6 conditions, a test program was initiated to investigate a number of different ignition schemes. Following is a list of the successful and unsuccessful techniques investigated.

#### Successful

1. High fuel flow
2. High back pressure
3. Cold gas injection in step
4. Cold gas injection at exit
5. An explosive charge in step
6. Staged fuel injection

#### Unsuccessful

1. Spark Plug in step
2. Hydrogen torch igniter in step

### 2) Successful Igniter Tests

#### a) High Fuel Flow

In Figure 182 the results of a successful ignition test at Mach 6 flight conditions are presented. In this test, the M = 2.7 arc tunnel nozzle - A was used along with the normal long row injector (G). As the fuel flow or equivalence ratio was increased, the (G) injector produced greater blockage of the main air stream producing auto ignition of the H<sub>2</sub> air mixture. Auto ignition occurred at ER = 1.97.

**CONFIDENTIAL**

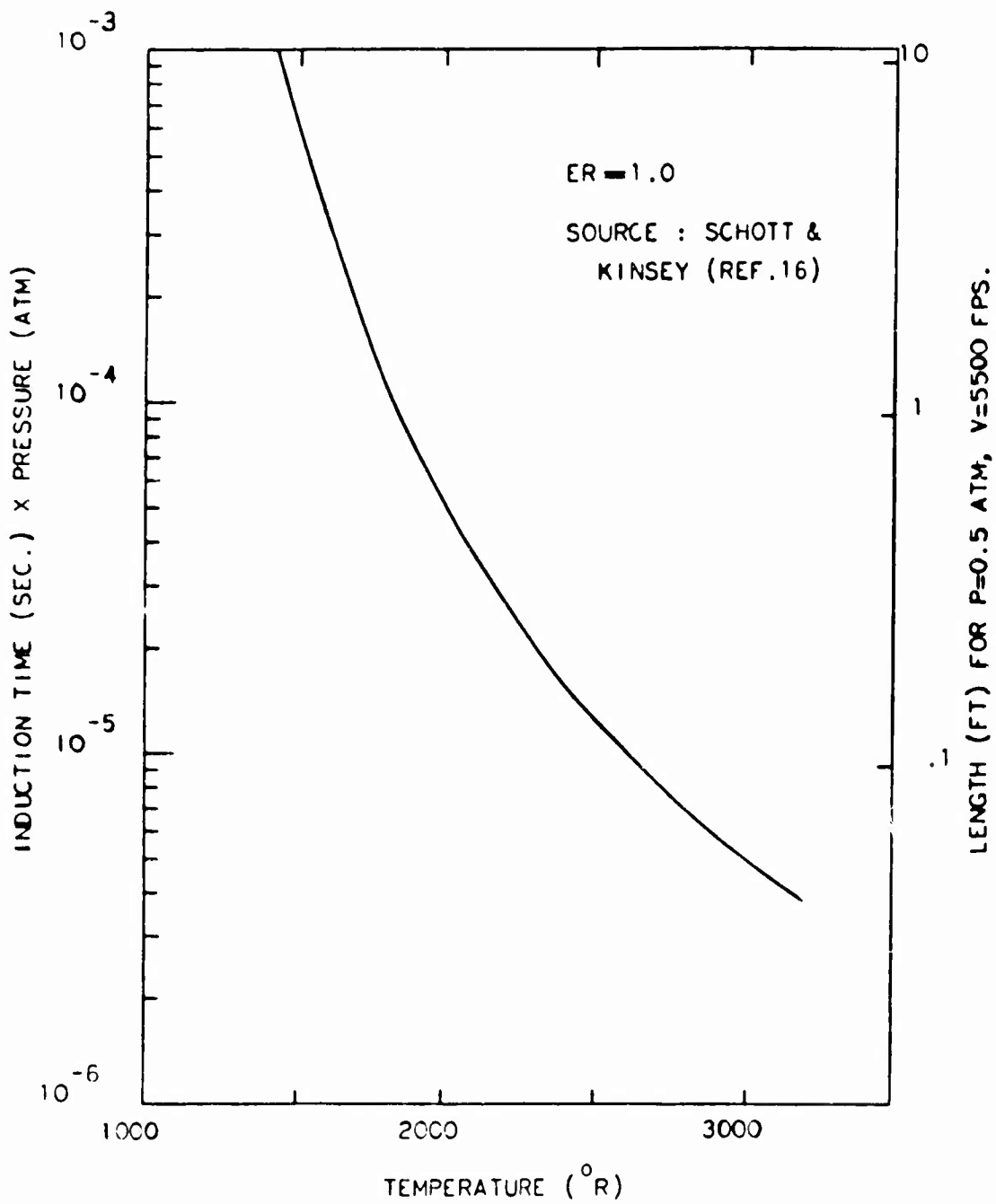
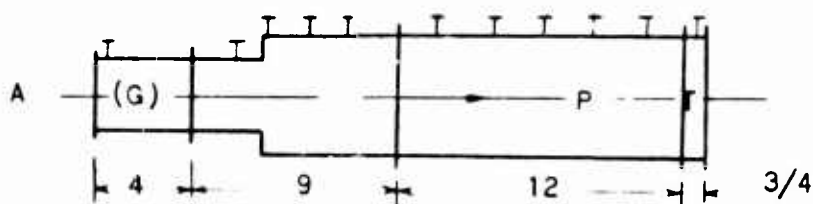
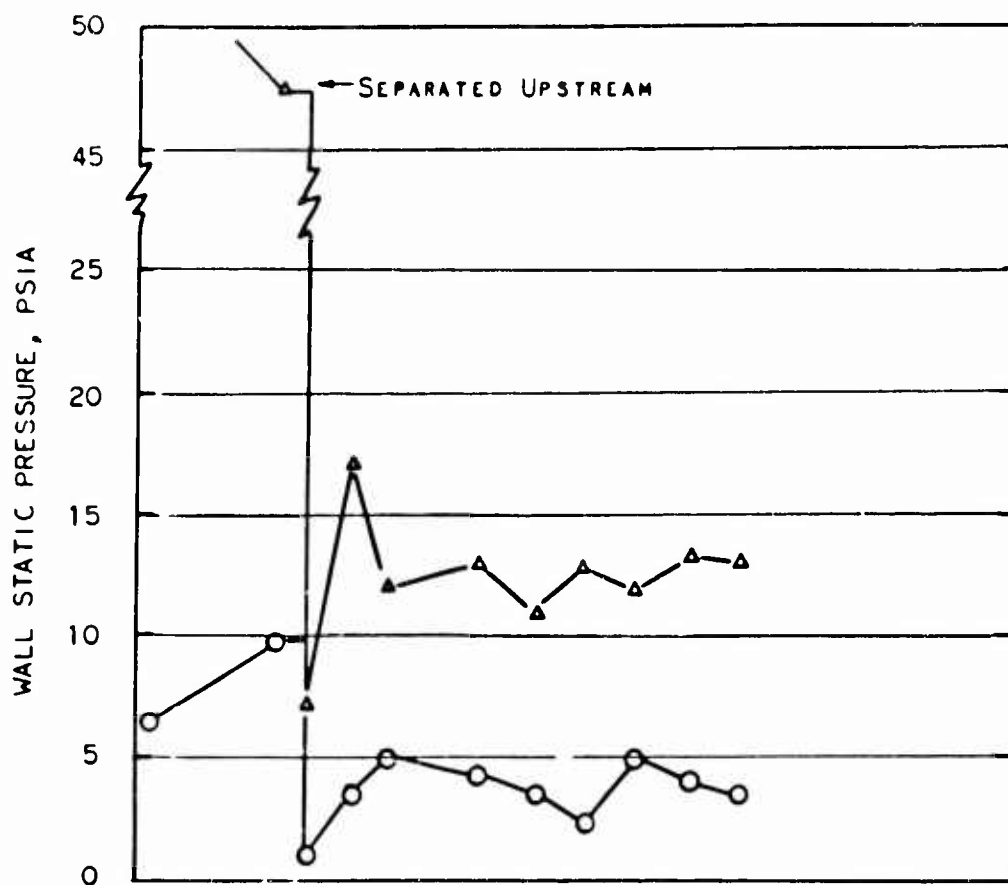
**CONFIDENTIAL**

Figure 181 - Predicted Ignition Delay for Hydrogen-Air

**CONFIDENTIAL**

**CONFIDENTIAL**

SYMBOL	$H_{T2}$	$M_p$	ER
○	744	5.9	.4
△	744	5.9	1.97

Figure 182 - High Fuel Flow Ignition

**CONFIDENTIAL**

**CONFIDENTIAL****b) High Back Pressure**

Previous to the ignition tests reported in this study, ignition at Mach 6 flight conditions had been achieved only by increasing the facility back pressure. This high back pressure resulted in boundary layer separations in the combustor and high pressure subsonic regions for ignition in the wake of the separations. A test was conducted to evaluate ignition in the wake of the separations. A test was conducted to evaluate ignition by increasing back pressure at low equivalence ratios. Figure 183 indicates the results of this test where ignition occurred at  $ER = .363$ .

**c) Cold Gas Injection in Step**

A jet of high pressure cold air was injected through an injector port that was downstream of the step at Mach 6 flight conditions. The results of the cold gas injection are presented in Figure 184 for a number of different burner and injector configurations. It can be seen from Figure 184 that using the upstream injectors (H) or (G) the cold gas injection produced separation of the approach airstream. In a flight vehicle such a separation would unstart the engine inlet. By using an injector positioned downstream of the step the cold gas injection produced ignition in the burner without causing separation upstream of the step.

This ignition technique accomplishes ignition by increasing local static pressures and temperatures by locally blocking a large portion of the available flow area, and by creating shock waves that propagate across the stream.

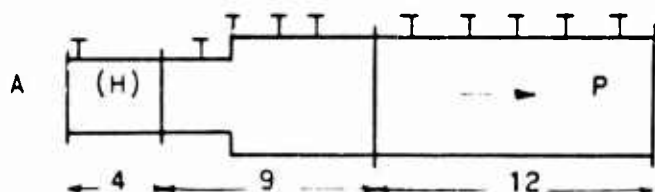
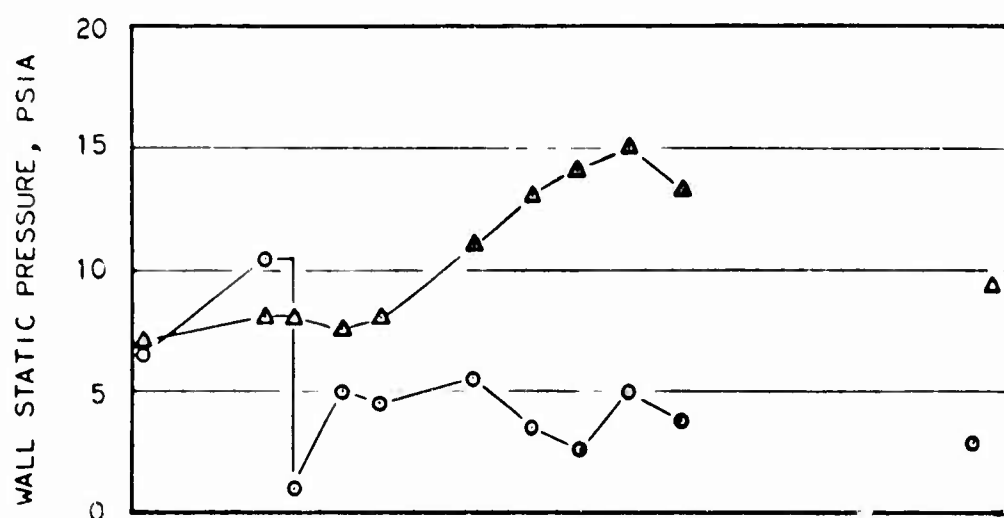
**d) Cold Gas Injection at Burner Exit**

Injection of a large volume of high pressure cold gas at the exit plane of a burner successfully produced ignition in the burner. In this case the fuel injectors were upstream of the step but the burner approach flow was not separated. The effects of the gas injection at the exit on pressure distribution are shown in Figure 185. The effects of cold gas injection on the burner are similar to the effects of high back pressure, as seen from the similarities of the pressure traces of Figures 185 and 183.

**e) An Explosive Charge in Step**

A .38 caliber blank cartridge with a 10 grain smokeless powder charge, was fired into the step region and resulted in ignition of an  $H_2$  air mixture at Mach 6 flight conditions. In Figure 186 the results of two tests using the .38 cartridge are presented. The results show that using the upstream injector (H), the .38 cartridge caused upstream separation, but using the downstream injectors (E) the .38 cartridge did not cause upstream separation. This result of upstream separation using upstream injectors is similar to the results of using cold gas injection in the step region in conjunction with upstream

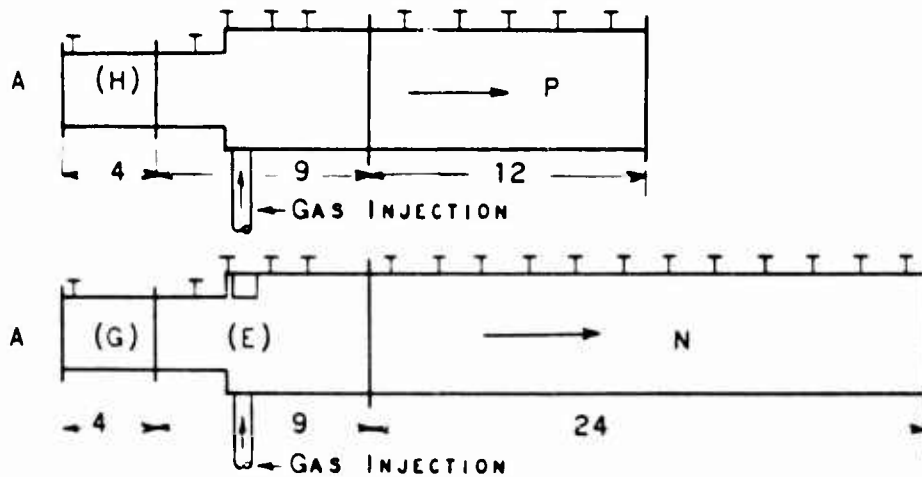
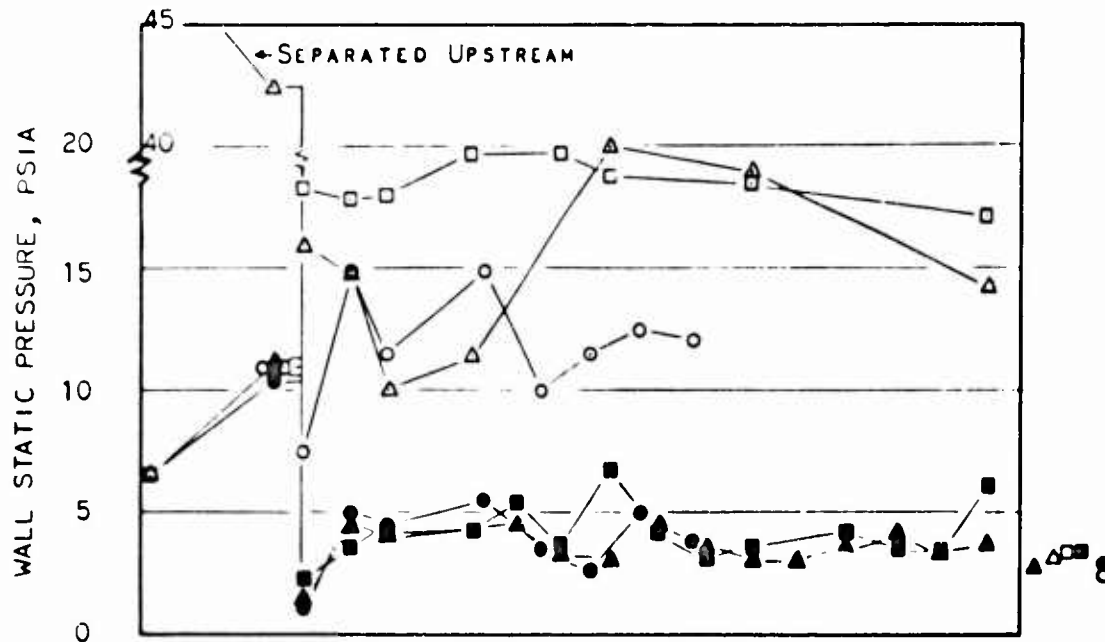
**CONFIDENTIAL**

**CONFIDENTIAL**

SYMBOL	$M_{12}$	$M_P$	ER
o	698	5.69	.72
Δ	753	5.93	.36

Figure 183 - High Back Pressure Ignition

**CONFIDENTIAL**

**CONFIDENTIAL**

SYMBOL	$M_{T2}$	$M_P$	$ER_{(H)}$	$ER_{(E)}^*$	$ER_{(G)}$
●	698	5.69	.72		
○	732	5.84	.77		AFTER INJECTION
■	751	5.92		.5	
□	742	5.89		.5	AFTER INJECTION
▲	742	5.89			.6
△	765	5.99			.54 - AFTER INJECTION

(\* ONLY 2 OF THE 4 (E) INJECTORS OPERATING)

Figure 184 - Cold Gas Injection In Step

**CONFIDENTIAL**

**CONFIDENTIAL**

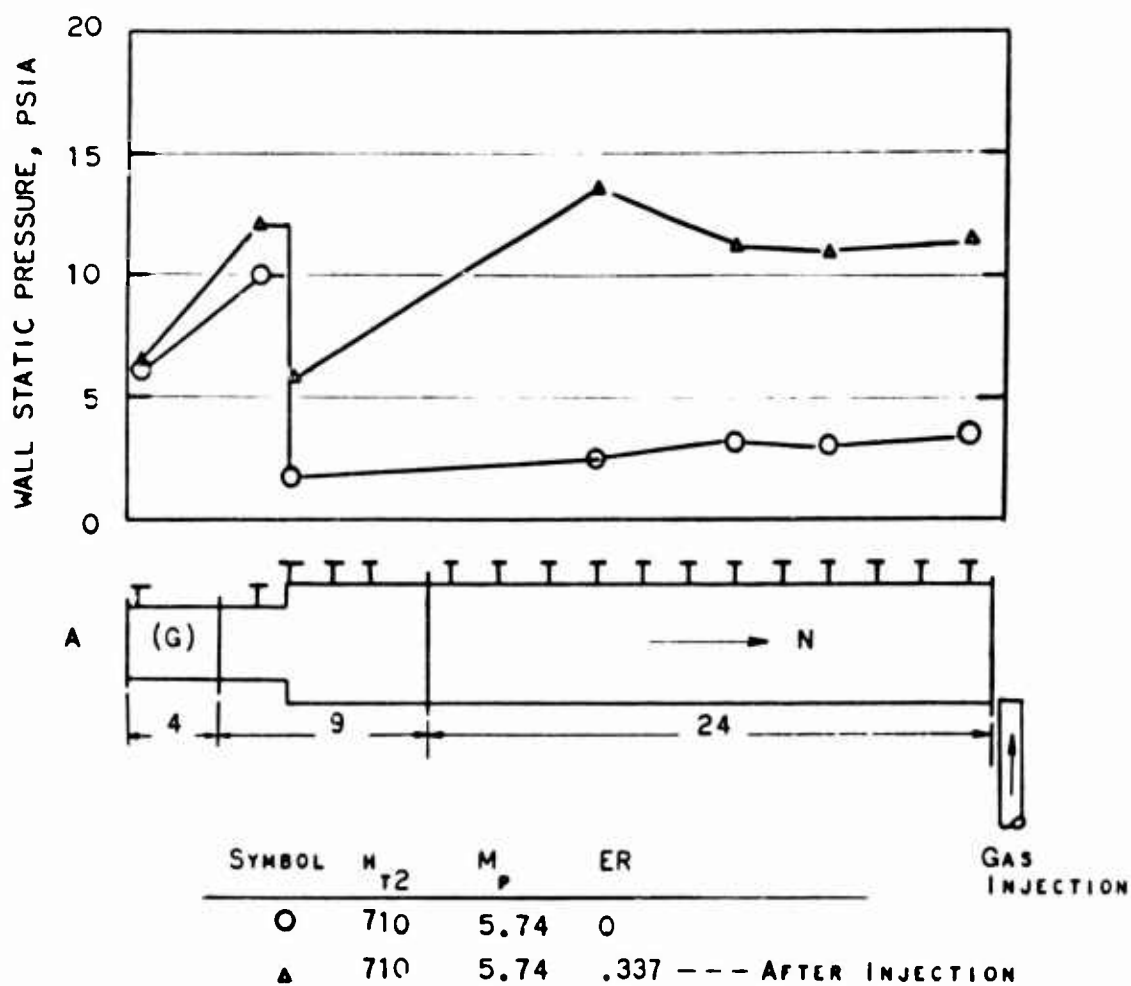
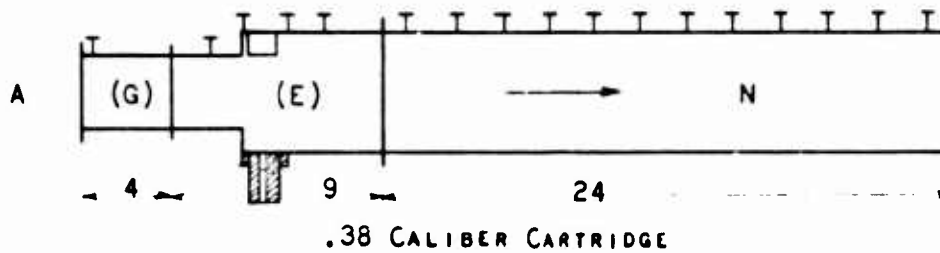
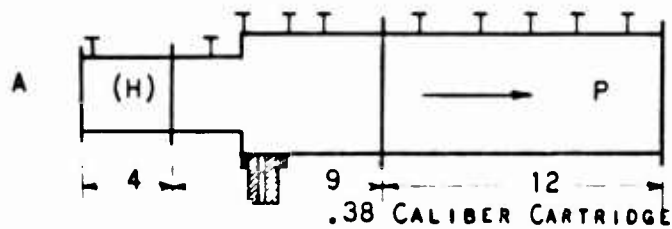
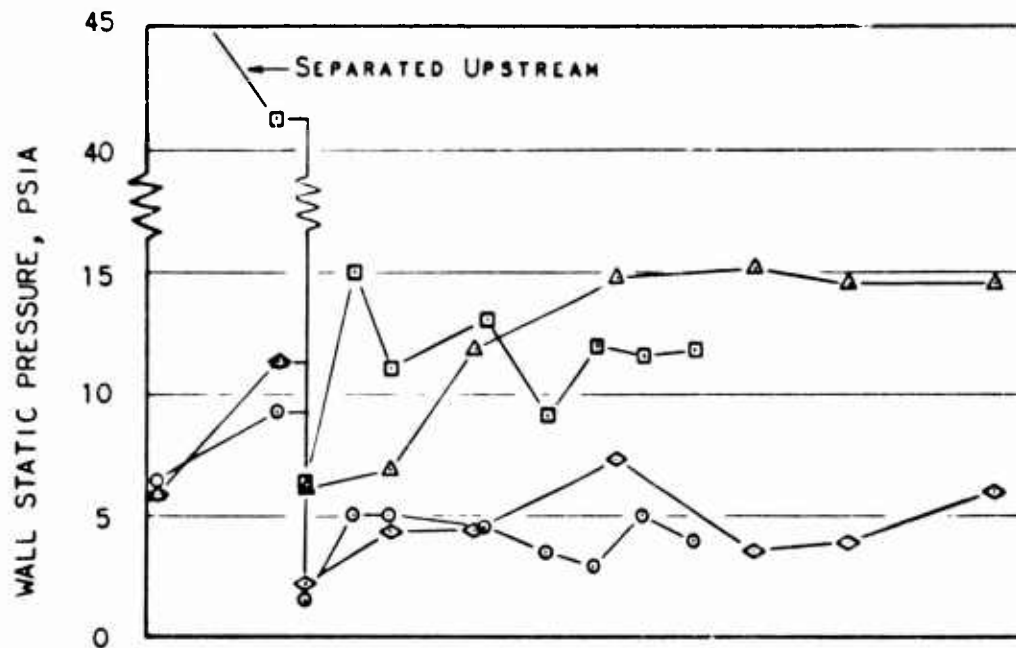


Figure 185 - Cold Gas Injection At Exit

**CONFIDENTIAL**

**CONFIDENTIAL**

SYMBOL	$M_{T2}$	$M_P$	$ER_{(H)}$	$ER^*_{(E)}$	
750		5.92	.75		
765		6.0	.76		AFTER FIRING .38
743		5.89		.5	
744		5.9		.5	AFTER FIRING .38
(* ONLY 2 OF THE 4 (E) INJECTOR OPERATING)					

Figure 183 - Explosive Charge In Step

**CONFIDENTIAL**

**CONFIDENTIAL**

injectors shown in Figure 184.

i) Staged Fuel Injection

Injection of fuel from injectors downstream of the step at the same time that a small amount of fuel is injected from injectors upstream of the step satisfactorily produced ignition at Mach 6 flight conditions. The results of a test using the (G) upstream injector and the (E) injectors downstream of the step are shown in Figure 187. The flow disturbance due to the (E) injectors ignited the mixture from the upstream (G) injector.

3) The Recommended Igniter System

The two stages of fuel injectors provided for performance also provide a satisfactory ignition technique. It was established in these component tests that although a single fuel injector system would not auto ignite at the burner inlet at  $M = 6$  conditions, a penetrating jet would initiate combustion in a stream which was already carbureted from an upstream injector. With an equivalence ratio between 0.1 and 0.5 from the upstream injectors, the downstream injectors should auto ignite. It is recommended that this technique be adopted for the 6-12 vehicle. If any difficulties occur in lighting the engine, a flare or explosive charge, such as used in component tests, could be incorporated into the design.

3. Combustor Design Considerations

a. Description of the Problem

The function of the combustor is to accept a stream of air from the engine's induction system and a stream of hydrogen from the structural cooling system, to mix and chemically react these streams in the most efficient manner possible, and to discharge the resulting stream of combustion products to the exhaust system in a condition to provide maximum thrust.

The engine induction system delivers air to the combustor through six nearly circular ducts spaced about the periphery of the engine. Each duct is approximately 4.45 inches in diameter. The properties of the air stream vary with flight speed, as shown in Figure 188. The air stream is very non-uniform, having thick boundary layers developed on the long compression surfaces of the inlet. The properties shown are those of a true one-dimensional equivalent of the air stream, defined as a uniform stream having the same stagnation enthalpy, mass flow, total momentum and area as the actual stream. This equivalent stream is used by one-dimensional cycle analysis computer programs to calculate the correct thrust produced by the engine.

To properly perform its function, the combustor must not alter the properties of the air stream delivered to it by the induction system.

**CONFIDENTIAL**

L

**CONFIDENTIAL**

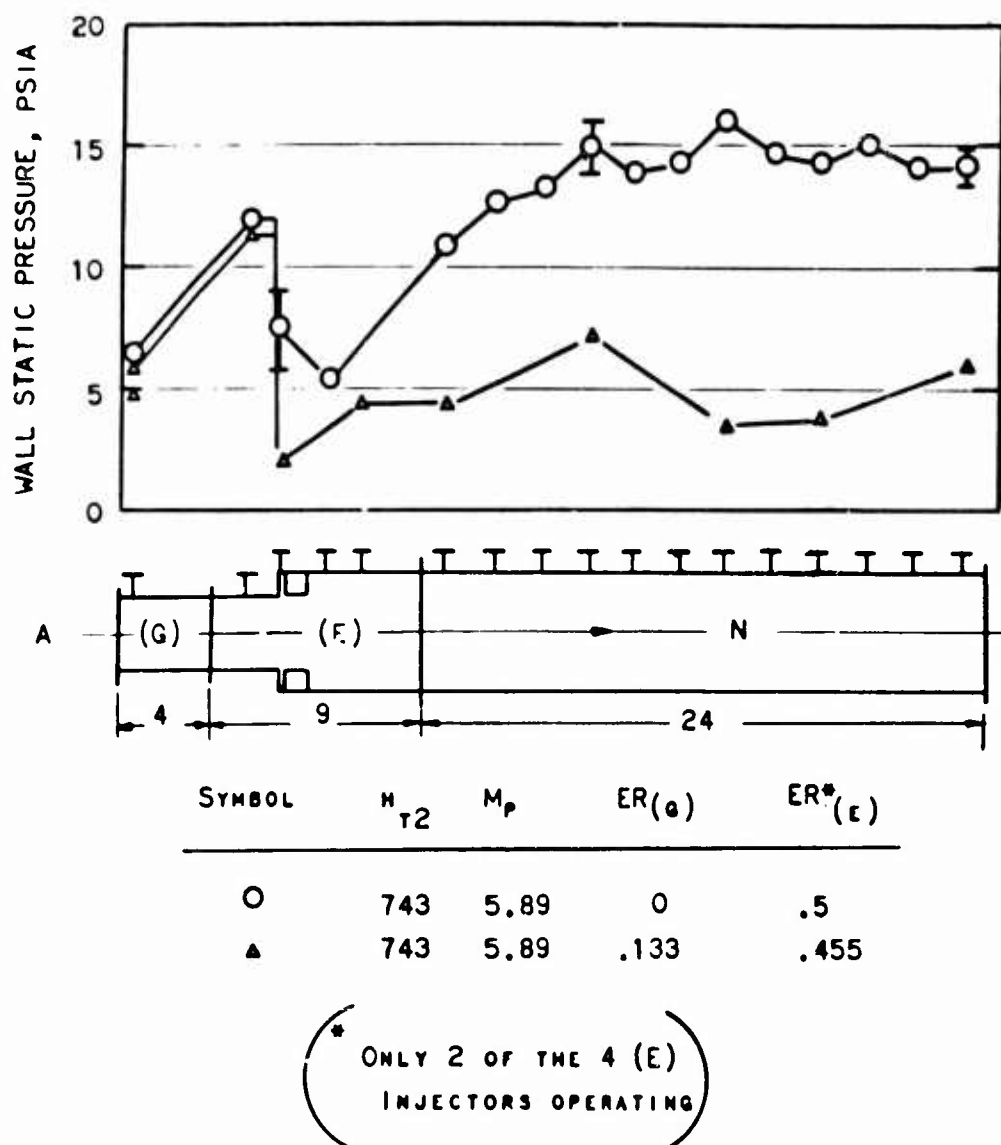


Figure 187 - Staged Fuel Ignition

**CONFIDENTIAL**

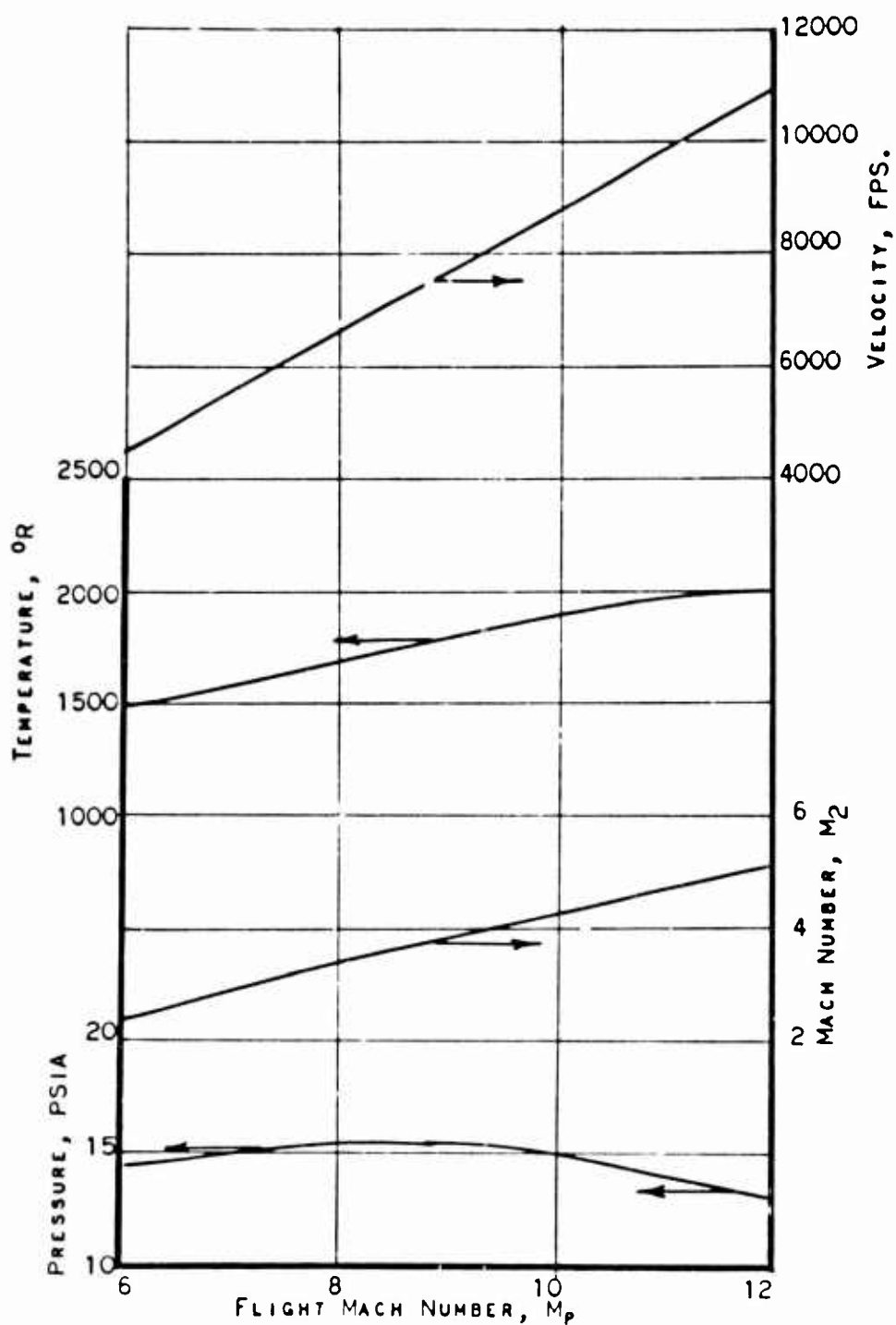
**CONFIDENTIAL**

Figure 188 - Burner Inlet Conditions

**CONFIDENTIAL**

**CONFIDENTIAL**

The mass flow and temperature of the hydrogen supplied to the combustor are dependent upon the demands of both the combustor and the structural cooling system. The functions of the combustor are most easily performed when the fuel temperature is high. Structural containment considerations limit the maximum fuel temperature to about 2000°R. At low flight speeds, the flow demanded by the combustor to produce adequate engine thrust is greater than can be heated to 2000°R by the cooling system, and a lesser temperature must be accepted. At high flight speeds, the cooling system must supply more fuel than is needed by the combustor in order to limit fuel temperature to 2000°R.

The variation of hydrogen flow and temperature with flight speed is shown in Figure 189. The fuel flow is expressed as equivalence ratio, defined as the fuel flow divided by the exact flow required to react with all the oxygen in the air stream.

The combustor must accept the hydrogen at the lowest pressure possible. Pumping hydrogen at high pressure requires much auxiliary power, and the pressure loss through the structural cooling system is great.

The efficiency with which the processes of mixing and reaction are accomplished within the combustor depends not only upon the degree of completion of the processes attained, but also upon the drag forces exerted upon the flow in accomplishing the processes. Minimizing drag forces requires that the combustor be as short as possible, with a minimum of structure immersed in the stream. The combustor length must, however, be sufficient to allow space for fuel tankage within the flight vehicle.

The combustor discharge is a single, circular duct, located concentrically within the engine. The entrance to the exhaust nozzle is adjustable to fit the combustor discharge. The nozzle provides no additional geometric constriction to the flow.

To produce maximum thrust when expanded through the exhaust nozzle, the combustor discharge stream must be as uniform as possible, and must have the smallest possible fraction of its total energy in the form of latent chemical energy. Chemical reactions left to be accomplished in the exhaust nozzle must be minimized.

#### b. Combustor Modes

##### 1) Supersonic Combustion

Supersonic combustion, as defined herein, is a process in which air enters a duct at supersonic velocity, fuel is injected into, mixes and reacts with the air stream in such a manner that the flow within the duct remains effectively supersonic, and the products of combustion depart from

**CONFIDENTIAL**

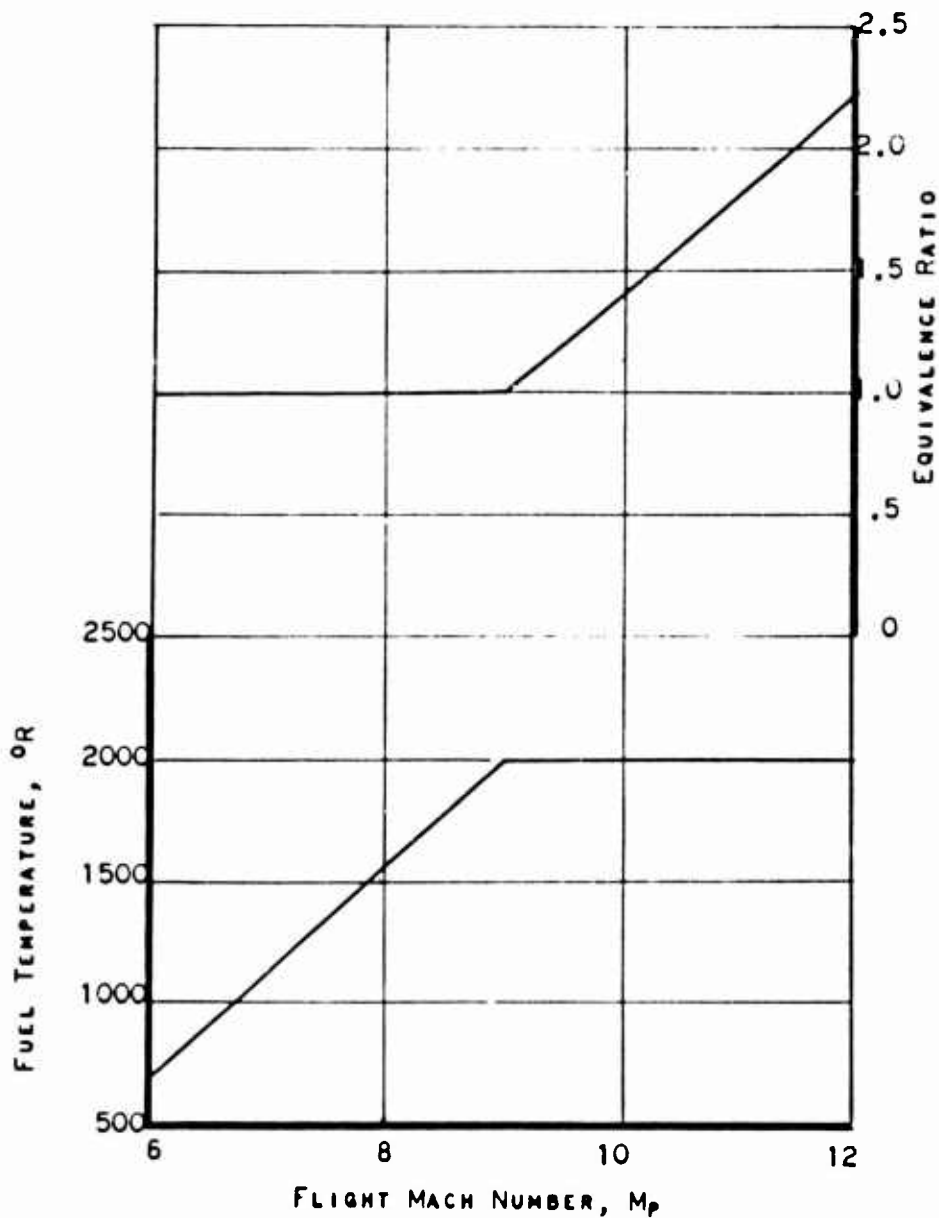
**CONFIDENTIAL**

Figure 189 - Fuel Conditions

**CONFIDENTIAL**

**CONFIDENTIAL**

the duct at principally supersonic velocity. The flow within the duct may have significant regions of subsonic flow without violating this definition. These regions are normally found in the shear layers adjacent to the duct walls, in wake regions aft of struts or wall steps, and in regions of separated flow in the vicinity of fuel injection points. Much of the energy conversion (burning) may occur in subsonic regions. As long as the properly integrated total momentum of the entire stream is greater than the minimum required to pass the flow, the flow is considered effectively supersonic, and the process of supersonic combustion exists.

The definition of a flow as being effectively supersonic or effectively choked, based on its total momentum, was discussed at length in a previous section entitled "Arc Tunnel Combustor Tests; Summary of Performance Measurements". It was shown that a uniform (one-dimensional) flow having a given mass flow, total energy and area required, by continuity, a total momentum not less than a minimum value. A stream having the minimum total momentum was termed "choked", and its velocity was sonic. Streams having greater than minimum total momentum were unchoked, and were either subsonic or supersonic. It was also shown that the minimum total momentum for a non-uniform stream could differ from that of a uniform stream having the same mass flow, area and total energy.

A stream having greater than the minimum total momentum will be either subsonic or supersonic, depending on the subsequent processes to be negotiated by the stream. Generally the stream can be subsonic only if the flow is choked at some location downstream from the point of consideration, or if the flow discharges to a high-pressure environment. If the flow discharges unchoked to a low-pressure environment, as is the case with supersonic ramjet combustors, the flow naturally seeks the lower-pressure supersonic condition.

A ramjet flight Mach number increases, the static temperature in subsonic combustors increases beyond the point where heat can be released by burning hydrogen and air. At high temperatures, the hydrogen does not burn completely to water, but reacts with air to form dissociated species such as H, OH and O. The large amount of chemical energy normally converted to sensible energy by hydrogen combustion is realized only when all of the hydrogen is converted to water.

Figure 168 is a plot showing the percent of the heating value of the fuel that can be converted to sensible heat by stoichiometric combustion to equilibrium conditions. At ten atmospheres pressure, 50% of the heat is released at 5900°R which is the combustor exit total temperature at  $M = 8$  flight conditions. At 6500°R, no heat is released; however, an enthalpy equal to the heating value of the fuel is converted to the chemical energy of dissociation of the exhaust

**CONFIDENTIAL**

**CONFIDENTIAL**

products. At higher static temperature, instead of releasing heat, the injected hydrogen will actually absorb heat from the air by dissociating into atomic hydrogen.

From this viewpoint, subsonic burners operating at very high inlet static temperatures are, therefore, no burners at all. Part or all of the chemical heat release occurs in the exhaust nozzle as the static temperature drops due to expansion. The subsonic section provides only mixing of fuel and air. In exhaust nozzles, the rate of expansion may be too fast to provide adequate reaction time at the static temperature conditions where recombination can occur.

Engine performance may be improved at higher Mach flight conditions if the inlet does not compress to subsonic conditions before combustion. This technique provides the following advantages:

- (1) The total pressure loss in the engine inlet is reduced.
- (2) The supersonic combustor can be designed to complete the combustion reactions by providing adequate length and reaction time at static temperature conditions at which combustion can take place.
- (3) The lower combustor pressures typical in supersonic combustors permit operation at lower altitudes before structural pressure limits and heat transfer limits are exceeded. Thus, at the static temperatures where burning occurs (supersonic Mach numbers), higher static pressures can be provided in a SCRAMJET combustor than is provided by the process noted in the preceding paragraph where heat release occurs in the exhaust nozzle. The increase in static pressure level results in greatly accelerated combustion rates.

For maximum engine performance, the combustion process should occur at the minimum velocity consistent with the other requirements of the system. If the combustor exit area is too large in comparison with the entrance area, the flow will tend to accelerate during the combustion process, and the combustion entropy rise will be unnecessarily high. For this reason, the combustor area ratio should be maintained at the minimum value for which the exit static temperature is consistent with acceptable dissociation levels.

Another reason for limiting the area ratio of the supersonic combustor is the desirability of maintaining steep pressure gradients in the mixing region. It is known that steep gradients have a strongly beneficial

**CONFIDENTIAL**

**CONFIDENTIAL**

effect on the process of mixing fuel with air. Pressure gradients are maximized by constricting the flow during combustion. The compression shock waves creating the pressure gradients induce no losses in the system if caused only by the various combustion processes.

Supersonic combustion is useful only at high flight speeds, where the combustor inlet stagnation enthalpy and Mach number are sufficiently high to prevent thermal choking in the combustor. At lower flight speeds, (Mach 6-8), thermal choking due to combustion occurs at usefully high equivalence ratios. This thermal choking, if not properly controlled, can cause the airflow to "back up" in the combustor until the excess spills from the induction system. If properly controlled, thermal choking can be used to improve combustor performance, as discussed in the next section.

## 2) Transonic Combustion

Transonic combustion as defined herein, is a process wherein air enters a duct at supersonic velocity and fuel is injected into, mixes and reacts with the air stream in such a manner that the stream becomes choked at one or more axial locations within the combustor. The flow at the choked location is in general, highly heterogeneous, but behaves as would a uniform stream at sonic velocity. The flow at the burner exit is either choked or effectively supersonic.

Transonic combustion occurs at moderate flight speeds (Mach 6-8), where the combustion heat release is significantly large compared to the total energy of the flow. Its occurrence depends to a lesser extent upon the Mach number of the burner entrance stream, although choking can occur with infinite inlet Mach number if the inlet total energy is sufficiently low.

Thermal choking, if properly controlled, can be strongly beneficial to the performance of the combustor. Control of the transonic combustor generally requires diverging walls, either in the combustor itself, or in the engine's induction system, downstream of the point of maximum contraction. When thermal choking occurs at a point in a duct, further increase in the sensible energy of the flow requires that the total momentum of the flow increase in order to maintain flow past the choked point. The flow "piles up" ahead of the choked point, the boundary layers separate and increase the pressure of the core flow.\* If a rearward-facing wall surface has been provided ahead of the

---

\* This increase in pressure is not to be mistaken for the type of compression which takes place in the engine inlet, where increase in pressure is accompanied by a decrease in stream-flow total momentum. While the increase in momentum in the combustor does provide higher engine performance by providing higher wall forces, this increase in performance is not related to the increase in performance which results from a pressure rise due to increased inlet contraction ratio.

**CONFIDENTIAL**

**CONFIDENTIAL**

choked point, the increased pressure reacts with this surface to provide the required increase in total momentum. If sufficient divergence is provided, the choked flow can be sustained throughout a wide range of sensible energy. The separated regions vary in pressure and extent to supply the demand for total momentum.

Excessive choking of the transonic combustor is detrimental to the performance of the engine. Excessive choking results from excessive heat release in the choked combustor creating a demand for more total momentum than can be supplied by the diverging walls provided. When this occurs, the separations advance forward of the point of minimum area. Since the increased pressure reacting with forward-facing surfaces produces a reduction of total momentum the separations advance unchecked along the compression surfaces of the inlet until the excess mass flow is spilled overboard. It is thus essential that sufficient internal divergence be provided to contain the separations within the combustor, with the desired amount of heat release.

The separations and shock waves preceding the choked point in a transonic combustor are not indicative of thrust losses in the system. The entropy rise incurred by these combustion-induced shocks is an integral part of the necessary entropy rise associated with heating of the high-velocity stream. This becomes obvious upon consideration of the process of one-dimensional simple heating of a perfect gas. In this process, known as Rayleigh line flow, the total temperature of the gas increases in a constant-area frictionless duct. The mass flow and total momentum of the gas remain constant.

The state of a one-dimensional perfect gas flow is determined by the generalized irreversible flow function derived in Appendix I:

$$N(\gamma, M) = \frac{RT_0}{\gamma g} \left( \frac{w}{F} \right)^2 \quad (62)$$

This function attains a maximum value at the sonic point:

$$N^* = N(\gamma, 1) \quad (63)$$

For Rayleigh line flow, with  $w$  and  $F$  constant,

$$\frac{N}{N^*} = \frac{T_0}{T_0^*} \quad (64)$$

**CONFIDENTIAL**

**CONFIDENTIAL**

Thus, for a given Mach number at the inlet to the duct, choking will result from a definite total temperature ratio.

Two approaches to the choked duct exit may be postulated, for a given supersonic entrance Mach number. The first is the fabled shock-free combustion, in which the Mach number decreases steadily with heat addition to unity. In the second, a normal shock is assumed to stand at the entrance, and the subsonic Mach number downstream from the shock increases steadily with heat addition to unity. In the normal shock process,  $T_0$ ,  $w$  and  $F$  all remain constant, so that the value of  $N$  does not change.  $N^*$  is a function of  $\gamma$  alone. Obviously, the same total temperature ratio is required to choke the flow after the normal shock as was required to choke the shock-free flow. Further, both choked flows have identical values of  $N^*$ , therefore, are at the same state. The entropy gains of both processes are equal. The entropy rise of the normal shock, added to the entropy rise of the subsequent subsonic heat addition, exactly equals the entropy rise of the supersonic heat addition process.

Transonic combustors, properly stabilized, have been tested and found to provide excellent performance. The separated flows and strong pressure gradients preceding the choked point have a powerfully beneficial effect on the mixing process. The use of transonic combustion, where possible, is highly desirable. The somewhat conflicting requirements of large burner area ratio for transonic combustion at moderate flight speeds and small area ratio for supersonic combustion at high flight speeds present a design problem.

### 3) Subsonic Combustion

Subsonic combustion is a process in which air enters a duct at subsonic velocity and fuel is injected, mixed and reacted at low speed. If the exhaust nozzle following the combustor is of the converging-diverging type, the burner exit stream is subsonic. If the exhaust nozzle only diverges, the burner exit stream is choked.

With a converging-diverging exhaust nozzle, the subsonic combustor shows good advantage at low flight speed, where burner temperatures cannot reach levels of excessive dissociation. The advantage arises from minimization of combustion entropy rise at the low combustion velocities. When the burner exit is choked, much of this advantage is lost.

The transonic combustor may become a subsonic combustor if the separations preceding the choke point are stabilized sufficiently ahead of the point of fuel injection. While some improvement in wall pressure may be gained by this means, much of the mixing benefit of the transonic combustion is lost. The principle mixing-promoting pressure gradients occur ahead of the fuel injector, where there is no fuel to mix.

**CONFIDENTIAL**

**CONFIDENTIAL****c. Combustor Features****1) Area Ratio**

The area ratio of a SCRAMJET combustor is optimized, when the burning is initiated at the smallest permissible flow area consistent with engine inlet unstarting, and when the subsequent divergence achieves substantial recombination of the dissociated products of combustion, while minimizing the high friction losses associated with the small burner inlet area.

Cycle calculations have been used to study the effects of burner area ratio on performance for many postulated vehicles. These results can be generalized to a considerable extent. For frictionless combustors with equilibrium nozzles, cycle calculations predict higher performance for constant area than for any diverging area combustor. Combustion at the highest temperature and pressure and at the lowest Mach number gives the best performance.

Diverging area combustors are adopted in spite of the cycle advantage of constant area, to avoid inlet unstarting at low flight Mach numbers and because of chemical kinetic considerations of nozzle freezing. At flight  $M = 6$  conditions, constant area passages with stoichiometric burning cannot pass the flow and the inlet unstarts.

One-dimensional calculations show that for stoichiometric combustion the engine inlet unstarts, the flow in the inlet passages goes subsonic, and the inlet spills more than the design spill flow. It has been shown (see discussion of Figure 157) that under some conditions a two-part or two-dimensional flow can pass through a slightly smaller flow area, than the equivalent mixed one-dimensional flow. However, because the pressure rise due to combustion will encourage considerable mixing of the flow, it is appropriate to treat the one-dimensional calculation as an effective limit.

Even at lower fuel flow conditions or at higher flight Mach number conditions, where one-dimensional mass flow continuity is not violated, the inlet may still unstart. Boundary layer separations propagating upstream from the high static pressures generated by the combustion can unstart an inlet. This limit may be more severe for engines where the fuel is injected close to the minimum contraction area. For vehicles which inject the fuel far downstream of the minimum contraction area, as in the design vehicle, inlet data taken with any method of back pressuring should be adequate for determining the limits of unstart. Angle-of-attack further increases the tendency to unstart by creating pressure distributions and fuel/air distributions around the circumference that can locally initiate inlet unstarting.

**CONFIDENTIAL**

**CONFIDENTIAL**

At conditions where there is no risk of the combustion pressure rise unstarting the engine inlet, the combustion should be partly completed in a constant-area burner inlet section. Because of the high friction loss in the constant area section, divergence should begin before combustion is entirely complete.

In addition to the cycle prediction of high performance for constant area burning, the pressure rise generated in the constant area section can be a valuable aid for achieving good mixing of fuel and air. The wake mixing theory discussed in this report indicated a large increase in mixing rate due to a pressure rise just downstream of the injectors. As can be seen in Figure 56, a factor of two increase in the pressure decreased the lengths required for mixing by a factor of five, for the example of sonic fuel velocity in the arc tunnel.

Component tests at air enthalpies simulating  $M = 9 - 10$  flight, exhibited increased burning when the constant area section was made long enough. This increased burning is attributed to the increased mixing rate and also to the effects of higher static temperature and static pressure on ignition and combustion rates.

As the combustion exhaust gases expand into the exhaust nozzle, the static temperature of the gas drops. This permits those exhaust products which are dissociated at these high temperatures, to partly recombine. In general, exhaust nozzle expansions are at too rapid a rate for the dissociated species in the combustion exhaust to recombine as the temperature in the nozzle drops. By providing a gradual expansion in the early part of the expansion, most of the dissociated species can be recombined. In the work on this contract this gradual early expansion has been treated as a combustor function. The exhaust nozzle is handled as a frozen expansion in cycle calculations. With this cycle assumption the optimum combustor is one with diverging area. The rate of area divergence near the downstream end of the combustor is selected from chemical kinetic calculations to give the best possible recombination.

Contracting area combustors have not been given significant consideration. A contracting area combustor involves a design with an increased risk of unstarting the inlet. Frequently such a design could be improved simply by doing more contraction in the inlet before beginning the combustion.

**CONFIDENTIAL**

**CONFIDENTIAL****2) Burner Length****a) Friction Loss**

Short combustors are desirable for minimizing heat transfer, friction loss and engine length and weight. The combustor length is determined by the requirements to achieve mixing of fuel and air and to complete the burning process. However, in supersonic combustors the friction loss and heat transfer can be so great as to result in significant compromises with mixing and combustion requirements.

Identification of optimum compromises are accomplished with the aid of cycle calculations and appropriate treatment of component data. For vehicle design studies, the friction loss and heat transfer effects are accounted for in the cycle calculations. In comparative evaluations of combustors in component tests, the friction loss is included in the over-all EtaNT performance parameter. Combustors with high friction loss have a lower EtaNT or thrust potential.

The flow cross section shape of the combustor is one significant variable affecting friction loss. For the same length of combustor, an annular combustor passage has more friction loss than a burner of circular cross section. However, insofar as the burners are mixing limited rather than reaction limited, an annular combustor can be shorter. Several circular burners have more friction loss than a single burner with circular cross section having the same length, but again mixing limited combustors can be made shorter in smaller diameters.

**b) Mixing**

Extensive effort has gone into the study of mixing of fuel and air in supersonic flows, and reasonable mixing has been demonstrated in General Electric component tests, documented with freestream gas samples. Mixing theory is inadequate to treat all aspects of the mixing problem. Most of the theories in the literature treat a single mixing mechanism and are confined to constant pressure fields. An approach based on a single shear mechanism was identified under previous contracts, and a machine program was written for handling certain problems. The approach treats cocurrent flow, density difference and combustion. Static pressure fields are treated independent of the machine program as an effect on the velocity field and resulting velocity shear gradients. Either axisymmetric or two-dimensional problems can be solved, but the method does not treat overlapping mixing fields or mixing fields affected by the presence of a wall. The findings of the penetration study in this report, permits the flow field after injection to be defined. By approximating the penetrated jets as a two-dimensional cocurrent flow, the problem can be reduced to simple wake equations which do not require machine program calculations.

**CONFIDENTIAL**

**CONFIDENTIAL**

Figure 61 presented previously, showed the mixing efficiency to be expected to a constant pressure field for a wall injector configuration.

Static pressure gradients generated by the combustion affected the mixing efficiencies by changing the momentum defect of the mixing wakes. These same penetration and mixing calculations can be applied to other configurations including configurations with fuel injection struts.

Perhaps the most useful approach for shortening mixing length is by utilization of the static pressure rise generated by the combustion. This static pressure rise increases the velocity difference between the low Mach number injected fuel and the supersonic airstream, thus increasing the mixing rate. By designing the burner divergence or the fuel staging to achieve the maximum pressure rise that can be maintained just downstream of the fuel injectors, high mixing rates should result. The wake mixing theory predicts that when the pressure rise is upstream of the fuel injection station the effect on mixing is eliminated. In this case, turbulence or mixing, is generated by the pressure rise due to its action on the wall boundary layer, an effect not included in the wake mixing analysis presented in this report. This effect on wall boundary layers was not examined analytically under the present contract.

Reduction in mixing length by utilization of a strong pressure rise also provides high static pressures and temperatures early in the burner that shorten the chemical kinetic requirements on burner length.

c) Chemical Kinetics

The chemical reactions of interest in a combustor are of two types: auto-ignition reactions and heat-releasing reactions.

The freestream static temperatures expected at the burner inlet at  $M = 6$  flight conditions are too low for auto-ignition to occur. However, once the fire is lit locally, the ignition can propagate by mixing as a turbulent diffusion flame. Also pressure rise near the burner inlet generated by the downstream combustion process, increases the static temperature at the inlet, in some cases resulting in auto-ignition temperatures. The basic problem of igniting the burner is discussed later.

The heat releasing reactions are not as sensitive to burner inlet temperature as the ignition reactions, but are very sensitive to pressure level. The combustor inlet pressures for most missions of interest are high enough to result in efficient combustion in short constant area lengths. These constant area combustors are mixing limited, not reaction limited.

**CONFIDENTIAL**

**CONFIDENTIAL**

However, the recombination of dissociated exhaust species which takes place in the upstream portion of the nozzle or in the final portion of a diverging combustor is limited by the pressure. The recombination reactions are the identical reactions that release heat in the combustion process and can be treated with the same calculations.

Machine programs for simultaneously solving the chemical kinetic equations are available. These calculations show that very high altitude flight missions are unsatisfactory, requiring excessively long combustion lengths. An abbreviated equation is used routinely by the General Electric Company in cycle calculations to prevent the selection of missions or configurations which are significantly limited in combustor efficiency. These same machine programs can be used for calculating the progress of reaction through the exhaust expansion. Abbreviated calculation programs, which identify the point in the nozzle where the reactions effectively freeze, are also available for estimating the recombination in a nozzle or diverging burner. Figure 190 is an example of freezing point calculations, these calculations used the rate constants that Lezberg (30) found to agree with experimental measurements in an exhaust nozzle. The curve represents the rate of expansion for which the freezing criteria is just met. Also shown on the figure is the expansion for a burner divergence equivalent to a  $1.67^\circ$  half angle cone. It is seen that the predicted kinetic freezing point occurs just at the end of this burner.

As the area ratio of the combustor is increased, the theoretical dissociation level decreases. At some point in the expansion (the freezing point) the pressure drops too low for the chemical species to recombine. This limit can be extended by increasing the length of the expansion region and by decreasing the rate of expansion. In general, the expansion rate in the exhaust nozzle is much faster than the burner divergence and the reactions are frozen in the exhaust nozzle expansion.

#### d) Vehicle Geometry Limitations

Frequently, combustor lengths are determined by mechanical features of the vehicle design. Examples are: the length of a structural strut; the length of a translating part; the length required to get from inlet annulus to centerburner; or the fuel tank length. Also once the combustor length or envelop for a vehicle design is established, further burner optimization is confined to other features of the burner. The combustor designer can optimize within a fixed length by diverging the combustor in the excess length, thus reducing friction loss and maximizing recombination, or by utilizing this length for mixing around the circumference, thus correcting any initial maldistribution of fuel and air. For very over-rich conditions, film cooling of the walls could conceivably be used in the region downstream of the

**CONFIDENTIAL**

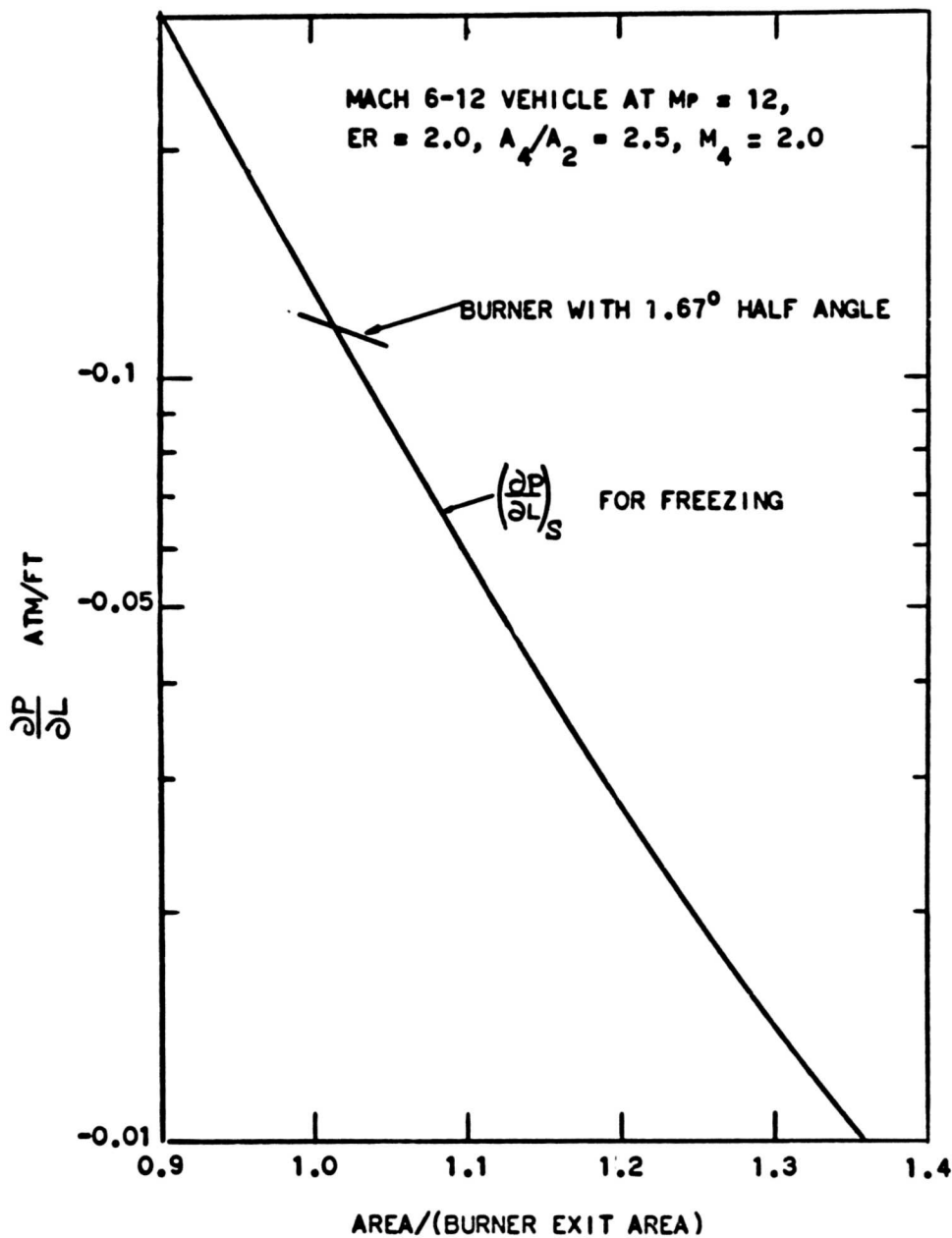
**CONFIDENTIAL**

Figure 190 - Freezing Point Calculations, (Rate of Change of  
 Pressure With Length for Freezing Near Burner Exit)

**CONFIDENTIAL**

**CONFIDENTIAL**

burner pressure rise to reduce skin friction loss and cooling loads.

The general shape of the burner, annular vs. circular was affected to some extent by arc tunnel testing considerations. It is desirable to select a final design very close to a configuration tested in the arc tunnel. The arc tunnel facility is particularly well suited for testing combustors with circular cross section. Testing a large annular burner in the arc tunnel would be more difficult. This arc tunnel consideration, therefore, contributed to the decision to design the burner for the 6-12 vehicle with a circular cross section rather than annular.

### 3) Fuel Injection

#### a) Struts and Wall Injectors

Fuel injection struts in a supersonic stream are objectionable for several reasons. They generate form drag losses as well as friction loss. They are difficult to cool and create severe structural problems. At the beginning of this contract, it was not known whether adequate mixing could be obtained without fuel injection struts. However, the aim of the program was to first investigate combustor designs that depended on injection from the walls of the combustor. Cold flow tests on penetration indicate that wall injectors can penetrate a substantial distance into the duct. Mixing theory predicts that these penetrated jets mix adequately, if sufficient length is available. Combustor tests verified the adequacy of mixing in long ducts. If much shorter L/D's were to be achieved, fuel injection struts would be investigated. This only seems desirable in very large ducts where mechanical problems may be minimized.

Combustors that are designed to mix across only the distance between struts will have significant  $f/a$  profiles at the burner exit, resulting from the initial air distribution at the burner inlet. Burners with wall injectors are designed to mix over greater radial distances, almost across the combustor. This tends to minimize problems associated with the initial radial air distribution. The 6-12 vehicle utilizes wall injectors. However, the six barrels approaching the centerburner are similar to a round duct with six radial struts. Fuel injection from the approach barrel walls is very similar to injection from struts and this principle is utilized in the design.

In addition to the advantageous placement of fuel by the use of struts, strut wakes provide a significant mixing mechanism. The end of the six barrels also provides this mechanism with much of the momentum defect in the approaching boundary layers contributing to the generation of mixing phenomena.

**CONFIDENTIAL**

**CONFIDENTIAL****b) Geometry**

Cold flow penetration tests indicated that some improvement in penetration over that obtained for a round hole could be obtained by making the hole have a low aspect ratio shape. Any geometry that provided low aspect ratio achieved this improved level; long-rows-of-holes as well as slots. Thus a mechanically convenient configuration can be selected. The low aspect ratio injectors can be made sonic; a shaped supersonic hole is not required for good penetration.

The injectors should be choked, but high pressure is not required for penetration. As indicated in the cold flow studies, the penetration is dependent on the mass flow per injector, but independent of the design pressure. This permits the fuel injectors to be designed to give minimum back pressure to the fuel system, thus minimizing pumping requirements.

Figure 191 is a fuel injector pressure schedule for a set of cycle conditions calculated for a 6-12 vehicle. The injector flow area was set to just choke the injectors at the  $M = 8$  condition assuming that the combustion process had increased the local freestream static pressure to twice the cycle value for the burner inlet. The pressures at other conditions were those required to pass the flows indicated in the cycles.

Figure 63 is a plot of penetration for a set of cycle conditions in the 6-12 vehicle. It is seen that the penetration remains relatively constant over the entire mission. This simplifies injector design. A single configuration provides suitable penetration at all conditions.

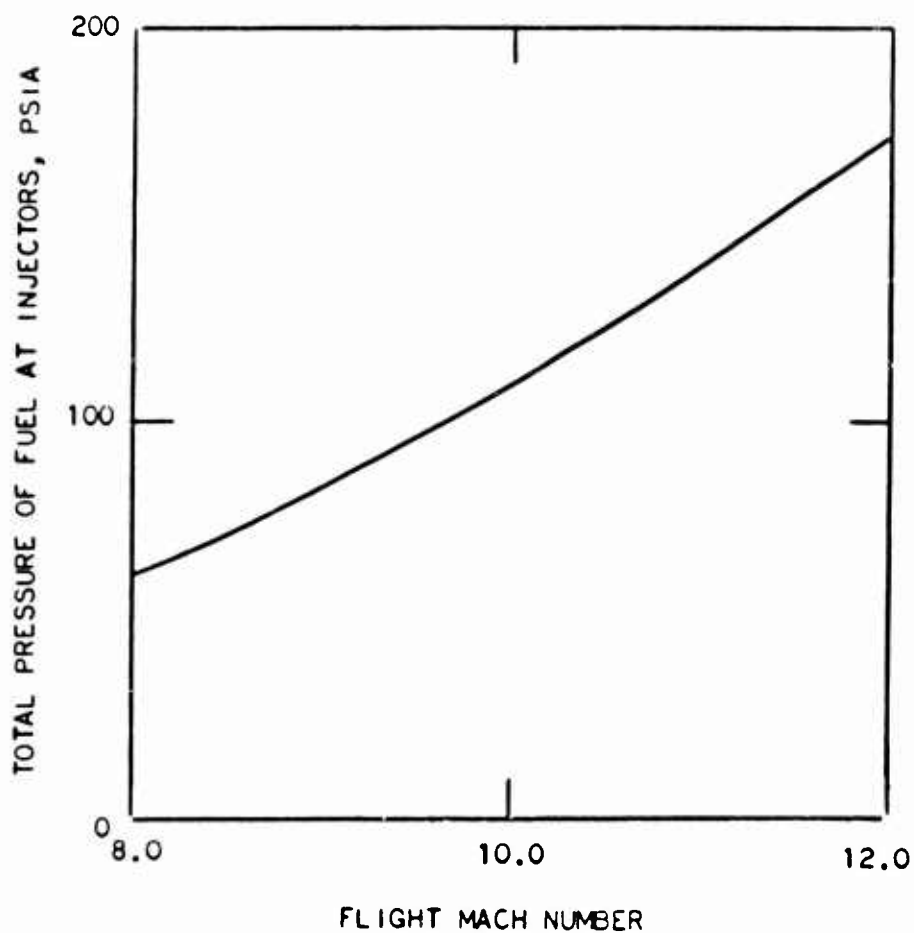
**c) Location**

The best performance will be achieved by burning at the lowest possible Mach number, or in the smallest possible flow area. This is limited by inlet unstating at low flight Mach numbers. Combustion in a diverging area combustor at  $M = 6$  and in a constant area combustor of  $M = 12$  can be accomplished by incorporating two sets of fuel injectors, one upstream of the other.

**d. The Recommended Combustor Design****1) Design Features**

In discussing Combustor Design Considerations, Task IID, in the mid-contract report for the previous SCRAMJET contract, written in December 1963, (Reference 8), it was stated that, "The available knowledge is too incomplete to design an operable SCRAM combustor at this time". Today both the experimental background and theoretical understanding of the

**CONFIDENTIAL**

**CONFIDENTIAL**CYCLE CONDITIONS

MP	ER	FUEL TEMP., °R
8	1.0	1555
10	1.41	2000
12	2.21	2000

Figure 191 - Maximum Fuel Injection Pressure  
(For Upstream Injectors)

**CONFIDENTIAL**

**CONFIDENTIAL**

phenomena are adequate for designing a flight combustor. Extensive experimental data are available simulating flight Mach numbers from 6-9. Experimental component tests simulating the  $M = 10$  to 12 range are lacking for performance estimates and experimental data at  $M = 9$  to 10 have indicated increasing difficulty with increasing Mach number, for diverging burners. However, some tests at  $M = 10$  to 10.5 have indicated encouraging results for burners with a constant area inlet section.

The objective of this contract was to identify a workable design rather than a completely optimized burner. This resulted in a conservative approach with effort directed at establishing good reliability for the recommended design with accurate performance estimates based on extensive test data. Close similarity to burners tested in the arc tunnel was incorporated in the recommended design.

a) Area Ratio

Figure 192 shows the burner contour in the 6-12 vehicle, a diverging area combustor with area ratio of 2.09. Although constant area gives high performance at conditions where it can be applied, at  $M = 6$  one-dimensional continuity is violated in constant area at a fuel equivalence ratio of one.

A smaller area ratio than 2.09 could have been selected without violating continuity; but the 2.09 area ratio limits the pressure rise at the burner inlet to a value that will not separate the approach boundary layer. A pressure limit of twice the approach stream static pressure was assumed to be satisfactory based on unpublished test results on inlet Model 28, together with observations from arc tunnel combustor tests. The pressure limit for  $M = 6$  operation was used to determine the burner area ratio. The average axial wall force was calculated by performing cycle calculations for Mach 6.0 flight conditions, assuming  $M = 1$  flow at the burner outlet. Although the burner area ratio was made small to optimize performance at  $M = 6$  conditions, the area ratio also provides significant recombination at the high flight Mach number conditions.

b) Divergence Rate

The burner begins in the six ducts that feed the central duct. The initial section of the burner is approximately constant area. This constant area permits the combustion to generate a significant pressure rise upstream of the diverging area region at the high flight Mach numbers, thus increasing the mixing and burning rates and resulting in high wall forces and high Mach numbers at the burner exit.

Sudden expansion exists where the six burner inlets come together into the central duct. This sudden expansion is in the burner not only for the mechanical simplicity of avoiding fairings in making this

**CONFIDENTIAL**

CONFIDENTIAL

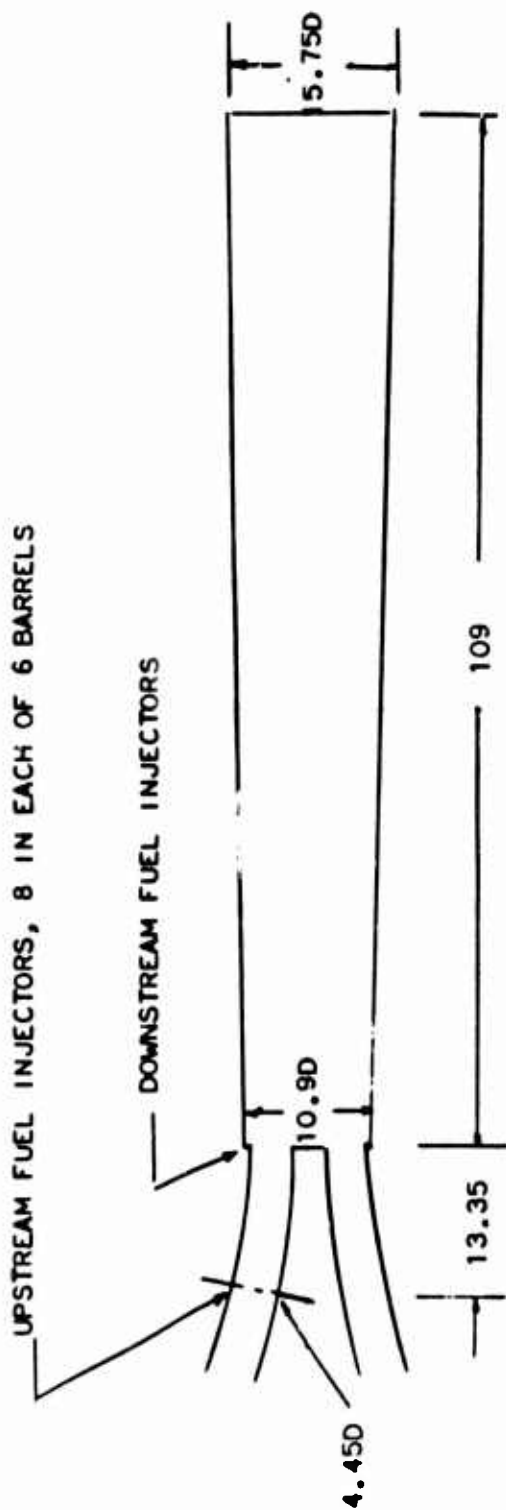


Figure 102 - Burner Contour (Mach 6-12 Vehicle)

CONFIDENTIAL

**CONFIDENTIAL**

transition, but also to help contain the combustion generated pressure rises at low Mach number. The final portion of the burner is diverging to further relieve the pressures created by the combustion process and to permit gradual expansion of the burned gases to lower temperatures where the dissociated exhaust products partly recombine before entering the exhaust nozzle. This sudden expansion and subsequent divergence have a very close relation to the step cone (R) tailpipe, which was extensively tested in the arc tunnel tests and presented in previous sections of this report.

c) Combustor Length

The over-all length of the combustor was set to achieve appreciable mixing and recombination before entering the exhaust nozzle. The length is the same L/D used in most of the arc tunnel combustor tests and the performance is, therefore, well documented.

The length of the combustor was affected to a considerable extent by vehicle fuel volume considerations. It was not possible to reduce burner friction loss by shortening the combustor since this would shorten the proposed engine and reduce its fuel capacity below that required to fly the 6-12 vehicle. Thus, the combustor selected was not actually optimized on a thrust potential basis; i. e., the reduction in friction loss for a shorten combustor was not balanced against the loss in combustion efficiency to select an optimum length. Shorter lengths might be desirable to reduce the cooling requirements on the fuel, but this optimization was also not incorporated.

By making use of the six inlet barrels as fuel injector struts, the effective L/D of the combustor is increased beyond the tested value of 10. The good performance obtained in component tests could probably be achieved in a burner having a length somewhat shorter than the indicated length. However, the extra length will be needed to achieve the indicated performance if significant mal-distribution of airflow between inlet barrels exists due to engine angle-of-attack.

Application of mixing theory calculations to estimate for length, indicate adequate length and that substantial combustion should be completed in the six barrels upstream of the centerburner at M = 8-12 conditions.

d) Fuel Staging

Two sets of fuel injectors are provided. At M = 6 the fuel is injected near the transition from six barrels to one burner. The other fuel injector is placed as far upstream as possible without running the risk of unstarting the engine inlet.

**CONFIDENTIAL**

**CONFIDENTIAL**

The injectors are a low aspect ratio configuration each consisting of a long row of holes. These injectors could be built the same as those in the "R" tailpipe arc tunnel tests, however, a configuration improvement is recommended. Ground testing before flight can be used to verify these changes in the vehicle. The long row of holes can be made from six holes instead of 12 or 14. The cold-flow penetration correlations indicate that this will penetrate, as well as, longer rows, at the injection pressure designed for the engine. This reduced number holes simplifies the mechanical problems of construction and reduces the chances of fuel hole plugging.

The number of injectors for low Mach number flight could be modified to take advantage of the injection struts provided by the partitions between the six barrels, but this modification is incorporated in the recommended design only for the high-flight-Mach number or upstream fuel injector stage.

These injectors are designed to give sonic choked hydrogen flow at the injector throat, at all conditions.

A second stage of fuel injectors is provided upstream of the first to achieve higher performance at the higher Mach numbers. As flight Mach number increases from  $M = 6$  to near  $M = 8$ , some of the fuel is diverted to the upstream injector. This upstream burning results in increased wall forces and improved performance. By  $M = 10$  the downstream injectors are completely shut off. The six barrels act like six short constant-area mixing and combustion chambers that feed a single recombination chamber. This single centerburner also mixes any mal-distribution of fuel and air coming from the six barrels.

The upstream fuel injectors have a larger flow area than the downstream injectors. This area is larger to carry the hotter, higher equivalence fuel flows at the high Mach numbers. Tentatively, the injection holes in both stages are angled at  $30^\circ$  to the wall to provide some downstream fuel thrust. Subsequent mechanical considerations may alter this plan.

Test configurations AHmR and BHmR were functionally similar to the aft stage of the recommended combustor design with the forward stage inoperative. Configuration AHmR was capable of operation with equivalence ratios up to at least 0.7 at simulated Mach 6 flight conditions, without separating the burner inlet stream (Figure 139). Configuration BHmR demonstrated high performance at enthalpy levels simulating Mach 7.8 flight (Figure 170), indicating that the forward stage is not needed in the flight speed range of Mach 6.0 - 7.8. Introduction of some fuel into the forward stage in the upper part of this range would have no adverse effects, however.

**CONFIDENTIAL**

**CONFIDENTIAL**

At simulated flight speeds in excess of Mach 7.8, the performance of Configuration BHmR deteriorated, as evidenced by reduced thrust potential (Figure 170) and low levels of wall static pressure (Figure 147). Performance was restored by moving part of the fuel injection upstream in Configuration BHmGR. This is seen in the wall static pressure data from tests of this configuration (Figures 153 and 154). Test Configuration BHmGR was geometrically similar to both stages of the recommended combustor design, although its "forward stage" was foreshortened.

Ideally, sufficient fuel would be injected in the forward stage to maintain choked flow at its exit, where possible. Practically, however, several factors may limit the useful flow through the forward stage to lesser values. One of these is the physical blockage of the aft stage fuel jets, located at the exit from the forward stage. This three-dimensional mass addition effect will cause choking of the forward stage at a lower fuel flow than would otherwise occur. Another factor is the pressure gradient negotiable by the boundary layers of the combustor inlet stream. If excessively steep gradients are induced in the forward stage, the boundary layers may separate upstream into the induction system. In the latter respect, the boundary layers of the combustion test vehicle were probably more stable than those to be encountered in the engine.

At a flight speed of Mach 10 or higher, it is expected that the inlet stream to the forward stage will have sufficiently high enthalpy and velocity so that all the fuel can be injected into the forward stage without adversely affecting the induction system. This is substantiated by the relatively weak pressure gradients observed in the forward part of Configuration BHmGR at high enthalpy test conditions (Figure 154).

At flight speeds between Mach 7.8 and Mach 10, the fuel must be divided between the forward and aft stages, to limit the pressure gradients in the forward stage to levels tolerable to the induction system. The wall static pressure data of Figure 153 obtained from Configuration BHmGR at test conditions simulating Mach 8.9 flight, provide information useful in estimating the correct flow split. Two sets of data obtained at similar equivalence ratios (1.15-1.17) are shown. In one set, 84% of the fuel was injected from injector Hm, located ahead of injector G. The pressure in the forward portion of the combustor increased by a factor of six in a distance of four inches. This gradient is considered dangerously steep. It is feared that in the engine, this pressure rise would separate the boundary layer and propagate upstream into the induction system. In another set, only 17% of the fuel was injected from the forward injector. The pressure increased by a factor of only four in the first four inches of the burner. This gradient was caused primarily

**CONFIDENTIAL**

**CONFIDENTIAL**

by separations induced by the second fuel injector, since little fuel was injected from the first. The gradient would have been even more gentle had the second injector been located further downstream, and had the second injector directed its fuel obliquely into the airflow, instead of perpendicularly.

Of the two sets of data, the first showed evidence of excessive fuel from the forward injector, and the second showed evidence of insufficient fuel from the forward injector. It is estimated that 50% of the fuel injected from the forward injector would have produced optimum performance at this test condition.

Two considerations other than performance affected the design decision on the selected fuel splits between the two stages. It is desirable to maintain choked flow in the fuel injectors, and to confine fuel split valves to on-off valves rather than infinitely variable control valves. If the injectors are choked at a very low equivalence, 0.1-0.3 for example, then the resulting injection pressures at high equivalence ratios will be excessive. A minimum flow limit of 0.3 equivalence ratio to either injector was adopted.

The division of fuel between the two stages of the recommended combustor design is prescribed as shown in Figure 193. In the range of flight speeds between Mach 6 and Mach 7.8 all fuel is injected into the aft stage. From Mach 7.8 to Mach 9.5, the fraction of total fuel injected into the forward stage is increased linearly from 30% to 70% of the total fuel. This variation can be approximated by step changes. Above Mach 9.5 all fuel is injected into the forward stage.

e) Ignition

The two stages of fuel injectors provided for performance also provide the needed ignition technique. It was established in component tests that although a single fuel injector system would not auto-ignite at the burner inlet at  $M = 6$  conditions, a penetrating jet would initiate combustion in a stream which was already carbureted from an upstream injector. With an equivalence ratio between 0.1 and 0.5 from the upstream injectors, the downstream injectors should auto ignite. If any difficulties occur in lighting the engine, a flare or explosive charge such as used in component tests could be incorporated into the design.

2) Combustor Performance Over the Flight Map (Mach 6 to 12)

a) Efficiency, Wall Force and Friction from Mach 6 to 9 Tests

Of the various combustor configurations tested, the step-cone burners (Configurations AHmR, BHmR and BHmGR) resemble most closely the recommended combustor design. The measured performance

**CONFIDENTIAL**

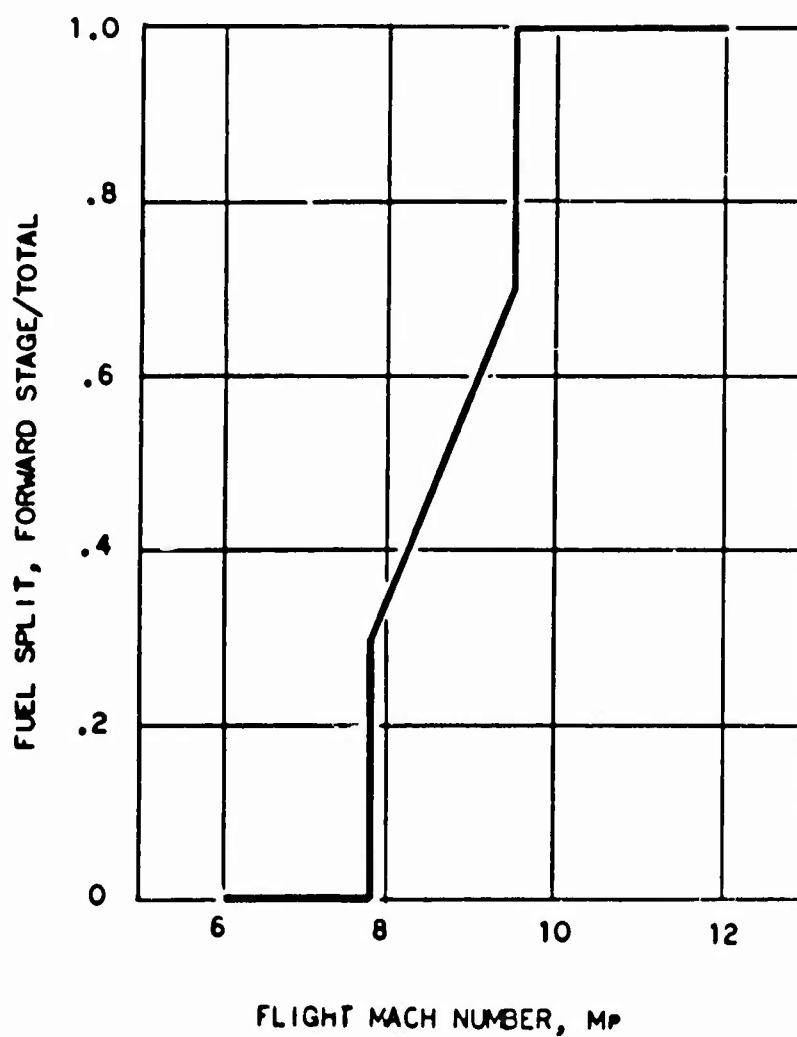
**CONFIDENTIAL**

Figure 193 - Fuel Staging for Recommended Combustor Design

**CONFIDENTIAL**

**CONFIDENTIAL**

of these burners may be used to predict the performance of the recommended combustor design, together with supporting data from other configurations. The predicted performance trends are also consistent with trends identified by calculations from mixing theory.

The combustion efficiency of Configuration AHmR at a simulated flight speed of Mach 7.8 was .75 at  $ER = .99$  and .84 at  $ER = 1.19$ . Configuration BHmR, which had a more realistic burner inlet Mach number for this enthalpy level, showed an efficiency of .75 at  $ER = .98$ , closely comparable with that of Configuration AHmR. These values appear in Table VII and Figure 169.

At higher enthalpy level, simulating Mach 8.4 flight, the combustion efficiency of Configuration BHmR degenerated to .66 at  $ER = 1.08$ . This reduced efficiency is evident in the low level of the wall static pressures measured during the test (Figure 147). In the test of Configuration BHmGR, which injected fuel further upstream from the step, the high level of wall static pressures indicative of high efficiency was restored (Figure 153), and was maintained at higher enthalpy levels, up to a simulated flight speed of Mach 10 (Figure 154). This is considered good evidence that by proper fuel staging, the efficiencies can be maintained at the flight Mach 7.8 level as flight speed is increased up to at least Mach 10.

The estimated combustion efficiency for the recommended combustor design based on component test results is shown in Figure 194, plotted as a function of equivalence ratio for various flight speeds, and in Figure 195, plotted as a function of flight speed for  $ER = 1.0$ . At low flight speeds, up to Mach 6.8, the efficiency level is expected to equal the high efficiencies attained by the step combustors (.90), due to the high mixing achieved in the transonic combustion mode. From Mach 6.8 to 7.8 the efficiency is expected to decline gradually to the level measured in the combustor tests at enthalpy levels simulating Mach 7.8.

At Mach 7.8 the variation of combustion efficiency with equivalence ratio is predicted to be as shown in Figure 194. The efficiency is expected to decrease approximately linearly with  $ER$  from a value of .90 at  $ER = .5$  to .74 at  $ER = 1.0$ . This trend was shown by the step combustor test data at this enthalpy level (Figure 169). Above stoichiometric, the efficiency is expected to increase with  $ER$  through a value of .84 at  $ER = 1.2$ . This trend was established from the step-cone combustor test data. It is interesting to notice that a minimum combustion efficiency near stoichiometric is also predicted from mixing theory as can be seen in Figure 64.

**CONFIDENTIAL**

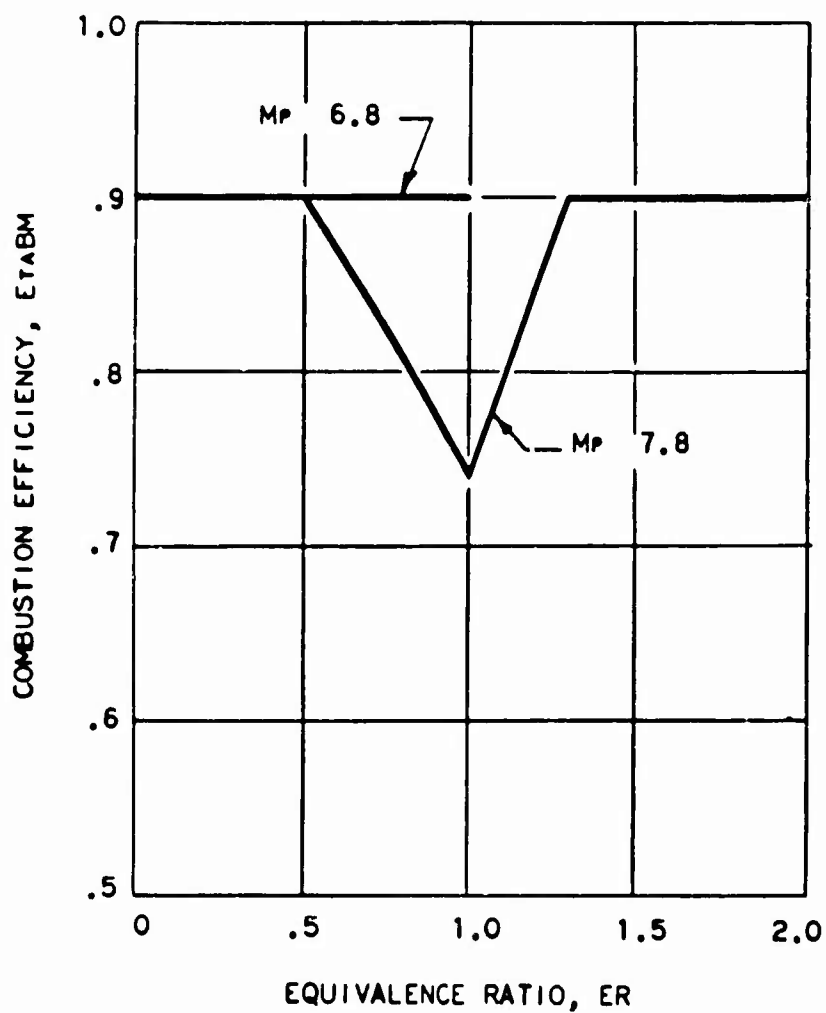
**CONFIDENTIAL**

Figure 194 - Predicted Combustion Efficiency of  
Recommended Combustor Design

**CONFIDENTIAL**

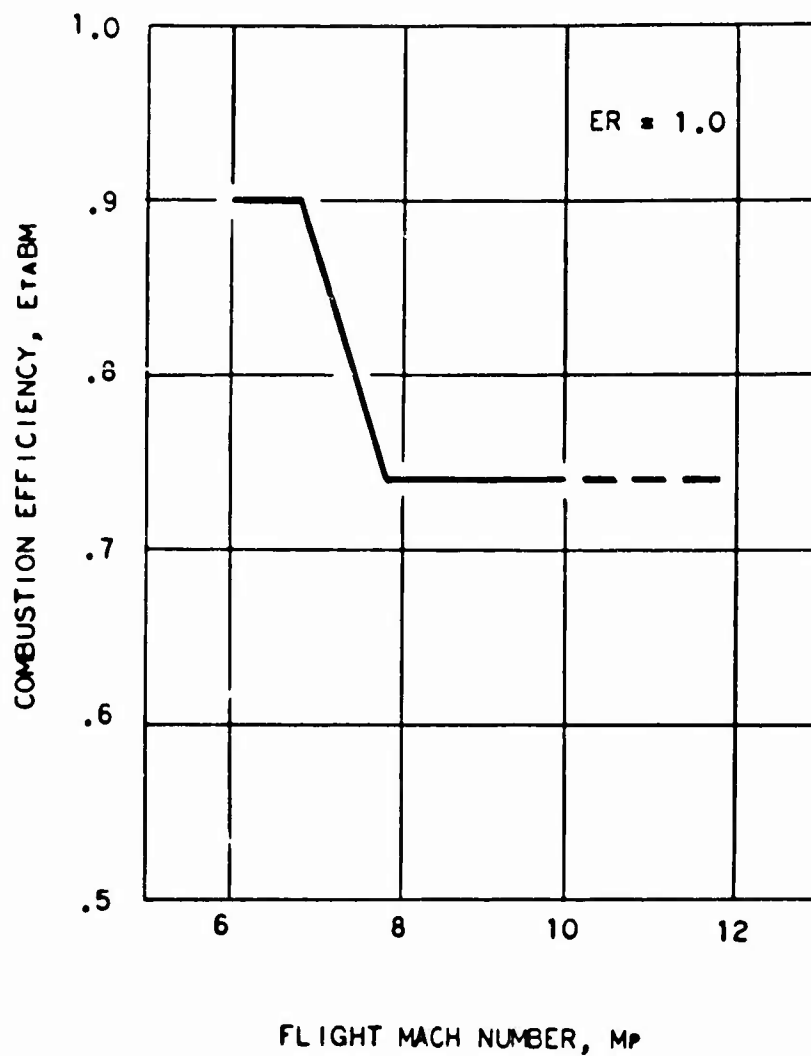
**CONFIDENTIAL**

Figure 195 - Predicted Combustion Efficiency of Recommended  
Combustor Design

**CONFIDENTIAL**

**CONFIDENTIAL**

Proper fuel staging, together with increasingly higher fuel temperatures, are expected to maintain the combustion efficiency at its Mach 7.8 level as flight speed is increased up to Mach 10. Beyond Mach 10, prediction of the efficiency trend is more uncertain, as no test data are available at these conditions. However, if the combustor pressure rise at  $M=12$  flight conditions can be made to occur in a short distance downstream of the fuel injector as was accomplished at  $M=10$ , Figure 154, then equivalent mixing rates and equivalent combustion efficiencies can be expected for the two Mach numbers.

The combustion efficiencies shown in Figure 194 for  $M=7.8$  to  $M=12$  are close to the values that were used for most of the mission studies that were done during the contract. The combustion efficiencies used for the final performance calculations were higher than these values. These higher values were predicted for the vehicle to account for an expected improvement in mixing in the vehicle.

Mixing is better in the vehicle due to the presence of six combustor inlets instead of one, and to the greater fuel penetration that occurs with the hotter fuel at the higher flight Mach numbers. Penetration of a given quantity of fuel increases when the fuel temperature increases. Component tests in the arc tunnel were confined to 500-550 R fuel. Part of the performance losses in the component tests were due to lean center regions that could have been corrected with increased penetration. The burner inlet in the component tests was a single duct. In the vehicle at high Mach number, fuel will be injected in six inlet barrels, having a total number of injectors six times as great as in the component tests. This increased number of injection points results in an improvement in mixing in the centerburner. The centerburner has the same  $L/D$  as in component tests.

Figure 196 is the performance level used in the final cycle calculations. This includes the performance increases above the component test level that is expected in the vehicle. Cycle calculations using this performance level also use an assumption of frozen nozzle expansion. No recombination of the exhaust gases takes place in the exhaust nozzle, the composition is frozen at the burner exit.

The mean pressure on the walls of a diverging combustor has an important effect on its over-all performance. In the step combustors tested, only the pressure acting on the step face influence the combustor performance. The test data (Figure 156) showed that this pressure was invariably low unless the step combustor were operated in the transonic mode. With the conical combustors and the step-cone combustors, however, the area divergence was distributed along the length of the burner, and the effective wall pressures were much higher.

**CONFIDENTIAL**

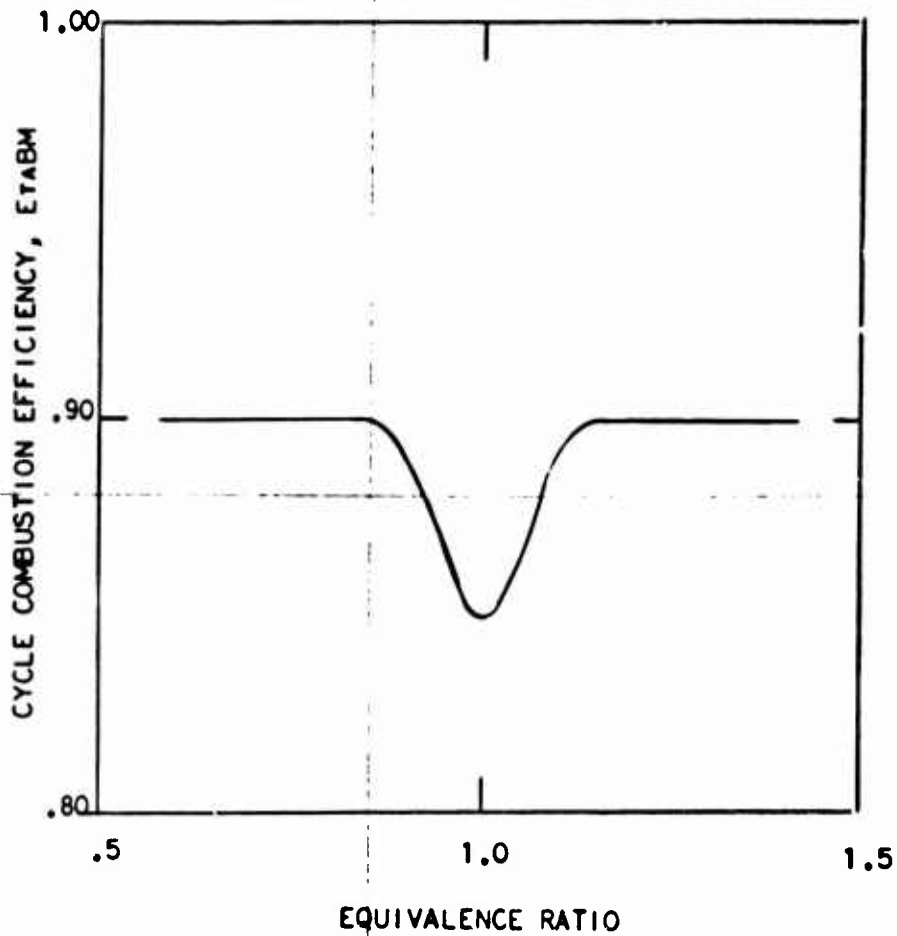
**CONFIDENTIAL**

Figure 196 - Cycle Performance Level

**CONFIDENTIAL**

**CONFIDENTIAL**

Inspection of the wall pressure data for the step-cone combustors Figures 139, 140, 145 through 149, 153 and 154 reveals that the mean pressure acting on the step and the diverging walls was in many cases approximately equal to the burner exit pressure. Since the step-cone combustor most closely resembles the recommended combustor design, these data are considered directly applicable.

The cycle program assumes that the burner is choked at the exit at  $M=6$  conditions. For the recommended design, this results in a calculated wall force that is less than the burner exit pressure giving a conservative performance calculation. At higher Mach numbers, the cycle analysis program uses a weighting factor,  $K$ , to define the combustor wall pressure in terms of the inlet and exit pressures:

$$P_w = P_4 + K(P_2 - P_4)$$

A cycle input value of  $K=0$  which is consistent with the experimental measurements would cause the cycle program to use a wall pressure equal to the burner exit pressure. The resulting performance level would be higher than the currently used cycle value of  $K=.5$ , which is a wall pressure equal to the average of burner inlet and exit pressures. Thus the cycle calculations that have been made are slightly conservative with respect to this performance parameter, in the range of the experimental measurements. The proper value to use above  $M=10$  is not established.

The remaining parameters affecting combustor performance are wall friction and the related length of the burner. The friction coefficients measured in the combustor tests averaged .0025, with considerable scatter. These data do not justify a deviation from the value of .00265 presently assumed in cycle analyses.

b) Applicability of Performance Parameters to Cycle Analyses

In dealing with thrust producing machines, the thermodynamic calculations are conventionally reduced to one-dimensional quantities at the entrance and exit of each component. That is, quantities such as pressure and temperature are invariant across the area in question for simplicity of calculation. In the actual component, these quantities (such as pressure and temperature) ordinarily vary significantly across the area in question. The problem of creating one-dimensional equivalents is the well-known averaging problem. Historically, jet propulsion devices have dealt with flow at subsonic  $M$  numbers and with flows which were close to uniform in the case of high performance components. In these subsonic flows, the

**CONFIDENTIAL**

**CONFIDENTIAL**

type of solution to the averaging problem frequently adopted introduced errors in the component performance numbers, but these errors were small relative to the inefficiencies in the high performance component, and these errors were not always sought out and isolated.

SCRAMJET cycle calculations involve a momentum balance across the combustor component. This balance utilizes impulse functions and forces on walls. The one-dimensional values used in the cycle should, therefore, represent the correct impulse function at the burner inlet and burner outlet. This is correctly accomplished if the thermodynamic quantities used to obtain one-dimensional averages are: area, massflow, total momentum and energy (or total enthalpy).

In general, calculation of the correct average quantities, which allow the above four quantities to be correct, will result in fictitious values for the other thermodynamic state quantities such as entropy, velocity, static temperature, static pressure, etc. These fictitious quantities, which may not appear anywhere in the actual profile measurements, are neither cause for alarm nor are they cause to discard the above averaging procedure. The true static temperatures and pressures which are of interest in estimating initial chemical reaction rates, must be determined independently of the one-dimensional cycle calculation; the entropy which is associated with certain common definitions of inlet efficiency, must also be determined independently of the cycle. With this approach for the cycle calculations, the inlet efficiencies that describe the burner inlet conditions are lower than those determined by some other techniques for averaging the burner inlet profile measurements. Also less inlet contraction is involved than for calculations which attempt to agree with the measured burner inlet static pressure or the entropy when this agreement is achieved by assuming an effective flow area rather than the true physical area of the flowpath.

In the first one-dimensional cycle calculations presented for the recommended 6-12 vehicle, the component performances are reported in terms of average quantities in which massflow, momentum, energy and area are implicit. The pressure forces on the burner walls and the forces between the wall and the airstream due to friction loss are input to the cycle independently of the one-dimensional average quantities. The "Combustion momentum loss" or "total pressure loss" is properly accounted for in the combustor momentum balance without the need for a specific cycle input.

The parameters of combustion efficiency ( $\eta_{BM}$ ) friction coefficient ( $C_f$ ), and wall pressure factor ( $K$ ), used to describe the performance of the test combustors and to predict the performance of the

**CONFIDENTIAL**

**CONFIDENTIAL**

recommended combustor design, can be used directly as input to cycle analysis computer programs to predict engine performance over the flight map. Although the thrust potential ( $\text{Eta}_{\text{NT}}$ ) is used extensively in the combustor analysis work, it is not used as input to cycle analysis. It is, however, a parameter descriptive of the over-all performance of the combustor, showing the combined effects of the other parameters, and is generated in a manner closely parallel to the cycle analysis techniques.

Particular effort was required to derive the combustion efficiency from the test data so that it would be compatible with the definition used in cycle calculations. The cycle analysis program assumes one-dimensional flow of a gas in chemical equilibrium. The exit stream from an inefficient combustor is defined, not by computing a non-equilibrium flow, but by using a flow in chemical equilibrium. The stagnation enthalpy of this flow is reduced by a fraction of the nominal heating value of the fuel equal to the inefficiency. The combustion inefficiency is thus taken as heat lost from the otherwise ideal system.

In reducing the test data, a hypothetical exhaust nozzle having an area ratio near that used by current study engines was assumed to have followed the test combustor. The non-uniform, non-equilibrium combustor exit stream was expanded through this hypothetical nozzle in a fairly rigorous manner to determine its thrust. A hypothetical one-dimensional, equilibrium stream having the same stagnation enthalpy, equivalence ratio, mass flow, area and total momentum as the combustor exit stream was then expanded through the hypothetical nozzle. The stagnation enthalpy of the hypothetical stream was reduced until the nozzle produced the same thrust as with the test combustor's exit stream. The amount by which the stagnation enthalpy was reduced, taken as a ratio to the heating value of the fuel, defined the combustion inefficiency ( $1 - \text{Eta}_{\text{BM}}$ ).

The quoted values of combustion efficiency, when input to the cycle analysis program, will produce the correct thrust from the exhaust nozzle.

e. Generalizations of the Recommended Design

1) Mach 3 to 6

To extend the operable range of the combustor to lower Mach numbers, the burner area ratio must be increased or the equivalence ratio must be increased or the equivalence ratio must drastically reduced. Increasing the burner area ratio for low Mach number operation does not eliminate the need for maintaining combustion in the smaller area for high performance at  $M = 6$ .

**CONFIDENTIAL**

**CONFIDENTIAL**

To accomplish both tasks,  $M=6$  and also lower Mach numbers, an additional fuel injector stage is required, positioned in a larger flow area region downstream of the  $M=6$  injectors, followed by additional burner length. Variable inlet and combustor geometry are also possible solutions.

At the lower Mach numbers ignition will be more difficult, and flame stabilization and flame spreading between fuel injectors will have to be considered in the design.

## 2) Mach 12 and Above

With increasing flight Mach number, the length of the constant area section at the burner may need to be longer to achieve good mixing. The pressure rise may require longer lengths for development because of the reduced angle of shock waves at higher Mach numbers and the pressure rise may be less because of the smaller burner temperature-rise ratio that may be involved. The increased difficulty of mixing resulting from the more gradual and lesser pressure rise may involve significant performance losses. One encouraging observation with respect to mixing is associated with the initial fuel conditions. Although the airflow is at high Mach number and its velocity is not much affected by static pressure gradients, the fuel injected from a penetrating jet, may have an effective downstream Mach number between zero and one.

A static pressure gradient just downstream of the fuel injectors can have a big effect on the resulting mixing, just as was discussed in this report for  $M=6$  conditions. Also, at the higher Mach numbers, higher equivalence ratios may be involved, relieving considerably the uniformity of fuel required.

To minimize friction loss and heat transfer loads it may be necessary to design shorter burners. Film or transpiration cooling may become an essential part of the design to further minimize friction and heat transfer problems.

## 3) Effects of Size

The combustor is easily scaled to larger sizes. In contrast to some other types of burners which do not scale easily, these SCRAMJET burners are mixing, rather than reaction limited, and all dimensions can be scaled, the length as well as the diameter. The effects of Reynolds number on the mixing are negligible, and have an effect only insofar as they effect the vehicle performance through boundary layer effect on the walls. To obtain equivalent operation, all dimensions must be scaled, the length as well as the diameter of the duct and the diameter for the fuel injector parts.

Although the combustor is basically mixing limited, a small performance improvement is predictable with increasing size, due to the

**CONFIDENTIAL**

**CONFIDENTIAL**

increased chemical reaction lengths available in the recombination region of the burner or exhaust nozzle.

#### D. CONCLUSIONS & RECOMMENDATIONS

##### 1. CONCLUSIONS

###### a. Demonstrated Performance Levels

Combustor performance adequate to accomplish the flight test vehicle's mission was demonstrated experimentally with test conditions simulating flight speeds to Mach 7.8.

Combustors designed with an abrupt increase in area by a factor of 2.5 showed high combustion efficiency and excellent resistance to inlet interference, but at simulated flight speeds above Mach 7, they suffered low wall pressure.

Combustors having an area increase by a factor of 2.5 by means of a straight taper showed high wall pressures at high simulated flight speeds, but were more subject to inlet interference and suffered lower combustion efficiency than the step combustors. High wall pressures were obtained without steep pressure gradients. Reduced efficiency was attributed to the absence of steep pressure gradients.

Combustors designed with an area ratio of 2.0, accomplished via a small step followed by a straight taper, provided both high wall pressure and high combustion efficiency with conditions simulating flight speeds up to Mach 7.8. Resistance to inlet interference at low flight speeds was acceptable. Maintenance of high performance levels at flight speeds above Mach 7.8 required shifting the combustion to a constant-area duct located ahead of the diverging combustor. This was true in tests which were conducted with simulated flight speeds up to Mach 10.

Appending an exhaust nozzle to the test combustors did not alter their performance. The composition of the exhaust gas departed from equilibrium during the nozzle expansion.

###### b. Increased Knowledge

###### 1) Ignition

Auto ignition of hydrogen jets with a total temperature of 500°R is unreliable at flight speeds less than Mach 7.7, even though the jets are directed normal to the air stream. Ignition is easily effected by any device that momentarily chokes the combustor, such as an air blast, a fuel surge, or a short-duration, solid-propellant gas generator. Ignition occurs because

**CONFIDENTIAL**

**CONFIDENTIAL**

of the high static pressure and static temperature created in the fuel/air mixture. A jet injecting normally into a fuel/air mixture produces a shock wave in the mixture which ignites the fuel. This last mechanism was recommended as the ignition device for the vehicle because two fuel injector stages were considered desirable for performance reasons. Once initiated, combustion is easily sustained at low flight speeds provided sufficient fuel is burned to thermally choke the combustor. This was demonstrated at simulated flight speeds as low as Mach 5.2, however, the low flight speed limit was not investigated.

## **2) Jet Penetration**

A simple but general correlation of cold-flow penetration data was obtained, useable for designing combustor fuel injectors. Configurations giving greater penetration than round 90° holes were identified, including a configuration injecting a 30° to the stream, which provides some downstream thrust. These improved configurations were used in arc tunnel combustion tests, and were incorporated into the design of the 6-12 vehicle.

The shape of the jet strongly influences its penetration at low injection pressures; jets greatly elongated in the airflow direction penetrate farther than nearly circular jets.

## **3) Fuel Distribution**

Fuel injectors having eight fuel jets spaced about the periphery of the cylindrical air duct produced uniform fuel distribution in the air stream ten diameters downstream when mixing was assisted by strong pressure gradients in the duct. With lesser pressure gradients, the radial distribution was uneven, rich near the walls and lean in the center.

Without strong pressure gradients to assist mixing, attainment of uniform fuel distribution requires over-stoichiometric fuel flow, high fuel temperature, or injection struts.

Injectors having only four points of injection required stronger pressure gradients to attain uniform distribution. Without strong pressure gradients, the fuel distribution was uneven circumferentially, as well as, radially.

A unified penetration and mixing theory was developed and the observed beneficial effect of pressure gradients on mixing was explained theoretically.

## **c. Projected Performance Levels**

With continued development effort, a combustion efficiency of .90 is believed attainable at all flight conditions.

**CONFIDENTIAL**

**CONFIDENTIAL**

An upper limit to attainable efficiency is imposed by the necessity of cooling the burner walls requiring a temperature profile in the burner exit stream.

## 2. RECOMMENDATIONS

Flight test experience with a SCRAMJET combustor in a hypersonic ramjet is needed to verify the results of component ground tests, provide data at conditions unattainable in ground test facilities, and identify areas requiring further development. The available data provide sufficient background for the reliable aerothermo design of the combustor for such a flight test.

Techniques should be investigated for extrapolating performance data from combustor tests to conditions unattainable in ground test facilities. These techniques should include design of combustion experiments representative of higher flight speeds than those directly simulated.

Test experience is needed with geometric configurations different from the cylindrical burners tested here. Annular combustors are of particular interest. This additional experience would permit the technology from this engine to be extrapolated to other proposed engine configurations proposed for this Mach 6-12 mission, as well as, for other missions.

The development of techniques for measuring combustor performance and of facilities for better simulation of flight conditions should be continued.

Component ground test of a flight-weight, fuel-cooled combustor would provide added assurance of success of the flight test mission.

**CONFIDENTIAL**

REFERENCES

1. "Analytical and Experimental Investigation of Advanced Air-Breathing Engines; Final Report" - Propulsion Laboratory, Research and Technology Division, AFSC, Report APL-TDR-64-21, May 7, 1964. Confidential
2. Colley, W. C. and Kenworthy, M. J., "Exploratory Experiments on Mixing and Burning of Hydrogen Jets in Supersonic Air Streams" - General Electric Company, TIS Report R62FPD394, January 1963. Confidential
3. "Equations, Tables and Charts for Compressible Flow", NASA Report No. 1135, Ames Research Staff, Ames Aeronautical Laboratory, Moffett Field, California, 1953.
4. Erickson, L. H. and Bell, "Optimum Design Investigation of Secondary Injection Thrust Vector Control, Thiokol TW 965-12-61, AFSC-TR-61-1, 1962. Confidential
5. Zukoski, E. E. and Spald, F. W., "Secondary Injection of Gases into a Supersonic Flow", California Institute of Technology, Pasadena, California, AIAA Preprint No. 64-110, January 29-31, 1964.
6. Strike, W. T., Schueler, C. J. and Deitering, J. S., "Interactions Produced by Sonic Lateral Jets Located on Surfaces in a Supersonic Stream", AEDC Report TDR63-22, April 1963.
7. Vranos, A. and Nolan, J. J., "Supersonic Mixing of Helium and Air", Pratt and Whitney Aircraft - Presented at the 31st 'Bumblebee' Propulsion Panel Meeting at Applied Physics Laboratory, May 1964. Confidential
8. "Analytical and Experimental Investigation of Advanced Air-Breathing Engines; Mid-Term Technical Report" - Propulsion Laboratory, Aeronautical Systems Division, July - December 1962. Confidential
9. Dowdy, M. W. and Newton, Jr., J. F., "Investigation of Liquid and Gaseous Secondary Injection Phenomena on a Flat Plate with  $M=2.01$  to  $M=4.54$ ", Jet Propulsion Laboratory, California Institute of Technology, Pasadena, California, Technical Report No. 32-542, December 23, 1963.

AF APL-TR-65-103

References (continued)

10. "Analytical and Experimental Investigation of Advanced Air-Breathing Engines; Mid-Term Technical Report" - Propulsion Laboratory, Aeronautical Systems Division, AFSC, Report ASD-TDR-63-193, January 1963. Secret
11. "Analytical and Experimental Investigation of Advanced Air-Breathing Engines; Fourth Quarterly Progress Report" - July 1963. Secret
12. "Advanced Air-Breathing Engines" - Air Force Aero Propulsion Laboratory, AFSC, Report APL-TRD-64-21 Volume II: Experimental Investigation; May 1964. Confidential
13. Colley, W. C. "Loss Mechanisms in Supersonic Combustion Systems" - General Electric Company, Design Memorandum DM63-117, May 1963.
14. Colley, W. C. and Lingen, A., "Supersonic Combustor Performance Criteria" - General Electric Company, TIS Report R64FPD143, May 1964. Confidential
15. Henderson, R. L., "Equilibrium Gas Boundary Layer Program", General Electric Company, AETD - Unnumbered Memorandum, December 18, 1964.
16. Rubins, P. M. and Rhodes, R. P., "Shock-Induced Combustion with Oblique Shocks - Comparison of Experiment and Kinetic Calculations", AIAA-ASME Hypersonic Ramjet Conference, Naval Ordnance Laboratory, White Oak, Maryland, April 1963.
17. Mossey, P. W., "Hypersonic Arc Tunnel Static Temperature Measurement System" - General Electric Company, TIS Report R64FPD282, November 1964.
18. Winovich, W., "On the Equilibrium Sonic-Flow Method for Evaluating Electric-Arc Air-Heater Performance", NASA TND-2132, March 1964.
19. Mossey, P. W., "Comparison of Calculated and Observed Sodium Line Reversal Temperature on Hy Arc Runs 110 and 111" - General Electric Company, Design Memorandum DM64-483, September 1964.
20. Korst, H. H., Chow, W. L., and Zumwalt, G. W., "Research on Transonic and Supersonic Flow of a Real Fluid at Abrupt Increases in Cross Section", University of Illinois ME Technical Report 392-5, December 1959.

References (continued)

21. Townend, L. H., "Some Effects of Stable Combustion in Wakes Formed in a Supersonic Stream" - Royal Aircraft Establishment (Farnborough) Technical Note Aero. 2872, March 1963.
22. Bowyer, J. M. and Carter, W. V., "Separated Flow Behind a Rearward-Facing Step With and Without Combustion", AIAA Journal, Volume 3, No. 1, pp. 181-183, January 1965.
23. Spalding, D. B., and Tall, B. S., "Flame Stabilization in High Velocity Gas Streams and the Effect of Heat Losses at Low Pressures", The Aeronautical Quarterly, Volume V, September 1954.
24. Zakkay, V. and Krause, E., "Mixing Problems with Chemical Reactions", Aeronautical Research Laboratories, Office of Aerospace Research, USAF, Report No. ARL 63-109, June 1963.
25. Collinson, E. S., "Turbo-Propulsion Combustion System Exploratory Development Program - Phase I Report," 1 April 1964 through 31 December 1964, General Electric Company TIS Report R64FPD341, January 1965.
26. Schlichting, H., Boundary Layer Theory, McGraw-Hill Book Co., Inc., London: Pergamon Press LTD, Karlsruhe: Verlag G. Braun, 1955.
27. Hinze, J. O., Turbulence, McGraw-Hill Book Company, Inc., New York 1959.
28. Keagy, W. R., and Weller, A. E., "A Study of Freely Expanding Inhomogeneous Jets", Proc. Heat Transfer and Fluid Mechanics Inst., Berkley, California, 1949.
29. Hawthorne, W. R., Weddell, D. S. and Hottel, H. C., "Mixing and Combustion in Turbulent Gas Jets", Third Symposium on Combustion Flame and Explosion Phenomena, Baltimore, Maryland, The Williams and Wilkins Co., 1949.
30. Lerberg, E. Q., and Franciscus, L. C., "Effects of Exhaust Nozzle Recombination Performance" NASA presented at AIAA-ASME Hypersonic Ramjet Conference, Naval Ordnance Lab., White Oak, Md., April 2, 3-25, 1963.
31. Schott, G. L. and Kinsey, J. L., "Kinetic Studies of Hydroxyl Radicals in Shock Waves. II. Induction Times in the Hydrogen-Oxygen Reaction", The Journal of Chemical Physics, Volume 29, No. 5, November 1958.

## APPENDIX I

### DERIVATION OF GENERALIZED IRREVERSIBLE FLOW FUNCTION

Consider the one-dimensional flow of a perfect gas past a point in a duct. The gas has the equation of state

$$p = \rho RT \quad (1)$$

where  $P$  = static pressure, lbf/ft<sup>2</sup>

$\rho$  = density, lbm/ft<sup>3</sup>

$R$  = 1545.4/m, gas constant, ft.lbf/lbm°R

$m$  = molecular weight, lbm/mole

$T$  = static temperature, °R

The equation of continuity of mass is

$$w = \rho AV \quad (2)$$

where  $w$  = flow, lbm/sec

$A$  = flow area, ft<sup>2</sup>

$V$  = velocity, ft/sec

Combining (1) and (2),

$$w = pAV/RT \quad (3)$$

The sonic velocity of a perfect gas is

$$a = \sqrt{\gamma gRT} \quad (4)$$

where  $\gamma$  = ratio of specific heats

$g$  = gravitational constant = 32.174 ft.lbm/lbf sec<sup>2</sup>

The Mach number is defined as

$$M = V/a \quad (5)$$

Combining (3), (4), and (5),

$$w = p A M \sqrt{\frac{\gamma R}{R T}} \quad (6)$$

The well known relationship between total (adiabatic stagnation) temperature and static temperature is

$$\frac{T_0}{T} = 1 + \frac{\gamma - 1}{2} M^2 \quad (7)$$

Using (7), equation (6) can now be written

$$w = p A M \sqrt{\frac{\gamma R}{R T_0} \left(\frac{T_0}{T}\right)} = p A M \sqrt{\frac{\gamma R}{R T_0}} \sqrt{1 + \frac{\gamma - 1}{2} M^2} \quad (8)$$

The total momentum (impulse function, stream thrust) is defined as:

$$F = pA + wV/g \quad (9)$$

Combining (3) and (9),

$$F = pA + \frac{pAV^2}{gRT} = pA \left(1 + \frac{V^2}{gRT}\right) \quad (10)$$

Using (4) and (5),

$$F = pA (1 + \gamma M^2) \quad (11)$$

Eliminating the product  $pA$  between (8) and (11), the desired function is obtained:

$$N = \frac{RT_0}{\gamma g} \left(\frac{w}{F}\right)^2 = \frac{M^2 \left(1 + \frac{\gamma-1}{2} M^2\right)}{(1 + \gamma M^2)^2} \quad (12)$$

The function  $N$  reaches a maximum when  $M = 1$ :

$$N^* = \frac{1}{2(\gamma + 1)} \quad (13)$$

Conveniently, the ratio

$$\frac{N}{N^*} = \frac{2(\gamma + 1) M^2 \left(1 + \frac{\gamma-1}{2} M^2\right)}{(1 + M^2)^2} \quad (14)$$

is identical to the oft-tabulated function  $T_0/T_0^*$  for Rayleigh - line flow (constant  $w$ ,  $F$ ,  $\gamma$ , and  $R$ ).

Confidential

Security Classification

DOCUMENT CONTROL DATA - R&D		
(Security classification of title, body of abstract and indexing annotation must be entered when the overall report is classified)		
1. ORIGINATING ACTIVITY (Corporate author) Flight Propulsion Division General Electric Company Cincinnati, 15, Ohio		20. REPORT SECURITY CLASSIFICATION Confidential
		23. GROUP Group 4
3. REPORT TITLE ANALYTICAL AND EXPERIMENTAL EVALUATION OF THE SUPERSONIC COMBUSTION RAMJET ENGINE (U) VOLUME II		
4. DESCRIPTIVE NOTES (Type of report and inclusive dates) Final Technical Report - Period June 1964 through June 1965		
5. AUTHOR(S) (Last name, first name, initial) Authorized by: Aerospace Propulsion Systems Operation Advanced Engine and Technology Department		
6. REPORT DATE 1 December 1965	7a. TOTAL NO. OF PAGES 370	7b. NO. OF REFS 31
8a. CONTRACT OR GRANT NO. Contract No. AF33(615)-1586 PROJECT NO. BPSN 4 (6399 - 651E)	9a. ORIGINATOR'S REPORT NUMBER(S) General Electric - R65FPD184	
	9b. OTHER REPORT NUM(S) (Any other numbers that may be assigned this report) AFAPL-TR-65-103	
10. AVAILABILITY/LIMITATION NOTICES In addition to security requirements which apply to this document and must be met, each transmittal outside the agencies of the U.S. Government must have prior approval of the Air Force Aero Propulsion Laboratory, RTD, WPAFB		
11. SUPPLEMENTARY NOTES		12. SPONSORING MILITARY ACTIVITY Air Force Aero Propulsion Laboratory Research and Technology Division Air Force Systems Command, USAF
13. ABSTRACT This was an experimental and analytical investigation to supply design information for the aerothermo design of a supersonic combustor for a flight test vehicle. The penetration of fuel jets into a supersonic stream was investigated in a cold flow supersonic wind tunnel and combustion tests of scale model combustors were conducted in General Electric's Hypersonic Arc-Tunnel. Combustion tests of several configurations identified a burner having adequate performance characteristics for achieving the vehicle mission. The aero-thermo design of the vehicle combustor was based on this tested configuration. Volume II of this three volume report is devoted to investigations of "Fuel Injection and Combustion" in supersonic airstreams.		

DD FORM 1473

Confidential

Security Classification

Security Classification

14	KEY WORDS	LINE A		LINE B		LINE C	
		ROLE	BY	ROLE	BY	ROLE	BY

INSTRUCTIONS

1. **ORIGINATING ACTIVITY:** Enter the name and address of the contractor, subcontractor, grantee, Department of Defense activity or other organization (corporate author) issuing the report.

2a. **REPORT SECURITY CLASSIFICATION:** Enter the overall security classification of the report. Indicate whether "Restricted Data" is included. Marking is to be in accordance with appropriate security regulations.

2b. **GROUP:** Automatic downgrading is specified in DoD Directive 5200.10 and Armed Forces Industrial Manual. Enter the group number. Also, when applicable, show that optional markings have been used for Group 3 and Group 4 as authorized.

3. **REPORT TITLE:** Enter the complete report title in all capital letters. Titles in all cases should be unclassified. If a meaningful title cannot be selected without classification, show title classification in all capitals in parentheses immediately following the title.

4. **DESCRIPTIVE NOTES:** If appropriate, enter the type of report, e.g., interim, progress, summary, annual, or final. Give the inclusive dates when a specific reporting period is covered.

5. **AUTHOR(S):** Enter the name(s) of author(s) as shown on or in the report. Enter last name, first name, middle initial. If military, show rank and branch of service. The name of the principal author is an absolute minimum requirement.

6. **REPORT DATE:** Enter the date of the report as day, month, year, or month, year. If more than one date appears on the report, use date of publication.

7a. **TOTAL NUMBER OF PAGES:** The total page count should follow normal pagination procedures, i.e., enter the number of pages containing information.

7b. **NUMBER OF REFERENCES:** Enter the total number of references cited in the report.

8a. **CONTRACT OR GRANT NUMBER:** If appropriate, enter the applicable number of the contract or grant under which the report was written.

8b. &c. &d. **PROJECT NUMBER:** Enter the appropriate military department identification, such as project number, subproject number, system numbers, task number, etc.

9a. **ORIGINATOR'S REPORT NUMBER(S):** Enter the official report number by which the document will be identified and controlled by the originating activity. This number must be unique to this report.

9b. **OTHER REPORT NUMBER(S):** If the report has been assigned any other report numbers (either by the originator or by the sponsor), also enter this number(s).

10. **AVAILABILITY/LIMITATION NOTICES:** Enter any limitations on further dissemination of the report, other than those

imposed by security classification, using standard statements such as:

- (1) "Qualified requesters may obtain copies of this report from DDC."
- (2) "Foreign announcement and dissemination of this report by DDC is not authorized."
- (3) "U. S. Government agencies may obtain copies of this report directly from DDC. Other qualified DDC users shall request through \_\_\_\_\_."
- (4) "U. S. military agencies may obtain copies of this report directly from DDC. Other qualified users shall request through \_\_\_\_\_."
- (5) "All distribution of this report is controlled. Qualified DDC users shall request through \_\_\_\_\_."

If the report has been furnished to the Office of Technical Services, Department of Commerce, for sale to the public, indicate this fact and enter the price, if known.

11. **SUPPLEMENTARY NOTE:** Use for additional explanatory notes.

12. **SPONSORING MILITARY ACTIVITY:** Enter the name of the departmental project office or laboratory sponsoring (paying for) the research and development. Include address.

13. **ABSTRACT:** Enter an abstract giving a brief and factual summary of the document indicative of the report, even though it may also appear elsewhere in the body of the technical report. If additional space is required, a continuation sheet shall be attached.

It is highly desirable that the abstract of classified reports be unclassified. Each paragraph of the abstract shall end with an indication of the military security classification of the information in the paragraph, represented as (TS), (S), (C), or (U).

There is no limitation on the length of the abstract. However, the suggested length is from 150 to 225 words.

14. **KEY WORDS:** Key words are technically meaningful terms or short phrases that characterize a report and may be used as index entries for cataloging the report. Key words must be selected so that no security classification is required. Identifiers, such as equipment model designation, trade name, military project code name, geographic location, may be used as key words but will be followed by an indication of technical content. The assignment of links, rules, and weights is optional.

Security Classification